NBS SPECIAL PUBLICATION 326

Accurate Characterization of the High-Pressure Environment

U.S. DEPARTMENT OF COMMERCE
National Bureau of Standards

UNITED STATES DEPARTMENT OF COMMERCE • Maurice H. Stans, *Secretary*
NATIONAL BUREAU OF STANDARDS • Lewis M. Branscomb, *Director*

Accurate Characterization of The High-Pressure Environment

Proceedings of a Symposium held at the National Bureau of Standards, Gaithersburg, Md., October 14–18, 1968

Edited by

Edward C. Lloyd

Institute for Basic Standards
National Bureau of Standards
Washington, D.C. 20234

National Bureau of Standards Special Publication 326

Nat. Bur. Stand. (U.S.), Spec. Publ. 326, 343 pages (March 1971)
CODEN: XNBSA

Issued March 1971

For sale by the Superintendent of Documents, U.S. Government Printing Office
Washington, D.C. 20402 (Order by SD Catalog No. C 13.10:326). Price $4.50

Abstract

The volume contains 38 papers prepared for the Symposium on Accurate Characterization of the High-Pressure Environment held on October 14–18, 1968, at Gaithersburg, Maryland, under the sponsorship of the National Bureau of Standards and the Geophysical Laboratory of the Carnegie Institution of Washington. The papers are presented with the discussions that occurred during the sessions. The book also includes reports of several informal committees of the conferees on choices of reference pressure materials and on other matters relevant to improved measurement and calibration. The Symposium was intended to provide an authoritative survey of problems and techniques presently in use or proposed for precise high-pressure measurement and for temperature measurement at high pressure.

Key words: Accurate measurement; equation-of-state; fixed points; high pressure; high-pressure equipment; instrumentation; pressure scale; shock wave technique; temperature.

Library of Congress Catalog Card No. 79-706140

Contents

SESSION V

Chairman: C. W. Beckett

SESSION VI

Choirman: F. R. Boyd, Jr.

SESSION VII

Chairman: R. Roy

APPENDIX

Symposium on
Accurate Characterization of the High Pressure Environment
Oct. 14–18, 1968

Photograph Key

1. John C. Bowen
2. M. van Thiel
3. George Jura
4. D. B. McWhan
5. R. Kaneda
6. C. Susse
7. M. Contre
8. G. Kennedy
9. H. Young
10. P. St. Pierre
11. Ikuo Kushiro
12. A. S. Kusubov
13. S. Akimoto
14. H. P. Bovenkerk
15. Ivan Getting
16. Willis Mock, Jr.
17. U. O. Hutton
18. D. H. Chung
19. M. F. Rose
20. A. Jayaraman
21. R. S. Kirk
22. Tom Clark
23. Naoto Asami
24. I. L. Spain
25. O. B. Verbeke
26. Naoto Kawai
27. Daniel Decker
28. F. R. Boyd, Jr.
29.
30. Eugene Hryckowian
31. Harold D. Stromberg
32. J. Houck
33. W. A. Bassett
34. Francis Bundy
35. S. Minomura
36. Charles Beckett
37. Robert Zeto
38. Renato Bautista
39. Boris Vodar
40. David H. K. Mao
41. Alvin van Valkenburg
42. G. R. Barsch
43. P. H. Abelson
44. Charles Bosco
45. M. C. Krupka
46. Rene Cavailhe
47. D. L. Hamilton
48. A. Lacam
49. R. H. Wentorf
50. G. S. Kell
51. E. C. Lloyd
52. M. C. Gilbert
53. A. Taylor
54. Alan Webb
55. Leon Thomsen
56. Albert Holt
57. C. B. Sclar
58. H. M. Strong
59. Marilyn S. Werkema
60. D. J. Pastine
61. J. D. Barnett
62. R. E. Hanneman
63. J. R. Hastings
64. Leo Merrill
65. G. A. Samara
66. P. D. Calvert
67. Eric Lundblad
68. O. Jones
69. H. Tracy Hall
70. G. E. Duvall
71. M. Cowperthwaite
72. L. C. Towle
73. J. Haygarth
74. Stanley E. Babb
75. F. Seifert
76. G. S. James
77. Rustum Roy
78. Jac Paauwe
79. Elvin M. Compy
80. Eugene Shull
81. Gene J. Scott
82. Ian MacGregor
83. D. P. Johnson
84.
85. Paul J. Freud
86. J. Jackson
87. James L. Cross
88. Y. A. Atanov
89. Z. P. Chang
90. Peter Bell
91. W. J. Carter
92. P. N. La Mori
93. A. Cezairliyan
94. E. V. Zolotykh
95. Donald H. Lindsley
96. J. L. England
97. C. E. Weir
98. Henry O. A. Meyer
99. K. Vedam
100. Peter L. M. Heydemann

This Proceedings volume includes all the papers, for which manuscripts were received, presented during the Symposium on Accurate Characterization of the High-Pressure Environment, October 14 to 18, 1968. In addition, the Appendix includes one panel discussion and reports of three informal committees, and two papers prepared subsequent to the meeting as an extension of discussions during the meeting. There were several informal presentations during the symposium for which no manuscripts were prepared, including opening remarks by the Session Chairmen and a keynote discussion by the opening speaker.*

The Symposium was intended to provide an authoritative survey of problems and techniques presently in use or proposed for precise high-pressure measurement and for temperature measurement at high pressure. It was hoped that a tentative consensus could be reached by the conferees on several important aspects of the measurement of high pressures and high temperatures, and a panel and three committees, whose reports appear in the Appendix, were established for this purpose. Since the list of prospective participants represented the majority of the high-pressure laboratories in the world, it was felt that the floor discussions would be of particular value. Thus, time priority was given during the sessions to the discussion, and both a stenotype record and a magnetic tape record were made of all discussions. Edited versions of these discussions appear with the papers. The Symposium organizers feel that these arrangements were successful, and it is hoped that the added value of the Proceedings volume will compensate for the delay in publication which is due, in part, to the extensive editing and correspondence required with the conference participants.

While no formal "referee system" has been used for the papers, it is felt that the discussion accompanying the papers has served this purpose in many cases, at least on important points.

The organizing group included C. W. Beckett, E. C. Lloyd, and D. P. Johnson of the National Bureau of Standards, and F. R. Boyd, Jr., and P. Bell of the Geophysical Laboratory, Carnegie Institution of Washington. Dr. Beckett acted as General Chairman. Enthusiastic cooperation of Dr. P. H. Abelson of the Carnegie Geophysical Laboratory and A. van Valkenburg of the National Science Foundation gave important support to the effort.

The staff of the NBS Office of Technical Information and Publications, particularly Mr. R. T. Cook, made important contributions to the successful arrangements for the conduct of the Symposium. Mrs. Barbara Mayo-Wells has prepared the text material for the printers, with the assistance of the Graphic Arts Section under Mr. C. F. Peters in preparing the illustrations and graphs. Mr. Raymond Gates of that Section prepared the key to the group photograph of the participants.

Special thanks is due Miss Judy Eyler of the NBS Mechanics Division Office for her untiring efforts before, during, and after the Symposium in efficiently handling many of the essential details concerned with arrangements for participants and preparation of the Proceedings volume.

EDWARD C. LLOYD

February 15, 1971

*Dr. H. G. Drickamer, University of Illinois, opened the symposium with a discussion concerning the role of high pressure calibration in scientific research.

*Introduction and Summary**

The importance to science and technology of precise measurements characterizing the high-pressure environment is demonstrated by the rapidly increasing activity in research, development, and industrial technology, involving such measurements. It has already become apparent that at an appropriate time it would be desirable to reach agreement on a pressure scale somewhat analogous to the temperature scale, over the range from 5,000 to 200,000 bars, and possibly higher pressures. Such a scale would be particularly helpful in coordinating the results being reported by the many laboratories now engaged in research involving the high pressure environment. Accuracy of measurement of elevated temperatures at high pressures is also limited, and the need for development of additional reference techniques for temperature measurement up to 2000 K at high pressures should be assessed.

This symposium was intended to provide an authoritative survey of precise measurement problems and techniques now in use or proposed. It was hoped that the symposium would permit critical evaluation of the need for efforts toward the development of improved measurement standards, and identification of probable fruitful lines of investigation toward establishment of such standards. The survey should provide the information needed to evaluate the feasibility of obtaining early agreement on a provisional pressure scale.

The symposium was attended by about 140 participants from the United States and abroad. Other countries represented included Canada, England, France, Japan, South Africa, the Soviet Union, Sweden, and West Germany. Thirty-eight papers were presented, and four panel sessions held, covering research at high pressures in static systems and in shock wave experiments.

The tone of the meeting was effectively set by the opening speakers, who emphasized the importance of improved accuracy in measurements at high pressures and in calibrations relevant to such measurements. The point was made that in current work, involving a wide range of phenomena and many types of apparatus, a series of "interlocking" standards is needed.

About one-fourth of the papers dealt with matters relevant to selection of reproducible and reversible reference points on the pressure scale—so-called "fixed points"—indicated by phase changes in selected substances. The importance attached to establishing such agreed-on fixed points was indicated by these papers and the discussions throughout the week. On the final day these matters were considered by an informal committee, and the following outline of the report of this committee and of the ensuing floor discussion summarizes the informal consensus reached.

It was recommended that phase transitions and accompanying pressures shown in table 1 be used as pressure fixed points. The fixed points recommended represent equilibrium values.

TABLE 1.

Transition	Fixed-point pressure (kilobars)	Present estimated uncertainty (kilobars)
Mercury freezing point at 0 °C	7.569	0.002
Bismuth I to II transition at 25 °C	25.50	0.06
Thallium I to II transition at 25 °C	36.7	0.3
Barium I to II transition at 25 °C	55	2
Bismuth III to V transition at 25 °C	77	3

Users are to consider the fixed points as exact. The values of "present estimated uncertainty" are given only to indicate the range within which a value may be expected to shift as a result of improved measurements in the future. The reproducibility of pressures based on these phase changes may be better or poorer than these uncertainties and, in any given case, depends strongly on technique. It is the responsibility of the experimenter to establish reproducibility and hysteresis for his own apparatus and technique, and the relationship between his experimental values and the above equilibrium values.

In addition to the five points listed in table 1 covering the pressure scale up to 77 kbar, a consensus was reached that the cesium II to III and III to IV transitions on *increasing pressure* be taken as 42.5 kbar and 43.0 kbar, respectively, with a present estimated uncertainty of 1 kbar, and that the tin I to II transition be tentatively used as a fixed point with an equilibrium transition value of 100 kbar and a present estimated uncertainty of 6 kbar.

In addition to the fixed point of 7.569 kbar at the freezing pressure of mercury at 0 °C, the committee favored use of the mercury melting curve to establish other reference pressures up to 15 kbar, corresponding to the freezing pressure of mercury at about 36.8 °C. It recommended that such reference pressures be based on the Simon equation, adjusted to agree with the value 7.569 kbar at 0 °C as follows:

*Largely from a meeting report by the same authors appearing in Science **164**, 860–2 (May 16, 1969).

$$P = 38227 \left[\left(\frac{T}{234.29} \right)^{1.1772} - 1 \right]$$

where T is the temperature in K on the International Practical Temperature Scale (1948), and P is the pressure in bars. Small adjustments in this equation will be needed when the new temperature scale, IPTS 1968, is used.

Several pressure scales derived from equations of state of cubic solids were proposed at the meeting. Both metallic and nonmetallic substances, such as the cesium halides, were considered. Sodium can be treated most accurately from the theoretical viewpoint, but its high chemical reactivity is inconvenient. Aluminum can be treated by quantum mechanical methods if parameters are adjusted to fit some of the observed properties. Both aluminum and copper have been investigated experimentally as standards in shockwave measurements. These metals also could be used as standards in x-ray measurements.

The new data on copper and aluminum shock standards have been used to reevaluate the equation of state of several other metals that have been used in determination of pressure based on x-ray measurements of lattice constants.

Sodium chloride has been used most often as a reference material in recent applications of x-ray methods for estimating pressure. An informal committee on equation of state standards considered requirements in this application such as high compressibility, low yield strength, chemical stability, availability of accurate data over a wide range of pressure, and other properties. The committee selected sodium chloride first, with copper and aluminum as alternates.

Four evaluations of data relevant to the sodium chloride scale now are available, including two which were presented. In these evaluations differences in reported pressures are less than the combined errors (about 4 percent) at pressures from 25 to 300 kbar. When these sodium chloride scales are combined with x-ray data on sodium chloride media in which transitions of bismuth and barium have been studied, the computed transition pressures lie within the uncertainties indicated in the table above for barium and for bismuth III to V.

The committee recommended that a single sodium chloride scale be adopted and that it be adjusted to give values of pressure as close as possible to those selected for the fixed points. An average of the two most recent sodium chloride scales would very nearly fulfill these requirements. An exact fit of selected fixed points appears unlikely without arbitrary adjustments in the equation of state. Nevertheless, a provisional sodium chloride scale consistent to within experimental error with the fixed points selected for the region below 100 kbar is attainable and, if accepted, could be very useful.

The committee suggested more comprehensive theoretical and experimental investigations of the equation of state of cubic solids in order to improve currently available scales. In particular, changes in the vibrational energy states of solids with volume are required in order to obtain accurate theoretical formulations of the equation of state and related properties.

Temperature in high-pressure experiments is normally measured by thermocouples. However, pressure affects the relation between electromotive force and temperature for a thermocouple, provided there is a thermal gradient within the pressurized region. The reality of this effect is readily shown by subjecting two dissimilar thermocouples (such as Pt-Pt 10 percent Rh and chromel-alumel) to the same conditions of high temperature and pressure and monitoring the difference in apparent temperature. In various solid-media apparatus there are differences on the order of 25 °C between the apparent temperature simultaneously read by chromel-alumel and Pt-Pt 10 percent Rh couples at 1000 °C and 40 kbar.

Quantitative evaluation of these effects is most difficult. Direct determinations have been made both in internally heated, solid-media apparatus and in externally heated, gas apparatus. The latter results have not thus far been extended to sufficiently high pressures to permit critical comparison with the solid-media results. Indirect methods have utilized a comparison of phase boundaries determined by experiment with boundaries calculated from thermochemical data. Temperatures determined by thermocouples have also been compared with those determined by the thermal noise technique.

All investigators agree that the pressure effect on the chromel-alumel couple is less than ~ 5 °C in the range up to 1000 °C and 40 kbar. Unfortunately, this couple is considerably less stable than Pt-Pt 10 percent Rh in high-pressure cells due to chemical contamination and strain effects. All investigators also agree that the effect of pressure on the Pt-Pt 10 percent Rh couple is considerably larger and that the magnitude of the effect increases with both increasing temperature and increasing pressure. Estimates of the pressure correction for this couple range up to 35 °C at 1000 °C (for a cold seal at 0 °C) and 40 kbar, but there are sizable differences in the results of various investigations in this range.

A conference concerned with the accuracy of pressure and temperature measurement at high pressures must necessarily be concerned with the "nuts and bolts" of high-pressure experimentation. A number of developments in technique were described which considerably extend the range, quality or accuracy of high-pressure measurements.

Liquid cells have been constructed for use in piston-cylinder and multi-anvil apparatus which permit measurements under perfectly hydrostatic conditions to be made at pressures up to 50 kbar at room temperature. These cells are jacketed with plastic or stainless steel and are filled with liquids

or mixtures of liquids such as pentane, isoamyl alcohol, and methanol. Such cells have remarkable mechanical stability and can be cycled over a wide pressure range. Their use eliminates shearing stresses which are inevitably present in systems employing solid pressure media and which in some instances affect the thermodynamic properties of materials under investigation. An analogous technique for high temperatures is to use molten glass as a pressure medium. Experience with molten Pyrex in high-pressure cells suggests that thermocouples are more stable in such an environment than with more commonly used ceramic insulation.

Until recently the pressure range of single-stage, piston-cylinder apparatus was limited to approximately 50 kbar. This limitation was imposed by the crushing strength of unsupported, carbide pistons. However, such pistons will support stresses up to 80 kbar if the ratio of the unsupported length of the piston to its diameter is kept considerably below 1. Failure along 45-degree shear planes is thus inhibited. A variation of this technique which permits greater stroke is to segment the unsupported length of the piston with binding rings. These binding rings slide back along the piston as they make up on the face of the pressure vessel during the compression stroke.

The possibility of using second-order phase transitions as secondary calibration standards has aroused considerable interest. Second-order transitions proceed without volume discontinuities and theoretically without hysteresis. The change in Curie temperature with pressure is promising in this regard although the effects thus far studied are rather small. For example, the dT/dP slope of the Curie temperature curve for nickel is 0.35 °C per kilobar. Other materials, such as ferrites, may show larger effects.

New developments in shockwave research now permit a derivation of the fusion curve (P versus T) of copper extending into the million-bar range. When combined with accurate measurements of temperature and pressure in the static high-pressure range (1100 to 1300 °C and 0 to 60 kbar) the fusion curves of several substances, such as copper, silver, and others, could be used for *in situ* checking of calibrations of high-pressure, high-temperature apparatus. However, in a broader perspective, accurately determined fusion curves may permit solution of some rather fundamental questions in geophysics and astrophysics involving extrapolation of phase diagrams to very high pressure and high temperature.

The kinetics of shockwave processes are being investigated from several viewpoints. These include lattice dynamic models of shocks in solids and experimental investigation of nonequilibrium processes at relatively low shock strengths in many cases. The behavior of shocks in regions of phase changes are especially interesting. The rate at which such changes occur depends upon the types of lattices involved and the orientation of the lattice with respect to the direction of the shock. From the viewpoint of pressure standards, additional studies of the transformation of iron at about 126 kbar were reported in the meeting.

The symposium was sponsored by the National Bureau of Standards and the Geophysical Laboratory of the Carnegie Institution of Washington. Expenses were covered by a grant from the National Science Foundation.

Edward C. Lloyd
Charles W. Beckett
Institute for Basic Standards,
National Bureau of Standards,
Washington, D.C.

Francis R. Boyd, Jr.
Geophysical Laboratory,
Carnegie Institution of Washington,
Washington, D.C.

Chairman: P. H. Abelson
Geophysical Laboratory
Carnegie Institution of Washington

Hydrostatic Pressures of 50 kbar in a Piston-Cylinder Device: Measurement of Pressure and Characterization of the Pressure Medium

A. Jayaraman and R. G. Maines

Bell Telephone Laboratories, Incorporated, Mountain Avenue, Murray Hill, New Jersey 07974

A method suited for making resistivity and other electrical measurements to 50 kbar hydrostatic pressure, using a conventional piston-cylinder device, is described. In this method a Teflon cell is used to contain the pressure medium, which is a 1:1 mixture of *n*-pentane and isoamyl alcohol. After the fluid mixture freezes (at about 46 kbar), further advance of the piston results in uniaxial stress. However, this can be readily relaxed by heating the medium to 70 °C. The resultant isotropic pressure distribution stays when the pressure medium is cooled back to room temperature. The technique of probing the pressure distribution inside the cell, as well as pressure calibration procedure, is described.

1. Introduction

A technique for generating hydrostatic pressures in excess of 30 kbar using a conventional piston-cylinder device was recently described [1].[1] In this, a Teflon cell contained the pressure medium, and leads were brought out of the cell for electrical measurements. The hydrostatic pressure limit of about 38 kbar was dictated by the freezing of the pressure medium at this pressure at room temperature. To evaluate friction correction, the Bi I → II transition at 25.4 kbar was used and it was shown that true pressure could be obtained from the indicated pressure by multiplying the latter with the ratio $P_{\text{tr}}\text{Bi I}\rightarrow\text{II}/P_{\text{indicated}}$ at the transition point. In the present paper, efforts to extend the hydrostatic pressure regime to 50 kbar, the methods used to characterize the pressure medium, and the measurement of pressure will be described.

2. Experimental Arrangement

Figure 1 is a schematic of the Teflon cell assembly in position in the pressure chamber, while Figure 2 shows the Teflon cell and lead arrangement in some detail. The materials used and the dimensions of the cell are given in the figure. Consistent with lower frictional correction and effective containment of the fluid, the optimum wall thicknesses for the ½-in and 1-in diam Teflon cells are 50 and 100 mils respectively. The ⅛-in-thick Teflon disk shown in the figure (see fig. 2) next to the cap serves the purpose of an additional seal. In the bottom side of the Teflon cell next to the piston, we use a 10-mil-thick steel shim as an additional seal and this permits the use of a longer cell. We find that leakage problems are virtually eliminated by slightly offsetting the drilled holes in the Teflon disk with respect to the holes drilled in the cap.

3. Characterization of the Pressure Medium

The pressure medium could be conveniently characterized by following the piezoresistance effect of an *n*-type silicon plate. The piezoresistance [2–5] effect relates the change $\delta\rho$ of the resistivity tensor to the stress tensor. For a cubic substance, the piezoresistance coefficient π can be described in terms of its 11, 12, and 44 components, referred to the coordinate axes chosen along the cubic directions. In the case of hydrostatic stress $-\delta\rho/\rho = P(\pi_{11}+2\pi_{12})$, where P is the pressure in dynes/cm^2 and the best value for the coefficient $(\pi_{11}+2\pi_{12})$ is about 3.1×10^{-12} cm^2 dyn^{-1} for *n*-silicon [6]. For the uniaxial stress and the current and field directions as used in our experiments, the appropriate component is $\pi_{21}=\pi_{12}$ which has the value -53.4×10^{-12} cm^2 dyn^{-1} for *n*-silicon. Because of this large difference in piezoresistance for the hydrostatic and uniaxial stresses, any deviation from hydrostaticity shows readily in the resistivity versus pressure curve of a (100) oriented *n*-type silicon plate. It should be noted here that the piston-cylinder geometry favors a uniaxial stress distribution, after the pressure medium freezes.

[1] Figures in brackets indicate the literature references at the end of this paper.

Paper presented at the Symposium on Accurate Characterization of the High-Pressure Environment, held at the National Bureau of Standards, Gaithersburg, Md., October 14–18, 1968.

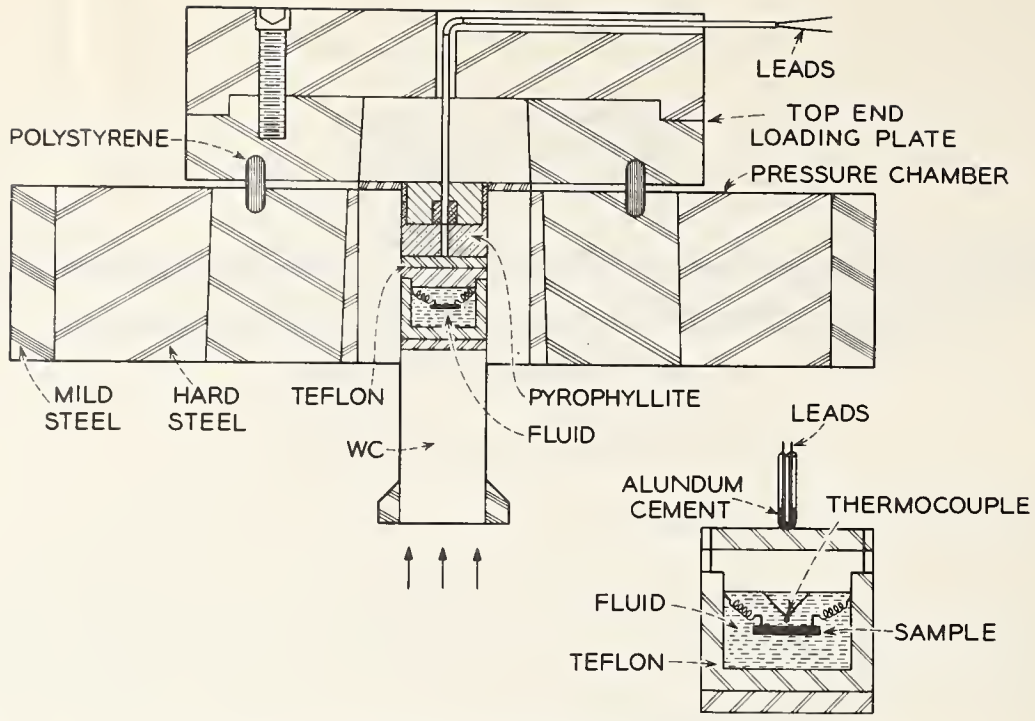

FIGURE 1. *Teflon cell assembly inside the pressure chamber.*
The diagram to the right is an enlarged view of the cell.

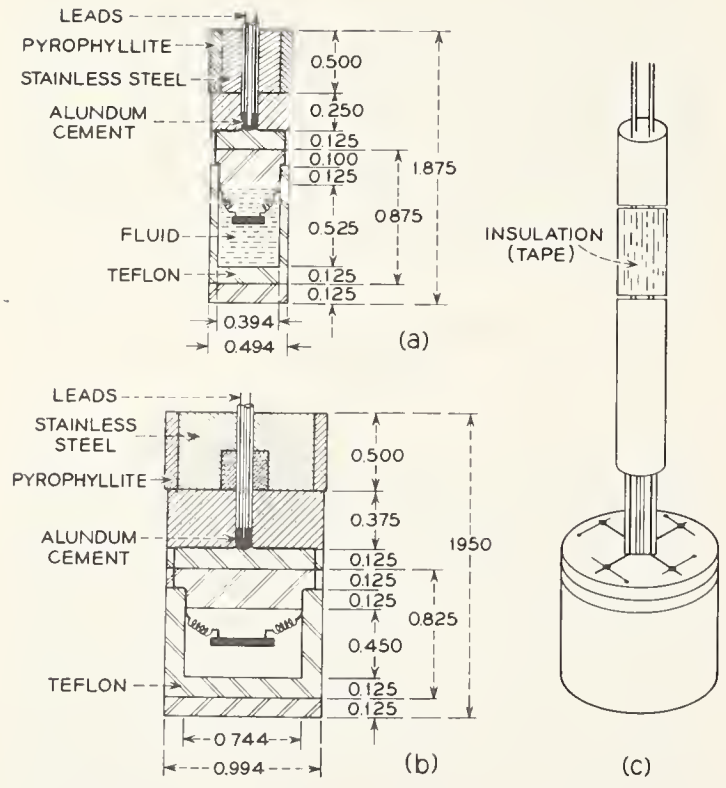

FIGURE 2. *The dimensions of the parts in inches, for ½-in and 1-in diam (O.D.) Teflon cell assembly.*
The connection of leads from inside the cell to the leads carried by the ceramic tubing are shown to the right.

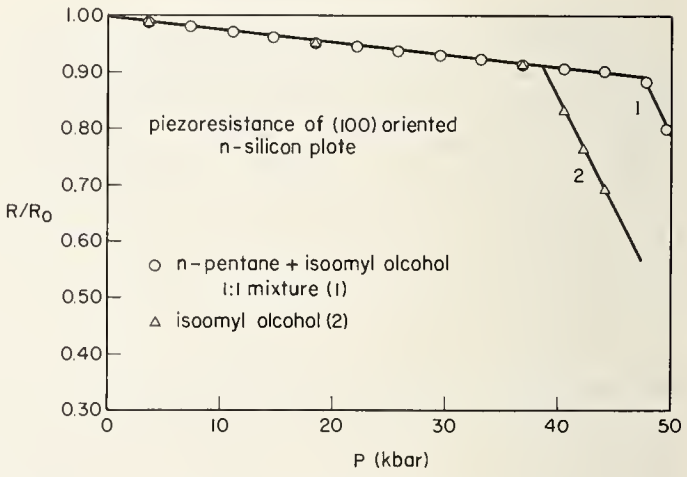

FIGURE 3. *Resistivity ratio of an n-type, (100) oriented silicon plate, plotted as a function of pressure.*

We used in our experiments a phosphorus-doped ($\rho = 4.4$ ohm cm) silicon sample of square geometry (160 mils to a side and 15 mils thick) cut parallel to the (100) crystal plane. (The advantage of using silicon is that there are no other conduction band minima, excepting the ones located near the [100] directions in k space. Further, the resistance response of n-silicon is almost linear with pressure.) The plate was oriented inside the Teflon cell with the plane perpendicular to the axis of the piston-cylinder geometry, so that when uniaxial stress appeared, it was in the direction normal to the (100) plane. Ohmic contacts were made at the four corners of the plate to which copper leads were soldered. Two adjacent leads were used for current while the opposite two served as potential leads. Since the change of resistance $\Delta\rho$ is small, both the current and potential measurements have to be very precise. A very convenient arrangement is to use a well stabilized current source in conjunction with a potentiometer, such as the Leeds and Northrup K3 for potential measurement. In figure 3 is shown the measured resistivity ratio plotted as a

function of pressure for a 1:1 mixture of *n*-pentane and isoamyl alcohol (curve 1) and for pure isoamyl alcohol (curve 2) as pressure medium.

The R/R_0 versus pressure plot shows an abrupt change of slope near 38 kbar, when isoamyl alcohol is used as the pressure medium, and near 45 kbar when the *n*-pentane + isoamyl alcohol (1:1 ratio) mixture is used as the medium. This change of slope is due to the appearance of uniaxial stress perpendicular to the (100) plane of silicon, after the pressure medium freezes. Above the freezing point, almost the whole of the applied stress appears as uniaxial stress. We find that this uniaxial stress can be relaxed by heating the pressure medium to about 70 °C. Resistance measurements on *n*-silicon obtained after heating and cooling back to room temperature fall on the extension of the hydrostatic data, showing thereby that the heating and cooling procedure is an effective method to restore hydrostatic stress distribution, after the pressure medium solidifies.

In describing the Teflon cell technique in earlier publications, it was stated that the 1:1 mixture of *n*-pentane and isoamyl alcohol solidifies at about 38 kbar. However, our present results show this to be incorrect. The reason for the discrepancy is due to the fact that *n*-pentane evaporates from the mixture somewhat rapidly and after a length of time, only isoamyl alcohol is left behind. This is what has apparently happened to the mixture used in previous experiments.

4. Pressure Measurement

For pressure calibration we have used the freezing point of mercury [7] at 22 °C (11.85 kbar), the Bi I–II [8] transition at 22 °C (25.4 kbar), the transition in thallium [9] at 22 °C (37 kbar) and the Cs II–III transition at 42.5 kbar. All the transitions fall within the freezing pressure of *n*-pentane–isoamyl alcohol mixture. In figure 4 is plotted the true pressure in kbar against the indicated pressure (computed from the dial gauge) using the above-mentioned three fixed points. The linear relationship between the two pressures shows that the friction correction is proportional to the pressure indicated; $P_{\text{true}} = (0.925)P_{\text{ind}}$. The multiplying constant is highly reproducible for the cell dimensions and geometry shown in figure 2 and for *n*-pentane-isoamyl alcohol as pressure medium. Thus the measurement of pressure is straightforward.

As a further check of the accuracy of our calibration, we have compared the resistance data obtained at Harvard by Kosicki and Paul on a sulfur-doped

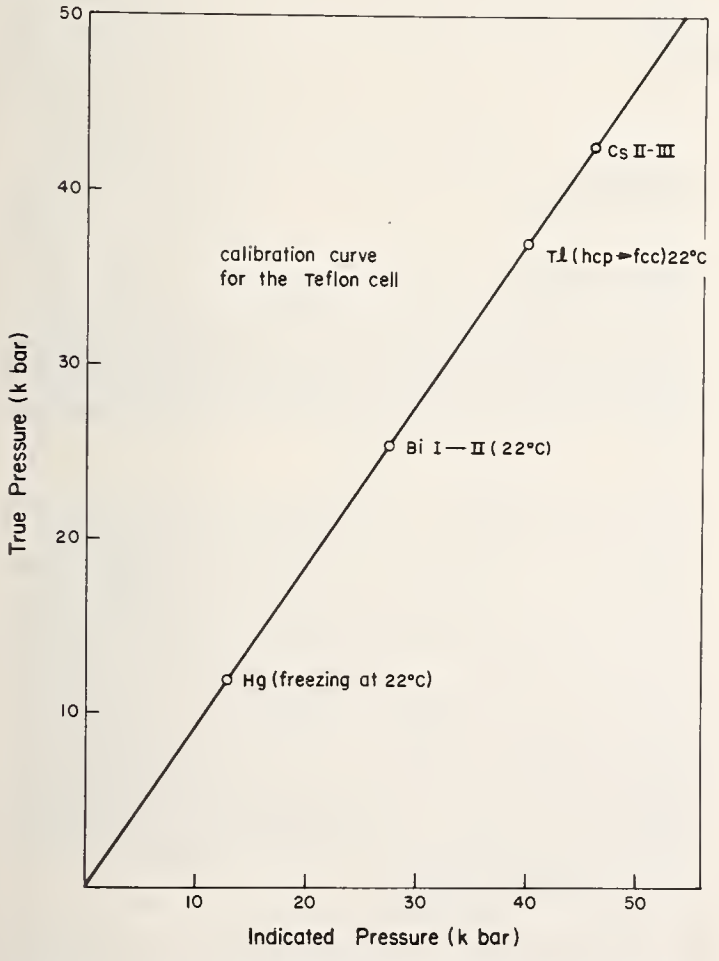

FIGURE 4. *Pressure calibration with the freezing point of* Hg *at 22 °C (11.85 kbar),* Bi I–II *transition (25.4 kbar), the transition in* Tl *at 37 kbar, and* Cs II–III *at 42.5 kbar.*
The ordinate gives the true pressure and the abscissa the applied pressure.

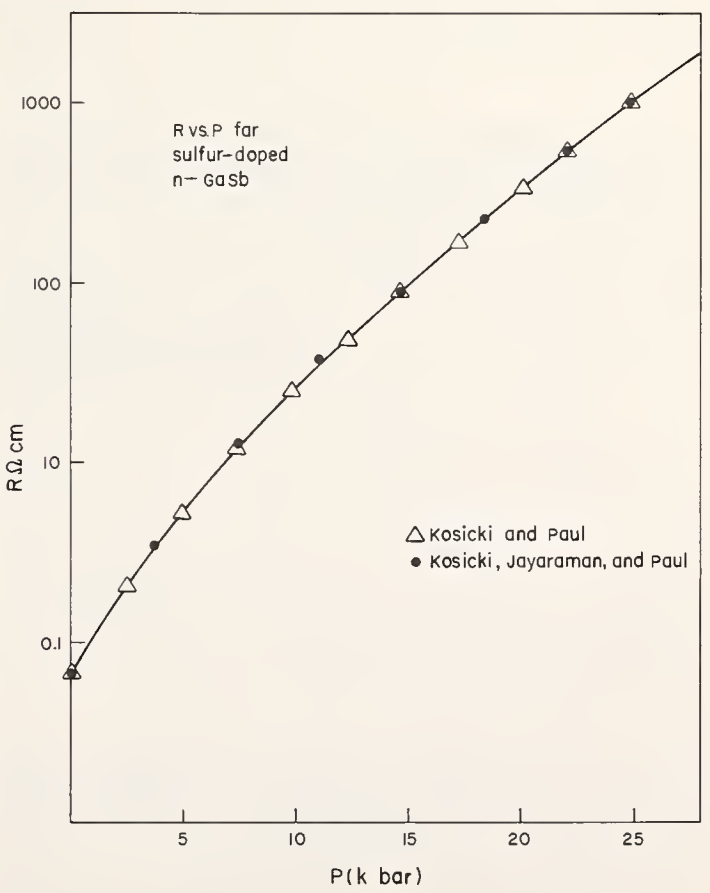

FIGURE 5. *Comparison of the resistivity of sulfur-doped* n-GaSb *measured in Harvard University Bridgman-type hydrostatic apparatus and in the piston-cylinder device (Teflon cell technique).*

385-762 O - 71 - 2

n-GaSb in a Bridgman apparatus (calibrated using a manganin gauge), with resistance measurements on the same sample in our hydrostatic setup. The results of these measurements are in very good agreement (see fig. 5). We estimate that our pressures are true to within one percent.

5. Conclusion

With the present technique it is possible to study the transport properties of metals and semiconductors at least up to 50 kbar hydrostatic pressure, at room temperature. This extension of the hydrostatic pressure range may be expected to yield valuable information, particularly on the energy band structure of semiconductors. Such usefulness has already been demonstrated at least in two cases. Using the technique of pressure generation detailed above, the energy of the higher-lying conduction band minima and the associated electron mobilities have been determined in GaSb [10] and Ge [11, 12].

6. Acknowledgment

It is a pleasure to thank Dr. B. B. Kosicki for helpful discussions and for the data on sulfur-doped GaSb, measurements on which were made in a Bridgman type hydrostatic apparatus at Harvard University. We would also like to thank Mrs. I. Kocserha for providing ohmic contacts on many of the silicon slices.

7. References

[1] Jayaraman, A., Hutson, A. R., McFee, J. H., Coriell, A. S., and Maines, R. G., Rev. Sci. Instr. **38,** 44 (1967).
[2] Smith, C. S., Phys. Rev. **94,** 42 (1954).
[3] Morin, F. J., Geballe, T. H., and Herring, C., Phys. Rev. **105,** 525 (1957).
[4] Herring, C., Bell System Tech. J. **34,** 1 (1955).
[5] Keyes, R. W., in Solid State Physics **11,** 187 (1960). (Seitz and Turnbull, Eds., Academic Press).
[6] Smith, A. C., Tech. Report H-P.-2 from the Division of Engineering and Applied Physics, Harvard University (1958), pp. 46–49.
[7] Bridgman, P. W., Proc. Am. Acad. Arts Sci. **47,** 347 (1911).
[8] Heydemann, P. L., J. Appl. Phys. **38,** 2640 (1967).
[9] Kennedy, G. C., and La Mori, P. N., J. Geophys. Res. **67,** 851 (1962).
[10] Kosicki, B. B., Jayaraman, A., and Paul, W., Phys. Rev. **172,** 764, (1968).
[11] Jayaraman, A., Kosicki, B. B., and Irvin, J. C., Phys. Rev. **171,** 836 (1968).
[12] Jayaraman, A., and Kosicki, B. B., in Proc. 9th Intern. Conf. on Physics of Semiconductors (Vol. 1, p. 47, 1968).

DISCUSSION

R. E. Hanneman (*General Electric Research and Development Center, Schenectady, New York*): What are the upper limits in pressure and temperature in using your technique?

G. C. Kennedy (*Institute of Geophysics and Planetary Physics, University of California, Los Angeles, California*): There is an interesting extension of this technique to higher temperatures. We have been doing experiments for several years in which the sample is immersed in molten glass. Glasses are available that melt from 150 °C on up to quartz 1800 °C. An advantage is the self-sealing of leaks. When a leak occurs it is stopped by the glass freezing off. Molten glasses work beautifully at 1200 °C to 1500 °C. We characteristically run our experiments in molten pyrex, and it is a hydrostatic medium under good conditions.

H. T. Hall (*Brigham Young University, Provo, Utah*): I have a question about the calibration and the effect of friction. I presume that the calibration was made on rising pressure. How much friction do you have, and where is it located?

This hydrostaticity-detecting device is interesting. Have you done experiments with Bridgman's mixture of iso-pentane and *n*-pentane in this device? While your present mixture appears to be limited to about 50 kilobars, I believe that there is evidence that higher pressures can be reached with Bridgman's mixture.

S. E. Babb, Jr. (*University of Oklahoma, Norman, Oklahoma*): On the matter of the pressure-transmitting liquid, Bridgman used impure pentane to 30 kilobars. The purity greatly affects the degree of subcooling, and I am suggesting that the pentane becomes a subcooled liquid.

H. G. Drickamer (*University of Illinois, Urbana, Illinois*): I doubt if necessarily the mixture is subcooled. A very long time ago we made some viscosity measurements at one atmosphere, down to the freezing point. We found that if you are careful the mixtures can be supercolled 10 to 15 degrees, but the viscosity goes up enormously as the freezing point is approached. In general, you have some kind of eutectic. If you are really subcooling, you will get the kind of things you did with the silicone. I think you have a low melting-point eutectic of some kind, and you are above the melting point on that particular mixture.

R. H. Wentorf, Jr. (*General Electric Research and Development Center, Schenectady, New York*): I remember once talking with Bridgman on the use of pentane. He said that when he used very pure pentane in his equipment it broke. A mixture is

best, because you get the well-known depression of freezing point with most organic mixtures, and some kind of eutectic. Bridgman went back to the conglomeration of different kinds of molecules in order to get the low freezing point he wanted.

R. Zeto (*U.S. Army Electronics Command, Fort Monmouth, New Jersey*): I would like to point out two problems in the calibration procedure. In your hydrostatic system you are calibrating on the initiation of the transformation which is not the real equilibrium point measured by Bridgman and Heydemann. At the bismuth I–II point there is a ½ to 1 percent error involved. Also, if you are changing pressure in 1 kilobar increments there is an additional uncertainty due to overpressurization. This can lead to an error of up to 4 percent for the bismuth I–II point.

We use an equivolume mixture of normal-pentane and iso-pentane without indication of freezing to 50 to 60 kilobars. We find this pressure medium to be hydrostatic and can cycle any number of times.

J. D. Barnett (*Brigham Young University, Provo, Utah*): I would like to know what your time scale is both on these piezoresistance effects and also on the bismuth transitions. Let me suggest that on your bismuth transition the time scale is dramatically influencing the hysteresis effect, as you will see from Zeto's paper. A difference of the order of several hundred bars, at least, can occur depending on how fast the pressure is changed.

M. Contre (*Commissariat a l'Energie Atomique, Paris*): I am concerned about your use of Teflon. Metals under pressure become elastic. Teflon becomes fragile under pressure. Has this caused trouble in your apparatus?

AUTHORS' CLOSURE

In reply to Dr. Hall: All the measurements and calibrations were done with increasing pressure. At 25.4 kilobars the friction was equivalent to 2 kilobars, and I think was mainly wall friction between the piston and cylinder. We have not tried to relieve this since we are able to correct for it.

Concerning use of a mixture of iso-pentane and *n*-pentane, we have tried this but we encountered leakage problems.

In reply to Dr. Zeto: We make sure that the temperature rises minimally. Since the bismuth I-II transition on the phase diagram has a fair slope, a definitely lower pressure would exist at the calibration point if an appreciable temperature rise occurs.

In reply to Dr. Contre: I think Teflon can be used at temperatures up to 200 °C or 300 °C quite easily. We have repeatedly experimented in the range up to 100 °C but have not done many experiments above that. At higher temperatures, the problem of leakage becomes more serious, particularly when electrical leads are brought out.

We have had no trouble with Teflon due to its becoming fragile. Our experience is that this material can be cycled many times to 50 kilobars, and it comes out in fairly good shape. There is some deformation. I think Teflon is probably one of the best materials to use for this kind of experiment. It's better than any metal, especially when electrical leads are to be brought out.

Ultrasonic and Dilatometric Measurements at Very High Pressures

Peter L. M. Heydemann and James C. Houck

National Bureau of Standards, Washington, D.C. 20234

A short-cylinder and piston assembly and its use for dilatometric and ultrasonic measurements on solids and liquids at pressures up to 40 kbar are described. All necessary corrections for the evaluation of measurements are discussed and the systematic uncertainties are given. It is demonstrated that ultrasonic methods can significantly reduce the uncertainties in the determination of density and bulk modulus of both solids and liquids.

Key words: Bulk modulus; density; dilatometric measurements; high pressure; liquids; solids; ultrasonics.

1. Introduction

Simple piston and cylinder assemblies are widely used to compress solids and liquids [1][1] and to study their mechanical, electrical, magnetic, and optical properties over a range of pressures of up to about 60 kbar. We have developed a particularly economical high-pressure cylinder and have also used ultrasonic methods extensively in connection with high-pressure investigations on solids [2] and liquids [3]. In the present report we investigate the systematic uncertainties of such measurements. Although we are dealing with our particular setup, the uncertainties and corrections discussed are nevertheless representative of this general type of equipment. The magnitude of the uncertainties is in many cases larger than was previously expected.

In investigating the estimated systematic uncertainties of ultrasonic measurements on compressed materials, we believe we can demonstrate the relatively greater accuracy that can be achieved—under favorable conditions—with such methods.

2. Piston and Cylinder Assembly

2.1. For Ultrasonic Measurements in Solids

Figure 1 shows a piston and cylinder assembly for ultrasonic and dilatometric measurements on polycrystalline materials and on polymers. The cylinder consists of tungsten carbide with 6 percent cobalt binder. It has a bore of about 1.2 cm diameter and is about 1 cm long. A steel ring, press-fitted with 1.2 percent interference on the carbide cylinder, provides radial support. The normal stress at the cylinder-support ring interface is approximately 11 kbar. At the upper end the cylinder is closed with a tungsten carbide backup plate, and at the lower end with the tungsten carbide piston. The assembly is clamped against the top platen of the press (not shown in fig. 1) for axial support of the cylinder. A washer is used to transmit most of the clamping force to the tungsten carbide cylinder. A clamping stress of 14 kbar at the faces of the cylinder is sufficient to support the cylinder at internal pressures up to 40 kbars. No attempt has been made so far to generate higher pressures.

A ram concentric with the one supplying clamping force is used to press the piston into the sample. A handle is provided as part of the piston stack for rotation under load. Travel of the piston stack is monitored by two dial indicator micrometers arranged diametrically on either side of the piston. The travel of the piston stack is measured at a point immediately below the lowest surface shown in figure 1 relative to the surface on which the lower face of the bridge plate rests. Rather large corrections have to be applied to obtain the advance of the front end of the piston relative to the cylinder from the dial indicator readings (see sec. 5).

The piston is fitted with about 5-μm diametral clearance into the cylinder. Delta (anti-extrusion) rings are used for very soft materials.

An ultrasonic transducer is cemented to the backup plate as shown in figure 1. Several backup plates with different lengths and with shear or longitudinal transducers are usually at hand in the laboratory. In cases where simultaneous

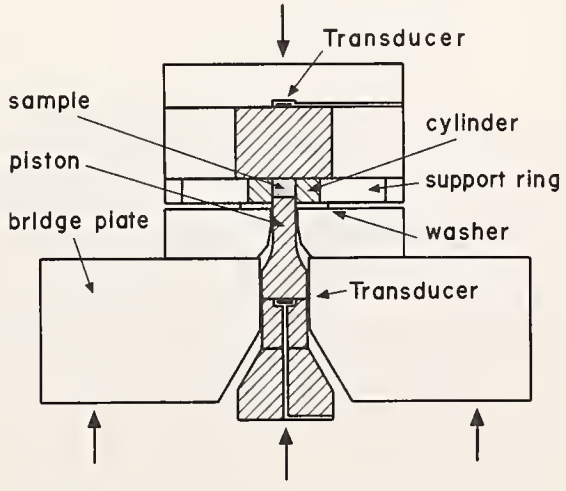

FIGURE 1. *Piston-cylinder assembly for solids.*

[1] Figures in brackets indicate the literature references at the end of this paper.

Paper presented at the Symposium on Accurate Characterization of the High-Pressure Environment, held at the National Bureau of Standards, Gaithersburg, Md., October 14–18, 1968.

measurement of shear and longitudinal wave propagation times is imperative, a stepped piston as shown in figure 1 is used. This carries a transducer at its larger rear surface. In all other cases, the expensive stepped piston is replaced by two tungsten carbide pieces of 2.54 cm and 1.27 cm diameter. The transducers are accommodated in recesses of the adjoining parts. Electrical leads are brought out through radial grooves to BNC connectors mounted on the outside of the assembly. Since the transducers are not subjected to mechanical stress from the high pressure on the sample, a glyceryl phthalate resin (Glyptal 1202 varnish), or a cyanoacrylate cement (Eastman 910), are sufficient to make bonds.

Samples are often precompacted into the cylinder in an auxiliary press and then machined inside the cylinder for plane and parallel surfaces. Alinement of the piston stack is carefully checked prior to each measurement.

2.2. For Ultrasonic Measurements in Liquids

Figure 2 illustrates the assembly used to contain liquids in the cylinder. The cylinder is lined with a polyethylene (PE) sleeve. The length of the liner is slightly smaller than the length of the cylinder, so that the piston can enter and close the lower end of the cylinder. Liquid is filled into the cylinder with piston and cylinder *in situ* in the press. The backup plate is then put in place and the assembly is clamped.

If the bulk modulus of the liquid is smaller than that of polyethylene, as is the case with most liquids (see, for example, water in fig. 3), then the piston will push against the sleeve as the contents of the cylinder are compressed. This small excess of stress in the piston-sleeve interface over the hydrostatic pressure in the cylinder is sufficient to seal the liquid, even at pressures as high as 40 kbar.

The extent to which this excess stress reduces the internal hydrostatic pressure below the nominal pressure computed from ram force and effective area, was investigated at two pressures. The melting pressure of ice VI at about 22 °C was measured as a function of the wall thickness of the sleeve. There was no discernible variation of the nominal pressure with sleeve wall thickness. Considering the accuracy of pressure determination, to be discussed later, we assume that at the melting pressure of ice VI of about 9200 bar at room temperature, the internal pressure is reduced by less than one percent below the nominal pressure by polyethylene sleeves with wall thickness as large as 0.25 cm.

Two kinds of experiments were made at the Bi I-II transition pressure. In the first experiment, about 0.11 cm^3 of polycrystalline bismuth was placed inside the polyethylene sleeve. The rest of the volume was filled with isoamyl alcohol. The Bi I-II transition pressure was then determined for three different sleeve wall thicknesses. The result is shown in figure 4. Plotted (X) for each of five experiments is the mean of the nominal pressures at which transition was observed under compression

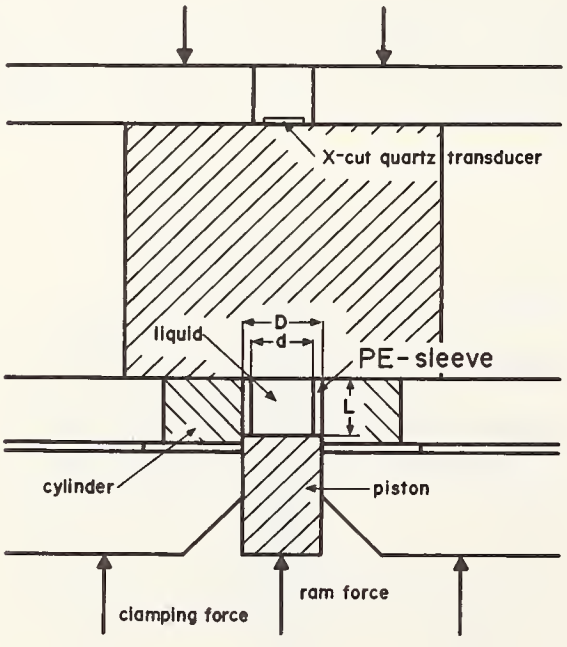

FIGURE 2. *Piston-cylinder assembly for liquids.*

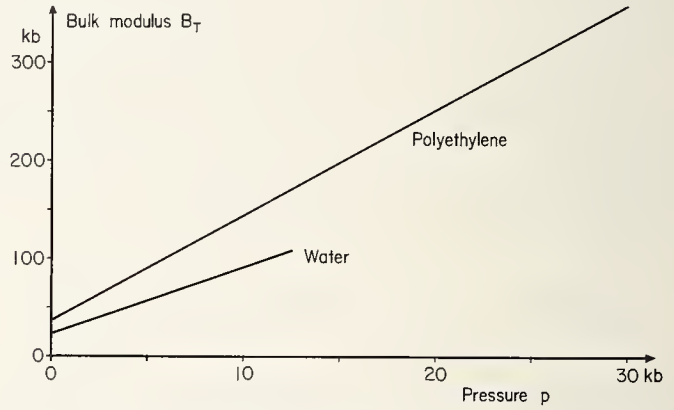

FIGURE 3. *Bulk modulus* B_T *of water and polyethylene as function of pressure.*

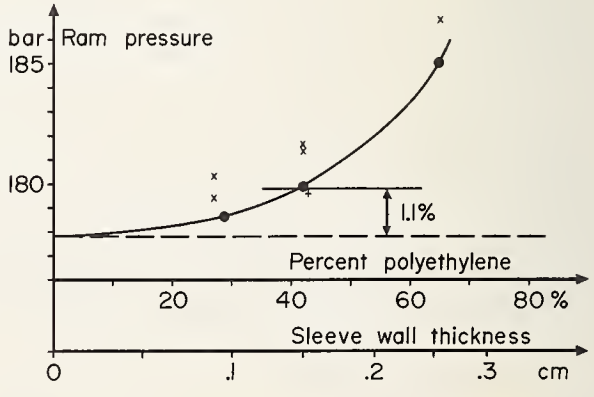

FIGURE 4. *Ram pressure necessary to reach the* Bi I-II *transition as function of the sleeve wall thickness.*

and decompression against the volume of polyethylene in percent of the total volume contained in the cylinder at zero pressure. With no polyethylene present the curve should extrapolate to a ram pressure of 177.8 bars corresponding to an internal pressure of about 25,660 bars, the Bi I-II transition pressure at 22 °C [4].

In the second experiment, an electrical lead was introduced into the cylinder through the backup plate, as shown schematically in figure 5. The change of electrical resistance of a bismuth wire connected to the electrical lead and to ground was used to detect the transition. The results are also plotted in figure 4. In three cases (●) isoamyl alcohol was used as pressure transmitting liquid, and in one case (+) methanol was used. The compression of both liquids to 25 kbar is quite similar [5, 6]. At this pressure the volume of methanol is 67 percent and that of isoamyl alcohol is 70 percent of their volumes at atmospheric pressure. Different curves in figure 4 would be expected for liquids of widely different bulk modulus. For the most frequently used sleeve wall thickness of 0.15 cm, the pressure correction amounts to only 1.1 percent at 25 kbar.

The pressure on liquids contained in these polyethylene sleeves can be cycled several times between zero pressure and pressures leading to compressions V/V_0 of less than 0.75. We have often been amazed about the repeatability of these measurements, which usually is within the sensitivity of both the dilatometric and the ultrasonic measurement. No such repeatability was found when, in the beginning of this development, polytetrafluoroethylene was used as sleeve material. In this latter case very significant plastic deformation occurred even at moderate compressions.

3. Ultrasonic Measurements and Typical Results

It is difficult to maintain parallelism of better than 30 s between the front and rear face of the samples in the assemblies of figures 1 and 2. Therefore, the ultrasonic measurement can not be of the precision of which it is inherently capable [7]. In most of our experiments, a wave train of about one-half μs duration with a carrier frequency of about 10 MHz was emitted from the transducer. The reflections from various interfaces in the acoustic path are picked up by the transducer, amplified and displayed on the screen of an oscilloscope. Times between pulses or echoes are then determined using a calibrated sweep delay. The echo pattern is often complex because of the number of interfaces. Multiple reflections usually further complicate the pattern. A typical echo pattern is shown and interpreted in figure 6.

Although we have not made any attempt to study ultrasonic attenuation as a function of pressure, the amplitude ratio of echoes and transmitted pulses is often recorded during a measurement.

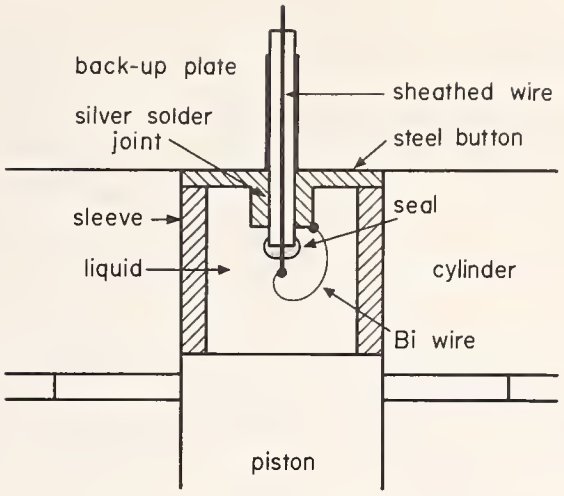

FIGURE 5. *Electrical feedthrough.*

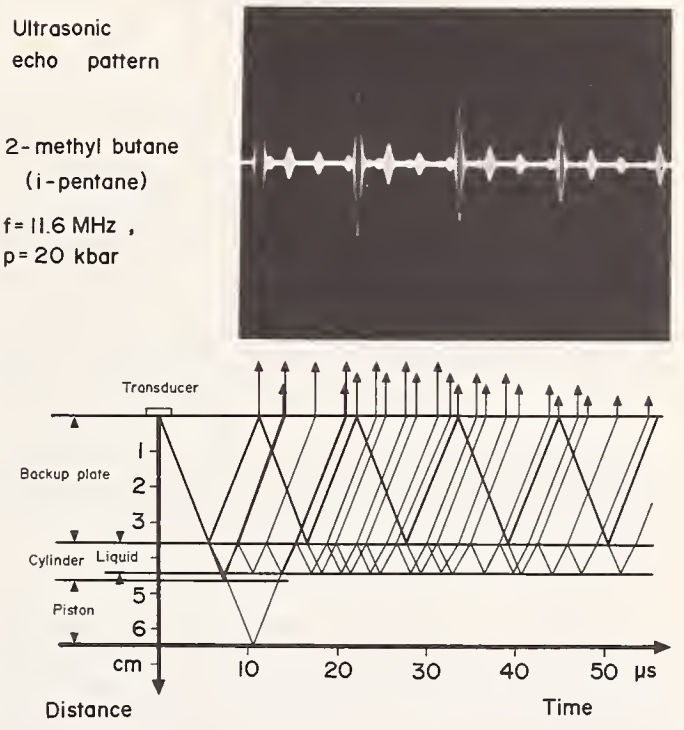

FIGURE 6. *Ultrasonic echo pattern from isopentane (2-methyl butane) at 20 kbar.*

Sample echo sequences are marked with groups of arrows of equal length.

Significant changes of this ratio are observed at phase transitions in solids (fig. 7, compare also [23]), or in the vicinity of the glass transition of certain liquids. In the first case this change of the signal amplitude is a facile way of detecting a transition. In the second case it indicates the increase of the viscosity as the glass transition is approached.

Both with liquids and many solids, times between pulses are usually measured to within ± 5 ns. These times are usually reproduced to within better than 10 ns from one pressure cycle to the next. When multiple echoes can be observed the transit time τ can often be determined to a few nanoseconds.

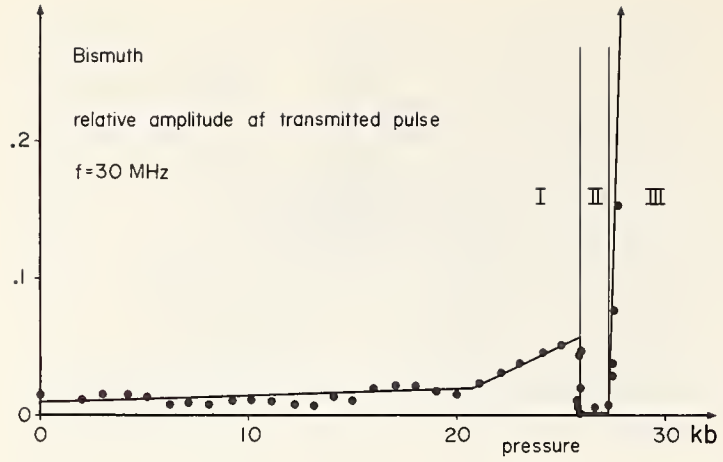

FIGURE 7A. *Variation of amplitude of reflected pulses at the* Bi I-II *transition.*

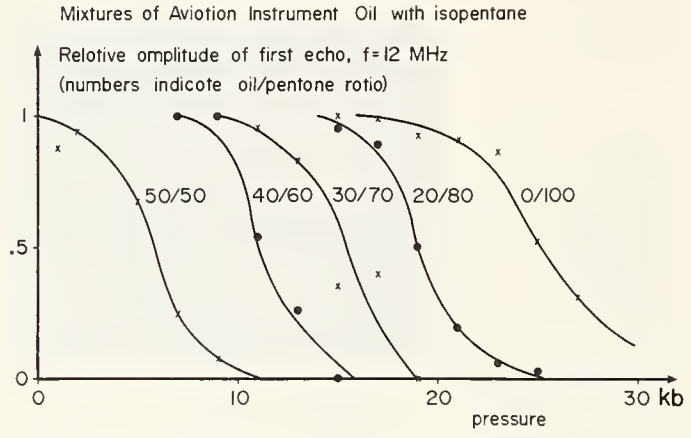

FIGURE 7B. *Variation of amplitude of reflected pulses in the vicinity of the glass transition of mixtures of aviation instrument oil with isopentane.*

Difficulties arise with materials showing large anisotropy of the speed of sound along different crystallographic axes, particularly when the grain size is large compared to the wavelength. This leads to high attenuation due to scattering and also to disintegration of individual echoes into a group of smaller echoes. Figure 8 demonstrates this effect with an example of the transmission of a 30 MHz wave train through a bismuth sample of about 1 cm length. Such samples are ground to a fine powder, passed through a 325-mesh sieve, and precompressed into the cylinder. Nevertheless, after one or two pressure cycles, very significant grain growth is observed. Similar effects have been observed in other materials.

4. Determination of Pressure

The internal pressure $\bar{p}$ for an upstroke is calculated from

$$\bar{p}=R(1+\beta_r\bar{p}_r)(1-\beta_{cyl}R\bar{p}_r)[\bar{p}_r-(a+b\bar{p}_r)] \qquad (1)$$

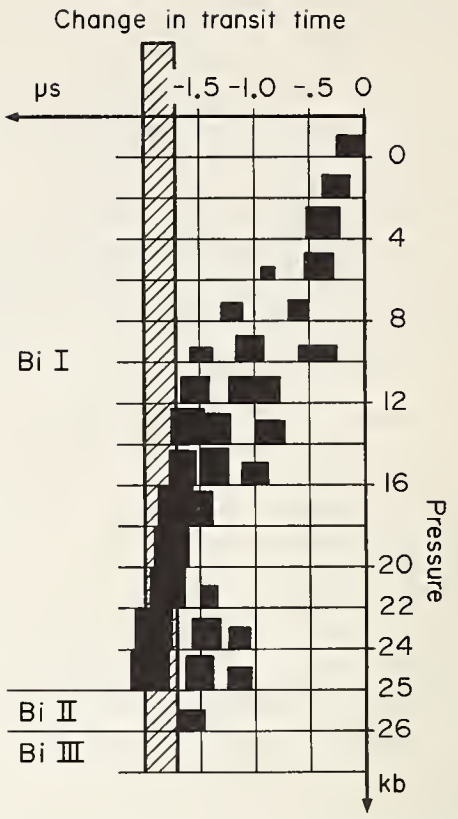

FIGURE 8. *Ultrasonic pulse transmission through bismuth showing the effect of changing grain structure: separation of pulse into two or more components.*

Areas of black rectangles indicate width and amplitude of pulses. Hatched area shows very large pulse amplitude in Bi III.

where a bar above or below a symbol denotes rising or falling pressure respectively, and where

R is the ratio of ram area to piston area,
$\bar{p}_r$ is the ram pressure,
$1+\beta_r\bar{p}_r$ is a correction factor for ram cylinder expansion,
$1-\beta_{cyl}\bar{p}_rR$ is a correction factor for high-pressure cylinder expansion,
a is a parameter representing the reduction of internal pressure due to friction extrapolated to zero ram pressure, and
b is a parameter representing the change of the internal pressure due to friction per unit ram pressure.

Both β_{cyl} and R depend to some extent on the seal in the high-pressure cylinder (effective area) and on the fraction of cylinder length exposed to high pressure. The reduction of the internal pressure due to friction is determined by including several small loops in the upstroke or downstroke as illustrated in figure 9. The friction data obtained from these loops on the upstroke are fitted to the equation

$$\text{reduction of internal pressure}=R(a+b\bar{p}_r). \qquad (2)$$

On the downstroke a special provision has to be made for correction in the range where the reversal

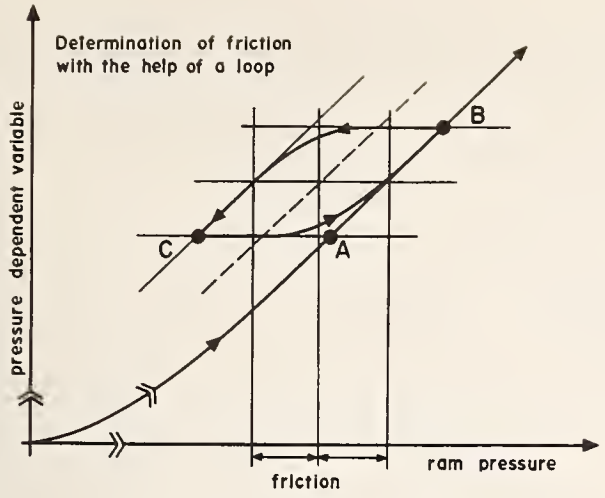

FIGURE 9. *Determination of friction.*

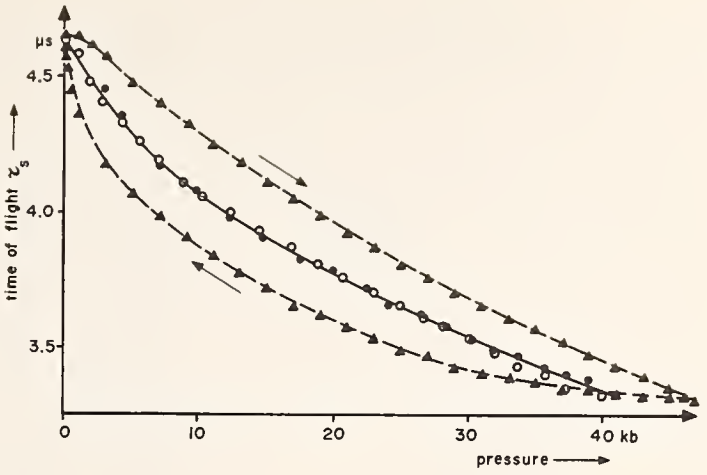

FIGURE 10. *Dependence of time of flight of ultrasonic pulses on pressure with and without correction for friction.*
Open circles upstroke, dots downstroke, both corrected for friction, triangles without correction for friction.

of friction takes place (B to C in fig. 9). An exponential function was found to describe the friction reversal very well.

$$\underline{p} = R(1+\beta_r \underline{p}_r)(1-\beta_{cyl} R \underline{p}_r)[\bar{\underline{p}}_r + (a+b\underline{p}_r) - 2(a+b\underline{p}_r)\exp[-F(p_{r,max}-\underline{p}_r)]], \quad (3)$$

where F is a factor chosen to fit the friction reversal (it is determined with the help of the OMNITAB FIT instruction [17] and taken to be constant for a particular kind of experiment), and

$p_{r,max}$ is the maximum ram pressure applied during the run.

The mass M of the ram piston reduces the internal pressure by MgR/A, where g is the acceleration due to gravity and A is the area of the ram. A similar correction must be applied for oil head in the line connecting the ram and the gage measuring the ram pressure.

Figure 10 illustrates how ultrasonic data taken during one full pressure loop are reduced to a curve of transit time versus internal pressure by applying eqs (2) and (3) to the upstroke and downstroke ram pressure.

Typical values for the constants in eqs (1) and (3) taken from measurements with polyethylene sleeves are:

$$R = 146.12$$
$$\beta_r = 7.5\times10^{-7}\ \text{bar}^{-1}$$
$$\beta_{cyl} = 5.0\times10^{-7}\ \text{bar}^{-1}$$
$$a = 2.62\ \text{bar}$$
$$b = 0.035$$
$$F = .013$$
$$p_{r,max} = 248\ \text{bar}$$

In these runs no rotation was used to relieve friction. The friction at the highest ram pressure therefore amounts to about 4.5 percent of the ram pressure.

The systematic error in the internal pressure p is determined from the total differentials of eqs (1) and (3). The terms of the total differential for $\bar{p}$, the uncertainties in individual constants or variables, and their contributions to the total uncertainty are listed in table 1. We believe that this list contains all of the significant contributions to the systematic uncertainty.

The uncertainty contribution of the ram-to-piston area ratio could be reduced by determining the diameter of the high-pressure cylinder with higher accuracy. The contribution of the ram cylinder expansion is obviously negligible. The expansion of the high-pressure cylinder makes by far the largest contribution to the total uncertainty in the pressure determination. We have described ultrasonic measurements of cylinder expansion in an earlier paper [2], and are presently planning further experiments to determine more accurately the expansion of cylinders under pressure. If necessary, the contribution of the ram pressure measurement can be reduced by replacing the Bourdon gage, used by us, with a piston gage. The contribution of friction can be reduced considerably by rotation of the piston.

In this computation of internal pressure we assume that friction on an upstroke equals that on a downstroke at a given internal pressure, if the loop is reasonably small. The loop should be large enough to develop friction fully in both directions of piston travel. When liquids are pressurized in a polyethylene-lined cylinder, small loops close within the precision of our measurement. This is not the case for many solids.

A solid under pressure in this apparatus is not under hydrostatic pressure, but is under axial loading by the piston and radial loading by the reaction

TABLE 1. *Total differential of* $\bar{p}$ *and contributions to estimated uncertainty of* $\bar{p}$.

Terms of total differential	Uncertainty of the variable	Contribution to total uncertainty at 30 kbar
$(1+\beta_r\bar{p}_r)(1-\beta_{cyl}R\bar{p}_r)[\bar{p}_r-(a+b\bar{p}_r)]dR$	0.1 (ram area to piston area ratio)	20 bar
$R\bar{p}_r(1-\beta_{cyl}R\bar{p}_r)[\bar{p}_r-(a+b\bar{p}_r)]d\beta_r$	1.5×10^{-7} bar^{-1} (ram cylinder exp.)	1 bar
$R^2\bar{p}_r(1+\beta_r\bar{p}_r)[\bar{p}_r-(a+b\bar{p}_r)]d\beta_{cyl}$	1×10^{-7} bar^{-1} (high-pressure cylinder exp.)	98 bar
$R(1+\beta_r\bar{p}_r)(1-\beta_{cyl}R\bar{p}_r)(1-b)d\bar{p}_r$	0.275 bar (ram pressure)	38 bar
$R(1+\beta_r\bar{p}_r)(1-\beta_{cyl}R\bar{p}_r)da$	.2 bar (friction)	29 bar
$R(1+\beta_r\bar{p}_r)(1-\beta_{cyl}R\bar{p}_r)\bar{p}_r db$	.002 (friction)	64 bar
Total uncertainty of $\bar{p}$ at $\bar{p}=30$ kbar		250 bar or 0.8 percent

force of the cylinder walls. This nonhydrostatic stress distribution can result in axial stress components exceeding radial stress components by the yield strength of the material on increasing pressure, and the reverse on decreasing pressure. This causes the size of the displacement versus pressure loops to be dependent on the extreme pressure to which the sample has been subjected [8, 9]. Therefore, we do not expect a large downstroke to come close to points C (fig. 9) of small loops included in an upstroke, if solid material is compressed. With liquids contained in polyethylene sleeves the downstroke does, however, approach points C closely.

5. Evaluation of Dilatometric Measurements

The advance of the piston into the cylinder cannot be measured directly with mechanical means. Instead, the travel of a piece in the lower part of the piston stack is measured relative to the support of the large bridge plate (fig. 1). Two diametrically arranged dial indicator micrometers are read to 0.00001 in (0.25 μm) and their readings averaged. A three-point measurement with gages spaced 120° would be preferable to the present setup, as it would permit detection of tilt of the piston stack around any axis.

To arrive at the advance of the front end of the piston relative to the cylinder, several corrections have to be applied. The complete equation used for an upstroke is

$$\Delta L = L(p) - L_0 = h_0 - h(p) + \phi\bar{p}_r + \eta\bar{p}_r^2 + \gamma[1 - e^{-\epsilon\bar{p}}r] + \beta_{cyl}L_0p \qquad (4)$$

where ΔL is the adjusted change in sample length;

$L(p)$ is the adjusted length of the sample at pressure p;

L_0 is the length of the sample at zero pressure;

h_0 is the dial gage reading at zero pressure;

$h(p)$ is the dial gage reading at ram pressure $\bar{p}_r$;

$\phi\bar{p}_r$ and $\eta\bar{p}_r^2$ are corrections for compression of the piston stack and distortion of other parts (the square term was omitted from most equations in this paper because its contribution is negligible)

$\gamma[1 - e^{-\epsilon\bar{p}}r]$ is a correction for initial slack in the setup at low pressures, and

$\beta_{cyl}L_0p$ is a correction for the effect of cylinder expansion which adjusts the length to the length the sample would have in a rigid cylinder, permitting the use of $L(p)/L_0$ for V/V_0.

Typical values for the terms of eq (4) are:

$L_0 = 0.85$ cm

$\phi = 1.5\times10^{-4}$ cm bar^{-1}

$\eta = 1.0\times10^{-8}$ cm bar^{-2}

$\gamma = 6.7\times10^{-3}$ cm

$\epsilon = 0.005$ bar^{-1}

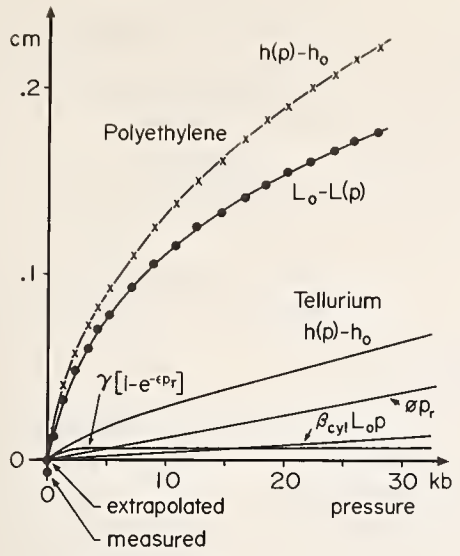

FIGURE 11. *Sample length and correction terms as function of pressure for polyethylene and tellurium.*

The dial gage reading $h(p)$ increases as the piston advances. Figure 11 illustrates the relative magnitude of the terms of eq (4) with data taken from a run with polyethylene as sample material. The curve for $h(p)$ shows a large change at very low ram pressures. This is mainly due to slack between various parts of the piston stack, which is picked up rapidly as the ram pressure increases. The fact that this large initial change is not due to sample compression only is illustrated in figure 12. Here the cylinder was omitted, and the piston is pushing directly against the tungsten carbide backup plate. Even after all the slack is eliminated, the piston stack is further compressed. This compression can be computed from the stress-dependent elastic constants and the dimensions of the parts involved. We prefer, however, to use the data shown in figure 12 to obtain the correction terms by fitting the equation

$$h(p) = h_0 + \gamma[1 - e^{-\epsilon \bar{p}_r}] + \phi \bar{p}_r + \eta \bar{p}_r^2 \qquad (5)$$

to the experimental data to determine h_0, γ, ϵ, ϕ, and η. Zero weight is assigned to h_0, since a reasonable zero pressure dial indicator reading cannot be obtained either with, or without, sample and cylinder. From the curve fitting operation, an extrapolated value for the zero pressure dial indicator reading h_0 is obtained.

To solve eq (4), a value for h_0 has to be chosen by extrapolating the $h(p)$ versus p_r curve to $p_r = 0$. This is, however, often a very arbitrary value, which may be off from the true value by as much as 0.005 in. A refined way of arriving at a value for h_0 closer to the true value will therefore be discussed below. With the sample length L known as a function of pressure, we can now proceed and determine the density and bulk modulus. Assuming that a solid sample was used we have

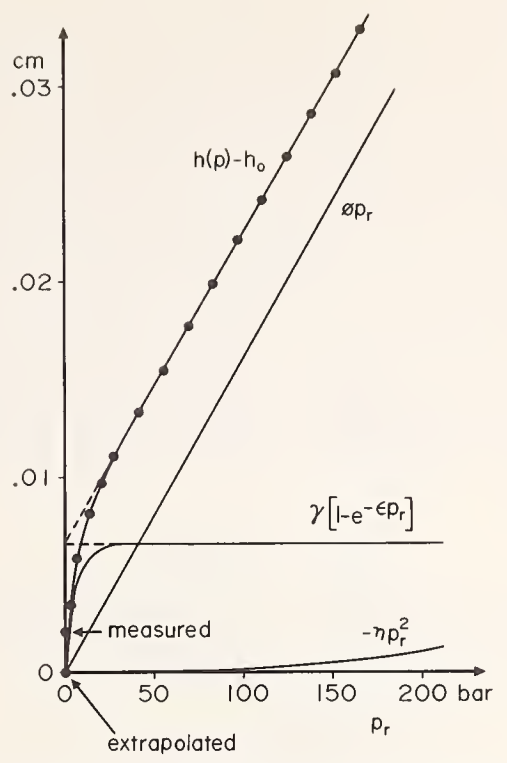

FIGURE 12. *Elastic distortion of piston stack.*

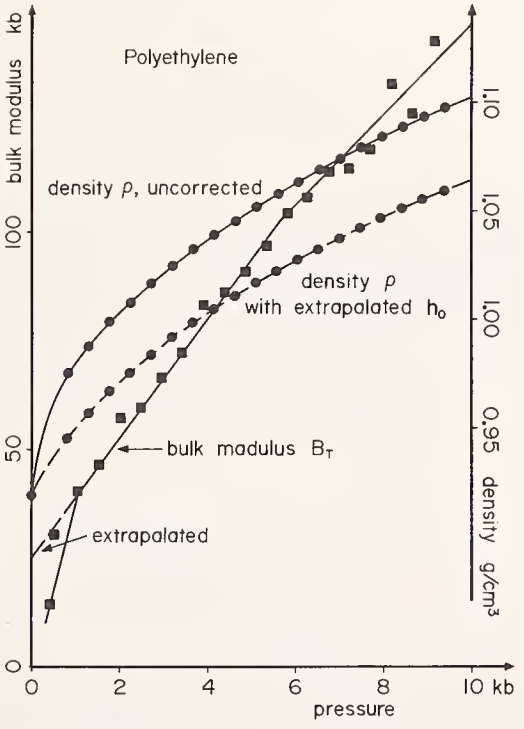

FIGURE 13. *Bulk modulus and density of polyethylene. Influence of extrapolated zero pressure dial indicator reading.*

$$\rho(p) = \frac{L_0}{L(p)} \cdot \rho_0 \qquad (6)$$

where $\rho(p)$, ρ_0 are the densities of the sample material at pressure p and at $p = 0$, and

$$B_T(p) = -L_0 \frac{\Delta p}{\Delta L(p)} \qquad (7)$$

where $B_T(p)$ is the isothermal bulk modulus. Figure 13 shows the results for the data used in figure 11. A quick glance at the $\rho(p)$ curve does not reveal any noteworthy effects. The $B_T(p)$ curve shows a break at the low-pressure end, while the rest of the curve is more nearly a linear function of pressure. If more runs than this one are compared, it appears that this break varies widely from run to run. It is, in fact, the arbitrary choice of h_0 which affects the lowest point of the $B_T(p)$ curve, since it appears as the difference of two similar values $h(p)$ and h_0 in the denominator of eq (7). Experience shows that B_T is a linear function of pressure at least for compressions up to $V/V_0=0.85$. If we assume that for a limited range

$$B_T(p)=B_0+B_1p \tag{8}$$

we can rewrite eq (4) and extrapolate h_0 from some value of $h(p)$ taken at a higher pressure but from within the range where eq (8) holds

$$h_0=h(p)-\frac{L_0}{B_1}\ln\frac{B_0+B_1p}{B_0}-\phi\bar{p}_r - \gamma[1-e^{-\epsilon p_r}]-\beta_{cyl}L_0p, \tag{9}$$

noting that

$$\frac{L(p)-L_0}{L_0}=-\int_0^p\frac{dp}{B_0+B_1p}=-\frac{1}{B_1}\ln\frac{B_0+B_1p}{B_0}. \tag{10}$$

This extrapolation has been made for the data in figure 11 and the extrapolated value for h_0 is indicated on the ordinate.

The extrapolated value for h_0 was then used to recompute $L(p)$, $\rho(p)$, and $B_T(p)$. The dashed lines in figure 13 indicate the improved values.

The computation of $\Delta L=L(p)-L_0$ for a downstroke is quite similar except that no correction needs to be made for pickup of slack. Therefore, we have for the downstroke

$$\Delta L=L(p)-L_0=h_0-h(p)+\phi\bar{p}_r+\beta_{cyl}L_0p. \tag{11}$$

If the sample is a fluid contained in a polyethylene sleeve, $L(p)$ is determined as above. $L(p)\frac{D^2\pi}{4}$, with D diameter of the cylinder, is the total volume of sample plus sleeve. The volume of the polyethylene to be subtracted from the total volume is

$$V_{PE}(p)=V_{o,PE}\left[1-\frac{1}{B_{1,PE}}\ln\frac{B_{0,PE}+B_{1,PE}p}{B_{0,PE}}\right] \tag{12}$$

where $V_{PE}(p)$, $V_{0,PE}$ are the volume of polyethylene at pressure p and at $p=0$, respectively,

and $B_{o,PE}$, $B_{1,PE}$ are the coefficients of a linear bulk modulus equation analogous to eq (8).

Furthermore, $V_{0,PE}=\frac{D^2-d^2}{4}\pi L_0$, where d is the inside diameter of the polyethylene sleeve.

The volume of the fluid then is

$$V_{Fluid}(p)=\frac{D^2\pi}{4}L(p)-\frac{D^2-d^2}{4}\pi L_0\left[1-\frac{1}{B_{1,PE}}\ln\frac{B_{p,PE}+B_{1,PE}p}{B_{0,PE}}\right], \tag{13}$$

the density is

$$\rho_{Fluid}(p)=\rho_{Fluid}(o)\frac{V_{Fluid}(o)}{V_{Fluid}(p)} \tag{14}$$

and the bulk modulus is

$$B_{T,Fluid}(p)=-V_{Fluid}(o)\frac{\Delta p}{\Delta V_{Fluid}}. \tag{15}$$

Again an extrapolation for h_0 will be necessary. It is complicated somewhat by the presence of two different materials in the cylinder. The expression to be used is

$$h_0=h(p)-L_0+\frac{L_0}{D^2}\left[(D^2-d^2)\left(1-\frac{1}{B_{1,PE}}\ln\frac{B_{0,PE}+B_{1,PE}p}{B_{0,PE}}\right)+d^2\left(1-\frac{1}{B_{1,Fluid}}\ln\frac{B_{0,Fluid}+B_{1,Fluid}p}{B_{0,Fluid}}\right)\right] -\gamma[1-e^{-\epsilon\bar{p}r}]-\phi\bar{p}_r-\beta_{cyl}L_0p. \tag{16}$$

The systematic uncertainty of $L(p)$ for a solid sample is determined from the total differential of eq (4). The significant terms of the differential and their contributions to the systematic uncertainty are shown in table 2 for 2 kbar and 30 kbar internal pressure. We believe this to be a complete list of all significant contributions. The total systematic uncertainty in the determination of $L(p)$ is about 0.4 percent at 2 kbar and 1 percent at 30 kbar. As in the determination of pressure, one of the largest contributions comes from cylinder expansion. The term $\bar{p}_rd\phi$ is related to the compression of the piston stack. It could be reduced significantly if all measurements were referred to, say, $p=2000$ bar, as is frequently done by other researchers [10] following Bridgman's example [5] to avoid the difficulties arising from the initial pickup of slack in the setup.

The large uncertainty in the determination of the bulk modulus from dilatometric data is demonstrated in table 3 (compare also fig. 11). Listed are the most significant terms only. A variation of all dial gage readings $h(p)$ by the same amount in the same direction does not have any influence on $B_T(p)$, which depends on the difference between two readings. Likewise, B_T at some high pressure is not affected by a variation in h_0.

TABLE 2. *Significant terms of the total differential of* L(p) *and their contributions to the systematic uncertainty of* L(p)

Terms of differential	Uncertainty of the variable	Contribution to systematic uncertainty	
		at 2 kbar	at 30 kbar
dh_0	0.00075 cm } (piston stack travel)	0.0007	0.0007
dh	.00025 cm }	.0003	.0003
$d\gamma$	.00075 cm (slack)	.0007	.0007
$L_0 p d\beta_{cyl}$	10^{-7} bar^{-1} (cylinder exp.)	.0003	.0025
dL_0	0.0013 cm (sample length)	.0013	.0013
$\bar{p}_r d\phi$	1.5×10^{-5} cm bar^{-1} (stack compr.)	.0003	.0033
Total systematic uncertainty		0.0036 cm or 0.4 percent	0.0088 cm 1 percent

TABLE 3. *Contributions to systematic uncertainty of* B_T *of tellurium at 35 kbar*

Uncertainty of variable	Contribution to total systematic uncertainty
$d\beta_{cyl}=10^{-7}$ bar^{-1} (cylinder exp.)	17 kbar
$dL=0.008$ cm (sample length)	0.5 kbar
$d\phi=1.5\times10^{-5}$ cm bar^{-1} (stack compr.)	141 kbar
Total systematic uncertainty	159 kbar or 26 percent of $B_T=590$ kbar

These contributions to the total systematic uncertainty of B_T were not determined from differentials but from variation of input data of the computer program used to evaluate B_T. The reference value for B_T was obtained from ultrasonic measurements with appropriate corrections to convert from adiabatic to isothermal conditions.

6. Evaluation of Ultrasonic Measurements

The ultrasonic transit times τ measured for longitudinal waves (τ_l) and transverse waves (τ_t) in solids are readily converted into velocities by division into the measured length $L(p)$ of the transit path

$$c_l(p)=\frac{L(p)}{\tau_l(p)}, \qquad c_t(p)=\frac{L(p)}{\tau_t(p)}.$$

We must note, however, that $L(p)$ as defined in eq (4) is corrected for cylinder expansion and that for accurate evaluation τ has to be corrected for the same effect so that, with $\alpha_{cyl}=1+\beta_{cyl}p$,

$$c_l=\frac{L(p)}{\tau_l(p)\,\alpha_{cyl}}, \qquad c_t=\frac{L(p)}{\tau_t(p)\,\alpha_{cyl}}. \tag{17}$$

The adiabatic bulk modulus B_S [24] is

$$B_S(p)=\frac{\rho(p)L^2(p)}{\alpha^2_{cyl}}\left(\frac{1}{\tau_l^2(p)}-\frac{4}{3}\cdot\frac{1}{\tau_t^2(p)}\right) \tag{18}$$

and since in a rigid cylinder or when suitable corrections are applied

$$\rho(p)=\rho_0\cdot\frac{L_0}{L(p)} \tag{19}$$

we have

$$B_S(p)=\frac{\rho_0 L_0 L(p)}{\alpha^2_{cyl}}\left(\frac{1}{\tau_l^2(p)}-\frac{4}{3}\cdot\frac{1}{\tau_t^2(p)}\right) \tag{20}$$

The conversion of the adiabatic modulus B_S to the isothermal modulus B_T is made with the relations

$B_S = B_T^*(1+\alpha_P\gamma_G T)$,

$$B_T^* = -V\frac{dp}{dV} \sim B_T = -V_0\frac{dp}{dV} \qquad (21)$$

where α_P is the thermal coefficient of volume expansion, γ_G is the Grüneisen constant,

$$\gamma_G = \frac{\alpha B_S}{\rho c_p} = \frac{\alpha c^2}{c_p},$$

and

T is the temperature in K.

The problems encountered in the determination of γ_G have been treated in several recent papers [11, 12, 13]. If literature values for γ_G are not available for the temperature and pressure range in question, we can replace γ_G by γ_S at least for simple solids from the modified Slater equation [13]

$$\gamma_S = \frac{1}{3} - \frac{1}{3}\frac{\partial \ln c_l}{\partial \ln (1/\rho)} - \frac{2}{3}\frac{\partial \ln c_t}{\partial \ln (1/\rho)} \qquad (22)$$

or we can determine γ_G as described below for fluids from measurements along at least three isotherms. Often the term $T\alpha_P\gamma$ is small compared to unity and can be assumed to be constant.

Because of the large uncertainty in the determination of sample length [22] it may be advantageous to eliminate $L(p)$ in eq (20) and to compute B_S or B_T from ultrasonic data only. We note that the variation of $L(p)$ with pressure for solids is relatively small

$$L(p) = L_0\left[1 - \int_0^p \frac{dp}{B_T(p)}\right]. \qquad (23)$$

We can therefore replace $B_T(p)$ under the integral by $B_S(p)$ assuming $\alpha_P\gamma_G T \ll 1$ and, after combining eqs (20) and (21), write for $B_T(p)$

$$B_T(p) = \frac{\rho_0 L_0^2}{\alpha_{cyl}^2(1+\alpha_P\gamma_G T)}\left[\frac{1}{\tau_l^2(p)} - \frac{4}{3}\frac{1}{\tau_t^2(p)}\right]\left[1 - \int_0^p \frac{dp}{\frac{\rho_0 L_0 L(p)}{\alpha_{cyl}^2}\left[\frac{1}{\tau_l^2} - \frac{4}{3}\frac{1}{\tau_t^2}\right]}\right]. \qquad (24a)$$

Furthermore, we can assume that $L(p)$ under the integral in the correction term is constant and equal to L_0. Whence it follows for B_T determined from ultrasonic measurements alone:

$$B_T(p) = \frac{\frac{1}{\tau_l^2(p)} - \frac{4}{3}\cdot\frac{1}{\tau_t^2(p)}}{\alpha_{cyl}^2(1+\alpha_P\gamma_G T)}\left[\rho_0 L_0^2 - \int_0^p \frac{\alpha_{cyl}^2 dp}{\frac{1}{\tau_l^2(p)} - \frac{4}{3}\frac{1}{\tau_t^2(p)}}\right]. \qquad (24b)$$

The significant terms of the total differential of B_T are listed in table 4, together with their contributions to the systematic uncertainty of the bulk modulus of tellurium at 35 kbar. The total systematic uncertainty is 9.3 kbar, which is about 1.6 percent of the bulk modulus ($B_T = 590$ kbar). This result compares very favorably with the large uncertainty shown in table 3 for the same material but from isothermal measurements. Even if we allow for a larger uncertainty of the term $\alpha_P\gamma_G T$, which was not considered in table 3, the ultrasonic method is superior in those cases where ultrasonic measurements can be made.

We have not, for example, been able to make ultrasonic measurements in polyethylene or in the low-pressure form of polytetrafluorethylene because of high attenuation. In the high-pressure polymorph of polytetrafluorethylene, ultrasonic attenuation is quite low and ultrasonic measurements could be made and evaluated, if the density were accurately known at some pressure above the transition.

A word of caution must be said, however. The solid samples in the piston and die assembly are subject to shear stresses, which may introduce enough anisotropy to invalidate the ultrasonic method [21]. This method should therefore only be used for materials which have small shear strength, small grain size, and a high degree of crystal symmetry.

With liquids, no such problems exist, and it is therefore quite interesting to apply the ultrasonic method to liquids contained in the polyethylene sleeve described above.

Only longitudinal waves can be used. As in the evaluation of eq (20) above, we choose not to use the experimentally determined $L(p)$ because of its rather large uncertainty. Instead, bulk modulus, speed of sound, and density are determined from ultrasonic data alone.

The volume of the fluid V_f at pressure p is

$$V_f(p) = V_{fo}\exp\left[-(1+\alpha_P\gamma_G T)\int_0^p \frac{dp}{B_S(p)}\right], \qquad (25)$$

where $V_{fo} = d^2\pi L_0/4$ is the fluid volume at ambient pressure.

If the adiabatic bulk modulus of the fluid

$$B_S(p) = \left(\frac{L(p)}{\alpha_{cyl}\tau(p)}\right)^2 \rho(p) \qquad (26)$$

is not known as a function of pressure, a first approximation is made

$$B_{S,1}(p) = \left(\frac{L_0}{\alpha_{cyl}\tau(p)}\right)^2 \rho_0. \qquad (27)$$

With this approximation we can now proceed to determine the approximate volume of the fluid $V_{f,1}$ at pressure p. The volume of the polyethylene sleeve is obtained from previous isothermal meas-

TABLE 4. *Significant terms of the total differential of* B_T *determined from ultrasonic measurements, and their contribution to the systematic uncertainty of* B_T *of tellurium at 35 kbar*

Terms of differential	Uncertainty of variable	Contribution to systematic uncertainty
$2\rho_0 L_0\left(\frac{1}{\tau_l^2(p)}-\frac{4}{3}\cdot\frac{1}{\tau_t^2(p)}\right)dL_0$	0.0013 cm (sample length)	2210 bar
$\frac{2\rho_0 L_0^2}{\tau_l^3(p)}d\tau_l$	5×10^{-9} s (transit time of longt. mode)	5150 bar
$\frac{8\rho_0 L_0^2}{3\tau_t^3(p)}d\tau_t$	10^{-8} s (transit time of transv. mode)	1925 bar
Total systematic uncertainty.....		9285 bar or 1.6 percent of $B_{T(35\text{ kbar})}=590$ kbar.

urements of the bulk modulus fitted to a linear function of pressure (see eq (12) and fig. 3).

From the sum of these volumes divided by the cross-sectional area we obtain a first approximation for the length of the fluid column

$$L_1(p)=\frac{V_{PE}(p)+V_{f,1}(p)}{D^2\pi/4}. \tag{28}$$

A first approximation for the density is obtained from

$$\rho_{f,1}(p)=\rho_{f0}\frac{V_{f0}}{V_{f,1}(p)}. \tag{29}$$

The first approximation length and density are now introduced into eqs (25, 26) and the computation is repeated. This iteration is performed until the change of the computed data from one cycle to the next falls below a specified value. With water as a test substance and pressures up to 12.5 kbar, four iteration cycles were usually sufficient.

If measurements are made along three isotherms, γ_G can be determined directly [14, 15, 16] by first computing the approximate volume along the isotherms and then calculating

$$\gamma_G=\frac{\alpha_P c^2}{c_P} \tag{30}$$

with $\alpha_P=\frac{1}{V}\left(\frac{\partial V}{\partial T}\right)$ and $\left(\frac{\partial c_P}{\partial P}\right)_T=-T\left(\frac{\partial^2 V}{\partial T^2}\right)_P$.

An iteration process such as described above but with two loops can be used to compute complete and very accurate equation-of-state data over the entire pressure-temperature plane.

We have made ultrasonic measurements on various liquids at pressures up to 40 kbar. Data obtained for water along the 22 °C isotherm are used to illustrate the merits of the method. The bulk modulus data obtained from the iteration process using the experimental transit time data [3] were fitted to a linear function of pressure. The OMNITAB [17] POLYFIT instruction was used for the least squares fit. The result of the least squares fit for B_S and p in bar is

$$B_S=23{,}222+6.677p.$$

The standard deviation of the fit was 743 bar. This equation was integrated assuming constant $\alpha_P\gamma_G T$ and converted to density. The density is plotted in figure 14. For comparison, density data from the works of P. W. Bridgman [18, 19] and L. H. Adams [20] are entered. Our data are also in good agreement with the data by Vedam and Holton [16], who used a fixed-path length interferometer. This method provides greater accuracy but is limited to much lower pressures.

Table 5 lists the contributions of various experimental data to the total uncertainty of density, velocity, and bulk modulus of water at 10 kbar. It is very interesting to note that the major uncertainties do not come from the transit time measurement, but from the pressure measurement and the determination of the initial length of the polyethylene sleeve. This is even more obvious, when the transit time τ is determined with the pulse superposition method rather than from a simple delay measurement. Pulse superposition will permit estimated uncertainties of less than one nanosecond with a resultant contribution to the total uncertainty of the bulk modulus of less than 80 bar.

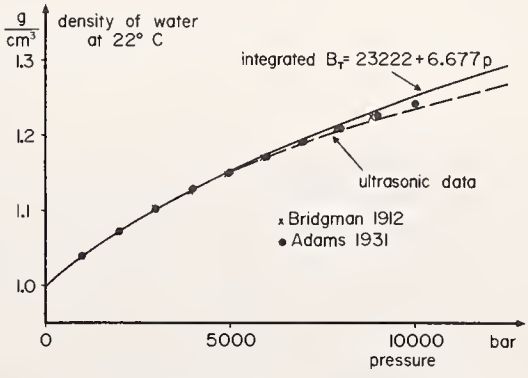

FIGURE 14. *Density of water as function of pressure.*

TABLE 5. *Contributions of uncertainties in experimental data to the total uncertainty of the ultrasonically determined equation of state of water (at 10 kbar)*

Experimental quantity	*Uncertainty of experimental quantity*	*Contribution to total uncertainty of*		
		Density	*Velocity*	*Bulk modulus*
p	90 bar (ram pressure)	0.00156 g/cm³	5.5 m/s	478 bar
L_0	0.004 cm (sample length)	.00186 g/cm³	11.5 m/s	633 bar
$B_{0,PE}$	1200 bar (bulk modulus of PE)	.00017 g/cm³	1.6 m/s	96 bar
$\alpha_P\gamma_G T$	0.0007 (Grüneisen constant)	.00021 g/m³	0.4 m/s	9 bar
ρ_0	0.0005 g/cm³ (density at $p=0$)	.00047 g/cm³	.3 m/s	52 bar
τ	5×10^{-9} s (transit time)	.00064 g/cm³	6.6 m/s	402 bar
Others		.00025 g/cm³	4.5 m/s	149 bar
Total uncertainty		0.00516 g/cm³ or 0.4 percent	30.4 m/s 1.1 percent	1819 bar 2 percent

$\rho_{(10\ \text{kbar})}=1.235$ g/cm³ $C_{(10\ \text{kbar})}=2705$ m/s $B_{T(10\ \text{kbar})}=90350$ bar.

7. Conclusions

The present evaluation of systematic uncertainties of dilatometric measurements in simple piston and cylinder assemblies demonstrates the large influence of the deformation of the piston stack (term ϕp_r) and of the expansion of the high-pressure cylinder (term $L_0 p\beta_{cyl}$) on the systematic uncertainties of density and bulk modulus derived from such measurements. It also shows the relatively greater accuracy that can be achieved by using ultrasonic methods under favorable conditions to determine the mechanical properties of the compressed materials. It appears that the development of improved dilatometric methods is imperative and that cylinder expansion and piston stack distortion have to be known much better before more sophisticated ultrasonic methods are employed.

8. References

[1] Jayaraman, A., Hutson, A. R., McFee, J. H., Coriell, A. S., Maines, R. G., ASME Annual Meeting 1966, Paper No. 66–WA/PT–10.

[2] Heydemann, P., Houck, J. C., J. Res. NBS **71C**, No. 1, 11 (1967).

[3] Heydemann, P., Houck, J. C., J. Appl. Phys. **40**, No. 4, 1609 (1969).

[4] Heydemann, P., J. Appl. Phys. **38**, No. 6, 2640 (1967), and J. Appl. Phys. **38**, No. 8, 3424 (1967).

[5] Bridgman, P. W., Proc. AAAS **74**, 399 (1942).

[6] Bridgman, P. W., Proc. AAAS **44**, 38 (1913).

[7] McSkimin, H. J., Andreatch, P., JASA **34**, No. 5, 609 (1962).

[8] Pistorius, C. W. F. T., Rapoport, E., Clark, J. B., Rev. Sci. Instr. **38**, No. 12, 1741 (1967).

[9] Tamayama, M., Eyring, H., Rev. Sci. Instr. **38**, No. 8, 1009 (1967).

[10] Weir, C. E., J. Res. NBS **53**, No. 4, 245 (1954).

[11] Bartels, R. A., Schuele, D. E., J. Phys. Chem. Solids **26**, 537 (1965).

[12] Anderson, O. L., J. Phys. Chem. Solids **27**, 547 (1966).

[13] Pastine, D. J., Phys. Rev. **138**, A767 (1965).

[14] Holton, G., J. Appl. Phys. **22**, 1407 (1951).

[15] Holton, G., Hagelberg, M. P., Kao, S., Johnson, W. H., Jr., JASA **43**, No. 1, 102 (1968).

[16] Vedam, R., Holton, G., JASA **43**, No. 1, 108 (1968).

[17] Hilsenrath, J., et al., OMNITAB, A Computer Program for Statistical and Numerical Analysis, NBS Handbook 101 (U.S. Government Printing Office, Washington, D.C., 1966).

[18] Bridgman, P. W., Proc. AAAS **48**, 307 (1912).

[19] Bridgman, P. W., J. Chem. Phys. **3**, 597 (1935).

[20] Adams, L. H., J. Am. Chem. Soc. **53**, 3769 (1931).

[21] Smith, R. T., Ultrasonics **1**, 135 (1963).

[22] Montgomery, P. W., Montgomery, C., Wald, D. A., Rev. Sci. Instr. **38**, No. 8, 1073 (1967).

[23] Matsushima, S., Special Contributions, Geophysical Institute, Kyoto University, No. 5, 117 (1965).

[24] Bergmann, L., Der Ultraschall (S. Hirzel Verlag, Stuttgart, 1954), p. 562.

DISCUSSION

P. M. Bell *(Geophysical Laboratory, Carnegie Institution of Washington, Washington, D.C.)*: There are three ways to measure ultrasonic transit times in an experiment of this type: a variable, calibrated delay for a comparison pulse, the pulse superposition or phase comparison techniques; and a direct delay for a comparison pulse; the pulse superposi- method. But I think your sample length of about 1 cm is too short for that and I am surprised that you get the stated accuracy. Have you used frequencies above 10 MHz?

G. C. Kennedy *(Institute of Geophysics and Planetary Physics, University of California, Los Angeles, California)*: The aim of your investigation was to develop better compressibility measurements. We have been working on the evaluation of precise shock wave data. These data are incredibly

good, far better than most of the people who made them think they are. The difficulty, of course, lies in the reduction of the Hugoniot to isothermal conditions. Depending on who evaluates one and the same curve you get different results. The problem comes down to the variation of Grüneisen gamma with volume.

We have measured the specific volume of ten compressible substances to three significant figures. These include indium, calcium, potassium, and so on. We find that our data agree to three significant figures with data derived from shock wave measurements, if the Dugdale-MacDonald relation for the volume dependence of gamma is used.

For indium at 50 kbar our specific volume is 0.841, from shock waves we obtain 0.841. Bridgman's value is 0.802 or something like that. Bridgman's values for gold and zinc agree both with our numbers and with those derived from shock wave data.

Since with the Dugdale-MacDonald relation for Grüneisen gamma shock wave and static experiments yield the same results, we now have a way to determine the variation of gamma by measuring isothermal compressibilities and comparing these with shock wave data. Our derived variation agrees with Dugdale-MacDonald.

As a result tables of compressibilities of a large number of standard substances are now being recomputed at Livermore.

L. Thomsen *(Columbia University, Palisades, New York):* In a paper by Orson Anderson and myself we have derived yet another expression for the Grüneisen parameter as a function of density which avoids all of the special assumptions that go into the various curves which Dr. Kennedy just drew. This paper will be presented on Wednesday morning and we should then be able to pursue this discussion considerably further.

D. J. Pastine *(U.S. Naval Ordance Laboratory, White Oak, Maryland):* There is not any magic formula that will give you the volume dependence of the Grüneisen parameter. Formulas like the Dugdale-MacDonald relation are essentially one-mode approximations. There are, however, relations which relate the Grüneisen parameter to other readily measurable thermodynamic quantities. These will give you the first and second derivative with respect to volume at low pressure.

AUTHORS' CLOSURE

In reply to Dr. Bell: We have in a few cases of samples with low attenuation and the perfectly alined endfaces used the more accurate phase comparison method. Usually we make a direct determination of pulse spacing with the help of a calibrated sweep delay. The position of the unmodulated rf-pulse is read at the peak of the pulse. This reading is reproducible to within 10 ns. We also expect it to be reproduced when we return to the same pressure setting following a small loop. The time between pulses measured in this way is equal to twice the transit time through the sample. However, in many cases five or more echos are observed and the actual transit time can then be determined to much better than 10 ns. Measurements are usually made at 10 to 12 MHz, but occasionally we go as high as 30 MHz.

In reply to Dr. Kennedy: If you have very accurate isothermal data for the bulk modulus then we can also use our ultrasonic data and, of course, thermal expansivity data, to determine the Grüneisen parameter. We have tried this with our isothermal data. But the accuracy of our isothermal data, especially in the case of liquids, was not high enough to yield really meaningful results.

The purpose of our paper was to emphasize how much the accuracy of the determination of the equation-of-state parameters can be improved by using ultrasonic methods. This is particularly true in those cases where the ratio of isothermal to adiabatic bulk modulus is close to unity. In all other cases we do have to rely on somebody's data for the Grüneisen parameter.

385-762 O - 71 - 3

Characterization of the Bismuth I-II and Barium I-II Points Under Hydrostatic Pressure

R. J. Zeto, H. B. Vanfleet*, E. Hryckowian, and C. D. Bosco

Institute for Exploratory Research
U.S. Army Electronics Command, Fort Monmouth, N.J. 07703

Hydrostatic pressure experiments were made which have new and important relevance to high-pressure calibration in both liquid and solid pressure systems for the bismuth I–II and barium I–II points on the high-pressure scale. The bismuth I–II transformations were characterized and the mechanism of the solid-state reactions was related to pressure calibration. The strain hysteresis commonly associated with the bismuth I–II point was shown to be invalid and was alternatively explained on the basis of a thermally activated nucleation and growth mechanism which was demonstrated to govern these transformations. With hydrostatic pressure, initiation of the bismuth I–II transformation was observed as a function of kinetic times as long as 15 hours while pressure and temperature were maintained constant. The transformation behavior was a function also of the microstructure, purity, and thickness of the sample. The bismuth I–II transformation was not necessarily sharp with respect to kinetic time. As long as 42 hours were observed for completion of the transformation with very thin samples. Under hydrostatic pressure the bismuth I–II equilibrium point was not midway between the initiation of the I–II and II–I transformations but was located appreciably closer to the former transformation. The bismuth I–II calibration point was correlated between liquid and solid pressure systems. For solid systems it was shown that the "apparent" hysteresis was completely one-sided toward the low-pressure side and that the equilibrium point coincided with the initiation of the I–II transformation which should be employed as the pressure calibration point. The bismuth I–II region of indifference was characterized with respect to nature of the sample and manner of measurement. An experimental technique was indicated by which the center of the region of indifference was reproducible within ±5 bars. The barium I–II point was measured at 56.27 kbar on the basis of a manganin gage under hydrostatic pressure.

1. Introduction

The current high-pressure scale is based upon fixed-point pressures of solid-solid phase transformations. Although the bismuth I-II point at 25.380 kbars at 25 °C is fundamental to the high-pressure scale and is universally employed for high-pressure calibration, very little work has been done to characterize the nature of the $I \rightleftharpoons II$ phase transformations upon which the fixed-point calibration pressure is based. In view of experience and theory on the variable nature of solid-solid phase transformations, such a characterization and relation to the calibration pressure is warranted, both for hydrostatic pressure systems which calibrate on the equilibrium point and for solid pressure systems which calibrate on the initiation of the transformations. This is particularly important for ultimate accuracy of the bismuth I-II calibration point in the former pressure systems in which pressures can be measured with a sensitivity of 1 bar. The behavior of the phase transformations can certainly be expected to display an influence on the calibration point in terms of this degree of sensitivity of pressure. More practically important at the present time is the resolution in terms of phase transformation theory of the several different calibration procedures employed in solid pressure systems. During the last several years in the high-pressure laboratory at Fort Monmouth, a unique hydrostatic pressure capability was developed with a hexahedral press, and hydrostatic pressure experiments were made which have new and important relevance to high-pressure calibration in both solid and liquid pressure systems for both the bismuth I-II and barium I-II points on the high-pressure scale. In view of the

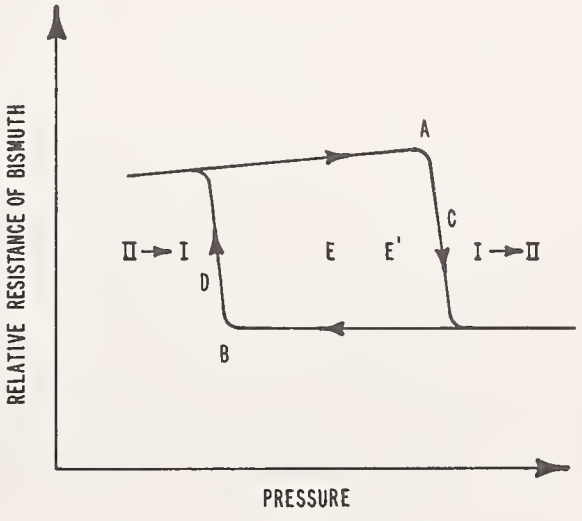

FIGURE 1. *Schematic representation of the relative resistance of bismuth for increasing and decreasing pressure in the vicinity of the I-II calibration point.*

*On Sabbatical Leave from Brigham Young University, Provo, Utah.

Paper presented at the Symposium on Accurate Characterization of the High-Pressure Environment, held at the National Bureau of Standards, Gaithersburg, Md., October 14–18, 1968.

large amount of information which resulted from these experiments, the important results pertinent to pressure calibration and the goals of this conference are presented in the manuscript in summary form. More elaborate discussion and experimental detail will be orally presented and will be submitted to J. Appl. Phys. and to J. Phys. Chem. Solids in the near future.

To place the results of the present paper in context, it is helpful to review briefly the present concept of the bismuth I-II and II-I transformations. A perusal of the literature reveals that the general nature of these transformations, whether examined by means of electrical resistance, volume change, or x-ray measurements in either liquid or solid pressure-transmitting systems, can be schematically depicted as in figure 1 for the vicinity near the calibration point. With increasing pressure on a sample composed completely of bismuth I, the I-II transformation initiates at a pressure corresponding to *A*. After sufficient overpressurization to completely convert all bismuth I to bismuth II, decreasing pressure causes the II-I transformation to initiate at a pressure corresponding to *B*, which is substantially lower than *A*. Both transformations occur isobarically in liquid systems but may have to be pressurized to completion in solid systems. Thus the transformations to completion, *C* and *D*, exist as illustrated for solid systems but are vertical for liquid systems. The pressure interval between points *A* and *B* is commonly denoted as a hysteresis for the transformations. In liquid systems this pressure interval has been reported to have an average value of about 0.71 kbar [1][1], whereas in solid systems the value is observed to be much larger and is of the order of kbars due to the attendant and additional hysteresis of the pressure-transmitting medium, e.g., pyrophyllite or AgCl. The transformations can be made to reverse over a much smaller pressure range near the equilibrium pressure if the hysteresis is entered, either by reducing pressure during the I-II transformation or by increasing pressure during the II-I transformation, so that both phases are in intimate contact.

In his liquid system, Bridgman [2] measured a pressure range of about 60 to 100 bars within which the transformation would not perceptibly run in either the I-II or the II-I direction and denoted this pressure range as the region of indifference. It is generally assumed, primarily because of a lack of data, that the equilibrium pressure, *E*, is situated halfway between the pressures at which the I-II and II-I transformations occur when measured either at the hysteresis or at the region of indifference. Several investigators [3, 4], however, have stated that such an occurrence might not be true with respect to the hysteresis, but in fact might be located at a higher pressure, *E'*.

[1] Figures in brackets indicate the literature references at the end of this paper.

2. Experimental

The basic apparatus was a hexahedral press with 2000-ton-capacity rams and a cubic pressure chamber 2.25 inches on an edge. Hydrostatic pressures were generated within a stainless steel cell which contained an equal-volume liquid mixture of normal- and iso-pentane. The stainless steel cell was situated within a pyrophyllite cube. As force was applied to the pyrophyllite cube, the cell experienced the uneven solid pressures within the cubic volume, but the sample within the stainless steel cell was exposed only to those forces transmitted by the liquid. The original hydrostatic pressure cell [5] was improved to increase its reliability and usable high-pressure volume ($^7/_{16}$ in diam $\times 1$ in length) and to give 10 electrical leads for measurement from the hydrostatic pressure chamber. This capability of volume and leads permitted four-terminal measurements, simultaneous comparison of several samples in the same experiment, and simultaneous measurement of manganin and samples. For example, one experiment comprised a manganin coil, mercury (for calibration of the coil), and four different bismuth samples. Four-terminal measurements were always made on manganin and also on the samples whenever possible. The resistance of the manganin coil was measured with a Leeds and Northrup Model 8069 G–2 Mueller Bridge with a sensitivity of ± 0.1 mΩ, which, for our coils, was equivalent to about ± 0.5 bar. Quantitative experiments were conducted with a properly seasoned and calibrated (mercury L-I and bismuth I-II points at 25 °C) manganin gage. Relative pressures from an uncalibrated manganin coil sufficed for the examination of qualitative features of the mechanism of the bismuth I-II and II-I transformations. The sample parameters investigated were purity (six nine's versus two nine's), microstructure (single crystal versus polycrystal), and thickness (0.040 in diam versus 0.013 in diam). Samples were monitored with a sensitivity of at least 0.1 percent either by means of a Keithley Model 150A microvoltammeter with the output recorded on a Varian Model G–11 strip chart recorder, or directly by means of a four-channel Model 240 Brush oscillograph-recorder. In order to avoid heating the samples, the current level was adjusted such that the power through the sample was kept at approximately 1.54×10^{-5} W. Temperature was measured to 0.001 °C by means of a platinum resistance thermometer immersed in a well of water which made contact through a brass plug with the anvil bearing on the pressure cell. Temperature corrections to 25 °C were applied for the resistance of manganin and for the temperature coefficient of 50 bars/deg C for the bismuth I-II point.

3. The Bismuth I-II Point Under Hydrostatic Pressure

3.1. The Apparent Hysteresis*

The hysteresis has important relevance to pressure calibration in solid pressure systems which comprise the bulk of pressure apparatus in current use. Two calibration procedures are generally employed in these systems: in one procedure only the I-II transformation pressure is measured and the calibration point is associated with point *A* in figure 1, and in the other procedure both the I-II and II-I transformation pressures are measured and the calibration point is associated with point *E* in figure 1. Obviously these are different calibrations, and pressures reported on the basis of the one type of calibration will be different than those pressures based on the other type of calibration. To resolve this discrepancy it has been suggested [4] that the former calibration method should add a pressure corresponding to one-half of the hysteresis width, i.e., *A-E* in figure 1. In any case, all of this type of calibration in solid pressure systems depends upon the hysteresis (both for bismuth and for the pressure medium) exhibiting a fixed and reproducible value.

Two publications [1, 4] associate a real hysteresis with the bismuth I-II point, but each also implies the possibility of a thermally activated nucleation and growth mechanism. Since a fixed strain mechanism and a thermally activated mechanism are mutually exclusive of one another, and in view of the obvious importance of the hysteresis for solid pressure calibration, it was considered desirable to conduct hydrostatic pressure experiments to determine the mechanism of the I-II and II-I transformations and the basis of the hysteresis. Actually, results published in the literature appeared to indicate a nucleation and growth type of mechanism. Also, our general experience with multiple cycles in the hydrostatic system failed to reproduce a closed loop with respect to resistance or to reproduce either boundary with respect to pressure and cast additional doubt on a fixed strain basis for the nature of the hysteresis *A-B* as represented in figure 1. It was of particular interest to determine whether or not this pressure hysteresis was real, i.e., if the initiation of the transformations beyond the equilibrium point was dependent upon a fixed strain energy which would yield a fixed pressure interval *A-B*. The alternative explanation of this pressure interval as being due to a thermally activated nucleation and growth mechanism requires that the pressure interval *A-B* be time dependent.

Experiments made under hydrostatic pressure showed that the hysteresis *A-B* of figure 1 was not a real strain hysteresis but was time dependent according to a thermally activated nucleation and growth mechanism.

*See also "Interpretation of initiation pressure hysteresis phenomena for fixed-point pressure calibration", Zeto and Vanfleet, J. Appl. Phys. (1970, in press) for later and more complete analysis.

By holding a sample composed completely of bismuth I at constant pressure and temperature below that represented by point *A* in figure 1, the I-II transformation initiated as a function of kinetic time. The observation of waiting periods prior to initiation of the I-II and II-I transformations at constant temperature and pressure within the apparent hysteresis has been noted numerous times for the I-II transformation and also for point *B* and the II-I transformation. Furthermore the pressure coefficient of the waiting periods for the I-II transformation, for example, was consistent with a thermally activated nucleation and growth mechanism; longer waiting periods were observed for lower pressures toward the equilibrium pressure. For the I-II transformation, point *A* was located with a very slow pressurization rate of 1 bar/min and then on different cycles pressure was maintained constant at various lower values. Waiting periods as long as 15 hr at constant pressure and temperature were measured prior to initiation of the I-II transformation. The waiting periods can be explained as a direct consequence of the kinetic time for nucleation of the new phase in a solid state transformation. In the vicinity of 150 to 200 bars over the equilibrium pressure, the pressure coefficient of the waiting periods appeared to be very large, about −6 min/bar. The waiting periods for the II-I transformation did not vary in a consistent manner with hydrostatic pressure. The initiation pressure of this transformation appeared to be dependent on the pressure with which the I-II transformation was overpressurized.

Hydrostatic pressure experiments in which several different samples were simultaneously examined and recorded showed very clearly that the transformation behavior was a function of sample purity, microstructure, and thickness. At constant pressure and temperature, appreciably different waiting periods for initiation of the I-II transformation were observed for different samples. Also, the times required for complete transformation to bismuth II varied not only from sample-to-sample but also as a function of the holding pressure. Slower transformation rates were observed for lower holding pressure in accordance with a nucleation and growth mechanism. Dramatically slow transformation rates were measured for very thin samples. For example, a bismuth strip sample 0.0004 in thick required about 42 hr for complete transformation, whereas under the same conditions in the same experiment a bismuth strip sample 0.011 in thick transformed completely in 1 hr. In the literature, "sharpness" of the transformations is sometimes invoked as a criterion for "hydrostaticity" of pressure, but the role of kinetic time in a solid-solid transformation must not be overlooked. Even though the transformations occur isobarically in a hydrostatic pressure system, the transformations may be very sluggish with respect to kinetic time. The slow transformation rates are further support for a thermally activated nucleation and growth mechanism. The fastest initiation and

transformation rates were observed with thick (0.040 in diam) polycrystalline samples.

All evidence from these hydrostatic pressure experiments was consistent with a thermally activated nucleation and growth mechanism. The hysteresis which is generally associated with the bismuth I-II point is not a real strain hysteresis but is actually an apparent hysteresis due to a large activation energy for nucleation and/or growth and the sluggish rates of a solid-solid phase transformation. This apparent hysteresis is variable with respect to kinetic time, pressurization rate, and sample characteristics. The assumption that the bismuth I-II equilibrium point is centered within the apparent hysteresis is also invalid. The relationship of the equilibrium point within the apparent hysteresis for liquid pressure systems was determined and is illustrated in figure 2. The apparent hysteresis *A-B* was found with a slow and constant pressurization rate and was then entered as described earlier for the measurement of the region of indifference within which is the equilibrium and calibration point. The region of indifference was not at all midway between the initiation pressures of the I-II and II-I transformations but was located appreciably toward the I-II side. The calibration point, *E*, was about 150 bars below point *A* which corresponded to about 1/3 of the pressure interval *A-B* in the liquid system. The transformations to completion, *C* and *D*, are represented as vertical lines since each transformation occurred isobarically. The initiation pressure of the II-I transformation, point *B*, was not reproducible on different pressure cycles and after completion of this transformation the initial bismuth I resistance was not recovered. Additional evidence of the variable nature of point *B* is shown in the next section.

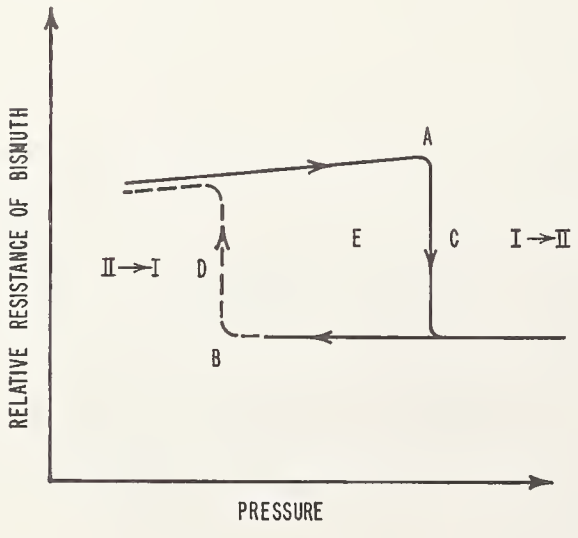

FIGURE 2. *Schematic representation of the relative resistance of bismuth for increasing and decreasing pressure in the vicinity of the I-II calibration point under hydrostatic pressure.*

Superficially these results have serious and detrimental implications for pressure calibration in solid pressure systems since the "hysteresis" is not a stable transformation feature upon which to fix a calibration. Consider, however, a nucleation and growth mechanism in the context of general experience with the kinetics of solid-solid phase transformations. The observed waiting periods at constant pressure and temperature may be associated with induction times for the nucleation of the new phase. It is known that scratching or grinding a material will reduce and remove an induction period, lower the activation energy for nucleation, and facilitate the nucleation rate of the new phase. Clearly, a scratching and grinding effect on the bismuth sample can be expected from the solid pressure medium and this would tend to eliminate the waiting periods observed under hydrostatic pressure. Theoretically, then, it would be expected that initiation of the I-II transformation in a solid pressure system should take place at a pressure which corresponds, or at least is close to, the real equilibrium point. Evidence that this correlation is valid is presented in the next section.

3.2. Correlation of the Calibration Point Between Liquid and Solid

An experiment was designed to test the transformation hypothesis just mentioned in the previous section. An experiment in the hydrostatic pressure cell was conducted with two identical bismuth samples: one sample was directly exposed to the pentane-mixture pressure medium and the other sample was completely embedded in an epoxy solid (about 0.040 in wall thickness) which in turn was directly exposed to the same pentane-mixture pressure medium. These samples were simultaneously examined in the same experiment and gave a direct comparison of the bismuth I $\rightleftharpoons$ II transformations for a specimen subjected to a hydrostatic pressure and one subjected to a solid pressure-transmitting medium. The samples were first pressure cycled with a slow, constant pressurization rate of about 15 bars/min in order to determine the apparent hysteresis for both samples. In cycling the samples, pressure was taken well beyond the bismuth II-III transformation in order to insure the presence of only one or the other of phase I and II at the initiation of the transformations. The true equilibrium pressure was then measured with the sample which was directly exposed to the hydrostatic pressure medium.

The correlation of the bismuth I-II equilibrium point within the apparent hysteresis for liquid and solid pressure-transmitting media is schematically illustrated in figure 3. The equilibrium point, *E*, measured with the sample in the liquid medium corresponded within a few bars to the pressure, A_S, at which the bismuth I-II transformation initiated

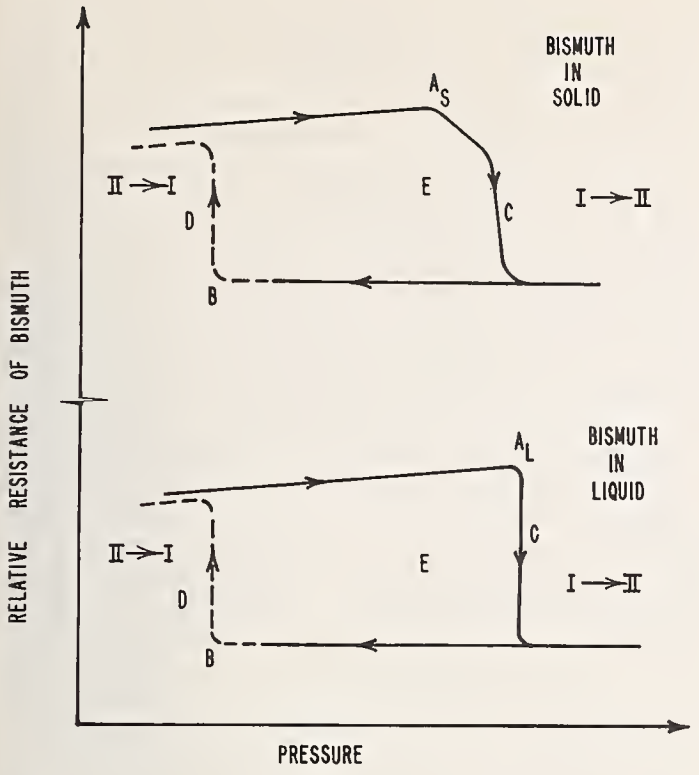

FIGURE 3. *Location and comparison of the equilibrium point in solid and liquid pressure transmitting media for the bismuth I ⇌ II transformations.*

in the sample which was embedded in the solid pressure transmitting medium. Verification of the theory of the mechanism of the transformation was obtained and these results provided striking correlation between liquid and solid pressure systems for pressure calibration at the bismuth I-II point. The hysteresis observed in solid pressure systems is completely one-sided towards the II-I transformation. In solid pressure systems, calibration should be conducted with a slow pumping rate and should be fixed to the initiation of the bismuth I-II transformation.

This phenomenon was investigated in another experiment in which an AgCl pressure-transmitting medium was employed. The same effect was clearly evident, although it was less pronounced than for bismuth in epoxy. Comparison of the transformation curves from initiation to completion of the transformation, C, revealed a dependence on the nature of the pressure transmitting media. This observation was consistent with a thermally activated nucleation mechanism in which nucleation of the new phase was accelerated by the pressure medium which was more non-isotropic, i.e., from pentane to AgCl to epoxy. Initiation of the I-II transformation occurred at the highest pressure, A_L, for the bismuth sample in the liquid medium. The II-I transformation, D, was very fast in all cases but the initiation of this transformation, B, occurred at a much lower pressure when the II-I transformation was preceded by the II-III transformations in the pressure cycle. In this case the equilibrium point, E, was located about the same pressure interval below A_L as when the II-III was not included in the pressure cycle, but A_L-E became only about one-sixth of the apparent hysteresis A_L-B.

3.3. The Region of Indifference Equilibrium Point

The region of indifference comprises the equilibrium point and is employed for pressure calibration in hydrostatic pressure systems. According to Bridgman [2], the region of indifference is measured as the pressure range over which the transformations can be made to run in opposite directions when starting from a pressure at which no transformation is perceptible. The region of indifference is determined with about equal amounts of both phases I and II present in the sample. Nucleation is no longer a consideration as the apparent hysteresis and the transformations can be made to reverse over a pressure range less than 100 bars. Although hydrostatic pressure systems comprise the minority of pressure apparatus in current use, there are an increasing number of laboratories utilizing these systems in which small pressure changes of about 1 bar can be measured with a manganin pressure gage. This precision cannot be utilized for pressure calibration with a comparable accuracy, however, since the equilibrium point has not been characterized with respect to the purity, microstructure, and thickness of the sample, the width of the region of indifference, the pressure direction of measurement, and the variation of the equilibrium point with respect to the relative proportions of bismuth I and bismuth II present in the sample. The pressure calibration point must be evaluated and considered in the context of the solid-solid phase transformation upon which it is based. General experience with high-temperature transformations shows that transformations in the solid state are influenced by these factors mentioned above. Characterization of the I-II equilibrium point is therefore important for the ultimate accuracy of hydrostatic pressure calibration, particularly in terms of the current techniques which measure pressure with a sensitivity of 1 bar. Hydrostatic pressure experiments were made to bear on such a characterization.

The technique which was experimentally employed to investigate the region of indifference was as follows. The sample potential was recorded for 15-min intervals at constant pressure. After the completion of an individual sample trace, pressure was altered either up or down in increments of 5 to 8 bars and the sample potential was again monitored for about 15 min at each pressure. The rate traces of sample potential versus time were zero within the region of indifference, positive for the II-I transformation, and negative for the I-II transformation. The manganin resistance was measured at the beginning and at the end of each trace and was

monitored on the recorder simultaneously with the sample trace. Pressure was constant within 1 bar over the duration of each rate record of the sample. The I-II and II-I boundaries of the region of indifference were noted as the pressure at which the sample rate trace deviated from zero in the negative and positive direction, respectively. The equilibrium pressure was then taken at the center of the region of indifference. By this procedure and with the sample and manganin sensitivity employed, 20 bars was commonly measured for the width of the region of indifference. This is the smallest region reported to date.

With respect to the equilibrium point the question arises as to the existence of a pressure region or a single pressure value over which or at which the transformation will reverse. Theoretically there cannot be a single value of pressure for the equilibrium point. The bismuth I-II point is based on a solid-solid phase transformation in which strain energy is a thermodynamic variable. In the phase rule sense, this extra degree of freedom means that the transformation must occur over a range of pressures at constant temperature instead of at a single pressure as normally expected for a pure compound. While greater sensitivity than that employed in the present investigation might reveal a region of indifference less than 20 bars, the region of indifference will nevertheless not be zero. The small value of 20 bars, however, is favorable for utilization of the bismuth I-II transformation for high-pressure calibration. In terms of this discussion, the nature of the region of indifference is based on the strain energy resulting from the volume change between phases I and II and this is really the strain hysteresis for the bismuth I-II point.

The nature of the region of indifference with respect to pressure direction of measurement was investigated with a polycrystalline bismuth sample of six nine's purity and 0.040 in diam. Since the determination of an equilibrium point should be made by approach from each side of the equilibrium, there are two possible ways in which the region of indifference may be measured: (1) I-II in the up-pressure direction and II-I in the down-pressure direction, and (2) I-II in the down-pressure direction and the II-I in the up-pressure direction. Four determinations were made by each method with 45 to 55 percent bismuth I present in the sample for each determination, and the results favored the former procedure as employed by Bridgman. The width of the region of indifference determined in this manner was 20 ± 6 bars, whereas a region of indifference of 27 ± 12 bars was determined by the latter procedure. The average of each set of four determinations gave the same absolute value for the center of the region of indifference for each method of measurement.

If the region of indifference is a strain hysteresis, as mentioned above, then this region could be a function of the relative proportions of bismuth I and bismuth II present in the sample. Consequently, measurement of the equilibrium point for high-pressure calibration might likewise be a function of the phase composition of the sample. To examine this phenomenon the region of indifference was measured at bismuth I proportions between about 20 and 80 percent with a polycrystalline sample of six nine's purity and 0.040 in diam. In this percentage range the widths of the region of indifference, about 20 bars in each case, overlapped. For bismuth I proportions between about 20 and 60 percent, the centers of the region of indifference were within about 5 bars of each other; however there appeared to be a definite bias, about 10 bars, towards lower pressures for the measurements at higher proportions of bismuth I. This effect was also observed for different samples with larger grain size (single crystal) and less purity (two nine's). In terms of the sensitivity of our pressure and sample measurements, this bias appears to be real, although it is difficult to make such a conclusion with certainty for such small pressure values in view of possible and unknown systematic errors of measurement. Investigation of this point by other laboratories seems desirable. In any case, it appears that highest reproducibility (several bars) of the calibration point is achieved when the pressure is adjusted so that about 50 percent of phase I exists in the sample when the region of indifference is measured.

As indicated above, the region of indifference was investigated as a function of the purity (six nine's versus two nine's), microstructure (single crystal versus extruded polycrystal), and thickness (0.040 in diam versus 0.013 in diam) of the sample. The center of the region of indifference was reproducible within ± 3 bars with respect to microstructure and thickness. Surprisingly, but favorable for pressure calibration, there was very little difference between six nine's and two nine's purity, the center of the region of indifference being about 10 bars higher for the less pure sample. The widths of the region of indifference overlapped for all samples. The most noticeable effect of these sample characteristics was that the width of the region of indifference became twice as large as a function of sample thickness from 0.040 in diam to 0.013 in diam, even though the center of the region was the same in each case. This width of the region was even 50 percent larger (about 70 bars) when measured by method (2) rather than by method (1) mentioned earlier. For all samples except the latter, the width of the region of indifference was about 20 bars.

The results described above have the following relevance to hydrostatic pressure calibration with the bismuth I-II point. First of all, the calibration point is reproducible at least within 50 bars regardless of pressure direction of measurement, proportion of bismuth I in the sample (between 20 and 80 percent), and sample characteristics (within the sample variation investigated) of purity, microstructure, and thickness, except for the wide region

for very thin samples. With the exception noted, all of these factors displayed their influence within ±25 bars of the calibration point. The influence of these factors on the nature of the I-II transformations has been assumed to be negligent in previous high-pressure calibration, but these factors have a basis in phase transformation theory and in experience with high-temperature transformations and it is comforting to have experimental verification of the extent of their influence. These results further indicate that the absolute reproducibility and accuracy for pressure calibration could be reduced to about ±5 bars for the center of the region of indifference and to about ±13 bars for the complete width of the region of indifference by employing a pressure and sample sensitivity comparable (or better) than that in this work and if the calibration is conducted starting with a pure single crystal sample about 0.040 in diam and by measuring the region of indifference after the manner of Bridgman with about 40 to 60 percent bismuth I present in the sample.

4. The Barium I-II Point Under Hydrostatic Pressure

Most high-pressure measurements above 40 kbar depend upon a calibration curve based on the barium I-II point. The importance of the point for accurate high-pressure measurements is clearly evident, particularly for pressures greater than 60 kbar. The barium I-II point has been measured [6, 7, 4, 8] with piston-cylinder devices and rotating free-piston techniques and with tetrahedral apparatus and x-ray techniques in conjunction with equation-of-state. In view of the present uncertainty associated with the calibration pressure for this transformation, the hydrostatic pressure cell described earlier was employed to provide an independent measurement of the barium I-II point, this one with hydrostatic pressure and based on a calibrated manganin pressure gage.

Pressure is hydrostatic to the extent that the viscosity of the pressure medium permits a fast relaxation time for bulk stresses. The pressure-transmitting medium in the hydrostatic pressure cell was a 1:1 volume mixture of normal- and iso-pentane in which pressures equalized by viscous flow through a prescribed capillary tube in times of the order of seconds at 50 kbar and of minutes at 60 kbar [5]. An approximate value of 10^8 poise at 60 kbars has been measured for this pressure medium [9]. The pressures generated at the barium I-II point were hydrostatic within this context.

The relative resistance change, $\Delta r/r_0$, of a properly seasoned manganin coil was calibrated with pressure by means of a quadratic equation

$$P = A(\Delta r/r_0) + B(\Delta r/r_0)^2.$$

whose coefficients A and B were determined by a two-point calibration with the accepted pressures and the measured relative resistance change of the manganin coil for the mercury L-I [10] and bismuth I-II [11] transformation at 25 °C. At the barium point slow pressurization rates were employed and adequate time for pressure equilibrium was allowed. The manganin relative resistance associated with the region of indifference of the barium I-II transformation was measured and the pressures corresponding to the width of the region of indifference were calculated from extrapolation of the manganin calibration curve. Using this same experimental and extrapolation technique, good agreement was obtained for measurement of the thallium II-III calibration point.

The width of the barium I-II region of indifference was 2.32 kbars according to manganin. This width is appreciably larger than the region of indifference measured with this same technique for bismuth I-II and thallium II-III, and is probably a reflection, at least to some extent, of the decreasing degree of "hydrostaticity" of the pressure medium. Nevertheless the pentane-mixture pressure medium is certainly more hydrostatic than the solid systems employed for the barium I-II point, and the present measurement of the region of indifference is the smallest reported for this transformation. According to the usual procedure the equilibrium pressure was determined from the center of the region of indifference and was 56.27 kbars. This value is 2.5 kbars lower than the presently accepted value of 58.8 kbars employed for high-pressure calibration. Based on this data, therefore, either the presently accepted equilibrium pressure for the barium I-II transformation is high by about 2.5 kbars or the curvature of the manganin curve changes quite sharply between 37 and 59 kbars. Several other recent measurements of this transformation have indicated that this calibration point should be lowered. Both of these measurements, 54.4 kbar [4] and 55.0 kbar [8], are still lower than the value obtained on the basis of manganin.

The results presented earlier for the comparison of the bismuth I-II point in solid and liquid pressure media have an interesting and potentially significant implication for measurement and calibration at the barium I-II point. If the mechanism of the barium I-II transformation is one of thermally activated nucleation and growth then, analogous to phase transformation theory and verification in the case of bismuth I-II, in solid pressure systems one would expect the real equilibrium point to be closer to initiation of the barium I-II transformation than to the average of the I-II and II-I initiation pressures, particular in view of the very wide pressure interval measured between these transformations in the solid systems.

5. Acknowledgment

Grateful acknowledgment is expressed to Dr.

H. H. Kedesdy for his encouragement during the course of this work, to Mr. G. E. Tomes for his able assistance with the experiments, and to Mr. F. J. Becker for his expert machining of the materials needed for the experiments.

6. References

[1] Davidson, T. E., and Lee, A. P., Trans. Met. Soc. AIME **230**, 1035 (1964).
[2] Bridgman, P. W., Proc. Am. Acad. Arts Sci. **74**, 1 (1940).
[3] Roy, R., 6th International Conference on the Reactivity of Solids, J. Wiley & Sons, New York, N.Y. (Jan. 1969).
[4] Jeffery, R. N., Barnett, J. D., Vanfleet, H. B., and Hall, H. T., J. Appl. Phys. **37**, 3172 (1966).
[5] Barnett, J. D., and Bosco, C. D., Rev. Sci. Instr. **38**, 957 (1967).
[6] Bridgman, P. W., Phys. Rev. **48**, 893 (1935).
[7] Vereshchagin, L. F., Zubova, E. V., Buimova, I. P., and Burdina, K. P., Soviet Physics-Doklady **11**, 585 (1967) (English translation), Dokl. Acad. Nauk, S.S.S.R. **169**, 74 (1966), (original Russian).
[8] Haygarth, J. C., Getting, I. C., and Kennedy, G. C., J. Appl. Phys. **38**, 4557 (1967).
[9] Barnett, J. D., and Bosco, C. D., J. Appl. Phys, **40**, 3144 (1969).
[10] Boren, M. D., Babb, S. E. Jr., and Scott, G. J., Rev. Sci. Instr. **36**, 1046 (1965).
[11] Kennedy, G. C., and LaMori, P. N., J. Geophys. Res. **65**, 741 (1960).

DISCUSSION

G. S. Kell (*National Research Council of Canada, Ottawa, Canada*): We measured the phase equilibrium between ice-I and ice-III and got a similar sort of result in that as you increased the pressure the transformation is rather sharp. When you lower the pressure, you can lower the pressure by hundreds of bars, without the transformation going back. We explained this by saying that as you lower the pressure, the low-pressure phase gives mechanical support to the high-pressure phase, which is then at a higher pressure than the hydrostatic pressure in the system.

Now I ask: Could this sort of phenomen apply in your case or, if not, is it possible that we have completely misdiagnosed our system? The phenomenon is quite asymmetric that as you raise pressure, once your transformation starts it runs to completion. As you go from high to low, it can be undershot many hundreds of bars and, if fact, perhaps you always have high-pressure nuclei left.

J. D. Barnett (*Brigham Young University, Provo, Utah*): You say you experience more consistency going from I-II than II-I. Is this not just due to the fact that generally you always run that transition going I-II initially and, therefore, you have no nuclei in the II phase at all? If you would cycle several times in the region of transition, wouldn't you get as much variability going either way? If you were to go to 50 kilobar and come back, then would it be reproducible? I wouldn't want to leave the impression that the II-I transition is inherently unreliable. It looked as though, if you go to high enough pressure or low enough pressure, and get far enough away from the transition so that no nuclei are present at all, it would be reproducible either way.

R. E. Hanneman (*General Electric Research and Development Center, Schenectady, New York*): Perhaps it would be instructive if we discussed the nucleation expressions and maybe it would become clearer as to why this hysteresis can occur on either side, in principle. If one simply takes the normal nucleation type expression, one obtains a pre-exponential term which I have shown to be essestially pressure-independent.[1] One obtains the pressure dependence in the activation energy for the nucleation term. As you increase the super-pressure at fixed temperature, the critical nucleus size becomes smaller.

The main point is that these are heterogeneously nucleated transitions and not homogeneously nuated systems; in order to heterogeneously nucleate a tetragonal phase versus an orthorhombic phase the terms that go into the heterogeneous nucleation barrier would be different going toward the orthorhombic phase versus toward the tetragonal phase. For instance, we have an interfacial energy term that goes into the nucleation expression. This term can be much more pronounced in either direction, depending on a specific heterogeneous nuclei present, be it the cell walls or impurities in the system. So I would submit we cannot assume the hysteresis would always be on the low side. It could be either way for transitions in different materials.

One other point related to this is if you use a homogeneous nucleation you end up with the largest possible activation pressure or super-pressure needed, so one might explore around and look for the most heterogeneous nuclei that you can find to minimize the hysteresis. In other words, you are working with a purposely dirty system, if you will, in terms of surface contact properties.

Another possibility would be working with a calibration type system where the free energy driving force versus super-pressure is very large and, therefore, as you go up just a little bit in super-pressure, it will enormously decrease the activation of free energy needed to nucleate the process.

As you run a bismuth transition at a higher temperature, if this model is correct at all, then the region should converge between hysteresis loops

[1] R. E. Hanneman, in Reactivity of Solids, John Wiley & Sons, Inc., New York, edited by J. W. Mitchell et al., pp. 789–802 (1969).

because your activation barrier for nucleation is dropping.

S. E. Babb, Jr. (*University of Oklahoma, Norman, Oklahoma*): It seems to me, if you are interested in measuring pressures better than say a tenth of a kilobar, that you have got all kinds of problems with this region of indifference. It is not clear where the center is in terms of technique. For example if I measure a region of indifference of 70 bars, it is not clear that my 70 overlaps your 20.

I suggest if it is at all possible, when you are interested in pushing towards the bars, you should avoid the solid-solid transition for calibration. Therefore, in the 20-kilobar region, I would like to suggest, on the basis of Kennedy's measurements, we go to melting and gallium.

R. Roy (*Pennsylvania State University*): I wish to expand on a point related to Dr. Hanneman's remark. There is little question that the phases formed either up or down pressure are in general heterogeneously nucleated. However, what is seldom considered is, the nature of the phase nucleated. The way we write our equations misleads us into thinking that each phase comes out in some thermodynamically standard state as a single crystal. Experimentally, in most cases even a single crystal will transform into an array of microscopic crystals with all kinds of residual strains, enormous grain boundary energies and possible orientation. (Very often so-called semiconductor-metal transitions only measure the low resistivity of the grain boundaries). Hence we actually observe the transition $A \rightarrow B^*$. Conversely on the down pressure cycle depending on how well annealed the sample is, we certainly observe a reaction of the type $B^* \rightarrow A^*$ or $B \rightarrow A^*$.

The free energy differences between A and A^* and B and B^* may be sufficient to cause a displacement of a few degrees or bars of the equilibrium curve. (In the case of MgO, the difference can be equal to 10 percent of the total enthalpy, see Weber and Roy, Am J. Sci. **263**, 668 (1965). Even in atmospheric pressure work we do not know a transition any better than ± 1 °C in the very best cases; perhaps to ± 0.2 °C in quartz. Hence I believe that we are up against the limitations of the physical realities involved and will not be able to obtain meaningful improvement of precision or accuracy beyond the point now reached by these authors.

F. P. Bundy (*General Electric Research and Development Center, Schenectady, New York*): I have a question on the mechanics. You showed very, very slow increase and decrease in pressure with time. I wondered, if you are reading the pressure on the manganin gage in the fluid cell, whether you observed any jumps? Most apparatuses where you have solid gaskets, and so on, between the flanges and punches will go by steps. Did you observe that? The phenomenon I am referring to is stick-slip in the solid portion of the cell between the punches and the gaskets, and the punch faces and the pyrophyllite, as you increase the force on the punches. Did you observe jumps in the cell pressure due to the stick-slip phenomenon? The pressure in the center of the cell doesn't necessarily go smoothly.

AUTHORS' CLOSURE

In reply to Dr. Kell: We do not believe that the large under-pressurization of the equilibrium pressure required for initiation of the bismuth II-I transformation was due to mechanical support from the low-pressure phase to the high-pressure phase, primarily since the under-pressurization was completely eliminated when pressure was released before the I-II transformation was completed such that phase I was present in the sample. Also the II-I transformation always proceeded to completion even after initiation instead of halting due to the increase of pressure or mechanical support caused by the volume change. Actually in our system we measured a pressure increase of about 10 to 20 bars concomitant with the transformation but completion was attained nevertheless. Also it seems unlikely to us that the formation of the first amounts of the transformation could cause a higher pressure in the matrix of the high-pressure phase equivalent to the 1.5 kbar under-pressurization observed in some cases.

In reply to Dr. Barnett: Our data showed that the initiation of both the I-II and II-I transformations were a function of the microstructure of the sample and we suggest that the II-I transformation is more sensitive to this variable. We believe that this effect is real, since we pressure-cycled the same sample in the same experiment many times and for the I-II transformation only on the first pressure cycle there was no possibility for phase II nuclei present in phase I. In order to insure as best we could that only one phase was present in the sample prior to the measurement of any initiation pressure, the sample was generally allowed to sit overnight at a pressure several kilobars from the equilibrium pressure. Under these conditions it seems unlikely that residual nuclei of the old phase remained in the sample although, of course, we cannot be unequivocally certain. Perhaps the II-I transformation would be more reproducible by going to the 50 kbar or some other pressure but the sample microstructure can also be expected to be a function

of the pressure treatment of the sample, particularly in solid pressure media. Fortunately for pressure calibration with the bismuth I⇄II point the results that we presented showed that the initiation pressure of the II-I transformation should not be included in the calibration technique in any case.

In reply to Dr. Hanneman: Our data were related specifically to the bismuth I⇄II transformations and we agree entirely that for other transformations the location of the equilibrium pressure between the initiation pressures is characteristic of the particular material and may be toward either the high- or the low-pressure side, it being less likely to be centered due to the factors involved in the nucleation process of each transformation. More detailed discussion of the present results in terms of the thermodynamic and kinetic aspects of phase changes will be found in the separate publications of this work. We also believe that nucleation of these transformations is heterogeneous but regarding the use of impurities to facilitate nucleation it should be mentioned that one must be careful that the purity and the calibrant do not form a two-component system so that the equilibrium pressure is altered. In this context we showed that initiation of the I-II transformation occurred first in two nine's purity bismuth versus six nine's purity bismuth but the important point for calibration was that the equilibrium pressures measured for the same samples differed by less than 10 bars and were within the experimental uncertainty of the determinations. Also it should be emphasized that the initiation of the bismuth I-II transformation is important for calibration only for pressure systems in which the equilibrium pressure, that is the true calibration point, cannot be measured. Our data showed that, in solid pressure-transmitting media, the initiation pressure of this transformation with slow pressurization rates corresponded quite closely to the equilibrium pressure and provides a good calibration. We have not yet examined bismuth I ⇄ II above room temperature, but at higher temperatures we also would expect to observe a smaller pressure interval between the initiation pressures with convergence of the initiation pressures toward the region of indifference.

In reply to Dr. Babb: We agree in principle that a solid-liquid transformation rather than a solid-solid transformation would be better for calibration, since then there would be no region of indifference and also initiation would always occur at the equilibrium pressure. We have just commented on the favorable coincidence of the initiation and equilibrium pressures for bismuth I-II in solid media and also we extensively examined the width and reproducibility of the region of indifference and found it to be quite satisfactory for calibration. We made 28 determinations of the region of indifference as a function of the purity, microstructure, and thickness of the sample, of the pressure direction of measurement, and of the relative proportions of the two phases present in the sample. The standard deviation of the center of the region of indifference for these 28 determinations was ± 0.008 kbar, which appears to be good evidence that the region of indifference should be reproducible from laboratory to laboratory.

In reply to Dr. Roy: We agree that the region of indifference of bismuth I ⇄ II is a good calibration point even though it is a solid-solid transformation. Although a solid-liquid transformation with zero region of indifference is ultimately desirable, the width of the region for bismuth I-II is smaller than the present accuracy of absolute measurement and also compares favorably with the precision of temperature measurements if one considers from *P-T* equilibrium boundaries a rough equivalent of 50 to 100 bars per degree.

In reply to Dr. Bundy: For the slow pressurization and depressurization rates of 1 to 25 bars/min that were employed for detection of initiation of the transformations and for the slower rates employed for the region of indifference measurements, jumps in the liquid cell pressure were only observed when the hydraulic pressure behind the rams was increased externally to purposely change the cell pressure. These jumps in the cell pressure were probably not due to stickslip in the pyrophyllite since there was no noticeable time delay between the external hydraulic pumping and the response of the manganin recording. After manganin started to change due to the external pumping the manganin increased smoothly and leveled off at the new value without discrete jumps in the recorded manganin trace except in very infrequent cases. In these cases the jump in the trace was always less than the increment in the pressure rate. The sensitivity of the recording was such that pressure changes of 1 bar were clearly perceptible. Consequently for slow pressure rates the external pressure changes appeared to be accommodated in the pyrophyllite part of the pressure chamber and gaskets by relaxation rather than by discrete stick-slip phenomenon.

Chairman: E. C. Lloyd

National Bureau of Standards
Washington, D.C. 20234

The Upper Bismuth Pressure Calibration Point[1]

J. C. Haygarth, H. D. Luedemann[2], I. C. Getting, and G. C. Kennedy

Institute of Geophysics and Planetary Physics, University of California, Los Angeles, California 90024

The Bi III-V and IV-V equilibrium boundaries were studied by monitoring electrical resistance changes. Extrapolation of the III-V data to 25 °C yields an equilibrium transition pressure of 77.5 ± 1.0 kilobar (kbar). The extrapolation also agrees within experimental error with the pressure of 78.2 kbar determined in a separate experiment at 22 °C. The use of the transition as a calibration point is discussed, and a procedure for estimating the compression-stroke transition pressure from the equilibrium transition pressure is proposed.

1. Introduction

In this paper, we describe a redetermination of of portions of the bismth III-V and IV-V equilibrium boundaries, with particular emphasis on a more accurate estimation of the pressure of the bismuth III-V transition at room temperature.

2. Experimental Procedure

End-loaded piston-cylinder apparatus as described by Boyd and England [1][4] was used, with modifications to enable it to reach higher pressures. The pressure vessel used in this study had a core of tungsten carbide cemented with 6 percent cobalt (Carboloy 883). It was found that Carboloy 883 cores suffered a maximum of 0.1 percent permanent enlargement of the bore diameter after exposure to the highest pressures, only one-tenth of that suffered by Carboloy 55A. The pistons, diameter 1.270 cm, were of Carboloy 999, which contains 3 percent cobalt binder. The phase transformations were detected by following the electrical resistance of the sample. The setup is shown in figure 1. Silver chloride was used as a pressure-transmitting medium.

There was no visible evidence of reaction between the bismuth and silver chloride. Examination of the samples after the runs with an electron microprobe failed to reveal the presence of any silver in the bismuth.

The resistance of the sample was followed by passing a constant current through it and observing the change of potential difference across it. The potential drop across the sample was suitably biased and displayed on one channel of a two channel Honeywell "Electronik 16" recorder with a sensitivity of 1 mV. full scale deflection. Changes of resistance of about 0.5 percent of that due to the III-V transition were detectable.

The transition temperature at a given compression was found by raising the temperature until the transition was partially completed, then reducing the temperature until the back reaction began to run. A dead span temperature interval in which the

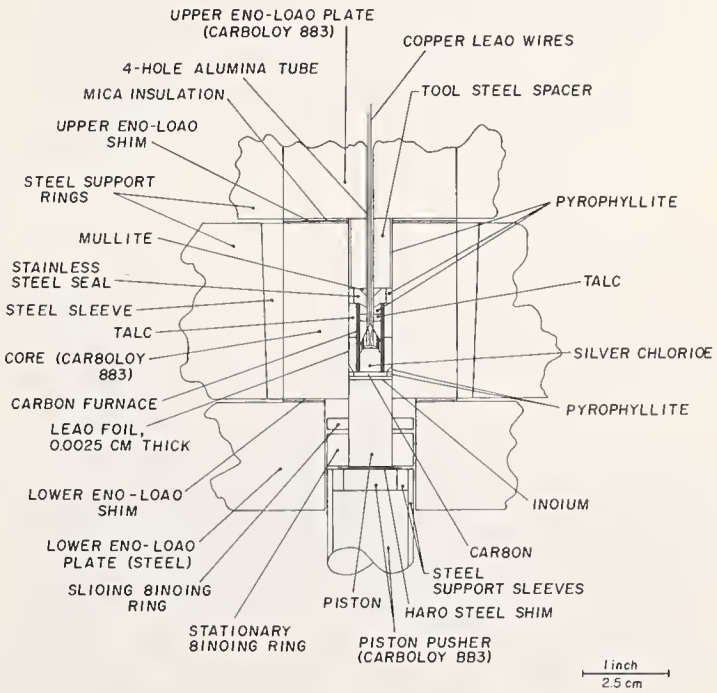

FIGURE 1. *Apparatus and sample assembly.*

[1] Publication #674, Institute of Geophysics and Planetary Physics, University of California, Los Angeles.

[2] Present address: Institut fur Physikalische Chemie und Elektrochemie, Universitat Karlsruhe, 75 Karlsruhe, Kaiserstrasse 12, W. Germany.

[3] Figures in brackets indicate the literature references at the end of this paper.

Paper presented at the Symposium on Accurate Characterization of the High-Pressure Environment, held at the National Bureau of Standards, Gaithersburg, Md., October 14–18, 1968.

reaction does not run detectably in either direction with both phases present was found. This temperature interval was independent of the relative amounts of the two phases present. It ranged in size from about 4° at the lowest temperature to about 0.5° near the triple point for the III-V boundary, and was 0.5° for the IV-V boundary near the triple point and less at higher temperatures. The transition temperature was taken as the mid-point of this interval. This method of locating the boundary is referred to later as the isobaric method.

The III-IV boundary was detected, and found to be associated with large hysteresis, confirming the findings of Klement et al. [2]. The hysteresis was so large that occasionally the metastable III-V boundary was observed in the neighborhood of the III-IV-V triple point. The III-IV reaction was so sluggish that no attempt was made to delineate accurately the equilibrium boundary.

The III-V boundary was also studied at a number of constant temperatures by cycling the pressure. This is referred to later as the isothermal method.

The III-V boundary was also observed at room temperature using a setup similar to that described for the barium transition [3]. In this case the pressure was varied continuously at about 0.2 kbar per second.

In all experiments, the pressure of the oil activating the hydraulic ram that drove the piston was measured with a Heise Bourdon-type gage.

3. Results and Discussion

The data from the isobaric experiments were in the form of thermocouple emf's and oil-pressure values for measurements taken on compression and decompression. They were plotted and resulted in two similar curves whose separation was the double-valued friction. It ranged from about 1.2 kbar at the highest temperature to 1.6 kbar near the triple point for the IV-V boundary, and from about 1.6 kbar near the triple point to about 3.0 kbar at the lowest temperature for the III-V boundary. On the assumption that the friction was symmetrical, the mean of compression and decompression values was taken at fixed values of thermocouple emf.

The results are plotted in figure 2. Circles represent points from the isobaric measurements, except that points on the metastable projection of the III-V boundary are shown as squares. Triangles denote points derived from the isothermal experiments, and the point represented by a diamond is the result of the room temperature experiment.

The data for the isobaric experiments, in which the equilibrium transition temperature was measured, were fitted to polynomials of degree two through ten using a least-squares technique with the U.C.L.A. IBM 360 computor. For both the III-V and IV-V boundaries the standard deviation was essentially constant for all the polynomials of second degree and above.

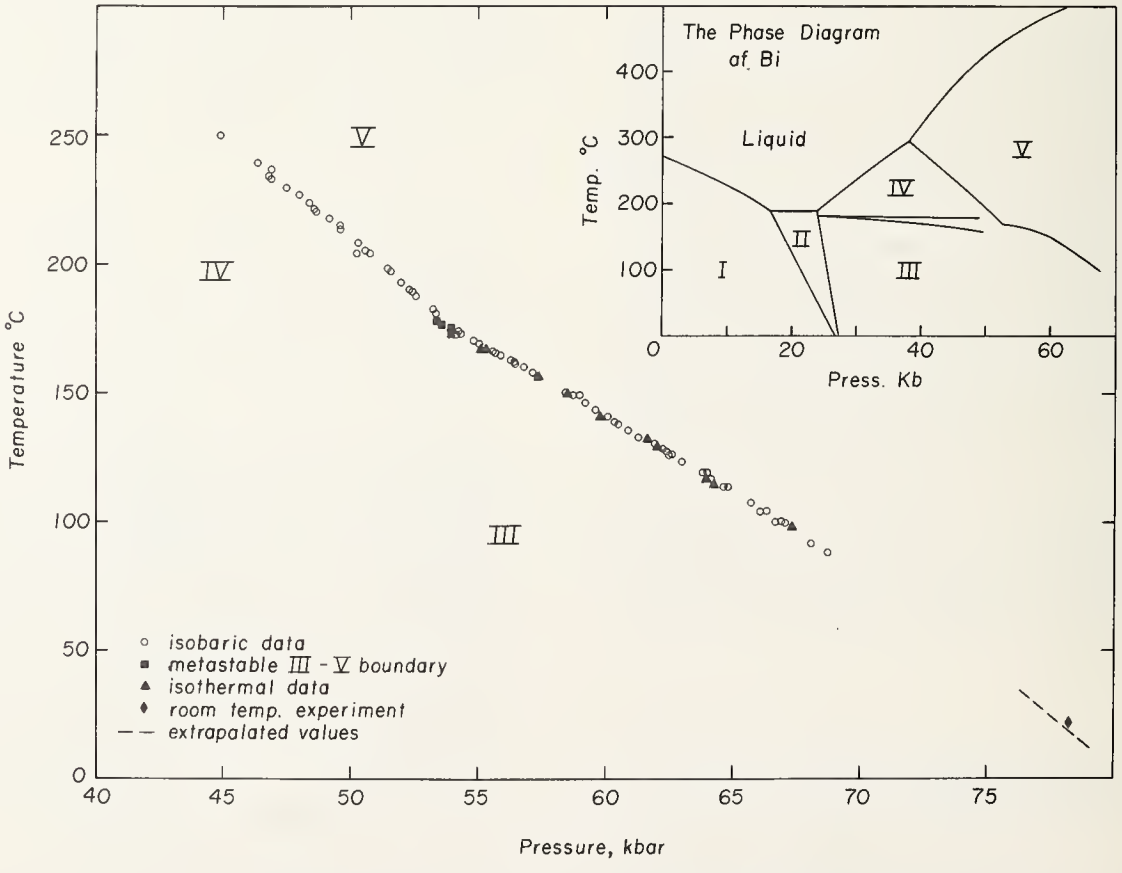

FIGURE 2. *Bismuth* III-V *and* IV-V *equilibrium boundaries.*

With P in kilobars and T in °K, the second degree equations were

$$P_{III-V} = 96.343 - 1.4431 \times 10^{-3}T - 2.0774 \times 10^{-4}T^2$$

and

$$P_{IV-V} = 54.192 + 1.0425 \times 10^{-1}T - 2.3354 \times 10^{-4}T^2.$$

The standard deviations were 0.08 kbar and 0.09 kbar respectively. Combination of these expressions gives the III-IV-V triple point coordinates as 174.6°, 54.3 kbar, which compares well, expecially as to temperature, with the result of Klement et al. [2], 174°, 52.6 kbar.

Equations for the III-V boundary give the value for the transition pressure at 25°, as 77.5 kbar; and predicted an abolute zero transition-pressure of 96.343 kbar. The extrapolated transition pressure at 22° is 77.9 kbar, in good agreement with the measured value of 78.2 kbar.

The pressure proposed for the III-V equilibrium boundary at 25° is 77.5 ± 1.0 kbar, allowing for absolute uncertainties in both pressure and temperature determinations. The standard deviation of the data from the expression with which they were extrapolated is less than one-tenth of the accuracy estimation. Previous estimates of the III-V transition pressure at room temperature have ranged from 88 to 90 kbar by Bridgman [4] and Vereshchagin et al. [5] to 73.8 ± 1.3 kbar by Jeffery et al. [6]. The consensus of recent opinion has favored a value near 80 kbar as reported by Klement et al. [2], Stark and Jura [7], and Giardini and Samara [8].

Of the four [2, 4, 6, 7] papers in which the estimated pressure is assumed to be the equilibrium pressure, only two [2, 4] describe the use of apparatus appropriate to measuring pressure directly. The others [6, 7] describe techniques in which an indirect method of calibration was used. The value of 78 to 82 kbar suggested by Klement et al. [2] was tentative and based on a long extrapolation of sparse data obtained in double-stage piston-cylinder apparatus, where pressure determinations are less certain than with single-stage apparatus. Considering this, the agreement with the present result is good. The fact that Bridgman [4] reports a value about 10 kbar above the present value is consistent with the finding that Bridgman overestimated the pressures of a number of transitions frequently used as calibration points [3, 9]. It is difficult to discuss the values reported by the other workers because of the indirect pressure calibration procedures [6, 7, 8] and the fact that the equilibrium pressure was not determined in all cases [5, 8].

On room temperature compression, Bi III persists about 2 kilobars beyond the equilibrium transition pressure into the Bi V field. Thus in normal calibration experiments the III-V transition may actually be detected a few kilobars above the equilibrium value reported above.

4. Acknowledgments

We wish to thank Dr. W. Klement for many helpful discussions, and Mr. L. Faus and Mr. J. Yamane for their skill and patience in machining the many intricate parts required. We are also indebted to the Army Research Office, Durham, North Carolina for partial financial support under contract DA-31-124-ARO-D.

5. References

[1] Boyd, F. R., and England, J. L., J. Geophys. Res. **65**, 741 (1960).
[2] Klement, W., Jr., Jayaraman, A., and Kennedy, G. C., Phys. Rev. **131**, 632 (1963).
[3] Haygarth, J. C., Getting, I. C., and Kennedy, G. C., J. Appl. Phys. **38**, 4557 (1967).
[4] Bridgman, P. W., Proc. Am. Acad. Arts Sci. **74**, 425 (1942).
[5] Vereshchagin, L. F., Zubova, E. V., Buimova, I. P., and Burdina, K. P., Soviet Phys.-Docklady **11**, 585 (1967).
[6] Jeffery, R. N., Barnett, J. D., Vanfleet, M. R., and Hall, H. T., J. Appl. Phys. **38**, 3172 (1966).
[7] Stark, W., and Jura, G., ASME paper 64-WA/PT-28 (1965).
[8] Giardini, A. A., and Samara, G. A., J. Phys. Chem. Solids **26**, 1523 (1965).
[9] Kennedy, G. C., and La Mori, P. N., J. Geophys. Res. **67**, 851 (1962).

DISCUSSION

R. Zeto (*U.S. Army Electronics Command, Fort Monmouth, New Jersey*): I would like to point out that likely you have a systemic pressure error in the isothermal III-V measurements due to the fact that, in changing pressures and temperatures, only about one minute was allowed to observe whether a transformation occurred from one phase to the other. For pressure calibration with sluggish transformations, kinetic time at constant pressure should be allowed for initiation of the transformation; otherwise the observed initiation pressure is erroneously high, depending on the pressure required to overcome the kinetic barrier to nucleation.

R. E. Hanneman (*General Electric Research and Development Center, Schenectady, New York*): The nucleation theory predicts that as the temperature rises the dead band or hysteresis region will become narrower, and the fact that the dead band is down to a small pressure interval at the temperature of the triple point indicates that in this particular case nucleation time does not have too important an effect.

R. Roy (*Pennsylvania State University, University Park, Pennsylvania*): Referring to the bismuth phase diagram, are you sure that the metastable projections between III and IV are, in fact, between the same phases? What is the evidence that the reverse transition is between the same phases as the transition in the forward direction? In looking into similar systems in detail we have found tremendous complexity. So I am asking a general question as to whether we should all make the assumption that when *A* goes to *B*, then *B* goes back to *A*, when in cases like germanium and sulfur we find there are many, many phases involved.

P. N. La Mori (*Battelle Memorial Institute, Columbus, Ohio*): I would like to raise a question concerning the pressure correction you made for lateral expansion or dilation of the piston under pressure. I have made some measurements at 40 kilobars in a similar type system using a 6 percent cobalt pressure vessel. Both by calculation from elastic constants as well as from measuring compressibilities of known materials, I found a correction of approximately 1.4 percent at 40 kilobars. In your work at 80 kilobars I believe the correction should be at least as large.

G. S. Kell (*National Research Council of Canada, Ottawa, Canada*): You put weight in your argument on the fact that your midpoint values with isothermal and isobaric changes were the same. Do you have a proof for this?

AUTHORS' CLOSURE

We agree with Dr. Zeto that our uncertainty in determining transition temperatures and pressures could have been further reduced by our spending more time on the measurements. However, in our isobaric measurements we determined the transition temperatures with both phases present, and we believe that this procedure allowed us to approximate the equilibrium temperatures with the precision quoted. In our experiments at constant temperature, the pressure was varied in increments of ½ kbar every ½ minute or ½ kbar every 2½ minutes. The variation of rate did not affect the values of transition pressures obtained, and the transition pressures determined in this way agreed with those determined in the isobaric experiments. The important point in this work is that the transition pressure at 25° for the III–V transition is shown to be near 77.5 kbar, rather than 89 kbar as previously accepted, and certainly not as low as 73 kbar.

In reply to Dr. Roy: The evidence we have that the metastable III-V boundary is observed just below the III-IV-V triple-point pressure is that on heating Bi III or cooling Bi V under these conditions we observed on occasion a single resistance change whose magnitude was equal to that of the III-V transition at pressures above the triple point, rather than two distinct resistance changes corresponding to the III-IV (or IV-III) and IV-V (or V-IV) transitions. The reason why the metastable projection of the III-V boundary may be observed at all is that while the III-V and V-III transitions occur rapidly with little hysteresis under these conditions while the III-IV and IV-III reactions are very sluggish with large hysteresis, and the V-IV reaction is slower than the V-III reaction and shows some hysteresis. Thus, it is possible to heat Bi III into the stability field of IV without IV forming, and as soon as the metastable projection of the III-V boundary is crossed, Bi V forms. Because of the sluggishness associated with the V-IV reaction, Bi IV does not form at once. Similarly, rapid cooling of Bi V will result in formation of Bi III just below the triple point pressure; Bi IV does not have time to form before the metastable projection of the III-V boundary is crossed.

In reply to Dr. La Mori: We feel that the discrepancy between his and our estimate of the dilation of the piston under pressure may be due to the fact that we used a grade of cemented tungsten carbide containing only 3 percent cobalt. We estimated the effective area of the piston by taking the diameter of the piston after the experiment, and making a correction for the elastic enlargement due to the axial load, and for the thickness of the indium layer between the pressure vessel wall and the piston. The magnitude of the correction to the diameter of the piston at 80 kbar was thus about +0.6 percent of the initial diameter. It is important to realize that the effective diameter may be calculated by consideration of the piston alone, since it is under radial constraint by the pressure vessel, and the two are thus separated only by the indium layer, whose thickness may be measured.

In reply to Dr. Kell: We made the assumption that the mechanical components of the total friction are symmetrical for compression and decompression. The fact that the mean of the compression and decompression values for the isothermal and isobaric determinations coincide would appear to indicate that the hysteresis for the transition itself is also symmetrical.

Optical Interferometry at High Pressures*

K. Vedam

Materials Research Laboratory, The Pennsylvania State University, University Park, Pennsylvania 16802

After a brief review of the present status of optical interferometry at high pressures, the experimental technique of measuring the variation of refractive index with pressure to 7 and 14 kbars with one- and two-stage optical pressure vessels respectively, is described along with some typical results obtained. The need for such measurements on liquids and gases which are used as fluid pressure media is emphasized.

1. Introduction

It is well known that optical interferometry is one of the standard techniques by which one can make precision measurements on the optical path length and its variation with parameters like temperature, pressure, etc. This article describes a brief review of the state of the art today in the field of optical interferometry at high pressures.

A glance at the literature reveals that the optical interferometric technique has been applied mainly in the study of pressure dependence of the refractive index of gases [1],[1] liquids [2, 3], and solids [4]. Since most gases and liquids solidify even at moderately low pressures of the order of 5 to 10 kbars, such measurements were perforce limited to this range. Even in the case of solids the upper limit of pressures that can be safely employed is rather limited, due to the inherent low strength of the optical windows in the pressure vessel. By using a two-stage pressure vessel with sapphire optical windows it is possible to increase the upper limit of pressure only to about 15 kbars—or at best to 20 kbars. Even so, one can carry out precise, reproducible measurements which often yield linear relationship between pressure and the change in refractive index. In view of the reasons mentioned above this article will deal mainly with the experimental procedure and results obtained with solids. However, with slight modification the same techniques and procedures are valid for liquids and gases as well.

2. Experimental Procedure

2.1. Single-Stage Optical Pressure Vessel

Until recently most of the experiments were conducted with a single-stage optical pressure vessel, which is described below in detail. In principle, the experimental method of measuring the variation of refractive index of solids with pressure involves the adaptation of Ramanchandran's [5] interferometric technique to an optical high-pressure vessel, and is somewhat similar to the techniques described by Cardona, Paul and Brooks [6] and Waxler and Weir [4]. A schematic drawing of the experimental arrangement is shown in figure 1. The experimental sample to be studied is suitably cut or cleaved, ground, and polished to be nearly optically parallel, so that one can easily observe localized interference fringes of the Newtonian type produced by interference of light reflected from the two surfaces of the crystal plate. The final dimensions of the specimens are usually about 0.8×0.8×0.3 cm. In the case of birefringent crystal the edges of the specimen are usually made parallel to the principal axes. In the case of cubic crystals as well as with isotropic solids, no such crystallographic orientation is necessary. The surfaces of the crystal were silvered by an aluminum evaporation process so as to increase the reflectivity and thus render the fringes sharp.

The optical pressure vessel is of conventional design with a single-crystal alumina window whose optically flat polished surface presses against a matched optically flat steel plug as shown in figure 1. Seals at other closures have been effected using Daniels' armored O-rings [7]. A combination of Buna-N Tetraseal and a flat ring of copper have also been found to be equally effective seals at these pressures. The *c*-axis of the alumina window is parallel to the direction of propagation of light. The pressure-generating system employed for these

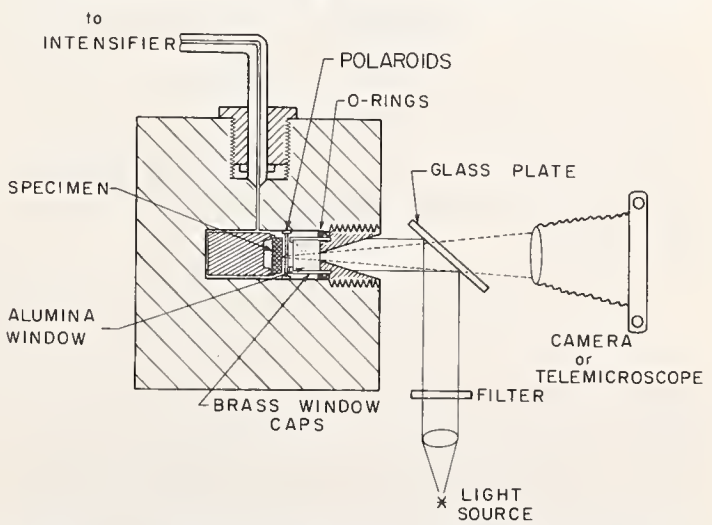

FIGURE 1. *Schematic diagram of the experimental arrangement, for measurement of the variation of refractive index of sclids with pressure.*

*Work supported by a grant from the National Science Foundation, Grant No. GK-1686-X.

[1] Figures in brackets indicate the literature references at the end of this paper.

Paper presented at the Symposium on Accurate Characterization of the High-Pressure Environment, held at the National Bureau of Standards, Gaithersburg, Md., October 14–18, 1968.

385-762 O - 71 - 4

measurements is a fairly conventional screw pump in conjunction with a Harwood intensifier. Sovasol, an optically transparent and colorless fluid marketed by Mobil Oil Company, was used as the fluid pressure medium. The pressure was read on a 16-in-diam 100,000 psi, Heise gage which itself was calibrated by a deadweight piston gage with an estimated accuracy of 3 parts in 100,000.

The specimen, supported suitably in the bomb, is illuminated with parallel light from a sodium lamp or a low-pressure mercury arc with appropriate filters. In the case of birefringent crystals, a sheet polarizer assembly is kept suitably oriented, between the alumina window and the specimen. This allows the measurements to be made with appropriately polarized light without any interference from the birefringence of the optical window. The localized interference fringes are observed in the telemicroscope for measurements in the visible region of the spectrum.

As the specimen is subjected to hydrostatic pressure both the thickness and the refractive index of the specimen change, with a consequent shift of the fringes across a fiducial mark on the specimen. The change in the refractive index Δn can be evaluated from the well known interference formula

$$\Delta n = \frac{p\lambda - 2n \cdot \Delta t}{2t_0} \tag{1}$$

where p is the number of fringes shifted, t_0 the initial thickness of the specimen, Δt the change in thickness of the specimen due to the applied pressure, and λ the wavelength of light employed. In actual practice the values of Δn and Δt at each pressure (corresponding to some known fringe shift) are evaluated from a programmed calculation on an IBM 360 and the value of n corrected by this Δn before it is used for the computation of $\Delta n'$ for the additional pressure producing the next fringe shift.

Since the pressure employed is fairly large, Δt the change in the thickness of the specimen, is evaluated with the help of the nonlinear theory of elasticity developed by Murnaghan [8], Birch [9], and others [10]. According to this theory, if the deformation produced by the applied stress τ_{ij} does not involve any rotation, as is the case in our present measurements that employ hydrostatic pressures only, then τ_{ij} can be expressed in terms of η_{ij} as (Barsch [11])

$$\tau_{ij} = C_{ijkl}\eta_{kl} + D_{ij,\,klmn}\eta_{kl}\eta_{mn}, \tag{2}$$

where

$$D_{ij,\,klmn} = 1/4\ (C_{inkl}\delta_{jm} + C_{jnkl}\delta_{im} + C_{imkl}\delta_{jn} + C_{jmkl}\delta_{in} + C_{ilmn}\delta_{jk} + C_{jlmn}\delta_{ik} + C_{ikmn}\delta_{jl} + C_{jkmn}\delta_{il} - 2C_{ijkl}\delta_{mn} - 2C_{ijmn}\delta_{kl} + 2C_{ijklmn}), \tag{3}$$

and C_{ijkl} are the second-order elastic constants, C_{ijklmn} are the Brugger's third-order elastic constants. In the case of cubic crystals and isotropic solids under hydrostatic pressure P, eq (2) reduces to

$$\tau = P = -(c_{11} + 2c_{12})\eta + \left(c_{11} + 2c_{12} - \frac{1}{2}c_{111} - 3c_{112} - c_{123}\right)\eta^2 \tag{4}$$

where η the Lagrangian strain is given by

$$\eta = \frac{1}{2}\,\frac{(t_0 - \Delta t)^2 - t_0^2}{t_0^2} \tag{5}$$

and the usual convention of replacing the index pairs 11, 22, . . . 12 by 1, 2 . . . 6 has been adopted for the suffixes of the elastic constants.

In the case of crystals of symmetry lower than cubic system, eq (2) reduces to second-degree equations in the principal strains and hence the strain components cannot be determined in a closed form. However, starting from the approximate values obtained by neglecting the higher order terms, we can easily compute the true values by an iterative procedure with the help of a computer. Thus, whenever data on third-order elastic constants are available the foregoing equations can be used to evaluate Δt and hence Δn.

The third-order elastic constants are available for only very few crystals. On the other hand, Bridgman [12] has made extensive measurements of the linear and volume compressibilities and their variation with pressure of a number of solids and fitted his data with quadratic equations of the type

$$\frac{L - L_0}{L_0}_1 = (\Delta L/L_0)_1 = -a_1P + b_1P^2 \tag{6}$$

and

$$\frac{V - V_0}{V_0} = (\Delta V/V_0) = -aP + bP^2. \tag{7}$$

Using his values of a and b, the change in the thickness of the sample and hence the value of Δn can again be evaluated.

Typical Results and Discussions

Figure 2 shows the results obtained on the variation of the refractive indices of CaF_2, BaF_2, and β-PbF_2 with pressure to 7 kbars for λ5893 Å. While some crystals like CaF_2 [16], MgO [17], α-Al_2O_3 [18], diamond [19], etc., exhibit a perfectly linear behavior in the pressure range investigated, some others like BaF_2 [16], the alkali halides [20], vitreous silica [21], α-quartz [22], etc., exhibit a nonlinear variation of the refractive index with respect to

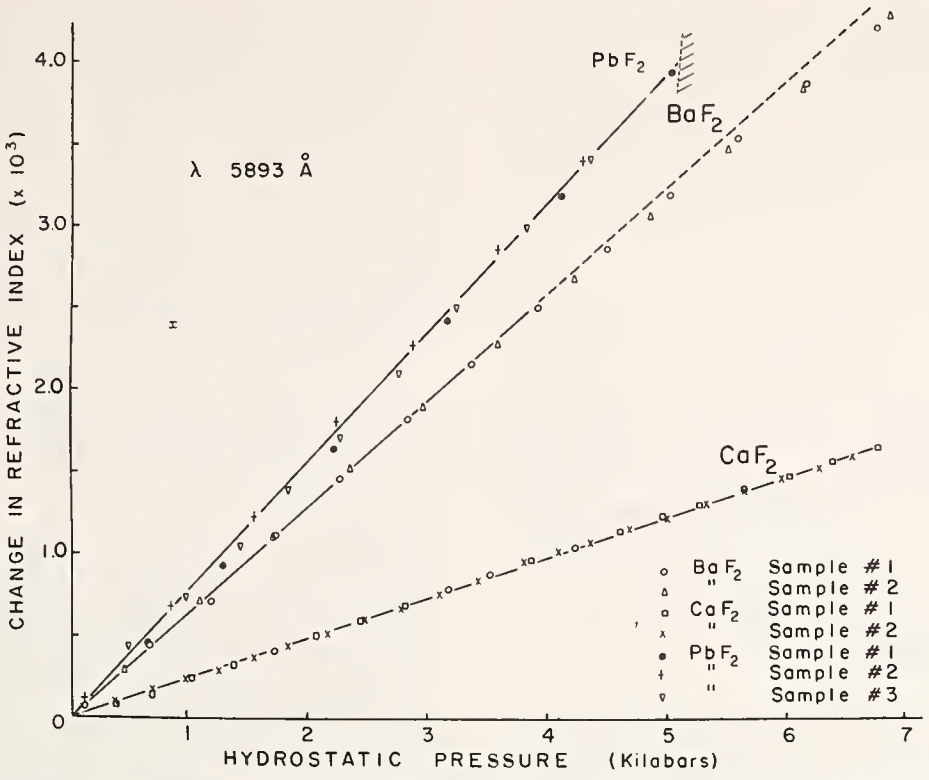

FIGURE 2. *Variation of the refractive indices of* CaF_2, BaF_2, *and* β-PbF_2 *with hydrostatic pressure* (T = 22 °C).

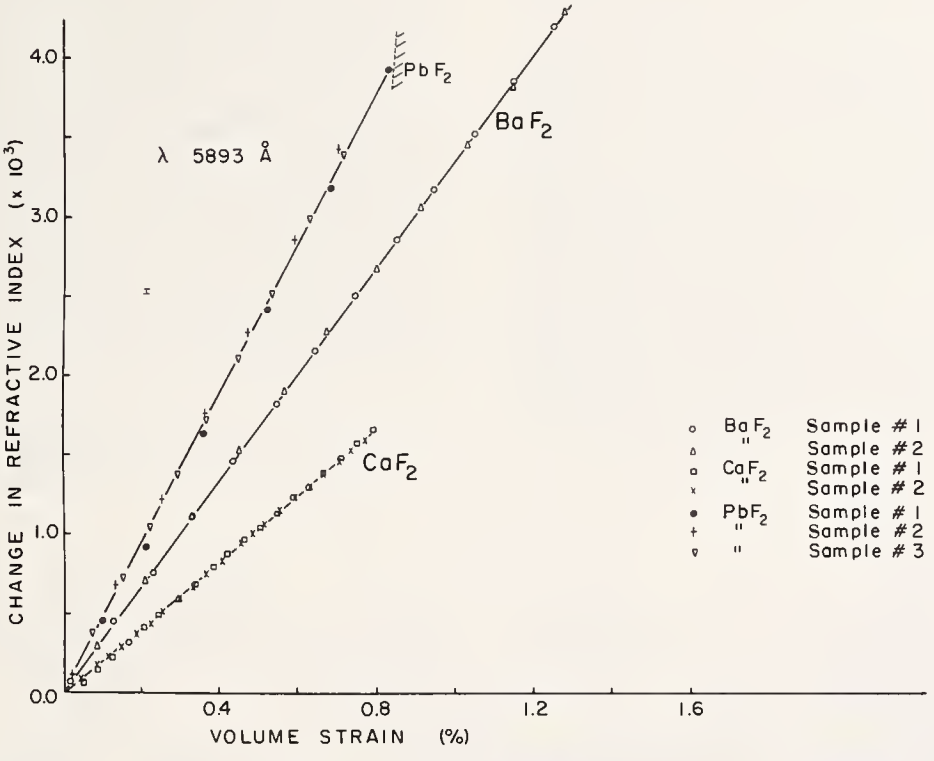

FIGURE 3. *Variation of the refractive indices of* CaF_2, BaF_2, *and* β-PbF_2 *with Lagrangian strain* (T = 22 °C).

pressure, particularly at high pressures. But the same results are found to show a perfectly linear dependence between Δn and the volume strain when the latter is computed, using the nonlinear theory of elasticity, as can be seen from figure 3 for the case of BaF_2. In the case of potassium iodide [20], even though the total volume strain is as high as 9 percent, the linear relation between Δn *and* $\Delta V/V_0$ is still found to be valid. A somewhat similar linear relationship between the isothermal volume strain and the melting temperature of various materials has been found by Kraut and Kennedy [23], even for strains as large as 60 percent in some cases. However, this does not mean that such a linear rela-

tion between the change in refractive index Δn and the Lagrangian strain will be valid universally. On the contrary, pronounced nonlinearity between Δn and the strain is observed even at fairly low strain levels in α and β-ZnS, CdS, etc., for λ5893 Å indicating the influence of the nearness of the absorption edge in these cases. This aspect has been dealt with elsewhere [24] and will not be described further here.

During the course of these studies, some crystals like β-PbF_2 [16], rubidium halides [25], etc., exhibited phase transitions at high pressures and by this interferometric technique it has been possible to measure the variation of the refractive index of these crystals with pressure up to the phase transition point, as in the case of the cubic form β-PbF_2 (fig. 2) which transforms irreversibly to the orthorhombic modification α-PbF_2 at 4.8 kbars at 23 °C.

2.2. Two-Stage Optical Pressure Vessel

A two-stage optical pressure vessel shown schematically in figure 4 has recently been constructed and put into operation for pressures up to 14 kbars. The principle of operation of this vessel is essentially similar to the single-stage vessel described earlier except for a few slight modifications. The two single-crystal alumina optical windows are positioned in such a way that at any time no one window experiences a pressure difference greater than 10 kbars. The telemicroscope used to observe the localized fringes in the single-stage vessel (fig. 1) has been replaced by a vidicon camera attached to a TV monitor. Such a procedure has two distinct advantages, namely (*i*) safety of the operating personnel and (*ii*) capability of carrying out these measurements over a wide spectral range from ultraviolet to the near infrared, just by changing the vidicon tube. Since sovasol, the fluid pressure medium used in the single-stage vessel, solidifies around 8 kbars, plexol 262, or *n*- or iso-pentane is used in the two-stage vessel. For studies in the ultraviolet, *n*- or iso-pentane are preferable over plexol 262 in view of their increased transparency at shorter wavelengths.

Figure 5 shows a typical result obtained on a Type I diamond with the two-stage vessel. Above 7 kbars the pressure was read with a manganin cell in conjunction with a Carey Foster's Bridge. It is seen from figure 5 a perfectly linear behavior between Δn and pressure and strain is observed in the case of diamond for λ5893 Å.

2.3. Optical Interferometry as an Interpolation Device in High-Pressure Techniques

From the above survey of the status of optical interferometry at high pressures, it is seen that all the work so far has been limited to pressure systems which employ gas or a liquid as the pressure medium and further only to the pressure range where pure hydrostatic pressures can be realized. This is understandable, for, under quasihydrostatic conditions normally attained at much higher pressures, the experimental sample (which itself acts as the interferometer), will be subjected to shearing stresses as well, in addition to the hydrostatic stress component. This invariably results in an irreversible plastic deformation of the specimen. If interferometric measurements are carried out under such circumstances it is doubtful whether any meaningful physical interpretation can be made from the results so obtained. In other words, optical interferometry can be used as an interpolation device for precision measurement of pressure only in the region where it is possible to develop pure hydrostatic pressures. One possible exception may be the use of materials like Diamond as the interferometric sample and fairly soft materials like AgCl or NaCl for the pressure medium, so that

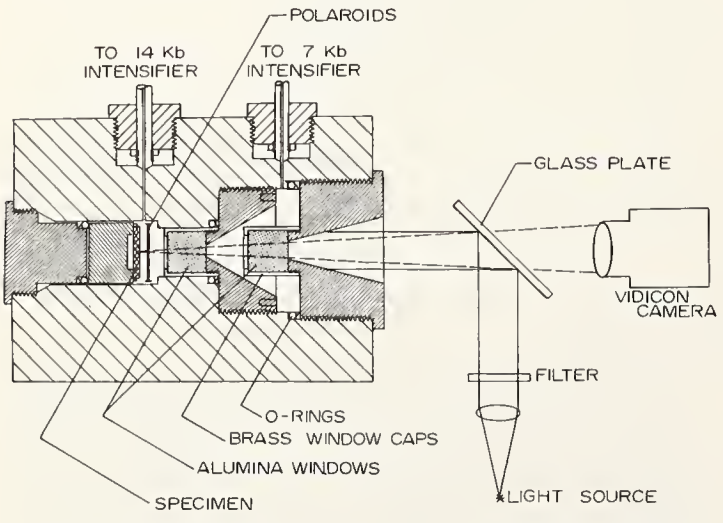

FIGURE 4. *Schematic diagram of the experimental arrangement with two-stage optical pressure vessel.*

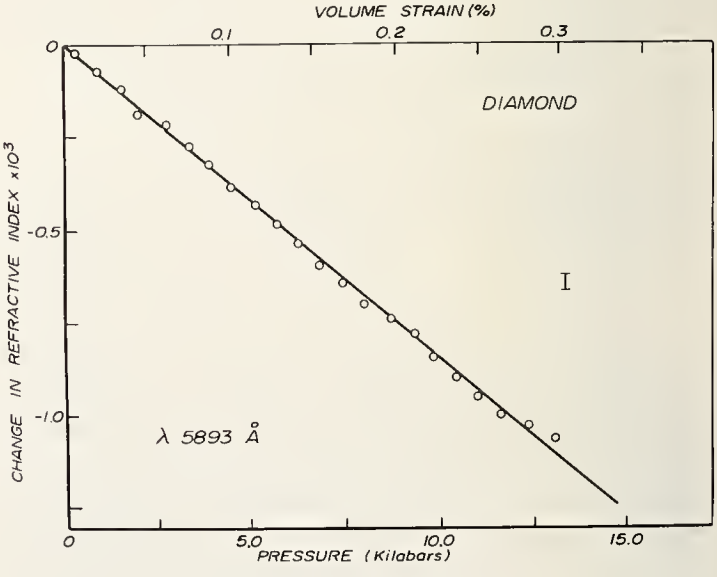

FIGURE 5. *Variation of the refractive index of Type I Diamond, with pressure* (T = 22 °C).

the permanent shear deformation under quasihydrostatic pressures can be minimized. Further, it would be advantageous to use suitable crystallographic orientation of the sample such that the stress-optic birefringence introduced by the shear stresses is either zero or negligible. In any case, further research work in this direction is necessary before any definite statements can be made.

Having thus limited our range to the region of pure hydrostatic pressures attainable in the laboratory it will be useful to consider the relative merits of gas, liquids, and solids on which the interferometric measurements can be made to obtain an accurate value of the pressure being used. As mentioned earlier, the use of solids for this purpose is not particularly advantageous, even though one can use a material with a perfectly linear relationship between pressure and the parameter measured. This is due to the fact that the elastic constants of the material and their variation with pressure must be known rather precisely. However, at any particular pressure, if one is interested in small deviations or fluctuations of the pressure the interferometer can be used with advantage, since then one is interested only in a slight shift of the fringes which can be measured with precision.

Here again the use of a liquid or gas would definitely be more advantageous. For then one can use Fabry-Perot etalons as the interferometers, with their easy capability of measuring fringe shifts of the order 0.01. Furthermore, since the compressibility of these materials is much greater than that of solids, the change in the refractive index for them is larger by 2 to 3 orders of magnitude. Thus, even though the elastic constants of the etalon-spacer material may not be known precisely, the error introduced on this account will be negligible.

However, experimental data on the variation of the refractive index of gases [1] and liquids [3] are at present limited to rather low pressures of only 1 to 3 kbars. Thus, this type of measurement, particularly on such gases and liquids which are currently used as fluid pressure media, appears to be a fruitful line of investigation.

3. Acknowledgments

The author would like to express his sincere thanks to Professor Rustum Roy for his kind interest and encouragement, to Professor G. R. Barsch for the many stimulating discussions, and to Messrs. E. D. D. Schmidt, T. A. Davis, and J. L. Kirk for carrying out some of the measurements reported.

4. References

[1] Michels, A., and Botzen, A., Physica **15,** 769 (1949) et seq.; de Groot, S. R., Rev. Opt. **28,** 627 (1949).
[2] Rosen, J. S., J. Opt. Soc. Am. **37,** 932 (1947).
[3] Waxler, R. M., and Weir, C. E., J. Res. NBS **67A,** 163 (1963); Waxler, R. M., Weir, C. E., and Schamp, H. W., Jr., ibid. **68A,** 489 (1964).
[4] Waxler, R. M., and Weir, C. E., ibid. **69A,** 325 (1965); Vedam, K., Schmidt, E. D. D., Myers, M. B., and Roy, R., ASME Publ. No. 66–WA/PT–3 (1966).
[5] Ramanchandran, G. N., Proc. Ind. Acad. Sci. **25A,** 208 (1947).
[6] Cardona, M., Paul, W., and Brooks, H., J. Phys. Chem. Solids **8,** 204 (1959).
[7] Daniels, W. B., Rev. Sci. Instr. **28,** 1058 (1957).
[8] Murnaghan, F. D., Finite Deformation of an Elastic Solid (John Wiley & Sons, Inc. New York, 1951).
[9] Birch, F., Phys. Rev. **71,** No. 11, 809 (1947).
[10] Hearmon, R. F. S., Acta Cryst. **6,** 331 (1953); Nran'yan, A. A., Sov. Phys. Solid State **6,** 936 (1964); Barsch, G. R., Report No. 5., Contract No. Nonr–656(27) (1963), unpublished.
[11] Barsch, G. R., ibid. Report No. 8 (1963), unpublished.
[12] Bridgman, P. W., The Physics of High Pressure (G. Bell and Sons, Ltd., London. 1958), p. 149.
[13] Anderson, O. L., J. Phys. Chem. Solids. **27,** 547 (1966).
[14] Murnaghan, F. D., Proc. Nat. Acad. Sci. **30,** 244 (1944).
[15] Thurston, R. N., J. Acous. Soc. Am. **41,** 1093 (1967).
[16] Schmidt, E. D. D., and Vedam, K., J. Phys. Chem. Solids **27,** 1563 (1966).
[17] Vedam, K., and Schmidt, E. D. D., Phys. Rev. **146,** 548 (1966).
[18] Davis, T. A., and Vedam, K., J. Appl. Phys. **38,** 4555 (1967).
[19] Schmidt, E. D. D., Kirk, J. L., and Vedam, K., Am. Min. **53,** 1404 (1968).
[20] Vedam, K., Schmidt, E. D. D., Kirk, J. L., and Schneider, W. C., Mat. Res. Bull. **4,** 573 (1969).
[21] Vedam, K., Schmidt, E. D. D., and Roy, R., J. Am. Ceram. Soc. **49,** 531 (1966).
[22] Vedam, K., and Davis, T. A., J. Opt. Soc. Am. **57,** 1140 (1967).
[23] Kraut, E. A., and Kennedy, G. C., Phys. Rev. **151,** 668 (1966).
[24] Davis, T. A., PhD. Thesis, Pennsylvania State University (1968).
[25] Vedam, K., and Schmidt, E. D. D., J. Mat. Sci. **1,** 310 (1966).

DISCUSSION

P. M. Bell (*Geophysical Laboratory, Carnegie Institution of Washington, Washington, D.C.*): Have you made measurements on the change in index of refraction of glass as a function of pressure?

O. E. Jones (*Sandia Laboratory Albuquerque, New Mexico*): I believe there has been some work on change of index of refraction of glass under shock loading, particularly by the Stanford Research Institute people. Ahrens [J. Appl. Phys. **37,** 4758 (1966)] did this on liquids. Then last year at the Paris meeting on high dynamic pressures I think there were some results reported on alpha quartz. How do your results correlate with these made, in general, at quite a bit higher pressure levels?

J. L. Cross (*National Bureau of Standards, Washington, D.C.*): In referring to the accuracy of the pressure measurements, you mentioned the use of a 100,000 psi Heise gage calibrated by a deadweight piston gage with an estimated accuracy of 3 parts in 100,000. I know of no piston gage capable of this accuracy in this pressure range and, in any event, I think that the dial gage could not be used with this accuracy.

B. Vodar (*Laboratoire des Hautes Pressions, Centre National de la Recherche Scientifique, Bellevue, France*): The method of measuring pressure by change in refractive index is presently being done by Coulon at the University of Marseilles, at pressures up to about one kilobar or possibly higher.

Voice from the floor: Presumably there is a relationship between refractive index and volume change that comes about because the index of refraction is related to the polarizability of the system and the density. Thus, in selecting materials for pressure calibration purposes, you would want to pick materials in which the dimensions of the atoms, which are being polarized, are small compared to the interatomic separation between atoms. Presumably, the deviation for cadmium sulphide occurred because the spacing between atoms was of the same order of magnitude as the atomic diameters.

AUTHOR'S CLOSURE

Yes, we have carried out measurements on vitreous silica. In this case the refractive index increases linearly with pressure up to about 4 kbars, thereafter it increases nonlinearly. It is interesting to note that at high pressures the points fall above the extrapolated straight line. This is unlike the crystalline materials where the points fall below the line. This unique feature of glasses arises from the *increase* in compressibility with pressure as the voids are closed. We have made measurements on vitreous silica only to 7 kbars. At higher pressures, perhaps 30 or 40 kbars, when all the voids are closed the refractive index will increase at a slower rate with pressure.

I have not compared my results with those observed from shock loading experiments referred to by Dr. Jones. Under shock loading conditions in solids significant shear stresses are present, making the conditions unlike those in my work. Further, the shock experiments yield values under adiabatic conditions whereas the hydrostatic measurements yield the isothermal values. The difference between these two can be significant, particularly in the case of liquids.

In the choice of materials for pressure measurement by refractive index change, the departure from linearity of many substances is an important problem. In many substances the refractive index decreases with pressure due to the fact the polarizability of the ions or the atom is itself a function of interatomic distances. In the case of gases, where the atoms are widely separated, you would expect the linearity to hold good. Unfortunately it does not.

Equipment for Generating Pressures up to 800 Kilobars

Naoto Kawai

Department of Material Physics, Faculty of Engineering Science, Osaka University, Toyonaka, Osaka, Japan

A type of high-pressure apparatus has been developed which extends considerably the range of attainable very high static pressure. It consists basically of a sphere segmented into tapering truncated pistons. Hydrostatic pressures in the sample chamber in the centre of the sphere have reached 800,000 bars (11,600,000 psi). Pressures of over one million bars should be possible with the present technology. Some new and interesting results from high-pressure studies are described.

1. Apparatus and Method

The apparatus consists basically of a metal solid of revolution segmented into a number of tapering sections. The preferred and usual form is a sphere, but a solid cylinder has also been used [1, 2].[1] The general array of pistons is illustrated in figure 1. The actual model for an eight-piston sphere is shown in figure 2(a). The regions where four pistons meet are flattened and covered by corner caps. The sections act as multipistions, directing an external stress towards the center. The innermost apex of each piston is truncated to form a polyhedral sample chamber. The assembly of pistons acts as a pressure intensifier, with the stress on an enclosed sample being a function of the ratio of its surface area and the outer area of the multipiston sphere.

An inter-piston separation, initially several millimeters, is necessary to allow inward motion of the pistons. The pistons are separated by a distribution of compressible spacers, usually pyrophyllite. A sample holder is machined to surround the sample, and fit in the central chamber (see fig. 1). It converts the stress directed by the pistons to an approximately hydrostatic pressure. Pyrophyllite, essentially $Al_2O_3 \cdot 4SiO_2 \cdot H_2O$, is favoured for such application because of its good compressibility but high coefficient of friction and shear strength. Such a sample holder preserves its shape and can hold the sample firmly to a temperature of over 2500 °C.

The metal sphere is sealed in two thick hemispherical rubber shells (see fig. 3). The appropriate wire leads, for measurement of temperature, electrical resistance, etc., are circuited out, and the sphere is rested on a support cylinder. The whole assembly is then placed in a high-pressure oil reservoir. In the experimental setup used, a confining oil pressure of 4 kilobars may be produced in the reservoir chamber, using a uniaxial hydraulic press (Mitsubishi Atomic Power Industries, rated at 2,000 tons). With this external pressure acting on the jacketed sphere, the multipistons move inward and exert a stress on the material in the central sample chamber.

[1] Figures in brackets indicate the literature references at the end of this paper.

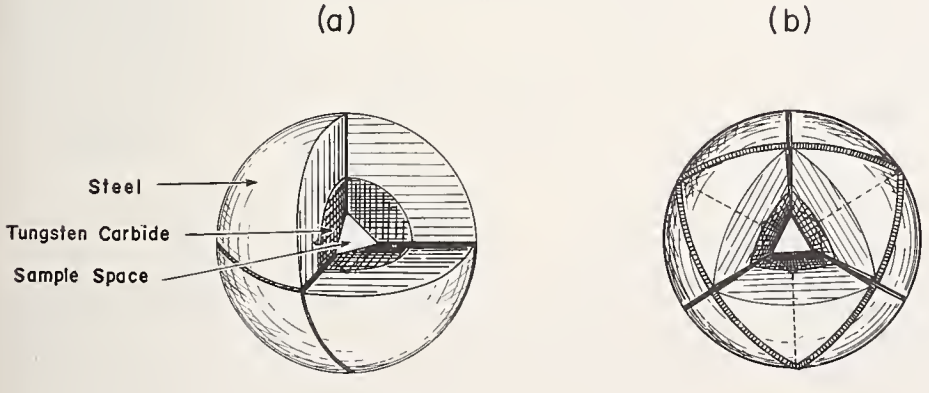

FIGURE 1.

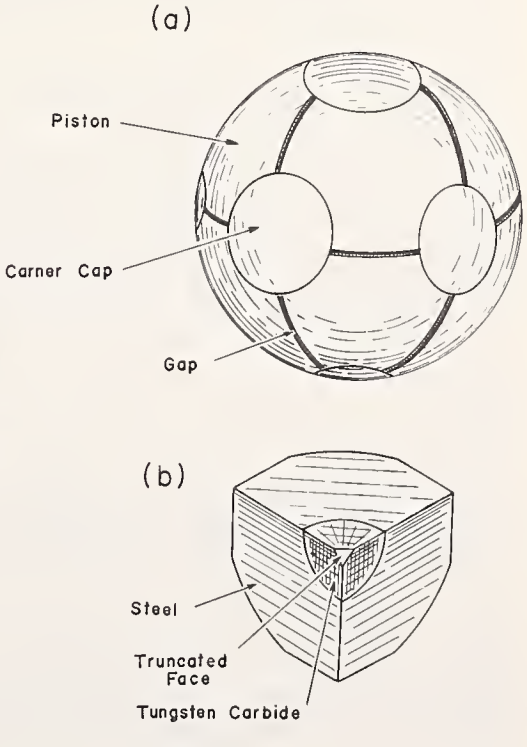

FIGURE 2.

Paper presented at the Symposium on Accurate Characterization of the High-Pressure Environment, held at the National Bureau of Standards, Gaithersburg, Md., October 14–18, 1968.

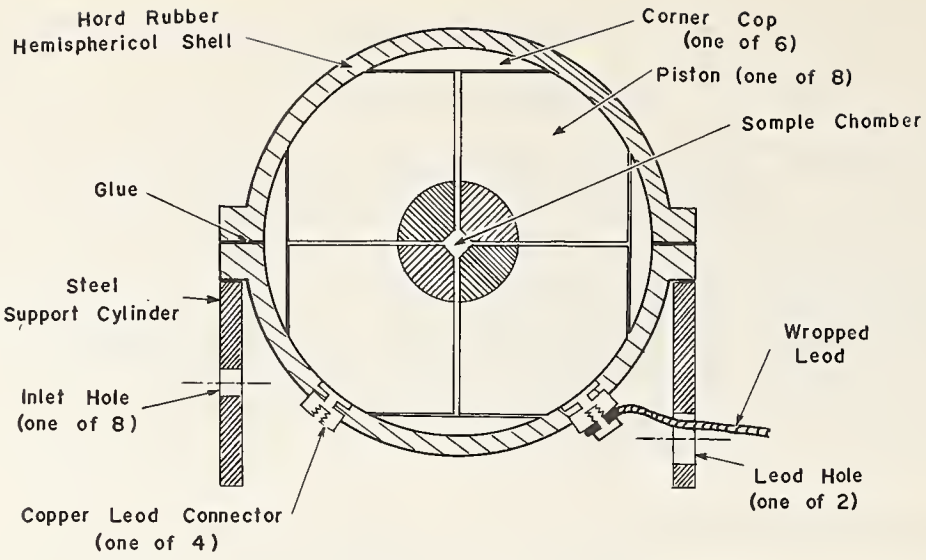

FIGURE 3.

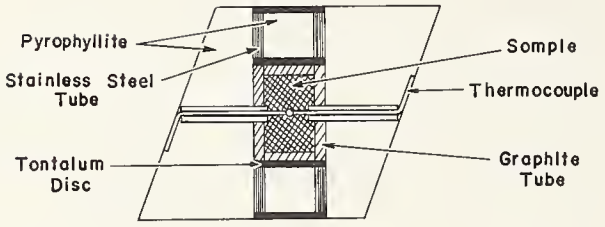

FIGURE 4.

With increasing stress, the material in the gasket structure between the pistons, and some of that enclosing the sample, is extruded outward between the pistons. As the pistons move closer together as well as inwards, this filler becomes thinner. It thus inhibits further outflow of the material from the sample space, and supports the inner portion of the pistons laterally.

The large radial pressure gradient means that only the inner region of the pistons need be made of the hardest, most expensive material. The flow of the gasketing material acts to confine the pistons laterally where the stress is most concentrated. This discourages their destruction by compressive failure and shear, and lateral ductile flow. No appreciable plastic deformation has occurred on the truncated piston inner faces, whereas this is frequently the case at a pressure of a few hundred kilobars for apparatus with only two opposed pistons.

The sample space may be equipped with instrumentation to monitor experimental proceedings. Figure 4 shows a sample prepared for thermal treatment. It is confined in an octahedral pyrophyllite block. A graphite heater and thermocouple are enclosed. The electric leads are taken out between pistons, through a seal in the rubber shell, and through the wall of the oil reservoir. A pressure-calibrating unit may similarly be imbedded in the sample space. In conjunction with application of pressure, the temperature of a sample may be elevated to about 2,000 °C.

2. Calibration and Capability

There are many known indicators for calibrating pressure. There are phase changes as evidenced by an abrupt decrease in volume, sudden changes in electrical resistance, and second-order transitions such as resistance maxima. Some calibration points are listed in table 1. One aspect of using resistance measurements for calibration is that there are two

TABLE 1. *Some transitions for calibration of pressure, based on changes in volume* (ΔV) *and electrical resistance* (ΔR) *at 25 °C.*

Conditions	Substance	Transition pressure
		(*kilobars*)
Abrupt ΔV	KBr	18.0
	KCl	20.2
	AgCl	88
Abrupt ΔV and ΔR	Bi	25.3, 26.8, 89
	Tl	37
	Ba	59
Abrupt ΔR	Fe	133
	Ba	144
	Rb	193
	GaAs	250
Resistance maximum	Cs	42
	Ca	375
	Rb	425
	CdS	465

causes of a change in resistance. There is the effect of pressure on the specific resistance, and the change due to possible alteration of the specimen shape in the sample chamber.

In experiments here, a good reproducibility has been obtained for calibration. The calibration is dependent on the particular apparatus used, because of different relative sizes of sample chambers, and on the arrangement of inter-piston spacers. The values of extreme pressure are deduced by extrapolation, since there is a lack of known reference points at the very high experimental pressures obtainable. The calibration is sufficiently uniform to make this procedure of extrapolation acceptable. The calibration of pressures above about 500 kilobars, however, is presently not well known. More known pressure-dependent changes at very high pressure are needed. These could be discontinuous changes such as volume or resistance changes, or continuous changes such as in resistivity or solubility of one component in another.

The maximum pressure attainable depends on the radius of the sphere and the amount of truncation at the centre. The smaller the central sample spacer, the higher the possible pressure. It also apparently depends on the number of pistons in the assemblage. It may be noted that the eight pistons of the spheres described here are more than in any of the other types of apparatus mentioned earlier. However, in a sphere the more numerous the pistons are, the smaller their apex angle becomes. This gives less support to the highly stressed piston apex regions, and allows failure at a lower stress. This problem is counteracted by the pressure of some gasketing material on the inner flanks, but optimum results are not obtained by continuing to increase the number of pistons.

The first sphere, constructed about three years ago, had a diameter of 8 cm. The maximum pressure obtained with it was about 200 kilobars. The highest operating pressure used since then has been 800 kilobars, in the large-diameter, small-sample-chamber sphere. This does not necessarily represent the maximum pressure feasible with these particular pieces of apparatus.

The extension of the range of pressure in the future will most likely require pressure intensification by multi-stage apparatus. Now being constructed is a design of multi-stage piston assemblages, with a central octahedral sample space. This cascaded device is expected to allow a central hydrostatic pressure in excess of 1 megabar (about 14,500,000 psi).

3. Conclusion

The apparatus described extends considerably the range of possible very high static pressures. The apparatus has significant advantages over other existing devices. It opens the way for further research into the nature and properties of substances under great pressures. For example, the deep interiors of the earth and other planetary bodies are pressure regimes. It is estimated that conditions in the earth vary from a pressure of 10 kilobars and temperature of 500 °C at a depth of 20 miles beneath the surface to a pressure of 1,700 kilobars and temperature of about 3,000–4,000 °C at a depth of 1,800 miles. The latter is at the earth's solid mantle–liquid core boundary. The presently available pressure of 800 kilobars corresponds to a depth of about 1,200 miles.

The new technology described here provides a means for probing further into the realm of superpressure science. It should allow investigation of material, properties, and phenomena as yet unknown.

4. Acknowledgment

Many thanks are due to the members of the working group who have been particularly involved in development of the high-pressure apparatus and research—Messrs. K. Hirooka, E. Itoh, and S. Endoh.

5. References

[1] von Platen, Baltzar, A multiple piston, high pressure, high temperature apparatus, Modern Very High Pressure Techniques, pp. 118–136, R. H. Wentorf, Editor (Butterworths, 1962).

[2] Kawai, Naoto, A static high pressure apparatus with tapering multi-pistons forming a sphere. I, Proc. Japan Acad. **42**, 385–388 (1966).

DISCUSSION

F. P. Bundy (*General Electric Research and Development Center, Schenectady, New York*): After the sample chamber has been pressurized to, say, 400 or 500 kilobars, and then unloaded, do the pistons remain as integral pieces or do they fracture?

In estimating pressures in the 200 to 400 kilobar region, I would suggest that you try the iron cobalt alloys. I have more faith in the linearity of these materials than in the linearity of cadmium sulfide.

P. N. LaMori (*Battelle Memorial Institute, Columbus, Ohio*): What are the dimensions of your apparatus?

F. R. Boyd, Jr. (*Geophysical Laboratory, Carnegie Institution of Washington, Washington, D.C.*): Would you tell us the grade of carbide that you used, and whether any failures of the carbide have occurred?

J. D. Barnett (*Brigham Young University, Provo, Utah*): I note your use of the cadmium sulfide transition for calibration of your apparatus in the 400 kilobar range. The reliability of a transition reported by Drickamer in CdS is questionable. I have done considerable work on calibration in a tetrahedral apparatus up to about 100 kilobars, and have found the relationship between true pressure and load to be very nonlinear, the curve becoming almost flat at the higher loads. We used samples of about the size you used—around 4 mm on an edge—and our equipment was capable of applying a load of 600 tons force to each ram. The pressure was monitored continuously by an x-ray beam on sodium chloride. We find that in apparatus of this type most of the ram force is taken by the gaskets, with the pressure reached in the sample being correspondingly limited.

G. Jura (*University of California, Berkeley, California*): Concerning your high calibration point, there has been a reported bismuth transition at 415 to 425 kilobars. Did you look for that one?

AUTHOR'S CLOSURE

In reply to Dr. Bundy: When the pressure is relieved the pistons remain together, but they are easily separated by hand.

In reply to Dr. La Mori: In our present apparatus the outside diameter of the sphere is 250 mm, and the diameter of the central sample chamber is 2 mm. The area ratio is thus 15,000.

In reply to Dr. Boyd: The tungsten carbide used for the piston contains 3 percent cobalt. We have not experienced breakage, and we believe that this is due to the lateral pressure of the gaskets exerted on the pistons. This is unlike the situation with two flat pistons (Bridgman anvils) in which relatively large deformations take place at 200 or 300 kilobars. Our gaskets are initially about 2 mm in thickness, and after pressure has been applied are found to be 0.1 to 0.2 mm in thickness.

Concerning Dr. Barnett's comment: His apparatus had only four pistons while ours had eight, which I believe would reduce the load taken by the gaskets. We hope to adapt the apparatus to use x-rays, and to use sodium chloride as a reference material.

In reply to Dr. Jura: We could not find a bismuth transition in the 400 kilobar region.

Manganin Resistance Gages as Accurate Instruments for High-Pressure Measurements

Yu. A. Atanov and E. M. Ivanova

All-Union Research Institute for Physical and Radiotechnical Measurements, Moscow Region, Mendeleevo, U.S.S.R.

The rapid development of modern science and technology foretells the wide application of high hydrostatic pressures from 20 to 40 kbar in the near future. The measurement of pressures in this range is usually carried out by manganin resistance gages. Many authors, however, report different metrological characteristics of individual manganin gages and present widely differing values of pressure coefficient, reproducibility, stability, nonlinearity, etc. There is no common basis for the selection of interpolation and extrapolation equations relating the change of resistance of a manganin gage with the measured pressure.

In this work an attempt is made to investigate the scatter of metrological characteristics of a large group of identical manganin gages by means of an absolute free piston gage, to find the best extrapolation equation and to evaluate possible errors of pressure measurements over 15 kbar.

1. Manganin gage

The spiral-wound manganin coil is mounted in the groove of a ceramic holder which is fixed to the closure plug. Overall dimensions of the completed coil are 9.5 mm o.d. and 7 mm height. The diameter of the wire is 0.08 mm. The nominal coil resistance is 40 Ω. Pieces of 0.12-mm copper wire are welded to the ends of the manganin coil. Soldered copper joints improve the stability of the gage.

Seventy-two gages were manufactured. The same batch of manganin wire was used. The completed gages were seasoned at temperature + 140 °C for at least 80 hr with periodic dipping into the liquid nitrogen bath (− 196 °C). Usually the high-voltage pulse technique [1] [1] is used for seasoning of manganin gages in our laboratory. In this method, however, it is difficult to control precisely the temperature of seasoning, which influences the value of the pressure coefficient. In view of the fact that we tried to minimize the scatter of gage characteristics, it was decided to use the low-temperature seasoning. After seasoning the average decrease of the gage resistance was equal to 0.28 percent of the initial value. Any additional seasoning did not change appreciably the gage resistance. This is of course the evidence of satisfactory seasoning.

2. Calibration of the Manganin Gages Against the Free Piston Gage

Twenty-four gages were taken from the group for calibration against the 15-kbar free piston gage having the precision of 1 part in 1,000. Four gages were being placed in the pressure vessel at the same time. The temperature was maintained at 25 ± 0.1 °C. The measurements were taken every 1 kbar. To reduce the errors associated with the setting of the temperature equilibrium in the pressure vessel the readings were registered 3 to 4 min after every application of pressure. Every gage was calibrated three or four times.

3. Pressure Coefficient of Resistance

The pressure coefficient of resistance $k=\frac{1}{R_0}\frac{\Delta R}{P}$ is one of the fundamental characteristics of manganin gages. (Here R_0 is the resistance of a manganin gage at atmospheric pressure, ΔR the increment of resistance at pressure P.) The pressure coefficients of all gages decrease with pressure over 4 kbar (fig. 1). Below 4 kbar the behavior of pressure coefficients is irregular. In most cases the values of pressure coefficients increase with pressure in this range, so there is the maximum in k-versus-p curve. Since k values decrease practically linearly with pressure, the calibration data were analyzed on the basis of the second-order expression $P=\alpha\Delta R+\beta(\Delta R)^2$, where α and β are constants

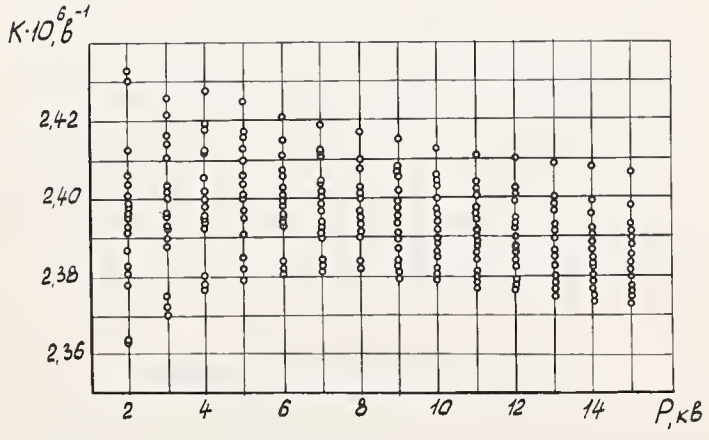

FIGURE 1.

[1] Figures in brackets indicate the literature references at the end of this paper.

Paper presented at the Symposium on Accurate Characterization of the High-Pressure Environment, held at the National Bureau of Standards, Gaithersburg, Md., October 14–18, 1968.

found by the least squares method. The expression fits the calibration data with an accuracy better than 0.1 percent. The pressure coefficient can be written then

$$k=\frac{1}{R_0}\frac{1}{(\alpha+\beta\Delta R)}\simeq\frac{1}{\alpha R_0}\left(1-\frac{\beta\Delta R}{\alpha}\right)=k_0(1-\gamma\Delta R) \tag{1}$$

where $k_0=\frac{1}{\alpha R_0}$ is the pressure coefficient of the gage at $P\to 0$, and $\gamma=\frac{\beta}{\alpha}$ the slope of the k-versus-ΔR plot. The scatter of metrological characteristics can be judged by the scatter of k_0 and γ values. For the gages calibrated the average pressure coefficient $\bar{k}_0=2.41\cdot10^{-6}$ bar^{-1}, the standard deviation σ_{k0} being $0.013\cdot10^{-6}$ bar^{-1}. At higher pressures the scatter of k values diminishes. This is the consequence of a correlation existing between k_0 and γ values of individual gages. The corresponding values for γ were:

$$\bar{\gamma}=0.00698, \qquad \sigma_\gamma=0.00201.$$

The measured pressure can be expressed through the pressure coefficient obtained in eq (1)

$$P=\frac{\Delta R}{R_0}\frac{1}{k}=\frac{\Delta R}{R_0}\frac{1}{k_0(1-\gamma\Delta R)}. \tag{2}$$

The substitution of k_0 and $\bar{\gamma}$ into eq (2) gives the approximate interpolation equation for any gage out of the group investigated:

$$P=\frac{\Delta R}{R_0}\frac{1}{2.41\cdot10^{-6}(1-0.00698\Delta R)}.$$

The experimental pressures were compared with pressures calculated from the approximate equation for 4, 12, and 15 kbar. The mean difference is 19.6 bars (or 0.49 percent) for 4 kbar. The corresponding values for 12 and 15 kbars are 40.2 bars (0.33 percent and 45.8 bars (0.31 percent).

The pressure seasoning of the gages was carried out in apparatus of the piston-cylinder type, permitting generation of hydrostatic pressures up to 30 kbar in the 30 cm^3 cell. k versus P plot is presented on figure 2. The average pressure coefficient $\bar{k}_0$ showed no change after pressure seasoning and the standard deviation σ_{k_0} decreased to $0.007\cdot10^{-6}$ bar^{-1}. The new averaged equation for the group of pressure-seasoned gages is

$$P=\frac{\Delta R}{R_0}\frac{1}{2.41\cdot10^{-6}(1-0.00678\Delta R)}. \tag{3}$$

The maximum difference between the experimental pressures and calculated from eq (3) is less than 0.5 percent at pressures from 4 to 15 kbar. In other words, eq (3) can be used for measurements of pressures with an accuracy 0.5 percent with any manganin gage of the group in the range from 4 to 15 kbar.

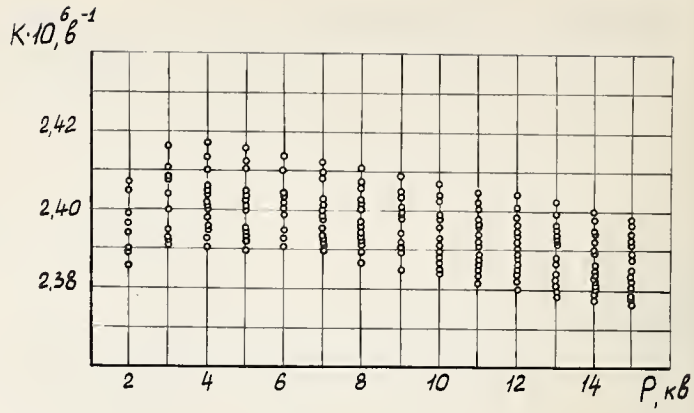

FIGURE 2.

4. Intercomparison of Manganin Gages

The intercomparison of manganin gages over 15 kbar was accomplished in the same 30 kbar hydrostatic apparatus. The measurements were carried out at the room temperature without any temperature control. The readings of four to six gages were registered at certain pressure in the cell. In all, 23 gages were intercompared. As a rule, after the release of pressure the R_0 values were higher than initial ones but in a few hours they recovered completely.

The treatment of data was as follows. The general equation (3) was used to get the pressure values from the readings of individual gages. The scatter of pressure values thus obtained was then calculated for every pressure at which the intercomparison was carried out. The maximum deviation from the mean value is less than 0.49 percent in the range from 15 to 28 kbar. If the individual equations are used for each gage which were found from the results of calibrations against the free piston gage, the corresponding maximum deviation will be 0.12 percent.

5. Conclusions

The results obtained show that the scatter of pressure coefficients of resistance does not increase with pressure in the range from 15 to 28 kbar. The manganin gages exhibit very good stability and reproducibility in this range. It goes without saying that the intercomparison of identical resistance gages does not permit determination of the total error of pressure measurements over 15 kbar. The 0.12 percent deviation cited above can be associated with the random error of measurements. Neverthe-

less the analysis of the pressure dependence of the pressure coefficient $k=f(P)$ in the range from 4 to 15 kbar makes it possible to claim rather low systematic error of pressure measurements over 30 kbar by means of extrapolation equations of the type (3). For most practical needs, one can successfully use such extrapolation equations with the constants determined from the calibration data. Undoubtedly, for high-precision experiments one needs to correct the constants of the extrapolation equation on the basis of the mercury melting pressure scale. At the moment such a comparison is being prepared in our laboratory. We expect that manganin gages calibrated against the mercury melting pressure scale will have the total error less than 1.5 percent in all the range of hydrostatic pressures to 40 kbar.

Reference

[1] Alexeyev, K. A., Atanov, Y. A., and Burova, L. L., The Proceedings of the Institutes of the Committee on Standards, **75** (135), 44 (1964).

DISCUSSION

J. L. Cross (*National Bureau of Standards, Washington, D.C.*): On the matter of the departure from linearity of the pressure vs. resistance characteristic of manganin, we have observed a second-order effect of opposite sign from that reported by Adams and Goranson.[1] I believe that this is probably due to our use of a strain-free coil configuration. The elimination of residual strains in the wire may have a large effect on the linearity observed, particularly at lower pressures. This may mean that taking our zero at atmospheric pressure may not be the most desirable way to use manganin gages. It may be desirable, when possible and when the accuracy required warrants it, to base the calibration upon points taken at elevated pressures only.

A matter that hasn't received much attention is the fact that the temperature coefficient of resistivity of manganin is a function of pressure, so that the temperature of the resistivity peak of manganin increases as the pressure goes up, and in order to do the best work with manganin, it may be necessary to include the temperature and the resistivity dependency on temperature in the calculations.

J. D. Barnett (*Brigham Young University, Provo, Utah*): I notice that you season the manganin coils by the Bridgman technique of cycling between annealing temperature and liquid nitrogen. Is this your standard procedure, or have you used other seasoning techniques?

AUTHORS' CLOSURE

From the results of our measurements we felt that behavior of the manganin coils below four kilobars was not representative of the behavior at higher pressures. Accordingly, when the data below four kilobars was not used all the curves of pressure coefficient of resistivity vs pressure had slopes of the same sign.

On the matter of temperature effects on the pressure coefficient of resistivity, we believe there are too many other sources of error to justify strict temperature control. If you work in the range from say 20 to 40 degrees Celsius, you are on the flat portion of the temperature dependence of resistivity, and the error due to the instability of temperature is very low as compared with the other sources of instability. Of course, the flat portion of the curve moves with the pressure, but we do not take this into account.

In reply to Dr. Barnett: The objective of this investigation was to obtain a large group of manganin gages with very similar characteristics. We tried to obtain a very homogeneous group of manganin gages. That is why we used the Bridgman cycle. But usually when we do the work in our lab with standard 100-Ω resistance gages, we use the very fast technique of temperature seasoning. It is a sort of standardized procedure in our laboratory. It takes just a few milliseconds for the pulse from a capacitor bank to flow through the gage. The temperature is raised for a very small time up to 500 °C. After that, the residual stresses are eliminated and stability of zero resistance is very good. We also tried to stabilize our manganin gages subjecting them simultaneously to very high pressures and high temperatures, but results were not satisfactory.

[1] L. H. Adams, R. W. Goranson, and R. E. Gibson, Construction and Properties of the Manganin Resistance Pressure Gauge, Rev. Sci. Instr. **8**, No. 7, 230–235 (July 1937).

Chairman: F. P. BUNDY
General Electric Company
Schenectady, New York

A Critical Review of the Effect of Pressure on Thermocouple emf's

R. E. Hanneman, H. M. Strong, and F. P. Bundy

General Electric Research and Development Center, P. O. Box 8, Schenectady, New York 12301

The effects of high pressure on the emf's of thermocouples are critically reviewed and best currently available thermocouple corrections are presented. The important factors affecting these thermocouple corrections are discussed, including pressure-temperature gradients, contamination, and deformation. A novel method for simultaneous and continuous *in situ* measurement of pressure and temperature within a high-pressure cell through use of dual thermocouples is briefly described.

1. Introduction

As high-pressure research has progressed in the past few years to include more quantitative experiments, the need for more accurate measurement of temperature and pressure has become more critical. Temperature is a particularly sensitive variable because of its importance in numerous thermally activated processes prevalent in materials. Since thermocouples provide the primary means for *in situ* temperature measurement in most high-pressure experiments carried out at elevated temperatures, the effect of pressure on the electromotive force (emf) of thermocouples is often very important.

The central purpose of this paper is to review critically our current knowledge of the effects of pressure on the emf of thermoelectric materials and to discuss the consequences of these effects on the accurate *in situ* measurement of temperature at high pressure. In addition, the concept of using thermocouples to monitor continuously any local, *in situ* pressure changes will be described.

2. Determination of Pressure Effects on Thermoelectricity

The current theoretical understanding of thermoelectricity and the electronic properties of metals and alloys is inadequate to permit any reliable quantitative calculations of the effect of pressure on thermal emf's. Thus, we must rely upon experimental determinations of the effect of pressure on thermoelectric behavior.

2.1. Moderate Temperature-Hydrostatic Pressure Range

The pressure effects on thermal emf's of metals and alloys have been measured in hydrostatic systems by either single wire or composite thermocouple methods. Bridgman [1][1] carried out the first measurements of the effect of pressure on thermal emf's of various materials using the single wire method illustrated in figure 1a. Bridgman's results were accurate to within a few percent for the conditions studied (0 to 12 kbar and $T_2 - T_1 = 100\,°C$). His work included some 20 metals and alloys but his measurements did not include most of the thermocouple materials commonly used.

Bell, England, and Boyd [2] have recently extended the single wire hydrostatic method to meas-

[1] Figures in brackets indicate the literature references at the end of this paper.

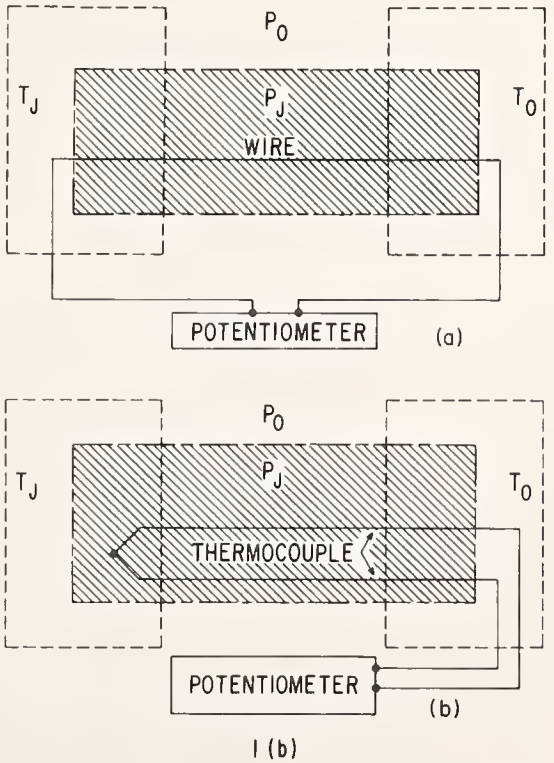

I (b)

FIGURE 1. *(a) Schematic diagram of Bridgman single-wire method for determination of pressure dependence of thermal emf. (b) Composite thermocouple method for measuring pressure effects on thermocouples.*

Paper presented at the Symposium on Accurate Characterization of the High-Pressure Environment, held at the National Bureau of Standards, Gaithersburg, Md., October 14–18, 1968.

ure accurate corrections on Pt–Pt 10 percent Rh and chromel-alumel thermocouples up to ~10 kbars and ~500 °C. The magnitude of the corrections obtained is in reasonably good agreement with experimental data from non-hydrostatic experiments to be discussed later in this section. Since a detailed paper by Bell et al. [2] on these results is included in this symposium, no further discussion of their results needs to be included here.

The related composite thermocouple method for measuring the pressure effects on thermocouples in a hydrostatic system is shown schematically in figure 1(b). This method was first attempted by Birch in 1939 over the limited pressure interval 0 to 4 kbars and for temperatures up to ~470 °C [3]. Unfortunately, Birch failed to take into account that only that part of the temperature gradient lying within the pressurized zone can contribute to the pressure correction of thermocouples. Thus, his deduced corrections were substantially smaller than the true ones. It is perhaps fair to remark that at least several other researchers have been caught by the same trap in attempts to measure pressure effects on thermocouples.

Bloch and Chaisse [4] have correctly used the composite thermocouple method to determine the effect of pressure on copper-constantan thermocouples over the range 0 to 5 kbars and −196° C to 89° C. This is the most reliable data available for low-temperature work and it is of particular interest for quantitative hydrostatic studies of magnetic and crystallographic transitions at low temperatures. Their copper-constantan results are in excellent agreement with Bridgman over the limited mutual range of measurement. Figure 2 summarizes some of the best current data available for thermocouple corrections obtained from hydrostatic systems.

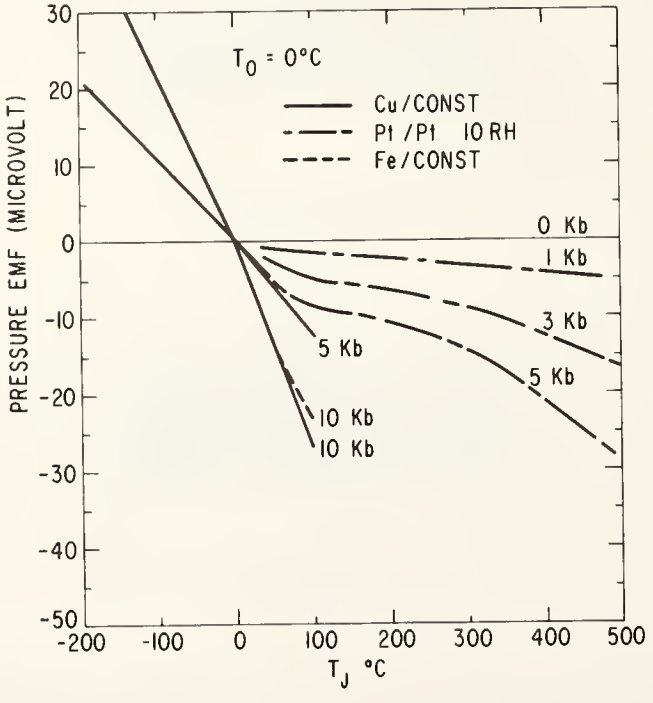

FIGURE 2. *Compilation of some key pressure corrections for thermocouples from hydrostatic systems.*

In both of the above methods of measurement the pressure gradient in the seal regions from P_J to P_0 is essentially isothermal. In addition, the internal temperatures T_J and T_0 are at the same temperature as the known external baths. As the internal pressure is increased from the atmospheric pressure P_0 to a higher value, P_J, the thermal emf output of a composite thermocouple (or single wire) will continuously deviate from its corresponding value at P_0 for fixed values of T_J and T_0. Thus, accurate, absolute corrections for pressure effects on thermocouples can be obtained. The available physical properties of seal and pressure vessel materials have restricted measurements under the above hydrostatic circumstances to pressures less than about 15 kbars and temperatures of no more than several hundred degrees.

2.2. Higher Pressure-Temperature Range

2.2.1. General Problems

Thermocouple corrections at much higher pressures and/or temperatures than discussed above are often needed. Such corrections have been achieved with much experimental difficulty using non-hydrostatic systems but they are only approximate because of: (1) uncertainties in the absolute pressure associated with non-hydrostatic systems used, (2) lack of a precise knowledge of the temperature within the high-pressure region, (3) non-isothermal pressure seals and (4) other effects including plastic deformation. In general, the higher the superimposed range of temperature and pressure the more difficult it is to obtain reliable, approximate corrections.

These and other problems in achieving accurate high pressure-high temperature measurement using thermocouples have been discussed by Hanneman and Strong [5, 6]. They show that chemical contamination of thermocouples can frequently occur within high-pressure cells at elevated temperatures and that this can strongly alter the output of a thermocouple. Chromel-alumel thermocouples are particularly susceptible to sizable high-temperature drift with time in pyrophyllite cells, while Pt/Pt 10 Rh thermocouples appear to be relatively inert.

The magnitude of the effect of plastic deformation (such as experienced within seal regions of non-hydrostatic cells) upon the thermal emf of Pt/Pt 10 Rh and chromel/alumel was found generally to be within a few percent of the total pressure correction at high pressures. As long as a high resistance insulating tubing such as BN or alumina surrounds thermocouple wires at high temperatures, the electrical shunting effect on thermocouple output should be negligible.

One of the most important modifications of

thermocouple corrections that can vary from one type of cell to another is the presence of temperature gradients within a pressure gradient region. The total pressure-induced contribution to the emf of a thermocouple is given by the following general expression[6]:

$$\partial E_p = \int_{T_0}^{T_J} \left[\frac{\partial Q}{\partial P}\right] P(\tau)\, dT \qquad (1)$$

where $\partial Q/\partial P$ is the pressure dependence of the thermopower of the couple and $P(\tau)$ is the pressure-temperature function along the thermocouple path into the cell. One can independently express P in terms of T in eq (1) without explicitly including the distance variable, since both follow continuous paths simultaneously. The quantities T_J and T_0 are the internal couple junction temperature and the temperature where the pressure drops to atmospheric pressure, P_0, respectively. The quantity $\partial Q/\partial P$ is, to a first approximation, a constant for the most common thermocouple materials and ∂E_p is nearly proportional to a temperature shift. Thus, the resultant decrease in temperature correction produced by a superimposed pressure-temperature gradient is approximately proportional to the normalized area under a plot of the temperature-pressure path of that thermocouple. Figure 3 shows schematically a diagram of a typical temperature-pressure path of a thermocouple (i.e., $T_0\ CD$) in a typical cell. The area ADT_0T_J corresponds to the maximum theoretical correction if seals were isothermal. The ratio CDT_JT_0/ADT_JT_0 is the fraction of the maximum correction applicable to the particular cell and P_J, T_J, and T_0 of interest. Correction modifications due to the superimposed pressure-temperature gradient effects sometimes exceed 10 percent of the total temperature correction. The above types of gradient modifications apply to both relative and absolute pressure-induced thermocouple corrections in any kind of apparatus.

Actual measurement of the approximate pressure-temperature gradient function along a thermocouple path within any given cell assembly is a difficult problem. To determine approximate temperature gradients within a cell and its seal region, thermocouples are placed with their junctions in a series of positions from the center of the cell sequentially toward the seal. The raw mv values of all thermocouples (and hence the approximate temperatures) along the path are determined from experiments where both the cell pressure and internal temperature are varied over the desired range. Care must be taken so that the extra thermocouples do not substantially alter the temperature gradients within the cell. The pressure gradients within a cell can be similarly approximated by a series of localized pressure calibrations as described earlier by Hanneman and Strong [6]. In carrying out such experiments, it should be borne in mind that the local pressure within a non-hydrostatic cell at fixed applied load can be dependent upon the temperature.

2.2.2. Methods of Determination and Results

Three major classes of measurement methods have been utilized to evaluate absolute emf corrections in non-hydrostatic systems including: (1) a modified Bridgman method [7], (2) direct thermal noise technique [8], and (3) indirect, self-consistent, calibration methods [5].

Modified Bridgman Method. A modified Bridgman method was used in a key study by Bundy to obtain thermocouple corrections over a much wider pressure range than previously studied (e.g., 0 to 72 kbars) [7]. Figure 4 illustrates schematically the

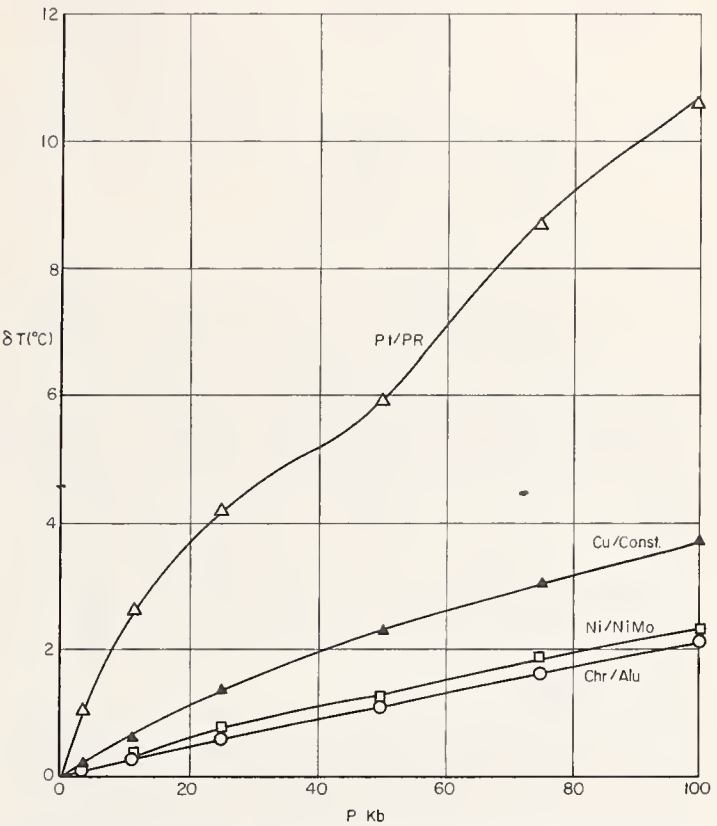

FIGURE 3. *Schematic of the pressure-temperature profile along a thermocouple path in typical and ideal high-pressure cells.*

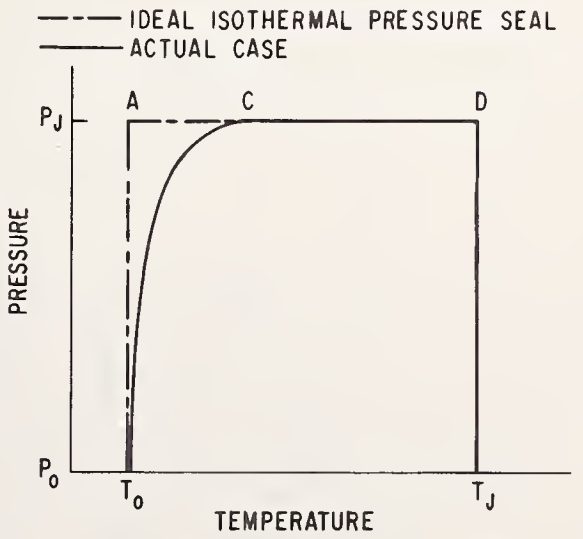

FIGURE 4. *Schematic diagram of modified Bridgman method for measuring effect of pressure on thermal emf's.*

385-762 O - 71 - 5

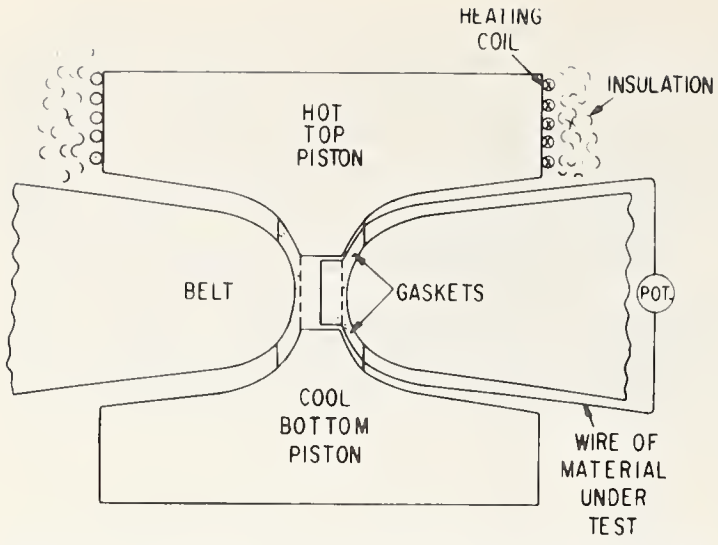

FIGURE 5. *Summary of pressure corrections for thermocouples for temperature gradient of 100 °C in non-hydrostatic range by the modified Bridgman method.*

Bundy apparatus. The maximum temperature gradient that could be achieved by this apparatus was approximately 100 °C because of the sizable thermal conductivity of the system between the hot and cold pistons. It was shown that errors due to a small temperature gradient in the seal regions of the cell did not exceed 5 percent of the thermocouple corrections obtained. Bundy's results for three common types of thermocouples are shown in figure 5. Recent similar measurements by I. Fujishiro, H. Mii, and S. Sakaida [9] have recently extended the single wire alumel data of Bundy out to 130 kbars for a 100 °C gradient with an opposed anvil apparatus.

Getting [10] has attempted the very challenging task of obtaining absolute thermocouple corrections for Pt/Pt 10 Rh couples up to 40 kbars and 1000 °C by the single wire modified Bridgman technique in a piston cylinder apparatus. Although these experiments have met with the great difficulties inherent in obtaining accurate corrections in this high-temperature range, some approximate corrections have been deduced. While in common agreement with nearly all workers over the range 0 to 100 °C up to 40 kbars these results do come into substantial disagreement with other higher temperature measurements to be described later as well as extrapolations of the lower pressure high-temperature measurements of Bell et al. [2].

Since all of the methods described so far have relied essentially upon external heat sources for the known temperature gradients set up within the high-pressure cell, the corresponding range of experimental results have been mostly restricted to rather limited temperature differentials within the cells, especially at higher pressures. In order to extend thermocouple corrections to the important region of higher temperatures at high pressures, new methods of measurement using internally heated cells have been devised. These will be described in the next two sections of this paper.

Thermal Noise Method. Studies using the thermal noise method to obtain thermocouple corrections at high pressure and temperature have recently been initiated [8]. Briefly, this method is based on the fundamental principle that a small pressure independent thermal noise is present in a resistor (or conductor). This may be given by:

$$(\Delta E)^2/(R\Delta f) = 4kT$$

where $(\Delta E)^2$ is the mean squared voltage fluctuations in a conductor of resistance R measured over the frequency interval Δf, and kT is the usual thermal energy term [11]. Experiments using this technique are very difficult, as they require extremely low noise measurement circuitry and a low noise ambient. Furthermore, d.c. heating is necessary in internally heated high-pressure cells to hold noise to a tolerable level. Thus, salt type cells cannot be used because of electrolysis effects. Since the magnitude of the mean voltage fluctuations is of the order of a microvolt per 1000 °K, measurements must be carefully made.

The most notable results to date at high pressure and temperature using the thermal noise method are those of Wentorf [8]. He has determined approximate corrections for Pt/Pt 10 Rh thermocouple up to 1000 °C and 40 kbars. The very limited data available are in reasonable agreement with the absolute corrections of Hanneman and Strong [6] obtained by a totally different approach that is described in the next section. For example, at 40 kbars and 1000 °C the absolute correction to a Pt/Pt 10 Rh thermocouple determined by Wentorf is +40 °C compared to a value of +36 °C deduced previously by Hanneman and Strong.

Indirect Self-Consistent Methods. The most extensive approximate determinations of absolute type pressure corrections for thermocouples have been obtained from indirect, self-consistent measurements. Until recent advances in low-noise electronics made the thermal noise technique possible, only indirect type measurements could be used to obtain corrections in the important range of high temperature at high pressure.

The first major effort to determine corrections in this region was that of Hanneman and Strong [5], who used the following indirect methods to deduce approximate absolute couple corrections: (1) comparison of experimental and thermodynamically calculated results of the effect of pressure on numerous single-component phase transformations and diamond growth from metal-carbon systems, and (2) correlation of results of high-pressure–high-temperature diffusion data. The scheme upon which the first class of indirect methods was carried out can be described most simply by referring to figure 6. This figure shows schematically three independent types of phase transformation common to various systems at high pressure. The solid curve A with a very steep temperature-pressure transfor-

mation boundary is typical of phase changes with a large ratio of volume change to entropy change, such as graphite to diamond. Solid curve B shows a transformation with a relatively low slope (dT/dP), which is typical of melting curves of metals with low volumes of fusion. Solid curve C depicts a transformation with a volume decrease on going to the higher temperature phase. Typical examples of this transformation include the melting of many semiconductors and the $\alpha \leftrightarrow \gamma$ transformation in iron. The dashed lines are representative of uncorrected, experimental curves that are found for each of the types of transformations. By designing a high-pressure cell to measure simultaneously two or more phase transformations (of different types) within the central isobaric pressure region, approximate thermocouple corrections to obtain a best fit of both sets of data can be deduced. Such data provide not only the approximate temperature corrections at pressure, but also the temperature coefficient of the internal cell pressure at fixed load. A series of such experiments over various pressure-temperature ranges with a variety of different materials permits a reasonable self-consistent approximation of absolute thermocouple corrections of a given type of thermocouple. The most sensitive types of combinations of transformations are A versus C or B versus C, since the C transitions have opposite slopes to the other two types. Numerous experiments of the above types have been carried out by Hanneman and Strong with self-consistent results.

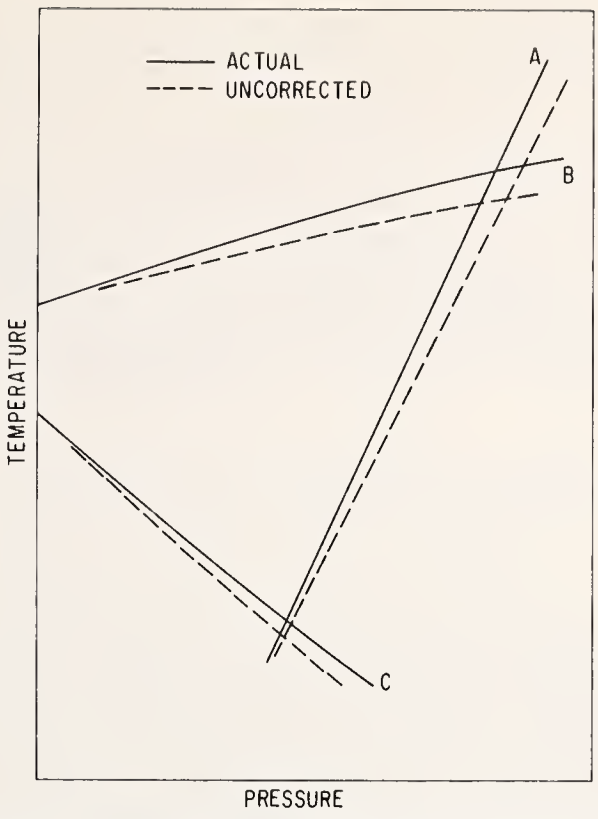

FIGURE 6. *Schematic diagram of various types of phase transformations used in indirect determinations of thermocouple corrections.*

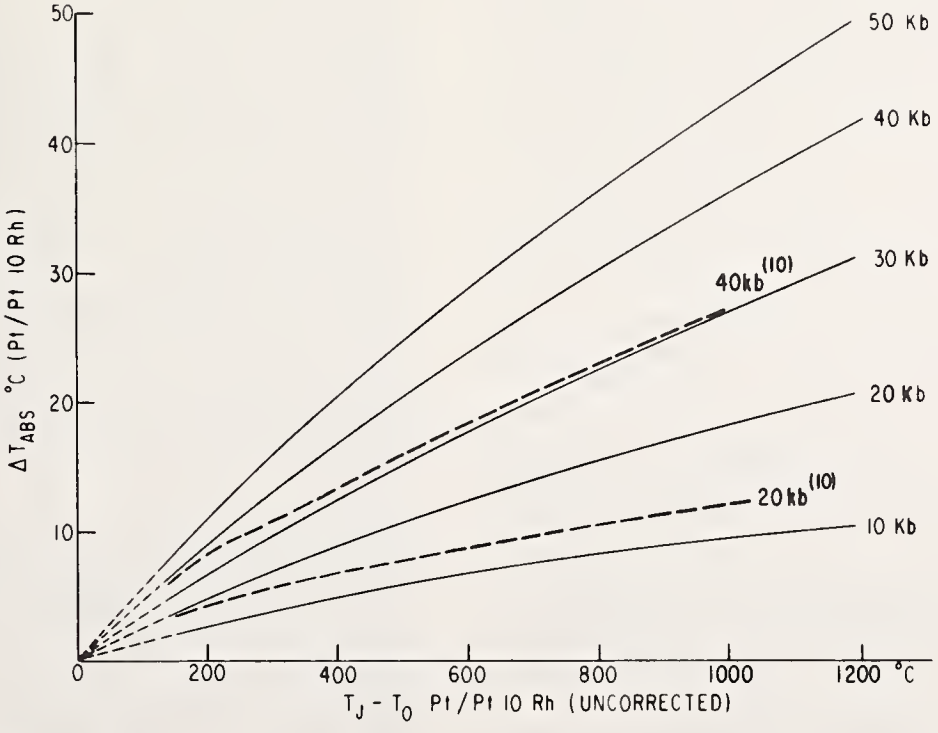

FIGURE 7. *Present approximate absolute pressure corrections for Pt/Pt 10 Rh thermocouples up to 1300 °C and 50 kbar for gradient factor equal to unity.*

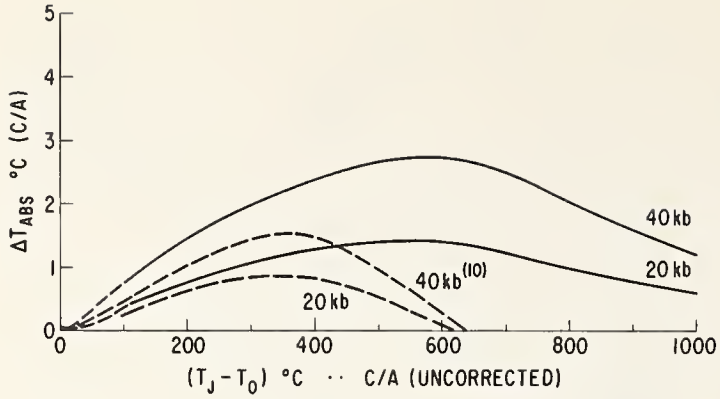

FIGURE 8. *Approximate absolute pressure corrections for chromel/alumel thermocouples up to 40 kbar and 1000 °C.*

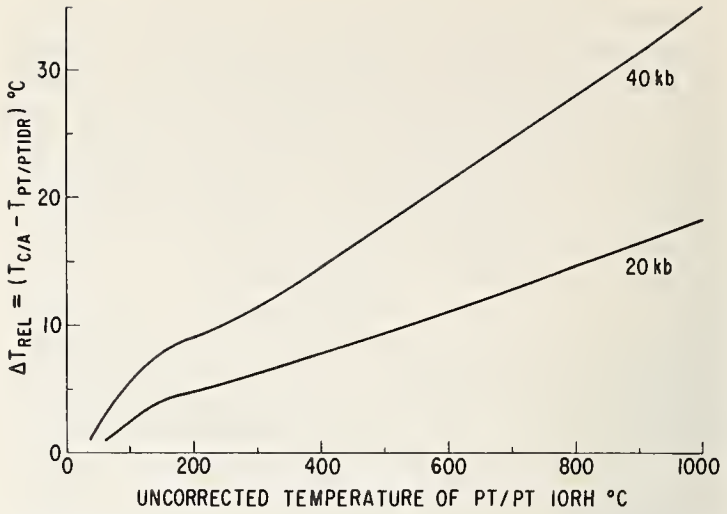

FIGURE 9. *Approximate relative corrections between Pt/Pt 10 Rh and chromel/alumel thermocouples up to 1000 °C at 20 and 40 kbar intervals. Gradient factor equal to unity.*

The second independent method they used to test the approximate magnitude of the thermocouple corrections was based on high-pressure diffusion experiments and theory. This approach has two indicators of the size of the correction. The first is to find, by a best fit of data, the appropriate temperature correction at a given pressure and composition which gives a constant value of activation volume for diffusion, V^*, over the temperature range of experimental data while maintaining a linear log D_p versus $1/T$ plot, where D_p is the diffusion coefficient at a pressure P and temperature T. The second approach is based upon a comparison of the value V^* calculated from the experimental atmospheric and high-pressure diffusion coefficients at fixed temperature with that obtained from experiments in the hydrostatic range and from theory. The approximate absolute thermocouple corrections deduced from diffusion data in the iron-vanadium and iron-nickel systems at 20 and 40 kbars are in reasonably good agreement with those obtained up to 1300 °C by the other methods described above (i.e., within ~ 20 percent). Further details on the diffusion analysis are treated in reference [5]. A complete plot of the approximate absolute corrections for Pt/Pt 10 Rh couples deduced from the best fit of all the indirect data of Hanneman and Strong and the thermal noise results of Wentorf adjusted for a pressure gradient factor of unity are presented in figure 7. Corresponding approximate absolute corrections for chromel/alumel couples are shown in figure 8. The corrections shown should be added to the uncorrected temperature. For comparison the Getting-Kennedy corrections [10] are shown as dashed lines in figures 7 and 8.

3. Effects of Pressure on the Relative Differences Between Various Thermocouples

The relative correction differences due to pressure-induced effects on thermocouples can be deduced by simply subtracting the known absolute corrections of two different types of thermocouples at a given temperature and pressure. In the limited pressure-temperature region where hydrostatic measurements have been made and for small thermal gradient regions (i.e., $\Delta T \leq 100$ °C) this yields satisfactory relative corrections because the absolute corrections are fairly reliable.

In the more uncertain high-pressure–high-temperature region, more accurate relative correction measurements can be obtained by direct experiments than can be deduced from absolute data. Such experiments have been reported for a direct comparison of chromel-alumel versus Pt/Pt 10 Rh couples by Hanneman and Strong [6] and by Peters and Ryan [12].

In order to obtain direct relative data at high temperature, two different types of thermocouples are brought into an internally heated high-pressure cell via equivalent pressure-temperature paths. Their junctions are both placed at the same position (i.e., pressure and temperature) and the wires are insulated throughout the cell. When the emf outputs of the two different thermocouples are referred to standard thermocouple tables, there is an apparent temperature discrepancy which increases with pressure at a given temperature. These data, together with a knowledge of the approximate cell pressure and internal gradients, permit a good approximation of relative corrections.

The best approximate relative corrections (for a pressure-temperature gradient correction factor of unity) for Pt/Pt 10 Rh versus chromel/alumel couples are shown in figure 9. The estimated accuracy of these relative measurements is approximately ±10 percent. Since these data are more reliable than any absolute corrections at high temperatures, any absolute data obtained on both types of couples must be in approximate agreement with the data in figure 9 if it is correct. Limited additional

relative correction data has been published for Pt/Pt 13 Rh and iron/constantan [5].

More extensive measurements of relative thermocouple corrections, especially at higher temperatures and pressures and for other types of couples, are needed. These data will be particularly helpful for the direct quantitative comparison of the published results of various workers on the same physical phenomena who have used different thermocouples. In this regard, it is urged that workers evaluate the pressure-temperature gradient effects in their cells and beware of the other sources of errors from thermocouple measurements described earlier in this paper.

4. Discussion and Conclusions of Absolute Corrections

The present theoretical knowledge of thermoelectricity and electronic properties of metals is insufficient to predict quantitatively the pressure dependences of thermocouples. We have shown that quantitative measurements of corrections for the pressure-induced deviations of thermocouples are very difficult in the high-pressure–high-temperature regime.

The most accurate corrections to date have been obtained in the range −200 to several hundred degrees centigrade and 0 to 15 kbars where hydrostatic cells can be used and deformation, contamination, and other problems can be minimized. A summary of some of the key results is shown in figure 2. Many of the results in this region are accurate to within a few percent.

Outside of the hydrostatic pressure range, the next most reliable data to date have been obtained from the modified Bridgman technique within a limited temperature range (0 to 100 °C). These results are generally believed to have an accuracy of better than 10 percent. Some of these by data are shown in figure 5.

The uncertainties in absolute corrections rise substantially in the range up to 50 kbars and 1300 °C where approximate corrections have been proposed. Nearly all of the indirect and thermal noise data [5, 6, 8] are compatible with the corrections given in figures 7 and 8. In addition, the magnitude of the corrections are compatible with extrapolations from lower pressure data achieved from direct determinations [2, 7].

As shown in figure 7, the Getting-Kennedy corrections [10] determined by the modified Bridgman approach do deviate substantially at higher temperatures from the other methods mentioned above. Although these corrections are of the same sign and magnitude as those from work in this laboratory, they are smaller by nearly one-half at the highest temperatures mutually examined. Possible inherent errors in the Getting-Kennedy approach would tend to make their corrections as lower limit values, whereas the thermal noise method would tend to give upper limit values. Thus, the actual absolute corrections probably lie somewhere in between the solid and dashed curves in figures 7 and 8.

Until more quantitative measurements can be carried out, it appears that one could obtain reasonable but approximate absolute corrections by averaging between the dashed and solid lines given in figures 7 and 8, and applying liberal error limits which span both sets of corrections. More accurate and complete measurements are clearly needed for better absolute corrections, but such tests will be very difficult.

5. Simultaneous and Continuous *in situ* Measurement of Pressure and Temperature

One of the major problems in research and applied technology in the area of high pressure has been the lack of an accurate, reliable method for continuous and simultaneous *in situ* measurement of high pressures and temperatures. Since accurate thermodynamic or kinetic studies under high pressure require a means of independently evaluating the true pressure and temperature at the sample, preliminary work in our laboratory was undertaken to develop a reliable, convenient method to accomplish this requirement.

Pressure measurement in most previous high-pressure investigations has relied completely on precalibration methods, which use first-order phase transformations of standard materials at room temperature to determine the relation between external press load and internal cell pressure for a given apparatus and cell geometry. In some cases approximate continuous measurements of pressure have been possible by use of resistance measurement of manganin or similar wire, but this is limited to < 250 °C and is sensitive to several variables. For various reasons, the apparent pressure based upon press load in a subsequent experiment often does not indicate the true internal cell pressure. For example, the pressure within a high-pressure cell varies as a function of temperature and time due to thermal expansion, phase changes in the sample holder or specimen, gasket leakage, and relaxation of stresses in the apparatus. Concurrently, the measurement of the true temperature in an internally-heated, high-pressure cell requires a knowledge of the effect of pressure on the electromotive force of thermocouples as described above.

By ulilizing two different thermocouples which have differing, known pressure dependences, one can uniquely monitor continuously both pressure and temperature within any high-pressure cell. In this method the junctions of two different thermocouples are placed together at the desired location in a high-pressure cell and both couples are surrounded by insulating material leading out of the

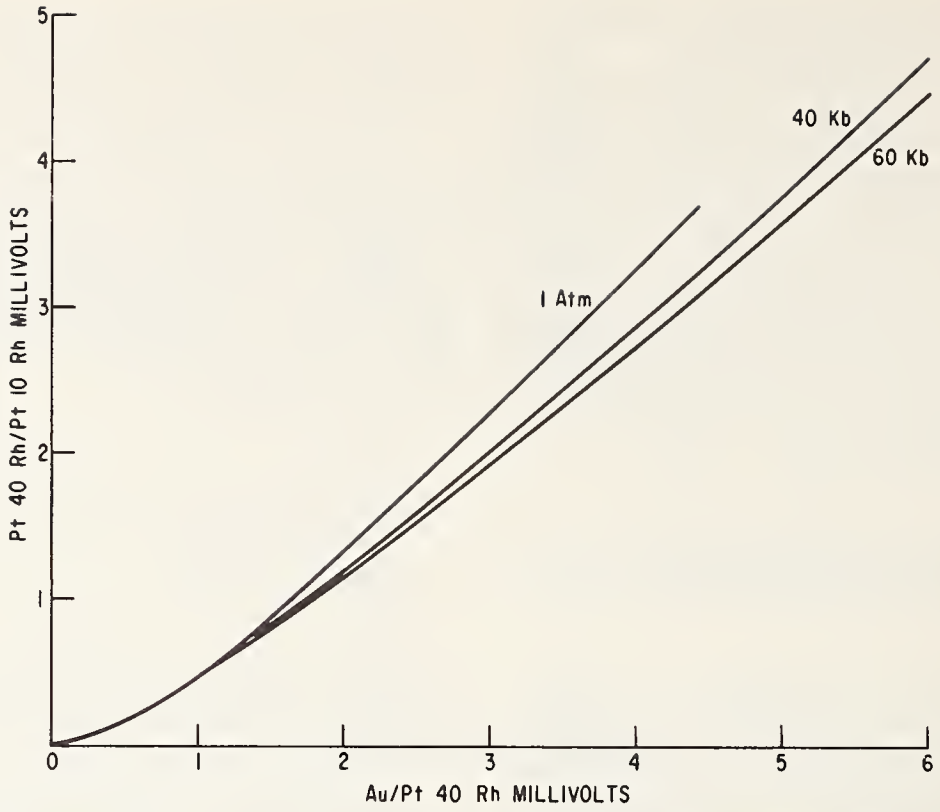

FIGURE 10. *Direct mv versus mv comparison of two different thermocouples for* in situ *pressure determination within a high-pressure cell.*

(Pt 40 Rh/Pt 10 Rh versus Au/Pt 40 Rh couples.)

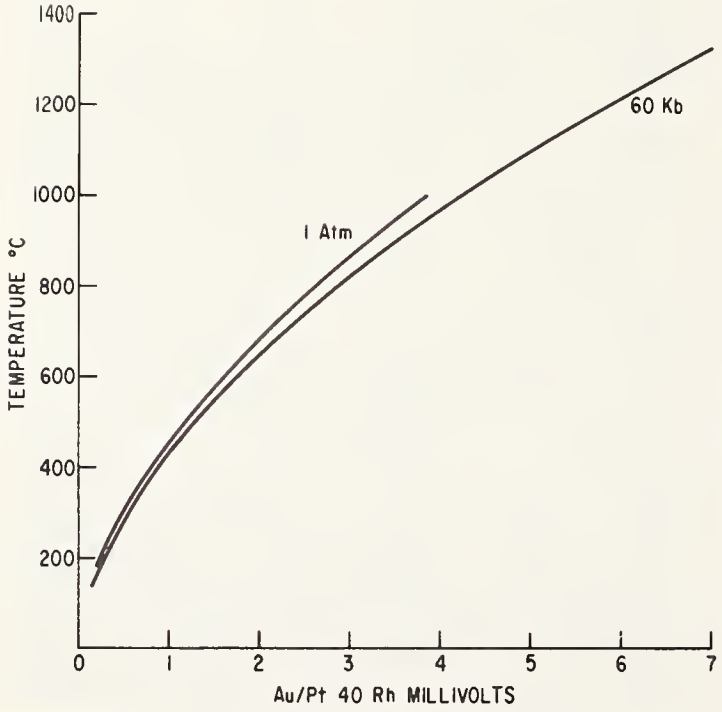

FIGURE 11. *Pressure effect on calibration of Au/Pt 40 Rh thermocouples for temperature determination.*

cell to cold junctions. These leads are then connected to sensitive potentiometers or other devices for accurately reading the emf output of both thermocouples. Such measurements require choice of thermocouple materials which will not be susceptible to chemical contamination drift. Figures 10 and 11 show the approximate pressure effects for Pt 40 Rh/Pt 10 Rh and Au/Pt 40 Rh thermocouples which have been used for simultaneous *in situ* measurements of pressure and temperature. The concurrent placement of both thermocouple emf's on figure 10 fixes the pressure. Then, by reference to a more detailed graph similar to figure 11, the corresponding temperature can be directly determined. Such determinations have absolute accuracies only as good as the absolute corrections available for thermocouples. However, relative changes of pressure within a cell during a given experiment can be seen to less than a kilobar under optimum circumstances [13].

6. References

[1] Bridgman, P. W., Proc. Am. Acad. Arts Sci. **53**, 269 (1918).
[2] Bell, P. M. England, J. L., and Boyd, F. R., Carnegie Institution: Ann. Rept. of Director Geophys. Lab., No. 1499, pp. 545–7 (1967); also The effects of pressure on platinum/platinum 10% rhodium and chromel-alumel thermocouples, this symposium.
[3] Birch, F. Rev. Sci. Instr. **10**, 137 (1939).
[4] Bloch, D., and Chaisse, F., J. Appl. Phys. **38**, 409 (1967).
[5] Hanneman, R. E., and Strong, H. M., J. Appl. Phys. **36**, 523 (1965).
[6] Hanneman, R. E., and Strong, H. M. J. Appl. Phys. **37**, 612 (1966).
[7] Bundy, F. P., J. Appl. Phys. **32**, 483 (1961).
[8] Wentorf, R. H., Temperature measurement by thermal noise at high pressures, this symposium.
[9] Fujishiro, I., Mii, H., and Sakaida, S. Bull. Jap. Soc. Appl. Phys. **37**, 621 (1968).

[10] Getting, I. The effect of pressure on the E.M.F. of the thermocouple, this symposium.
[11] Garrison, J. B., and Lawson, A. W., Rev. Sci. Instr. **20**, 785 (1949).
[12] Peters, E. T., and Ryan, J. J., J. Appl. Phys. **37**, 933 (1966).
[13] Hanneman, R. E., and Strong, H. M., New applications of duplex thermoelectric measurements in metals and alloys under high pressure-high temperature conditions, G.E. R&DC report 65-RL-3913X (Mar. 1965).

DISCUSSION

D. B. McWhan (*Bell Telephone Laboratories, Murray Hill, New Jersey*): Are there any data on pressure corrections for thermocouples using some of the newer materials, such as chromel versus gold-iron, at low temperatures? This thermocouple has a sensitivity of 15 μV per degree at 4 K.

M. C. Krupka (*Los Alamos Scientific Laboratory, University of California, Los Alamos, New Mexico*): Do you have any information in the relative correction of an increased rhodium content couple—for example a Pt-Pt 13 percent Rh couple?

I. Getting (*Institute of Geophysics and Planetary Physics, University of California, Los Angeles, California*): In some work I did on platinum-rhodium alloys other than platinum 10 percent rhodium, I found that the absolute correction increases slightly as the rhodium content increases. Within the uncertainties of our measurements, the correction could be taken to increase linearly with the rhodium content.

G. C. Kennedy (*Institute of Geophysics and Planetary Physics, University of California, Los Angeles, California*): In applying two thermocouples to measurement of the pressure by means of the differences in pressure effect on thermo-emf, wouldn't the most sensitive pressure-measuring device be obtained by using a couple made of a metal of minimum compressibility versus a metal of maximum compressibility?

I'd like to comment on the indirect method of measuring the pressure correction for a thermocouple. A number of years ago you published a suggestion as to the size of the correction, and the basis of it was the difference between the computed thermodynamic diffusion slope of a boundary and the measured slope. One of the boundaries used was the germanium melting curves that we published. We had also just done eight other melting curves. For over half of our curves, a comparison of the thermodynamic computed slopes versus measured slopes would suggest a thermocouple correction in an opposite direction. My view is that the uncertainties of the thermodynamic parameters are such that from data of this sort little can be said about thermocouple corrections. Finally, in very careful experiments with well-characterized materials and thermodynamic parameters, I believe that useful, approximate thermocouple corrections can be obtained by comparison of experiments and calculation. This is demonstrated by comparing our previous results with those from "direct" methods reported at this Conference.

H. Tracy Hall (*Brigham Young University, Provo, Utah*): In some multi-anvil devices it is convenient to make a thermocouple lead connection directly to an anvil rather than to bring the wire out. This is particularly true in a cubic press. Now, in a cubic type of press with an internal heater containing a charge of good thermal conductivity—diamond powder or something like that—leads have been brought out to the anvil surface and then enfolded in a metal, nickel in one instance, so that the contact is between platinum-platinum rhodium wire and nickel. Then the nickel is in contact with the tungsten-carbide (6 percent cobalt) anvil.

If you make a temperature calibration in the usual way by controlling power input (say watts of electric power) versus thermocouple temperature taken from the tables, you will obtain a certain curve using these nickel tabs. Now if the ends of the thermocouple wire are enfolded in, say, copper tabs, the result will be different. And I suppose if you pick some other metal it would still be different.

Because of the high symmetry of this system, it would appear that pressure gradients ought to be pretty much the same in all cases, and the temperature at the anvil surfaces ought to be about the same. At 1500 degrees there is about a 40-deg C difference between results using copper and using nickel. The difference increases as you go to higher and higher temperatures. At 400 or 500 degrees, there's not much difference. At 1000 degrees, there may be 20 deg C difference. Wherein would you say lies the cause of this discrepancy? What effect is there that gives you those differences? What would be the basis for choosing a metal for the tabs so that the temperature correction is very small?

A. Taylor (*Westinghouse Research Laboratory, Pittsburgh, Pennsylvania*): I'm wondering whether we are really looking at the problem from the right point of view. Rather than saying what the temperature is at a particular pressure, should we not state what the pressure is at a particular temperature?

If, from your curves, the temperature is approximately 40 degrees off at 1500 degrees, that is only a relatively small percentage error in the temperature. But at that temperature, a nominal pressure of about 60 kilobars in the tetrahedral anvil press can, in a matter of a few seconds, drop from let's say 60 kilobars down to only 40 kilobars, and you might never know it from the outside conditions.

So the question really is: How can we measure the pressure at these high temperatures rather than the temperature at the high pressures?

AUTHORS' CLOSURE

In reply to the question by McWhan: I believe that data on copper-constantan from −200 °C to room temperature is significantly better than any other in this temperature range. Thus, determination of the relative correction between copper-constantan and other couples would be worthwhile. No direct data on pressure corrections of chromel versus gold-iron couples at cryogenic temperatures has been obtained to my knowledge.

In reply to Dr. Krupka: The effect of increased rhodium content in Pt–PtRh couples is to increase the correction slightly on going from 10 to 13 percent Rh. Some explicit results are given in our 1965 paper (ref. 5).

In reply to Dr. Kennedy: Selection of metals of high and low compressibility for pressure-measuring thermocouples would not necessarily give the greatest sensitivity.

The thermopower, Q, of a material can be given by:*

$$Q=\frac{\pi^2}{3}\frac{k^2T}{e}\left\{\frac{\partial \ln A}{\partial \epsilon}+\frac{\partial \ln \lambda}{\partial \epsilon}\right\}_{\epsilon_F}$$

where k, T, and e have their usual meanings and A and λ are the effective area of the Fermi surface and the electron mean face path, respectively, evaluated at the Fermi energy ϵ_F. Although the pressure dependences of A and λ are not known sufficiently well in real metals and alloys to predict the effect of pressure on thermocouples, it is instructive to estimate the order of magnitude of the effect.

Applying the free electron approximations to the terms in A and λ and differentiating with respect to pressure, it follows that:

$$\frac{dQ}{dP}\approx \alpha\frac{\pi^2k^2T}{e}\frac{\beta}{\epsilon_F}$$

where α is factor of the order of unity, β is the isothermal compressibility, and the other terms have the previously stated meanings. Substituting in typical values of $T\sim 1{,}000$ °K, β of the order of 10^{-12} to 10^{-13} cm²/dyne, and $\epsilon_F\sim$ few eV and using equation (1) in the text, emf corrections of the order of 0.1 to 1 mV are indicated at 50 kbar, for example, for a given metal. Thus the total expected pressure dependence of a thermocouple should be of this magnitude or smaller, since it will arise from differences in (β/ϵ_F) of the two materials used.

In the situation described by Dr. Hall, if the pressures are really about the same in the two cases, and if there is not a significant temperature gradient through the metal, then one is forced to assume that the difference between results with nickel tabs and copper tabs is due to stress effect, deformation, or something of this sort. Chemical contamination could be also rather important. A further key to the cause of the discrepancy might be obtained by studying the effect of copper and of nickel tabs as a function of time.

In choosing materials for the tabs, I would favor materials which are as chemically inert as possible and which keep the temperature-pressure gradients as small as possible.

In reply to Dr. Taylor's question: I would submit that for quantitative work, *in situ* measurement of both pressure and temperature are important. That is why I presented the dual thermocouple idea in my paper. Thus an *in situ* pressure drop would be immediately noticeable.

In addition to phase diagram definition under pressure which seems to have been of most past concern, it's clear to me that thermally activated processes including nucleation, growth, diffusion, and other kinetic processes are going to require increasingly accurate *in situ* characterization of both temperature and pressure. In these latter processes an error of 40 °C in 1,000 °C to 1,500 °C would generally lead to much greater errors than, say, 10 kbars out of 50 kbars.

*J. M. Ziman, Electrons and Photons (Oxford Univ. Press, London, 1960).

The Effect of Pressure on the Thermal Emf of the Platinum/Platinum 10 Percent Rhodium Thermocouple

P. M. Bell, F. R. Boyd, Jr., and J. L. England

Geophysical Laboratory, Carnegie Institution of Washington, Washington, D.C. 20008

Temperature in high-pressure experiments is usually measured by thermocouples, which are themselves subjected to pressure. The effects of pressure on the thermoelectric properties of these thermocouples are significant in many experiments, and they need to be quantitatively understood. This problem has become acute with the development of solid-media pressure apparatus capable of operating at temperatures up to 2,000 °C and pressures of 100 kbar or more. Corrections for the effects of pressure on thermal emf may be as much as 50 to 100 degrees under these extreme conditions. Other papers in this volume discuss the evaluation of these effects by experiments with solid pressure cells in the pressure range above 10 kbar (Hanneman, Strong, and Bundy, p. 53; Getting and Kennedy, p. 77). The purpose of the present study has been to provide more extended data for the region below 10 kbar, which can be explored with an externally heated gas apparatus. Measurements that can be made with gas apparatus are limited in range, but they are inherently more accurate than measurements with solid-media apparatus. It is hoped that the data obtained in the present study will provide a useful base for the solid-media experimentation.

Early measurements with gas apparatus on the effects of pressure on thermal emf by Bridgman (1918) were remarkably precise but extended to only 100 °C and 12 kbar. Unfortunately Bridgman did not study most of the alloys that are currently used for thermocouples in high-temperature, high-pressure experiments. He formed a thermocouple by pressurizing part of a continuous homogeneous wire. One pressure seal was heated, while the other was cooled to 0 °C for reference. In such an experiment—now called a "single-wire experiment"—the absolute pressure effect is measured directly for a given element or alloy.

Birch (1939) has provided data on chromel/alumel and platinum/platinum 10 percent rhodium thermocouples to 580 °C and 4 kbar. He subjected these thermocouples to nitrogen pressure in steel tubes immersed in a lead bath and compared their emf readings with those from reference thermocouples at the same temperature but at atmospheric pressure. As discussed by Bundy (1961), Birch did not cool the pressure seal in his apparatus to 0 °C, and hence he did not observe a maximum or "absolute" effect.

In the present study a platinum/platinum 10 percent rhodium thermocouple was subjected to nitrogen pressure in a tube, one end of which was heated by an electrical furnace while the other end was cooled to 0 °C in an ice bath (fig. 1). The emf of the pressurized thermocouple was read as a function of pressure relative to a second platinum/platinum 10 percent rhodium thermocouple heated to the same temperature but held at atmospheric pressure. The data obtained are "absolute" in that they are tied to a 0 °C reference. Most modern high-pressure apparatus does not have pressure seals at 0 °C, and practical applications of these data will generally require correction for the temperature of the pressure seal.

Paper presented at the Symposium on Accurate Characterization of the High-Pressure Environment, held at the National Bureau of Standards, Gaithersburg, Md., October 14–18, 1968.

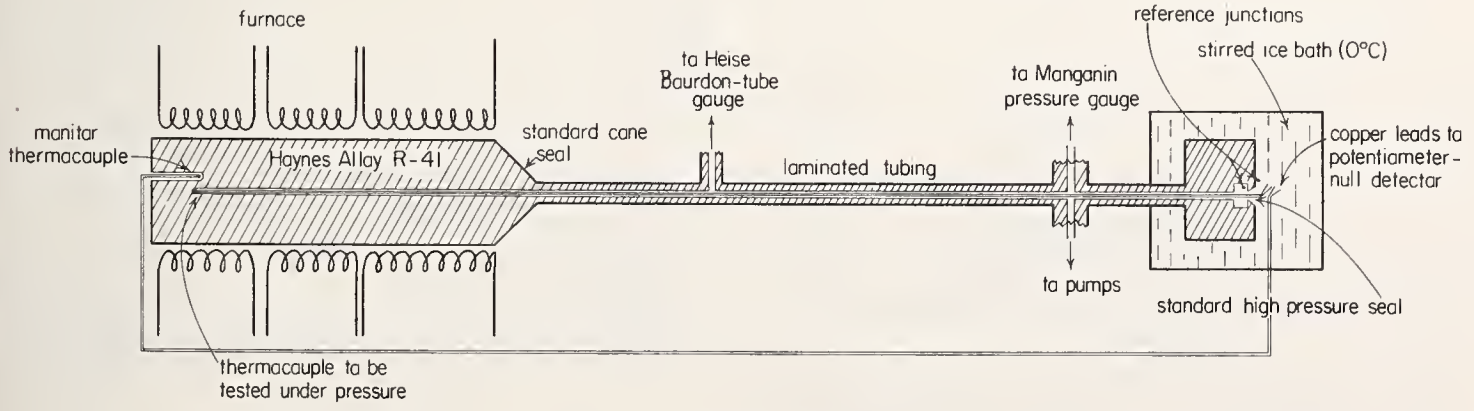

FIGURE 1. *Gas apparatus used for the measurement of the effect of pressure on the thermal emf of the platinum/platinum 10 percent rhodium thermocouple.*
The pressure medium used was nitrogen.

1. Apparatus

The apparatus is designed for the range 1000 °C and 13 kbar, but most of the experiments reported here were made in the range up to 5 kbar. The pressure vessel (René 41) containing the pressurized thermocouple was heated in an external electric furnace constructed to have a thermal gradient less than 1°/in at the hot spot and capable of precise control. The monitor thermocouple at atmospheric pressure was located in a small cavity in the outside end of the pressure vessel. Leads from both thermocouples were brought into a stirred ice bath in which the pressure seal was suspended. Two additional thermocouples were employed, one in the ice bath itself and another on the high-pressure side of the cold pressure seal. Emf differences between pressurized and unpressurized thermocouples were measured with a potentiometer-null detector combination, which can be read to 1×10^{-8} V.

Readings were taken at constant temperature at intervals of pressure up to 10 kbar. The temperature difference between the hot junctions of the pressurized thermocouple and the monitor thermocouple was reduced to about 0.1 °C. The ΔT observed at atmospheric pressure at the start of an experiment drifts slowly during the experiment, apparently owing to the large increase in conductivity with pressure of the gas. Thus observed ΔT readings required a small correction for shift of the base. Data were not accepted if the potential difference of the pressurized and unpressurized cold-junction thermocouples indicated a temperature difference of greater than 0.01 °C.

2. Results

Pressure decreases the thermal emf of a platinum/platinum 10 percent rhodium thermocouple, requiring a positive correction to the reading of the thermocouple for some pressure above atmospheric. This effect is not linear with pressure or temperature, but its magnitude increases with both pressure and temperature.

Figure 2 shows the experimental data in a series of isotherms ranging up to 509 °C, and these data are plotted again in figure 3 as isobars. Some of the points (fig. 2) were repeated in a series of heating and cooling cycles and were found to be reproducible to better than a microvolt. The maximum effect

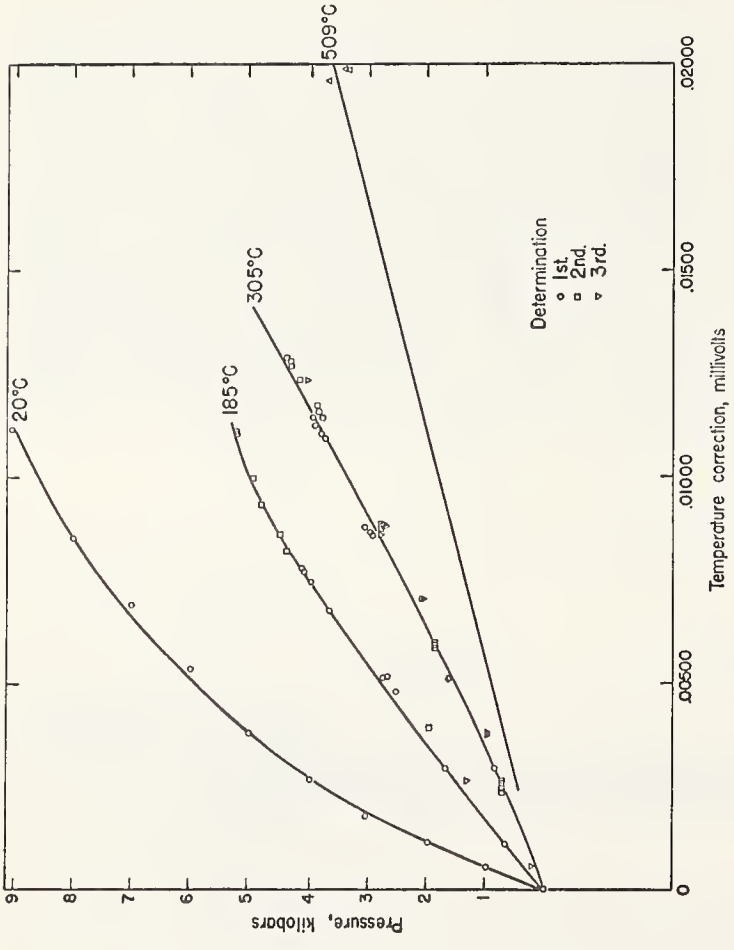

FIGURE 2. *Measurements of the change in emf (negative) of a platinum/platinum 10 percent rhodium thermocouple with pressure.*

The cold junction and pressure seal were at 0 °C. This correction must be added to the observed emf of a pressurized couple to give the true temperature.

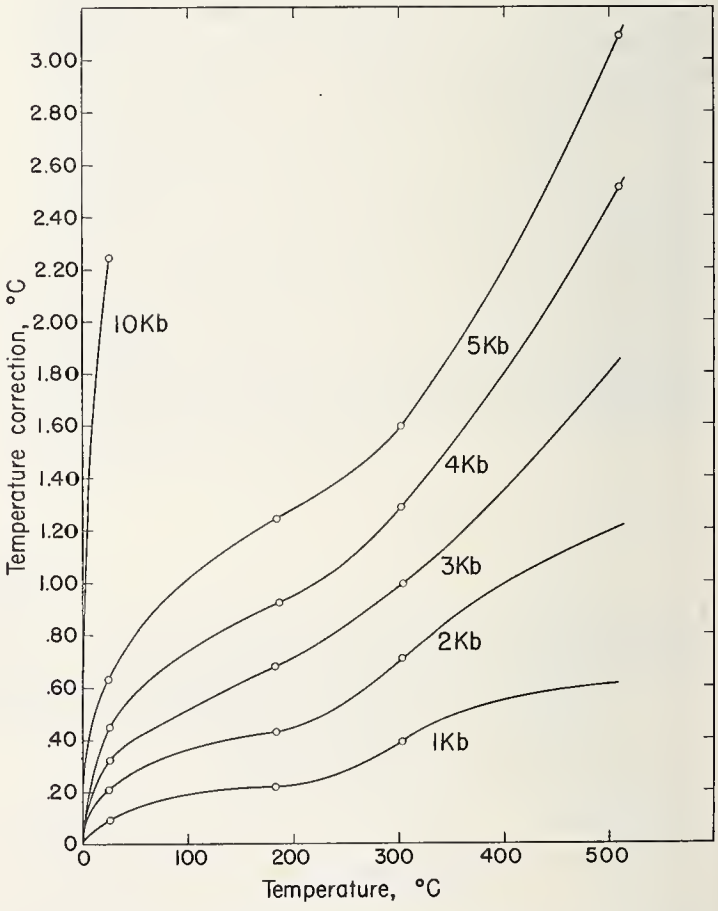

FIGURE 3. *Measurements in fig. 2 plotted as isobars.*

This correction must be added to the observed emf of a pressurized couple to give the true temperature.

observed was 20 μV at 509 °C and 3.5 kbar, corresponding to an apparent ΔT of 2 °C. Birch's determination (*op. cit.*, fig. 2) shows about 13 μV at this same pressure and temperature. The difference between present results and Birch's measurement is most likely due to the fact that the pressure seal was cooled to 0 °C in our experiment but was at some temperature above room temperature in his determination. Present results agree in sign and are roughly comparable in magnitude to results extrapolated from solid-media experiments at much higher pressures. Our results must be extended to higher pressures and temperatures, however, before meaningful quantitative comparisons with the solid-media data can be made.

3. References

[1] Birch, F., Thermoelectric measurement of high temperatures in pressure apparatus, Rev. Sci. Instr. **10**, 137–140 (1939).

[2] Bridgman, P. W., Thermoelectromotive force, Peltier heat, and Thompson heat under pressure. Proc. Am. Acad. **53**, 267–386 (1918).

[3] Bundy, F. P., Effect of pressure on emf of thermocouples, J. Appl. Phys. **32**, 483–488 (1961).

[4] Getting, I. C., and G. C. Kennedy, The effect of pressure on the emf of the thermocouple. This volume, p. 77.

[5] Hanneman, R. E., H. M. Strong, and F. P. Bundy, A critical review of the effect of pressure on thermocouple emf's. This volume, p. 53.

Pressure Dependence of the Thermoelectric Power of Thermocouple Materials

Paul J. Freud and Phillip N. La Mori

Battelle Memorial Institute, Columbus Laboratories, 505 King Avenue, Columbus, Ohio 43201

Single-wire measurements of the pressure dependence of the thermoelectric power were made hydrostatically to 8 kbar for chromel, alumel, copper, and constantan and in a piston cylinder apparatus to 40 kbar for chromel, alumel, platinum, and platinum 10 percent rhodium. The temperature interval covered for the hydrostatic measurements was −195 °C to 290 °C and for the piston cylinder measurements it was 30 °C to 380 °C. A detailed discussion is given of the pressure-temperature distribution within the piston cylinder cell. Pressure emf values are presented with an uncertainty of ±7 percent.

1. Introduction

Measurements of the pressure dependence of the thermoelectric power (T.E.P.) have been made on a number of thermocouple materials using the single-wire technique. The objective of this work was to establish a pressure and temperature range in which the pressure dependence of the T.E.P. could be determined to an accuracy required for normal thermocouple use. Therefore the main emphasis of this study was to define the pressure and temperature conditions of the high-pressure cell rather than to push for the extremes of pressure-temperature conditions. A number of high-pressure cell configurations were investigated and calibrated before we arrived at a configuration using solid AgCl for the main pressure column. The temperature distribution within the high-pressure cell was determined carefully, since the calculation of the pressure dependence of the T.E.P. is crucially dependent upon how the pressure and temperature are distributed within the measuring cell.

We believe that it is valuable to restate the concepts involved with the use of thermocouples under high-pressure conditions so that a clear understanding of the important parameters is established. The simplest way to look at thermal emf's is to imagine the thermocouple circuit as divided up into small segments each with a particular ΔT across it. An emf will be induced across the segment which is proportional to ΔT. The proportionality constant is the thermoelectric power (α) of the material being used. The total thermal emf of the circuit is determined by summing all the emf's from each segment. Thus,

$$V=\sum \alpha_i \Delta T_i \rightarrow \oint \alpha(T)\,dT. \qquad (1)$$

Figure 1a is a schematic diagram of a typical thermocouple circuit used in a high-pressure environment. The circuit consists of two dissimilar wires which go from ambient pressure through pressure seals into the high-pressure and high-temperature environment. The seal is represented by the crosshatched region, and in this region the pressure increases from the ambient pressure to the high interior pressure. For this analysis it is assumed that the sealing region is isothermal. The errors introduced when this assumption is not valid are discussed later.

The temperatures of significance in this circuit are the reference temperature T_0, the temperature of the seal region, T_1, and the junction temperature, T_2.

The T.E.P. of a given material is in general a function of temperature and pressure and can be written as the sum of a pressure-independent term and a pressure-dependent term:

$$\alpha_a=\alpha_a(T)+\Delta\alpha_a(p, T). \qquad (2)$$

The subscript refers to the particular material in question. The first term is the T.E.P. of the material at zero pressure, and the second is the change in the T.E.P. due to pressure. The second term is also a function of temperature. If we integrate the emf around the circuit shown in figure 1a, the following

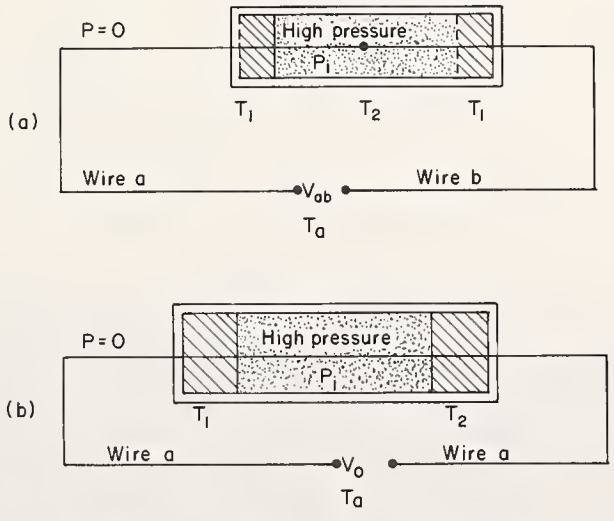

FIGURE 1. (a) *Schematic diagram of thermocouple circuit for high-pressure apparatus.*
(b) *Schematic diagram of high-pressure single-wire circuit.*

Paper presented at the Symposium on Accurate Characterization of the High-Pressure Environment, held at the National Bureau of Standards, Gaithersburg, Md., October 14–18, 1968.

expression results:

$$V_{ab}=\oint \alpha dT=\int_{T_0}^{T_1}\alpha_a(T)dT+\int_{T_1}^{T_2}[\alpha_a(T)+\Delta\alpha_a(p_i,\,T)]dT+\int_{T_2}^{T_1}[\alpha_b(T)+\Delta\alpha_b(p_i,\,T)]dT+\int_{T_1}^{T_0}\alpha_b(T)dT.$$

This reduces to the following when the pressure-independent and pressure-dependent terms are separated:

$$V_{ab}=\int_{T_0}^{T_2}[\alpha_a(T)-\alpha_b(T)]dT+\int_{T_1}^{T_2}[\Delta\alpha_a(p_i,\,T)-\Delta\alpha_b(p_i,\,T)]dT. \quad (3)$$

The first term is just the emf, V_0, which would be induced in the circuit at zero pressure (the value tabulated for the temperature interval $T_0 \rightarrow T_2$), and the second term is the additional emf induced due to the wires being pressurized to p_i. Note that the temperature interval over which the pressure-dependent term is integrated is the seal temperature to junction temperature.

To measure the change in the T.E.P. as a function of pressure, the circuit in figure 1b can be employed. This circuit is used for the so-called single-wire experiment, an accurate means of measuring the T.E.P. pressure dependence. In this circuit, a single wire is brought into a high-pressure vessel through an isothermal pressure seal at a temperature T_1 and is brought out through a similar seal at a temperature T_2. The induced voltage, using eqs (1) and (2), is the following:

$$V(p_i)=\int_{T_0}^{T_1}\alpha_a(T)dT+\int_{T_1}^{T_2}[\alpha_a(T)+\Delta\alpha_a(p_i,\,T)]dT+\int_{T_2}^{T_0}\alpha_a(T)dT=\int_{T_1}^{T_2}\Delta\alpha_a(p_i,\,T)dT. \quad (4)$$

The pressure correction term for a thermocouple circuit, the second term of eq (3), can therefore be determined by performing the single-wire experiment for each material of the thermocouple pair.

The problem of simultaneous pressure gradient and temperature gradient which normally exists in a pressure seal and throughout a solid-media device will modify this treatment. Equation (4) is still valid but the variation of $\Delta\alpha(p,\,T)$ has to be taken into account, since the pressure is not constant over the temperature interval within the cell. Hanneman and Strong [1][1] have provided a means of approximating the amount of uncertainty involved when the simultaneous gradients exist. They approximate $\Delta\alpha(p,T)$ where A is a constant and $p(T)$ is the internal pressure written in terms of the temperature. This is possible since T and p are both functions of position within the cell and therefore one can be written as a function of the other. To determine the uncertainty associated with this problem, one has to determine the function $p(T)$. In other words the pressure and temperature gradients within the high-pressure cell have to be established. Equation (4) reduces to

$$V=A\int_{T_1}^{T_2}p(T)dT, \quad (5)$$

which is a constant times the area under the curve $p(T)$ versus T. The error introduced by assuming no pressure gradients where there are temperature gradients is just the difference in area between the actual $p(T)$ versus T curve and the area calculated if it is assumed that $p=p_{\max.}$ from T_1 to T_2 and is zero everywhere else.

We have made a detailed analysis of the pressure and temperature distribution in our piston cylinder cell and have established the $p(T)$ relation so that the area is determined to an accuracy of 2 percent.

2. Experimental Procedure

2.1. Hydrostatic Measurements

Single-wire measurements were carried out both in a hydrostatic gas apparatus to 8 kbar, and in a piston-cylinder solid-media apparatus to 40 kbar. A schematic diagram of the hydrostatic apparatus is given in figure 2. The materials measured were standard 36-gage teflon-coated thermocouple wire. The wires were threaded through the 0.6-mm-diam. bore of a stainless steel high-pressure tubing. One end was brought out to ambient pressure through a frozen gas U-tube seal which is immersed in liquid nitrogen. Argon, which is used as the pressure medium, is solid in liquid nitrogen and therefore acts as the pressure seal around the wires coming out of the U-tube. The temperature of this seal is therefore fixed at 78 °K.

The high-temperature seal is made by silver soldering the thermocouple wire a small distance into the high-pressure tubing. Since this region of tubing is maintained strictly isothermal, no error in the thermal emf is produced by shorting out this section of the thermocouple wire with another material. The high-pressure tubing in this region is surrounded with a tight-fitting, thick-walled copper cylinder which insures that no temperature gradients will exist across the silver solder seal. The thermocouple circuit is grounded at this point while the rest of the circuit and the potentiometer are insulated from ground.

[1] Figures in brackets indicate the literature references at the end of this paper.

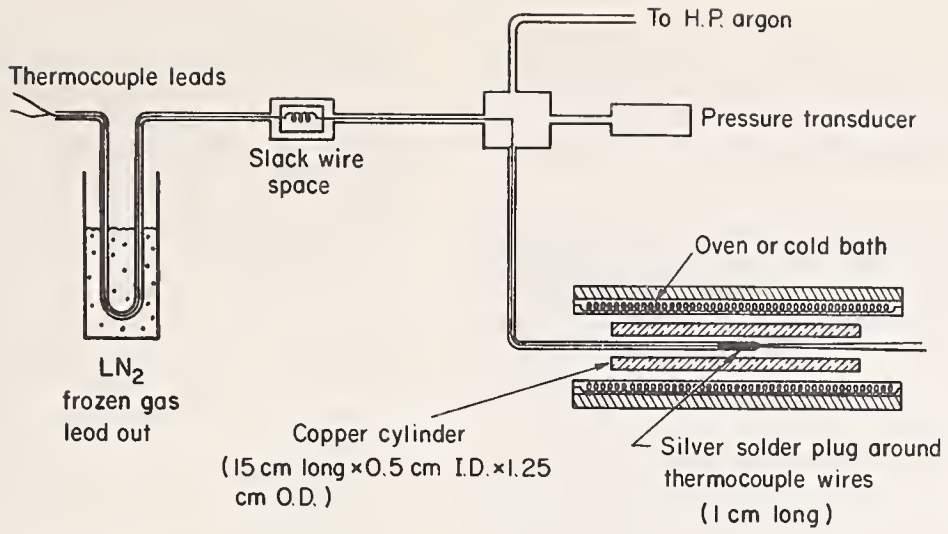

FIGURE 2. *Hydrostatic pressure apparatus for measuring single-wire high-pressure thermal emf.*

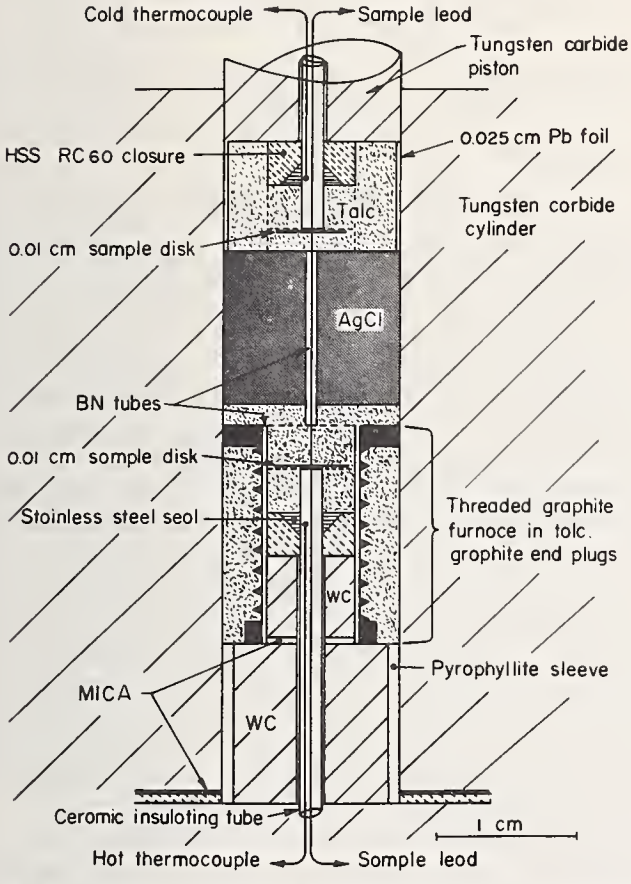

FIGURE 3. *Piston cylinder high-pressure cell for measuring single-wire high-pressure thermal emf.*

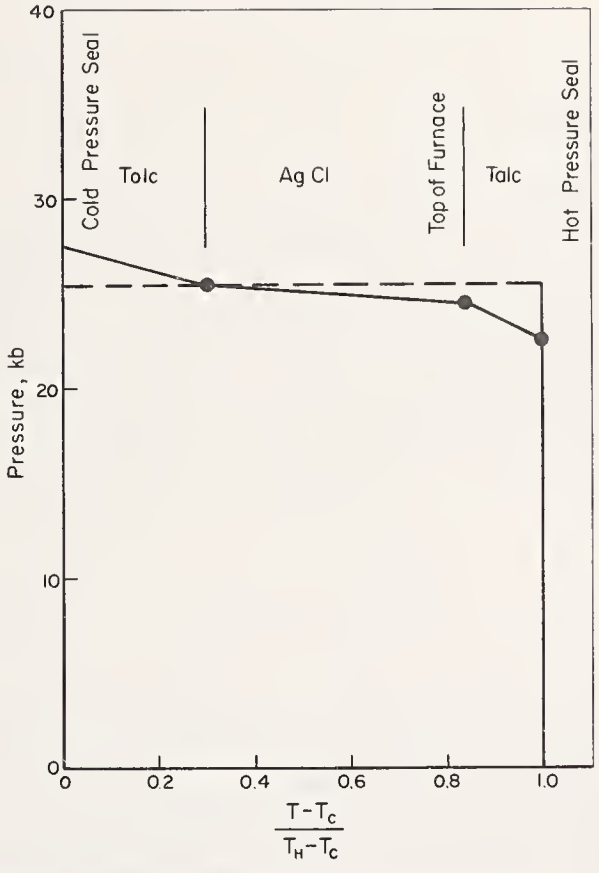

FIGURE 4. *Pressure temperature distribution in piston cylinder high-pressure cell.*

Pressure was generated with a three-stage intensifier system and was measured with a strain gage transducer, which had been calibrated against a manganin coil. The maximum temperature was limited to 300 °C due to the strength of the silver solder plug. At the dry ice point the pressure was limited to 5 kbar due to the freezing of argon. At all higher temperatures the maximum pressure used was 8 kbar. A space was provided between the low- and high-temperature ends for some slack wire so that straining of the wires due to movement in the cold seal would be minimized.

2.2. Piston Cylinder Measurements

The piston cylinder measurements were made in an apparatus of standard design and of dimensions 1.27 cm diam × 5.08 cm long. The cylinder material was 94¼ percent WC 5¾ percent cobalt binder (Plansee 850). Figure 3 shows a schematic cross section of the cell design for this experiment.

The design of the cell is obviously quite important and the key to success or failure of the experiment. The cell had to provide the conceptual physical ideas discussed in the introduction with minimum

deviations from the ideal. Therefore, one requirement was to make the pressure seals as sharp as possible and/or as isothermal as possible. Additionally the pressure gradient over the temperature gradient in the high-pressure cell was to be kept to a minimum.

The reasons for these requirements are illustrated in figure 4. If the pressure seals are infinitely sharp and there is no pressure gradient in the high-pressure cell, the dashed line represents the $p(T)$ versus T relation. This is the ideal or perfect experiment. The pressure emf is proportional to the area under the curve.

The actual experimental conditions are shown as the solid line. The points on the graph have been measured in our cell by use of thermocouples and the bismuth transitions. This will be discussed in detail below. The effects of the slight temperature gradient across the pressure seal have not been indicated on the graph. The area under the dashed curve is proportional to the value of the effect we want to measure. We have chosen the experimental pressure to be the pressure of the talc-AgCl interface (piston end) as this gives the best representation of the true area.

The pressure calibration was an important factor influencing the final design of the cell shown in figure 3. Large pressure gradients over the temperature gradients inside the high-pressure region would cause large uncertainties in the results. We originally started with a cell using talc as the pressure media, quite similar to that of Getting and Kennedy [2]. This would correspond to replacing the AgCl in our figure 3 with talc. A wire of bismuth 0.03 cm diam $\times$ 0.6 cm long was placed axially in the furnace from the seal to the top of the furnace. The bismuth $1 \rightarrow 2$ transition started at 32 kbar force/area on the compression stroke and took 7 kbar to complete. Using this design we found it impossible to go beyond the end of the bismuth $2 \rightarrow 3$ transition without danger of piston failure (44 kbar on the piston). If the bismuth wire extended the length of the cell the maximum pressure of the $1 \rightarrow 2$ transition should remain the same but the gradient would be extended from 7 kbar to 12 kbar. This would seriously compromise the determination of area in a $p(T)$ versus T plot and thus the final results.

An improvement was noted by replacing 0.64 cm of the talc at the furnace end with AgCl. Here the bismuth $1 \rightarrow 2$ transition started at 28 kbar room pressure but still took 7 kbar to complete. The bismuth $2 \rightarrow 3$ transition was complete at 39 kbar on the piston. Another improvement was made by going to the configuration in figure 3 except that the BN was 0.32 cm diameter. In this setup the $1 \rightarrow 2$ transition started at 27.5 kbar and took 6 kbar to complete. For the first time the bismuth 2 resistance had a flat portion. The bismuth $2 \rightarrow 3$ transition was complete at 36 kbar on the piston.

The majority of the large ΔP from start to finish of the transitions can be attributed to the ΔV of

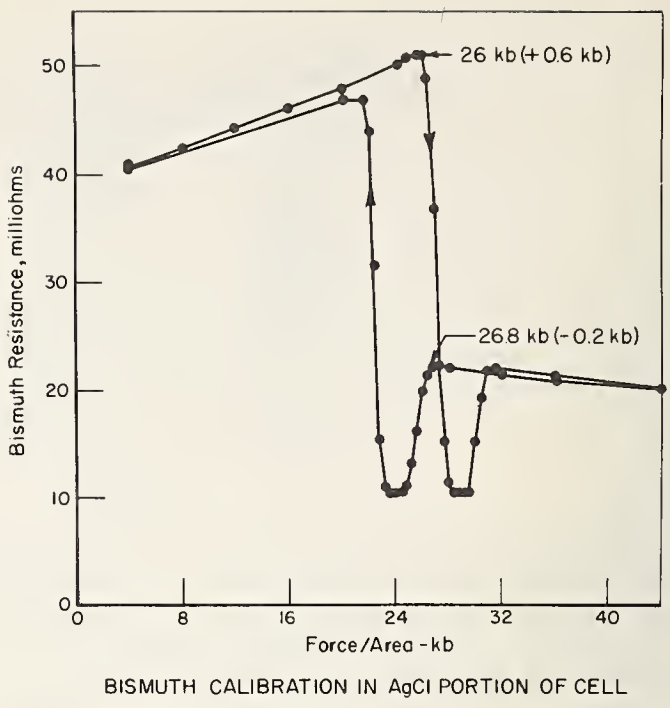

FIGURE 5. *Pressure calibration for* AgCl *column in high-pressure cell.*

transition. As the metal transforms it decreases in volume. The shear strength of the talc is large enough so that pressure must be added to the system to force the talc to follow the bismuth. Boyd and England's [3] result using a 0.033 cm diam Bi wire in 0.32 cm diam AgCl in talc confirm this. Here the smallness of the ΔV of the small bismuth wire and the weakness of the surrounding AgCl cause the ΔP of the transition to be about 1.5 kbar.

Our setup used AgCl as the pressure media. However, it was necessary to protect the thermocouple wires from the reactivity of AgCl, so they were sheathed in BN. BN is stronger than AgCl and therefore reacts to pressure in a similar manner to talc. We quickly found that the diameter of the BN was critical to the ΔP of transition. Figure 3 shows our final configuration with a 1 mm BN sleeve and a 0.3 mm wire. Figure 5 shows the bismuth pressure calibration for this cell with the Bi wire in the 1 mm BN sleeve in the AgCl portion.

The ΔP of transition in this configuration is about 2 kbar and the bismuth $2 \rightarrow 3$ transition completes at 31 kbar force/area. This represents a considerable improvement over the all talc cell originally tried (7 kbar and 44 kbar). In the actual experiment the wire of thermoelectric material does not undergo a ΔV; therefore, the ΔP down the wire is less than 2 kbar. Bridgman has shown AgCl to have a shear strength of 0.8 kbar at 25 kbar. This is the lower limit ΔP to be expected along the AgCl with no BN. Based on measurements made with other diameter BN tubes and the pressure calibrations discussed above, we find the ΔP along the wire in the AgCl to be 1.0 to 1.5 kbar. For figure 4 we have used the value of 1.0 kbar. Using our measurements of pressure drop in the talc portions of the hot and cold end

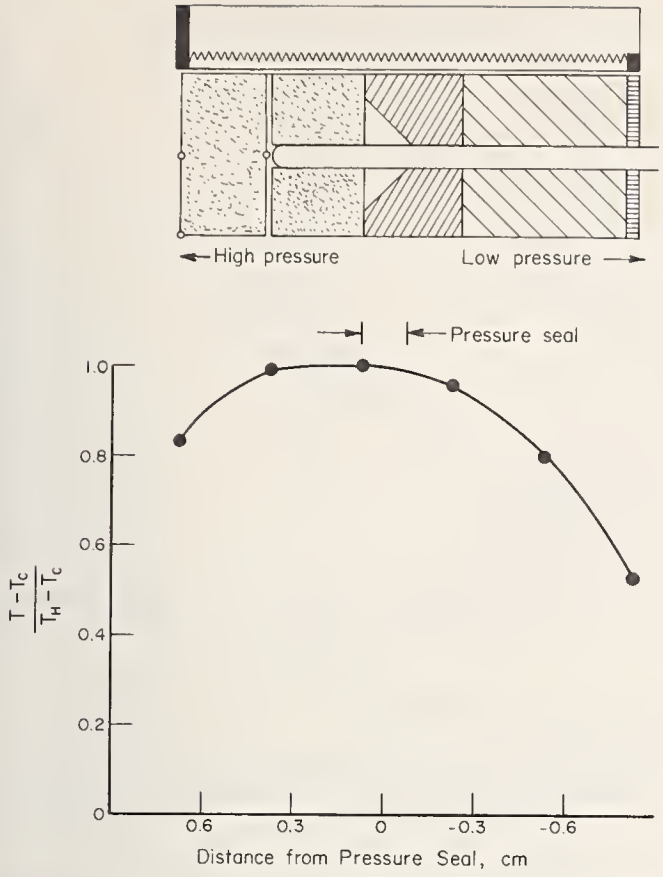

FIGURE 6. *Temperature distribution in the region of the high-temperature seal in the piston cylinder cell.*

of the cell and the similar results of Boyd and England [3], we estimate the ΔP to be 2 kbar in the talc.

Figure 6 shows the temperature calibration for the furnace end of the high-pressure cell. These data were taken in two runs of four thermocouples each; the middle two thermocouples were common to both runs. All the temperature calibration data as well as the experimental data reported in this paper were taken after the cell had been cycled to 40 kbar pressure. It was necessary to do this in order for the temperature calibration to remain constant from run to run and also during a run. This was also useful in checking for failures in the experimental setup.

All the information is shown in figure 4. It is important to notice that the talc portions contribute little to the measurement or its uncertainty and tend to cancel out. The most important effect comes in the AgCl portion of the cell. As long as the pressure and temperature gradients are small or well-known here, the uncertainty of the measurement is small. If the pressure calibrations at room temperature are valid for high temperature the uncertainty of the method is less than 2 percent when the pressure is evaluated in the AgCl portion.

The location of the high-temperature thermocouple is shown in figure 3. Examination of figure 6 shows that this is the location of maximum temperature in the cell. A great deal of care was taken to keep the location of this thermocouple as well as the cold thermocouple in place. The ceramic tube was epoxied to the stainless steel at the start of the experiment. The seal design quickly locked the ceramic tube in place as pressure was applied. All runs were inspected for movement of the thermocouple. This was not a problem at temperatures to 400 °C. We occasionally had movement before using the epoxy but never after; those runs were discarded. It will be necessary to modify the high-temperature seal for work at higher temperatures.

Behind the seal was a tungsten carbide bushing whose I.D. was slightly larger than the ceramic tubing. The high compressive strength of the WC was used to keep the pressure on the wire at 1 atm.

Because the magnitude of the pressure emf's are 10's to 100's of microvolts, it is necessary to measure the voltage to an accuracy of 1μV. Large currents in the vicinity of the thermoelectric element could induce voltages and limit the accuracy of the measurements. AC pickup would require filters, etc. We have specially designed our high-temperature furnace to eliminate or reduce these problems.

The furnace shown in figure 3 is a graphite spiral in the talc. This is accomplished by making a graphite screw which is threaded and cemented into the talc and then has the center machined out. The resistance of our furnace was about 30 Ω. We were able to reach 400 °C with only 3 A current. This low current and coil geometry combine to eliminate problems with induced voltages in the experiment. This is a much more desirable configuration than the solid carbon resistance tube heater normally used in high-pressure experiments.

We have described in detail the high-pressure cell and its calibration, since it is imperative to establish accurately the pressure-temperature distribution within the cell before any valid interpretation of pressure emf's can be made.

2.3. Measurements

2.3.1. Hydrostatic Experiments

Measurements were taken of four thermocouple materials: chromel, alumel, copper, and constantan. The cold seal was maintained at 78 K and the high-temperature seal was maintained at a number of fixed temperatures between 190 K and 560 K. With the temperature interval between the seals fixed, the pressure was varied between 0 and 8 kbar and the induced emf was measured at each pressure. In all cases, the induced emf was linear with pressure so only the slope of the emf versus p plot is presented. To insure that spurious readings generated in the frozen gas seal were not included in the data presented, the emf generated over the smallest temperature interval (i.e., 78 K to 190 K) was subtracted from all the measurements at larger temperature intervals. This eliminated any spurious readings arising from the frozen gas seal, since they would be independent of the temperature of the high-temperature seal. The reproducibility of the

385-762 O - 71 - 6

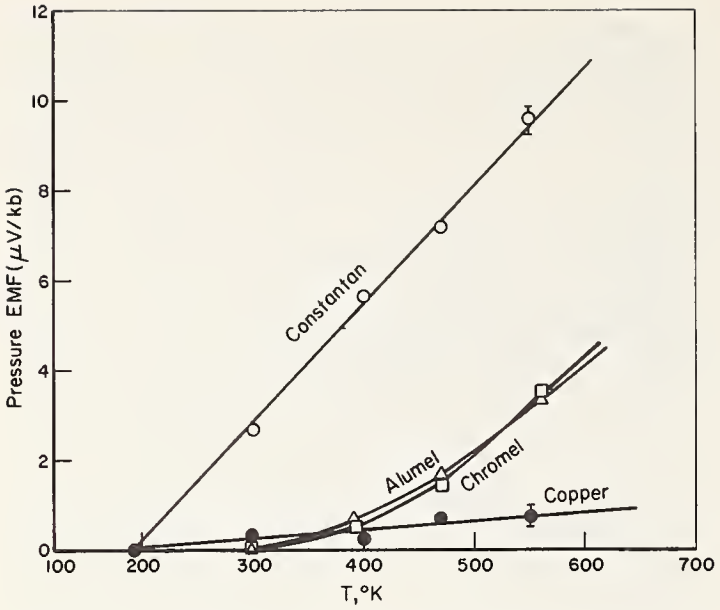

FIGURE 7. *Pressure emf per kilobar for temperature interval 190 K→ T measured in hydrostatic apparatus.*

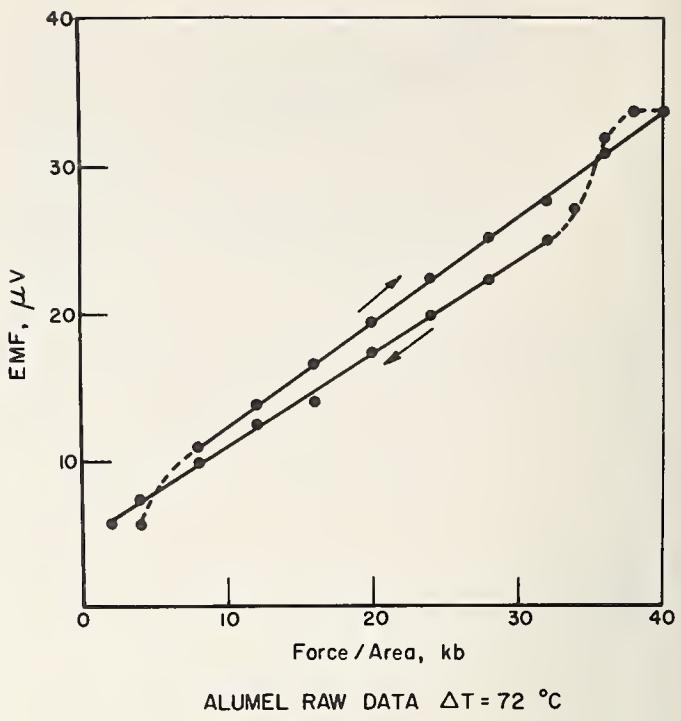

FIGURE 8. *Pressure emf as a function of pressure for alumel at a constant temperature interval in piston cylinder apparatus.*

data showed that if spurious emf's are generated, they were consistent from run to run. The data are therefore presented in figure 7 in terms of the emf per kilobar generated by temperature intervals of 190 K to T where T ranges to 560 K. Scatter in the data introduced an error of ± 0.25 μV/Kbar which is the total error of the measurement.

2.3.2. Piston-Cylinder Experiments

Measurements were made in the piston cylinder apparatus on chromel, alumel, platinum, and platinum-10 percent rhodium wires using the cell described above. Attempts were made initially to fix the pressure and measure the pressure emf as a function of temperature interval between the seals. This method proved to be difficult since the pressure and pressure distribution could not be maintained at a constant value due to thermal expansion of the cell upon heating and a subsequent redistribution of friction forces within the cell. All data reported here were therefore taken as induced emf versus pressure at constant temperature intervals between the hot and cold seal. The agreement between the two sets of data was satisfactory, however.

The pressure on the axis of the cell undergoes an unusual cycle due to the presence of the highly incompressible tungsten carbide column that makes up the high-temperature seal. As the piston advances, the pressure at the top of this column increases rapidly, compared with the pressure in the rest of the cell. This continues until the pressure medium cannot support the stress gradient generated. Further piston advances increase the pressure uniformly throughout the cell. On the pressure release, the opposite effect occurs with the pressure decreasing rapidly at the top of the seal column. This pressure cycle will exhibit the opposite of the

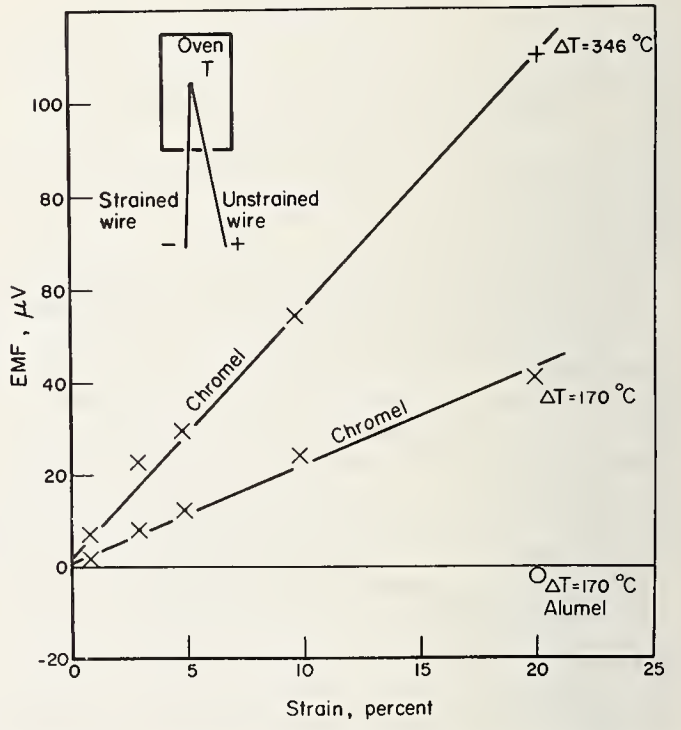

FIGURE 9. *Effect of strain on the thermal emf of chromel thermocouple wire.*

normal hysteresis cycle of a piston cylinder. Figure 8 shows the pressure emf for alumel at a fixed temperature interval between the seals as a function of the piston pressure. The reverse hysteresis effect is quite apparent.

Another effect was found when the chromel wire was measured. At zero pressure a negative emf was measured in the circuit with a fixed temperature difference maintained between the seals. The effect

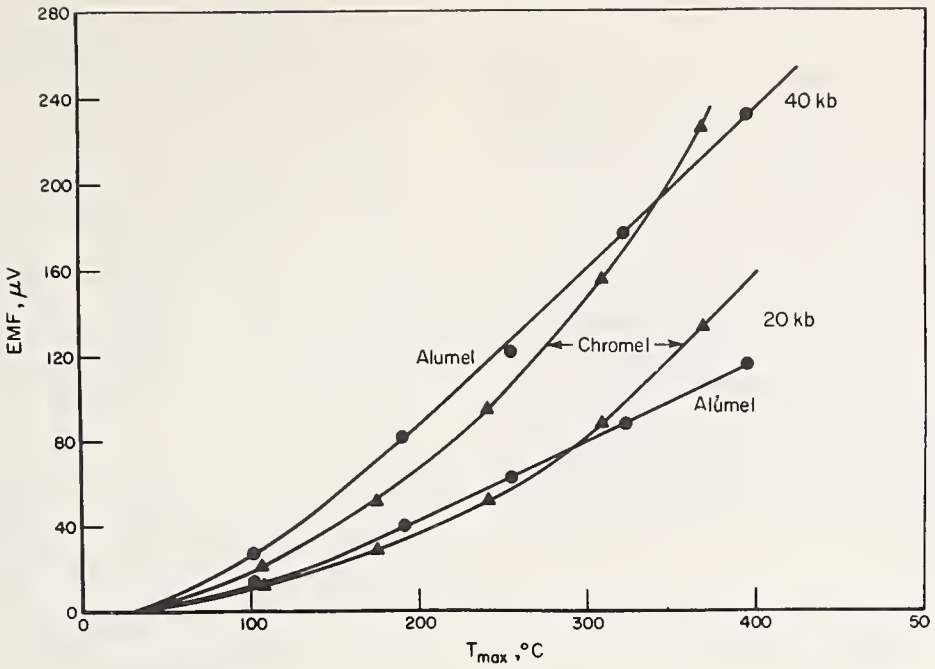

FIGURE 10. *Chromel and alumel pressure emf as a function of temperature interval at 20 kbar and 40 kbar.*

of pressure was to decrease this negative emf toward zero. It was found that chromel wire is quite strain sensitive and that in preparation it had been strained slightly. Tests were made using a strained and unstrained chromel wire as a couple. Figure 9 shows that the resulting emf is a linear function of permanent strain and is about linear in temperature difference. Similar strain tests were made with the alumel, platinum, and platinum-10 percent rhodium wire, but no measurable strain-induced emf was detected. Hanneman and Strong [4] have reported that they found no measurable strain-induced emf for all four materials. Our experiments show that chromel is strain sensitive.

In solid-media, high-pressure apparatus, the methods used to bring leads out of a high-pressure cell generally result in a high degree of permanent deformation of the lead wires. Therefore, caution should be used when using chromel-alumel couples, since an emf can be induced by the strain effects of the chromel. However, the amount of temperature correction is small, compared with the total emf of the couple. For instance, if a gradient of 350 °C exists across a 10 percent strained wire, the resulting error would be only 1.5 °C. To minimize this error, the high-pressure cell should be designed so that regions of high strain are in regions of low-temperature gradient.

Measurements were taken over a temperature range 30 to 400 °C and a pressure range of 0 to 40 kbar. The pressure dependence of the emf was obtained from the raw data, e.g., as shown in figure 8, using only the data where apparatus friction effects were known. These would correspond to the straight-line sections in figure 8. On the compression

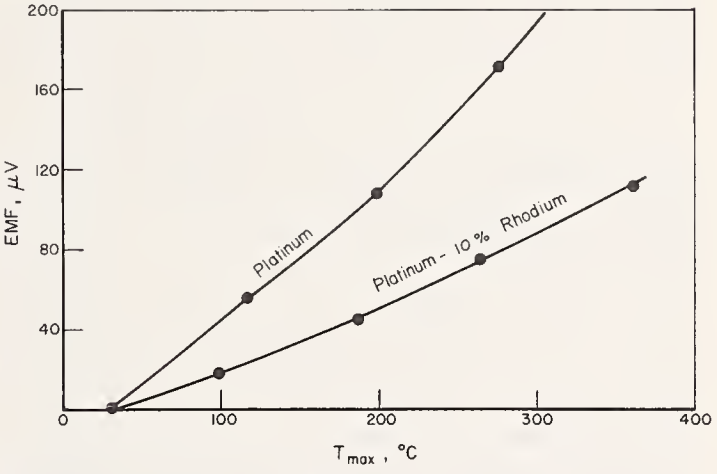

FIGURE 11. *Platinum and platinum 10 percent rhodium pressure emf as a finction of temperature interval at 40 kbar.*

curve this gives data to the highest pressures and on the release curve gives data to the lowest pressure. The curves rarely went through the origin as they should. This was attributed to apparatus friction and/or small spurious emf's in the circuit. This offset from zero was always small except for the chromel. The chromel offsets from 0 emf at 0 pressure could be accounted for by the above mentioned strain effects.

The curves were first displaced so that they went through the origin. The compression and decompression curves were then corrected for the compression and decompression values of the bismuth transitions. These results were averaged to give the final curve of emf versus pressure at a fixed temperature interval. During the experimental cycle ΔT drifted somewhat. Each individual experimental

point was corrected to a constant ΔT before the above data reduction was made.

For all temperature intervals, the cold seal was at a temperature above 30 °C. Therefore an additional correction to the final curves was made so that they would all correspond to temperature intervals of 30 °C $\rightarrow T$.

In general data were taken at ΔT's of approximately 75 °C, 150 °C, 200 °C, 275 °C, 325 °C for each material with about 20 pressure data points at each temperature. We estimate the uncertainty of the data in the piston cylinder experiments to be approximately 5 percent. This results from differences in the compression and release data. Added to the 2 percent error in the area determination of $p(T)$ versus T plots, we believe that the measurements are good to ± 7 percent.

3. Results and Discussion

The hydrostatic pressure results are given in figure 7 for the four materials investigated. The induced emf for a fixed temperature interval was found to be a linear function of pressure for all four materials within the accuracy of the measurements (0.25 μV/kbar). For the copper and constantan wires, the induced emf per kilobar was also a linear function of temperature interval up to an interval of 190 to 560 K. On the other hand, the induced emf per kilobar for chromel and alumel was zero between 190 and 300 K, and then increased nonlinearly above 300 K. Values of emf are considered positive when the low-temperature seal side of the circuit in figure 1b is positive.

The piston cylinder results are given in figure 10 for chromel and alumel and in figure 11 for platinum and platinum-10 percent rhodium. It was found that over the temperature intervals investigated alumel and platinum had a pressure emf at constant temperature intervals which was linear with pressure up to 40 kbar. A nonlinear pressure dependence was found for Pt10Rh and chromel, both of which became less sensitive to pressure at higher pressure. Due to this nonlinear pressure dependence, the results are also tabulated in table 1.

The comparison between the piston cylinder results and hydrostatic results on the chromel and alumel wires indicates the two methods give the same results within the experimental error. For a temperature interval of 30 to 300 °C the piston cylinder results at 10 kbar show a pressure emf of 39 ± 3 μV for alumel and 43 ± 3 μV for chromel, while the hydrostatic results if extrapolated from 8 kbar to 10 kbar yield 36 ± 3 μV for alumel and 39 ± 3 μV for chromel. Also, it is seen that over this temperature-pressure range the pressure emf of chromel is equal to that of alumel within the experimental error for both the hydrostatic experiment and the piston cylinder experiment. This shows that the two methods of measuring the pressure emf give consistent results.

TABLE 1. *Pressure emf (μV) for temperature interval 30° → T (°C) of pressurized wire*

T, °C	10 kbar	20 kbar	30 kbar	40 kbar
		alumel		
100	6	13	18	26
200	21	43	63	86
300	39	78	117	157
400	58	117	174	234
		chromel		
100	5	10	14	19
200	20	37	53	68
300	43	82	119	148
400	87	165	226	280
		(chromel)-(alumel)		
100	−1	−3	−4	−7
200	−1	−6	−10	−18
300	+4	+4	+2	−9
400	+29	+48	+52	+46
		platinum		
100	12	23	34	46
200	28	57	84	114
300	45	90	135	181
400	62	124	186	248
		platinum 10 percent rhodium		
100	5	11	16	20
200	14	27	38	50
300	25	48	68	90
400	35	72	105	130
		(Pt10Rh)-(Pt)		
100	−7	−12	−18	−26
200	−14	−30	−46	−64
300	−20	−42	−67	−91
400	−27	−52	−81	−118

Other measurements are available for comparison with our results, but we will only comment in general about them.

Bundy's [5] single-wire experiment gave consistently higher emf values than ours for alumel, platinum, and platinum 10 percent rhodium. His chromel value was negative which was probably the result of the strain effect described above.

Bloch and Chaissé [6] measured Cu-Constantan hydrostatically and their results agree with ours

within our experimental error of $\pm .25$ μV/kbar.

Bridgman's [7] single-wire experiments on constantan and copper yielded pressure emf's which were the same as ours within our experimental error.

The comparative measurements of Hanneman and Strong [4] on Pt-Pt10Rh versus chromel-alumel couples at 40 kbar with a temperature interval of 0 to 400 °C are within 10 percent of our results. Their absolute values [8] for Pt-Pt10Rh are higher than our values by 30 percent which is outside of their stated experimental limits. In addition their chromel-alumel corrections are positive while ours are negative.

Of the results presented at this conference, our results are most easily compared with those of Getting and Kennedy [2]. The agreement is within experimental errors for Pt, Pt10Rh, and alumel. For chromel, their results are lower than ours by a significant amount (the order of 30 percent at 20 kbar and $\Delta T = 0 - 400$ °C). It appears that the strain effect described above could be the cause of this discrepancy. However, our hydrostatic results are in agreement with our piston cylinder data within an error limit of ± 7 percent. Since no strain effects are present under the hydrostatic conditions, the agreement of our two sets of data indicates our piston-cylinder chromel data to be more accurate than that of Getting and Kennedy.

4. Conclusions

We have only discussed the data, and the data gathering procedure so far, but have not described how to use the data. In the introduction, eq (3) shows that as the result of the pressure dependence of the thermoelectric power, an additional emf is generated in a thermocouple circuit if the pressurized region is in a region of changing temperature. It was also shown that single-wire experiments could measure directly the amount of additional emf generated. To utilize the single-wire results, one must know the temperature of the thermocouple junction in the high-pressure cell and the temperature of the seal where the pressure drops to zero. The internal temperature is measured by the uncorrected emf generated in the two-wire circuit. This temperature is the uncorrected temperature, but for purposes of determining the amount of the correction, it is accurate enough. The seal temperature must be determined independently and in the case of certain belt and piston cylinder cell designs, this temperature can be considerably higher than ambient. Thus, having established the temperature interval from seal to high-temperature region (it is the temperature interval which is needed, not just the difference) and having established the pressure, one can determine the amount of additional emf induced in the thermocouple circuit from an isobaric plot of pressure emf vs. temperature interval, such as figures 10 and 11 or table 1. The total emf induced in the thermocouple pair is just the difference between the two pressure emf's. The sign convention here is important. The pressure emf is positive if the high-pressure seal at the low-temperature side of the single-wire circuit is positive. This is the case for all materials we measured. The pressure emf for the wire of the pair which is negative (constantan, alumel, platinum) is subtracted from the pressure emf of the wire which is positive (copper, chromel, platinum, 10 percent rhodium). The resulting emf is subtracted from (or added to, if it is negative) the measured emf of the circuit to arrive at the zero pressure emf which can be converted to temperature from a standard table. By adopting this convention, no ambiguity will result when applying the pressure correction. By leaving the corrections in terms of emf values instead of temperature values, one can easily apply the correction needed for his particular high pressure cell with its own particular seal temperature, reference temperature, and thermocouple materials.

Although the data presented in this work are over a limited temperature range, we have determined a region of pressure and temperature where well-defined experimental conditions were established and where pressure emf's were measured to an accuracy needed for precision thermocouple applications.

5. References

[1] Hanneman, R. E., and Strong, H. M., J. Appl. Phys. **36**, 523 (1965).

[2] Getting, I. C., and Kennedy, G. C., The Effect of Pressure on the EMF of the Thermocouple, this volume.

[3] Boyd, F. R., and England, J. L., J. Geophys. Res. **65**, 741 (1960).

[4] Hanneman, R. E., and Strong, H. M., J. Appl. Phys. **37**, 612 (1966).

[5] Bundy, F. P., J. Appl. Phys. **32**, 483 (1961).

[6] Bloch, D., and Chaissé, F., J. Appl. Phys. **38**, 409 (1967).

[7] Bridgman, P. W., Proc. Am. Acad. Arts. Sci. **53**, 269 (1918).

[8] Bundy, F. P., A Critical Review of the Effect of Pressure on Thermocouple EMF's, this volume.

The Effect of Pressure on the E.M.F. of Thermocouples

Ivan C. Getting and George C. Kennedy

Institute of Geophysics and Planetary Physics,
University of California, Los Angeles, California 90024

A schematic diagram of a thermocouple as installed in a typical high-pressure apparatus is shown in figure 1. There is, of course, no effect on the reading of a thermocouple if the temperature of a thermocouple junction at high pressure is the same as the temperature at which the elements emerge from the high-pressure environment to the low-pressure environment. However, in many installations, the temperature at which the thermocouple emerges from the high-pressure environment is vastly different than the temperature of the thermocouple junction. Thus substantial effects on the emf of the thermocouples may be expected. Pressure thus creates various thermocouple junctions between compressed and uncompressed segments of the thermocouple elements.

Both Bridgman and Bundy have examined the emf generated by a thermocouple of compressed and uncompressed segments of the same wire. However, these measurements have been taken to modest limits of temperature and pressure. It was the aim of the present investigation to carry the measurements on to very high pressures and temperatures.

In our experiments a tungsten carbide bushing with a small axial hole was used to hold pressure off the test wires over part of their length so that the emf of a compressed-uncompressed thermocouple could be measured. A furnace was used to heat the junction. Compressed-uncompressed junction temperatures were measured with separate thermocouples. Our measurements were limited by the pressures and temperatures at which the tungsten carbide sleeve failed. This experiment, which we call the single-wire experiment, is shown schematically in figure 2 and a detailed drawing of our experimental arrangement is shown in figure 3. The emf of various wires thus can be measured and the results combined algebraically to give the correction for a thermocouple made of any two elements at high pressures with a junction at one temperature and pressure seal at a different temperature.

Our experiments were conducted in an end-loaded piston-cylinder apparatus to a maximum pressure of 30 kbars and a temperature of 1000°. A coaxial graphite resistance heating element was used to heat the junction of the compressed versus uncompressed wire under study. It is, of course, necessary to show that the pressure drop across the junction is isothermal and the zones of temperature drop

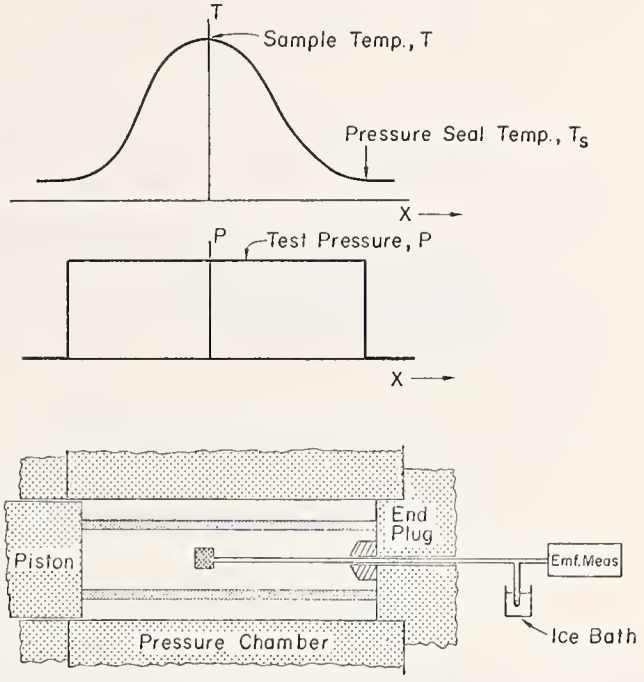

FIGURE 1. *Schematic view of typical high-pressure cell with temperature and pressure distributions.*

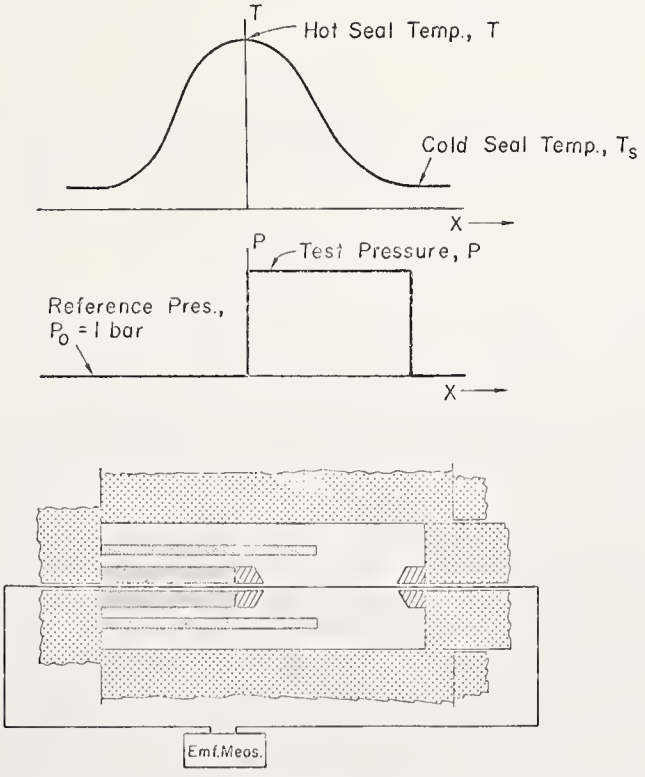

FIGURE 2. *Schematic view of single-wire experiment cell with temperature and pressure distributions.*

Paper presented at the Symposium on Accurate Characterization of the High-Pressure Environment, held at the National Bureau of Standards, Gaithersburg, Md., October 14–18, 1968.

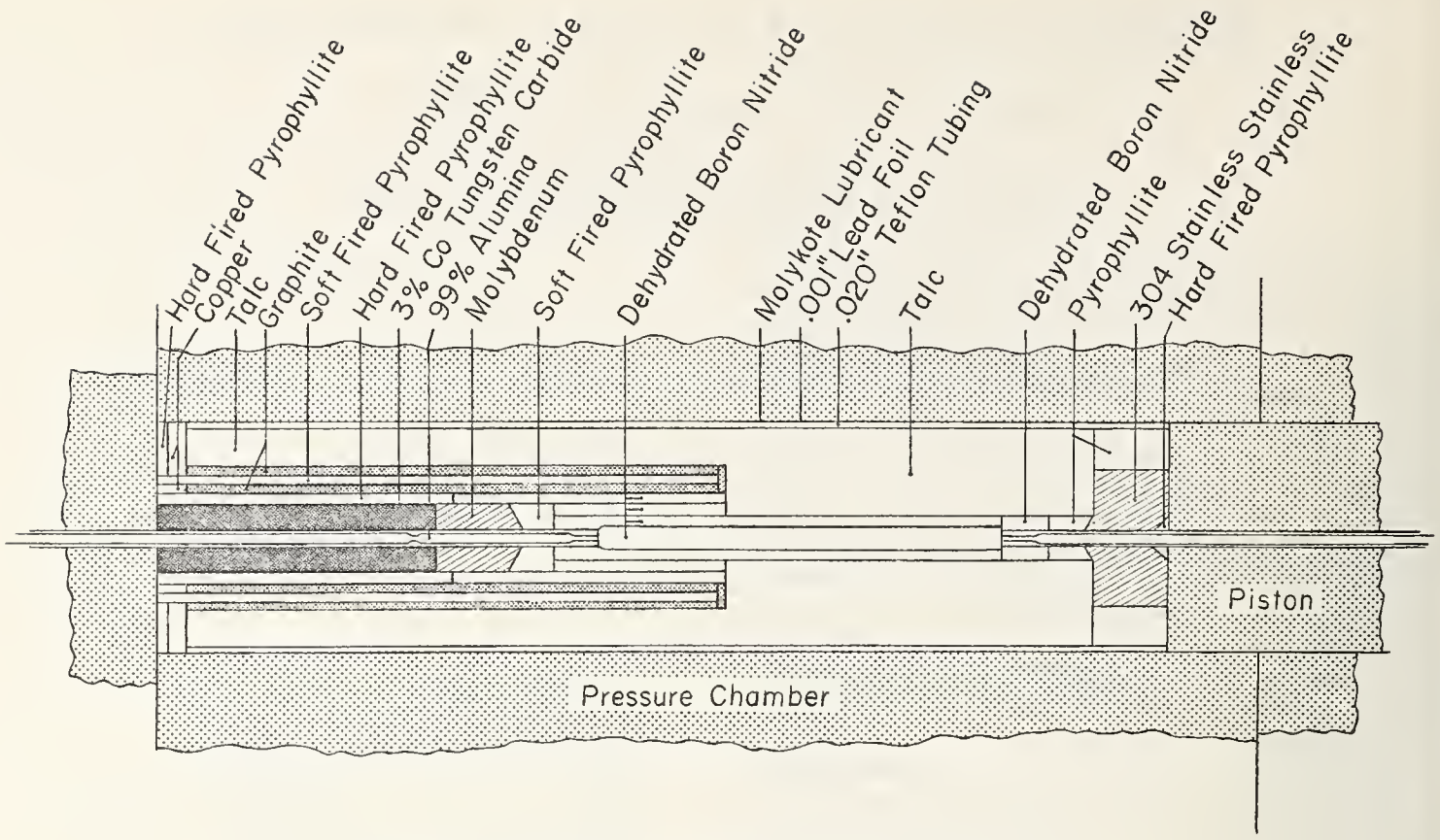

FIGURE 3. *Detailed view of single-wire experiment pressure cell.*

inside the cell are isobaric. Thus, six thermocouples not shown in figure 3, were located in two groups of three spanning the seal regions. It was shown that the temperature variation across the seals was less than 3 percent of the hot seal temperature. Bi I-II transition experiments at room temperature led to an expected 3-kb maximum pressure difference within the cell.

In figure 4 we show experimental results at 10, 20, and 30 kbars up to temparatures of 900°. These results are the plots of the emf generated by single-wire experiments on platinum minus the emf generated by the single-wire experiments on platinum-10 rhodium.

The temperature axis shown in figure 4 represents the difference in temperature between the hot junction of a thermocouple and the temperature where the thermocouple wires merge from the high-pressure apparatus. In our particular apparatus, when the hot temperature junction is at 1000° the cool seal, where the thermocouple emerges from the high-pressure apparatus, is at approximately 100 °C. The data are corrected for this rise in seal temperature and the results are presented in figure 5.

In most high-pressure apparatus, the seal temperature rises as the sample temperature rises. If the relation between these two temperatures is known, the correction for the effect of pressure in the thermocouple may be determined as shown in figure 6. In the example shown in figure 6, we assume a sample temperature of 800°, 30 kbars, and a seal temperature of 150°. The voltage correction applicable is the difference between the value at 800° and

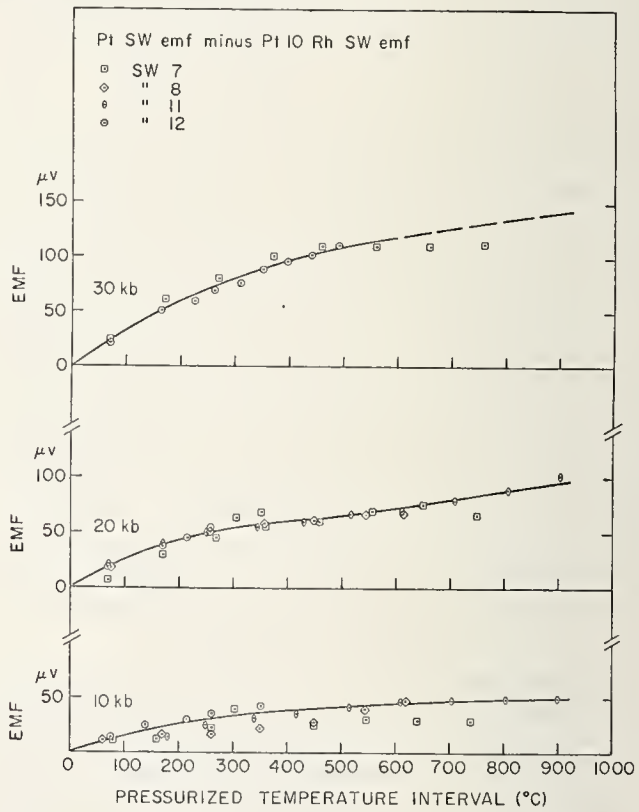

FIGURE 4. *Pt S.W. emf minus Pt 10 Rh S.W. emf.*

150°, here 110μV. To obtain the correction in degrees, the voltage correction must be divided by the relative Seeback coefficient at 800°, 10.8μV/°C. The correction is to be added to the observed value. The pressure seal temperature must be known for every

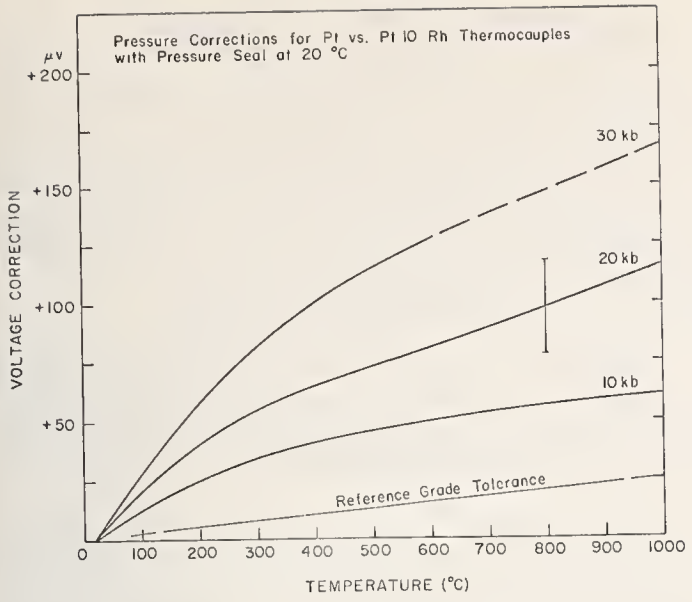

FIGURE 5. *Pressure corrections for Pt vs. Pt 10 Rh thermocouples with pressure seal at 20 °C.*

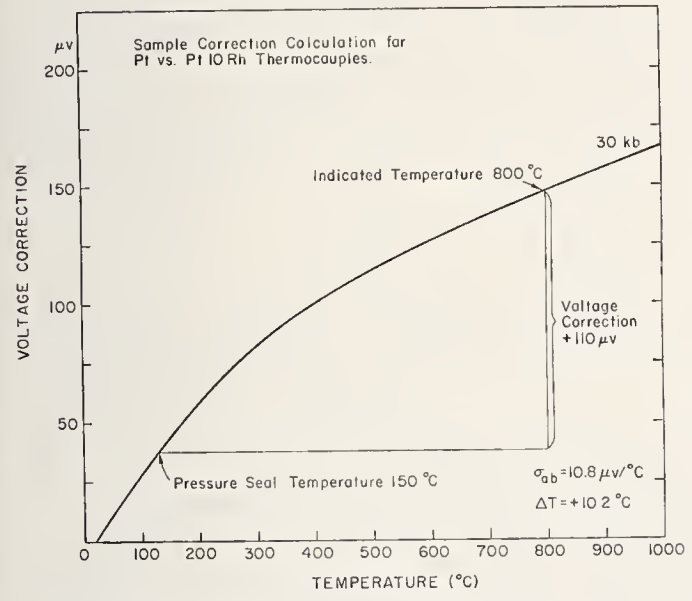

FIGURE 6. *Sample correction calculation for Pt vs. Pt 10 Rh thermocouples.*

temperature measurement to which these corrections are to be applied. Data for Chromel and Alumel thermocouple wires are shown in figure 7. Here, as before, the data presented are the algebraic differences between the voltages observed in single wire experiments on each of the two thermoelements. Unfortunately, in some of the runs chemical contamination of the thermocouple elements took place. These erratic readings are also presented. The solid curves are drawn through results believed to be from runs where no contamination took place. A smooth plot with the pressure correction for Chromel-P versus Alumel thermocouples with the pressure seal at 20° is shown in figure 8. The relative Seeback coefficient for Chromel/Alumel is nearly constant at about 40μV/°. Thus, for temperatures up to about

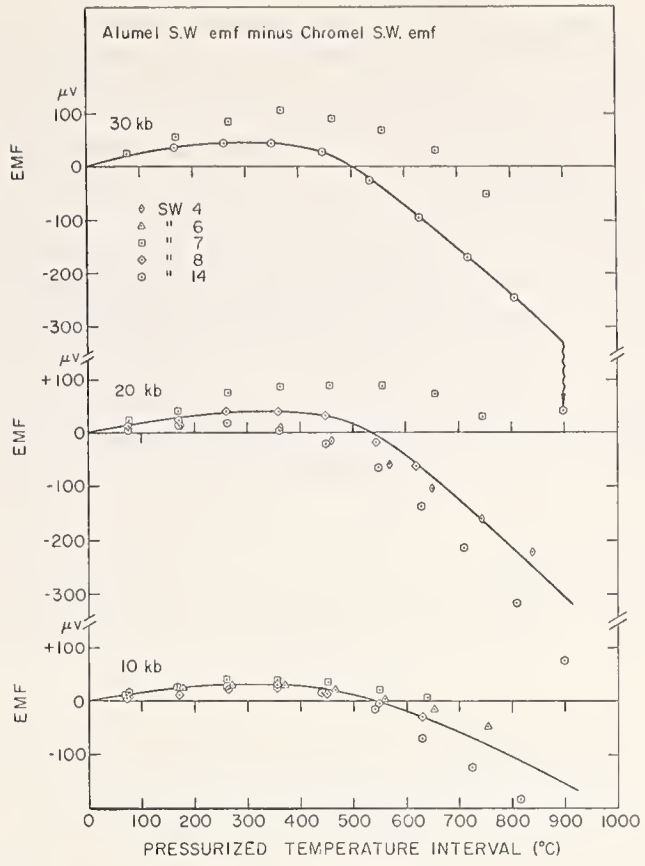

FIGURE 7. *Alumel S. W. emf minus Chromel S. W. emf.*

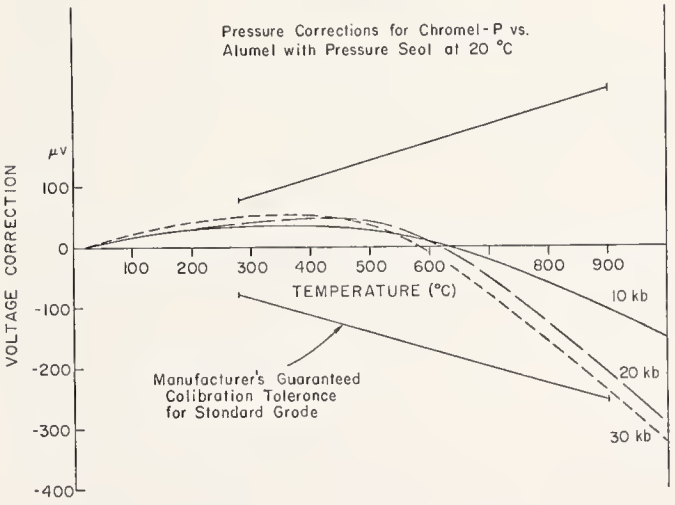

FIGURE 8. *Pressure corrections for Chromel-P vs. Alumel with pressure seal at 20 °C.*

600°, the corrections for Chromel-Alumel thermocouples are less than 2°. For pressure seal temperatures other than 20° the corrections are calculated by the same method demonstrated in figure 6.

Because of some uncertainties in the pressure of the experiment and uncertainties in the temperature as well as a small temperature gradient to the pressure seal we estimate a maximum certainty in the final corrections to be about ±3° at the highest pressures and temperatures of the measurement. Proportionately the uncertainty is less at lower values.

In typical high-pressure experiments where ceramic tubes surround the thermal elements, stress distribution can make the corrections uncertain by very much larger amounts. In a number of our runs, grossly non-hydrostatic conditions were noted along the thermocouple wire where bits of ceramic tubing pressed against the wire or alternatively protected the wire from pressure. Thus, if precise temperature measurements are made at high-pressure, care must be taken to insure pressure uniformity along the thermocouple wires in the high-pressure environment. Chemical deterioration of the thermocouple wires can often introduce error several magnitudes greater than the error introduced by ignoring the effect of pressure on the thermocouple.

As a final check on the accuracy of these measurements, we intercompared platinum-10 rhodium thermocouples with Chromel-Alumel thermocouples at high pressures and temperatures. We find the difference in the reading of the two thermocouples in our intercomparison experiment to agree with the corrections we indicate for these thermocouple pairs within the stated uncertainty of the measurements.

Note added in press

Subsequent work on this problem has led to a slight revision of the data presented herein. A complete discussion of the experiment and the revised data are presented in J. Appl. Phys. Oct. 1970.

Temperature Measurement by Thermal Noise at High Pressures

R. H. Wentorf, Jr.

General Electric Research and Development Center, P.O. Box 8, Schenectady, New York 12309

The temperature of a small carbon resistor (700 to 3,000 Ω) in a high-pressure cell next to a Pt-Pt10 percent Rh thermocouple was measured by thermal noise. Runs were made at 40 and 50 kbar to temperatures of about 1,400 K. The results suggest that at the highest temperatures the thermocouple indicated temperatures from 40 to 60 K too low, in fairly good agreement with estimates made by other methods.

1. Introduction

Many interesting phenomena occur at high temperatures and high pressures, e.g., 1,500 K and 50 kilobars (kbar). However, it is difficult to determine pressure and temperature accurately at these conditions. [1][1]

One can mention two ways to determine the temperature inside a high-pressure chamber:

(1) One method is based on the equipartition of energy. The thermal agitation of the current carriers in an isolated resistor generates at its terminals a minute, fluctuating voltage known as thermal or "Johnson" noise [2, 3].

One may write:

$$\overline{E^2} = 4\,kTRB \qquad (1)$$

where $\overline{E^2}$ is the average of the square of the fluctuating voltage due to thermal agitation,

k is Boltzmann's constant,

T is the absolute temperature,

R is the value of the resistance,

B is the bandwidth of the frequencies for which E is measured; the frequencies are generally below 10^{14}Hz (optical).

Although it is simple in principle, the method demands careful attention to experimental details and it is not so convenient. Garrison and Lawson [4] demonstrated that the method could be used at high pressures.

(2) One might measure temperature by means of thermocouples. This common and simple method has some limitations. Apart from the annoyances of broken or corroded wires, one notes that metals change their electronic characteristics with pressure, and so the emf of a thermocouple depends on the pressure and temperature system to which it is exposed. A satisfactory theoretical treatment of this problem has not yet appeared, but several workers have made experimental measurements at moderate pressures or temperatures [5, 6, 7, 8, 9]. Hanneman and Strong [10] have estimated the effects of pressure on common thermocouples for more severe conditions.

One of the aims of the work reported in this paper is to measure the same temperature simultaneously by methods (1) and (2) and thereby help determine the effect of pressure on thermoelectricity.

2. Experimental Considerations

2.1. General

The apparatus was intended to provide a stable Pt-Pt10 percent Rh thermocouple at essentially the same pressure and temperature as a suitably isolated resistor whose Johnson noise could be amplified and measured. The temperature of the probe resistor could then be estimated by using eq (1), assuming that the observation period was long enough to obtain a sufficiently precise value of E^2.

Equation (1) could be used directly if one had an ideal noiseless amplifier of known, stable gain. For real, noisy amplifiers with somewhat unsteady gain, it is better to compare the signal from the probe resistor with that from a reference resistor which is at a known temperature and has the same resistance as the probe.

The amplifier noise (the first stage contributes the most) is simply added to the noise from the probe resistor; the sum appears in the output and is called $\overline{AE2}$ (amplified average E^2). Thus a plot of $\overline{AE2}$ versus T is linear, as shown in figure 1 for various values of the probe resistor R. The intercept at $T=0$ is the amplifier noise when the probe is at 0 K. For an ideal but noisy amplifier the intercepts for various R's would coincide and the slopes would be proportional to R. The amplifier used in this work was not ideal, for reasons to be given later, and so the intercepts did not coincide at $T=0$ and the slopes were not quite proportional to R because the effective bandwidth B changed with R. However, one still had the important linear relationship between T and $\overline{AE2}$ for a given R.

Thus the following experimental information was necessary to determine the temperature of the probe:

[1] Figures in brackets indicate the literature references at the end of this paper.

Paper presented at the Symposium on Accurate Characterization of the High-Pressure Environment, held at the National Bureau of Standards, Gaithersburg, Md., October 14–18, 1968.

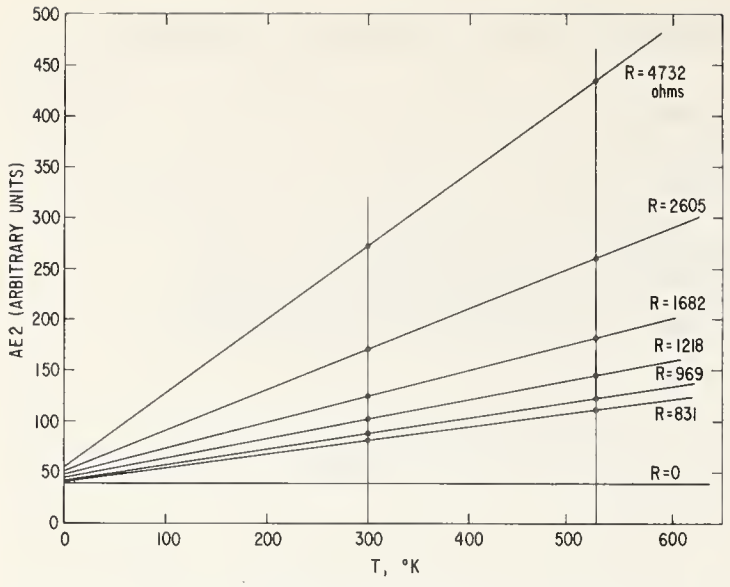

FIGURE 1. *Plot of* $\overline{AE2}$ *versus* T *for various probe resistances from 831 to 4732* Ω.

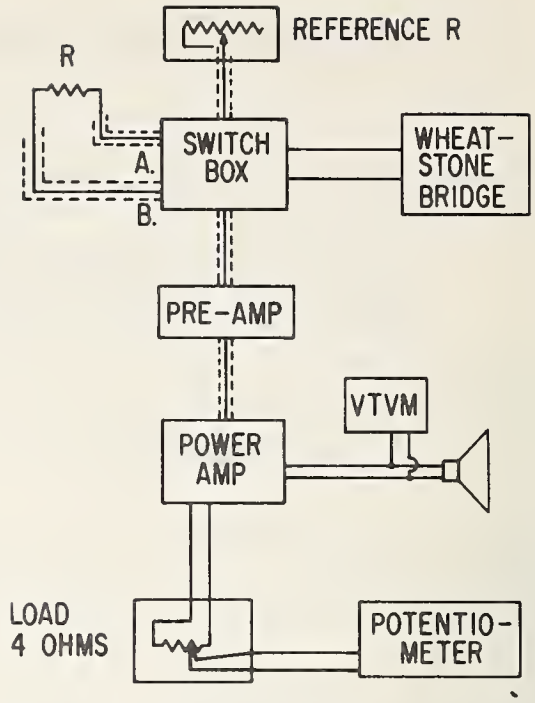

FIGURE 2. *Block diagram of amplifier and detector.*

(a) The resistance R of the probe;

(b) The amplifier output $\overline{AE2}$, averaged over a sufficiently long time, with the probe at the input;

(c) $\overline{AE2}$, with reference resistor, resistance R, at input;

(d) The temperature of the reference resistor (usually near 300 K);

(e) $\overline{AE2}$ with shorted input ($R=0$) to monitor the amplifier gain over periods of hours;

(f) A high probability that only a negligible amount of external noise had been included in $\overline{AE2}$ during the measurements of (a) through (e) above. External noise comes and goes, substantially independently of the experimenter's desires, and so one always seeks the minimum $\overline{AE2}$ values out of a large number of observations.

Figure 2 is a block diagram of the amplifier and switching arrangements used in this work. One can read about them in greater detail further along in the paper.

2.2. The Value of *R*

Consider eq (1) and let $R=1{,}000\ \Omega$, $T=1{,}000$ K, and $B=5\times10^4$. Then E^2 is about 2.8×10^{-12} V^2, and we can expect to deal with signals in the range 1 to 2 μV. Larger signals could be obtained from larger resistances, but there are practical limits:

1. The shunt capacitance of the system, of the order of 50×10^{-12} farad (F).

2. The finite input impedance of the amplifier.

3. Inside a high-pressure chamber the volume which is approximately isothermal is limited and subject to various stresses. Long, thick wires are impossible.

4. The resistor must be an electrically passive element and tolerably isolated from its surroundings. Available insulating materials at 1,500 K have maximum resistivities of about 10^6 ohm-cm and so can provide isolation of $10^6-10^7\ \Omega$.

Evidently many factors conspire to limit R to less than 5,000 Ω. For the range 100 to 10^5 Hz, it is difficult to achieve amplifiers with less noise than that of 500 ohms at 300 K. Thus suitable values of R appear to lie between 500 and 5,000 Ω. In this work values of R from 600 to 3,000 Ω were used.

2.3. The Value of *B*

Several factors limit the frequency band:

1. At frequencies above about 200 kHz one has problems with tuned circuits, stray capacitance, and feedback.

2. Ubiquitous 60 Hz power line frequencies and their harmonics make it wise to ignore frequencies below about 1,000 Hz.

3. The Miller effect operates to reduce the input impedance of the amplifier and/or limit the amplification of higher frequencies unless tuned circuits are used.

4. The time constants of the resistor used to measure $\overline{AE2}$ demand a small resistance which in turn demands a transformer to feed it; broad-band transformers do not operate too well above 100 kHz.

Thus the value of B comes to slightly less than 10^5 Hz. In this work the amplifiers used made the effective range for B to lie between 2 kHz and about 80 kHz; the cutoffs at eaeh end were not perfectly sharp but were more than 6 dB/octave.

The relative uncertainty in $\overline{AE2}$ is given by $(Bt)^{-1/2}$ where t is the observation time [4]. For $B=6\times10^5$, an observation time of 5 sec corresponds to an uncertainty of about 0.6×10^{-3}, i.e., 1 degree out of 1,500, which is well below the uncertainties from other causes.

3. Experimental Apparatus

3.1. The High-Pressure Sample

Figure 3 shows a sample arrangement which proved satisfactory. (Several other kinds were tried.) It fits in a "Belt" apparatus [11] with 19-mm-diam piston faces.

The probe resistor, R, begins life as a strip of Saran (polyvinyl chloride) about 0.013 mm thick, 0.13 mm wide, and 25 mm long. It is carbonized *in situ* at about 40 kbar to yield a resistance in the range 500 to 5,000 Ω, typically 1,000 Ω. The working length of the resistor is about 7.5 mm, well inside the walls of the heater tube, H. A rod of fused silica about 7.5 mm long and 0.36 mm diam lies alongside the Saran and fixes the working length. Two 0.25 mm platinum wires, a and b, butt against each end of the silica rod and connect the ends of the resistor to two 0.50-mm Formex-coated copper wires, A and B, which pass through the compressible stone gasket, F, to the outside. The Saran, silica, and parts of wires a and b lie in a Lucalox (Al_2O_3) tube about 0.38 mm I.D., 1.5 mm O.D., and 19 mm long. This tube is the most important electrical insulating barrier between the resistor R and the heater tube H. The Lucalox tube fits snugly inside a porcelain tube 2.5 mm O.D. and 19 mm long. This tube shields the Lucalox tube against mechanical intrusion of material from the heater H as the sample is crushed and sheared during compression and temperature changes. The two tubes are labeled I in figure 3.

The Pt-Pt10 percent Rh thermocouple is made from 0.25-mm wires c and d with the junction in the heated zone at J. Wires c and d lie in tubes of Lucalox and porcelain like the resistor, to help J be at the same temperature as the resistor. The 0.5-mm Pt and Pt10 percent Rh wires C and D pass through the gasket and connect c and d to a 0 °C cold junction and a Rubicon potentiometer. The thermocouple gave very little trouble.

The various tubes, etc. are carried at the midlength of a cylindrical sample holder PS, about 24 mm long and 19 mm diam, made of pyrophllite previously fired in air to about 750 °C to remove much of the water, etc., in the pyrophyllite which would attack the procelain and Lucalox at high temperatures. The heater tube H is pressed from a mixture of graphite and hexagonal BN (1:2 by weight), so that its hot resistance is about 0.15 Ω. It is about 24 mm long, 9.2 mm I.D., and 10.5 mm O.D. Copper disks 0.25 mm thick carry the heating current from the pistons. Inside the heater is a rod, PC, of fired pyrophyllite. After PC, H, and PS were assembled, two parallel holes 2.5 mm in diameter and 0.45 mm apart were bored through the assembly at the midlength to receive the various tubes, and then the wires, etc., could be inserted and fixed.

The heater tube H was heated by direct current from a bank of 12-V storage batteries via an adjustable series resistor. Electrolysis effects on the heater and pyrophyllite were negligible.

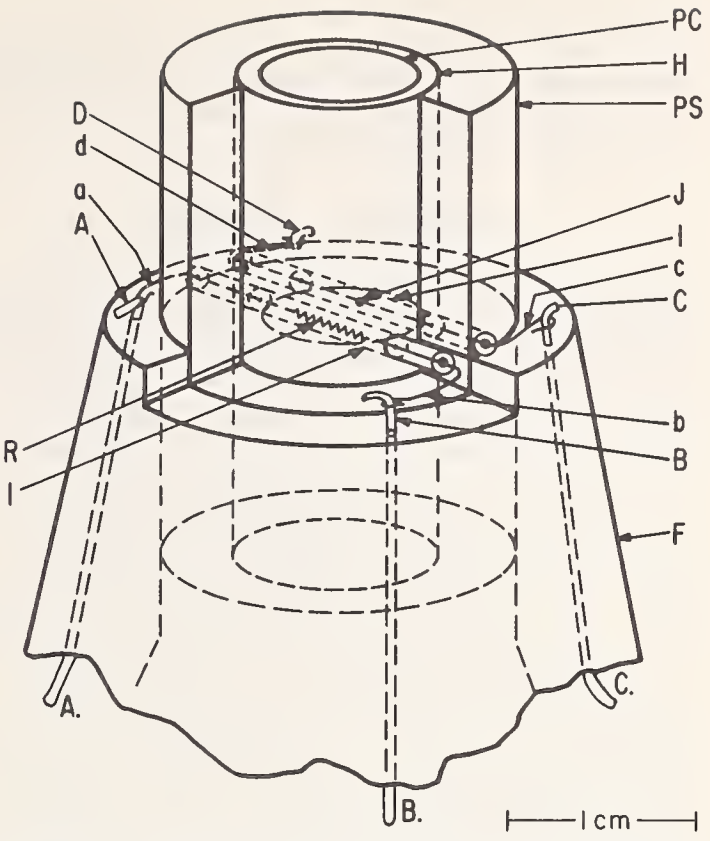

FIGURE 3. *High-pressure cell containing probe resistor (leads* A, B) *and thermocouple (leads* C, D).

The maximum furnace temperatures used were about 1,450 K. At temperatures much above this, the electrical isolation of the resistor was unsatisfactory, partly because of the enhanced conductivity of the insulation at high temperatures and partly because of the disruptions and intrusions from thermal expansion forces.

Leads A and B were connected by low-capacity coaxial cable to the switch box. Either A or B could be connected to ground of the system. The top piston (and hence the heater tube), the pressure chamber cyliner, and the press frame were also connected to ground. (The pistons are ordinarily insulated from the press frame by about 10^7 Ω.) Thus the probe resistor R had good electrostatic shielding. The resistance between lead A or B and the heater tube could be measured during a run by temporarily disconnecting the ground to the heater circuit. The resistance between A or B and ground was measured for every data point; any persistent differences indicated faulty isolation of R. (A portion of the voltage drop along the heater tube was then acting to bias the wheatstone bridge.) $\overline{AE2}$ was also measured for either lead A or lead B grounded, and persistent differences in these readings or wild, unsteady variations in $\overline{AE2}$ also indicated faulty isolation of R. Such data points were ignored.

The thermocouple leads C and D went to an ice bath where they joined copper wires to a Rubicon potentiometer. Usually lead D was grounded as a safeguard against feedback oscillation of the amplifier. The resistance between D and the heater tube

could be measured to insure that the thermocouple was suitably isolated, but the low resistance of the thermocouple wire reduces its isolation requirements below that of the probe resistor, and thermocouple isolation was not a problem.

3.2. Reference Resistor

The reference resistor was made of four rotary adjustable carbon strip resistors with resistances of 10 KΩ, 5 KΩ, 1 KΩ, and 500 Ω. They were connected in series and any reference value between 0 and 16,500 Ω could be selected with the aid of the wheatstone bridge. The resistors were mounted in a small aluminum box and connected to the switchbox by a piece of low-capacity coaxial cable having about the same length as that used to connect leads *A* and *B*, and adjusted so that the shunt capacity across the reference closely matched that across the probe. The reference temperature was read from a calibrated thermometer next to the box.

For calibration purposes, such as constructing the straight lines of figure 1, a number of metal film resistors on alumina cores were placed in a cavity in an aluminum block, together with a calibrated Pt-Pt10 percent Rh thermocouple, and heated over a gas flame to about 525 K maximum. A cool switch at the end of a stainless steel tube permitted one to select various resistances. This assembly replaced the probe *R* for calibration experiments.

3.3. Pre-amplifier

Figure 4 gives a circuit diagram of the pre-amplifier. It was built inside a small aluminum box and operated while buried in dry ice (195 K). Its dynamic input impedance, as determined by the value of input series resistance needed to reduce the output by half, went as follows:

kHz	5	10	20	50	60	80	100
kΩ	220	220	260	210	120	75	52

Cooling the pre-amplifier from 300 K to 195 K reduced the shorted input noise by 25 percent and increased the gain by about 10 percent with negligible effect on the bandwidth. The small input capacitor and the dynamic input impedance caused the amplifier gain spectrum to vary somewhat with input (probe) resistance.

3.4. Power Amplifier

3.4.1. First Section

A schematic diagram of the first section of the power amplifier is given in figure 5. A 1-μV signal at the pre-amplifier input appeared as a 0.1-V signal at the output of the first section of the power amplifier.

3.4.2. Second Section

A schematic diagram of the second (final) section of the power amplifier is shown in figure 6. This amplifier delivered a signal of about 1.5-W maximum to a 4-ohm output load resistor, to provide the $\overline{AE2}$ power in the detector described below. The output transformer must be of high quality to provide good frequency response.

3.5. Detector

If the fluctuating output voltage is impressed across a resistor, then the power dissipated in the resistor is proportional to $\overline{E^2}$ or $\overline{AE2}$. The power appears as heat, and a suitable resistor can thus be heated and its temperature measured by means of a thermocouple attached to the resistor.

A suitable resistor-thermocouple detector for this work was made from 0.13-mm-diam chromel and

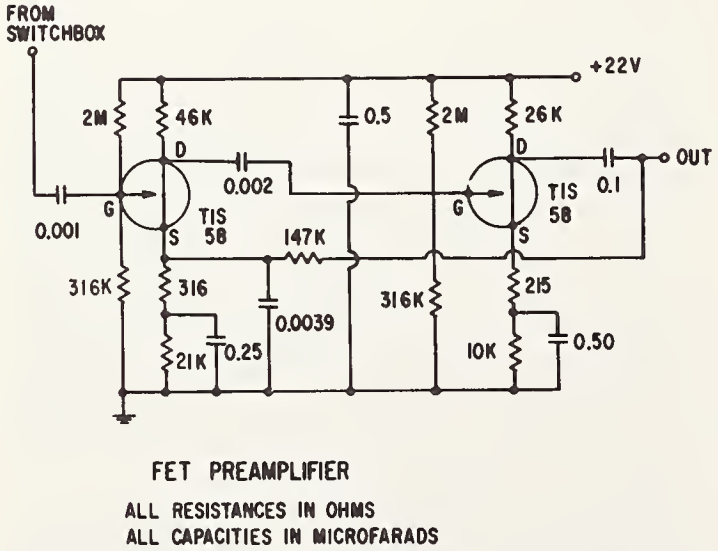

FIGURE 4. *Preamplifier.*
All resistances in ohms. All capacities in microfarads.

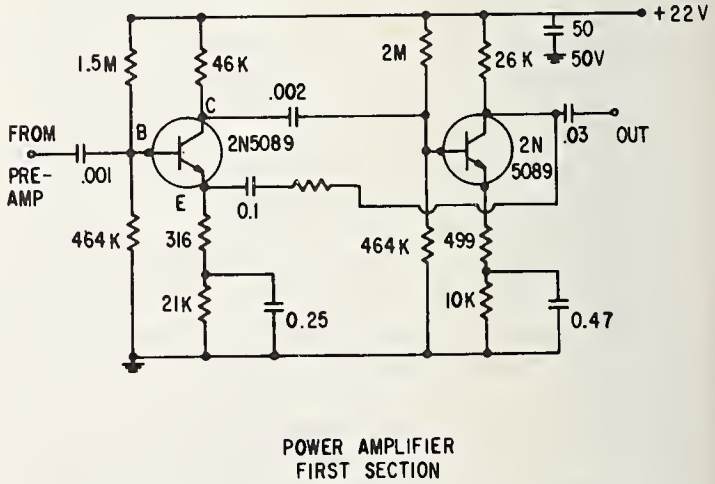

FIGURE 5. *Power amplifier, first section.*
All resistances in ohms. All capacities in microfarads.

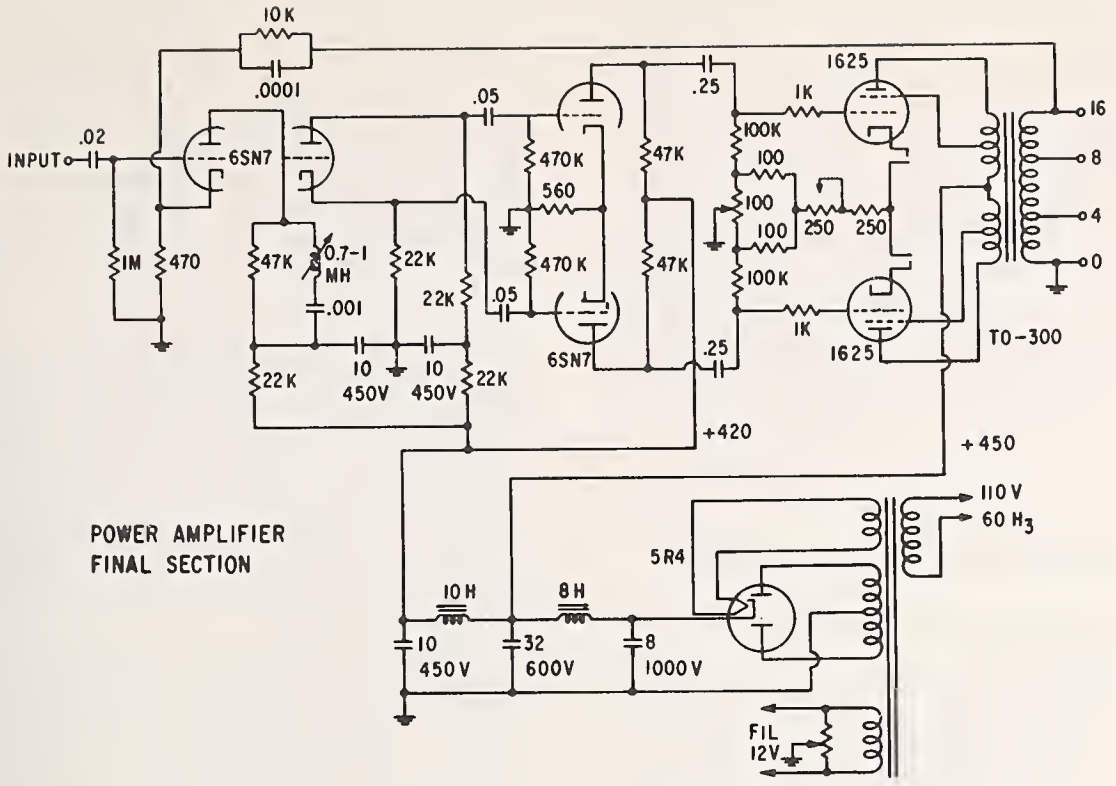

FIGURE 6. *Power amplifier, final section.*
All resistances in ohms. All capacities in microfarads.

alumel wires. Three pieces of chromel wire and one of alumel were fused together at one end in a small bead. A chromel-alumel pair was taken out as a thermocouple and the remaining chromel pair was wound non-inductively into a small helix with the bead inserted partway into the core of the helix so that the bead would be as hot as possible. The chromel pair was about 50 mm long and had a resistance of about 4 Ω. The ends of all four wires were soldered to terminals bolted through an aluminum plate and insulated from it by mica washers. The aluminum plate formed part of a sealed can which was immersed in an ice bath. Thus the resistor dissipated its heat to a sink at constant temperature and the thermocouple cold junction was kept at 0 °C. The can was electrically grounded.

The chromel wire load resistor was connected to the output of the power amplifier in series with a 100-μF capacitor. The potentiometer which measured the emf of the thermocouple was connected in series with a 1-H, 60-Ω choke. In this way the potentiometer was isolated from the amplifier.

This resistor-thermocouple detector had a thermal half-life of about 5 sec, a desirable value for both accuracy and waiting time in the presence of ambient noise, etc. Two were made and calibrated with the direct current heating, using the average of both current directions to cancel the effect of a small voltage drop across the thermocouple bead. The maximum calibration temperature was about 350 °C, produced by about 1 W, and in use the resistor temperature never exceeded about 230 °C, except when one detector was decisively incinerated by throwing the wrong switch.

3.6. Calibration of the Entire Electronic Apparatus

As remarked in section 2, a plot of $\overline{AE^2}$ versus T should be linear, and the slope of the line should depend upon R. Various practical considerations made it necessary to work with an imperfect amplifier and so the slope of the line was not exactly proportional to R. However, the dependence upon R was obtained in a series of experiments done at 1 atm with hot resistors having resistances in the range 831 to 4730 Ω at temperatures up to about 525 K, as mentioned in section 3.2. When the probe resistor and the reference resistor, both at one atmosphere, were at the same temperature, one could determine the small effects, e.g., 0.1 percent for 1600 Ω, of the slightly greater shunt capacitances for the probe—the noise from the probe was slightly less than expected. The noise measurements from the hot probes were used to construct the lines of figure 1. The ratio of line slope to resistance decreased by about 2.0 percent upon going from 830 to 4,730 Ω, in agreement with a simple circuit analysis and the measured dynamic input impedance of the amplifier.

A second type of calibration was performed as the last step in a high-pressure run after the pressure on

the probe resistor had been reduced to about 2 kbar. At this pressure the thermocouple error due to pressure is very small, and noise measurements could be obtained on the actual resistor which had been used at high pressure. The mechanical strains of decompression followed by heating limited the temperatures attainable with satisfactory isolation to about 1,000 K, and usually the probe resistance was much higher than it had been at high pressures, but these measurements permitted estimates of the effective shunt capacitance of the probe resistor as well as a partial check on the slope of the $\overline{AE2}$ versus T line and the performance of the amplifier and detector.

4. Experimental Procedure

4.1. Pressure Calibration

The pressures existing inside the high-pressure cell of figure 3 were estimated from the oil pressure driving the press ram pushing the pistons of the Belt apparatus. The apparatus was calibrated at room temperature by reference to the resistance transition in thallium at 36.7 ± 0.3 kbar. It was also calibrated at higher cell temperatures by comparing the emf of a Fe-Pt, 10 percent Rh couple with that of a Pt-Pt, 10 percent Rh couple according to the method of Strong et al. [12]. This method permits one to detect the $\alpha - \gamma$ transition in iron in the range 40 to 50 kbar at temperatures of about 900 K. The cold and warm calibrations agreed well for 40 kbar, but differed by a few kilobars at 50 kbar. There is much evidence of several kinds which indicates that the pressure inside a pyrophyllite cell changes in complicated ways in response to temperature changes, and so the actual pressure in the hot cells is not known to within 2 or 3 kbar. Further comments on this problem appear in section 6.

4.2. Gathering Noise Data

After the sample shown in figure 3 had been assembled and placed in the high-pressure apparatus, the pressure was increased to about 40 kbar and then the sample was slowly heated by direct current to reach about 1,350 K in 1 to 2 hr. Thereby the Saran strip was pyrolyzed and its resistance fell to something less than 3,000 Ω. After that the drift in resistance was slow enough to permit noise temperature measurements.

The noise temperature measurements were made in the following way. At some pressure and heating power level, after probe resistance and the cell thermocouple temperature became relatively steady, one could roughly balance the potentiometer which read the output resistor thermocouple temperature (which was related to $\overline{AE2}$), and then watch the galvanometer pointer on the potentiometer as it swung in response to the thermal noise signal and other electrical disturbances. In the absence of disturbances, the galvanometer pointer asymptotically approached a rest position according to the 5-sec thermal half-life of the output resistor, so that 30 sec of freedom from electrical disturbance was ample to establish a minimum emf value for the output resistor temperature.

Usually the disturbances were caused by switches, relays, commutating motors, ignition, etc., operating in other parts of the building. Some periods of the week were quieter than others, but disturbances were abundant even at midnight. The disturbances usually added about 1 percent to the output thermocouple emf, but not in a systematic way. The loudspeaker on the output helped one identify periods of intense disturbance during which measurement attempts were futile.

Usually 5 to 15 min of observation sufficed to establish the minimum output thermocouple emf between disturbances. Once this had been established, the Pt-Rh thermocouple emf and the probe resistance could be determined in about 15 secs; these two changed relatively slowly. Next the reference resistor was adjusted to the same resistance as the probe, and the output resistor thermocouple emf was determined for it. Fortunately this circuit was not so sensitive to disturbances. Finally the output resistor thermocouple emf was measured with the preamplifier input shorted, to monitor the amplifier behavior.

Following these steps, the probe resistor connections were reversed by means of the switchbox, e.g., lead A of the probe was grounded instead of lead B, and the foregoing procedure was essentially repeated. If all was well, the two sets of measurements were in substantial agreement, after allowing for slight changes in cell heating power. If the probe resistor was poorly isolated, the two sets of measurements did not usually agree very well and were ignored.

From time to time the resistances between probe and heater tube or between thermocouple and heater tube could be determined as a check on the isolation, and the reference resistor temperature was noted.

Thus one accumulated a number of values of output resistor thermocouple emfs, Pt-Rh thermocouple emfs, and probe resistances for various cell pressures and heating power levels.

The data were gathered first at a pressure of about 40 kbar and with falling temperature steps; then at 25 °C the pressure was increased to about 50 kbar and the temperature was increased in steps to a maximum (usually limited by isolation failure) and then decreased in steps (with improving isolation) to room temperature. Finally the pressure was reduced to a few kilobars and the temperature was raised and lowered as described in section 3.6.

4.3. Reduction of Data

The first step in obtaining useful information from the data was to convert all good output resistor thermocouple readings into $AE2$ values using the relationship determined by the calibration with direct current heating of the output load resistor.

Next, one took into account the effect of probe resistance on the slope of the line of $AE2$ versus T. (See fig. 1 and section 2.6.)

One also made small corrections to allow for the differences in shunt capacitance between probe and reference resistor, on the basis of the room temperature high-pressure data and the low-pressure, high-temperature data, for both of which the pressure corrections to thermocouples are negligible.

Finally one estimated the probe temperature using the linearity of the relationship between $AE2$ and T for each particular value of R observed. I.e., one knew two points on the straight line for a particular R and determined the T corresponding to a given $AE2$ on that line. The closer T is to the reference resistor temperature, the more accurately it can be fixed because the uncertainty in the slope of the line affects it less.

5. Results

Three satisfactory high-pressure runs occurred. The results are summarized in figure 7, for 40 kbar and falling T only, and in figure 8, for 50 kbar and rising and falling T. In these two figures the abscissa is the uncorrected temperature which one would obtain from the emf of a Pt-Pt, 10 percent Rh thermocouple, according to standard reference tables, without allowing for pressure effects, and the ordinate is the difference between the temperature estimated from thermal noise and the uncorrected Pt-Pt, 10 percent Rh temperature. The temperature estimated from thermal noise was always higher than that indicated by the uncorrected thermocouple. As noted in section 6.1.2 the effect of combined pressure and temperature gradients is to make the pressure corrections (the ordinates of figs. 7 and 8) from 5 to 10 percent too low.

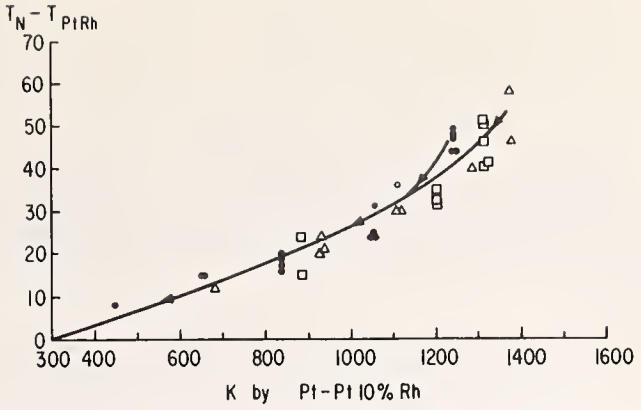

FIGURE 7. *Thermal noise estimated temperature minus Pt-Pt 10 percent Rh indicated temperature, versus Pt-Rh indicated temperature at 40 kbar; falling* T *only.*

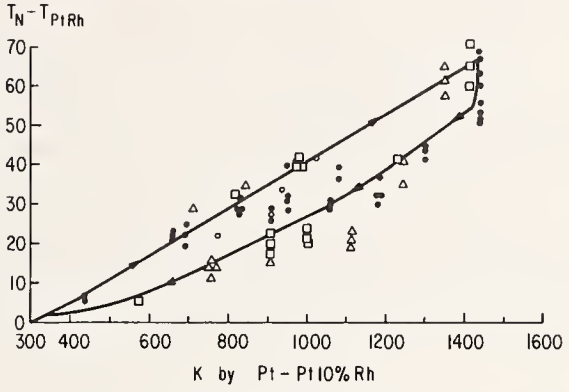

FIGURE 8. *Thermal noise estimated temperature minus Pt-Pt 10 percent Rh indicated temperature, versus Pt-Rh indicated temperature at 50 kbar.*

The upper line is for increasing temperature; the lower line is for decreasing temperature.

6. Discussion

6.1. Errors

6.1.1. Fluctuation Errors

The scatter of the points in figures 7 and 8 indicates that the experimental conditions were not as constant as one might have hoped in view of the pains taken. The scatter is associated with the use of high-pressure apparatus; at one atmosphere and 500 K the scatter in temperature estimation was about 1 K. The most probable causes for this scatter are the long-term (several hours) variations in ambient electrical noise, the variations in cell pressure resulting from temperature changes, and slight variations in cell construction.

Past experience with high-pressure, high-temperature reaction vessels has shown that the actual pressure in the cell depends on its pressure and thermal history [13]. The data indicate that the Pt-Rh thermocouple experienced a higher pressure during a slight temperature increase than it did during a temperature decrease, i.e., the thermocouple correction (ordinate of figs. 7 and 8) was larger for a slight increase in temperature. The points of figures 7 and 8 also indicate this same effect on a broad scale in that the thermocouple correction is generally larger for the ascending temperature path than for the descending path, so that the points fall on a rough loop instead of a line.

Even though as much care as possible was used during the construction of a cell, variations of from 0.2 to 0.4 mm in the positions of various elements were possible. Furthermore, one should not expect a cell made of such a wide variety of materials to compress in a uniform manner; instead, erratic motions are likely.

The emf of a thermocouple may be affected by the amount of cold work it suffers. Variations of

385-762 O - 71 - 7

several degrees in the indicated temperature may be produced by this effect [9, 14].

6.1.2. Systematic Errors

A likely cause for systematic error which can not be detected by general examination of the data is the generation of spurious extra noise by current flowing through the probe resistor due to imperfect isolation.

Such current noise power is generally inversely proportional to frequency and is not too important above 100 kHz. For most carbon resistors one expects about 1.5 μV per applied volt for the range 1 kHz to 100 kHz. In the high-pressure cell, if the isolation resistance is 100 times the probe resistance, e.g., 100 kΩ, and the spurious driving voltage is 1 percent of the total of 10 V, then the voltage on the probe available to produce current noise is about 10^{-4} V. The current noise would then produce about $1.5 \times 10^{-4}\,\mu$V of noise compared with the thermal noise of about 1.7 μV. But power, not voltage, is to be added or compared; on this basis the current noise contribution would be less than 10^{-8} of the thermal noise. Even if the probe resistor developed 100 times the usual current noise voltage, the contribution of current noise would be less than 10^{-4} of the total.

The above considerations notwithstanding, when the isolation resistance failed at high temperatures, the noise from the probe suddenly increased and became extremely erratic. It was not possible to measure the emf of the output resistor thermocouple because the galvanometer in the potentiometer was too restless.

Therefore it appears likely that extra current noise from the probe resistor was certainly not important below 1,000 K where the isolation resistance was excellent; and was probably not important up to the highest temperatures for which results are given in this paper.

In an ideal measurement of the effect of pressure on a thermocouple, the temperature gradient occurs at constant pressure and the pressure gradient occurs at constant temperature [6]. In the apparatus used in this work these ideal conditions did not occur. As figure 3 indicates, the thermocouple wires *C* and *D* experience the bulk of the temperature fall along their radial portions. At the internal joint where the wires begin to travel vertically in the gasket, the temperature was at most 250 °C, judging from the decomposition of traces of glue used in assembly. In this radial portion the pressure on the wires probably changes by less than 2 kbar, if other types of experiments are used as a guide. In their vertical travel through the gasket the wires encounter the major pressure drop to one atmosphere in a region having a temperature of about 70 to 100 °C when the hot junction is at about 1,400 K. The wire temperature finally drops to about 25 °C while the wires are at one atmosphere.

These considerations indicate that the ideal correction to a Pt-Pt, 10 percent Rh thermocouple for the effect of pressure would be somewhat larger than indicated in figures 7 and 8, probably 5 to 10 percent larger, because only about 90 to 95 percent of the temperature drop in the wires occurred at high pressure.

6.2. Comparison With Other Work

As mentioned in the Introduction, some work has been done on the effect of pressure on thermocouples at more moderate conditions of pressure or temperature than attempted here.

The Work of Bundy [6] shows that at a pressure of 50 kbar and a temperature of 100 °C, the Pt-Pt 10 percent Rh couple should indicate a temperature which is about 6 °C too cool. The present work agrees satisfactorily with this previous finding.

The work of Bell, Boyd, and England [8] carried out to temperatures of about 500 °C at pressures of 5 kbar shows that a Pt-Pt, 10 percent Rh thermocouple at 500 °C and 5 kbar should indicate a temperature which is about 3 °C too cool.

Freud and Lamori [9] estimate from their work that at 40 kbar and 300 °C the Pt-Pt 10 percent Rh thermocouple should read about 13 °C too low. This work is in satisfactory agreement.

The work of Getting (1968) shows that a Pt-Pt, 10 percent Rh thermocouple at 600 °C and 30 kbar should indicate a temperature which is about 13 °C too cool. This is about two-thirds the correction estimated from the present work.

Hanneman and Strong [10] and Bundy [14] considered a number of experimental phenomena at high pressures and temperatures such as diffusion in metals, melting curves of metals such as germanium, gold, iron, etc., and phase equilibria such as $\alpha - \gamma$ Fe and diamond-graphite to construct a self-consistent set of pressure corrections to thermocouples. Their estimates and the results of the thermal noise work in this paper are in fairly good agreement. E.g., for a pressure of 50 kbar and a temperature of 1,370 K, the foregoing authors estimate a correction of 47 K; the average correction found by the thermal noise method for the same nominal conditions is about 60 K. At 40 kbar and 1,270 K the foregoing authors estimate a correction of 36 K, and 40 K was found in the present work.

It appears that the present work is in satisfactory agreement with results found by other or earlier workers; the thermal noise temperature estimates tend to be somewhat higher, in agreement with the expectation that undetected extra noise may have been added to the thermal noise signal from the hot probe.

7. References

[1] Dachille, F., and Roy, R., Chapt. 9 of Modern Very High Pressure Techniques, R. H. Wentorf, ed. (Butterworths, Washington, 1962).

[2] Johnson, J. B., Phys. Rev. **32**, 97–109 (1928).
[3] Bell, D. A., Electrical Noise (Van Nostrand, London, 1960).
[4] Garrison, J. B., and Lawson, A. W., Rev. Sci. Instr. **20**, 785–794 (1949).
[5] Bridgman, P. W., Proc. Am. Acad. Arts Sci. **53**, 269 (1918). Or see his collected papers (Harvard, 1964).
[6] Bundy, F. P., J. Appl. Phys. **32**, 483–488 (1961).
[7] Getting, I. C., and Kennedy, G. C., The effect of pressure on the E.M.F. of the thermocouple, paper presented at this meeting.
[8] Bell, P. M., Boyd, F. R., and England, J. L., The effect of pressure on the thermal emf of the platinum/platinum 10 percent rhodium thermocouple, paper presented at this meeting.
[9] Freud, P. J., and LaMori, P. N., The effect of pressure on thermoelectric power of thermocouple materials, paper presented at this meeting.
[10] Hanneman, R. E. and Strong, H. M., J. Appl. Phys. **36**, 523 (1965); *Ibid.*, **37**, 612 (1966).
[11] Hall, H. T., Rev. Sci. Instr. **31**, 125 (1960).
[12] Strong, H. M., and Bundy, F. P., The use of iron and gold for calibration of higher pressure and temperature points, Report No. 68–C–402, General Electric R&D Center, Schenectady, N.Y. Paper presented at this meeting.
[13] Strong, H. M., Chapt. 5 in Modern Very High Pressure Techniques, R. H. Wentorf, ed. (Butterworths, Washington, 1962).
[14] Hanneman, R. E., Strong, H. M., and Bundy, F. P., A critical review of the effect of pressure on thermocouple Emf's, Report No. 68–C–367, General Electric R&D Center, Schenectady, N.Y. Paper presented at this meeting.

DISCUSSION

H. T. Hall (*Brigham Young University, Provo, Utah*): Are your results on corrections that are to be applied to platinum-platinum rhodium couples consistent with other results of your laboratory and with results of other laboratories?

I. Getting (*Institute of Geophysics and Planetary Physics, University of California, Los Angeles, California*): May I suggest that if you used a dc heater there is a likelihood of dc pickup on the thermocouple. We tried the Bridgman single-wire experiment with a dc furnace only once, due to unsatisfactory results from this cause.

Question from the floor: Does the insulating material surrounding the resistor have any effect on the noise voltage?

M. Waxman (*National Bureau of Standards, Washington, D.C.*): What is the ac loading on the noise resistor?

Would you comment on the integrating time, and describe the power fluctuations?

AUTHOR'S CLOSURE

On the question of agreement with results of others, the corrections I found agree pretty well with estimates of Hanneman and Strong, but are about 50 percent larger than Getting has found. I think that my results may tend to be high because of the extraneous noise from the environment, but I don't think they are 50 percent too high.

I was aware of the problem of dc pickup, and the data from one run was discarded because of this. However, I monitored the resistance between the thermocouple and the heater, and between the noise resistor and the heater and, at 1400 °C, these resistances were usually of the order of 10^5 to 10^6 Ω. The key to this high resistance was the use of a very pure shielded alumina insulator (Lucalox). I think that this is one of the best materials available.

The insulating material has no effect on the noise voltage because it is not carrying any current. While the insulating material does comprise a resistor in parallel with the noise resistor, they are both at the same temperature, and the only effect is that the resistance of the combination is slightly lower than that of the noise resistor alone.

The ac loading of the noise resistor depends, of course, on the preamplifier input impedance, and was of the order of 50,000 Ω. This affects the slope of the calibration curves, and requires a separate curve, done at low pressure, for each resistance range.

On the matter of integrating time, the time constant of the circuit was such as to give an integrating time of about 5 seconds. However, random fluctuations due to extraneous causes often required observations to be made over a period of 15 minutes or more in order to obtain three measurements, say, that had the same minimum, so that the integrating time might really be of the order of 10 to 20 seconds.

Chairman: G. E. DUVALL
Washington State University
Seattle, Washington

Equations of State for Sodium and Aluminum

D. John Pastine and M. J. Carroll

U.S. Naval Ordnance Laboratory,
White Oak, Silver Spring, Maryland 20910

Equations of state are calculated for sodium and aluminum. In each case this is done by first calculating the 0 K isotherm and then adding the thermal contributions to the pressure. The calculations in both cases are theoretical and very few experimental data are used. Comparisons of theoretical prediction and experimental data are very favorable.

1. Introduction

It seems wise to initiate any equation-of-state calculation with a general expression for the specific Helmholtz free energy, A. For, by this procedure, one can at least ascertain what it is that he must know to go further. Accordingly, since this article treats two elemental metals in the solid state, we will begin by writing the general equilibrium expression

$$A = A_0 + A_{\text{q.h.}} + A_{\text{a.h.}} \tag{1}$$

This equation is a legacy of statistical mechanics [1][1] and it is very helpful because it makes an orderly separation between three distinct contributions to A. In eq (1) A_0 is the total specific Helmholtz energy of the solid at absolute zero of the temperature, T, excluding all vibrational contributions. A_0 therefore has a definite value for every fixed configuration of the nuclei of a solid and is a function only of the relative positions of these nuclei. Under conditions of uniform pressure, P, the relative positions of the nuclei can in principle be specified completely by the specific volume v. Under these conditions therefore A_0 is a function of v only.

The quantity $A_{\text{q.h.}}$ in eq (1) is the contribution to A arising from thermal vibrations in the quasi-harmonic (q.h.) approximation. In this approximation, the normal vibration frequencies of the solid are assumed to be functions only of the mean nuclear positions and therefore do not depend explicitly on T. As in the case of A_0 these frequencies will be functions only of v if the pressure is uniform. $A_{\text{q.h.}}$ has the general form

$$A_{\text{q.h.}} = kT \sum_{i=1}^{3n} \{\theta_i/2T + \ln [1 - \exp (-\theta_i/T)]\} \tag{2}$$

where $\theta_i = hf_i/k$, h is the Planck constant, k is the Boltzmann constant, f_i is the ith normal mode frequency, and n is the number of atoms per gram.

The quantity $A_{\text{a.h.}}$ in eq (1) is the contribution due to anharmonic effects not already included (implicitly) in $A_{\text{q.h.}}$. It is therefore a correction to $A_{\text{q.h.}}$ which in essence accounts for the fact that the f_i cannot really be independent of T at constant volume. For most elemental metals at room temperature $A_{\text{a.h.}}$ is a very small correction, but in the case of sodium, it is significant at low pressures and therefore a crude (but effective) estimate will be made in this case. In subsequent sections of this article P, v, T equations of state are calculated for solid sodium and aluminum. In each case it is done by considering separately the important contributions of each term on the right side of eq (1).

2. The P, v, T Equation of State of Sodium

2.1. The Evaluation of A_0

Since in general $P(v, T) = -(\partial A/\partial v)_T$, then according to eq (1) the contribution of A_0 to the pressure is $P_0(v) = -(\partial A_0/\partial v)_T = -dA_0/dv$ where $P_0(v)$ is a function of volume only. It is convenient to express volume in terms of the dimensionless parameter $x = v/v_0$ where v_0 is the specific volume at $P = 0$ and $T = 0$ K. For sodium $v_0 = 0.9873$ cm^3/g. With this definition, the pressure becomes $P(x, T) = -\rho_0(\partial A/\partial x)_T$ where $\rho_0 = 1/v_0$ is the density at $P = 0$ and $T = 0$ K. Likewise the expression for

[1] Figures in brackets indicate the literature references at the end of this paper.

Paper presented at the Symposium on Accurate Characterization of the High-Pressure Environment, held at the National Bureau of Standards, Gaithersburg, Md., October 14–18, 1968.

P_0 becomes

$$P_0(x) = -\rho_0 \frac{dA_0(x)}{dx}. \tag{3}$$

From eq (3) it is clear that in the range of interest one need consider only those contributions to A_0 which change appreciably with volume and therefore contribute significantly to the pressure. For sodium this excludes a good deal. It excludes, for example, the necessity of accounting for the volume variation of the wave functions of the ten core electrons in each sodium atom [2]. This is because the core electrons are tightly bound relative to the valence electrons and are localized in a region of volume, v_c, which is small compared to the volume per atom, v_a, in the solid. The compression of core electrons is therefore unlikcly to become an important factor until $v_a \simeq v_c$, which in sodium corresponds to $x \simeq 0.2$ and a pressure of well over 500 kbars at room temperature. Therefore, for sodium, the calculation of $P_0(x)$ requires an evaluation only of the interaction energy between the singly charged atomic cores themselves, the interaction energy between cores and valence electrons, and finally the energy of the valence electrons themselves. Two small contributions to the core-core interactions can be established immediately. These are the repulsive contribution, A_0^R, due to the mutual overlap of core wave functions and the attractive contribution, A_0^W, due to the Van der Waals interaction. Reasonable semitheoretical expressions for the pairwise contributions to A_0^R and A_0^W already exist in the literature [3–5], and from these one finds

$$A_0^R = (130.92\times10^9)\ \exp\ [5.07\ (1-2.0611x^{1/3})]$$

ergs/g. (4)

and

$$A_0^W = -\ (0.1187\times10^9)/x^2$$

ergs/g. (5)

Equations (4) and (5) represent the results of calculations in which only nearest neighbor interactions are included. The remaining contributions to A_0 can be viewed as the sum of four conceptually distinct energies. These are as follows:

(1) $A_0^{g.s.}$, the contribution (ground-state energy) which one would have if all valence electrons were in the ground state (i.e., not translating throughout the lattice) and interacted with nothing save their respective ion cores;

(2) $A\mathfrak{h}$, a contribution (the Fermi energy) which occurs because the exclusion principle prohibits all the valence electrons from being in the same energy state;

(3) $A\mathfrak{h}^{ex.}$, a contribution (exchange energy) which results from interactions between electrons and degeneracies which occur because of their indistinguishability;

(4) $A\mathfrak{h}^{corr}$, a contribution (correlation energy) which arises because valence-electron motions are somewhat correlated because of the mutual Coulomb interactions.

Of these four energies, $A\mathfrak{h}$ is presently the easiest to evaluate. This is because the band structure of sodium has already been calculated in considerable detail. Bienenstock and Brooks (B–B), for example [6], have given sphericalized analytic relations connecting valence electron energy with wave vector in sodium for various values of the lattice parameter. The latter calculations are very detailed and are based on the quantum defect method. Since the Fermi surface of sodium is known to be very nearly spherical [7], the energy versus wave vector relations given by B–B can be used to obtain the (mean) Fermi energy for several values of the sodium lattice parameter by simple integrations over wave vector space. When this is done one finds in every case that the mean Fermi energy of compressed sodium remains within 3 percent of the free electron value for electrons of equivalent number density. The B–B calculations are particularly interesting because they were performed in several ways. One set of calculations, for example, includes the effects of core polarization and another does not. These inclusions and exclusions were made so as to discover their effect on theoretical shift of the Landé g factor for sodium.

The results are interesting in that the set of calculations which provides the best agreement with the pressure dependence of the experimentally measured g-shift is also the set for which the mean Fermi energy is closest to the free electron value. As a matter of fact, in this case the mean Fermi energy remains within 0.7 percent of the free electron value over a range of the lattice parameter which for sodium corresponds to 30 percent compression (i.e., $0.7 \leq x \leq 1.0$). The indications are, therefore, that for sodium A_0^f is very close to the free electron value, which is given by

$$A_0^f(x) = (81.511\times10^9)/x^{2/3} \quad \text{ergs/g.} \tag{6}$$

The closeness of A_0^f to the free electron value is not surprising. The free-electron-like nature of the metallic sodium valence electron has been emphasized by many authors for the past 35 years [8]. So far as the equation of state is concerned, it is a fortunate fact, because it makes it sensible to calculate $A_0^{ex.}$ and $A_0^{corr.}$ in the same approximation, especially since these terms are only small corrections to A_0^f. Expressions for the free electron exchange energy may readily be found in the literature. A particularly good treatment of this subject has been given by Gombás [9]. Estimates of the free electron correlation energy may also be found. Here, an analytic expression given by D. Pines [10] is used. Great accuracy is not attached to the latter expression (±20 percent) but, as it happens, for the monovalent alkali metals the two energies

$A_0^{ex.}$ and $A_0^{corr.}$ tend to cancel one another and as a result their sum contributes very little to either A_0 or P_0. The possible inaccuracy of $A_0^{corr.}$ is therefore not a matter of great concern. Using the literature mentioned above, one finds that for sodium [2]

$$A_0^{ex.}(x)+A_0^{corr.}(x)=10^9[41.2058/x^{1/3}-79.887$$

$$+35.7213\ \ln(3.933x^{1/3})-5.8515x^{1/3}] \quad \text{ergs/g.} \quad (7)$$

The constant term in (7) has been kept for the purpose of calculating the cohesive energy later on.

The ground-state energy $A^{g.s.}$ may be evaluated in either a semi-theoretical or a purely theoretical fashion. From the standpoint of accuracy, the semi-theoretical approach is most desirable because with this approach one can incorporate some of the observed experimental behavior in the final expressions for pressure. This can be done by constructing a reasonable and adjustable analytic expression for the ground-state pressure $P_0^{g.s.}$ and then manipulating the adjustable constants until satisfactory agreement is obtained between the theoretical and experimental 0 K isotherms. The theoretical 0 K isotherm $P_{00}(x)$ is given by the sum

$$P_{00}(x)=P_0(x)+P_0^v(x)$$

where $P_0^v(x)$ denotes the contribution of 0 K lattice vibrations. In the range $0 \leq P_{00}(x) \leq 20$ kbars, an accurate experimental isotherm can be obtained from the data of Beecroft and Swenson [11]. The big advantage of the semi-theoretical approach is that it permits errors arising either from small omissions or from inaccuracies in the expressions (4) through (7) to be absorbed in the adjustable constants of $P_0^{g.s.}$. This is particularly important at low pressures, where the theoretical isotherms are given by the small differences between relatively large quantities. In this region small errors in any of the terms contributing to the 0 K isotherm ($A_0^{corr.}$ for instance) are likely to show up in a conspicuous way. At higher pressures this is no longer true. Consequently in the higher pressure region one should expect good agreement between a purely theoretical calculation and a good semi-empirical estimate of the 0 K isotherm, provided of course that the error in each contributing term of the pure theoretical calculation is sufficiently small. It is therefore a good procedure to check the results of an analytic, semi-empirical calculation at high pressure by comparing them with the prediction of pure theory. This is the procedure which will be taken below.

As in the case with the other quantities which contribute to A_0, it is easy to obtain a reasonable analytic expression for $A_0^{g.s.}$. The first such expression was derived for the alkali-metals by Hellman and Kassatotschkin [12] (H–K) and in our units it has the form

$$A_0^{g.s.}(x)=10^9\{-435.273/x^{1/3}+(201.043z/x)[1$$

$$-(1+yx^{1/3})e^{-yx^{1/3}}]\} \quad \text{ergs/g} \quad (8)$$

where z and y are adjustable constants. The expression (8) is used in subsequent calculations because it is simple and analytic and because its theoretical basis is sufficiently sound. The development of eq (8) is based primarily on an approximation due to Wigner and Seitz [8] (W–S), according to which one assumes that $A_0^{g.s.}=n\times$(the ground state energy of one valence electron and one core contained in a spherical cell of volume v_a). Corrections to this approximation for sodium have been investigated in considerable detail and have been found in general to be quite small [13–14]. In the H–K development it is further assumed that ground-state wave function $\psi_{g.s.}$ is equivalent to that of a free electron (i.e., $\psi_{g.s.}^*\psi_{g.s.}=1/v_a$. The energy in a single cell E_a is then calculated with the expression

$$E_a=4\pi\int_0^{R_s}\psi_{g.s.}^*\varphi(R)\psi_{g.s.}R^2dR$$

where $\varphi(R)$ is the effective valence electron core-interaction, R is the distance from the center of the core (which coincides with the center of the spherical cell), and R_s is the cell radius. The adjustable constants appear in the expression for $\varphi(R)$, for which (H–K) used the form

$$\varphi(R)=-(e^2/R)[1-Ae^{-KR}]\,\text{ergs}. \quad (9)$$

Here e is the electronic charge in e.s.u. and the constants A and K must be determined from experiment. In eq (8), $z=(A/K^2)\times10^{16}\text{cm}^2$ and $y=KR_s^0$ where R_s^0 is the value of R_s at $v=v_0$. As mentioned previously z and y can be evaluated by forcing agreement (to within experimental error) between the theoretical expressions for $P_{00}(x)$ and the experimental 0 K isotherm. To do this it is necessary to jump ahead to the approximate expression for P_0^v derived in the next section, that is,

$$P_0^v(x)\simeq(0.5435)/x^{1.86}\ \text{kbar}. \quad (10)$$

With $A_0(x)$ given analytically by the sum of eqs (4), (5), (6), (7), and (8), and with P_0^v given by eq (10), the 0 K isotherm is easily derived from the relation $P_{00}(x)=-\rho_0\,dA_0/dx+P_0^v(x)$. When this is done and when z and y are adjusted to optimize agreement with experiment, one finds $z=0.43258$ and $y=6.71$. The results of this adjustment are shown graphically in figure 1, the complete analytic expression for the 0 K isotherm is given in Appendix A.

[2] The potential arising from the Coulomb interaction in the Hartree field is included in eq (7).

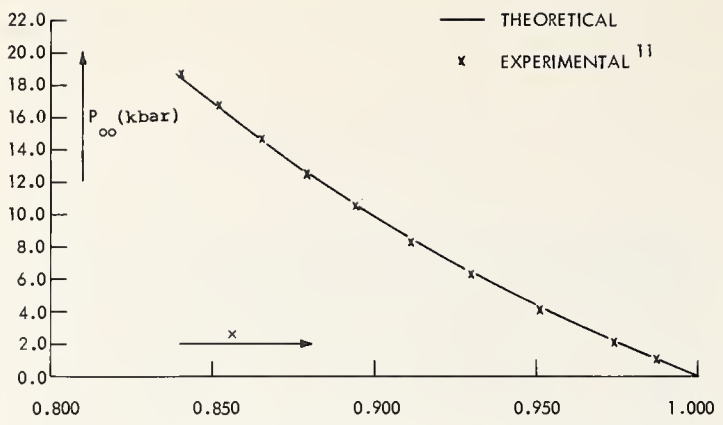

FIGURE 1. *The result of fitting the theoretical 0 K isotherm to the experimental data.*

As was mentioned earlier, there exist more purely theoretical approaches to the calculation of $A_0^{g.s.}$. Of these the most successful (for sodium) has been that of Wigner and Seitz [8]. These authors merely solved the Schrödinger equation for a single ground-state valence electron in the spherical W–S cell. An eigenvalue of the energy per valence electron, E_a, was assumed and the Schrödinger equation for $\psi_{g.s.}$ was numerically integrated until the proper boundary condition was met. In this case, the boundary condition compatible with the translational symmetry of the lattice requires [8] that $\psi'_{g.s.}(R_s)=0$. By solving the Schrödinger equation in this way (W–S) were able to generate the curve of E_a versus R_s or equivalently the relationship between $A_0^{g.s.}$ and x. The valence electron-core interaction used by (W–S) in the Schrödinger equation was one originally derived from spectroscopic data by Prokofjew. Here the W–S procedure has been repeated to obtain theoretical values of $A_0^{g.s.}$ and $P_0^{g.s.}$. These values are much more accurate (than those of (W–S)), since they were obtained by a computerized Runge-Kutta integration technique. In table 1 values of $A_0^{g.s.}$ and $P_0^{g.s.}$ calculated from eq (8) are compared with the theoretical (W–S) values as a function of x. It can be seen immediately that the agreement between the two sets of values is quite good to about 40 percent compression. This agreement implies several important things. First of all, it implies that the theory is sound and that all the analytic terms which contribute to $P_{oo}(x)$ are represented quite accurately. Secondly, it implies that the error in the calculated 0 K pressures should amount to little more than the difference between the theoretical and semi-theoretical values of $P_0^{g.s.}$.

At $x=0.6$ this difference is only 0.23 kbars, whereas the calculated pressure, P_{oo}, at this compression is 94.2 kbars. Since the analytic version of $P_{oo}(x)$ is forced to reproduce the correct (experimental) pressures below 20 kbars and since up to 94.2 kbars this same function agrees with the theoretical values of $P_{oo}(x)$ everywhere to within

TABLE 1. *Comparison of values of $A_0^{g.s.}$ and $P_0^{g.s.}$ calculated using the Prokofjew Potential for sodium with those calculated using (8).*

x	Prokofjew		Equation (8)	
	$A_0^{g.s.}$	$P_0^{g.s.}$	$A_0^{g.s.}$	$P_0^{g.s.}$
	(10^9ergs/g)	(kbar)	(10^9ergs/g)	(kbar)
1.0235	−347.10	−59.76	−347.71	−60.56
1.0133	−347.70	−60.19	−348.32	−60.86
0.9914	−349.02	−60.96	−349.64	−61.49
0.9701	−350.30	−61.66	−350.94	−62.09
0.9619	−350.80	−62.00	−351.45	−62.31
0.9215	−353.30	−63.34	−353.96	−63.37
0.8882	−355.40	−64.33	−356.06	−64.16
0.8569	−357.40	−65.14	−358.05	−64.80
0.7801	−362.40	−66.48	−363.02	−65.80
0.7374	−365.20	−66.46	−365.79	−65.78
0.6914	−368.20	−65.39	−368.77	−65.14
0.6441	−371.2	−62.80	−371.78	−63.41
0.6360	−371.70	−62.29	−372.29	−62.97
0.6009	−373.80	−60.27	−374.44	−60.50
0.5937	−374.20	−55.80	−374.86	−59.84
0.5367	−376.90	−40.65	−378.05	−52.50

0.8 kbars, it seems a fair conclusion that the analytic 0 K isotherm reproduces the true sodium isotherm with an accuracy of 2 percent up to pressures of 95 kbars. For pressures beyond about 95 kbars the two calculations begin to deviate significantly and one cannot be entirely sure which is the more correct. Estimates of accuracy are therefore limited to the region of $P_{oo}(x) \leq 95$ kbars. As a last test of the analytic 0 K isotherm, the theoretical bulk modulus and cohesive energy at $x=1$ are compared with the experimental values. The experimental cohesive energy of sodium is [16] 48.28×10^9 ergs/g at 0 K and the experimental bulk modulus is [11] 78.2 kbars. The theoretical values are 47.314×10^9 ergs/g and 79.0 kbars.

2.2. The Contribution of $A_{q.h.}$

At high temperatures ($\theta_i/T \ll 1$ for all i), the expression (2) for $A_{q.h.}$ has the limiting form

$$A_{q.h.}=kT\sum_{i=1}^{3n}\ln(\theta_i/T)\cdot \qquad (11)$$

This makes a contribution $P_{q.h.}$ to the pressure of an amount

$$P_{q.h.}(x,T)=\rho_0 3nk\,(\gamma_0/x)T$$
$$=3.293\,(\gamma_0/x)\,(T/300)\ \text{kbars} \qquad (12)$$

where $\gamma_0(x)=\frac{1}{3n}\sum_{i=1}^{3n}\gamma_0^i$ and $\gamma_0^i=-\frac{x}{f_i}\left(\frac{\partial f_i}{\partial x}\right)_T$

$$=-\frac{x}{f_i}\left(\frac{df_i}{dx}\right).$$

Although the form of eq (12) is quite simple, the theoretical evaluation of $\gamma_0(x)$ (quasi-harmonic Grüneisen parameter) is full of obvious difficulties and some rather drastic approximation must be made. This isn't really a cause for concern because it is already known [17] that for sodium near $x=1$, γ_0 should be of the order of unity and moreover should diminish with decreasing x. This means that at 40 percent compression ($x=0.6$) and room temperature (here $T=300$ K) the contribution of $P_{\text{q.h.}}$ should be no more than five kbars. Since at this compression $P_0(x)$ is 92.8 kbars, then a 50 percent error in γ_0 (which is quite unlikely) would lead at the most to a 2.6 percent additional error in the total pressure. In estimating $\gamma_0(x)$, therefore, one can afford to be a little crude. The approximation which will be used for $\gamma_0(x)$ is the (apparently accurate) "two-mode" approximation [18–20]. In this scheme, one replaces the unwieldy average over the $3n$ logarithmic derivatives of the normal mode frequencies, f_i, with an average over only two types of long wavelength acoustic modes. Of these two types of modes, one is purely longitudinal (p.l.) with a propagation velocity C_l, given by

$$C_l^2=xC_{11}^0/\rho_0 \tag{13}$$

where C_{11}^0 is the usual elastic constant, evaluated along the 0 K isotherm. The other type is purely transverse (p.t.) (having two independent directions of polarization) with a propagation velocity, C_t, given by

$$C_t^2=xC_{44}^0/\rho_0, \tag{14}$$

where C_{44}^0 is the usual elastic shear constant evaluated [21] at 0 K. Since as a solid is isostatically compressed, one expects the wavelength of a p.l. or p.t. mode to vary as $x^{1/3}$, then the propagation frequency of a p.l. mode, f_l, is given by $f_l \propto C_l/x^{1/3}$ and that of a p.t. mode, f_t, is given by $f_t \propto C_t/x^{1/3}$. With these relations for frequency and the expressions (13) and (14) for velocity, one can calculate

$$\gamma_0^l=-\frac{x}{f_l}\left(\frac{df_l}{dx}\right)=-\frac{1}{6}-\frac{x}{2C_{11}^0}\left(\frac{dC_{11}^0}{dx}\right) \tag{15}$$

and

$$\gamma_0^t=-\frac{x}{f_t}\left(\frac{df_t}{dx}\right)=-\frac{1}{6}-\frac{x}{2C_{44}^0}\left(\frac{dC_{44}^0}{dx}\right). \tag{16}$$

In the "two-mode" approximation, one assumes that the average $\frac{1}{3n}\sum_{i=1}^{3n}\gamma_0^i$ is given approximately by $\frac{1}{3n}\{n\gamma_0^l+2n\gamma_0^t\}$. In other words, the $3n$ values of γ_0^i are replaced by n of the type γ_0^l and $2n$ of the type γ_0^t. It remains now to compute C_{11}^0 and C_{44}^0 from theory.

For the alkali metals, the theory of the elastic shear constants C_{44}^0 and $\tilde{C}^0=(C_{11}-C_{12})/2$ has been developed by Fuchs [22]. According to Fuchs, the electronic contributions to C_{44}^0 and $\tilde{C}^0$ are given, respectively, by $53.2/x^{4/3}$ kbars and $7.146/x^{4/3}$ kbars. To the electronic term of C_{44}^0 one should add the contribution due to ion core-ion core repulsion [23] (this contribution can be neglected [23] in the case of $\tilde{C}^0$). When this is done the expressions which result for C_{44}^0 and $\tilde{C}^0$ are

$$C_{44}^0=\{53.2/x^{4/3}+(1654.6/x^{1/3}-312.1/x^{2/3})$$

$$\exp[5.07(1-2.0611x^{1/3})]\}\quad\text{kbar} \tag{17}$$

$$\tilde{C}^0=7.146/x^{4/3}\quad\text{kbar}. \tag{18}$$

With $\tilde{C}_0$ given by (18), C_{11}^0 can be calculated immediately from the identity

$$C_{11}^0=-x\frac{dP_0}{dx}+\frac{4}{3}\tilde{C}^0. \tag{19}$$

With (15), (16), (17), (18), and (19) an analytic expression for the theoretical $\gamma_0(x)$ can be constructed

TABLE 2. *Calculated values of* γ_0, γ_0', γ_0'', *and* $P^{\text{q.h.}}/(T/300)$ *as a function of* x *for sodium.*

x	γ_0 (Dimensionless)	γ_0' (Dimensionless)	γ_0'' (Dimensionless)	$P^{\text{q.h.}}/(T/300)$ (kbar)
1.06	0.895	0.214	0.957	2.784
1.05	0.893	0.205	0.933	2.803
1.04	0.891	0.196	0.905	2.824
1.03	0.890	0.187	0.897	2.845
1.02	0.888	0.178	0.891	2.867
1.01	0.886	0.169	0.875	2.890
1.00	0.884	0.161	0.845	2.913
0.96	0.879	0.128	0.788	3.015
0.92	0.874	0.097	0.745	3.130
0.88	0.871	0.068	0.693	3.259
0.84	0.869	0.042	0.640	3.406
0.80	0.868	0.017	0.596	3.571
0.76	0.867	−0.006	0.538	3.758
0.72	0.868	−0.026	0.473	3.970
0.68	0.869	−0.043	0.391	4.210
0.64	0.871	−0.057	0.290	4.483
0.60	0.874	−0.066	0.148	4.796

in the "two-mode" approximation.

The resulting values of $\gamma_0(x)$, its first and second derivative (γ_0' and γ_0''), and the function $P_{\text{q.h.}}/(T/300)$ are listed as functions of x in table 2.

In the low-temperature limit eq (2) has the form

$$A_{\text{q.h.}} = k \sum_{i=1}^{3n} \theta_i/2 = \sum_{i=1}^{3n} hf_i/2. \tag{20}$$

Using the Debye approximation [24] to estimate the right side of (20), one finds

$$A_{\text{q.h.}} \simeq (9/8)\ nk\ \theta_D(x)$$
$$= (4.0651 \times 10^6)\ \theta_D(x)\ \text{ergs/g} \tag{21}$$

where $\theta_D(x)$ is the Debye temperature which for sodium at $x=1$ is [25] $\simeq 152$ K. Now since the Debye temperature has the definition: $h\ f_{\max}/k$ where $f_{\max}$ is the highest normal mode frequency, then one should expect that the quantity

$$-(x/f_{\max})\, df_{\max}/dx = -(x/\theta_D)\, d\theta_D/dx$$

behaves very roughly as $\gamma_0(x)$ which, as it happens, is fairly constant (see table 2) with values remaining near 0.86. As a rough approximation it will do to set $-(x/\theta_D)\ \ d\theta_D/dx = \gamma_0(x) \simeq 0.86$. After integrating this expression one has

$$\theta_D(x) = \theta_D(1)/x^{0.86} = 152/x^{0.86}\ \text{K}. \tag{22}$$

By substitution (22) into (21) and differentiating, one can obtain an estimate of P_0^v which is the contribution of $A_{\text{q.h.}}$ to the pressure at 0 K. This is

$$P_0^v(x) = (0.5435)/x^{1.86} \qquad \text{kbar} \tag{23}$$

which is the expression already given in (10).

2.3. The Contribution of $A_{\text{a.h.}}$

From the outset it should be clear that $A_{\text{a.h.}}$ will modify the isothermal pressures near room temperature only in a minor way. In effect it is a small correction to a small correction.

It has already been said that in the quasi-harmonic (q.h.) approximation the f_i are assumed to be (for all practical purposes) functions of x only and that, in essence, $A_{\text{a.h.}}$ could be viewed as accounting for the temperature dependence of the f_i. If one finds therefore that some of the f_i vary appreciably with temperature at constant volume (i.e., if $(\partial \ln f_i/\partial \ln T)_x$ is not small compared to unity), then a correction should be made. In the case of the present calculation on sodium, consistency demands that whatever corrections are made should be made only on the frequencies (f_l and f_t) on the p.l. and p.t. modes used in the approximation of $A_{\text{q.h.}}$. The necessity of a correction in this case is easy to discover. Obviously, for the q.h. "two-mode" approximation to be perfectly correct it is necessary that C_l^2 and C_t^2 be given exactly by (13) and (14). In other words, it requires that the elastic constants C_{11} and C_{44} be functions of volume only (i.e., $C_{11} = C_{11}^0$; $C_{44} = C_{44}^0$). This is because in the q.h. approximation it is assumed that the f_i are independent of T, which implies that for a given x they are essentially the same at elevated temperature as they are on the 0 K isotherm. Consequently the temperature dependence of f_l and f_t will show up in the temperature dependence of C_{11} and C_{44}. More precisely one can write

$$\left(\frac{\partial \ln f_l}{\partial \ln T}\right)_x = \left(\frac{\partial \ln C_{11}}{\partial \ln T}\right)_x \tag{24}$$

and

$$\left(\frac{\partial \ln f_t}{\partial \ln T}\right)_x = \left(\frac{\partial \ln C_{44}}{\partial \ln T}\right)_x. \tag{25}$$

For sodium under normal conditions the derivatives on the right side of (24) and (25) can be evaluated from the experimental data of Diederich and Trivosonno [23]. From these data one finds $(\partial \ln C_{44}/\partial \ln T)_{x\simeq 1} = -0.351$ and $(\partial \ln C_{11}/\partial \ln T)_{x\simeq 1} = 0.0197$. This tells us immediately that in the "two-mode" approximation only the shear frequencies f_t will contribute appreciably to $A_{\text{a.h.}}$, the contributions of f_l being negligible by comparison. Since, as has been said, $A_{\text{a.h.}}$ will make only a small contribution, $P_{\text{a.h.}}$, to isothermal pressures, only a crude estimate of $P_{\text{a.h.}}$ is necessary. The most obvious way to make this estimate is simply to examine the correction to γ_0 which results from the temperature dependence of C_{44}. To do this one needs an expression for C_{44}, which gives the temperature dependence of C_{44}^0 at least to first order (i.e.,

$$C_{44} = C_{44}^0[1 + g(x)T],$$

where $g(x)$ is a function of x only). It is not hard to find such expressions [1] but unfortunately in the case of C_{44} the function $g(x)$ is not easily evaluated. One can, however, estimate the temperature dependence of the shear constant $\tilde{C} = \frac{1}{2}(C_{11} - C_{12})$. To first order in T it can be shown that

$$\tilde{C} = \tilde{C}^0(1 + \tilde{g}(x)T) \tag{26}$$

in which $\tilde{g}(x)$ is given roughly by [26]

$$\tilde{g}(x) = -s\gamma_0'/\tilde{C}^0 \tag{27}$$

where s is a positive constant.

Now since Fuchs [22] has pointed out that C_{44}^0 and $\tilde{C}^0$ should be almost exactly proportional to each other, then it seems reasonable to expect that the first-order temperature-dependent terms of C_{44} and $\tilde{C}$ are also simply related. As a matter of fact, from experimental data it is possible to deduce that for sodium

$$g(x) \simeq a\tilde{g}(x) + b \tag{28}$$

where a and b are constant. Daniels [27], for example, has shown experimentally that for sodium under normal conditions

$$C_{44}/\tilde{C} = \left(\frac{\partial C_{44}}{\partial x}\right)_T \Big/ \left(\frac{\partial \tilde{C}}{\partial x}\right)_T . \tag{29}$$

This implies directly that, for some range of isothermal compression, $C_{44} \propto \tilde{C}$; or, using the theoretical expressions for C_{44} and $\tilde{C}$,

$$C_{44}^0 (1 + g(x)T_0) = \delta \tilde{C}^0 (1 + \tilde{g}(x)T_0), \tag{30}$$

where δ is the proportionality constant and $T_0 = 300$ K. But Fuchs has shown (and also the experimental data) that $\tilde{C}^0/C_{44}^0$ is very nearly constant [28]. Therefore, setting the constant $\epsilon = \tilde{C}^0/C_{44}^0$, one can rearrange terms in (30) to obtain

$$g(x) = \delta\epsilon\tilde{g}(x) + (\delta\epsilon - 1)/T_0 = a\tilde{g}(x) + b. \tag{31}$$

Using (31) for $g(x)$ and (27) for $\tilde{g}(x)$, C_{44} becomes $C_{44} = C_{44}^0(1 + bT) - (sa/\epsilon)\gamma_0' T$. Setting $sa/\epsilon = \beta$ this becomes simply

$$C_{44} = (1 + bT) C_{44}^0 - \beta \gamma_0' T. \tag{32}$$

With eq (32) it is possible to obtain an expression for the first order effect of temperature on the derivative

$$-(\partial \ln f_t/\partial \ln x)_T = -1/6 - (1/2)\ (\partial \ln C_{44}/\partial \ln x)_T .$$

Using (32) for C_{44} and noting that the term containing the temperature is small relative to [29] $(1 + bT)C_{44}^0$ one can obtain (Note also, $bT \ll 1$)

$$-\left(\frac{\partial \ln f_t}{\partial \ln x}\right)_T \simeq \gamma_0^t + \mu\left[x\gamma_0'' - \gamma_0' \frac{d \ln C_{44}^0}{d \ln x}\right](T/300)/C_{44}^0 \tag{33}$$

where several constants have been lumped into μ. Viewed as a correction to γ_0 the second term on the right of eq (33), which we will call $\Delta\gamma^t$, contributes an amount $P_{\text{a.h.}}$ to the pressure, which is given by

$$P_{\text{a.h.}} = \rho_0 3nkT\Delta\gamma/x = 3.293(\Delta\gamma/x)(T/300) \quad \text{kbar} \tag{34}$$

where $\Delta\gamma = (2/3)\Delta\gamma^t$. The total pressure P_T due to thermal effects is therefore

$$P_T = P_{\text{q.h.}} + P_{\text{a.h.}} = 3.293(\gamma_0 + \Delta\gamma)(T/300)/x \text{ kbar}. \tag{35}$$

Since analytic expressions for γ_0 and C_{44}^0 have already been given, it is necessary only to evaluate μ. This can be done by demanding that the total pressure $(P_0 + P_T)$ be equal to zero at room temperature (300 K) and the observed value of volume [30] $(x = 1.043)$. In this way one obtains $\mu = 17.345$ kbar.

The evaluation of μ completes the P, v, T equation of state for sodium, but it is interesting to pursue the matter further and find the expression for $A_{\text{a.h.}}$ implied by eq (34). This is done in Appendix B, from which one finds

$$A_{\text{a.h.}} \cong -\mu(2.1674 \times 10^9)(T/300)^2(\gamma_0'/C_{44}^0) \text{ ergs/g}. \tag{36}$$

With eq (36) it is possible to calculate the total specific energy E in the high-temperature limit $(T \gg \theta_D)$ through the relation $E = -T^2[\partial(A/T)/\partial T]_x$. This gives us

$$E = A_0 + (3.25118 \times 10^9)(T/300)[1 + (2/3)\mu(T/300)\gamma_0'/C_{44}^0] \text{ ergs/g}. \tag{37}$$

With eq (37) one can make a more stringent test of the accuracy of $A_{\text{a.h.}}$ by calculating quantities more sensitive to it than the pressure. For example, one can calculate the specific heat at constant pressure, C_P, and compare it with the experimental [31] values. One can use the identity

$$C_P = C_v + \frac{\alpha x}{\rho_0}\left[P + \rho_0\left(\frac{\partial E}{\partial x}\right)_T\right] \tag{38}$$

where both $C_v = (\partial E/\partial T)_x$ and $(\partial E/\partial x)_T$ are given by eq (37) and $\alpha = 1/x(\partial x/\partial T)_P = (\partial P/\partial T)_x/[-x(\partial P/\partial x)_T]$ can be obtained from the P, v, T equation of state already derived.

In this manner C_P has been calculated (with small quantum corrections [32]) along the $P = 0$ isobar. The results are compared with experiment [31] in figure 2; the agreement is excellent. The derivative $(\partial C_P/\partial P)_T$ was also calculated under normal conditions and was found to have the value 1.657×10^{-4} cm³/g K. The experimental value is [33] 1.653×10^{-4} cm³/g K. The theoretical room temperature isotherm is compared with experimental data in table 3; values of $\Delta\gamma/(T/300)$ are also listed in this table.

The theoretical isothermal bulk modulus at 349 K and normal pressure was found to be 64.3 kbars; the experimental value [11] is 63.9 kbars.

The theoretical Hugoniot equation of state (which is somewhat sensitive to $\gamma_0 + \Delta\gamma$) was also calculated. An outline [34] of the procedure for doing so is given in Appendix C. The results are compared

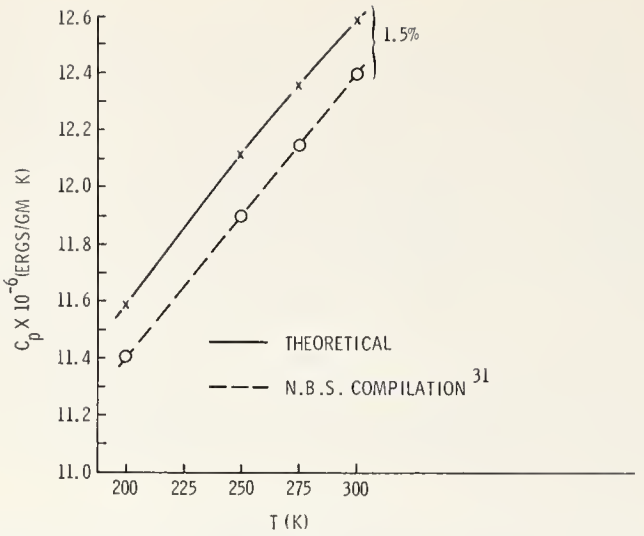

FIGURE 2. *Comparison of theoretical and experimental* C_p *values. The Dulong-Petit value is* $10.84 \times 10^{+6}$ ergs/g K.

with experiment [35] in table 4. The agreement is again excellent.

At this point it seems a fair conclusion that, for T in the neighborhood of room temperature, the theoretical isothermal equation of state for sodium gives pressures accurate to within 3 percent at a given volume in the range of compression ($0.6 \leq x \leq 1$).

3. The P, v, T Equation of State of Aluminum

3.1. The Evaluation of A_0

From the viewpoint of electronic structure, aluminum is in many ways similar to sodium. Like sodium, it has ten tightly bound core electrons which will contribute little to $P_0(x)$ for sufficiently small compressions. Also like sodium, it appears that the mean Fermi energy of aluminum is close to the free electron value. The band structure calculations of B. Segall, for example [36], indicate that for aluminum, $A_0^f = 0.976 \times$ the free electron value at the normal volume. Calculations for smaller volumes have not been carried out, but here it will be assumed that A_0^f stays near the free electron value for reasonably small compressions. We will therefore use the free electron approximation for $A_0^{\text{corr.}} + A_0^{\text{ex.}}$ and 0.976 of the free electron value for A_0^f. The appropriate expressions are

$$A_0^f = 10^9(734.35/x^{2/3}) \quad \text{ergs/g} \qquad (39)$$

and

$$A_0^{\text{corr.}} + A_0^{\text{ex.}} = 10^9[-170.755 + 91.283 \ln (2.9849x^{1/3}) - 59.162/x^{1/3} - 11.447x^{1/3}] \quad \text{ergs/g} \qquad (40)$$

where again $x = v/v_0$, and for aluminum [30] $v_0 = 0.36945$ cm^3/g. These expressions are somewhat different than eqs (6) and (7) for sodium. This is because, unlike sodium, aluminum has three valence electrons per atom. Also unlike sodium the inclusion of A_0^R and A_0^W in the expression for A_0 is unnecessary [37], as they make very small contributions to $P_0(x)$ for low compressions ($0.8 \leq x$). They have therefore been neglected. The remaining problem is that of evaluating $A_0^{\text{g.s.}}$ (in the W–S scheme).

TABLE 3. *Theoretical and experimental 300 K isotherms and values of* $\Delta\gamma/(T/300)$ *as a function of* x *for sodium.*

x	P(kbar)	P(kbar)	ΔP(kbar)	$\Delta\gamma/(T/300)$
	Theoretical	Experimental [a]	Approximate experimental error	(Dimensionless)
1.06	−1.034	.....	.....	0.290
1.05	−0.426	.....	.....	0.275
1.04	+0.206	.....	.....	0.260
1.03	0.883	.....	.....	0.250
1.02	1.591	1.51	±0.1	0.240
1.01	2.323	2.19	±0.1	0.229
1.00	3.081	2.92	±0.14	0.215
0.96	6.518	6.16	±0.20	0.176
0.92	10.637	10.07	±0.20	0.144
0.88	15.569	14.98	±0.30	0.115
0.85	19.92	19.50	±0.30	0.090
0.80	28.671	.....	.....	0.067
0.76	37.368	.....	.....	0.050
0.72	47.991	.....	.....	0.033
0.68	61.061	.....	.....	0.019
0.64	77.280	.....	.....	0.008
0.60	97.604	.....	.....	−0.003

[a] Reference [11].

TABLE 4. *The theoretical and experimental Hugoniots of sodium*

x	P_h(kbar)	P_h(kbar)
	Theoretical	Experimental [a]
0.7341	48.64	47.08
0.6762	71.06	70.47
0.6517	83.61	83.35
0.6404	89.67	90.54
0.6094	113.31	112.77

[a] Reference [35].

Unfortunately there exists as yet no Prokofjew potential $\varphi_P(R)$ for aluminum which will give the interaction between a single valence electron and the triply charged aluminum core. Without this interaction one cannot integrate the Schrödinger equation to obtain $A_0^{g.s.}$. The situation is not hopeless, however, because near the normal volume the pressure $P_0^{g.s.}$ for aluminum should depend primarily on the value of $\varphi_P(R)$, near $R = R_s$ and the integral of $\varphi_P(R)$ over the atomic volume v_a. This is so because of the free electron like behavior of the valence electrons in the region between cores.

For values of R greater than the approximate core radius R_C, $\psi^*_{g.s.}$ $\psi_{g.s.}$ should behave like $1/v_a$. In the region $R < R_C$ set $\psi_{g.s.} = \psi_1(R, R_s)$ where ψ_1 is the wiggly part of the wave function in the region of high kinetic energy. The energy per ground-state valence electron E_a is given by

$$E_a \simeq +4\pi \int_0^{R_C} \psi_1^2 \varphi_P(R) R^2 dR + \frac{4\pi}{v_a} \int_{R_C}^{R_s} \varphi_P(R) R^2 dR - \frac{4\pi\hbar^2}{2m} \int_0^{R_C} \psi_1^* \nabla^2 \psi_1 R^2 dR \qquad (41)$$

where m is the electron mass. The pressure contribution P_a arising from E_a is $P_a = -(1/4\pi R_s^2) dE_a/dR_s$ which according to (41) is given by

$$-4\pi R_s^2 P_a = +4\pi \int_0^{R_C} 2\psi_1 \psi_1' \varphi_P(R) R^2 dR - \frac{4\pi v_a'}{v_a^2} \int_{R_C}^{R_s} \varphi_P(R) R^2 dR + \frac{4\pi}{v_a} \varphi_P(R_s) R_s^2 - \frac{4\pi\hbar^2}{2m} \int_0^{R_C} (\psi_1^{*\prime} \nabla^2 \psi_1 + \psi_1^* \nabla^2 \psi_1') R^2 dR \qquad (42)$$

where $\psi_1' = d\psi_1/dR_s$ and $v_a' = dv_a/dR_s$. All the terms in (42) depend on integrals of $\varphi_P(R)$ over the volume except one which depends on $\varphi_P(R_s)$. Thus it can be expected that if $\varphi_P(R)$ is well known outside of the core and approximately inside the core (so that the integral of $\varphi_P(R)$ over v_C is reasonably accurate), then $P_0^{g.s.}$ can be well estimated. This is easy to demonstrate. If instead of the Prokofjew potential for sodium one substitutes $\tilde{\varphi}(R) = -(e^2/R)(1 + 10e^{-\bar{\alpha}R})$ ergs and adjusts $\bar{\alpha}$ so as to reproduce one theoretical value of $P_0^{g.s.}$, it is possible to closely reproduce the theoretical $P_0^{g.s.}$ curve for sodium in the range $0.6 \leq x \leq 1.0$. Calculations of this type have been carried out using $\bar{\alpha} = 4.3931 \times 10^8$ cm^{-1}. The results are shown in figure 3, where they are compared with values of $P_{g.s.}$ derived from the Prokofjew potential. This

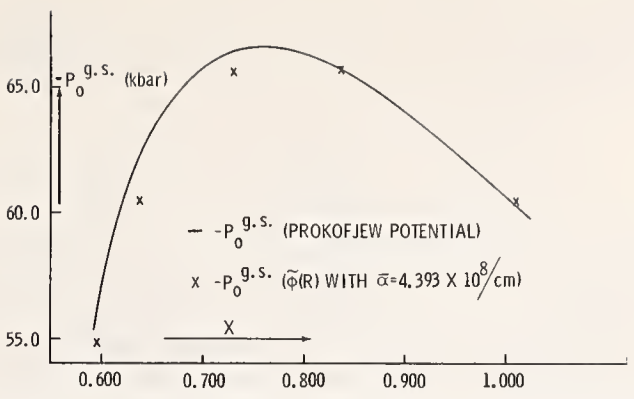

FIGURE 3. *Comparison between values of* $P^{g.s.}$ *calculated using Prokofjew potential with those calculated using* $\tilde{\phi}$(R).

TABLE 5. *Theoretical values of* $P_0^{g.s.}$ (x) *and* P_0 (x) *for aluminum*

x	$P_0^{g.s.}$	P_0
	(*kbar*)	(*kbar*)
0.9922	−1210.17	5.73
0.9852	−1218.85	11.93
0.9702	−1238.37	25.29
0.9606	−1251.05	34.38
0.9461	−1269.59	49.85
0.9311	−1289.70	66.44
0.9221	−1301.32	77.63
0.8941	−1338.12	115.75
0.8705	−1370.01	152.12
0.8389	−1412.04	209.70
0.8036	−1456.74	288.94
0.7950	−1467.47	306.86
0.7820	−1468.24	360.82

procedure works because near R_s (when $R_s > R_C$), $\tilde{\varphi}(R) \simeq -e^2/R$ and so is the Prokofjew potential. When $\bar{\alpha}$ is adjusted to reproduce one theoretical $P_0^{g.s.}$ value (calculated from the Prokofjew potential), it forces the average value of $\tilde{\varphi}(R)$ in the core region to have nearly the same value as the average of the Prokofjew potential itself. Aside from this, both potentials have the same value near $R = 0$, namely $-11e^2/R$. This is the procedure which will be used to find $P_0^{g.s.}$ for aluminum. In this case, however, α will be determined by adjusting $P_0^{g.s.}$ so as to force $P_0(x)$ to zero at the observed value of volume ($v_0 = 0.369$ cm^{3}g). For aluminum, therefore, the valence electron-core potential is taken as

$$\varphi(R) = -(e^2/R)(3 + 10e^{-\bar{\alpha}R}) \text{ ergs} \qquad (43)$$

where the three accounts for the triply charged aluminum core. To eq (43) one must add the potential contribution due to the presence (on the average) of two other valence electrons in the volume v_a. For a first approximation one can assume a

charge density of $-e/v_a$ per valence electron. In this approximation one must add to eq (43) the potential [38]

$$\varphi_1(R) = \left(\frac{e^2}{R_s^3}\right)[3R_s^2 - R^2] \text{ ergs.} \quad (44)$$

Using eqs (43) and (44), $P_0^{\text{g.s.}}$ was calculated for aluminum in the manner already described. The parameter $\bar{\alpha}$ was found to have the value $\bar{\alpha} = 4.3459 \times 10^8$ cm^{-1}. The results are given in table 5. The total pressure $P_0(x)$ is also given in this table.

3.2. The Calculation of $P_{\text{q.h.}}$

Unlike sodium aluminum is not well above the Debye temperature θ_D under normal conditions. For aluminum [39] $\theta_D \simeq 395$ K. For $T < \theta_D$ the contribution of eq (2) to $P_{q.h.}$ is

$$P_{\text{q.h.}} = (\rho_0/x)\sum_{i=1}^{3n}\gamma_i^0\epsilon_i + (\rho_0/x)\sum_{i=1}^{3n}\gamma_i^0(hf_i/2) \quad (45)$$

where $\epsilon_i = hf_i/[\exp(hf_i/kT) - 1]$ is the mean thermal energy of the ith mode. If one defines

$$\gamma(x, T) = \sum_{i=1}^{3n}\gamma_i\epsilon_i / \sum_{i=1}^{3n}\epsilon_i,$$

then eq (45) may be rewritten as

$$P_{\text{q.h.}} = (\rho_0/x)\gamma(x, T)E_T + (\rho_0/x)\sum_{i=1}^{3n}\gamma_i^0(hf_i/2) \quad (46)$$

where E_T is the thermal energy per gram

$$\left(\text{i.e., } E_T = \sum_{i=1}^{3n}\epsilon_i\right).$$

Barron [40] has pointed out that in most cases for $T > 0.3\theta_D$. $\gamma(x, T)$ is practically independent of T. Since the calculation here will be limited to $T > 0.3\theta_D$ then the first term on the right in eq (46) will be viewed as a product of E_T and a function of x only (i.e., $(\rho_0/x)\gamma(x)E_T$). The second term on the right of eq (46) is the contribution P_0^v of the 0 K vibration to the pressure. In a sense this has already been included in the calculation of $P_0(x)$ since the latter function was forced to zero at the observed value of volume at 0 K. At the observed value of volume (i.e., $x = 1$) it is the sum $P_0(x) + P_0^v$ which should be zero. Thus, in effect, P_0^v has been absorbed into the calculation of P_0, and for aluminum the calculated $P_0(x)$ should be approximately equal to $P_{00}(x)$. Consequently the second term on the right of eq (46) should not be included in the calculation of $P_{\text{q.h.}}$ for aluminum, and therefore when $0.3\theta_D \lesssim T < \theta_D$ one should expect that

$$P_{\text{q.h.}} \simeq (\rho_0/x)\gamma(x)E_T. \quad (47)$$

The evaluation of $\gamma(x)$ is somewhat simpler in the case of aluminum. This is because for aluminum one can expect $P_{\text{a.h.}} \simeq 0$ (this point is discussed in the next section) and therefore $P_T \simeq P_{\text{q.h.}}$. This in turn implies that $\gamma(x)$ can be obtained directly from eq (C–7) (see Appendix C) if one sets $\Delta\gamma = 0$ and $F = 1$. In other words one should expect that for aluminum

$$P_h = \{P_0 + (\rho_0\gamma(x)/x)[A_0(x_i) - A_0(x) + (E_T)_i]\}/[1 - \gamma(x)(x_i - x)/2x] \quad (48)$$

where $x_i = v_i/v_0$, v_i is the normal volume for aluminum ($v_i = 0.3740$ cm^3/g) and $(E_T)_i$ is the specific thermal energy under normal conditions [41] [$(E_T)_i = 1.636 \times 10^9$ ergs/g]. Since P_h can be obtained from experimental data and since $A_0(x_i) - A_0(x) = -\frac{1}{\rho_0}\int_x^{xi} P_0(x)dx$ [where P_0 is given in table 5 or by equation (52)], then $\gamma(x)$ can be calculated directly from (48). Calculations of this type have been carried out earlier by P. McKenna [43]. It should be noted that the latter computations were effected in such a way as to compensate for the effects of yielding on P_h at low shock pressures. The results of these calculations are given in table 6.

TABLE 6. *Calculated values of* $\gamma_0(x)$ *and* $P_{\text{q.h.}}$ *for aluminum.*

x	γ	$P_{\text{q.h.}}$ 300 K
		(*kbar*)
0.98	2.15	9.63
0.96	2.06	9.05
0.94	1.93	8.41
0.92	1.78	7.61
0.90	1.58	6.84
0.88	1.38	6.12
0.86	1.23	5.45
0.84	1.12	4.90
0.82	1.09	4.52
0.80	1.00	4.34

The latter data can be represented accurately by an expansion of the type

$$\gamma(x) = \gamma_0 + a(1 - x) + b(1 - x)^2 + c(1 - x^3) \quad (49)$$

where $\gamma_0 = 2.302$, $a = -3.86$, $b = -56.13$, and $c = 215.4$. Equation (49) reproduces the data of table 6 to within 10 percent for a given x.

To complete the expression for P_T it remains to evaluate $E_T(x, T)$. For this the Debye approximation [24] will be used according to which

$$E_T(x, T) = (2.771 \times 10^7)\theta_D(T/\theta_D)^4 \int_0^{\theta_D/T} \{y^3/(e^y - 1)\}dy \text{ ergs/g.} \quad (50)$$

The Debye temperature θ_D has been determined experimentally for aluminum by Raimondi and Jura [39]. These authors have found that

$$\theta_D = 395 \exp\{-1.78(0.9877\, x - 1)\}\text{K.} \quad (51)$$

By substituting eq (51) into eq (50), E_T can be calculated as a function of x and T. Values of $P_{\text{q.h.}}$ calculated at 300 K using eqs (47), (49), (50), and (51) are listed in table 6 as a function of x.

3.3. The Smallness of $P_{\text{a.h.}}$

As has been mentioned earlier, the relative smallness of $P_{\text{a.h.}}$ is indicated by the smallness of $(\partial \ln C_{44}/\partial \ln \mathcal{V})_x$ relative to unity. For sodium this derivative is $\simeq -0.3$, which leads to a contribution of about 20 percent to P_T (the thermal pressure) at low pressures. For aluminum the experimental data [43] indicate that $(\partial \ln C_{44}/\partial \ln T)_x \simeq -0.03$. This is a factor of 10 less than the value for sodium, indicating that C_{44} depends far more on volume than temperature. One should expect then that for aluminum $P_{\text{a.h.}}$ is quite small and $P_T \simeq P_{\text{q.h.}}$.

Assuming $P_{\text{a.h.}} \simeq 0$, the P, v, T equation of state for aluminum above the Debye temperature is then given by $P = P_0(x) + P_{\text{q.h.}}$. The theoretical room temperature isotherm of aluminum is given in table 7, where it is compared with two p-v points taken from Bridgman's [44] data, which have been corrected according to a suggestion of Jamieson [45, 46].

For convenience we have fit (by the method of least squares) the calculated values of $P_0(x)$ to an expression of the type

$$P_0(x) = K\{\exp[2b(1-x^{1/3})] - \exp[b(1-x^{1/3})]\}/x^{2/3}. \quad (52)$$

This expression eq (52) fits the calculated points in table 5 quite well (to within 0.65 kbar) in the range $(0.8 \leq x \leq 1.01)$ when $K = 627.1$ kbars and $b = 3.7721$. Equation (52) should be recognized as the result of assuming that $A_0(x)$ is given by a Morse function.

TABLE 7. *Comparison of the theoretical 300 K aluminum isotherm with corrected[a] Bridgman[b] data.*

x	(Theoretical)[c]	Corrected experimental
	P(kbar)	P(kbar)
1.01245	0.00	0.00
1.010	2.55	.....
1.000	10.11	.....
0.990	17.97	.....
0.980	26.34	.....
0.973	32.53	29.0 to 30.5
0.960	44.51	.....
0.950	54.39	.....
0.940	64.90	.....
0.930	75.96	.....
0.920	87.69	.....
0.919	88.94	87.5 to 88.5
0.900	113.38	.....
0.880	142.33	.....
0.860	174.95	.....
0.840	211.78	.....
0.820	253.39	.....
0.800	300.41	.....

[a] References [45] and [46].
[b] Reference [44].
[c] Using eq (52) for $P_0(x)$.

In the range $(0.9 \leq x \leq 1.01)$ $P_0^{\text{g.s.}}$ is represented accurately by the analytic relation

$$P_0^{\text{g.s.}} = -100 \ln [A + Bx + Ce^{-Dx}] - 1057.8/x^{4/3} \text{ kbar} \quad (53)$$

where $A = 26.9302$, $B = -16.4253$, $C = -208.096$, and $D = 3.4857$. In the range $(0.8 \leq x \leq 0.9)$ one must add the correction $-4131.4 + 9378.5x - 5322\, x^2$ kbars to $P_0^{\text{g.s.}}$ to obtain an accurate representation of the calculated values.

Appendix A. Analytic Form of the Sodium 0 K Isotherm $P_{00}(x)$

Since $P_0 = -\rho_0 dA_0/dx$ and $A_0(x)$ is the sum of several terms, it follows that P_0 is the sum of terms, each of which corresponds to one term in the expression for $A_0(x)$. Thus,

$$P_0(x) = P_0^{\text{g.s.}} + P_0^f + P_0^{\text{corr.}} + P_0^{\text{ex.}} + P_0^R + P_0^W. \quad (A\text{–}1)$$

Taking the appropriate derivatives of the terms in A_0, one obtains (units are kbars)

$$P^{\text{g.s.}} = -146.8015/x^{4/3} + 203.4154z[1 - (1 + yx^{1/3} + y^2x^{2/3}/3)e^{-yx^{1/3}}]/x^2 \quad (A\text{–}2)$$

where $z = 0.43258$ and $y = 6.71$;

$$P_0^f = 54.9861/x^{4/3}; \quad \text{(A–3)}$$

$$P_0^{\text{corr.}} + P_0^{\text{ex.}} = 13.9118/x^{4/3} - 12.0602/x + 1.9756/x^{2/3}; \quad \text{(A–4)}$$

$$P_0^R = 461.89\{\exp[5.07(1 - 2.0611x^{1/3})]\}/x^{2/3}; \quad \text{(A–5)}$$

and

$$P_0^W = -0.2404/x^3. \quad \text{(A–6)}$$

To obtain $P_{00}(x)$ one must add to $P_0(x)$ the vibrational pressure P_0^v at 0 K

$$P_0^v = 0.5435/x^{1.86}. \quad \text{(A–7)}$$

Appendix B. The Calculation of $A_{\text{a.h.}}$

According to eq (34),

$$P_{\text{a.h.}} = -\rho_0 \left(\frac{\partial A_{\text{a.h.}}}{\partial x}\right)_T = 2.1953(\Delta\gamma^t/x)(T/300) \quad \text{kbar} \quad \text{(B–1)}$$

where

$$\Delta\gamma^t = \mu\left[x\gamma_0'' - \gamma_0' \frac{d \ln C_{44}^0}{d \ln x}\right](T/300)/C_{44}^0. \quad \text{(B–2)}$$

An expression for $A_{\text{a.h.}}$ can be obtained quite simply by integrating eq (B–1) with respect to x. This results in

$$A_{\text{a.h.}} = -10^9(37.594)(T/300)^2\gamma_0'/C_{44}^0 + q(T) \text{ ergs/g} \quad \text{(B–3)}$$

where $q(T)$ is a general function of T only. The function $q(T)$ introduces either a constant or a pure function of T into the energy through the relation

$$E = -T^2\left[\frac{\partial(A/T)}{\partial T}\right]_x.$$

But general theoretical calculations of first order anharmonic effects in solids indicate that there is no pure function of T or non-zero constant which contributes to the anharmonic part of the energy [1]. Therefore for purposes of this development $q(T)$ can be set equal to zero and for $A_{\text{a.h.}}$ one can use the expression

$$A_{\text{a.h.}} = -10^9(37.594)(T/300)^2\gamma_0'/C_{44}^0 \text{ ergs/g}. \quad \text{(B–4)}$$

Appendix C. Calculation of the Theoretical Hugoniot

The shock Hugoniot is the locus of pressure volume points obtained through the shock compression of a solid. For a solid which is initially in the normal state, the stress, σ_h, specific energy, E_h, and compression, x, of the material behind a steady-state plane shock wave are related to the initial conditions through the exact conservation relations [34]

$$\sigma_h = \rho_o U_s U_P/x_i \quad \text{(C–1)}$$

$$x = x_i(1 - U_P/U_s) \quad \text{(C–2)}$$

$$E_h = E_i + x_i\sigma_h(1 - x/x_i)/2\rho_0 \quad \text{(C–3)}$$

where $x_i = v_i/v_o$, v_i is the normal specific volume, E_i is the initial specific energy, U_s is the velocity of shock propagation, and U_P is the velocity of matter in the shocked state. When the yielding stress of the solid is small compared to σ_h, then σ_h is (for all practical purposes) equivalent to a hydrostatic pressure P_h. In this case eq (C–3) becomes

$$E_h \simeq E_i + x_i P_h(1 - x/x_i)/2\rho_0. \quad \text{(C–4)}$$

But P_h should be given by the sum $P_0 + P_T$ or in the case of sodium

$$P_h = P_o(x) + 3.293\ (\gamma_0 + \Delta\gamma)(T_h/300)/x \text{ kbar} \quad \text{(C–5)}$$

where T_h is the temperature in the shocked state.

With eq (37) one can substitute for $(T_h/300)$ with the expression

$$10^9 \times 3.25118(T_h/300) = (E_h - A_0)/[1 + (2/3)\mu(T_h/300)(\gamma_0'/C_{44}^\circ)]. \quad \text{(C–6)}$$

By substituting eq (C–4) for E_h into eq (C–6) and then substituting eq (C–6) into eq (C–5) and solving for P_h, one can obtain the expression

$$P_h = \frac{P_0 + \rho_0(\gamma_0 + \Delta\gamma)[A_0(x_i) - A_0(x) + (E_T)_i]/(xF)}{1 - (\gamma_0 + \Delta\gamma)(x_i - x)/(2xF)} \quad \text{(C–7)}$$

where $F = [1 + (2/3)\mu(T_h/300)(\gamma_0'/C_{44}^0)]$ and $(E_T)_i$ is the specific thermal energy under normal conditions [i.e. $E_i = A_0(x_i) + (E_T)_i$]. For sodium

the quantity F decreases rapidly with volume at constant temperature. For example at $x = 0.8$ and $(T/300) \simeq 1$, $F \simeq 1.003$. As a consequence, little error results in setting F equal to unity in eq (C–7) provided T_h is less than about 2000 K. Since T_h is also contained in $\Delta\gamma$ in eq (C–7) an iteration is necessary to obtain P_h. One first sets $\Delta\gamma = 0$ in eq (C–7) and obtains values of P_h as a function of x. Then T_h is calculated as a function of shock compression via eqs (C–4) and (37). These same values T_h can be used to calculate $\Delta\gamma$, which can in turn be substituted into eq (C–7) to recalculate P_h, and so on. This is the procedure which has been used to calculate P_h for sodium.

References

[1] See for example Leibried, G., and Ludwig, L., Solid State Physics Advances in Research and Application, Vol. **12**, (Academic Press, New York, 1961).
[2] Brooks, H., Nuovo Cimento Suppl. **7**, 207 (1958).
[3] Born, M., and Mayer, J. E., Z. Physik **75**, 1 (1932).
[4] Mayer, J. E., and Helmoltz, W., Z. Physik **75**, 19 (1923).
[5] Fuchs, K., Proc. Roy. Soc. (London) **A153**, 622 (1936).
[6] Bienenstock, A., and Brooks, H., Phys. Rev. **136**, A787 (1964).
[7] See for example Schneider, T., and Stoll. E., Phys. Kondens Materie **6**, 135 (1967).
[8] Wigner, E., and Seitz, F., Phys. Rev. **43**, 804 (1933). See also ref. [2].
[9] Gombás, P., Die Statistische Theorie Des Atoms und Ihre Anwendungen (Springer-Verlag, Vienna, 1949).
[10] Pines, D., Nuovo Cimento Suppl. **7**, 329 (1958).
[11] Beecroft, R. I., and Swenson, C. A., J. Phys. Chem. Solids **18**, 329 (1961). Because of a small calibration error the pressures reported in this article should be increased by 3 percent [C. A. Swenson (private communication)].
[12] Hellmann, H., and Kassatotschkin, W., Acta Physicochim. URSS **5**, 23 (1936).
[13] Wigner, E., and Seitz, F., Phys. Rev. **46**, 509 (1934).
[14] See ref. [2], p. 203.
[15] A corrected version of the Prokofjew potential is given in ref. [8].
[16] To obtain the cohesive energy (at $x = 1$) the ionization energy of the free atom valence electron in (ergs/g) must be subtracted from $A_0(1)$.
[17] See, for example, ref. [11].
[18] Bijl, P., and Pullan, H., Phil. Mag. **45**, 290 (1955).
[19] White, G. K., and Anderson, O. L., J. Appl. Phys. **37**, 430 (1966).
[20] Pastine, D. John, Phys. Rev. **138**, No. 3A, A767 (1965).
[21] The elastic constants must be evaluated at 0 K because in q.h. approximation f_l and f_t (and therefore C_l and C_t) are assumed to be independent of T. It automatically follows that in this approximation the temperature dependence (at constant volume) of C_{11} and C_{44} must not be included in the calculation of the frequencies.
[22] See ref. [5].
[23] Diederich, M. E., and Trivisonno, J., J. Phys. Chem. Solids **27**, 637 (1966).
[24] See, for example, Mayer, J. E., and Mayers, M. G., Statistical Mechanics (John Wiley & Sons, Inc., New York and London, 1940).
[25] Martin, D., Phys. Rev. **139**, No. 1A, A150 (1965).
[26] Pastine, D. John, J. Phys. Chem. Solids **28**, 522 (1967).
[27] Daniels, W. B., Phys. Rev. **119**, 1246 (1960).
[28] This can be ascertained by relating the data in ref. [23] to the theoretical relations given here for C_0 and C_{44}.
[29] This can also be determined from the data in ref. [23].
[30] The specific volumes at 0 K for both sodium and aluminum can be calculated using the tables of Corrucini, R. J., and Gnieweck, J. J., Natl. Bur. Std. (US) Monograph No. 29 (1961).
[31] Corrucini, R. J., and Gnieweck, J. J., Natl. Bur. Std. (US) Monograph No. 21 (1960).
[32] Quantum corrections were made by multiplying C_v given by eq (37) by the factor $[1 - 1/20(\theta_D/T)^2]$. See for example ref. [24].
[33] Rodionov, K. P., Sov. Phys. Tech. Phys. **11**, 955 (1957).
[34] For more details on the physical properties of shock Hugoniots see Rice, M. H., McQueen, R. G., and Marsh, S. P., Solid State Physics Advances in Research and Application, Vol. **6** (Academic Press, New York, 1958).
[35] Rice, M. H., J. Phys. Chem. Solids **26**, 483 (1965).
[36] Segall, B., Phys. Rev. **124**, 1797 (1961).
[37] This is because of the smallness of the aluminum cores relative to the separation between them.
[38] It should be noted that this potential assigns all of the energy of interaction to the valence electron in question. This was done so that the resulting (after integrating the Schrödinger equation) valence electron energies could be compared with Hartree-Foch calculations on the free atom. Since each valence electron should be assigned only 1/3 of the interaction in eq (44), after each integration of the Schrödinger equation, an amount $1.2e^2/R_s$ was subtracted from the energy (i.e., two thirds of the total interaction between free electrons in a sphere of radius R_s).
[39] Raimondi, P. L., and Jura, G. J., Phys. Chem. Solids **28**, 1419 (1967).
[40] See for example Barron, T. H. K., Ann. Physics **1**, 77 (1957).
[41] The specific thermal energy under normal conditions can be obtained from the tables in American Institute of Physics Handbook (McGraw-Hill Book Co., Inc., New York, Toronto, and London, 1957).
[42] McKenna, P., and Pastine D. John, J. Appl. Phys. **39**, 6104 (1968).
[43] Lazarus, D., Phys. Rev. **4**, 545 (1949).
[44] Bridgman, P. W., Proc. Am. Acad. of Arts and Sci. **76**, 55 (1948).
[45] Jamieson, J. J., A discussion in High Pressure Measurement (Butterworths, Washington, 1963).
[46] Jamieson gave the separate volumes of NaCl and Al (in a mixture of NaCl and Al) measured accurately at two different pressure levels. Detailed calculations on the equation of state of NaCl (based on shock data) have been done by J. Fritz of Los Alamos, who has kindly given us the pressures corresponding to these two levels.

DISCUSSION

R. Grover (*Lawrence Radiation Laboratory, University of California, Livermore, California*): For sodium, there appears to be a lack of agreement between shock data, Bridgman's compressibility data, and equation of state values. I believe that some additional experimental or theoretical work would be desirable to resolve this.

L. Thomsen (*Columbia University, Palisades, New York*): You indicated that the pressure correction $P_{\text{a.h.}}$ (eq 34) arose from the temperature dependence of the eigenfrequencies. Now, the eigenfrequencies for all eigen vibrations are rigorously defined as functions of volume only, so this $P_{\text{a.h.}}$ is "correction" in which you made a two-mode

385-762 O - 71 - 8

approximation for gamma. To make this correction you introduced the velocities of sound. By introducing these velocities of sound you *introduce a pseudo*-temperature dependence of the eigenfrequencies which is then subtracted out again with your $P_{a.h.}$. Have I followed your logic correctly?

O. Anderson (*Columbia University, Palisades, New York*): From a theoretical point of view, which do you think we can rely most on in the long run: equations of state of aluminum, or of sodium chloride? Would you find that the equation of state of sodium has advantages theoretically over either of these?

R. H. Wentorf, Jr. (*General Electric Research and Development Center, Schenectady, New York*): Could calculated isotherms be readily calculated for sodium and aluminum at, say, 500 K and 1000 K, for possible use of these materials as high-pressure, high-temperature reference materials?

G. E. Duvall (*Washington State University, Pullman, Washington*): I'd like to make a comment which bears on this subject, remotely at least. For several years R. M. Rosenberg* at the University of California has done some remarkable work on the properties of lattices which have nonlinear forces connecting them. He has discovered some quite remarkable things about normal mode and eigenfrequencies. One of the things that astonished me was that there is not necessarily any correlation between the number of normal modes and the number of degrees of freedom in a system, once the linear force assumption is violated.

AUTHORS' CLOSURE

In response to Dr. Grover's comment: The lack of agreement with Bridgman's data depends to some extent upon which of Bridgman's data comparison is made with. There is reasonably good agreement with his 1945 data, as indicated in my paper [Phys. Rev. **166,** 703 (1968)]. There is a later set of Bridgman's data, however, with which agreement is poor.

Concerning Dr. Thomsen's comments: It is, of course, true that eigenfrequencies are rigorously functions of volume only. One can't have eigenfrequencies if the modes of vibration aren't independent. As soon as you add anharmonic content to the vibrational spectrum, that is as soon as you make the frequencies temperature-dependent, the normal modes start interacting and are no longer independent. However, it turns out in certain cases that, to a reasonable degree of approximation, you can look at these normal modes as having shifted in frequency due to anharmonic effect.

In response to O. Anderson: The question of whether equations of state are to be preferred for sodium, sodium chloride, or aluminum is a difficult one. I accept the accuracy limitations placed on the equation of state by Fritz and Decker. Perhaps the choice depends upon the circumstances in any particular case. If a very compressible substance is desired, use sodium; if a relatively incompressible material is needed, aluminum might be chosen. In the case of sodium chloride, distortion of the lattice probably occurs under pressure, and thus the actual pressures will not be the same as those predicted by the equation of state. This is not as likely to happen with sodium, because the pressures depend almost entirely on the volume.

In response to R. H. Wentorf: The isotherms at elevated temperatures are easily calculated. The 1968 paper referred to above describes calculation of any isotherm.

*On non-linear vibrations of systems with many degrees of freedom, Advances Appl. Mech. 9, 155–242 (1966).

An Atomistic Theory of Shock Compression of a Perfect Crystalline Solid

D. H. Tsai

National Bureau of Standards
Washington, D.C. 20234

Lattice dynamical calculations have been employed to study the process of compression of a perfect, two-dimensional, fcc lattice by a strong shock wave. The interaction energy between the lattice points is assumed to be the Morse-type potential function, and the interaction is assumed to extend to the fourth nearest neighbors. The formulation of the dynamical problem is described. The details of the computation of the shock wave stress and density profiles, shock velocity, energy density profile, local energy distribution, velocity distribution, and the components of the Grueneisen parameter are discussed. Of special interest is the thermal relaxation process behind the shock front. It is found that the relaxation time is not constant, and that the steady, relaxed region in the shock profile trails farther behind the shock front with increasing time. The implications of these results on the calculation of the high-pressure equation of state of a crystalline solid are examined.

Key words: Equation of state of solids; lattice dynamics; shock compression; shock wave; thermal relaxation.

1. Introduction

The study of high-pressure phenomena in solids has become important in recent years in connection with geophysical investigations of the earth's interior, studies of the cratering phenomena on terrestrial and lunar surfaces from meteoritic impact or from nuclear explosion, research and development in ballistics and high explosives, industrial manufacture of new high-pressure materials such as synthetic diamonds, and other related problems of interest to physics, geophysics, and technology. In all of these studies, a central problem is the equation of state of solids under high pressure and high temperature. In the laboratory, pressures up to several megabars, accompanied by temperatures of several thousand K, can be obtained by compressing a material by means of a strong shock wave. Such a shock wave may be generated by detonating high explosives placed next to the material, or by impact of a high-velocity projectile on the material, or by a combination of the two. These methods have been employed extensively in the past 20 years to study the shock compression of a variety of solids. From the dynamics of the shock wave propagation, and with suitable assumptions, the equation of state and other thermodynamic properties of these materials under high-pressure conditions have been obtained [1, 2, 3].[1]

We would like to discuss briefly the basic assumptions which are usually made in these studies. For the interpretation of the dynamics of the shock wave, two assumptions are usually employed: First, the compressed material behind the shock front is assumed to be in thermodynamic equilibrium. This implies that the shock stress profile is also steady in time. Second, the compressed material is assumed to have yielded completely, so that the stresses may be assumed to be hydrostatic. This is based on the observation that the stresses behind the shock front are usually many times higher than the yield strength of the material. These assumptions essentially reduce the solid to a fluid, obeying the continuum theory of fluid dynamics. With these assumptions, and with the aid of the Hugoniot relationships of conservation of mass and of momentum across the (steady) shock front, one easily obtains the pressure and density behind the shock front from the measured shock velocity and the particle velocity behind the shock front. An additional assumption giving the relationship between the Grueneisen parameter and density is then employed, and this directly allows the calculation of the *PVT* relationship for the material behind the shock front. The equation of state obtained this way is the Mie-Grueneisen equation of state.

A closer examination of these assumptions reveals a number of questions. In the first place, the yield strength referred to above is the static yield strength of the material. Under dynamic conditions, with the shock wave propagating at a supersonic velocity, the yield strength of the material probably is much higher, perhaps approaching the theoretical strength. In any event, yielding is known to be a strain-rate dependent phenomenon. If the material behind the shock front yielded to a hydrostatic condition, then it would be important to know the density and the stress histories behind the shock front before one could apply the Hugoniot relationships. The problem of time-dependent yielding under the transient condition of shock compression is very complex. To our knowledge, this problem has not been exhaustively studied either experimentally or theoretically in the high-pressure regime.

In addition to the yielding problem which may affect the stress profile behind the shock front, there is a basic question in the continuum assumption. A solid may be considered as a material made up of discrete particles (atoms) bound together rather in a

[1] Figures in brackets indicate the literature references at the end of this paper.

Paper presented at the Symposium on Accurate Characterization of the High-Pressure Environment, held at the National Bureau of Standards, Gaithersburg, Md., October 14–18, 1968.

regular pattern by attractive and repulsive interatomic forces acting at close range. It is the purpose of lattice dynamics to study the properties of such a solid on an atomistic scale, and to relate the microscopic properties to macroscopic properties. On this subject there exists a vast and distinguished body of literature. From a lattice viewpoint, the continuum approach would be valid if the wavelength of the shock wave were long compared with the lattice spacing. For waves of shorter wavelength, the discrete nature of the atoms causes a dispersive effect. Now a shock wave has high- as well as low-frequency components. Also, because of the anharmonicity in the interatomic forces, there is coupling among waves of different frequencies: for example, the wave front of a low-frequency compression wave has a tendency to steepen in the course of propagation and to generate high-frequency components. The effect should be especially pronounced in waves of large amplitude. Thus as the shock wave propagates into the solid, the dispersive effect should progressively cause the high-frequency components to separate out from the low-frequency components, so that the stress profile of the shock wave perhaps should change continuously with time. If this be the case, one would not be justified in using the Hugoniot conditions to calculate the stress and the density behind the shock front, without first investigating the process of approach to equilibrium.

A few authors [4, 5] also have studied the theoretical problem of the shock wave structure in a solid from a continuum viewpoint. They show that if a dissipative, viscous effect in the solid is postulated, then a steady shock wave profile is obtained. The thickness of the shock front in such a profile increases with increasing viscosity. In our opinion, these theoretical results are not satisfactory, because the physical nature of the viscous effect is not clear. As the viscous effect is reduced to zero, the theoretical solution produces a discontinuous shock front, but without the effect of dispersion.

The foregoing considerations have motivated us to study the process of shock compression of a solid from a more detailed, lattice dynamical viewpoint. In two earlier papers [6, 7], we have investigated the propagation of a strong, one-dimensional shock wave in a semi-infinite cubic lattice, with simple cubic, fcc or bcc configuration. Our main purpose was to study the role of the interatomic forces and the range of their interaction on the dynamics of the shock wave. For our purpose, we assumed different interaction energies ranging from the simple harmonic type of potential between nearest neighbors to the more complicated Morse-type potential with interactions extending to more distant neighbors. We further restricted the motion of the lattice points to only one- and two-dimensional motions by assuming certain symmetries of the relevant interatomic forces. Finally, we assumed that quantum mechanical effects were unimportant at high temperatures, and considered the lattice to be a simple system obeying classical mechanics. Under these assumptions and some others listed in our earlier papers [6, 7], we studied the dynamic response of the lattice following an impact at the face of the semi-infinite lattice model, by solving numerically the equations of motion of the lattice points. From the solutions we then obtained the density and stress profiles of the shock wave, as well as other properties such as the average energy density and the Grueneisen parameter in the compressed lattice.

Our earlier papers were rather brief, because of editorial requirements. In this paper, we would like to present a more complete account of our calculations, and to discuss additional results from our investigations of the lattice energy, thermal stresses, etc., with a view to examing in greater detail the problems of studying the equation of state of a shock compressed lattice by numerical computation, especially the problems of temperature rise behind the shock front, and of thermal relaxation.

It may be noted that our numerical approach to this problem is basically the same as that employed by Fermi, Pasta, and Ulam [8], Alder and Wainwright [9], Northcote and Potts [10], Rahman [11], and others, in their investigations of the dynamic behavior of lattices, solids, and liquids. Recently, Payton, Rich, and Visscher [12] have also studied the thermal conductivity of a lattice by numerical computation. The scope of this line of investigation is therefore quite broad. Numerical solutions suffer from rather well-known limitations. In our present problem cost considerations further restrict us to studying lattices of small sizes, and over short time intervals. From these solutions, it is not easy to develop a broad understanding of the various phenomena we wish to study. On the positive side, it is clear that in the absence of a more powerful mathematical theory which treats large anharmonic and perhaps also anisotropic effects in a large system of oscillators closely coupled in a complicated manner, we must continue to rely on the numerical solutions to provide insight to our problem. Fortunately, in the approximation of classical mechanics, our problem is fairly well adapted to numerical computation, and the results are often not difficult to interpret on physical or intuitive grounds. Thus if the validity of the lattice model could be established, then the numerical results clearly would be useful for the interpretation of experimental data, as well as for the development of mathematical theories.

In section 2, we outline the formulation of the mathematical problems of calculating the dynamics of the lattice under shock compression. In section 3, we discuss the numerical method of solution. In sections 4 through 9, we discuss the calculation of the properties of the lattice from the numerical solutions thus obtained. These include the density and the stress components, shock velocity, energy density and energy distribution, the problem of thermal relaxation, velocity distribution and the problem is fairly well adapted to numerical compu- of the Grueneisen parameter. In section 10 we give a

summary of the results and discuss our view on the problem of shock compression of solids in the light of our results.

2. Formulation of the Numerical Problem

In references [6 and 7], we have described briefly the formulation of the problem of the shock compression of a semi-infinite lattice constrained to one- and two-dimensional motions. In both cases, our problem was formulated as an initial-boundary value problem in a cartesian coordinate system which was stationary with respect to the uncompressed lattice. In the present report, we give a more detailed, alternative formulation of the same problem, in a cartesian coordinate system stationary with respect to the compressed lattice behind the shock front. This resulted in a slight simplification in the calculation of some of the properties of the compressed lattice. In every other respect, the two formulations are identical, because the relative velocity of the two coordinate systems, U_p, is constant.

We limit ourselves here to the case of an fcc, monatomic lattice.[2] The 100, 010, 001 directions are alined in the x, y, z directions respectively, and the face of the semi-infinite lattice is normal to the x axis. The lattice is constrained to two-dimensional motion, in the x and y directions, the motion in the z direction being identically zero, because an exact balance of the z component of the interatomic forces would follow from the assumed symmetry in the z direction. If there is also symmetry in the y direction, then the motion is reduced to the simple, one-dimensional case.

We assumed that the interatomic forces were central forces, and that the interaction energy ϕ between a pair of isolated atoms was given by the Morse potential function:

$$\phi = D\left\{\exp\left[-2ar_0\left(\frac{r}{r_0}-1\right)\right] - 2\exp\left[-ar_0\left(\frac{r}{r_0}-1\right)\right]\right\} \quad (1)$$

where D is the dissociation energy of the atom pair, a is a constant related to the "stiffness" of the potential, r is the separation distance of the atom pair, and r_0 is the separation distance at the potential minimum. If we define a "stiffness parameter" R_1 as that value of R $(=r/r_0)$ which makes ϕ equal to zero, then $ar_0 = \ln 2/(1-R_1)$. In the present paper, we assumed $R_1 = 0.7$. Earlier, we have also set R_1 equal to 0.8 and 0.9. In keeping with the treatment of lattice vibrations of crystals in the literature (see, for example, the review article by Slater [13]) we assumed that there was no damping in the interactions between the lattice points.

[2] We have also studied the bcc lattice in two-dimensional motion under comparable conditions, but we shall not specifically refer to the bcc results except in figure 5.

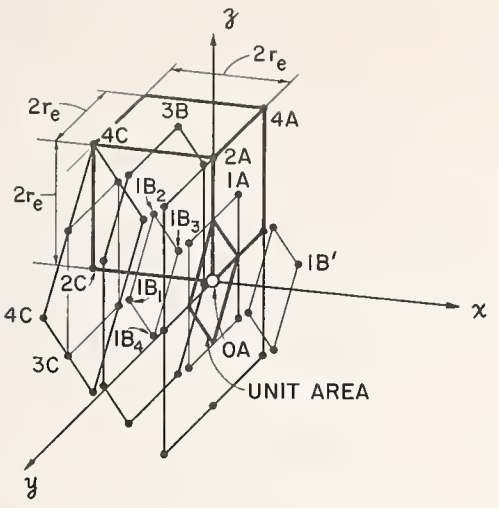

FIGURE 1. *A face-centered cubic lattice showing lattice point* OA *and some of its neighbors.*

The unit cell with dimension $2r_e$ in each direction, and with OA at a corner, is shown in heavy outlines. $1A$ and similar points in lattice plane A are the nearest neighbors of OA in plane A. Similarly for $2A$, $4A$ in lattice plane A; $1B$, $3B$ in lattice plane B; and $2C$, $3C$, $4C$ in lattice plane C. $1B'$ is in lattice plane B' which is on opposite side of OA from plane B. There is also a plane C' on opposite side of OA from plane C. The neighbors in B' and C', except for $1B'$, have been omitted in order to keep the figure simple. The unit area is formed by the perpendicular bisectors of OA and $1A$ in plane A, and is used in the calculation of stress across plane A.

To simplify our calculations, we assumed that the interaction engeries were pairwise additive, so that the total potential energy of an atom is given by

$$\Phi = \frac{1}{2}\sum_i \phi_i \quad (2)$$

where $i = 1, 2, \ldots$ denotes the various neighbors with which the atom interacts, and the factor 1/2 arises because each ϕ_i is shared between this atom and its neighbor. For our fcc lattice, we assumed that the interactions extended to the fourth nearest neighbors (fig. 1). These neighbors are in lattice planes two lattice spacings away from the atom in question, and according to the results of reference [6], with the Morse potential and $R_1 = 0.7$, neighbors farther than the fourth nearest neighbors, lying in planes three lattice spacings away, would have no appreciable effect on the propagation of the shock wave in the lattice.

We obtained the equilibrium configuration of the lattice by equating $\partial\Phi/\partial r$ to zero, and solving for the equilibrium lattice spacing $r = r_e$ based on interactions extending to the fourth nearest neighbors. For $R_1 = 0.7$, r_e was found to be 0.5313 r_0. The corresponding force constant in the x direction was $k = 10.5437 k_0$, where $k_0 = (\partial^2\phi/\partial r^2)_{r=r_0} = 2a^2D$ is the force constant for the iolated atom pair [6]. The longitudinal velocity of sound was $c = r_e(k/m)^{1/2} = 1.7252\ c_0$, where m is the mass of the atom, and $c_0 = r_0(k_0/m)^{1/2}$ is the longitudinal volocity of sound in a chain of atoms spaced at r_0 apart, and interacting with nearest neighbor interactions given by (1). We assumed that these properties extended throughout the semi-infinite lattice, and we ignored the surface effect near the face of the lattice.

Equations of motion. Under dynamical conditions, the force between an atom and its nth neighbor is given by

$$\left.\begin{aligned}(f_x)_n &= -(\alpha \partial\phi/\partial r)_n \\ (f_y)_n &= -(\beta \partial\phi/\partial r)_n\end{aligned}\right\} \tag{3}$$

where f_x and f_y are the x and y components of the interatomic forces, α and β are the cosines of the direction angles between r and the x and y axes, respectively. The total force on the atom is given by (3) summed over all the relevant neighbors,

$$\left.\begin{aligned}\mathscr{F}_x &= \sum_n (f_x)_n \\ \mathscr{F}_y &= \sum_n (f_y)_n\end{aligned}\right\}. \tag{4}$$

The equations of motion of the atom then become

$$\left.\begin{aligned}m\ddot{x} &= md^2x/d\tau^2 = \mathscr{F}_x \\ m\ddot{y} &= md^2y/d\tau^2 = \mathscr{F}_y\end{aligned}\right\} \tag{5}$$

where x and y are respectively the coordinates of the atom in question in the cartesian coordinate system.

Boundary conditions: For simplicity, we assumed that the x-y lattice plane was divided into strips running in the x direction, each strip containing N rows ($N=10$ to 50) of lattice points in the y direction. For the boundary condition in the y direction, we assumed that the solutions in two neighboring strips were mirror images of one another about the common boundary, and that the solution in the entire x-y plane was pieced together with these alternating strips of solutions. Actually, two slightly different conditions were used along the y boundaries: (a) In the majority of cases, we assumed that the mirror planes contained the first and the Nth row of lattice points, and the y components of the velocities of these points, therefore, were always equal to zero. The lattice points in the other rows of two neighboring strips were symmetrically disposed about the common boundary. (b) In some cases, we also moved the mirror planes one-half of a lattice spacing outward, so that the Nth row of the lattice points in one strip and the first row of the lattice points in the adjacent strip were mirror images of one another, and similarly for the $(N-1)$th row in the first strip and the second row in the next strip, etc. This was done in order to investigate the effect of the boundary condition on the details of the numerical solution, especially the velocity distribution.

The boundary condition described above is equivalent to assuming that the boundaries in the y direction are rigid and perfectly reflecting. An incident wave I_a impinging on the boundary is reflected as wave R_a of the same strength, $R_a=-I_a$. Similarly, an incident wave I_b impinging on this boundary from the other side is reflected as $R_b=-I_b$. If $I_a=-I_b$, then $R_b=I_a$ and $R_a=I_b$. Thus an alternative interpretation of the rigid boundary condition is that as an incident wave I_a reaches the boundary, it passes through the boundary without change as R_b, but I_a is always accompanied by $I_b=-I_a$ approaching the boundary symmetrically from the other side, and passing through the boundary as R_b. This situation is analogous to the "cyclic" boundary condition which is often employed. In the cyclic case, we assume that as I_a approaches the boundary of a lattice strip, $I_b=I_a$ simultaneously approaches the *opposite* boundary of the strip, I_b and I_a have the same direction, and cross the boundaries at exactly corresponding points.

Both the rigid and the cyclic boundary conditions are physcially unrealistic. Dean [14] has discussed the effects of these boundaries, as well as the effects of the "free" boundary, on the vibrational frequency of a lattice. He showed that for a large lattice, the effects of the different boundaries on the frequency spectra were small, approaching zero as the number of lattice points approached infinity. In several cases, we have compared the solution of a lattice with $N=10$ and that with $N=50$. The solution in the central strip (also 10 spacings wide) of the lattice with $N=50$ differed in minor details from the solution of the lattice with $N=10$, but the time-averaged dynamical behavior of the shock wave was not at all affected. With $N=10$, the boundary conditions (a) and (b) resulted in some difference in the velocity distributions in the transverse direction. However, with $N=50$, this difference became very small. Thus our results were in agreement with Dean's analysis, and the lattice with $N=10$–50 appeared to be wide enough for our purpose.

In the x direction, we assumed that the boundary condition at the face of the semi-infinite lattice was the same as that of (b) described above. As the shock wave propagated into the lattice, we terminated our calculations of the shock wave profile when the shock wave no longer produced an appreciable disturbance to the lattice points ahead of the shock front. We have also tried to isolate a piece of the shock compressed lattice, in order to study the problem of approach to equilibrium. This was done by replacing the boundary condition at the shock front with the boundary condition (b) inserted somewhere in the shock compressed lattice, and studying the time-development of the oscillations of the lattice now isolated by boundary conditions (b) on all four sides.

Initial conditions: To simulate thermal motion in the lattice before shock compression, we initially set the lattice in transverse motion by first displacing one or more of the interior lattice rows in the y direction from their equilibrium positions, and then allowing the lattice rows to oscillate freely as they sought to reestablish equilibrium. With the assumption of central forces, it was necessary to have lattice motion in the y direction to provide a mechanism for scattering longitudinal waves generated by the

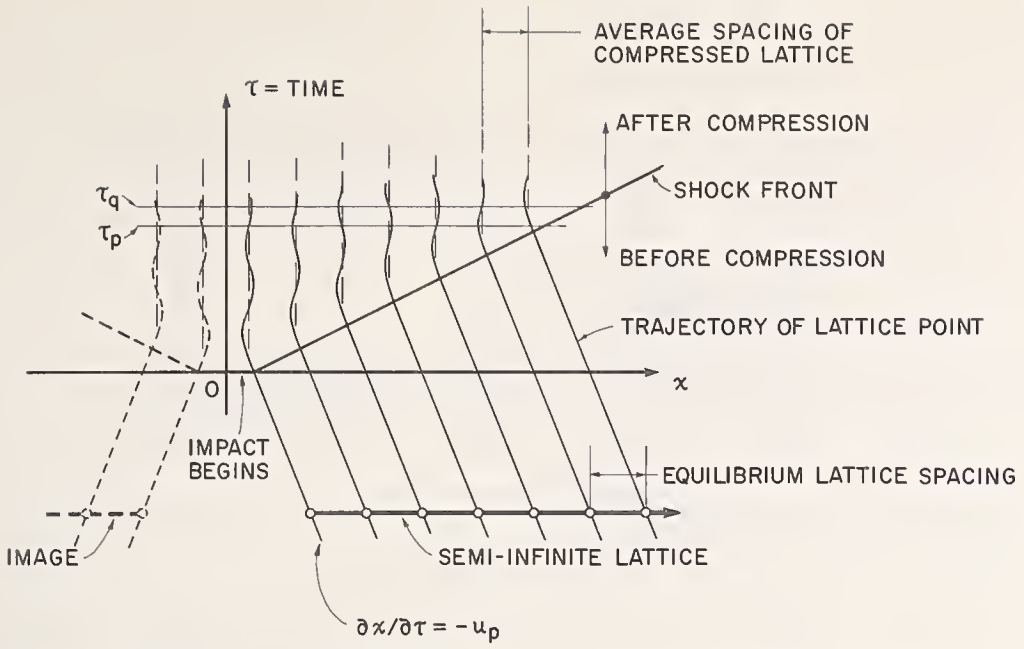

FIGURE 2. *Schematic diagram in the x-τ plane showing the events near the beginning of impact of a semi-infinite lattice with its image.*

shock wave in the transverse direction. We limited the "thermal" oscillations to the transverse direction purely for reasons of economy. In this way, it was necessary to calculate only the one-dimensional motion of plane waves in the y direction. As the shock wave moved in the x direction, the shock front would encounter the uncompressed lattice at various stages of transverse oscillations, so that the scattering of the shock wave in the y direction might be expected to become somewhat random, and thus simulating thermal scattering. To test this hypothesis, we tried several initial configurations, with different lattice rows displaced in different directions, but with the initial lattice energy kept constant. Our results again showed only minor differences in the details of the solutions, but the dynamical behavior of the shock wave was not affected.

In addition to the transverse "thermal" oscillations, we also set the lattice in motion in the $-x$ direction toward the origin of the coordinate system, with the x component of the velocity $\dot{x}=-u_p$ for all the lattice points. This was to simulate the conditions of impact: We imagined that the mirror image of this lattice was simultaneously (and symmetrically) moving in the $+x$ direction toward the origin from the other side, and with a uniform velocity $+u_p$, and we considered that the impact started when the faces of the two lattices were one equilibrium lattice spacing apart from one another. At this point we allowed the atoms in the two lattices to interact. As the separation became smaller than the equilibrium spacing, the repulsive potentials between the surface layers would decelerate these layers, and cause them to stop and rebound. Similarly, the interior layers would progressively decelerate and compress. By this process, we caused a shock wave to be generated at the interface, and the shock would propagate into the lattice as long as the lattice continued to move toward the origin. Figure 2 describes schematically in the x-τ plane the events near the beginning of the impact for a simplified, one-dimensional, semi-infinite lattice.

With these initial and boundary conditions, our problem was to calculate the position, velocity, and acceleration of all the lattice points affected by the shock wave, by solving the equations of motion at successive instants of time, τ_p, τ_q, etc. From these solutions, we study the details of the shock wave propagation and of the energy conversion, and calculate the properties of the compressed lattice.

3. Numerical Computation

It is convenient to work with dimensionless quantities. In table 1, we list the dimensionless quantities used in our calculations. Most of the symbols have been defined earlier. In addition, $R_a=ar_0=\ln 2/(1-R_1)$, $M_1=KR_aR_e$, σ_{xx} is the normal stress in the x direction, ρ is the density, and other symbols will be introduced as they are needed.

Numerical Method. In terms of the dimensionless variables, the equations of motion become

$$\left.\begin{aligned}\ddot{X}&=d^2X/dt^2=F_x/M_1\\ \ddot{Y}&=d^2Y/dt^2=F_y/M_1\end{aligned}\right\}. \tag{6}$$

We solved these equations numerically by the "improved Euler-Cauchy method" [15]: Consider two successive steps, p and q, in the t-X-Y coordinate system (fig. 3). For step p, at time t_p, points $1p$, $2p$, etc., are in an X-Y plane which contains the line X_p passing through the equilibrium positions of these points in the X direction. In this plane, there are also other points which are the neighbors of $1p$, $2p$, etc., but we do not show them here, in order to

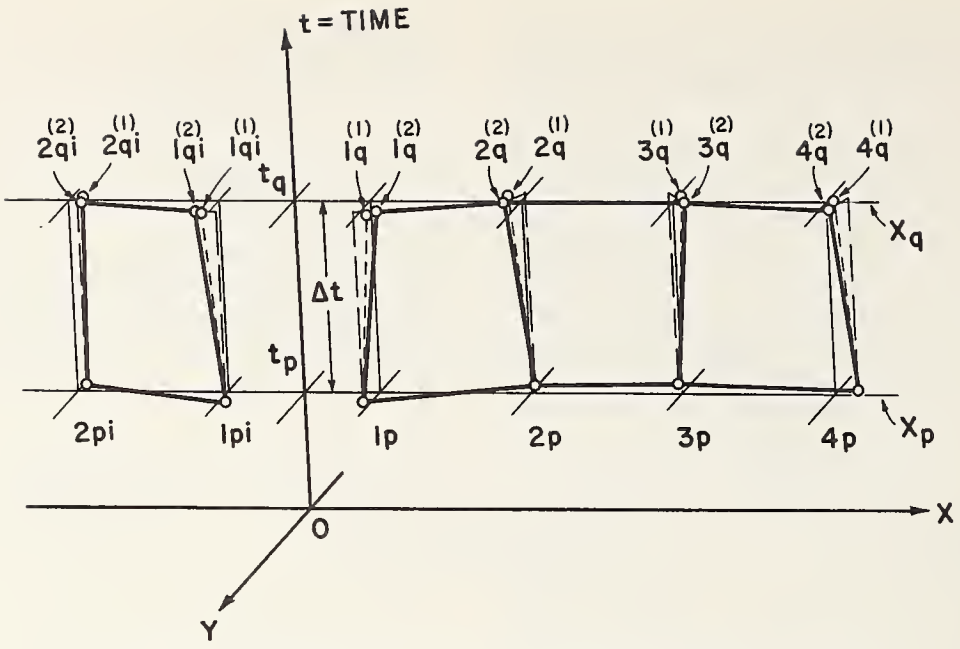

FIGURE 3. *Schematic diagram of the numerical procedure of iteration.*

keep the diagram simple. Point $1p$ is also in the surface layer of the semi-infinite lattice, and $2p$, $3p$, etc. are in the successive interior lattice planes. These planes are generally normal to X_p. Notice that for our fcc lattice, point $2p$ is actually the projection of the nearest neighbors of $1p$ and $3p$ onto the X-Y plane: these neighbors are physically in the $2p$th lattice plane, but they lie above and below the X-Y plane in the Z direction. With $1p$ and $3p$, they form a face of a primitive cell of the lattice. Similar considerations apply to points $4p$, $6p$, etc. In figure 3, we also show points $1pi$ and $2pi$ which are the image points of $1p$ and $2p$, respectively, about the plane $X=0$. The interactions between $1p$ and its neighbors, including those in planes $1pi$ and $2pi$, determine the boundary condition at the face of the lattice.

At step p, the position, velocity, and acceleration (X, Y; $\dot{X}$, $\dot{Y}$; and $\ddot{X}$, $\ddot{Y}$) of points $1p$, $2p$, etc., are

TABLE 1. *List of dimensionless quantities*

Dimensional quantity		Normalizing factor	Dimensionless quantity
Name	Symbol		
Equilibrium lattice spacing.....	r_e	r_0	$R_e=r_e/r_0$
Distance between lattice points.	$r=(r_x^2+r_y^2)^{1/2}$	r_e	$R=r/r_e=(R_x^2+R_y^2)^{1/2}$
Lattice point position.....	x, y	r_e	$X=x/r_e$, $Y=y/r_e$
Lattice point velocity.....	$u_x=\dot{x}=dx/d\tau$, etc.	c	$U_x=X=dX/dt=u_x/c$, etc.
Time.....	τ	r_e/c	$t=\tau c/r_e$
Velocity of sound.....	$c=r_e(k/m)^{1/2}$	$c_0=r_0(k_0/m)^{1/2}$	c/c_0
Potential energy.....	$\Phi=\sum_n \phi_n$	D	$E_p=\Phi/D$
Kinetic energy.....	$e_k=\frac{m}{2}(u_x^2+u_y^2)$	D	$E_k=R_aR_cM_1(U_x^2+U_y^2)$
Force.....	$\mathscr{F}_x=-\sum_n(\alpha\partial\phi/\partial r)_n$, etc.	$2aD$	$F_x=\mathscr{F}_x/2aD$, etc.
Force constants.....	k	$k_0=2a^2D$	$K=k/k_0$
Stress (see text).....	σ_{xx}, σ_{yy}, etc.	ρ_0c^2	$S_{xx}=\sigma_{xx}/\rho_0c^2$, etc.

known, either from previous calculations, or from the prescribed initial conditions. Step q follows step p at an interval Δt later, $t_q = t_p + \Delta t$. At time t_q, the line X_p has moved to the new position X_q, and $1p$, $2p$, etc., to $1q$, $2q$, etc., respectively. Our problem is to determine the position, velocity, and acceleration for points $1q$, $2q$, etc.

As a first approximation, we assume

$$\left.\begin{aligned} &\ddot{X}^{(1)}_{nq} = \ddot{X}_{np}, \qquad \ddot{Y}^{(1)}_{nq} = \ddot{Y}_{np} \\ &\dot{X}^{(1)}_{nq} = \dot{X}_{np}, \qquad \dot{Y}^{(1)}_{nq} = \dot{Y}_{np} \\ &X^{(1)}_{nq} = X_{np} + \Delta t \dot{X}_{np} + \tfrac{1}{2}(\Delta t)^2 \ddot{X}_{np} \\ &Y^{(1)}_{nq} = Y_{np} + \Delta t \dot{Y}_{np} + \tfrac{1}{2}(\Delta t)^2 \ddot{Y}_{np} \end{aligned}\right\} n = 1, 2, \ldots \quad (7)$$

The superscript (1) indicates the value of the first iterate. The subscripts np and nq for $n = 1, 2, \ldots$ correspond to the lattice points in figure 3.

To obtain improved values, we proceed as follows: Let us fix our attention on particle 1. From (7) we have the coordinates $X^{(1)}_{1q}$ and $Y^{(1)}_{1q}$ of particle 1 and those of its neighbors. Note that some of these neighbors are in the image planes $1qi$ and $2qi$, because particle 1 is next to the boundary at $X = 0$. If particle 1 is also next to a transverse boundary, then it also has neighbors in the image planes across the transverse boundary. The coordinates of these neighbors in the image plane are obtained from (7) by reflection. From these new position coordinates, we calculate new pairwise force components on particle 1 from (3). We then obtain the new total force components by summing the pairwise components over all the relevant neighbors according to (4). These are $F^{(2)}_{x1q}$ and $F^{(2)}_{y1q}$ in dimensionless form. The superscript (2) denotes the second iterate. From (6) we have

$$\left.\begin{aligned} \ddot{X}^{(2)}_{1q} &= F^{(2)}_{x1q}/M_1 \\ \ddot{Y}^{(2)}_{1q} &= F^{(2)}_{y1q}/M_1 \end{aligned}\right\}. \quad (8)$$

These are the improved values of the acceleration components for point $1q$. From (8), improved values of velocity and position may be obtained:

$$\begin{aligned} \dot{X}^{(2)}_{1q} &= \dot{X}_{1p} + \tfrac{1}{2}\Delta t(\ddot{X}_{1p} + \ddot{X}^{(2)}_{1q}) \\ \dot{Y}^{(2)}_{1q} &= \dot{Y}_{1p} + \tfrac{1}{2}\Delta t(\ddot{Y}_{1p} + \ddot{Y}^{(2)}_{1q}) \\ X^{(2)}_{1q} &= X_{1p} + \tfrac{1}{2}\Delta t(\dot{X}_{1p} + \dot{X}^{(2)}_{1q}) \\ Y^{(2)}_{1q} &= Y_{1p} + \tfrac{1}{2}\Delta t(\dot{Y}_{1p} + \dot{Y}^{(2)}_{1q}) \end{aligned} \quad (9)$$

We apply equations 3, 4, 8, and 9 repeatedly to all the lattice points, starting from $1q$ in the Y direction to cover the width of N rows, and then from $2q$, . . ., $3q$, . . ., etc., always using the newest available values of F_x, F_y; $\ddot{X}$, $\ddot{Y}$; $\dot{X}$, $\dot{Y}$; and X, Y. In this way, we extend the calculation in the X direction until we pass through the shock front and reach the region undisturbed by the shock wave (see fig. 2). To test this condition, we require that

$$|X^{(2)}_{nq} - (X^{(2)}_{(n-1)q} + 1)| < C, \text{ for two successive } n\text{'s} \quad (9a)$$

Here C is a prescribed tolerance. This completes the second iteration.

In the undisturbed region, there are of course the free oscillations in the Y direction set up initially to simulate the thermal energy in the lattice prior to the arrival of the shock wave. The iterative procedure for computing these thermal oscillations is identical to the procedure just described for the shock compressed region, except that we are concerned here only with the iteration of the motion in the Y direction, the motion in the X direction being given by the uniform motion with a velocity equal to $-U_p = -u_p/c$, as described earlier.

The third and higher iterates are obtained in the same manner. The computation for step q is terminated when the maximum change in the values of X_{nq} and Y_{nq} between successive iterations is less than the tolerance C:

$$\left.\begin{aligned} |X^{(k)}_{nq} - X^{(k-1)}_{nq}| &< C \\ |Y^{(k)}_{nq} - Y^{(k-1)}_{nq}| &< C \end{aligned}\right\} \text{for all } n\text{'s.} \quad (10)$$

Numerical Accuracy, Step Size, and Other Details of Computation. We employed a double-precision scheme for computing the positions of the lattice points in an effort to improve the numerical accuracy. This was necessary because the interatomic forces depended on the differences between the position coordinates of an atom and those of its immediate neighbors, and when the position coordinates assume large values, small errors in these coordinates would cause large uncertainties in the computed forces. Our scheme consisted simply in dividing each position coordinate into two parts: an integer part and a decimal part, and we performed the arithmetic operations separately for the two parts, and then combined them for the purpose of calculating the interatomic forces. In this way, we were able to keep the same number of significant figures (≈ 7 places) in the decimal part of the position coordinates through the entire calculation. The velocities and the accelerations of the lattice points all were of comparable magnitudes, less than unity. We used only the regular single-precision arithmetic for these quantities in order to conserve storage space in the computer.

The numerical accuracy was also affected by the tolerance C (9a and 10) and by the step size Δt, their choice being dictated by the accuracy requirement as well as the economy of computation. We used a value of 10^{-5} for C and 0.2 to 0.25 for Δt. These were found to be satisfactory in our earlier work [6, 7]. With $C = 10^{-5}$, 2 or 3 iterations were usually re-

quired for each step of Δt. A value of $\Delta t = 0.2$ corresponded to a step size of 10^{-14} s, if we took the period of a lattice oscillation at the highest frequency to be 10^{-13} s (wavelength $= 2r_e$), cf. Rahman [11].

We obtained a further check on the numerical accuracy from our study of the problem of approach to equilibrium of an isolated system of 25×25 lattice points taken from a lattice that was previously compressed by a shock wave. For such a system, the energy should remain constant in time. Our results showed that after 860 steps, at $\Delta t = 0.25$, the energy density had changed from 1.011424 to 1.010916, or 5 parts in 10^4.

Apart from the above investigations, we have not analyzed the problem of errors in our numerical method of integration, although the need for such an analysis clearly exists. In addition, we also should examine other numerical methods which may be more efficient than the improved Euler-Cauchy method of integration. These problems have now become important as our computation becomes lengthier with the increased size and dimensionality of the lattice.

The size of the lattice is determined by the size of the computer, and even more importantly, by the cost of computation. With a computer of 65×10^3 words (each word = 36 bits), we could study 3,000 lattice points by our present method of computation. In a two-dimensional array, our maximum lattice size was adjustable from 300×10 (X-Y dimensions) to 60×50. The 300×10 lattice was used mainly to study the propagation of the shock wave in the X direction, while the 60×50 lattice was used mainly to study the boundary conditions and the problem of approach to equilibrium. In both cases, we periodically recorded the computed values of position, velocity and acceleration of the lattice point on a magnetic tape, for later analyses of the stresses, energy density, velocity distribution, velocity autocorrelation, etc., of the compressed lattice. In the shock wave calculations, we have thus far carried the computation to a maximum time of $t = 160$ in the 300×10 lattice, with the shock front reaching about 205 lattice spacings from the face, but for most of the runs, we stopped at $t = 60$. Earlier, in a one-dimensional lattice with harmonic as well as anharmonic forces, we had carried the computation to $t = 1000$ [6], in order to investigate the steadiness of the shock stress profile. Finally, in the equilibrium calculations, we have carried the computation to $t = 250$ in the isolated 25×25 lattice mentioned earlier, but without definitely ascertaining that equilibrium had been established. The time required for this last calculation was about 4 hr.

4. Density and Stress Calculations

In the fcc lattice, if the unstrained equilibrium lattice spacing is r_e, then the normal density ρ_0 is $m/2r_e^3$, and the normal specific volume v_0 is $2r_e^3$ per lattice point. Under compression from external forces, the equilibrium lattice spacings of the deformed lattice become r_{ex} and r_{ey} ($r_{ez} = r_e$ in our two-dimensional case), so that the density ρ now is $m/2r_e r_{ex} r_{ey}$, and the specific volume is $2r_e r_{ex} r_{ey}$. In dimensionless terms, we define the relative density $\bar{\rho}$ and relative volume V as follows

$$\bar{\rho} = \rho/\rho_0 = r_e^2/r_{ex} r_{ey} \tag{11}$$

$$V = v/v_0 = r_{ex} r_{ey}/r_e^2 \tag{12}$$

$$\bar{\rho} = 1/V.$$

These are geometrical quantities, and are easily computed once the equilibrium positions of the lattice points are determined. If the lattice points oscillate, we can define the instantaneous local density and specific volume, and their local spatial and time averages. If the energy density in the shock compressed region should be non-uniform, we might expect the local average of the density and specific volume to differ, also, from the values of (11) and (12), since different parts of the lattice would have different thermal expansions. However, in the small lattice we studied, over relatively short time intervals, we could not detect any difference due to non-uniform energy density profile.

The calculation of the stress components in a lattice with the lattice points at rest at their equilibrium positions has been discussed in detail by Love [16]. The ideas are quite straightforward, and may be summarized as follows:

Consider the unit area A (fig. 1) constructed from the perpendicular bisectors between $0A$ and its nearest neighbors $1A$. The plane of A is normal to the x axis. We wish to calculate the normal component of all the interatomic forces (up to the fourth nearest neighbors, by assumption) which intersect A. This is the usual definition of the normal stress over A. We denote this by σ_{xxo} with the subscript o indicating that the lattice points are not oscillating. For clarity, we imagine the center of $0A$ (and those of $1A$, $2A$, $4A$) to be slightly to the right of A in the x direction. Then the interactions between $0A$ and its neighbors to the right ($1A$, $2A$, $4A$, $1B'$, etc.) do not intersect the plane of A, and need not be considered in the calculation of σ_{xxo}. The interactions between $0A$ and its neighbors to the left ($1B$, $3B$, $2C$, $3C$, $4C$, etc.) intersect A at its center, and the normal components of the interatomic forces (eq 3) all contribute to σ_{xxo}. The interaction between $1B'$ and $1B_1$ is like that between $0A$ and $4C$. This type of interaction also intersects A at the center, and the normal component therefore also contributes to σ_{xxo}. The interaction between $1B'$ and $1B_2$ is like that between $0A$ and $3C$. This type of interaction intersects A at the midpoint of an edge of A, and is shared between two adjacent areas having the edge in common, therefore only one half of the normal

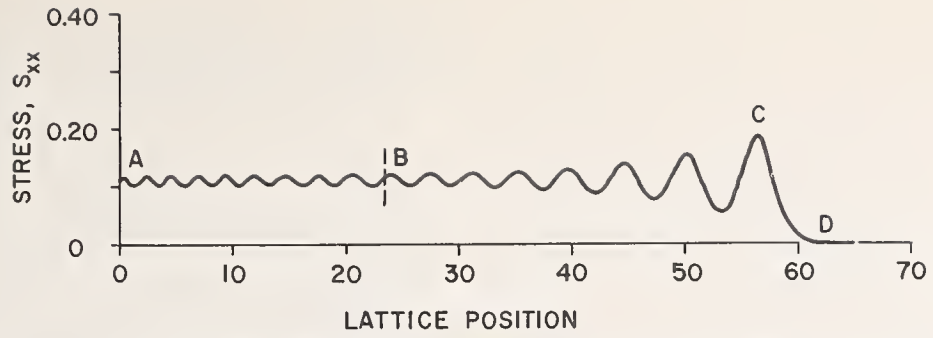

FIGURE 4. *Shock stress profile in a one-dimensional fcc lattice at* $t = 60$, $U_p = 0.1$, *other conditions as given for case* (8) *in figure 5.*

component contributes to σ_{xxo}. Finally, the interaction between $1B'$ and $1B_3$ is like that between $0A$ and $2C$. This type of interaction intersects A at a corner, and is shared among four adjacent unit areas having the point at the corner in common, therefore only one-fourth of the normal component contributes to σ_{xxo}. The resultant σ_{xxo} is the algebraic sum of all the components enumerated above. In a similar way, σ_{yyo} and other stress components may be calculated. We worked with dimensionless stresses. These were obtained by dividing the stress components by the factor $\rho_0 c^2$.

When the lattice points are oscillatory, we can calculate the instantaneous stress components σ_{xx} and σ_{yy} in the same way, except now some of the neighbors $1A$, $2A$ and $4A$ may be to the left of the plane of A, and their interactions with $0A$ also have to be considered. σ_{xx} and σ_{yy} now fluctuate in time and in space, so we must also calculate the appropriate time and space averages of the stress components: For example, σ_{xx} may be averaged over an area in the plane of A to give the instantaneous normal stress in the neighborhood of $0A$. This local stress averaged over time is the normal stress that would be measured on a macroscopic scale at point $0A$. If the lattice as a whole is not moving, the local macroscopic stress obtained this way would be the same over the entire lattice. The difference between the macroscopic stress σ_{xx} and σ_{xxo} is the thermal stress component in the x direction. Similarly for σ_{yy} and σ_{yyo}, etc. These may then be used for calculating the components of the Grueneisen parameter.

In reference [7], we also computed the macroscopic stress σ_{xx} by equating the work done by σ_{xx} per unit time (in a coordinate system which was stationary with respect to the uncompressed lattice) to the gain in the energy of the lattice per unit time, and solving for σ_{xx}. The stress obtained this way was the stress at the interface exerted externally on the lattice, and we were able to verify that this "external" stress was equal to the "internal" stress computed by the method described above. This was as it should be, since the interface did not have an average acceleration in either coordinate system. The disadvantage of the method of computing the external stress is that the motion of the boundary must have a component in the direction of the stress. If the boundary does not move, as in the case of the boundary in the y direction, then this method is not applicable. But the internal stress always can be calculated by the method outlined above.

5. Shock Profile, U_s versus U_p, and Summary of Earlier Results

Figure 4 shows the shock wave stress profile, S_{xx}, in a one-dimensional lattice at a certain instant of time. This was taken from reference [7]. It is a typical profile for a stable lattice. The stress profile in a two-dimensional lattice was found to be very nearly the same as in the one-dimensional lattice, when they were similarly compressed by a shock wave of the same strength (same U_p). We arbitrarily defined the position of the shock front as that point in the leading portion CD (fig. 4) at which the particle velocity was equal to zero in the coordinate system of figure 2. From the shock front position at successive instants of time, we determined the propagation velocity U_s of the shock wave.

Figure 5 shows the computed relationship between U_s and U_p for a large number of cases described in the caption of the figure. This figure was taken from reference [6], except that curve (8) for the fcc lattice, and curve (9) for the bcc lattice apply to both one- and two-dimensional cases. The dashed portion of curves (8) and (9) shows a change in the slope of the U_s versus U_p curve for the fcc and bcc lattices with $R_1 = 0.7$. At this point, $U_p = 0.5$, we found that both lattices showed an interesting instability.[3] This resulted when a lattice point with sufficient energy overcame the potential barrier of the neighboring lattice plane, and jumped into the neighboring cell. We observed that this jumping seemed to occur first in the x direction of shock propagation, and could take place also in the reverse direction, thus causing the lattice to "heal" itself. In the case of the two-dimensional bcc lattice, we also observed instabilities in the y direction, which followed those in the x direction in certain places

[3] We wish to point out that in reference [7], we did not notice the instability which also occurred in the two-dimensional fcc lattice, $R_1 = 0.7$, at $U_p = 0.5$. This was an error which we now wish to correct.

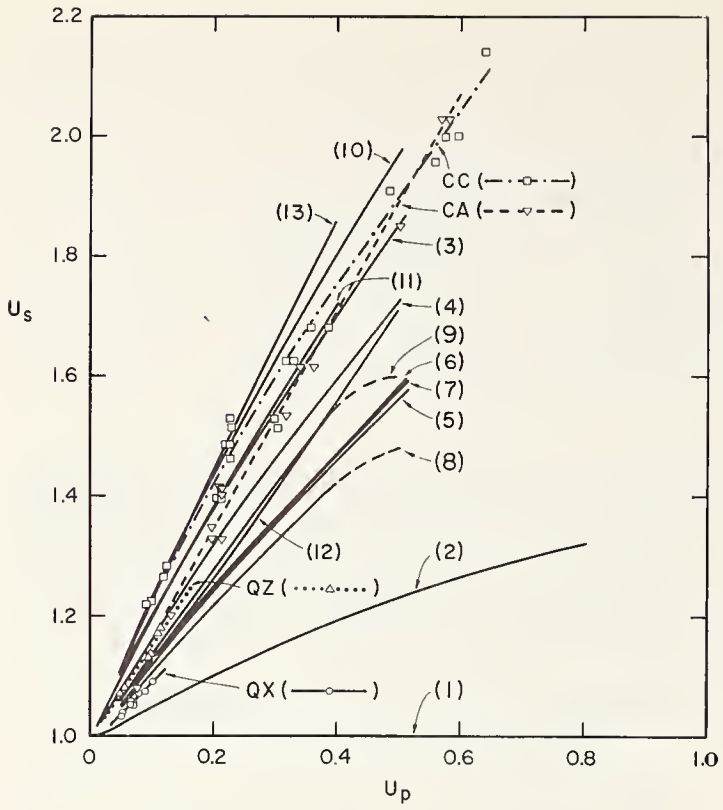

FIGURE 5. *Computed* U_s *versus* U_p.

The conditions for the various curves are given in the table below. All the curves apply to the one-dimensional lattice, except (8) and (9) which also apply to the two-dimensional lattice. Experimental data for graphite, *CA* and *CC*, for shock wave propagating in the *A* and *C* directions, are taken from Coleburn [17]. Experimental data for quartz, *QX* and *QZ*, for shock wave propagating in the *X* and *Z* directions, are taken from Wackerle [18].

Lattice	Linear chain	Square lattice	sc	sc	sc	fcc	bcc
Farthest neighbor taken into account	1st	2d	3d	6th	7th	4th	3d
Hooke's law [a]	[d] (1)						
Parabolic [b]	(2)						
Morse [c], $R_1 = 0.7$	(3)	(4)	(5)	(6)	(7)	[e] (8)	[e] (9)
Morse, $R_1 = 0.8$			(10)		(11)	(12)	(13)

[a] $f_x = k(r - r_0)$.
[b] $f_x = k(r - r_0) - (k'/r_0)(r - r_0)^2$, $k' = k$ for case (2).
[c] See eq (1)–(4).
[d] Numbers in parentheses refer to similarly numbered curves in the figure.
[e] Curves apply to both one- and two-dimensional lattices. Others apply to one-dimensional lattice only.

in the highly agitated region immediately behind the shock front. This caused a progressive disarrangement of the regular lattice structure, in a manner suggestive of the phenomenon of melting. Presumably a similar situation could occur in the three-dimensional lattice as well. In the one-dimensional case, since there was no motion in the y direction, instability in the y direction was of course not observed. We should note that these results are somewhat inconclusive, because in our computational program we did not take proper account of the changing role of the more distant neighbors after the instability first occurred. But up to this point, our results should be reasonably valid. The change in the slope of curves (8) and (9) is especially interesting, and may have a bearing on the interpretation of phase changes observed in shock wave experiments [3]. Further studies are needed to clarify the various details of our results. For this report, we shall not refer to this problem again, but shall confine ourselves only to the stable fcc lattice.

Figures 4 and 5 have been discussed in detail in references [6, 7]. For the sake of completeness, we give here a very brief summary of the main results: (a) We found that in both the one- and two-dimensional cases, the lattice was stable under fairly high compression, and that in the stable region, the computed U_s versus U_p in the two cases was very nearly identical. (b) The computed U_s was very sensitive to the assumed interatomic forces, and the assumed range of interaction. With realistic anharmonic forces, U_s increased with increasing U_p approximately in a linear manner, in good agreement with experimental results (fig. 5). This suggests the possibility of our using the shock wave data for evaluating the repulsive part of the interatomic forces and the range of their interaction, if the structure of the lattice is indeed the same as we have postulated. (c) The typical shock wave stress profile was made up of a steady shock front *CD* (fig. 4), a compressed region *AB* with high frequency, small amplitude oscillations trailing far behind the shock front, and a transition region joining the shock front and the compressed region. The transition region resulted from the interactions of waves of various frequencies generated at the shock front by the anharmonicity of the interatomic forces, and propagating in the dispersive lattice. With increasing time, the transition region also increased in extent. Thus we found that the shock profile was not steady in time, and that the stresses and specific volume we computed for region *AB* were different from those computed on the assumption that the solid was a continuum with a steady stress profile. (d) The computed relationships between the specific volume and the vibrational energy, and between the specific volume and the Grueneisen parameter were in qualitative agreement with published results from other investigations on three-dimensional solids.

The quantities we obtained in (d) above were those averaged over the entire shock wave profile. We would like to examine now in greater detail the problem of energy calculations, with a view to studying the temperature of the shock compressed lattice. Also, in (a) above, although the computed U_s versus U_p was the same for the one- and two-dimensional lattices, the details of the solutions were different. For example, in the one-dimensional case, there were no oscillations in the transverse direction and we would like to know how this would affect the temperature of the lattice. There are two parts to the temperature problem: the calculation of the local energy density and energy distribution in the lattice; and the study of the relaxation process and approach to thermodynamic equilibrium. Of these, the second part is the more difficult, and our results so far are still not extensive enough to give us a

clear understanding on the existence of thermodynamic equilibrium. In the following discussion, our conclusions bearing on this part of the problem are therefore necessarily somewhat tentative.

6. Energy Calculations

Two-dimensional lattice. The energy density e_{av} of a lattice of N lattice points may be defined as follows:

$$e_{av}=\frac{1}{N}\sum_{j}^{N}(\Phi_j+e_{kj})=\frac{1}{N}\sum_{j}^{N}(\Phi_j+mu_j^2/2) \quad (13)$$

where Φ_j is the potential energy of the jth lattice point computed from eq (2), and e_{kj} is the kinetic energy of the jth lattice point, and is equal to $mu_j^2/2$, where u_j is the velocity of the jth lattice point which an observer would see if he were attached to the lattice. N is associated with the region whose energy density we wish to calculate. A point on the boundary or at the shock front is counted as one half of a lattice point. In dimensionless terms, we have

$$E_{av}=e_{av}/D,\ E_{pj}=\Phi_j/D,\ E_{kj}=e_{kj}/D=R_aR_eM_1U_j^2.$$

Figure 6 shows the local energy density in the shock compressed region as a function of lattice position at several instants of time. The positions of the shock front at different times are marked by arrows at the top of the figure. N was taken to be 90 for each local region. The energy density computed this way fluctuated somewhat in different regions, especially near the shock front. If N were still smaller, say $N=9$, the local fluctuations would have been larger. For this discussion, we consider only the mean curves drawn through each set of computed points. These curves show that in the tail part of the shock profile (AB in fig. 4), the average energy density remained very nearly constant in time, and that in the front part of the profile (BC in fig. 4), the energy density increased toward a maximum at the shock front. Beyond the shock front, the lattice was not compressed, so that the energy density was simply equal to the average "thermal" energy given to the lattice as an initial condition. This is indicated by a line marked $E_{tho}=0.037$ on on the ordinate scale. As we have found earlier [7], the energy density averaged over the entire shock profile also remained constant in time. This is indicated by a line marked $\bar{E}_{av}=0.678$ on the ordinate scale. These results imply that the energy density profiles at different times were actually geometrically similar, i.e., we could reduce the different profiles to one by linear adjustments of the scale of the abscissa. The mean curves in this figure, in fact, have all been made geometrically similar this way. Their fit with the computed local energy densities is seen to be satisfactory.

Figure 7 shows a series of histograms of the local energy distribution at various instants of time, corresponding to the curves of figure 6. In each histogram, successive abscissas give the range of energy $(\Phi+e_k)$, and the ordinate gives the count of the lattice points in each energy range. The values of M gives the range of lattice positions covered by

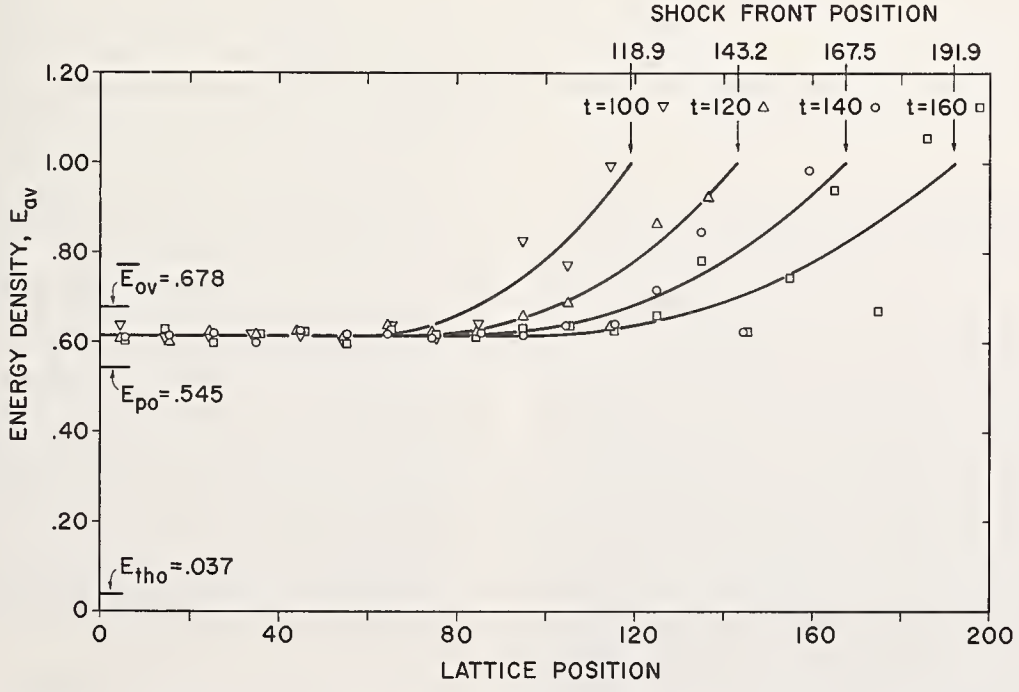

FIGURE 6. *Energy density profile in a two-dimensional fcc lattice under shock compression.*

$U_p=0.2$, other conditions as given for curve (8) in figure 5. E_{po} is the lattice energy at zero temperature. $\bar{E}_{av}$ is the energy density averaged over the entire shock profile. E_{tho} is the thermal energy initially contained in the lattice.

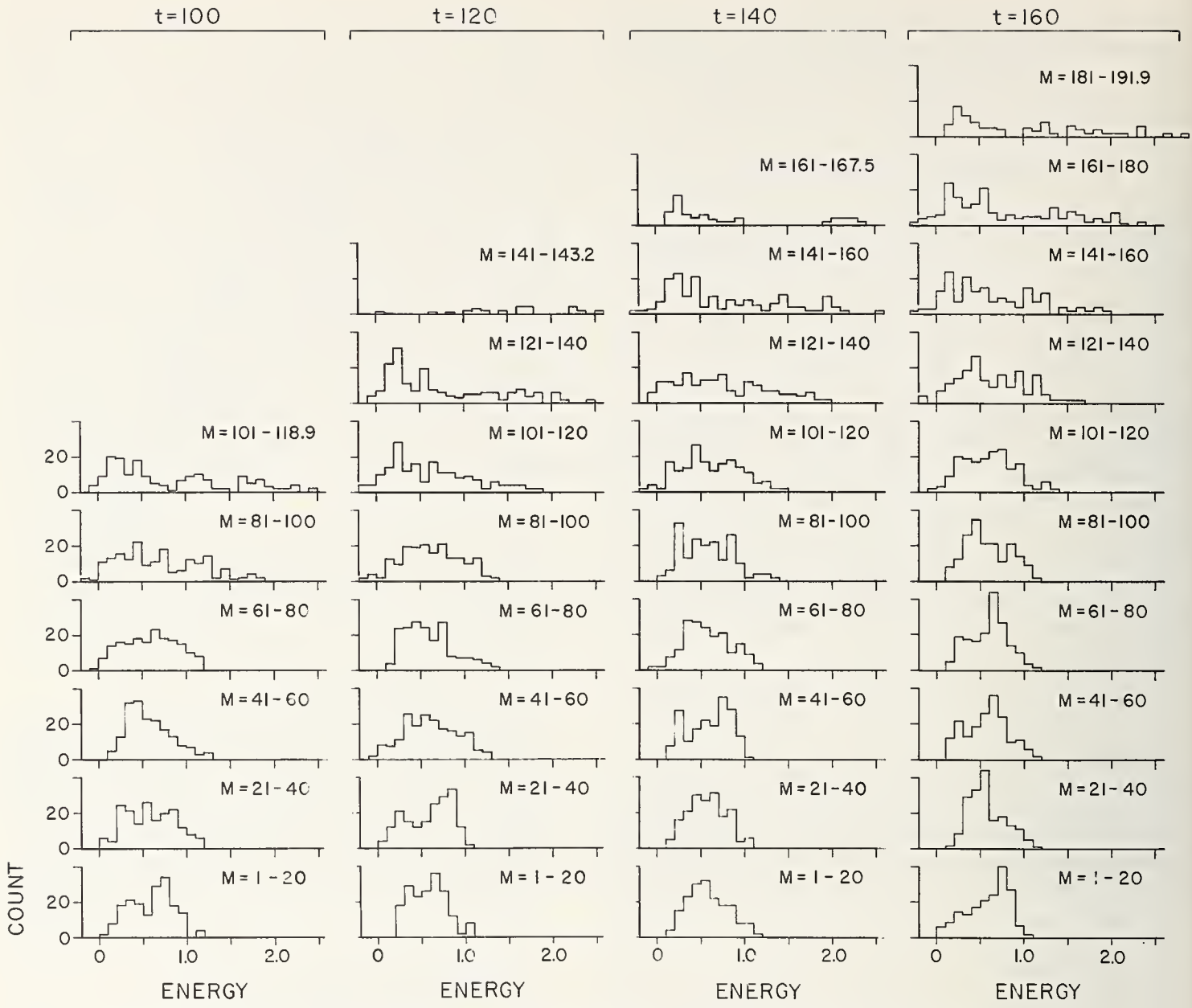

FIGURE 7. *Local energy distribution in the two-dimensional fcc lattice corresponding to the curves in figure 6.*

each histogram, as along the horizontal axis of figure 6. $M=1-20$ denotes the first 20 lattice columns, $M=21-40$ denotes the next 20 lattice columns, and so on, until the shock front is reached. The count in each block of 20 columns is 180 points. We shall designate each block by the first value of M.

The histograms in figure 7 clearly show the time and spatial development of the local energy distribution in the lattice under shock compression. For example, consider the block $M=121$ and its time development from $t=100$ to $t=160$. At $t=100$, the shock has not yet arrived at this position, and the energy distribution, not shown here, would have been the distribution corresponding to the "thermal" energy which the lattice initially contained, with the average value at $E_{tho}=0.037$, as in figure 6. At $t=120$, the shock front has just passed this block, and the energy distribution shows that a number of lattice points have now acquired higher energies. This distribution is typical for the part of the lattice near the shock front, cf., $M=141$ at $t=140$, $M=161$ at $t=160$. As the shock front passed farther into the lattice, the energy distribution of $M=121$ relaxed toward the distributions of those blocks at the tail end of the shock profile. For these blocks ($M=1$, 21, 41, and 61), the energy distributions exhibited fluctuations with respect to position and time. It is clear, however, that their spatial and time averages were very nearly the same, and, indeed, the average energy density for this region remained constant, as shown in figure 6.

In addition to the energy density, we are also interested in studying the vibrational energy, e_{vib}, of the lattice, defined as follows:

$$e_{vib}=e_{av}-\Phi_0 \tag{14}$$

where e_{av} is computed from eq (13) and Φ_0 is the

potential energy per lattice point in a lattice that is compressed to the same specific volume as in eq (13), but with all the lattice points at rest, so that the lattice is at zero temperature. In dimensionless terms, we have $E_{vib}=e_{vib}/D$, E_{av}, and $E_{po}=\Phi_0/D$. If E_{av} is the energy density of the lattice in thermal equilibrium, then E_{vib} computed this way is directly related to the temperature T of the lattice: in a two-dimensional lattice, $E_{vib}=2kT/D$, where k is the Boltzmann's constant.

We shall postpone the discussion of the question of equilibrium until section 8. For the present, it is seen from figures 6 and 7 that in region BC, E_{av} and the energy distribution were both relaxing with time, so that this region certainly was not in equilibrium. On the other hand, in region AB, both E_{av} and the energy distribution and therefore the value of E_{vib} remained very nearly constant in time, so that it is possible to define a steady-state temperature based on E_{vib}. In figure 8, we have plotted the computed $\Delta E_{vib}=E_{vib}-E_{tho}$ as a function of the relative volume V. This figure is similar to figure 2 of reference [7], except that E_{vib} now is computed from E_{av} for the local region AB (fig. 4) whereas in reference [7], E_{vib} was computed from E_{av} for the entire shock profile. For comparison, we have also plotted Pastine's results [20] on aluminum. Pastine employed a fcc lattice model with nearest neighbor interactions, and assumed a Morse potential function with $R_1=0.78$, and uniform compression in three dimensions. His method for computing temperature was also different from ours. We converted his computed temperatures to ΔE_{vib}, by setting $\Delta E_{vib}=3k\Delta T/D$. With these qualifications in mind, we found our results in qualitative agreement with Pastine's.

One-dimensional lattice. The results for the one-dimensional case were rather different. For a linear lattice with harmonic interactions between nearest neighbors, subject to boundary conditions similar to those employed here, there is an exact solution [19] given by the Bessel function of the first kind. For such a solution, the lattice points at the tail end of the shock profile become non-oscillatory as t approaches infinity, and there is no temperature rise in the compressed lattice. Our numerical results for this case indeed agreed with these conclusions, within the accuracy of our calculations. For example, for $U_p=0.2$, at $t=100$, we found that the local energy was distributed about an average value of $E_{av}=0.02$ over the entire shock profile. Near the shock front, the width of the distribution was about ± 15 percent of E_{av} and this width decreased steadily toward the tail of the shock profile. Presumably, after a very long time, the distribution would shrink to a single line at $E_{av}=0.02$. The value of E_{vib} which we calculated was effectively zero.

For a linear lattice with anharmonic interactions, E_{av} no longer remained constant over the entire shock profile but decreased from a maximum at the

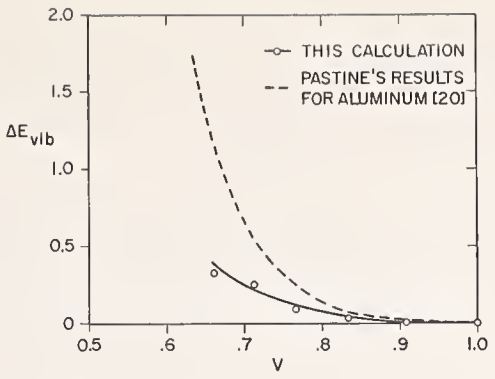

FIGURE 8. *Computed* ΔE_{vib} *versus* V *in region* AB *for the two-dimensional fcc lattice under shock compression, under conditions given for curve (8) in figure 5.*

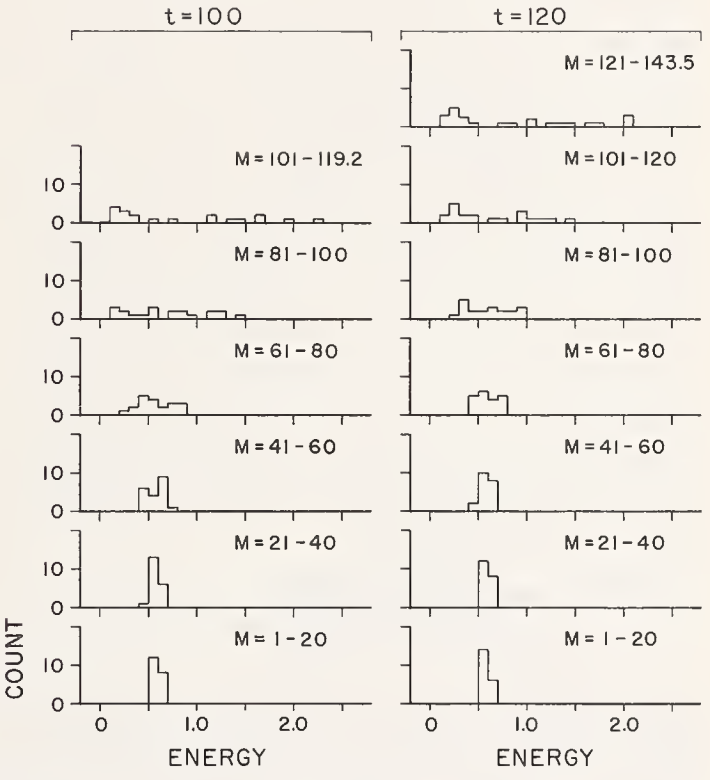

FIGURE 9. *Local energy distribution in a one-dimensional fcc lattice under shock compression.*

$U_p=0.2$, other conditions are the same as those given in figure 6.

shock front toward the steady value at the rear of the shock profile, as in the two-dimensional case (fig. 6). In fact, as was found in reference [7], the values of E_{av} averaged over the entire shock profile were nearly the same for the one- and two-dimensional cases. However, the energy distributions for the two cases were very different: for the anharmonic linear lattice, the energy distribution showed a tendency to become peaked at the local value of E_{av} toward the tail of the shock profile, similar to the harmonic linear chain, whereas in the two-dimensional (anharmonic) lattice, no such tendency was observed. This is shown in figure 9 which is to be compared with figure 7. It seems likely that after a long time, the energy distribution in the tail portion of the shock profile in figure 9

also would shrink to a single line at $E_{av}=0.545$. This means that there would not be any oscillation in that part of the lattice, and that the E_{vib} calculated from eq (14) and hence the temperature rise would be zero.

Suppose we now interpose a rigid boundary in the semi-infinite linear lattice to make it finite. Then the shock wave, upon reaching this boundary, would be reflected back and forth between the two boundaries and eventually the energies in the various modes would be equilibrated [10]. The energy density of the whole lattice would be $\bar{E}_{av}$, and there would be a corresponding E_{vib} and a temperature rise. It seems rather curious that in the one-dimensional lattice there should be no temperature rise in the tail part of the shock profile until after the shock wave has had a chance to be reflected from the rigid boundary, whereas in a two-dimensional lattice there should be a temperature rise upon the first passage of the shock. We do not have a simple physical explanation for this phenomenon. Apparently the transverse boundary condition for the one-dimensional model ($U_y=0$) has the effect of making the "temperature" in the transverse direction zero, and this also makes the "temperature" in the longitudinal direction zero behind a transient shock front. This suggests that the one-dimensional model is not realistic. The results of the two-dimensional model seem more reasonable, but we really should study the three-dimensional case in order to gain a deeper insight to this problem. For the present, in the discussion of the temperature rise behind the shock front, we limit ourselves to the two-dimensional case only.

7. Thermal Relaxation Behind the Shock Front

In the discussion of figure 4, we have noted our earlier results which showed that the transition region BC in the shock wave profile increased in extent as the shock front propagated into the lattice. We see from figures 6 and 7 that this transition region corresponds to a region in which the energy density relaxes from a maximum value at the shock front to a steady value in region AB. So the unsteadiness of the shock wave stress profile is associated with the relaxation of the energy density, and in our computation of the shock profile, we have also obtained a description of the relaxation process behind the shock front.

We may investigate the relaxation time behind the shock front by studying the velocity U_b with which point B moves behind the shock front. The geometric similitude of the energy density profiles (fig. 6) at different times indicates that region AB is a constant fraction of the shock profile, so that U_b is also a constant fraction of U_s.

The precise location of point B is difficult to determine from either the energy density profile or the stress profile. In a further attempt to distinguish region AB from BC, we also studied the velocity distribution of the lattice points in these regions. We found that in region AB the distribution of the velocity components U_x and U_y was nearly maxwellian, but in region BC, especially near the shock front, the distribution was non-maxwellian. Thus, by calculating the width of the distribution curve for the lattice, starting from the tail end of the shock profile and taking successively greater portions of the lattice toward the shock front, we could identify region AB as one with approximately constant width of the distribution curve, and region BC as one in which the width increased toward a maximum near the shock front. We used this method to locate point B, and computed the velocities of U_b at different values of U_p. The results are plotted in figure 10.

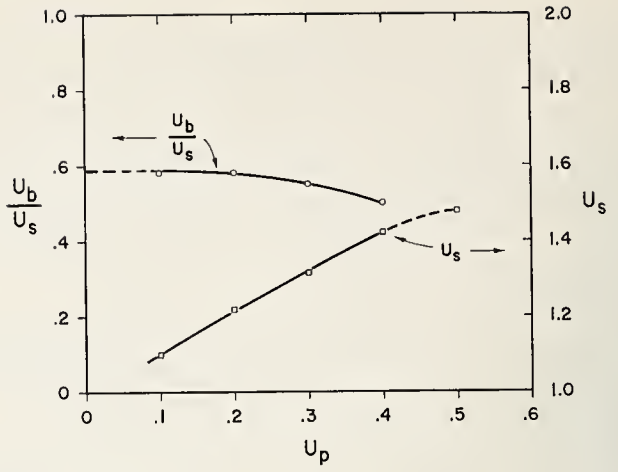

FIGURE 10. *Velocity of propagation of point* B, U_b, *plotted as* U_b/U_s *versus* U_p.

Figure 10 shows that U_b/U_s was approximately equal to 0.58 at low values of U_p, corresponding to low compression, and this value decreased to about 0.5 at $U_p=0.4$. If we consider AB to be a truly steady region, with a steady temperature given in figure 8, then these results give the propagation velocity of point B at the front of this steady region. The value of 0.58 is especially interesting: It is very nearly equal to $1/\sqrt{3}=0.5774$ which is the velocity of second sound in a crystal at normal pressure and low temperature [21]. We are naturally led to speculate that what we have computed here is the equivalent second sound in a crystal under high-stress, high-temperature conditions. Alternatively, we could consider BC as a region of thermal relaxation. Our results in figure 10 show that at higher shock compression (higher U_p and U_s) the relaxation region is a larger fraction of the shock profile.

8. Investigation of the Existence of Equilibrium in Region *AB*

Thus far our results show that in region AB the local averages of the following quantities remained uniform along the lattice and steady in time:

(1) Specific volume
(2) Stress components S_{xx} and S_{yy}
(3) Energy density and E_{vib}
(4) Energy distribution
(5) Approximately maxwellian velocity distribution.

However, even at $t=1000$ ($\approx 5\times10^{-11}$ s), the time of our calculation was short on a macroscopic scale (say 10^{-6} s or greater), so the question of the equilibrium properties of the lattice remains.

To study this problem, we investigated the time development of the velocity distributions. According to the principle of equipartition of kinetic energy in statistical mechanics (see, for example, Guggenheim [22]) the average kinetic energy in each classical degree of freedom is equal to $kT/2$ and the distributions of the velocity components are maxwellian. Hence the average widths (standard deviation) of the distribution curves should be identical. Figure 11a shows the distributions of the velocity components U_x and U_y when the lattice in region AB was compressed more in the X direction than in the Y direction. The velocity distribution in the X direction was also narrower. Thus in this case, we see that the "kinetic temperatures" have not been equilibrated.

We could adjust the final unit cell configuration by compressing the lattice statically first in the Y direction, and then dynamically by means of the shock wave in the X direction. Figure 11b shows that when the final unit cell configuration was more nearly square, the corresponding velocity distributions were more nearly equal.

Closer examination of figure 11b shows that the two velocity distributions were actually not identical, and one wonders whether this was due to the slight difference in the average spacings in the X and Y directions (0.846 in X and 0.850 in Y). To study this problem, we isolated a portion of the lattice in figure 11b, 25×25 lattice points in size, by introducing the boundary condition (b) (see section 3) on all four sides. We also adjusted the distances between opposite boundaries so as to make the average spacing in both the X and Y directions equal to 0.847. We then continued the computation with the conditions of figure 11b as the initial conditions. Our purpose was to observe the time development of the velocity distributions. Since the lattice was now identical in X and Y directions, we would expect that at equilibrium we would not be able to see any difference in the velocity distributions, or in any other property of the lattice, in the X and Y directions. A knowledge of the time required to reach equilibrium, starting from the conditions of region AB behind the shock front, is of considerable interest. Given this knowledge we could then carry out similar calculations over a similar time interval for the case of figure 11a with unequal strain and obtain a detailed description of the equilibrium condition appropriate to this case, assuming that the two cases required similar times to reach equilibrium after shock compression.

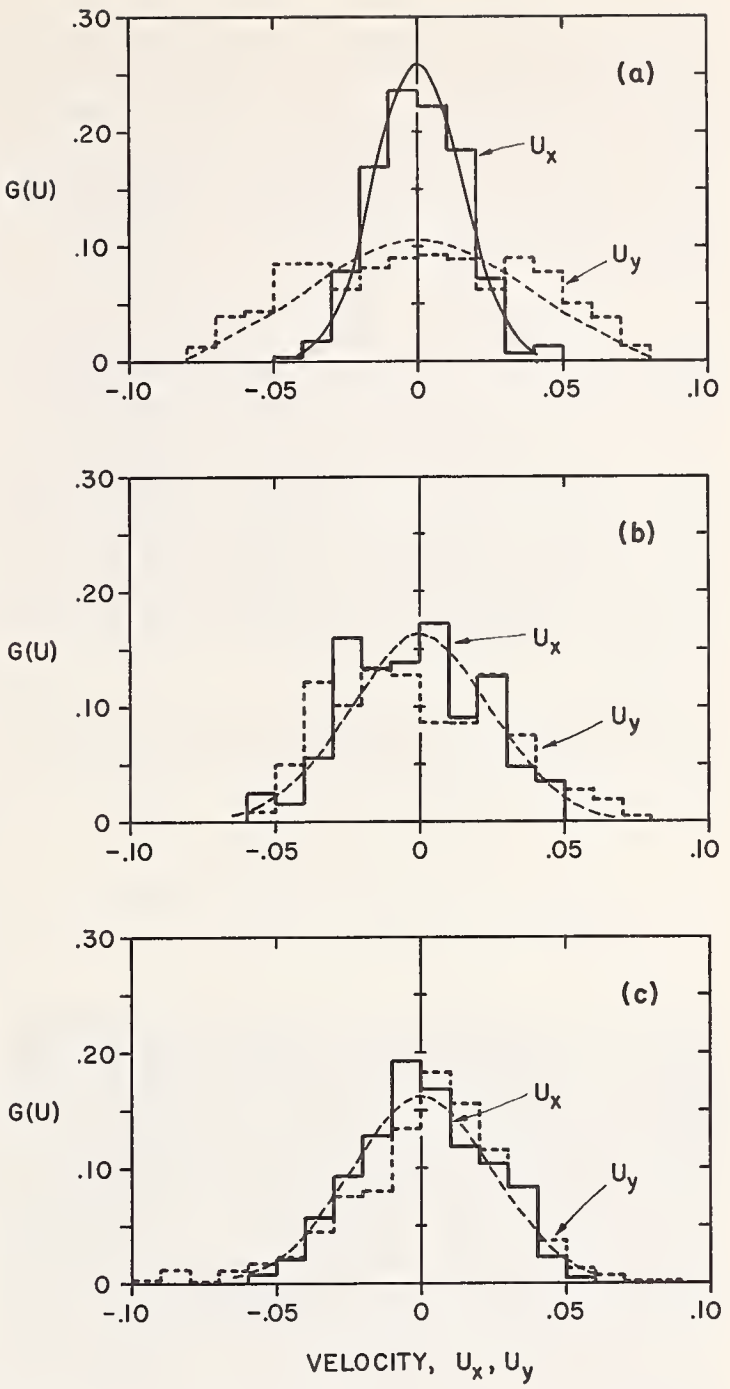

FIGURE 11. *Velocity distribution in three two-dimensional fcc lattices.*

The abscissa gives the range of the velocity components U_x and U_y. The ordinate gives the value of $G(U)$, the fraction of lattice points having velocity in a given range.

(a) Region AB of shock profile, $U_p=0.2$, $t=100$. AB is 60 lattice spacings in X direction and 10 lattice spacings in Y direction. $R_x=0.833$, $R_y=1.000$.

(b) Region AB of shock profile, $U_p=0.2$, $t=35$. AB is 25 lattice spacings in X direction and 50 lattice spacings in Y direction. $R_x=0.846$, $R_y=0.850$.

(c) Isolated lattice at $t=250$, 25 lattice spacings in both X and Y directions. $R_x=R_y=0.847$.

The data for figure 11b were obtained at $t=35$. Starting at this point with the isolated lattice, as described above, we carried the computation to a maximum of $t=250$. The velocity distributions at $t=250$ are shown in figure 11c. Comparing figures 11b and 11c, we see that during this time interval, the velocity distributions had not changed appreciably. The standard deviations for U_x were

385-762 O - 71 - 9

0.0245 at $t = 35$ and 0.0220 at $t = 250$, and those for U_y were 0.0274 at $t = 35$ and 0.0279 at $t = 250$. During this time interval, the velocity distribution also fluctuated, and the averages of all the standard deviations at the end of the interval, at $t = 250$, were 0.0213 for U_x and 0.0327 for U_y. Hence we must conclude that no appreciable equilibration had occurred during this time in the isolated lattice of figure 11c.

We should point out that the isolated lattice of figure 11c enclosed by reflecting boundaries on all four sides was not the same as the lattice of figure 11b which was in contact with region *BC* toward the shock front. The equilibration times for these two systems need not be the same, because in the closed system, equilibration could take place only through the exchange of energies among different modes that were coupled by anharmonic effects, but in the open system, in addition to the exchange of energies, it was also possible for the unequilibrated part to leave the system.

Within the limits of our numerical data, we have also calculated the velocity autocorrelation function which may be defined as [10]

$$\rho_i(t,T) = \frac{\int_0^T U_i(t+\tau)\cdot U_i(\tau)\,d\tau}{\int_0^T (U_i(\tau))^2 d\tau}, \quad T \gg t$$

where ρ_i is the velocity autocorrelation function of particle i, and $U_i(\tau)$ is the velocity of i at time τ. We shall not discuss the details of our results, but briefly, for a point near the middle of the lattice, we found that ρ_i did not decrease nearly so rapidly with t as in the cases studied by Rubin [23], by Northcote and Pott [10], and by Rahman [11]. This was consistent with our conclusion of lack of equilibrium in figure 11c, although it was also possible that we have not made T large enough compared with t.

If in figure 11b we did not achieve equilibrium in region *AB*, we were not very far from it either. Presumably, for some case not too different from that of figure 11b, we could obtain very nearly identical average velocity distributions in the X and Y directions. If we then followed this with additional calculations, as in figure 11c, for the isolated lattice, we would not expect to see appreciable change in the lattice even in long times, and we would conclude that for this case, we might have reached equilibrium. But then the question is why we should be able to reach equilibrium rapidly only in this particular case. This is a curious question to which we do not have an answer. Our basic difficulty at this moment is twofold: We do not have an adequate theoretical model of equilibrium for a small, anharmonic and anisotropic lattice, and we do not have enough numerical results to permit us to construct such a model. We also do not know how this possible lack of equilibrium affects shock wave calculations based on the assumption of equilibrium behind the shock front [1–5]. Further study of these problems and further numerical computation are therefore needed in order to achieve progress in this direction.

9. Grueneisen Parameter Calculations and Summary of Results

The components of the Grueneisen parameter (Grueneisen tensor) may be defined as follows [24]:

$$\left.\begin{aligned}\gamma_{xx} &= v(\sigma_{xx}-\sigma_{xxo})/e_{vib}\\ \gamma_{yy} &= v(\sigma_{yy}-\sigma_{yyo})/e_{vib}\end{aligned}\right\}$$
etc.

In dimensionless terms, we have

$$\left.\begin{aligned}\gamma_{xx} &= 2R_aR_eM_1V(S_{xx}-S_{xxo})/E_{vib}\\ \gamma_{yy} &= 2R_aR_eM_1V(S_{yy}-S_{yyo})/E_{vib}\end{aligned}\right\} \qquad (15)$$
etc.

Here σ_{xxo}, σ_{yyo}, etc. are the stress components when the lattice points are at their equilibrium positions and not oscillating, corresponding to the lattice at zero temperature.

The computed results for the steady region *AB* in our two-dimensional fcc lattice are listed in table 2 which also summarizes the other results. The values are averages over the time (t) period shown. For the isolated lattice, the averages were taken from the first step after $t = 35$ to $t = 250$, and these values are probably more reliable than the others because of the comparatively long time of averaging. Here, the unequal values of γ_{xx} and γ_{yy} for the lattice under equal compression ($R_x = R_y = 0.847$) indicate again the lack of equilibration in the X and Y directions. The other values of the γ components are less reliable because of the shorter time average, and, especially in the case of $U_p = 0.1$, because of the small differences between S_{xx} and S_{xxo}, S_{yy} and S_{yyo}, and E_{av} and E_{po}. There seems to be a systematic decrease of E_{po} with increasing time. We do not have sufficient data to say whether this trend would continue monotonically, or become oscillatory as the lattice rebounds under shock excitation.

Despite the above considerations, the differences between the γ components for the lattice with equal and unequal compression in the two directions are probably real. Specifically, at $U_p = 0.4$ and $R_x \neq R_y$, the specific volume of 0.712 was approximately the same as the specific volume of 0.719 with $R_x = R_y = 0.847$, but the γ components for these two cases differed by a factor of almost 3 or 4. Thus we see that the Grueneisen parameter depends not only on the specific volume, but also on the details of the state of strains (and of the stresses) in the crystal [25].

TABLE 2. *Summary of results*

U_p	t	U_s	Lattice spacing		Specific volume	Stress				E_{av}	E_{po}	E_{vib}	$\frac{U_b}{U_s}$	γ_{xx}	γ_{yy}
			R_x	R_y	V	S_{xx}	S_{xxo}	S_{yy}	S_{yyo}						
0.1	50	1.096	0.908	1.000	0.908	0.1103	0.1099	0.0500	0.0471	0.188	0.151	0.036	0.58	(0.7)	(1.3)
	70	1.101	0.908	1.000	0.908	0.1109	0.1094	0.0472	0.0468	0.188	0.152	0.037			
0.2	100	1.217	0.833	1.000	0.833	0.243	0.230	0.111	0.106	0.619	0.549	0.070	0.58	5.2	2.3
	120	1.216	0.833	1.000	0.833	0.241	0.230	0.113	0.106	0.618	0.546	0.072			
	140	1.219	0.834	1.000	0.834	0.245	0.229	0.112	0.106	0.617	0.544	0.073			
	160	1.221	0.834	1.000	0.834	0.246	0.228	0.112	0.105	0.619	0.541	0.078			
0.3	50	1.311	0.766	1.000	0.766	0.395	0.369	0.196	0.182	1.306	1.177	0.129	0.55	5.1	2.5
	60	1.317	0.767	1.000	0.767	0.396	0.367	0.194	0.181	1.303	1.168	0.135			
0.4	50	1.416	0.711	1.000	0.711	0.567	0.512	0.293	0.267	2.222	1.945	0.277	0.50	4.6	2.1
	60	1.423	0.713	1.000	0.713	0.570	0.508	0.293	0.264	2.223	1.922	0.301			
0.5	50	1.489	0.660	1.000	0.660	0.747	0.673	0.408	0.369	3.255	2.909	0.346		3.9	2.2
	60	1.470	0.660	1.000	0.660	0.734	0.673	0.406	0.369	3.284	2.908	0.376			
0.2	35	1.316	0.846	0.850	0.719	0.404	0.398	0.394	0.394	0.990	0.966	0.023			
Isolated lattice	250	—	0.847	0.847	0.717	0.402	0.400	0.401	0.400	1.011	0.964	0.047		1.2	0.8

10. Conclusions

We have discussed in some detail the dynamical response of a lattice under shock compression, and the associated problems of calculating the properties of the lattice from the dynamical solutions. Our results show that a perfect, two-dimensional lattice (fcc or bcc) is stable under fairly large one-dimensional strain, but under still larger compression, the lattice develops instabilities which are suggestive of melting. In the stable regime, the shock profile is made up of a relaxation region (*BC* in fig. 4) and a steady region (*AB* in fig. 4). The relaxation time is not constant, but increases with time, so that the steady region trails further behind the shock front with increasing time. In the steady region, the energy density, energy distribution, velocity distribution, stress components all remain steady with time. The computed steady-state temperature for this region increases with increasing compression (fig. 8). The propagation velocity of this region decreases with increasing compression (fig. 10), and at low compression, this velocity is about 0.5 to 0.6 times the longitudinal velocity of sound, or approximately equal to the velocity of second sound in a crystal under zero pressure. Our results do not show that there is equilibrium in this steady region. The computed Grueneisen components do not appear to be a function of the specific volume of the lattice alone, but show a strong dependence on the state of strains in the lattice. Finally, we found that although the energy density profiles in a one-dimensional lattice may be nearly identical to those in a two-dimensional lattice, the energy distributions in region *AB* in the two lattices are different: In the one-dimensional case, the energy distribution becomes narrower with increasing time, and presumably becomes a single line at very large times, so that there is no vibrational energy or temperature rise in a one-dimensional lattice; whereas in the two-dimensional case, we do not observe a similar narrowing of the energy distribution or a decrease of the vibrational energy with time. We therefore conclude that the one-dimensional model is not a realistic model for studying the energies of the lattice under shock compression.

The above conclusions apply to the two-dimensional lattice model. All real solids are three-dimensional, and probably imperfect, and at this moment we are unable to say what modifications are necessary before we can apply our results to the three-dimensional case. It is disturbing, nevertheless, that none of our results so far supports the usual assumptions of a continuum solid employed in the analysis of shock wave experiments. On the other hand, our computed relationships between U_s and U_p are in good agreement with experimental data over a wide range of experimental conditions. If this be taken as an indication of the "correct" interatomic forces used in our calculations, then the consequences also must be valid for the model

postulated. We must therefore extend our calculations and refine our model as we continue our study on an atomistic scale. For example, we should extend our calculations to the three-dimensional case and study its energy density and distribution. If we included imperfections in the three-dimensional model, we should be able to study the problem of stress relaxation under shock compression. Also, by propagating the shock wave in an arbitrary direction with respect to the crystalline axes, we could study the effect of shear on the temperature of the lattice. The stability problem and the melting phenomenon of a three-dimensional lattice are also important problems with some hope of experimental verification. Finally, the problem of equilibration is vital to the calculation of the equation of state and other properties of the lattice. These are very lengthy problems, but it seems clear that they must all be studied in comparable detail if we are to complement more effectively the vast amount of experimental work already in progress in this area.

11. Acknowledgments

The author wishes to thank Dr. M. Klein, Chief of the NBS Equation of State Section, for his interest in this work and for his support. The author has benefited from discussions with Dr. C. W. Beckett, Mr. L. Harr, Dr. M. Klein, Dr. R. MacDonald, Dr. R. Nossal, Dr. B. Robertson, and Dr. R. J. Rubin. Mr. J. Barnett provided invaluable assistance in the computational work in the latter part of this investigation.

12. References

[1] Rice, M. H., McQueen, R. G., and Walsh, J. M., Compression of solids by strong shock waves, Solid State Phys. **6**, 1–63 (1958).

[2] Deal, W. E., Jr., Dynamic high pressure techniques, in Modern Very High Pressure Techniques, ed. by R. H. Wentorf, Jr., pp. 200–227 (Butterworths, Washington, D.C., 1962).

[3] Alder, B. J., Physics experiments with strong pressure pulses, in Solids Under Pressure, ed. by W. Paul and D. M. Warschauer, pp. 385–420, (McGraw-Hill Book Co., New York, N.Y., 1963).

[4] Band, W., Studies in the theory of shock propagation in solids, J. Geophys. Res. **65**, 695–719 (1960).

[5] Bland, D. R., On shock structure in a solid, J. Inst. Math. Applications, London **1**, 56–75 (1965).

[6] Tsai, D. H., and Beckett, C. W., Shock wave propagation in cubic lattices, J. Geophys. Res. **71**, 2601–2608 (1966).

[7] Tsai, D. H., and Beckett, C. W., Shock wave propagation in a two-dimensional crystalline lattice, in The Behavior of Dense Media under High Dynamic Pressure, Symposium H.D.P., International Union of Theoretical and Applied Mechanics, Paris, September 1967, pp. 99–108 (Gordon and Breach, New York, N.Y., 1968).

[8] Ulam, S. M., A Collection of Mathematical Problems, pp. 109–113 (Interscience Publishers, Inc., New York, N.Y., 1960).

[9] Alder, B. J., and Wainright, T. E., Studies in molecular dynamics. I. General method, J. Chem. Phys. **31**, 459–466 (1959); II. Behavior of a small number of elastic spheres, J. Chem. Phys. **33**, 1439–1451 (1960).

[10] Northcote, R. S., and Potts, R. B., Energy sharing and equilibrium for nonlinear systems, J. Math. Phys. **5**, 383–398 (1964).

[11] Rahman, A., Correlations in the motion of atoms in liquid argon, Phys. Rev. **136**, A405–A411 (1964).

[12] Payton, D. N., Rich, M., and Visscher, W. M., Lattice thermal conductivity in disordered harmonic and anharmonic crystal models, Phys. Rev. **160**, 706–711 (1967).

[13] Slater, J. C., Interaction of waves in crystals, Rev. Mod. Phys. **30**, 197–222 (1958).

[14] Dean, P., Atomic vibrations in solids, J. Inst. Math. Applications **3**, 98–165 (1967).

[15] Collatz, L., The Numerical Treatment of Differential Equations, 3d ed., pp. 54–57 (Springer-Verlag, Berlin, 1960).

[16] Love, A. E. H., A Treatise on the Mathematical Theory of Elasticity, 4th ed., pp. 616–627 (The University Press, Cambridge, 1934).

[17] Coleburn, N. L., Compressibility of pyrolytic graphite, J. Chem. Phys. **40**, 71–77 (1964).

[18] Wackerle, J., Shock wave compression of quartz, J. Appl. Phys. **33**, 922–937 (1962).

[19] Bateman, H., Partial Differential Equations of Mathematical Pbysics, American ed., pp. 228–236 (Dover Publications, New York, N.Y., 1944).

[20] Pastine, D. J., An equation of state for face-centered cubic metals, J. Appl. Phys. **35**, 3407–3414 (1964).

[21] Chester, M., Second sound in solids, Phys. Rev. **131**, 2013–2015 (1963).

[22] Guggenheim, E. A., Boltzmann's Distribution Law, pp. 34–36 (Interscience Publishers, Inc., New York, N.Y., 1955).

[23] Rubin, R. J., Momentum autocorrelation functions and energy transport in harmonic crystals containing isotopic defects, Phys. Rev. **131**, 964–989 (1963).

[24] Pastine, D. J., Thermal expansion and structure of anisotropic monatomic solids, Phys. Rev. **148**, 748–758 (1966).

[25] Anderson, O. L., Some remarks on the volume dependence of the Grueneisen parameter, J. Geophys. Res. **73**, 5187–5194 (1968). See table 1, p. 5188 for acoustic transverse gamma and acoustic longitude gamma compared with thermal gamma and other calculated "gammas."

DISCUSSION

D. J. Pastine (*U.S. Naval Ordnance Laboratory, White Oak, Maryland*): Referring to figure 8, I would like to make the point that the upper curve ought to be reduced by one-third to compare with yours, because you are dealing with a two-dimensional calculation. This will put you in good agreement on the low end. If you take into account the more recent calculations, the upper curve will be lowered even a little more on the high compression side, so I think the agreement then will be very good between the two.

L. Thomsen (*Columbia University, Palisades, New York*): You said there was not thermal equilibrium. Is it possible to define a local thermodynamic equilibrium or an instantaneous thermodynamic equilibrium?

M. van Thiel (*Lawrence Radiation Laboratory, University of California, Livermore, California*): It is difficult at this stage to compare wave profiles from the calculation with experiment because our time resolution is much less than that which would

be required. It is possible, of course, that over this short a time scale the system has not equilibrated.

In figure 4, showing the wave profile, it looked as though your phonon spectrum from an analysis of the profile was peaked along certain frequencies. We also mentioned earlier that the coupling between the various modes is slow. It is possible, if you can put in the proper zero-point motion for the lattice, that the order that you start with will be disturbed enough that coupling between the various modes becomes easier.

AUTHOR'S CLOSURE

It is true that if we reduced the ordinates of Pastine's curve in figure 8 by one-third, our results would be more directly comparable, and the agreement would improve. However, it is not easy to assess the significance of the improved agreement, because of the differences between Pastine's model and ours, including the unequal compression and the apparently unequilibrated kinetic temperatures in the X and Y directions in our model. Moreover, Pastine's calculations did not consider the thermal relaxation process behind the shock front. His results therefore corresponded to

$$\Delta E_{\text{vib}} = \bar{E}_{\text{av}} - E_{\text{po}} - E_{\text{tho}}$$

(in fig. 6). Indeed, as we showed in reference [7], our ΔE_{vih} based on $\bar{E}_{\text{av}}$ was in fair agreement with Pastine's results. But there is a more serious difficulty: Our one-dimensional results showed that the oscillations in region AB tended to decrease to zero with increasing time, so that in this region the oscillatory (thermal) energy was not one-third of the three-dimensional value, but zero. This clearly indicates that the one-dimensional model was not suitable for studying the problem of temperature rise under transient compression. Whether this difficulty is completely removed in a two-dimensional model is uncertain at this moment.

On the question of local equilibrium, we found that the oscillations in the Y direction, introduced into the lattice initially to simulate thermal vibrations, interacted rather strongly with the large amplitude oscillations near the shock front, and equilibrated rapidly along themselves, even in region BC. The oscillations in the X direction equilibrated more slowly, not until they reached region AB, because of the combined effects of dispersion, and of the moving shock front which steadily lengthened the compressed region. In region AB, the amplitude of the oscillations and hence the anharmonic coupling between the X and Y directions were both small. Our results showed that if these oscillations were not equilibrated before they entered region AB, they would be slow in coming into equilibrium on the time scale of our calculation.

In order to try to find at least a partial answer to the question raised by van Thiel, we displaced different rows in our model by varying amounts before the shock arrived, so that the shock was going into a lattice which was vibrating in the transverse direction. This gives the possibility of some transfer of momentum in the transverse direction. The model still has a rather high symmetry, but what we have done probably simulates fairly well the zero-point vibrational energy or even room temperature vibrational energy in the solids studied experimentally.

Effect of 2024 Aluminum Alloy Strength on High-Pressure Shock Measurements*

M. van Thiel and A. Kusubov

Lawrence Radiation Laboratory, University of California,
P.O. Box 808,
Livermore, California 94550

A shock wave technique is described by which wave profiles may be determined in metals. Piezoresistive manganin gages were used to determine these profiles to 130 kbars in 2024 aluminum alloy. The data are consistent with the assumption that the Hugoniot is the hydrostat. A maximum of 28 kbars is obtained for the maximum yield strength on the release wave following the strongest shock. The derived loading-unloading curves in the pressure volume and pressure mass velocity planes indicate that errors of about 2 percent are produced by use of purely hydrostatic release paths.

When we determine an equation of state from shock wave data, we usually rely on the assumption that the strength of the material is small. We say then that, to a good approximation, the stress in the shock direction is the same as that in the other two directions. This is reasonable insofar as extrapolation of shock wave data to low pressures often yields bulk moduli in good agreement with sonic data. This assumption has, furthermore, been justified by the agreement of shock wave equations of state with Bridgman anvil data. We say this, knowing that Professor Kennedy at the University of California at Los Angeles, in cooperation with some of our coworkers at Lawrence Radiation Laboratory (LRL), have reopened the issue and have questioned the term "reasonable agreement." This is, of course what should happen when, with growing confidence in the validity of our measuring techniques, we can look more critically at possible discrepancies.

Disagreement with the assumption of fluid behavior of the high-pressure Hugoniot has, however, appeared earlier in the shock wave literature. Barker et al. [1][1] and Hartman [2] have shown that strength, indeed, is a factor—at least up to a pressure roughly equal to ten times the Hugoniot elastic limit. But Al'tshuler [3] demonstrated that, even at higher pressure, a sizable strength effect exists in the release process that follows a shock wave. The magnitude of this effect is described by Erkman and Christensen [4], by Barker [5], by the authors [6], and by some unpublished work of Wilkins at LRL. It is evident from this work that strength in metals, even above 100 kbars, cannot be ignored. This paper is intended to describe some further measurements taken by us (with manganin gauges) of the strength of the 2024 aluminum alloy at high pressures and the effect of this strength on the temperature and the shape of the release curve.

The method used here consists of measuring a wave profile. To understand this, we will consider loading and unloading curves in the pressure volume plane. The sample is initially compressed by a shock indicated by the dashed line in Figure 1a, where this loading curve is drawn to indicate a two-wave process. This double-wave process occurs for aluminum up to about 100 kbars, while above this pressure the (first) elastic wave, moving with a velocity corresponding to the Hugoniot elastic

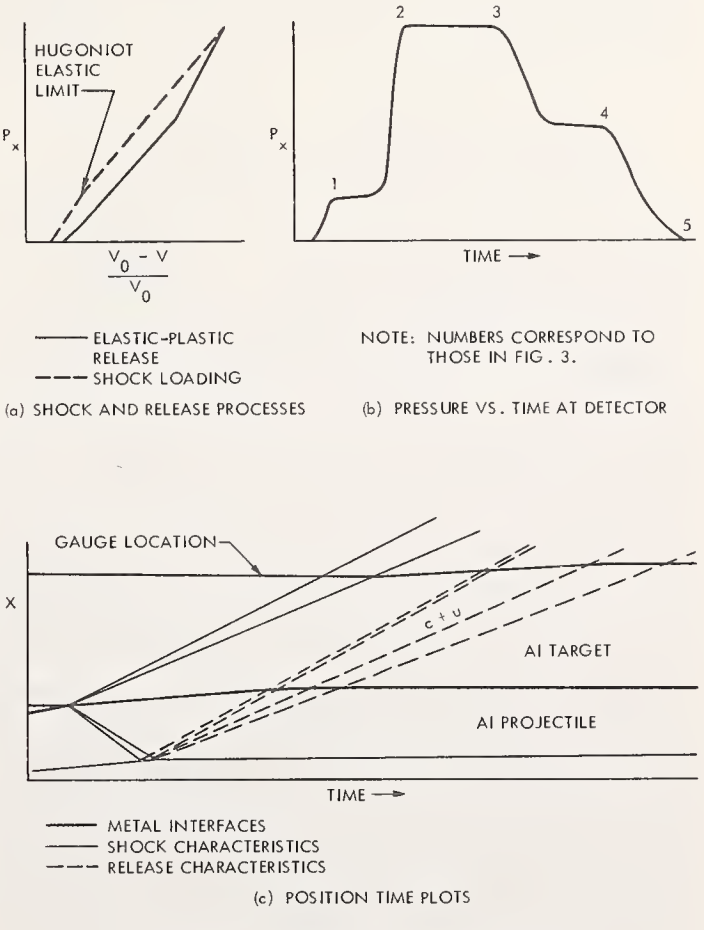

FIGURE 1. *Shock and release processes.*

* This work performed under the auspices of the U.S. Atomic Energy Commission.

[1] Figures in brackets indicate the literature references at the end of this paper.

Paper presented at the Symposium on Accurate Characterization of the High-Pressure Environment, held at the National Bureau of Standards, Gaithersburg, Md., October 14–18, 1968.

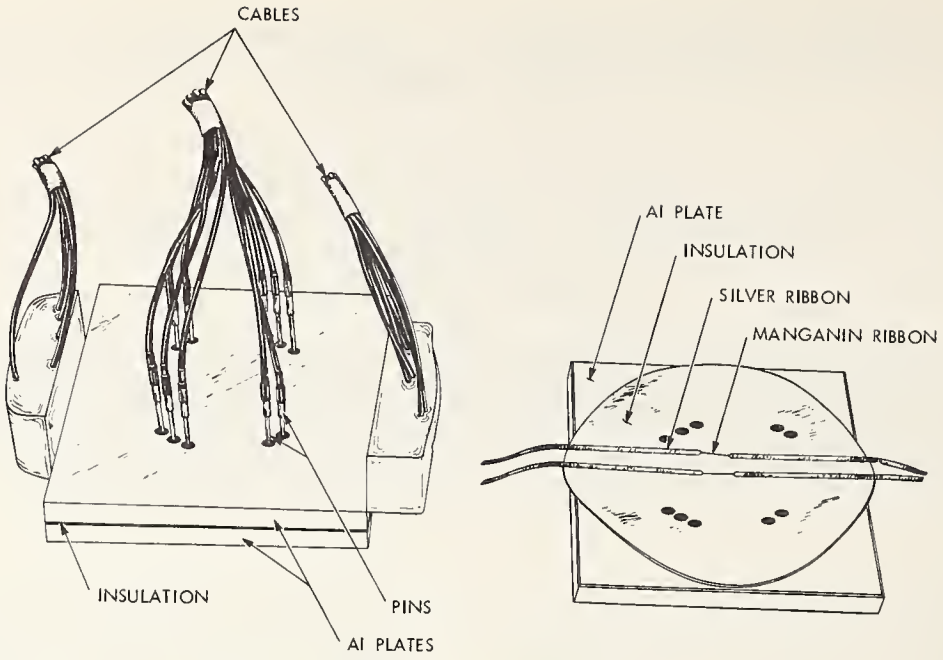

FIGURE 2. *Target assembly.*

limit (HEL), is overtaken by the plastic shock. When the wave starts unloading, simple elastic-plastic theory [7] indicates that initially the material unloads along an elastic release curve until the difference in the stresses in the x and y direction are sufficiently large to cause dislocation flow and yielding. Thereafter, the release curve is essentially that of a hydrostatically compressed material, and the slope, therefore, is given by the bulk modulus. In fact, this release curve is a nonisentropic adiabat, with the energy dependence

$$dE = -P_x dV = \frac{2}{3} Y(V) dV - \bar{P}(V) dV,$$

where Y is the von Mises yield strength. We also assume that the material can be described by a cubic or isotropic stress tensor.

The wave shape that each part of the loading and unloading curve implies is illustrated in figure 1b. Here we show the pressure as a function of time at a point in the sample. The velocity of the two loading waves is different, since there is a break in the loading curve at the yield point. The same is true of the unloading curve. Each portion of the loading and unloading curve is characterized by a velocity $dP_X/d\rho = c^2$. Therefore, once we have determined these velocities as a function of pressure, we can construct the hysteresis curve in the P, V plane.

The shock and release wave loci are illustrated in the time-space plane of figure 1c. A plate projectile impacts a target, sending shocks into the target as well as into the projectile. We have drawn these trajectories for the most general case, in which elastic and plastic shocks run at different speeds. A measurement of the velocity of these shocks then yields the two loading curves. Similarly, the detection of the unloading wave at an interface

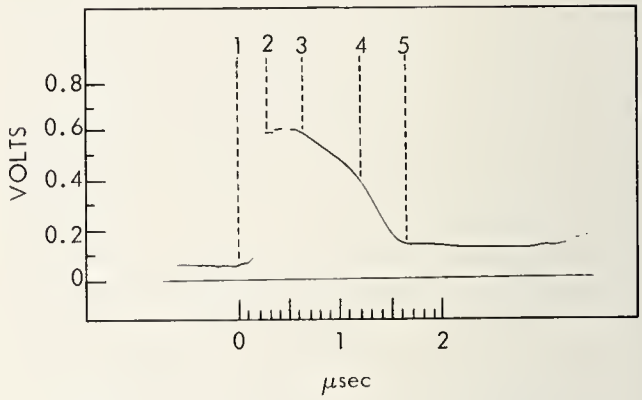

FIGURE 3. *Experimental manganin gauge record.*

(1) Elastic precursor
(2) Plastic shock
(3) Start of semi-elastic release wave
(4) Point at which release wave velocity is comparable to $(dP/d\rho)^{1/2}$
(5) End of release process

containing a pressure gauge yields the characteristics $c+u$, where u is the local mass velocity, and c is the desired velocity in the mass coordinate system. We can calculate u from the Riemann equation

$$\frac{du}{dP} = \left(-\frac{dV}{dP}\right)^{1/2} = \frac{1}{\rho c}$$

and solve for c by iteration. A characteristics code was written to make these calculations as well as to construct the P, ρ curves from the calculated c values.

The experimental assembly used by us is schematically represented in figure 2. Twelve-micron-thick manganin ribbons spot-welded to silver ribbons are placed between two 25-micron-thick insulating sheets of Kapton.[1] A small amount of oil is used to provide a hydrostatic environment for the gauge and to hold the gauge in place on the insulation during assembly. The Kapton insulation is

[1] DuPont polyimide film.

sandwiched between two aluminum plates that make up the target. Voltage and current leads soldered to the silver ribbons are potted in epoxy to strengthen the assembly. Pins are placed around the gauge area to measure projectile velocity and tilt. Shock velocities were not measured, since the projectile velocity and the known shock properties of the material yielded these to sufficient accuracy. All the c values were, therefore, obtained relative to the calculated velocity of the shock wave.

Figure 3 shows the results of a measurement. This is a voltage-time trace of the gauge output. The numbers indicate the various shock and release wave features mentioned earlier. A small disturbance produced by the elastic precursor is followed by the main shock wave. We do not believe that the gauge gives a good measure of the wave shape during the first part of the compression process, since initially it is not in intimate contact with its immediate environment. The behavior, therefore, is not reliable until any small gaps near the manganin gauge element have been eliminated. These gaps must certainly be closed when the release wave reaches the interface between plates where the gauge is located. We note here that the release process does not start with a simple elastic release wave. It starts as a ramp along which the velocity decreases rapidly, from a value that corresponds to a longitudinal modulus to one that corresponds to a bulk modulus. After that, the shape of the release wave is close to the one expected from the usual variation of modulus with pressure.

The gauge is used here in its most reliable mode; namely, as an interpolation device. This is possible, since the peak pressure can be determined from the known shock Hugoniot [8] and the measured projectile velocity. The pressure coefficients of resistivity obtained on the gauges used are somewhat lower than those determined by Keough [9] on gauges potted in epoxy. He obtained coefficients near 0.29 percent/kbar, while the values measured here were near 0.26 percent/kbar; i.e., closer to the statically measured coefficients.

A loading-unloading hysteresis curve calculated from these data is shown in figure 4. The pressure scale on the left shows a peak pressure of 131 kbars. At this shock pressure no elastic precursor exists, and the shock process is described by a single Rayleigh line. The large curvature of the release wave at high pressure is a direct consequence of the shape of the unloading curve in the region where a simple elastic release process was expected. While the initial slope yields a reasonable Poisson ratio, the slope rapidly decreases and goes over to a normal bulk decompression curve. It seems, therefore, that incipient yielding occurs almost immediately at the start of the release process.

Related to this observation is the question of the location of the hydrostatic release curve along which the stresses, both in the direction of the wave and

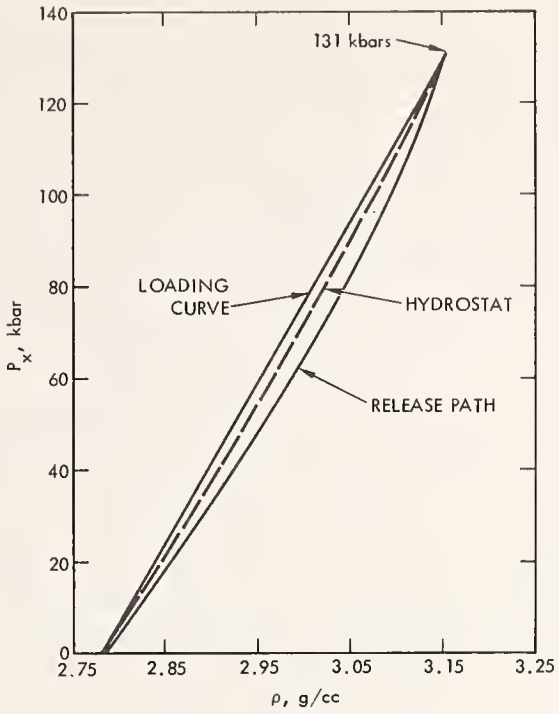

FIGURE 4. *Experimental loading and release curve with estimated hydrostat.*

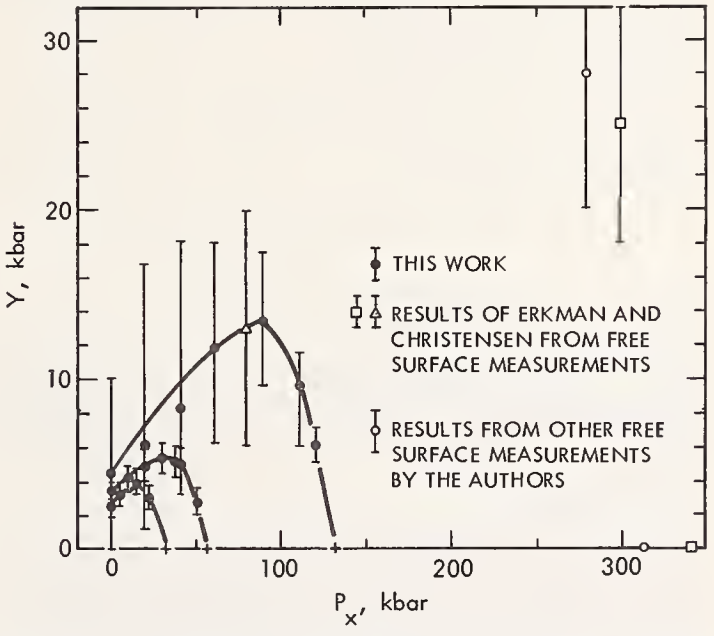

FIGURE 5. *Summary of experimental dynamic strength of 2024 aluminum alloy at high shock pressures.*

at right angles to it, are the same. The release curve must lie below this hydrostat before the direction of the resolved shear stress is such that it can cause dislocations to move. Since some yielding is observed at the very beginning of the release process, this suggests that the Hugoniot point from which the release starts is hydrostatic—or at least close to it. While this may seem surprising, there is no evidence to the contrary. In fact, it is known from double shock experiments [1, 10] that the Hugoniot does not lie on a shock yield surface. In these experiments, [1, 10] elastic compression waves resulted from a second shock immediately following

the first. Following this line of reasoning, we have drawn the hydrostatic release curve through the Hugoniot point. The total energy change along this hydrostat is equal to the change along the release curve plus a small residual energy at $P_x = 0$, due to the small elastic compression stresses that remain in the y and z directions (see Appendix for details of this calculation). After complete release, the final temperature is 51 °C – greater than the initial value. This is 24 °C higher than the final temperature obtained from an isentropic decompression. We will come back to temperature effects later.

In figure 5 we give a data summary of yield strengths obtained in the work described here, as well as three pertinent measurements taken earlier [4, 5], using a free surface technique to detect arrival and decay of the elastic wave. The data obtained by the latter method were reduced, assuming a simple elastic-plastic model. While not entirely correct, this model yields reasonable yield strengths. Turning first to the manganin gauge results, we note that, starting at the Hugoniot pressure (where, by our interpretation of incipient yielding, the yield strength is zero), the yield strength rapidly increases. This yield strength is 1.5 times the stress difference (ΔP_X) between the hydrostat and the release curve, consistent with the von Mises' yield criterion

$$\sum (P_i - P_j)^2 = 2Y^2,$$

and the assumption that

$$1/3 \sum_{1}^{3} P_i = \bar{P} = \text{hydrostatic pressure.}$$

Similar hardening of the sample during pressure release was observed by Barker [5], who used an interferometer method on a somewhat purer aluminum alloy (6061). But, as the release process approaches zero stress, the strength decreases, which is the reverse of what is expected from work-hardening.

From the other three measurements obtained with a free surface technique, it would appear that there is a gradual increase in the hysteresis or strength. If the peak strength levels off at about 28 kbars and then stays constant up to the melting point, we might speculate at what shock pressure melting should first be observed on the release curve. If the release process were isentropic, melting would occur at the foot ($P = 0$) of the release wave from a shock of 680 kbars or stronger. With a constant value of Y, the discrepancy from the isentropically calculated temperatures is roughly proportional to pressure above 300 kbars. This results in a reduction of the shock stress required to initiate melting. Using these data, a shock stress in excess of 520 kbars is sufficient to melt some portion of the sample on release. If the yield strength increases above 300 kbars, this number should further decrease.

One reason for the selection of 2024 aluminum alloy for the present study is its use as a standard to

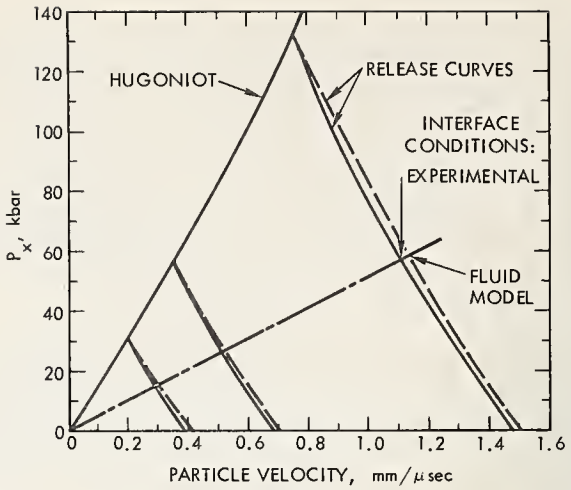

FIGURE 6. *Hugoniot and release curves in the stress-versus-particle velocity plane showing the difference in the interface condition between the duraluminum sample holder and a sample with dynamic impedance $\rho_0 U_s$ for isentropic and measured release curves.*

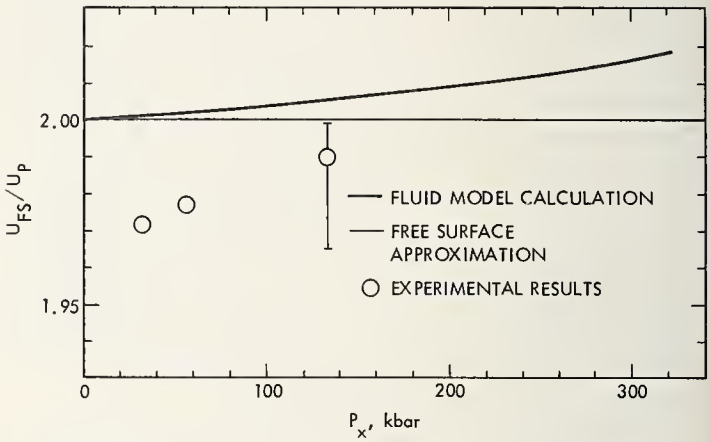

FIGURE 7. *The ratio of free surface-to-particle velocity.*

determine Hugoniots of other materials. To note how this is done, we turn to figure 6, where the data are reproduced in the stress-versus-mass velocity plane. The Hugoniot along which pressure increases with mass velocity behind the wave is represented by the solid line. Here the pressure of the experimental release curves decreases as the mass velocity increases. Calculated isentropic release curves obtained with a fluid model [11] are given by the dashed lines. These curves are used by many shock wave experimentalists to obtain the mass velocity behind a shock in a sample placed on an aluminum plate, through which this shock pressure was applied. The dynamic impedance line of the sample, which has a slope $\rho_0 U_s$ in this plane, meets the measured release curve at the correct pressure and mass velocity of the interface between the sample and the plate. In the example of figure 6, this is about 2 percent lower than would be indicated by the isentropic release curves.

Another, somewhat more approximate but quite convenient, method for determining the particle velocity behind a shock wave is the free surface approximation, where one assumes that the velocity achieved by the sample surface upon arrival of the shock is twice as large as the particle velocity. Those who have used this technique should turn to figure 7.

Here we show the ratio of the free surface velocity to the particle velocity as a function of the shock pressure. Again, a fluid model calculation [11] using the Grüneisen equation of state with the Dugdale-MacDonald [12] formulation for $(\partial P/\partial E)_V$ was used to derive the solid curve. Note that the free surface approximation becomes progressively worse at higher P_x according to this model. The three experimental release curves measured here, however, yield a value less than two. One may expect, however, that this approximation will hold at higher pressures than expected prior to now, because of the compensating effects of shock heating and strength. Barker [12] has observed deviations in 6061 aluminum of 5 percent at even lower pressures.

In summary, we note that the effective yield strength at high pressure increases drastically along the release curve, but that the Hugoniot appears to be hydrostatic, or nearly so. This strength increase causes small but noticeable errors in equation-of-state points measured by using hydrostatic release curves for the 2024 aluminum standard. The free surface approximation is similarly affected. It is also noted that melting will occur on the release waves of shocks weaker than those predicted from fluid models.

Appendix

We consider a plate which has been shock-compressed in the x-direction and subsequently decompressed to $P_x=0$. We wish to calculate the yield strength (the residual stress in the y and z directions) and the temperature.

The stress-strain condition after decompression to $P_x=0$ are defined by

$$\delta P_x=\delta P_1=0=C_{11}\delta\epsilon_1+2C_{12}\delta\epsilon_2 \tag{1}$$

$$\delta P_y=\delta P_z=\delta P_2=C_{12}\delta\epsilon_1+(C_{11}+C_{12})\delta\epsilon_2, \tag{2}$$

for an isotropic medium without shear. From eq (1),

$$\delta\epsilon_2=-\frac{C_{11}}{2C_{12}}\delta\epsilon_1, \tag{3}$$

since at the yield surface $\delta P_y=Y$ (the yield strength) we have from eqs (2) and (3)

$$Y=\left[-\frac{2C_{12}^2}{C_{11}}+(C_{11}+C_{12})\right]\delta\epsilon_2; \tag{4}$$

therefore

$$\delta\epsilon_2=\frac{C_{11}Y}{C_{11}^2+C_{11}C_{12}-2C_{12}^2},$$

and similarly,

$$\delta\epsilon_1=\frac{-2C_{12}Y}{C_{11}^2+C_{11}C_{12}-2C_{12}^2}. \tag{5}$$

For small $\delta\epsilon_i$ at the yield surface,

$$\frac{\delta V}{V}=\delta\epsilon_1+2\delta\epsilon_2$$

$$=2\cdot\frac{C_{11}-C_{12}}{C_{11}^2+C_{11}C_{12}-2C_{12}^2}\cdot Y, \tag{6}$$

and

$$Y=\frac{\delta V}{V}\cdot\frac{1}{2}\frac{C_{11}^2+C_{11}C_{12}-2C_{12}^2}{C_{11}-C_{12}}. \tag{7}$$

Therefore, by substituting eq (7) into eq (5), we get

$$\delta\epsilon_2=\frac{1}{2}\frac{\delta V}{V}\frac{C_{11}}{C_{11}-C_{12}}. \tag{8}$$

The adiabatic energy change to the yield surface is

$$\delta E=\frac{VY}{2}(\delta\epsilon_2+\delta\epsilon_3)=VY\delta\epsilon_2.$$

Now, substituting eq (7) and (8),

$$\delta E=\frac{V}{4}\left(\frac{\delta V}{V}\right)^2\frac{C_{11}(C_{11}^2+C_{11}C_{12}-2C_{12}^2)}{(C_{11}-C_{12})^2}. \tag{9}$$

If the plate was compressed from $V_0P_0E_0$ then decompressed back to V_f, E_f, with $P_x=0$ and $P_y=Y=P_z$, we must first estimate the thermal energy increase before we know the value of the total elastic volume change,

$$\frac{\delta V}{V}=\frac{V_0-V_f}{V}+\frac{1}{V}\left(\frac{\partial V}{\partial E}\right)_P\Delta E,$$

where the thermal energy change, ΔE, is the difference between the final and initial energy plus the elastic energy

$$\Delta E=E_f-(E_0+\delta E).$$

Since δE is usually small, the proper value of $(\delta V/V)$ and Y may be obtained in a few iterations.

NOTE: The analysis given here was made by estimating the elastic constants for duraluminum from

$$C_{11}=\rho_0v_L^2 \text{ and } C_{12}=\rho_0\frac{3v_B^2-v_L^2}{2},$$

with $v_L=0.63$ cm/μsec and $v_B=0.535$ cm/μsec.

Therefore, we have

$$C_{11}=1.1054 \text{ Mbar},$$

$$C_{12}=0.7971 \text{ Mbar},$$

$$\delta\epsilon_2=\frac{\delta V}{V}\cdot 1.94,$$

$$Y=\frac{\delta V}{V}\frac{1}{2}\frac{0.8324}{0.3083}=1.35\frac{\delta V}{V}\text{ Mbar},$$

and

$$\delta E=V\left(\frac{\delta V}{V}\right)^2(2.62)\frac{MB\cdot cc}{g}.$$

References

[1] Barker, L. M., Lundergan, C. D., and Hermann, W., J. Appl. Phys. **35,** 1203 (1964).
[2] Hartman, W. F., J. Appl. Phys. **35,** 2090 (1964).
[3] Al'tshuler, L. V., et al., J. Exp. Theoret. Phys. (USSR) **38,** 1061 (1960).
[4] Erkman, J. O. and Christensen, A. B., J. Appl. Phys. **38,** 5395 (1967).
[5] Barker, L. M., High Dynamic Pressure Symposium I.U.T.A.M., Sept. 11–15, Paris (1967).
[6] Kusubov, A. S. and van Thiel, M., J. Appl. Phys. **38,** 893 (1969).
[7] Morland, L. W., Phil. Trans. Roy. Soc. (London) **251,** 341 (1959).
[8] van Thiel, M., et al., Compendium of Shock Wave Data, UCRL–50108 (Clearing House for Federal Scientific and Technical Information, Natl. Bur. of Std., U.S. Dept. of Commerce, Springfield, Virginia) (1966 plus 1967 suppl.).
[9] Keough, D. D., Stanford Res. Inst., Report No. DASA–1414–1 (1964).
[10] Taylor, J., GMX–6, Los Alamos Scientific Laboratory, private communication (1968).
[11] Rice, M. H., McQueen, R. G., and Walsh, J. M., Solid State Phys. **6,** 59 (1958).
[12] Barker, L. M., private communication (1968).

DISCUSSION

O. E. Jones (*Sandia Laboratory, Albuquerque, New Mexico*): If you assume the von Mises yield criterion holds on unloading, then how can you explain the fact that work hardening doesn't occur on loading as well as unloading?

D. J. Pastine (*U.S. Naval Ordnance Laboratory, White Oak, Maryland*): I can understand how you calculate the P_x part of the curve on the release portion, and I understand how you calculated the energy difference between the release curve and what ought to be the hydrostat. But it isn't clear to me how you got the details of the release hydrostat.

G. E. Duvall (*Washington State University, Pullman, Washington*): I would like to comment on the strain rate effects. I understand that the construction of this release curve was based on the calculation of propagation velocities point by point in the profile that you showed. I assume that these propagation velocities were then calculated by assuming that you knew the form of the adiabat at the rear face of the driver and the position of the gage, and you could therefore calculate the time of propagation of each stress level from the rear face of the driver to the gage. I would suggest that if there were a strain rate effect in the aluminum, this could have a significant effect on the shape, and you might very well get a "smearing out" of what would otherwise be a discontinuity in the release curve.

AUTHORS' CLOSURE

In reply to Jones: I can think in terms of dislocations and dislocation tangles being produced. Let's consider the pressure-time plane. A shock front always has some finite width. And within this width there is some sort of stress-time or stress-strain profile. We know there are regions of very high strain rate and regions of lower strain rate. One would expect that the production rate of dislocations would certainly be different in these two regions.

The question is, whether dislocations will be trapped or restrained from further motion in the interval between their production and the stabilization of the stress at the top of the stress wave. If the production rate is very high during some portion of the loading process, some dislocations may be mobile at the top. We know that aluminum in the annealed state is a very soft material and has a strength of less than a kilobar. All we need to do to explain this profile is to say that the strength is less that a kilobar due to the presence of mobile dislocations. On the way down the process is considerably slower. The dislocation production and trapping rates are therefore more like those that occur in normal work-hardening processes.

In answer to Pastine: We assume the Riemann formulation for the actual release curve, which of course is strictly correct only if the state points on the wave are a function of stress only. Strictly speaking, it should be redone in detail for the viscoelastic model. The Riemann formulation used assumes that the mass velocity of the medium plus the sound velocity is a function of stress only. You need only one wave profile because it gives you all the stress states reached during the unloading process. So you get sound velocity versus pressure. The hydrostatic release curve is calculated using a Grüneisen equation of state and a Dugdale-MacDonald form for γ, similar to the method originally used by the GMX–6 group. This approach actually assumes that the Hugoniot state reached is hydrostatic.

On Duvall's comment: The actual deviations from the hydrostatic isotropic derivation Riemann made are not known at this time. We don't know how much the trajectory of each stress point in the position-time plane curves. All the reduction of velocity-time measurements or position-time measurements were done with this approximation so far. I haven't seen any good viscoelastic model that is better than that.

Calculation of Equation of State from High-Pressure Sound Velocity Data*

Albert C. Holt and Richard Grover

Lawrence Radiation Laboratory, University of California, Livermore, California 94550

We describe a method for calculating the Mie-Grüneisen equation-of-state parameters for simple metals from shock Hugoniot data and a knowledge of the volume variation of longitudinal sound velocity at high pressure. The theory is applied to the calculation of the equation of state of aluminum.

1. Introduction

Shock-wave experiments are useful for equation-of-state measurements because the quantities P, V, and E behind a plane shock front can be calculated unambiguously from the velocity U_s of the shock wave and the velocity U_p of the material behind the wave [1] [1]. Thus, by determining U_s as a function of U_p from the results of a series of experiments at different shock strengths, one obtains a line, the Hugoniot, on the PVE equation-of-state surface of the material. Measurement of the U_s (U_p) relationship has, for some time, been a routine matter at some of the nation's laboratories, and recent development of improved measuring techniques [2] insures that these experiments will continue to provide interesting and useful scientific information.

More recently, however, some shock-wave experimentalists have turned their attention to the measurement of material properties behind the shock front [3] and to observations of the evolution of the shape of the shock wave itself [4–5]. The most striking characteristics of this wave evolution are the effects of material rigidity and a number of useful measurements have resulted from this work; for example, the determination of material strengths for the case of one-dimensional strain. Some consequences of these particular measurements will be discussed in a later paper of this Symposium, by Jones and Graham [6].

Another material rigidity effect is the elastic release wave which overtakes the shock front from within the shocked material. This wave travels at the longitudinal sound speed for the shocked material, so that observation of the wave shape at successive points in the solid permits one to calculate the longitudinal sound speed at a point on the Hugoniot. The results from a series of experiments yields the variation of the longitudinal sound velocity along the Hugoniot line. As we have seen in the preceding paper, the shape of the elastic release wave can be used to estimate the corrections to the Hugoniot for the *material strength* of the shock compressed material.

*This work was performed under the auspices of the U.S. Atomic Energy Commission.

[1] Figures in brackets indicate the literature references at the end of this paper.

Paper presented at the Symposium on Accurate Characterization of the High-Pressure Environment, held at the National Bureau of Standards, Gaithersburg, Md., October 14–18, 1968.

The object of this paper is to utilize the high-pressure sound velocity data for simple metals to estimate the *thermal* corrections to shock data which are necessary to obtain isothermal compression curves. For this purpose, a thermal equation of state is derived from a modification of Slater's theory, and the theory is applied to recent release wave velocity data on aluminum.

2. Theory

We now proceed to make some assumptions about the nature of the solid and to show that these assumptions are sufficient to permit one to calculate the equation of state from Hugoniot data and the longitudinal sound velocity data mentioned in the introduction. We begin by assuming that the solid is described by the Mie-Grüneisen equation of state [7],

$$P-P^s(V)=\frac{\gamma}{V}[E-E^s(V)], \tag{1}$$

where γ is the Grüneisen parameter, V is the specific volume, P is the pressure, and E is the specific internal energy. The functions $P^s(V)$ and $E^s(V)$ represent the pressure and specific internal energy along the isentrope which crosses the Hugoniot at $P=0$. (Here, and in the remainder of the paper, "the Hugoniot" means that Hugoniot whose initial point is at $P=0$, $T=300$ K.) Further, we assume that γ is given by the modified Slater formula [9],

$$\gamma=\frac{1}{3}-\frac{1}{3}\frac{\partial \ln C_l}{\partial \ln V}-\frac{2}{3}\frac{\partial \ln C_t}{\partial \ln V}, \tag{2}$$

where C_l and C_t are the longitudinal and transverse sound speeds in the isotropic continuum approximation, and γ is regarded as a function of volume but independent of temperature.

Equation (2) improves on previous theories [8] in the following way: Instead of inferring the volume dependence of all the normal mode frequencies from the volume derivatives of the pressure, eq (2) infers this volume dependence from the actual volume dependence of the three acoustic modes in the isotropic continuum approximation. Thus we allow for different average thermal properties in the longitudinal and transverse modes of the lattice vibration of the solid. This improved theory is still

not adequate, however, for more complicated atomic systems such as diatomic solids which contain distinct optical modes of vibration whose behavior is not closely related to that of the acoustic modes. We refer to the metals which do not have these distinct optical modes as "simple" metals.

Finally, in this calculation we assume that the normal stress in the shock wave, given by the jump condition [1]

$$\sigma_N = U_s U_p V_0^{-1}, \tag{3}$$

(where σ_N is the stress normal to the wavefront and V_0 is the initial specific volume) is equal to the pressure behind the shock front. Thus we neglect the effect of stress anisotropy in calculating the pressure behind the shock front. For a more detailed calculation, one would correct σ_N to P as suggested in the preceding paper.

To derive expressions for γ, P^s, and E^s, we note that the pressure P_H and the energy E_H along the Hugoniot curve are known as functions of U_p and U_s by means of the jump conditions,

$$E_H = U_p^2/2 \tag{4}$$

and

$$P_H = U_s U_p V_0^{-1}. \tag{5}$$

The third jump condition,

$$1 - \frac{V}{V_0} = U_p/U_s, \tag{6}$$

and the experimentally determined relationship between U_s and U_p,

$$U_s = C + S_1 U_p + S_2 U_p^2, \tag{7}$$

are sufficient to determine E_H and P_H as functions of V along the Hugoniot. We could now, at least in principle, substitute E_H and P_H for E and P in eq (1) to obtain an identity in V among the three unknowns $\gamma(V)$, $P^s(V)$, and $E^s(V)$.

At this point, we allow eqs (6) and (7) to define the transformation to a new dimensionless variable, $x = U_p/C$, which will be used in place of V. By substituting eq (7) into eqs (4), (5), and (6), we obtain E_H, P_H, and V as functions of x, and on substituting these quantities into eq (1), we obtain the equation

$$\left\{\frac{1+(S_1-1)x+CS_2x^2}{1+S_1x+CS_2s^2}\right\}\left\{x+S_1x^2+CS_2x^3-\frac{V_0P^s}{C^2}\right\} = \gamma\left(\frac{x^2}{2}-\frac{E^s}{C^2}\right), \tag{8}$$

which holds identically in x. The quantities P^s, E^s, and γ in eq (8) are now functions of x which we would like to determine.

Because of the limited range of data available, adequate solutions to eq (8) can be found by means of a Taylor series expansion in x for P^s, E^s, and $\gamma(x)$. If we write

$$\frac{V_0P^s}{C^2} = ax + bx^2 + dx^3 + ex^4 + \ldots, \tag{9}$$

then the unknown coefficients a, b, d, . . . may be determined by substituting $\gamma(x)$, $E^s(x)$, and $P^s(x)$ into eq (8) and equating coefficients of equal powers of x. The expression for E^s follows easily, since

$$P^s = -\frac{dE^s}{dV}, \tag{10}$$

we have

$$E^s = -\int_{V_0}^{V} P^s(V')\,dV'. \tag{11}$$

By changing the independent variable in eq (11) and substituting P^s from eq (9), we obtain

$$E^s/C^2 = \frac{ax^2}{2} + \frac{b-2S_1}{3}x^3 + \frac{(d-2S_1b+3S_1^2a)}{4}x^4 + \ldots, \tag{12}$$

which is the desired expression for $E^s(x)$.

In order to determine $\gamma(x)$, given by eq (2), in terms of a, b, d, e, . . ., we suppose that $C_l(U_p)$, the longitudinal sound speed, has been measured at points lying on the Hugoniot, and we write

$$C_l/C = \alpha + \beta x + \delta x^2 + \ldots, \tag{13}$$

where α, β, δ . . . are obtained by fitting eq (13) to the experimental data. We will use eq (13) and the bulk modulus β_s, obtained by differentiating eq (9) to obtain a transverse sound speed C_t. An error is introduced here, since β_s is the bulk modulus on the isentrope, while C_l was measured on the Hugoniot. Strictly speaking, C_l should be corrected for the temperature difference between the two lines at constant volume (or constant x). In the appendix, we calculate $(\partial C_l/\partial T)_V$ for aluminum and find that the temperature correction from the Hugoniot to the isentrope would be much smaller than the other uncertainties in this calculation, and consequently we ignore this small difference.

The bulk modulus on the reference isentrope can be obtained from eq (9) by means of the differentiation,

$$\beta_s = -V\frac{dP^s}{dV} = -V(x)\,\frac{dx}{dV}\frac{dP^s}{dx} \tag{14}$$

and we obtain C_t by substituting eqs (13) and (14)

into the equation

$$C_l=\left\{\frac{3}{4}\left(C_l^2-V\beta_s\right)\right\}^{1/2}. \tag{15}$$

Finally, we obtain an expansion for γ from eq (2),

$$3\gamma=1+\frac{\beta}{\alpha}+\frac{B}{A}+\left\{\left(\frac{\beta}{\alpha}+\frac{B}{A}\right)(2S_1-1)+\frac{B}{A}\left(\frac{2\delta}{\beta}-\frac{\beta}{\alpha}\right)+\frac{\beta}{\alpha}\left(\frac{2D}{B}-\frac{B}{A}\right)\right\}\cdot x+\ldots, \tag{16}$$

where A, B, D, . . . are expansion coefficients for C_l^2 which are determined by eq (15). This expansion is given by

$$C_l^2/C^2=\frac{3}{4}\{A+Bx+Dx^2+\ldots\}, \tag{17}$$

$$A=\alpha^2-1,$$

$$B=2\alpha\beta-(4S_1-2),$$

and

$$D=2\alpha\delta+\beta^2-3CS_2-3d-(5S_1-1)(S_1-1).$$

The indicial equations for eq (8) require that

$$a=1, \tag{18}$$

$$b=S_1, \tag{19}$$

and

$$d=CS_2-\frac{S_1}{9}\left\{1+\beta/\alpha+\frac{B}{A}\right\}; \tag{20}$$

so that the desired expressions for P^s, E^s, and γ are obtained by substituting eqs (18)–(20) into eqs (9), (12), and (16).

3. Calculation

We now apply the theory from the first part of the paper to the problem of calculating the equation-of-state parameters for 2024 aluminum. For this calculation, we use the following values for the Hugoniot parameters of eq (7):

$$C=0.5282 \quad \text{cm}/\mu\text{s}$$

$$S_1=1.4922$$

$$S_2=-0.7229 \ \mu\text{s/cm}.$$

These values represent a least-squares fit to 300 data points obtained at Livermore up to pressures of about 800 kbar.

To obtain the coefficients for eq (13), we have combined results from four sources. The high-pressure sound velocity data came from the paper of Kusubov and van Thiel [7], which preceded this one on the Symposium program, and from an earlier paper by Erkman and Christensen [10]. These data are shown in figure 1. Because of the large uncertainties in this high-pressure data, we have used ultrasonic data [11, 12] to determine the intercept, α, and the initial slope, β. The curvature was obtained from the high-pressure sound velocity data. The three curves in figure 1 are fits to the data made in the following way: For curve A we made a least-squares fit to all of the high-pressure data by varying δ. This represents our best solution for the problem. Curves B and C were made by omitting, in the least-squares calculation, each of the last two data points successively. We use these two curves to test the sensitivity of the calculation to the data and to determine how the experimental uncertainties are reflected in the results of the calculations.

The most sensitive test of the theory is in the calculated values of γ. In table 1, we compare our values of γ_0 and $\partial \ln \gamma/\partial \ln V$ with values obtained from ultrasonic and thermodynamic data. We also include the values of γ_0 and $\partial \ln \gamma/\partial \ln V$ predicted from shock-wave data by means of the Dugdale-MacDonald theory. Our value of γ_0 is, like the acoustic value, not in good agreement with the value of γ_0 obtained from thermodynamic data. On the other hand, the value of $\partial \ln \gamma/\partial \ln V$ which we obtain is within 20 percent of the value of $\partial \ln \gamma/\partial \ln V$ obtained from acoustic data. Further, the acoustic values of γ_0 and $\partial \ln \gamma/\partial \ln V$ with values obtained from curves B and C, so that one can say that there is agreement within the uncertainty of the calculation. The large *experimental* uncertainties are

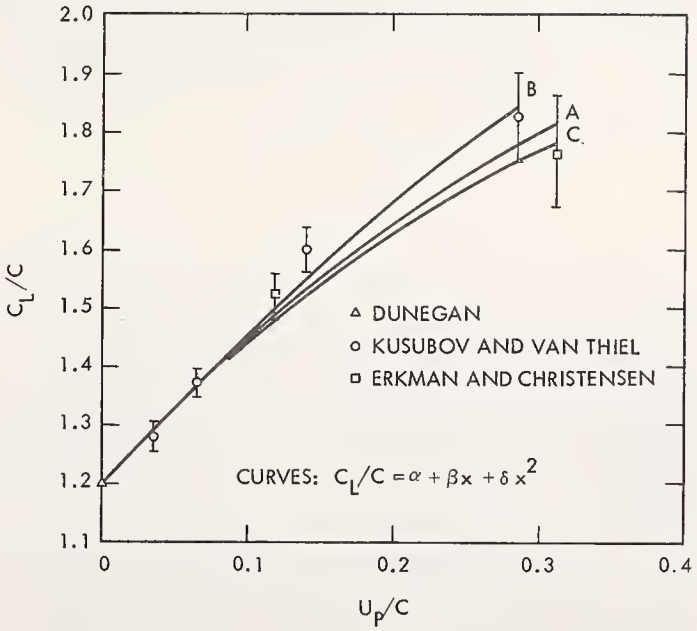

FIGURE 1. *Experimental values of the longitudinal sound velocities are given as a function of shock particle velocity.*

Both velocities are normalized to the quantity C, the $U_p=0$ intercept of the $U_s(U_p)$ relation. The parameters α and β for the curves were determined from ultrasonic data. The curvature, δ, is obtained by the method of least squares. Curves A, B, and C are used to test the sensitivity of the calculated quantities to the experimental results.

TABLE 1. *Values of γ_0 and $\partial \ln \gamma / \partial \ln V$ as obtained from thermodynamic, acoustic, and shock-wave data.*

The Dugdale-MacDonald value is calculated from shock-wave data by means of the Dugdale-MacDonald theory.

	Thermo-dynamic	Acoustic	Dugdale-MacDonald	This work		
				A	*B*	*C*
γ_0	2.13	2.68	1.98	2.97	2.97	2.97
$\frac{\partial \ln \gamma}{\partial \ln V}$		1.65	2.31	1.33	0.246	1.825

TABLE 2. *Comparison of the reference adiabat from this work with the same adiabat calculated by means of the Dugdale-MacDonald theory.*

V/V_0	Pressure (Mbar)		Energy ($\times 10^3$ — Mbar cm^3/g)	
	This theory	From DM γ	This theory	From DM γ
1.0000	0	0	0	0
0.9534	0.0416	0.0416	0.33	0.33
.9127	.0878	0.884	1.25	1.27
.8766	.1377	.1397	2.68	2.74
.8441	.1902	.1952	4.51	4.68
.8147	.2441	.2546	6.65	7.05
.7877	.2984	.3176	9.01	9.81
.7628	.3520	.3844	11.52	12.95

reflected in the wide spread in $\partial \ln \gamma / \partial \ln V$ from curves *B* and *C*.

Finally, we compare our reference adiabat with an adiabat calculated for the same Hugoniot data using the Dugdale-MacDonald γ. This is shown in table 2. The good agreement is not surprising since this adiabat must lie very close to the Hugoniot for the range of pressure we consider.

4. Concluding Remarks

We have shown how high-pressure sound velocity data can be used, at least in principle, to calculate Mie-Grüneisen equation-of-state parameters for simple metals. Although the results of the calculation for the case of aluminum are somewhat disappointing, we feel that there are two strong arguments in favor of pursuing this investigation further.

First, the calculation is an extension of the ultrasonic definition of gamma, which agrees well with the thermodynamic gamma for almost all metals except aluminum. This aluminum anomaly is not, at present, understood. Thus, the fact that high-pressure sound velocity measurements are available only for aluminum is singularly unfortunate. The calculation should be better on the average for other metals.

Second, if the error bars on the sound velocity data could be reduced and if the measurements could be extended to higher pressures, then numerical solutions of these equations can be carried out to yield the high-pressure behavior of γ. We believe that the high-pressure longitudinal sound velocity measurements can be extremely valuable for obtaining more reliable values of the Grüneisen γ.

5. Acknowledgments

This work has benefitted from conversations of the authors with Dr. E. B. Royce. We wish to thank Forrest Rogers for performing some of the equation-of-state calculations referred to in the text.

6. Appendix

The purpose of this appendix is to calculate $(\partial C_l/\partial T)_V$ in order to estimate the magnitude of the correction of C_l from the Hugoniot to the reference adiabat. To this end, we use the thermodynamic identity.

$$\left(\frac{\partial C_l}{\partial T}\right)_V = \left(\frac{\partial C_l}{\partial T}\right)_P + \left(\frac{\partial C_l}{\partial P}\right)_T \frac{\alpha}{\chi_T}, \tag{21}$$

where α is the coefficient of thermal expansion, and χ_T is the isothermal compressibility.

The values of $(\partial C_l/\partial P)_T$ and $(\partial C_l/\partial T)_P$ were calculated from the single crystal data of Schmunk and Smith [12] and that of Kamm and Alers [13] by means of the Voigt-Reuss-Hill-Gilvarry [14] averaging scheme. The values for α and χ_T were taken from the tables given by Gschneidner [15]. Using the values

$$\left(\frac{\partial C_l}{\partial P}\right)_T = 1.821 \times 10^{-3} (\text{cm}/\mu\text{s})\,\text{kbar}^{-1}$$

$$\left(\frac{\partial C_l}{\partial T}\right)_V = -0.747 \times 10^{-4} (\text{cm}/\mu\text{s})\,\text{K}^{-1}$$

$$\alpha = 7.23 \times 10^{-5}\,\text{K}^{-1}$$

$$\chi_T = 1.385 \times 10^{-12}\,\text{cm}^2/\text{dyne},$$

we obtain

$$\left(\frac{\partial C_l}{\partial T}\right)_V = 2.22 \times 10^{-5} (\text{cm}/\mu\text{s})\,\text{K}^{-1}.$$

Since the offset of the Hugoniot from the reference adiabat is on the order of hundreds of kelvins, we estimate that the error introduced by neglecting this difference is less than 1.0 percent. This is much smaller than the uncertainties in the measured values of C_l which we consider.

7. References

[1] Courant, R., and Friedricks, K. O., Supersonic Flow and Shock Waves, Chapt. 3, p. 121 (Interscience, New York, 1948).

[2] For example, see: Barker, L. M., Butcher, B. M., and Karnes, C. H., J. Appl. Phys. **37,** 1989 (1966). For a review, see: Doran, D. G., Measurement of Shock Pressures in Solids, Proc. High Pressure Measurements Symposium, New York, November 1962, p. 59, ed. A. A. Giardini and E. C. Lloyd (Butterworth, 1963).

[3] For example: Mitchell, A. C., and Keeler, R. N., Rev. Sci. Instr. **39,** 513 (1968). Also see: Duff, R. E., et al., Shock-Wave Studies in Condensed Media, Proc. IUTAM Symposium on Behavior of Dense Media Under High Dynamic Pressures, Paris, September 1967, UCRL–70247, Rev. 1.

[4] Some early work: Minshall, S., J. Appl. Phys. **26,** 463 (1955).

[5] For example: Fowles, G. R., J. Appl. Phys. **32,** 1475 (1961); Taylor, J. W., and Rice, M. H., J. Appl. Phys. **34,** 364 (1963); Lundergan, C. D., and Herrmann, W., J. Appl. Phys. **34,** 2046 (1963).

[6] Jones, O. E., and Graham, R. A., Shear Strength Effects on Phase Transition "Pressures" Determined from Shock-Compression Experiments.

[7] Kusubov, A. S., and van Thiel, M., Effect of 2024 Aluminum Alloy Strength on High-Pressure Shock Measurements.

[8] For a brief discussion see: Rice, M. H., McQueen, R. G., and Walsh, J. M., Solid State Phys. **6,** 1, p. 41 (1958).

[9] Pastine, D. J., Phys. Rev. **138,** A767 (1965).

[10] Erkman, J. O., and Christensen, A. B., J. Appl. Phys. **38,** 5395 (1967).

[11] Compendium of Shock Wave Data (UCRL–50108), ed. M. van Thiel, Vol. 1, Sec. A1, Art. 29–12, p. 1.

[12] Schmunk, R. E., and Smith, C. S., J. Phys. Chem. Solids **9,** 100 (1959).

[13] Kamm, G. N., and Alers, G. A., J. Appl. Phys. **35,** 327 (1964).

[14] Anderson, O. L., J. Phys. Chem. Solids **24,** 909 (1963).

[15] Gschneidner, K. A., Solid State Phys. **16,** 275 (1964).

DISCUSSION

D. J. Pastine (*U.S. Naval Ordnance Laboratory, White Oak, Maryland*): I would like to point out that in your model, Poisson's ratio is not independent of volume—that is, this approximation is not made—since a continuum is assumed in calculating the transverse and longitudinal sound speeds separately.

I would also like to make another point in favor of this approach. Your method and the one that I discussed earlier are independent methods, but the values obtained by the two approaches for the Gruneisen parameter are in good agreement.

L. Thomsen (*Lamont Geological Observatory, Columbia University, Palisades, New York*): One possible source of trouble with this formulation is in the high-frequency part of the dispersion curve where the ω versus λ curve bends over so that the acoustic velocity isn't well defined. In that case your expression for gamma is uncertain to the extent that the velocity is uncertain.

G. E. Duvall (*Washington State University, Pullman, Washington*): I inferred that van Thiel thinks that the slope of the release curve right at the Hugoniot point already indicates some plastic flow. If that were the case, his velocity, as indicated by the slope, would represent a smaller velocity than the actual elastic longitudinal velocity; I wonder if this would seriously alter your results.

AUTHORS' CLOSURE

As Mr. Thomsen points out, the velocity is not well defined at higher frequencies, and to some extent our agreement must be considered fortuitous. This seems, at least on the surface, to be a little surprising, but we hope that a further study may turn up a reason for this surprising agreement.

NOTE ADDED IN PROOF: The question raised by Dr. Thomsen may now be answered. Holt and Ross have calculated the individual normal mode gammas for several physically realistic interparticle force laws and for a wide range of densities (see Phys. Rev. **B1,** 2700 (1970)). The calculated values for the transverse modes are all very nearly equal to the average gamma for the transverse modes and conversely the individual mode gammas for the longitudinal modes are all very nearly equal to the average gamma for the longitudinal modes. Thus it appears reasonable to assume that the average gamma for the material is approximated by the weighted average of the longitudinal and transverse acoustic gammas. Since these calculations do not rely on the concept of an "acoustic velocity" one need not concern himself with the fact that an acoustic velocity is not defined near the boundaries of the Brillouin zone.

In reply to Dr. Duvall: I believe that the velocity right at the breaking point is the longitudinal sound velocity. There is some disagreement on this between myself and Dr. van Thiel.

385-762 O - 71 - 10

Shock Temperature Calculations for Silicone Fluid*

M. Cowperthwaite and J. H. Blackburn

Stanford Research Institute, Menlo Park, California 94025

The problem of calculating shock temperature indirectly from experimental data without assuming thermodynamic properties is formulated and solved theoretically. In principle, the $(e-p-v)$ and $(T-p-v)$ equations of state can be constructed in an overlapping domain of the $(p-v)$ plane from a family of Hugoniot curves centered at points of known energy and temperature.

Experiments were performed in an attempt to construct these equations of state for silicone fluid 210. Shock and free surface velocities were measured to determine Hugoniot curves in the 300-kbar regime, and energies and densities were measured from −30 to +260 °C along the atmospheric isobar to determine the initial states of the shock wave experiments. In practice, it was necessary to assume a form for the $(e-p-v)$ equation of state, since the differences in volumes between states on Hugoniot curves at the same pressure above 40 kbar were found to be comparable with the experimental error in measuring the volumes of each of these states. The data were fitted to a Mie-Grüneisen type $(e-p-v)$ equation of state with variable C_v and $(\partial p/\partial T)_v$, since Hugoniot points indicated a linear dependence of energy on pressure along an isochore, and C_v varied along the atmospheric isobar. Shock temperatures on the 25 °C Hugoniot were calculated at points of intersection with isentropes and by integrating with constant atmospheric pressure values of C_v. The position of the 296 °C isentrope limits the temperature calculation with isentropes to values below 522 °C and 58 kbar, and the values around 50 kbar are 8 percent lower than those calculated with the 25 °C value of C_v, since C_v increases along the Hugoniot curve. Temperature calculations above 58 kbar assumed the 296 °C value of C_v. Considerably more experimental work would be required over the entire pressure range to permit determining equations of state of silicone 210 without making assumptions.

1. Introduction

The use of shock waves to study the high-pressure environment in the kilobar regime is based on the assumption that thermodynamic equilibrium is established behind the shock, where material behaves as a perfect fluid. The method is limited at the present time, however, since the mechanical state variables can be measured in shock wave experiments but the thermal state variables cannot. Thus shock wave data are insufficient to determine an equation of state, and shock wave studies provide an incomplete characterization of the high pressure environment. In addition, shocked states are incomplete thermodynamic systems unless shock temperature can be determined, and their characterization is an equation of state problem equivalent to that of determining the temperature-pressure-specific volume $(T-p-v)$ equation of state. In practice, this problem has been solved by assuming thermodynamic properties that allow the unknown state variables to be calculated. More specifically, the form of a complete equation of state is assumed and shock wave data are used as boundary conditions to determine arbitrary functions that would otherwise be undefined. In some cases [1][1] the form of the complete equation of state is an explicit assumption, in others [2–4] it is implicit in the assumptions that enable the state variables to be calculated. But the significance of such a characterization depends upon the correspondence between the assumed and the actual thermodynamic properties of the material.

The present paper describes an attempt to determine shock temperature indirectly from experimental data so as to provide a complete characterization of shocked states without assuming thermodynamic properties. The problem of calculating shock temperature is formulated and solved theoretically. The equations governing shocked states and the identities of thermodynamics [5] are combined to define the experimental data required to construct equations of state without assuming their form. Dow Corning silicone 210 fluid was used as a test liquid.

2. Theory

We first pose the problem of shock temperature and formulate a theoretical basis for its solution. Let e, s, U, and u denote specific energy, specific entropy, shock velocity, and particle velocity, and let subscript o denote the constant state of stationary fluid in front of the shock. Then the Rankine-Hugoniot jump [6] conditions relating shocked and unshocked states,

$$vU = v_o(U-u) \tag{1}$$

$$uU = v_o(p-p_o) \tag{2}$$

$$puv_o = U(e-e_o+\tfrac{1}{2}u^2) \tag{3}$$

express the balance of mass, momentum, and energy

*This work was supported by Physical Research Laboratory, Edgewood Arsenal, under Contract No. DA-18-035-AMC-122(A).

[1] Figures in brackets indicate the literature references at the end of this paper.

Paper presented at the Symposium on Accurate Characterization of the High-Pressure Environment, held at the National Bureau of Standards, Gaithersburg, Md., October 14–18, 1968.

across the shock discontinuity, and the inequality

$$s(e, v) > s(e_o, v_o)$$

expresses the second law of thermodynamics for the irreversible shock process.

Eliminating U and u from eq 3 gives the Hugoniot equation [7]

$$e - e_o = \tfrac{1}{2}(p + p_o)(v_o - v). \tag{4}$$

If an $(e-p-v)$ equation of state satisfies the condition $(\partial^2 p/\partial v^2)_s > 0$, then eq (4) with $v < v_o$ defines the locus of compressed states on the $(e-p-v)$ surface that can be reached from an initial condition (e_o, p_o, v_o) by single shocks. The $(e-p-v)$ equation of state and eq (4) define this locus of shocked states as a curve in the (p, v) plane, $p = p_H(p_o, v_o, v)$, which passes through the point (p_o, v_o) and is called the Hugoniot curve centered at (p_o, v_o). The elimination of u from eqs (1) and (2) gives the equation of the Rayleigh line,

$$p - p_o = (U/v_o)^2(v_o - v). \tag{5}$$

Since a shocked state satisfies eqs (4) and (5), the intersection of the Hugoniot curve centered on (p_o, v_o) and the Rayleigh line of slope $-(U/v_o)^2$ passing through (p_o, v_o) defines the mechanical thermodynamic state (p, v) behind a shock propagating at constant velocity U into a stationary state (p_o, v_o).

With the assumption of thermodynamic equilibrium behind a shock, the state variables of a nonreacting shocked fluid satisfy the following thermodynamic identities:

$$de = Tds - pdv \tag{6}$$

$$T(s, v) = \left(\frac{\partial e}{\partial s}\right)_v \tag{7}$$

$$p(s, v) = -\left(\frac{\partial e}{\partial v}\right)_s \tag{8}$$

For thermomechanical processes, a knowledge of e, s, T, p, and v provides a complete characterization of a thermodynamic state. Thus, the $(e-s-v)$ equation of state is called complete because of the identities (7) and (8) that define the $(T-s-v)$ and $(p-s-v)$ equations of state, but all other equations of state among these variables are incomplete. The $(e-p-v)$ equation of state is incomplete because it cannot be used to calculate temperature and entropy without additional data. Similarly, the $(T-p-v)$ equation of state is incomplete because it cannot be used to calculate energy and entropy without additional data. However, a knowledge of any two incomplete equations of state provides a complete characterization because of the identities of thermodynamics.

The objective of the present work is to use shock wave and low-pressure data to characterize completely the high-pressure environment in the kilobar regime without additional thermodynamic assumptions. Since shock temperature cannot be measured directly with present-day techniques and cannot be calculated from knowledge of the energy along a Hugoniot curve, it is necessary to construct the $(T-p-v)$ equation of state. Such a construction must be based on the mechanical properties of shocked states. At present the only feasible way to achieve this objective is to construct the $(e-p-v)$ equation of state first, and then use it with the identities of thermodynamics to calculate the $(T-p-v)$ relationship. Hugoniot curves form the basis of the experimental method of constructing the $(e-p-v)$ equation of state using shock wave data; the relationship between the $(T-p-v)$ and $(e-p-v)$ equations of state forms the basis for calculating the temperature of shocked states.

2.1. The $(e-p-v)$ Equation of State

An experimental Hugoniot curve $p_H(p_o, v_o, v)$ is the locus of experimentally measured pressure-volume states produced by passing constant velocity shocks of various strengths into an initial state (p_o, v_o). The change in internal energy along a Hugoniot curve is given by eq (4). A family of Hugoniot curves, each of which is centered on a curve along which the energy change is known, is therefore sufficient to determine the $(e\text{-}p\text{-}v)$ equation of state over the domain of the $(p\text{-}v)$ plane covered by the Hugoniots.

In the present work we choose to measure a family of Hugoniots centered on the atmospheric $(p \approx 0)$ isobar, because the energy change can easily be measured along this cross curve.

2.2. Calculation of the $(T-p-v)$ From the $(e-p-v)$ Equation of State

Since the $(T-p-v)$ and $(e-p-v)$ equations of state are both incomplete, it is necessary to establish what additional data are required to calculate temperature when the $(e-p-v)$ relationship is known. It follows from thermodynamic identities that the $(e-p-v)$ and $(T-p-v)$ equations of state are related through the isentropes. The position of an isentrope in the $(p-v)$ plane is determined by the $(e-p-v)$ equation of state and the isentropic condition $de = -pdv$ obtained by setting $ds = 0$ in eq (6). The temperature along an isentrope is given as

$$T = T_i \exp\left[-\int_{v_i}^{v}\left(\frac{\partial p}{\partial e}\right)_v dv\right] \tag{9}$$

by integrating the identity

$$ds=\left(\frac{\partial e}{\partial T}\right)_v \frac{dT}{T}+\left(\frac{\partial p}{\partial T}\right)_v dv \qquad (10)$$

subject to the isentropic condition $ds=0$.

Thus to calculate the $(T-p-v)$ from the $(e-p-v)$ equation of state, it is necessary first to construct a family of isentropes in the $(p-v)$ plane and then to calculate temperature along them with eq (9). It is important to note that temperature cannot be calculated with eq (9) unless the temperatures T_i at particular points (p_i, v_i) on the isentropes are known. Measurement of the temperature along any curve which intersects the entire family of isentropes permits a value of T_i to be assigned to each isentrope. Thus the $(T-p-v)$ equation of state is determined in the domain of the $(p-v)$ plane covered by a family of isentropes. For a given $(e-p-v)$ equation of state, there is a thermodynamically consistent $(T-p-v)$ equation of state for each assignment of temperature along a nonisentropic curve.

Measurements of temperature and energy along the atmospheric isobar are sufficient to calculate the $(T-p-v)$ and $(e-p-v)$ equations of state from a family of Hugoniot curves centered on this isobar. However, the $(e-p-v)$ and $(T-p-v)$ equations of state will necessarily be specified over different but overlapping domains of the $(p-v)$ plane. The family of Hugoniot curves defines the domain where the $(e-p-v)$ equation of state is known, but the family of isentropes constructed from the $(e-p-v)$ relationship defines the subdomain where the $(T-p-v)$ equation of state is known.

3. Experiments

Dow Corning silicone 210 fluid (100 centistokes) was chosen because of its good thermal stability and its large coefficient of expansion. Static experiments were performed to measure the variation of density and specific enthalpy h, along the atmospheric isobar. Shock wave experiments were performed to determine a family of Hugoniot curves centered on the atomspheric isobar.

3.1. Static Measurements

The variation of volume with temperature at atmospheric pressure between −30 °C and 150 °C was measured with a density balance. A least squares fit for the data, with T in degrees Kelvin,

$$v^{-1}=1.2566+1.0577\times10^{-3}T+2.604\times10^{-7}T^2$$

was used above 150 °C to calculate initial conditions for the shock wave experiments. The standard deviation from the least squares fit is less than 0.1 percent of the largest volume measured.

The variation of specific enthalpy with temperature at atmospheric pressure between −26 °C and 318 °C was determined with a drop calorimeter. A least squares fit for the data with T in degrees Kelvin and $h=0$ at $T_1=298$ K is

$$h=16960(1/T-1/T_1)-0.09818(T-T_1)+4.842\times10^{-4}(T^2-T_1^2).$$

The standard deviation from the least squares fit is less than 3/4 percent of the largest enthalpy increment measured.

3.2. Shock Measurements

Four explosive shots were performed to obtain high-pressure equation of state data using an impedance match technique [1]. Each shot assembly contained both cold and hot liquid samples.

A cross section of an assembly showing the brass cells containing the liquid samples is illustrated in figure 1. Plane shocks were induced in the liquid samples by the interactions produced by a brass flier striking the cells. The driver system for the flier plate was a P–80 plane-wave lens in contact with a 4-in pad of high explosive. Shocked conditions in the liquid were varied by varying the composition of the explosive pad.

Direct measurement of shock velocity in the liquid and indirect measurement of the shocked condition in the brass at the cell-liquid interface suffice to calculate the shocked state in the liquid. The measurements were recorded on 70-mm Tri-X film with a Beckmann & Whitley 770 camera writing at a speed of 10 mm/μs; object-to-image ratio was 2.6/1 and the slit overwrite time was 0.01 μs. Figure 2 shows a detailed drawing of a streak camera view of the liquid cells. Changes of reflectivity of

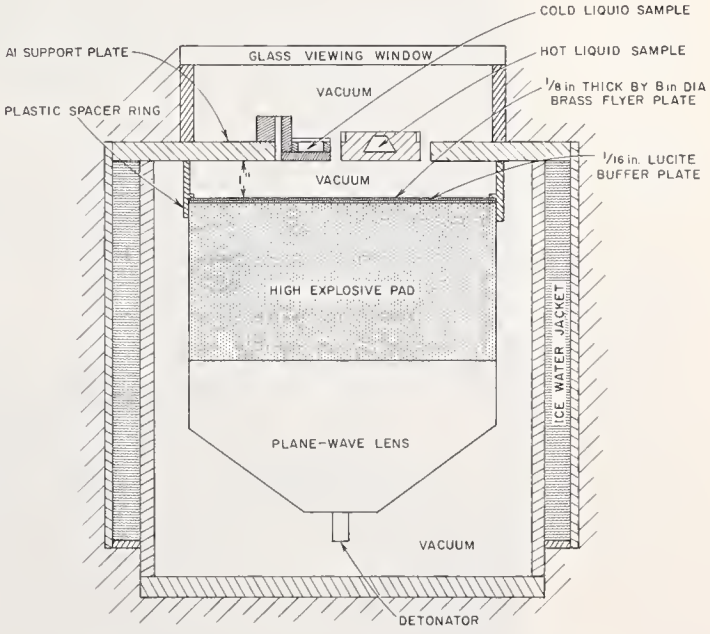

FIGURE 1. *Cross-section of shock experiment.*

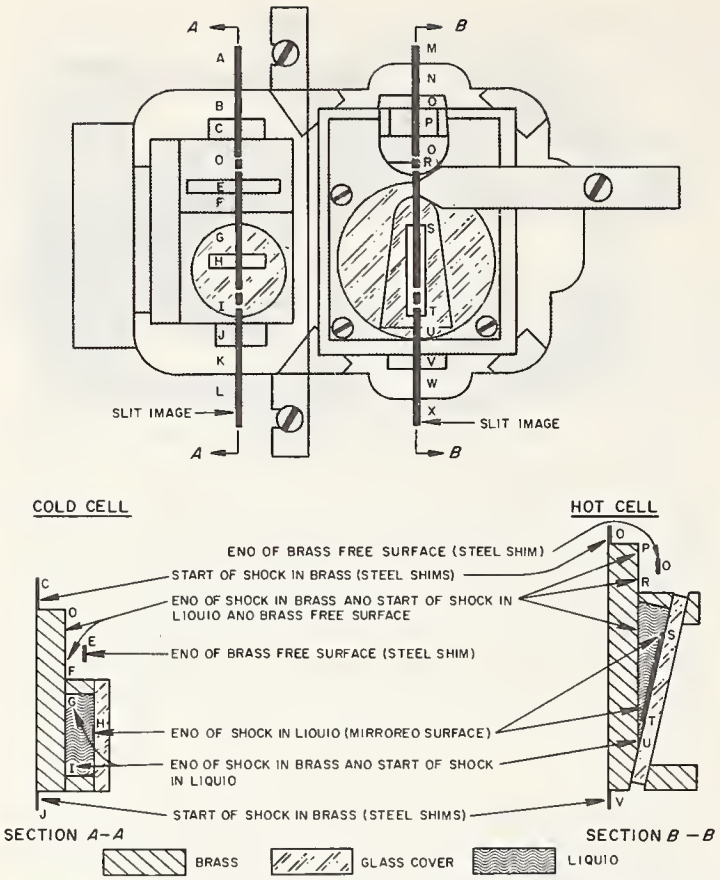

FIGURE 2. *Hot and cold cells: Camera view of hot and cold cells showing slit projection; and cross-sectional views through hot and cold cells along slit lines.*

the steel shims E and C, the brass surface DF, and the mirrored surface H produce signals that depict the series of events for the cold cell in the shock experiment. A typical streak record is shown in figure 3, where the letters identifying the signals match the letters in figure 2. The figure shows (a) the filter plate striking the cold cell at C and J; (b) the time of arrival of the shock at the surface of the brass at D, F, G, and I; (c) the time of arrival of the free surface of the brass at E; (d) entrance of the shock into the liquid at G and I; and (e) time of arrival of the shock at the liquid-glass interface at H. The shock velocity through the liquid was calculated from times recorded at G, I, and H. The shock velocity in the cold brass and its free surface velocity determine conditions at the brass-liquid interface. The shock velocity in the cold cell was calculated using the time differences of location C and D divided into a corrected thickness of the brass at location D. The corresponding free-surface velocity was calculated from times at D, F, and E. The time differences between locations were reduced by 0.022 μs to account for the transit time through the steel shim at location E. Similar calculations were made for the hot cell.

Pressure in the brass was calculated using eq (2) with $p_o = 0$ and with the particle velocity assumed to be one-half free surface velocity. Comparison of the calculated $(p - u)$ points for hot and cold brass

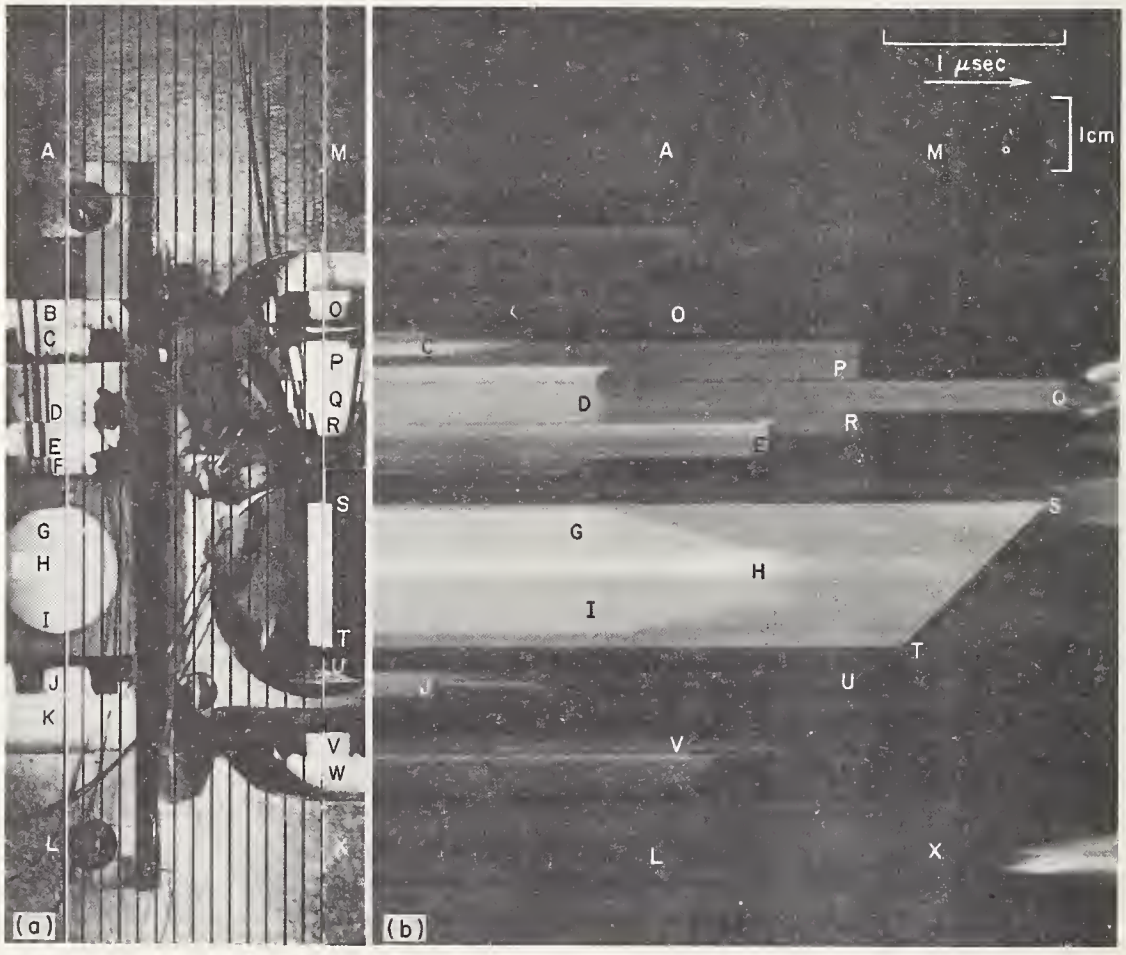

FIGURE 3. *Streak camera photographs: (a) Static; (b) Dynamic.*

TABLE 1. *Summary of shock-wave experiments*

SRI shot No.	Initial conditions			Shock measurements		Calculated shocked states		
	Initial temp.	Specific volume	Specific energies (ref. 0 at 25 °C)	Shock velocity [a]	Particle velocity	Pressure [b]	Specific volume [b]	Specific energy [b]
	(°C)	(cm^3/g)	(J/g)	(mm/μs)	(mm/μs)	(kbar)	(cm^3/g)	(J/g)
12,326	−32	0.983	−92	[c] 6.72 ± 0.02	3.18 ± 0.02	[c] 216 ± 2	[c] 0.518 ± 0.005	[c] 4952 ± 70
11,939	−20	.994	−71	6.91 ± 0.07	3.46 ± 0.03	240 ± 5	0.497 ± 0.009	5887 ± 84
12,228	−20	.994	−71	4.87 ± 0.05	1.87 ± 0.03	91 ± 2	0.611 ± 0.014	1684 ± 44
12,496	−10	1.004	−55	7.11 ± 0.04	3.11 ± 0.01	256 ± 2	0.494 ± 0.004	6474 ± 39
11,939	158	1.178	218	6.47 ± 0.06	3.56 ± 0.02	195 ± 3	0.530 ± 0.008	6548 ± 89
12,496	158	1.178	218	6.61 ± 0.02	3.72 ± 0.01	208 ± 2	0.516 ± 0.004	7225 ± 55
12,326	159	1.179	220	6.16 ± 0.04	3.28 ± 0.03	171 ± 3	0.550 ± 0.008	5607 ± 160
12,228	256	1.299	399	4.08 ± 0.02	1.94 ± 0.01	61 ± 1	0.679 ± 0.008	2290 ± 30
12,326	279	1.330	445	6.09 ± 0.07	3.31 ± 0.01	[c] 152 ± 2	[c] 0.606 ± 0.009	[c] 5927 ± 40
12,496	296	1.350	481	6.39 ± 0.05	3.91 ± 0.02	[c] 184 ± 3	[c] 0.526 ± 0.010	[c] 8095 ± 74

[a] Errors in shock velocity calculated by summing estimated errors in length and time measurements.
[b] Errors computed with absolute values of estimated errors; see ref. [9].
[c] Points omitted from analysis.

with the $(p-u)$ points of McQueen and Marsh [8] for brass initially at 20 °C shows that only the 20 °C Hugoniot curve need be considered for the impedance match calculations. The mirror-image approximation was used for the brass isentropes. Thus pressure and particle velocity at the brass-liquid interface were calculated at the intersection of the Rayleigh line for the liquid and the brass rarefaction curve, assumed to be a reflection of the Hugoniot curve through the measured free surface velocity. The specific volume of the shocked liquid was then calculated using eq (1), and the corresponding change of internal energy was calculated using the Hugoniot equation in the form $e-e_o=\frac{1}{2}u^2$.

The shock wave data are summarized in table 1. The precision of the data is controlled mainly by the pressure uniformity and planarity of the explosive driver system.

4. Construction of $(e-p-v)$ Equation of State

The limited number of experimental Hugoniot points and the restricted range of data along the atmospheric isobar prohibit the construction of an equation of state solely from experimental data. It is important, however, to use both shock wave and static data to indicate the most appropriate form of the $(e-p-v)$ equation of state. A graphic fit of Hugoniot data in the 200-kbar regime, without the three points from shots 12,326 and 12,496 that indicate crossing Hugoniot curves, suggests a linear dependence of internal energy on pressure along lines of constant volume-isochores; static data show that the partial derivative $(\partial e/\partial p)_v$ varies along the atmospheric isobar. Thus, the $(e-p-v)$ data were fitted to the form

$$e=pf(v)+g(v) \tag{11}$$

with $(\partial e/\partial p)_v=f(v)>0$ everywhere in the region of interest.

Additional properties of this model follow from thermodynamic relationships. The relationship between specific heat at constant pressure C_p and specific heat at constant volume C_v is

$$C_p=C_v[1+T(\partial v/\partial T)_p/f(v)] \tag{12}$$

and C_v is constant along an isentrope, since

$$\left(\frac{\partial C_v}{\partial T}\right)_s=\left(\frac{\partial^2 e}{\partial p^2}\right)_v\left(\frac{\partial p}{\partial T}\right)_v^2=0. \tag{13}$$

The equation for a Hugoniot curve centered at $(p_o=0,\ v_o)$ is

$$p[f(v)-\tfrac{1}{2}(v_o-v)]=g(v_o)-g(v) \tag{14}$$

the differential equation for an isentrope is

$$\left(\frac{\partial p}{\partial v}\right)_s=-\frac{p(1+df/dv)+dg/dv}{f(v)} \tag{15}$$

and the equation [9] obtained by formal integration of eq (15) shows that the first derivative of $g(v)$ must be positive, i.e., $dg/dv>0$. The rapid increase of pressure along an isentrope indicates that the $(e-p-v)$ relationship will satisfy the mechanical stability condition $(\partial p/\partial v)_s<0$ if $f(v)$ satisfies the condition $(1+df/dv)>0$.

Values of $f(v)$ in the specific volume range $0.994<v<1.35$ cm^3/g along the atmospheric isobar were calculated with the identity,

$$f(v)=-C_p\left(\frac{\partial v}{\partial p}\right)_s\left(\frac{\partial T}{\partial v}\right)_p \tag{16}$$

The values of C_p and $(\partial v/\partial T)_p$ were determined

experimentally. The values of $(\partial p/\partial v)_s$ were calculated from the sound velocity data of McSkimin [10], which were extrapolated to cover the range of initial temperatures used in the shock experiments. Values of $f(v)$ in the volume range $0.515 < v < 0.55$ cm^3/g were taken to be the slopes of $(e-p)$ isochores calculated from the Hugoniot curves. Values of $f(v)$ in the intermediate range were assumed to lie on a smooth curve because values of $(\partial e/\partial p)_v$ calculated in the neighborhood of 0.54 cm^3/g were approximately equal to the value calculated at 0.994 cm^3/g. Least squares fits of the data give the following expressions for $f(v)$:

$$f(v) = -23.055 + 23.134v \quad \text{if } v \geq 1.152 \text{ cm}^3/\text{g}$$

$$f(v) = 60.502 - 121.866v + 62.916v^2 \quad \text{if } 0.9693 \leq v \leq 1.152 \text{ cm}^3/\text{g}$$

$$f(v) = 1.3822 + 0.108v \quad \text{if } v \leq 0.9693 \text{ cm}^3/\text{g}$$

where the constants are given to a number of decimal places for computation.

Since $h = e = g(v)$ when $p = 0$, the measured enthalpies at atmospheric pressure give values of $g(v)$ in the volume range $0.985 \leq v \leq 1.66$ cm^3/g. A linear least squares fit for $g(v)$ in this volume range is given by the expression

$$g(v) = -16.107 + 15.517v.$$

For values of volume less than 0.985 cm^3/g, fits for $g(v)$ were generated by patching together the high-pressure Hugoniot data and the atmospheric data so as to satisfy the condition $dg/dv > 0$. The best least squares fits for $g(v)$ with a slight discontinuity in the slope at $v = 1.01316$ cm^3/g are:

$$g(v) = 2408.116 + 7566.432v - 7949.11v^2 + 2787.845v^3 \quad \text{is } v \leq 1.0136 \text{ cm}^3/\text{g}$$

$$g(v) = -16.107 + 15.517v \quad \text{if } v \geq 1.0136 \text{ cm}^3/\text{g}$$

The fits for $f(v)$ and $g(v)$ define the $(e-p-v)$ equation of state and allow calculation of Hugoniots centered on, and isentropes passing through points on the $p = 0$ isobar in the $(p-v)$ plane. The discontinuous change in slope of the $g(v)$ function at $v = 1.01316$ cm^3/g is manifest in the shape of these curves in the neighborhood of this volume.

5. Calculations

5.1. Construction of Hugoniot Curves and Isentropes

The Hugoniot curves centered on $p = 0$ at -20 °C, 25 °C, 158.5 °C, and 256 °C were calculated directly with eq (14). The isentropes passing through $p = 0$ at 25 °C, 158.5 °C, 256 °C, and 296 °C were constructed by integrating eq (15) numerically with a

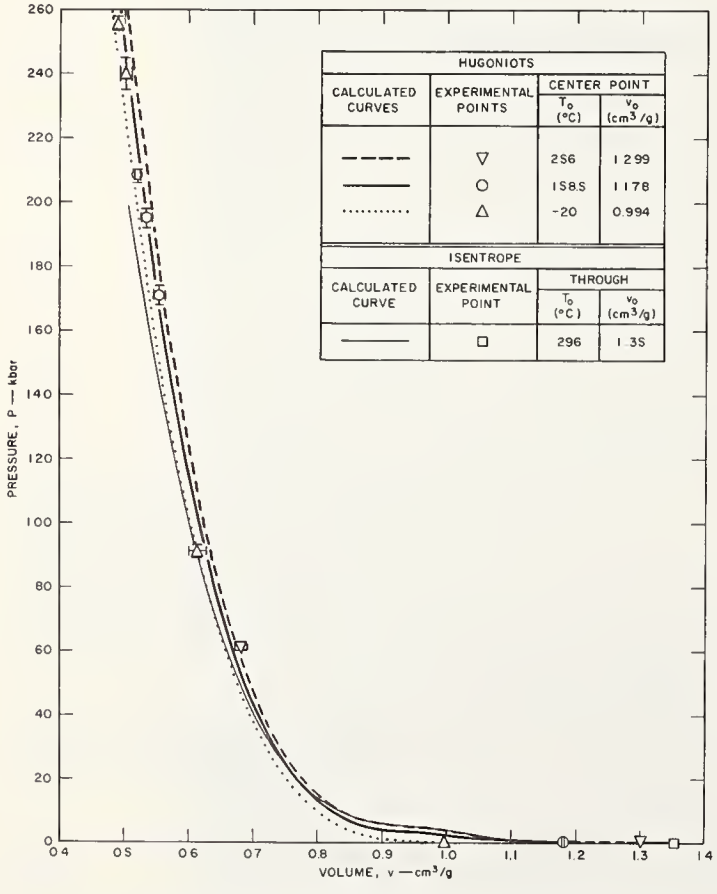

FIGURE 4. *Isentrope and three Hugoniots calculated for silicone 210.*

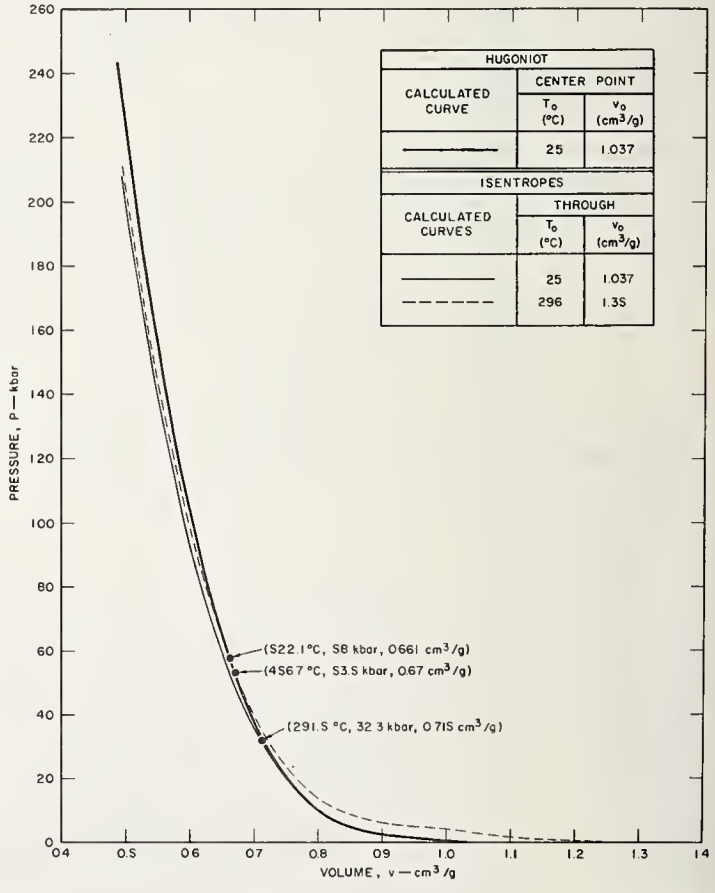

FIGURE 5. *Hugoniot and two isentropes calculated for silicone 210.*

Runge-Kutta technique. The −20 °C, 158.5 °C, and 256 °C Hugoniots and the 296 °C isentrope are shown in figure 4. The 25 °C Hugoniot and the 25 °C and 296 °C isentropes are shown in figure 5.

5.2. Calculation of Temperature

Equation (9) was used to calculate the temperature along the isentropes passing through 25 °C and 296 °C on the atmospheric isobar. The values of temperature along these isentropes are listed in table 2. Calculation of temperature at points where isentropes intersect the 25 °C Hugoniot defines values of shock temperature along this Hugoniot curve. The point of intersection (T_c=522.1 °C, p_c=58 kbar, v_c=0.661 cm³/g) of the 296 °C isentrope and the 25 °C Hugoniot is the highest point on the 25 °C Hugoniot where shock temperature can be calculated with the present data. The temperature on the 25 °C Hugoniot below 58 kbar can be calculated with the isentropes lying to the left of the 296 °C isentrope. The temperature where the 256 °C isentrope intersects the Hugoniot is 456.7 °C, and the temperature where the 158.5 °C isentrope intersects the Hugoniot is 291.5 °C.

It is not possible to calculate temperature on the 25 °C Hugoniot above 58 kbar without making further assumptions. The temperature along the Hugoniot above 58 kbar was calculated with constant C_v rather than by extrapolating the low-pressure data further. The equation for shock temperature [2] above a point (T_c, v_c) on a Hugoniot centered at (p_o=0, v_o),

$$TI = T_c + \frac{1}{2C_v}\int_{v_c}^{v} I\left[p+(v_o-v)\frac{dp}{dv_H}\right]dv \quad (17)$$

with

$$I = \exp\int_{v_c}^{v} dv/f(v)$$

was used to calculate temperature on the 25 °C Hugoniot above (T_c=522.1 °C, v_c=0.661 cm³/g). The integral term in eq (17) was evaluated numerically with a constant value of $C_v = 1.3735\times10^{-2}$ kbar cm³/g °C equal to the constant value along the 296 °C isentrope. Since C_v is constant along an isentrope, the significance of temperatures calculated with eq (17) depends on the variation of C_v with volume along the atmospheric isobar above v=1.35 cm³/g. In the case that C_v increases with increasing volume above v=1.35 cm³/g, it also increases with the increasing pressure along the Hugoniot curve, and the values of temperature calculated with eq (17) under the assumption of constant C_v would be upper estimates for shock temperature above 58 kbar. The values of temperature calculated with eq (17) are listed in table 3.

For comparison the method of Walsh and Christian [2] was also used to calculate temperature along the 25 °C Hugoniot curve with eq (17). The integral

TABLE 2. *Calculated temperature along the 25 °C and 296 °C isentropes*

Volume	25 °C Isentrope	296 °C Isentrope
(cm³/g)	(°C)	(°C)
1.35		296.0
1.29		300.4
1.25		304.0
1.19		310.8
1.15		316.4
1.09		328.5
1.05		339.7
1.0369	25.0	
1.01	29.4	353.9
0.969	38.0	371.6
.909	50.8	398.3
.849	64.3	426.1
.809	73.6	445.4
.749	88.0	475.4
.709	98.1	496.2
.649	113.7	528.5
.609	124.5	551.0
.549	141.3	585.9
.509	153.1	610.1

TABLE 3. *Calculated temperatures on the 25 °C Hugoniot above 58 kbar*

Pressure	Volume	Calculated with	
		$C_v = 1.9353\times10^{-2}$ kbar cm³/g °C $f(v) = 1.3822 + 0.10798v$	$C_v = 1.3735\times10^{-2}$ kbar cm³/g °C $f(v) = 1.7839$
		Temperature	Temperature
(kbar)	(cm³/g)	(°C)	(°C)
58.3	0.661	522.1	559.8
71.1	.641	541.4	698.8
85.7	.621	588.9	866.8
102.5	.601	640.3	1069.8
121.5	.581	725.4	1313.8
142.9	.561	839.3	1591.8
167.0	.541	986.4	1926.8
193.9	.521	1171.3	2316.8
223.8	.501	1397.3	2756.8

was evaluated under the assumption that C_v and $f(v)$ were constant along the Hugoniot curve and that the values of these constants were the values of C_v and $f(v)$ evaluated at 25 °C. The calculated temperatures where the 158.5 °C, 256 °C, and 296 °C isentropes intersect the 25 °C Hugoniot are 296.8 °C, 507.1 °C, and 561.5 °C. The values of temperature above 58 kbar calculated by this method are also listed in table 3.

6. Summary and Conclusions

Because of the scarcity and inaccuracy of experimental data, it was necessary to assume a simple form of the $(e-p-v)$ equation of state to calculate the thermodynamic properties of silicone fluid. The particular form of the $(e-p-v)$ relationship, $e=pf(v)+g(v)$ with $f(v)$ and $g(v)$ arbitrary functions of volume, was suggested from the shock wave data and also from the variation of $(\partial e/\partial p)_v$ along the atmospheric isobar. Values of $f(v)$ calculated from the shock wave data and values of $f(v)$ calculated from atmospheric static data with the identity $(\partial e/\partial p)_v=-C_p(\partial v/\partial p)_s(\partial T/\partial v)_p$ were used to calculate values of $f(v)$ in the volume range not covered by the experimental data. The values of $g(v)$ calculated from shock wave data, the values of $g(v)$ measured along the atmospheric isobar, and the condition $dg/dv>0$ were used to calculate values of $g(v)$ in the volume range not covered by experiment.

The Hugoniot curves centered at −20 °C, 25 °C, 158.5 °C, and 256 °C on the atmospheric isobar were calculated directly with the expression

$$p[f(v)-\tfrac{1}{2}(v_o-v)]=g(v_o)-g(v)$$

obtained by combining the Hugoniot equation with the $(e-p-v)$ equation of state. The calculated Hugoniot curves were consistent with experimental Hugoniot points up to a pressure of 240 kbar but then started to deviate from them. The isentropes passing through 25 °C, 158.5 °C, 256 °C, and 296 °C on the atmospheric isobar were calculated by numerically integrating the differential equation for an isentrope with a Runge-Kutta method; the temperature along these isentropes was calculated with the equation $T=T_i \exp -\int_{v_i}^{v} dv/f(v)$. Calculation of the temperature where the 158.5 °C, 256 °C, and 296 °C isentropes intersect the 25 °C Hugoniot curve defines values of shock temperature on this Hugoniot curve. The temperature T_c=522.1 °C at the point of intersection (p_c=58 kbar, v_c=0.661 cm³/g) of the 296 °C isentrope and the 25 °C Hugoniot is the highest temperature on the 25 °C Hugoniot that can be calculated from the data without additional assumptions. To put a possible upper estimate on shock temperature along the 25 °C Hugoniot above 58 kbar, the temperature was calculated by integrating along the Hugoniot curve with constant C_v. The method of Walsh and Christian was used to calculate temperature along the 25 °C Hugoniot above 0 kbar.

It is obvious from our calculations of the $(e-p-v)$ equation of state that many more experimental Hugoniot $(p-v)$ points are needed to construct an $(e-p-v)$ equation of state without first assuming its functional form. Indeed, to test the feasibility of constructing an equation of state from experimental data it would be necessary to determine, with accuracy, the positions of at least three Hugoniot curves in the $(p-v)$ plane. With well-defined Hugoniot curves it is possible to test the validity of thermodynamic assumptions such as $(\partial e/\partial p)_v=f(v)$, and if necessary to fit the data with more complicated functions. However, with a limited amount of Hugoniot data and the positions of the Hugoniot curves not well defined, it is not in general possible to test or to determine any thermodynamic properties conclusively. Specifically, it is not possible to test the validity of $(\partial e/\partial p)_v=f(v)$ with our data because the experimental Hugoniot points do not lie on isochores in the $(p-v)$ plane. Many more data points obtained with explosive driver systems producing an improvement in wave flatness and pressure uniformity are required to achieve a more definitive characterization of the $(e-p-v)$ surface.

The temperature calculations in this paper use more thermodynamic data than previous methods of calculating shock temperature. The shock wave Hugoniot data and the atmospheric data for silicone fluid span a larger domain of the $(p-v)$ plane than either the water data used by Rice and Walsh [3] or the metals data used by Walsh and Christian [2]. In the domain of the $(p-v)$ plane where it is possible to calculate temperature without making assumptions about specific heat, the present method of calculating temperature is considered to be better than methods based on the assumption of a constant specific heat. The comparison of temperatures on the 25 °C Hugoniot curve below 58 kbar calculated using the present method, with those calculated using the Walsh and Christian model based on the constancy of C_v and $(\partial e/\partial p)_v$ suggests that the Walsh and Christian model gives an upper estimate for shock temperature. The comparison of temperatures on this Hugoniot above 58 kbar calculated using the Walsh and Christian method but with different values of C_v substantiates this suggestion. However, the difference between the temperatures calculated above 58 kbar resulting from the difference between the numerical values of the constants emphasizes the problem of determining the temperature of shocked liquids. The fact that it is possible with the Walsh and Christian model to calculate different temperatures with a constant value of $(\partial e/\partial p)_v$ once again reflects the independence of the $(e-p-v)$ and $(T-p-v)$ equations of state. Because of the identity $(\partial e/\partial p)_v=C_v/(\partial p/\partial T)_v$, the $(T-v-v)$ equation of state is not determined

by an $(e-p-v)$ equation of state based on an experimental Hugoniot curve and the assumption of constant $(\partial e/\partial p)_v$. The constancy of $(\partial e/\partial p)_v$ provides no guarantee that C_v and $(\partial p/\partial T)_v$ are also constant. In fact different sets of values of C_v and $(\partial p/\partial T)_v$ that satisfy the condition of constant $(\partial e/\partial p)_v$ can be associated with different $(T-p-v)$ equations of state that will give different values of shock temperature.

It is concluded that the values of shock temperature calculated along the isentropes are more realistic than those that would be calculated with models based on less thermodynamic information.

7. Acknowledgments

The authors are grateful to Physical Research Laboratory, Edgewood Arsenal, for supporting this work under Contract DA-18-035-AMC-122(A), and thank Miss B. Loo for performing the numerical integration and plotting the diagrams.

8. References

[1] Rice, M. H., McQueen, R. G., and Walsh, J. M., Compression of solids by strong shock waves, Solid State Physics Vol. 6 (Academic Press, Inc., 1958).
[2] Walsh, J. M., and Christian, R. H., Phys. Rev. **97**, 1544 (1955).
[3] Rice, M. H., and Walsh, J. M., J. Chem. Phys. **26**, 824 (1957).
[4] Cowperthwaite, M., Am. J. Phys. **34**, 1025 (1966).
[5] Gibbs, J. W., The Scientific Papers of J. Willard Gibbs; Vol. 1, Thermodynamics (Dover Publications, New York, 1960).
[6] Zeldovich, Ya B., and Kompaneets, A. S., Theory of Detonation (Academic Press, New York & London, 1960), pp. 9–10.
[7] Courant, R., and Friedrichs, K. O., Supersonic Flow and Shock Waves (Interscience Publishers, New York, 1948).
[8] McQueen, R. G., and Marsh, S. P., Equation of state for 19 metallic elements and shock wave measurements to 2 megabars, J. Appl. Phys. **31**, 7, 1253–1269 (1960).
[9] Cowperthwaite, M., and Blackburn, J. H., Temperature of Shocked Liquids, Stanford Research Institute Special Tech. Rept. No. 14, Contract DA-18-035-AMC-122(A) (1967).
[10] McSkimin, H. J., J. Acoust. Soc. Am. **29**, 1185 (1957).

DISCUSSION

A. Holt (*University of California, Lawrence Radiation Laboratory, Livermore, California*): In your present work I assume that you have concluded that the Hugoniots lie too close to one another at high pressure to make this method valuable in obtaining equations-of-state. If this is true, would you say that this result would be found with other materials besides silicone?

D. J. Pastine (*U.S. Naval Ordnance Laboratory, White Oak, Maryland*): I would like to make the point that you can calculate the rate of change with temperature of the initial slope of the U_s-U_p relation, which gives you an idea of how the Hugoniots are going to change with temperature, and this turns out to be of the order of thermal expansions—that is, very small. So you could expect that for a 300 degree temperature change in metal the Hugoniot curves will be right on top of each other.

J. W. Forbes (*U.S. Naval Ordnance Laboratory, White Oak, Maryland*): I'm interested in your choice of brass as a material to shock as the bottom of your cells, because, in work by Nat Colburn and myself, we have found that due to preheating, brass gives a large anomalous effect as far as U_s-U_p relationship is concerned. We reported this a year ago at Bethlehem. It is also my understanding that McQueen and Marsh discontinued use of brass because they found it is too difficult to use as a standard. In our data the separations in Hugoniots show a decrease in shock velocity of perhaps up to 20 percent for the same free surface velocity. We don't understand exactly why.

G. E. Duvall (*Washington State University, Pullman, Washington*): Your curves were plotted in the $p-v$ plane, and all tend to fall on one another. If you plotted in the $p-T$ plane, they would have been nicely spread out. Or, better yet, a three-dimensional plot would be useful.

AUTHORS' CLOSURE

Reply to A. Holt: It is unfortunately true that at the present time the method is limited by the accuracy of the Hugoniot measurements and the close spacing of the Hugoniot curves which will be even more pronounced for heated solids. The way to obtain Hugoniot points away from the crystal density Hugoniot curves of metals is to shock porous samples of low density as in the equation of state work on aluminum performed at Stanford Research Institute by G. D. Anderson, A. L. Fahrenbruch, and G. R. Fowles.

Reply to D. J. Pastine: I agree.

Reply to J. W. Forbes: I don't understand why either. The brass was both heated and cooled in our experiments and corrections were made accordingly.

Reply to G. E. Duvall: I think that is an optimistic way to look at the data.

The Equation of State of Selected Materials for High-Pressure References*

W. J. Carter, S. P. Marsh, J. N. Fritz, and R. G. McQueen

University of California, Los Alamos Scientific Laboratory, Los Alamos, New Mexico 87544

1. Introduction

Establishing a standard for high-pressure dynamic shock wave work requires more than precise measurements of Hugoniot data. Indeed, although a $P-V$ relation may in principle be determined (at least under the Rankine-Hugoniot assumptions) in terms of mass, length, and time with arbitrary accuracy if sufficient care is taken, in order for the material to be useful as a standard it is also necessary to extend the equation of state into regions off the Hugoniot. For example, if the standard is to be used in other shock wave experiments it is necessary to calculate reflected shocks and isentropes in order to perform the impedance-matching calculations. If it is desired to transform the shock wave data to a form useful in static experiments, it is usually necessary to calculate isotherms. These calculations all assume knowledge of thermodynamic properties of the material in regions where such data are unobtainable at present. Although these calculations are not difficult, the necessity of extending the shock wave results to regions off the Hugoniot probably results in the major uncertainty in establishing a dynamic pressure standard.

The Los Alamos Scientific Laboratory has long been interested in establishing such a dynamic pressure standard. To this end, we have devised experimental techniques which measure directly both the shock velocity and material velocity needed to establish pressure-compression curves through the Rankine-Hugoniot equations. Although these techniques have been applied to a number of different materials, the direct or primary standards are now considered to be deoxidized copper and 2024 aluminum alloy. Once these primary standards are well established, it is possible in turn to measure the equation of state of other materials relative to the standards through the impedance match method. If the Hugoniot data obtained in this way are sufficiently well-determined, these materials may in turn be used as secondary standards, particularly if they have properties useful in static experimentation. A number of such materials are included in this report.

Familiarity will be assumed with the Rankine-Hugoniot equations and some of their consequences, as well as many of the techniques of dynamic high-pressure work. For a more detailed discussion of these questions, see reference [1].[1]

*Work done under the auspices of the U.S. Atomic Energy Commission.

Paper presented at the Symposium on Accurate Characterization of the High-Pressure Environment, held at the National Bureau of Standards, Gaithersburg, Md., October 14–18, 1968.

2. Direct Measurements of the Hugoniot Equation of State

2.1. Experimental Techniques

Perhaps the simplest yet potentially most accurate method of obtaining Hugoniot data is to measure the velocity of a shock front created by the symmetrical collision of two plates moving at known relative velocity. In the laboratory system, this can be done by explosively driving one plate (the driver) into a stationary one (the target); then the measurements of interest are the velocity of the driver at the time of impact (u_d) and the corresponding shock velocity in the target (u_s). Provided the target and driver are in the same thermodynamic state, symmetry requires that the particle or material velocity (u_p) behind the shock wave be equal to one-half the measured driver velocity. Varying the driver velocity by changing the driver thickness, the explosive system, or the length of free run between the driver and target then allows the Hugoniot locus in the u_s-u_p plane to be determined. The Rankine-Hugoniot equations centered at $P=0$

$$P=\rho_0 u_s u_p \tag{1}$$

$$\rho_0/\rho=V/V_0=(u_s-u_p)/u_s \tag{2}$$

$$E-E_0=1/2P(V_0-V) \tag{3}$$

then serve to transform the experimental data to other thermodynamic quantities such as pressure (P), density (ρ), or energy (E). The method has the obvious advantage that it is free of the necessity of calculating isentropes and the usual accompanying assumptions, and furthermore does not depend on zero-pressure thermodynamic data not directly obtainable in the experiment, such as thermal expansions and specific heats. These limitations are all inherent in the previous method used to establish dynamic standards through the measurement of free surface velocities [2, 3].

The experimental set-up is shown in figure 1. A sweeping image camera is used to record shock-wave arrival times by the flash gap technique developed by Walsh and Christian [4]. The shock velocity is determined in the usual way by measuring the

[1] Figures in brackets indicate the literature references at the end of this paper.

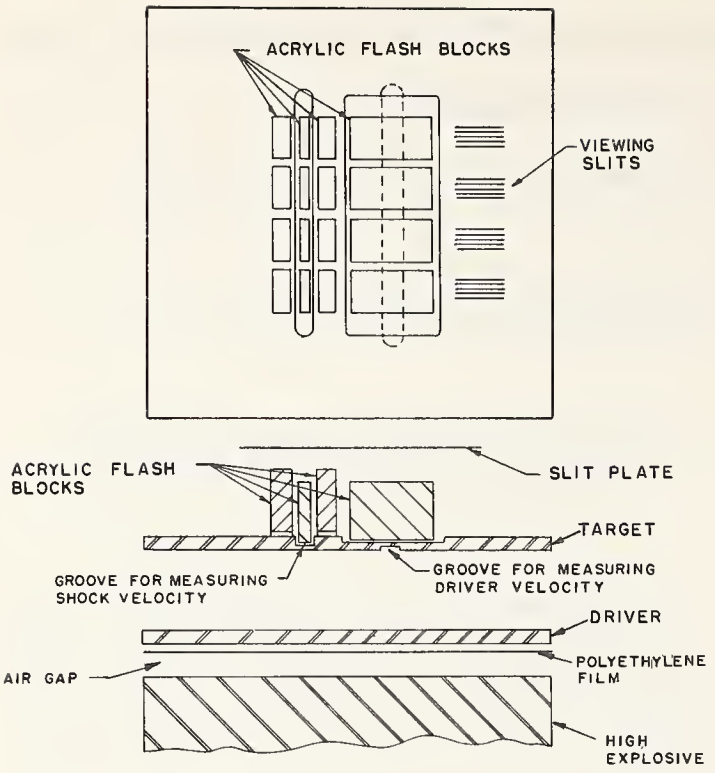

FIGURE 1. *Design of the experimental assembly used to obtain shock velocity-particle velocity data.*

The upper part of the figure shows the arrangement of the plastic flash blocks on the target plate which in effect give four independent sets of $u_s - u_d$ data points. The left hand side of the assembly is used to measure the shock velocity and the other side the driver velocity. Each set of blocks is viewed through four or five slits. The polyethylene film placed behind the driver plate helps prevent driver plate breakup before collision.

transit time of the shock wave through a known thickness of material. The driver velocity is determined by a differential measurement of the transit time of the front surface of the driver through a shallow groove milled on the back surface of the target plate. The resulting photographic trace is shown in figure 2.

As simple and straightforward as the technique appears to be, there are nevertheless a number of potential sources of error. Perhaps the most serious of these is the lack of hydrodynamic equilibrium in the shock, which of course is a property of the material and not of the technique. This will be discussed in more detail in section 2.3. Other sources of difficulty are the following:

1. The driver plate may not be moving at constant velocity at the time of impact. Studies have shown that a series of accelerations, caused by shock reverberations, are produced when a plate is driven by high explosives [5]. Hence, the driver velocity may not be constant as the driver moves through the groove and the measured particle and shock velocities will not be compatible. Whether or not an acceleration occurs as the driver is moving through the groove depends on such factors as the length of free run, thickness of the driver, and the pressure level produced by the high explosive assembly. These factors must all be considered in design of the shot assembly in order to minimize

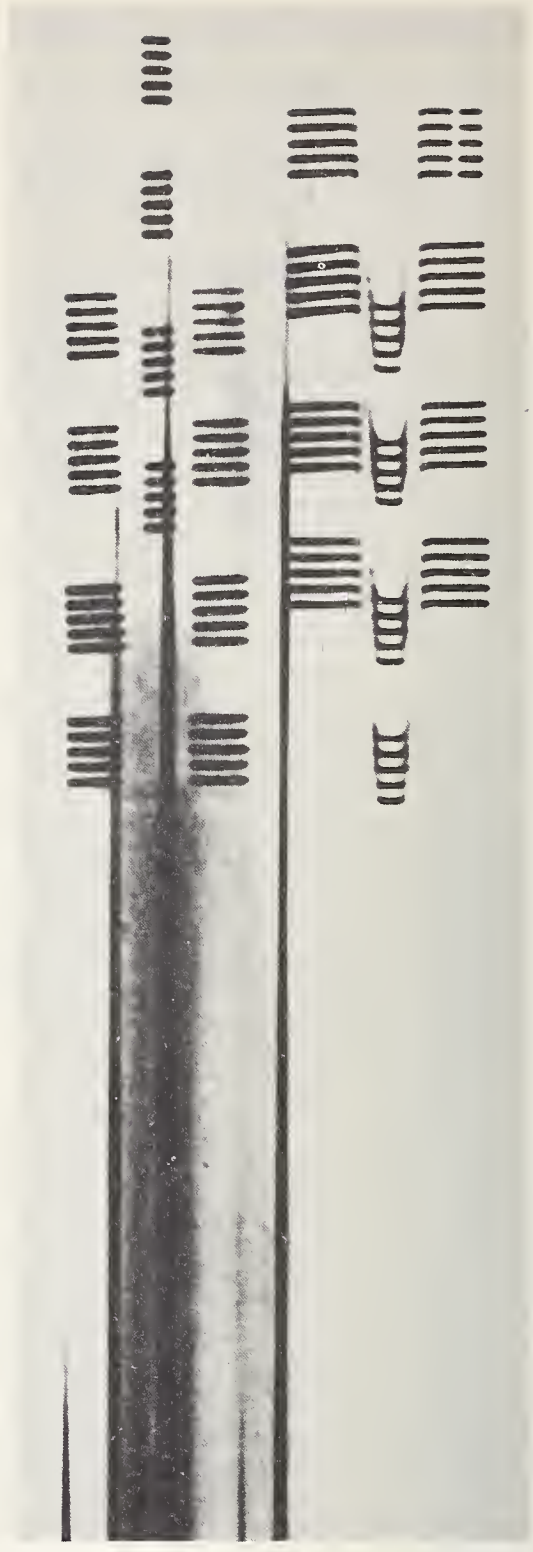

FIGURE 2. *An enlargement of a photographic record obtained using the assembly shown in figure 1.*

In this record, time increases downward; hence, the early traces on the left hand side represent the shock wave arrival at the bottom of the narrow groove. The corresponding reference traces establish the wave arrival at the top of the plate. Since the flash blocks on the right hand side are at a lower level, the reference traces for the u_d measurements arrive earlier. The offsets represent the difference in the driver-shock transit times through the small gap machined in the bottom of the plate.

such errors. However, one can guarantee that the initial shocks on both the shock and driver velocity sides of the plate are the same by machining the groove directly into the back of the target plates. Also, by placing the groove at this position, small pressure pulses present in the driver plate at col-

lision time are more likely to result in an increase in the driver velocity than an increase in the shock velocity. This is advantageous, since the $u_s - u_p$ Hugoniot is relatively insensitive to errors in the particle velocity, especially at low pressures.

2. Rarefactions from the rear surface and from edges in the assembly may give deceptively low apparent velocities. Since a shock is propagated both into the driver and into the target on collision, it is possible that the rarefaction wave from the rear of the driver may overtake the shock wave moving through the target before the measurements have been made. The catch-up ratio, r = target thickness/driver thickness, can be computed using the longitudinal wave velocity at pressure; these calculations show that values of r greater than 4 are suspect and should be avoided. For a given desired pressure level, this limits the thickness of the target plate and hence the accuracy of the experiment. This limitation, of course, is most stringent at high pressures. The width and depth of the groove must also be so tailored that sidewise rarefactions do not pinch off the wave front; this again limits the depth of the u_d groove and hence the accuracy of the experiment. This limitation is most stringent at low pressures.

3. The thermodynamic states of the driver and target may not be identical. This is certainly always the case, since the driver has been shocked while being accelerated but the target has not. However, a correction for this shock heating of the driver can be applied to the data if the shock history of the driver is known. This is done by recentering the known Hugoniot of the driver to an initial state of higher energy and lower density through the equation

$$E = E_H + (P - P_H)/\rho\gamma. \qquad (4)$$

This recentered Hugoniot is then used in an impedance match calculation to give the corrected value of u_p. At low pressures the correction in particle velocity is negligible. Since almost all the shock heating arises from the first strong shock from the high explosive, an attempt was made to minimize experimentally the magnitude of this pulse. A small air gap between the high explosive and the driver appears to accomplish this while not appreciably lowering the final driver velocity. This has the added advantage of reducing the tension waves due to the Taylor wave in the high explosive. Using thick layers of high explosive is also helpful in the latter respect.

Other errors in these experiments are probably random in nature, leading to scatter of about $\pm 1/2$ percent in shock velocity. These errors arise from the high degree of precision required in machining and assembly of the shots.

2.2. Hugoniot Data for 2024 Aluminum and Copper

It is obviously impractical to obtain Hugoniot data for all materials by the method outlined in the previous section. However, this method can be used to determine the Hugoniots of a few selected materials to be used as primary standards. Two of the most satisfactory materials serving as shock wave standards are deoxidized annealed Cu and 2024 Al alloy; these materials have therefore been

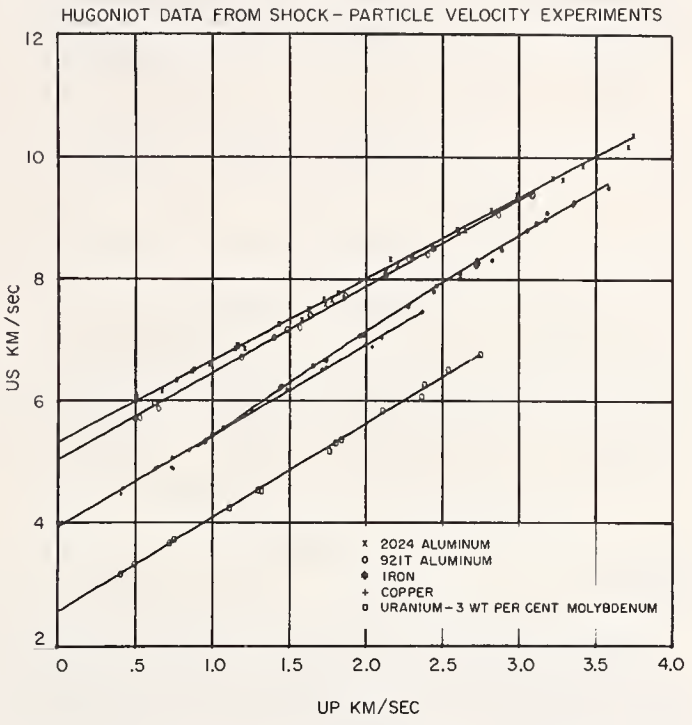

FIGURE 3. *Hugoniot* $u_s - u_p$ *data for 2024 Al, 921-T Al, Fe, Cu, and U-3 percent Mo alloy.*

Each set of data points was obtained by independent symmetrical collision experiments. The curves were obtained by the method of least squares.

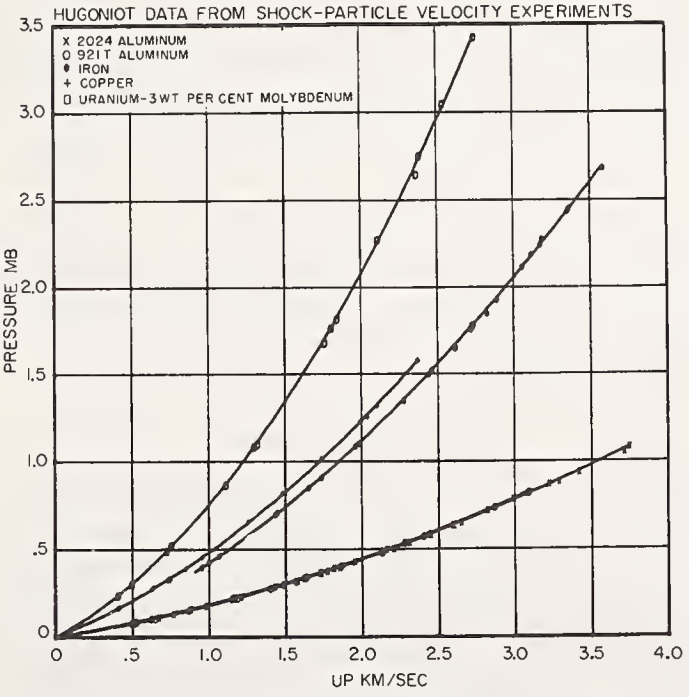

FIGURE 4. *Hugoniot* $P - u_p$ *data for the five standards.*

The curves drawn through the data were calculated from the $u_s - u_p$ fits shown in figure 3. In this plane the Hugoniots for the two Al alloys are indistinguishable. A substantial area of the $P - u_p$ plane is covered by these five materials, so that any unknown material can be studied by using a standard of comparable shock impedance. This minimizes errors arising from long extensions of isentropes and reflected shocks away from the Hugoniot.

TABLE I. *Thermodynamic constants at 293 K*

Material	Density	Thermal expansion	Specific heat	Debye temperature			Sound velocities			Grüneisen parameter
	ρ_0	α	C_p	θ	c_l	c_t	c_b	c_b(e.c.)	c_b(comp)	γ
	g/cm³	*deg⁻¹*	*ergs/g deg K*	*deg K*	*km/s*	*km/s*	*km/s*	*km/s*	*km/s*	
2024 Aluminum	2.785	21.8×10^{-6}	0.879×10^{7}	350	6.39	3.15	5.25 [14]			2.00
Copper	8.930	16.3	0.386	306	4.76	2.33	3.93 [14]	3.91 [15] 3.92 [16] 3.95 [17]	3.98 [8]	1.96
Silver	10.490	18.8	0.234	225				3.14 [15] 3.14 [18] 3.08 [19]	3.19 [8]	2.38
Sodium	0.968	20.8	0.122	160					2.54 [10] 2.61 [25]	1.17 1.17
Molybdenum	10.206	4.9	0.251	314	6.45	3.47	5.04 [14]	5.13 [15] 5.12 [20]	5.19 [8]	1.52
Palladium	11.991	11.8	0.238	220	4.57	2.06	3.90 [14]		3.80 [8]	2.26
Periclase	3.585	8.7	0.913	760	9.70	6.01	6.76 [14]	6.54 [15] 6.58 [21] 6.80 [22] 6.74 [23]	6.82 [10]	1.32
Magnesium	1.740	23.9	1.025	237	5.74	3.15	4.44 [14]	4.46 [24]	4.45 [9]	1.43

Thermal expansion and specific heat data were obtained from refs. [11–13].

The sound velocities c_l, c_t, and c_b are longitudinal, transverse and resultant bulk velocities obtained by the pulse-echo technique on polycrystalline samples. The velocity c_b(e.c.) is the bulk velocity calculated from measurement of elastic constants on single-crystal samples, while c_b (comp) is the bulk velocity from measurements of isothermal compressibility, transformed by us to adiabatic compressibility. References to original sources are indicated in parentheses.

thoroughly studied. In order to check the results and extend them to regions of higher impedance, similar studies have been performed on Fe and a high-density alloy of U and Mo. Finally, because of possible rigidity effects in the 2024 Al alloy, another aluminum alloy (921–T) with a very small elastic wave was also studied; unfortunately this material proved to be unusable because of large variations in porosity. The results of these Hugoniot measurements are shown in figures 3 and 4 for all five of these materials. Table 1 presents some of the important thermodynamic constants for Cu and 2024 Al as well as further selected materials. Table 2 lists the results of a linear least squares fit of the data in the form

$$u_s = c_0 + s u_p. \tag{5}$$

TABLE 2. *Coefficients of the Hugoniot Equation*

$$u_s = c_0 + s u_p$$

Material	c_0	s
	km/s	
2024 Aluminum	5.328	1.338
Copper	3.940	1.489
Silver	3.229	1.595
Sodium	2.629	1.223
Molybdenum	5.124	1.233
Palladium	3.948	1.588
Periclase	6.597	1.369
Magnesium	4.492	1.263

Values of the bulk sound velocities for these materials from compressibility, elastic constant, and ultrasonic measurements are listed in table 1; comparison with the leading coefficient in eq (5) shows excellent agreement for Cu but somewhat higher values of the Hugoniot intercept for the 2024 Al alloy. This is attributed to rigidity effects and is discussed in section 2.3.

In order to check the consistency of the measured shock velocity-particle velocity loci, we have tested each material against each of the others by the impedance match technique, using each in turn as a standard to remeasure the Hugoniot of all the others. The overall agreement is quite satisfactory and shows that all five standards satisfy this necessary condition. It should be remarked, in view of the wide range of impedances of these materials, that this cross-check is a stringent test of the individual Hugoniot loci and also a test of the adequacy of the values of the Grüneisen parameter γ listed in table 1 and the widely used assumption of constant $\rho\gamma$.

It is of interest to compare the results of these measurements with the free surface velocity measurements originally used to obtain the Hugoniots of

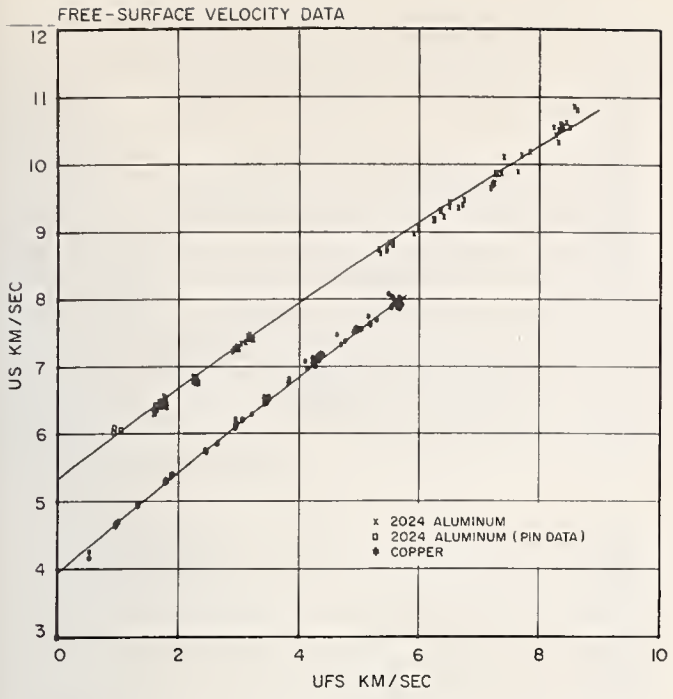

FIGURE 5. *Shock velocity-free surface velocity for 2024 Al and Cu.*

The data were obtained by flash-gap techniques quite similar to those described earlier. The solid curves were obtained by evaluating the Riemann integral along the isentropes calculated from the shock velocity-particle velocity Hugoniots.

the standards [3]. These measurements consisted of shock velocity-free surface velocity pairs obtained on the same shot. To obtain a $u_s - u_p$ Hugoniot from these, the Riemann integral

$$u_r = u_{fs} - u_p = \int_{V(P)}^{V(0)} [-(\partial P/\partial V)_s]^{1/2} dV \qquad (6)$$

was evaluated indirectly by an iterative procedure in which calculated free surface velocities were made to agree with experimental free surface velocities by varying the particle velocities. The isentropes were tied down along the zero pressure isobar by requiring the internal energy $E(V)$ at the foot of the rarefaction release wave to agree with that calculated from specific heat and thermal expansion data. In figure 5 the experimental $u_s - u_p$ data points are compared with the $u_s - u_{fs}$ locus calculated directly from eq (6) using the new shock velocity-particle velocity Hugoniots of Cu and 2024 Al. The agreement for Cu is satisfactory in view of the uncertainty in the zero pressure data and the approximations used in calculating the isentropes. 2024 Al, on the other hand, contains regions where the agreement is poor. These deviations are probably real and might reflect the effect of phase changes (melting and vaporization) that are not handled precisely in the calculated rarefaction release isentropes.

2.3. Effect of Rigidity

In order for the Rankine-Hugoniot equations to apply across a shock front, it is necessary that

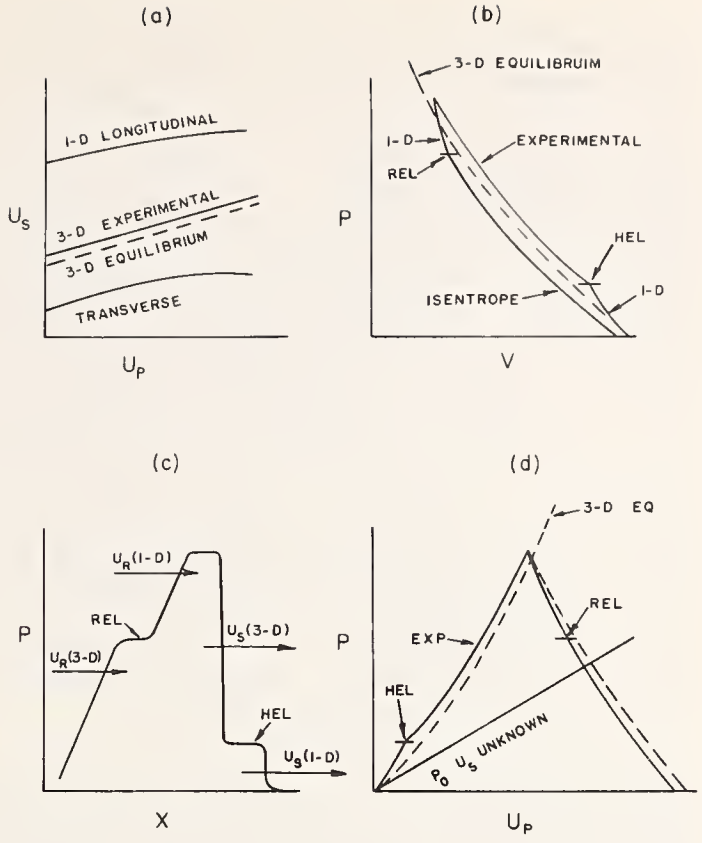

FIGURE 6. *The effect of rigidity on the Hugoniot curves.*

In (a) are drawn possible curves for the various wave velocity loci as a function of particle velocity. The upper curve represents a one dimensional Hugoniot and could be used to find the instantaneous longitudinal elastic wave velocity. The lowest curve represents the transverse wave velocity due to the shear modulus along the Hugoniot as a function of particle velocity. It has been established through static experiments that the shear modulus increases with pressure so it has been drawn with a positive slope. However, since the temperature along the Hugoniot increases in an exponential manner, this curve has been drawn with a downward curvature. If the material melts on the Hugoniot this curve will go to zero and the longitudinal and bulk velocity curves will coincide.

The remaining figures correspond to the lower pressure region of (a) where rigidity effects will be most pronounced. The relationship of the experimental Hugoniot and true release isentropes with the equilibrium Hugoniot is indicated in (b). Here HEL represents the Hugoniot elastic limit on compression and REL the elastic limit on the release wave. Figure (c) represents the type of pressure profile curve that would result from the collision of a finite driver plate with a target plate of the same material if its shock-wave equation of state were given by (b). Figure (d) is the $P - u_p$ transform of (b). In figures (b), (c) and (d) the relative amplitudes of the various waves are the same.

hydrodynamic equilibrium be obtained. Particularly at lower pressures, it is always possible that lingering effects of material rigidity can alter the ideal Hugoniot behavior. The behavior of a plane shock and rarefaction wave with rigidity present is sketched in figure 6. The pressure and volume are initially related by a one-dimensional equation of state, since initially there can be compression in one coordinate only. However, as the pressure increases, the deviatoric shear stress increases and the material begins to shear plastically, i.e., to relax to a three-dimensional equilibrium state. If the maximum resolved shear stress tolerable to the material is small compared with the shock stress, and if plastic flow can occur sufficiently rapidly (that is, if the relaxation time is small compared to the measurement interval), rigidity will have no pronounced effect on the Hugoniot and the material should exhibit true hydrodynamic behavior. However, if the material does not relax completely

385-762 O - 71 - 11

from the 1-D to the 3-D equilibrium Hugoniot, then all states on the experimental Hugoniot will be slightly stiffer than the hydrostat. This means that measured shock velocities will be higher than the true equilibrium Hugoniot and the resulting Hugoniot intercept in the $u_s - u_p$ plane should lie above the measured bulk sound velocity. As seen earlier, this is indeed the case for 2024 Al, where the Hugoniot intercept is 2.7 percent too high. Previous free surface velocity profiles measured here on 2024 Al and Cu by the dc capacitor technique have shown that the Hugoniot elastic limit, or dynamic yield point, of 2024 Al is about 5.5 kbar but is practically nonexistent for Cu [6]. An assumed residual stress of about 2 kbar in the expermental 2024 Al Hugoniot, when subtracted to obtain the equilibrium Hugoniot, allows the Hugoniot intercept and bulk sound velocity to agree. On the basis of the sound velocity, the small amplitude of the elastic precursor, and the very steep wave profile observed even at low pressures, it can be assumed that the experimental Hugoniot of Cu is representative of a true hydrostat.

If the material does not relax entirely to the equilibrium Hugoniot, an elastic precursor release wave which is even larger than the shock precursor should also be expected (see fig. 6). This should be manifested by a smaller free surface velocity than the true hydrostat would predict. Ideally, of course, in our experiments the free-surface and driver velocities should be equal in the low-pressure regime. Symmetrical-collision cannon shots using 2024 Al, however, show that free surface velocities are less than the projectile velocity [6]. High-pressure explosively driven experiments on 2024 Al, where the free surface velocity and the driver velocity were measured on the same shot, show a similar effect. Even at driver velocities up to 3 km/s, a deficit in free surface velocity of about 1 percent was

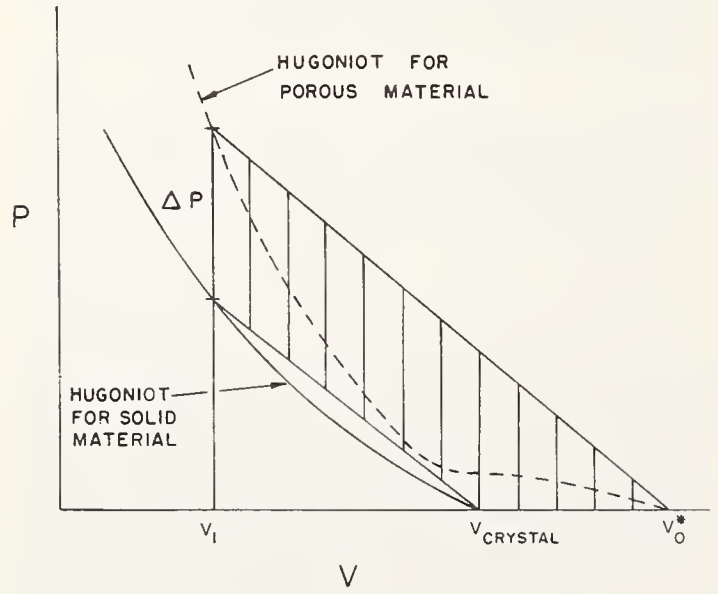

FIGURE 7. *Schematic to illustrate how porous materials can be used to measure the Grüneisen parameter.*

The difference in internal energy between the two Hugoniots at V_1 is indicated by the crosshatched area. The corresponding pressure difference is also indicated. By using samples of low initial densities, very high temperatures can be reached in the shock.

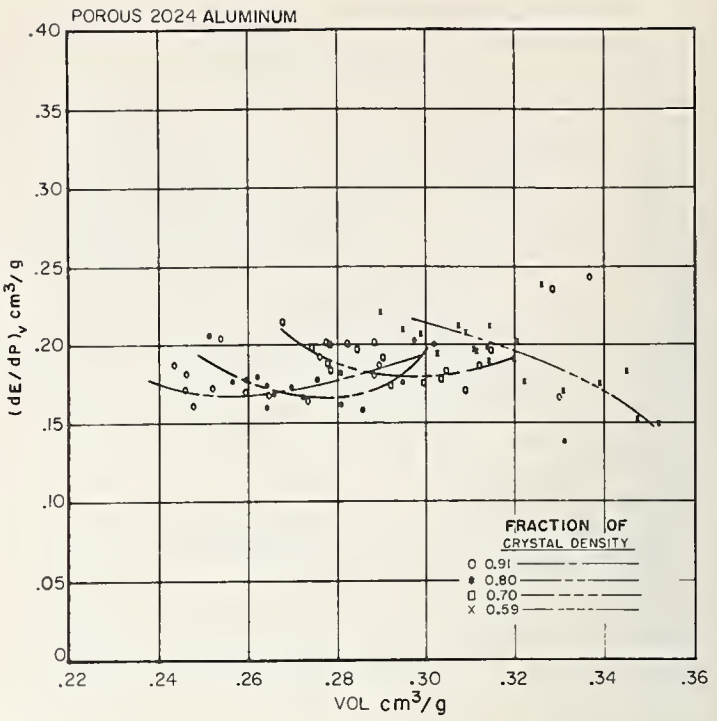

FIGURE 8. *Experimental values for* $(dE/dP)_V$ *versus volume determined from shock wave studies on porous 2024 Al.*

In this and the following figure each data point was computed from the shock-wave data for each porous sample and the fit of crystal density Hugoniot data. The curves were computed from least square fits of the $u_s - u_p$ data for each density group. Samples with lower initial densities represent average values of $(dE/dP)_V$ measured over larger temperature ranges at a given volume. Within the experimental accuracy there does not appear to be any measurable variation of γ with temperature. The general appearance of the data gives support to using the simple relationship $\rho\gamma$ constant.

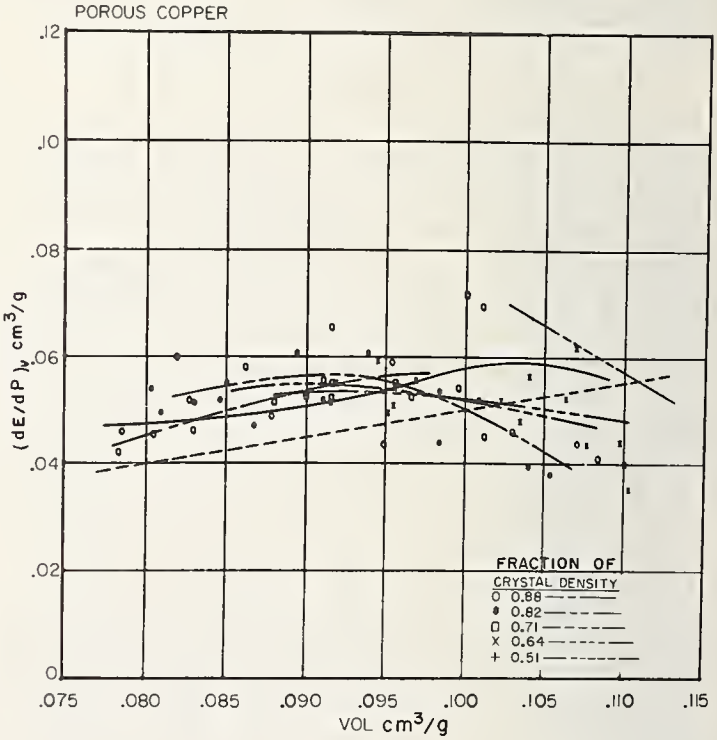

FIGURE 9. *Experimental values for* $(dE/dP)_V$ *versus volume determined from shock wave studies on porous Cu.*

In addition to the experimental curves the values of $(dE/dP)_V$ versus V obtained from the Dugdale-MacDonald relationship (solid line) and γ constant (dashed line) are also plotted. It can be seen that the data agree quite well with the Dugdale-MacDonald calculation. At small volumes experimental data lie well above the γ constant line, which is known to be a poor representation of the volume dependence of γ because it predicts vanishing sound speeds at large compressions.

found. Hence, elastic-plastic behavior is important in 2024 Al even at high pressures. Copper does not show this behavior except at very low shock pressures.

Rigidity must obviously play a role when 2024 Al is used as a standard for materials of lower shock impedance since the impedance match solution requires calculation of isentropes. It is not clear how a residual deviatoric stress will affect the results when a material of higher impedance, requiring calculations of reflected shocks, is used with such a standard. It is hoped that the increase in the shear modulus due to the offset in pressure is compensated by the increase in temperature also encountered in strong shock waves.

2.4. Experimental Studies on Porous Samples

In addition to a Hugoniot $u_s - u_p$ locus, it is necessary to know the properties of the Grüneisen parameter γ over wide regions of the $P-V$ plane in order for a material to be useful as a shock-wave standard. This is because the impedance match technique requires the calculation both of reflected shocks and of release isentropes. Experimentally, this is extremely difficult to do. One way of attempting this is to use porous samples of the material of interest in equation-of-state shots using the impedance match technique. An average value of the Grüneisen ratio is then determined by the pressure and energy offset from the crystal-density Hugoniot at a given volume through the relation (see eq (4))

$$\bar{\gamma}(V) = V\left(\frac{\Delta P}{\Delta E}\right)_V .$$

This is shown schematically in figure 7. The values of $(\partial E/\partial P)_V$ computed from the crystal density Hugoniot and the experimental data points are shown in figures 8 and 9 for 2024 Al and Cu respectively. Also shown in these figures are the smoothed results obtained by fitting the experimental data points with a quadratic $u_s - u_p$ fit which is then used to find the pressure and energy offsets from the crystal Hugoniot. It is obvious that the method is a very sensitive one, and the precision requirements to measure γ accurately are quite severe. However, there is no indication in these figures of a volume dependence of $(\partial E/\partial P)_V$, so that the results are compatible with the assumption of constant $\rho\gamma$.

It is possible to compute the Hugoniot of a porous material from the crystal density Hugoniot through the equation

$$P = P_H[1-(\rho\gamma)(V_0 - V)/2]/[1-(\rho\gamma)(V_0^* - V)/2] \quad (7)$$

which gives the pressure as a function of volume for a porous material centered at the volume V_0^*. Here V_0 is the initial volume of the crystal

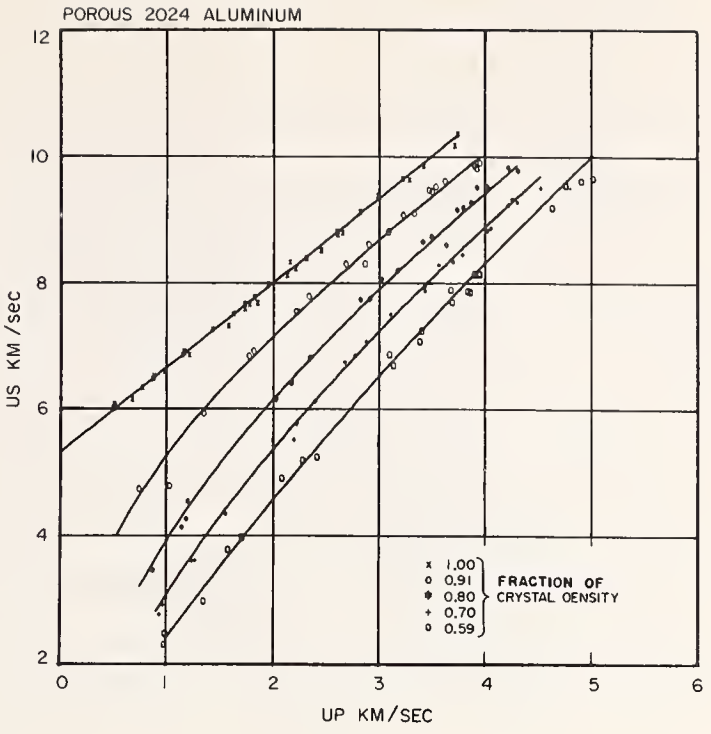

FIGURE 10. *Shock velocity-particle velocity data for porous 2024 Al.*

The curves were computed from the least square fit of the crystal density Hugoniot and a constant value of $(dE/dP)_V$, obtained from the γ and ρ in table 1, for the average initial density of each group of samples. The data were also corrected for deviations in initial density. In this and in figure 12 it can be noted that the calculated curves originate at $u_s = u_p = 0$. Thus the higher density curves have considerably more curvature in the low-pressure region. The low initial density curves become almost linear, since they are approaching the initial density $\rho_0 = \rho_{crys}\gamma/(\gamma+2)$ which yields a vertical $P-V$ asymptote at crystal density.

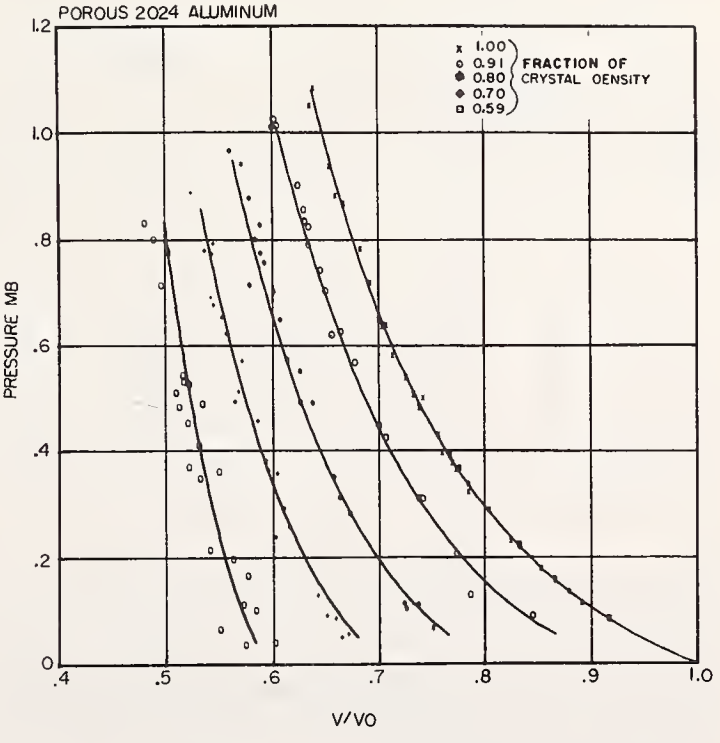

FIGURE 11. *Pressure versus relative volume for porous 2024 Al.*

In this and in figure 13 the curves are the $P-V/V_0$ transforms of the computed $u_s - u_p$ fits. The scatter in the data due to variation in density is more pronounced in these plots. V_0 in the figures refer to the average density of each group of samples. Although the compression is large for these low initial density samples, the final densities are not. The approach to the asymptotic density is quite apparent.

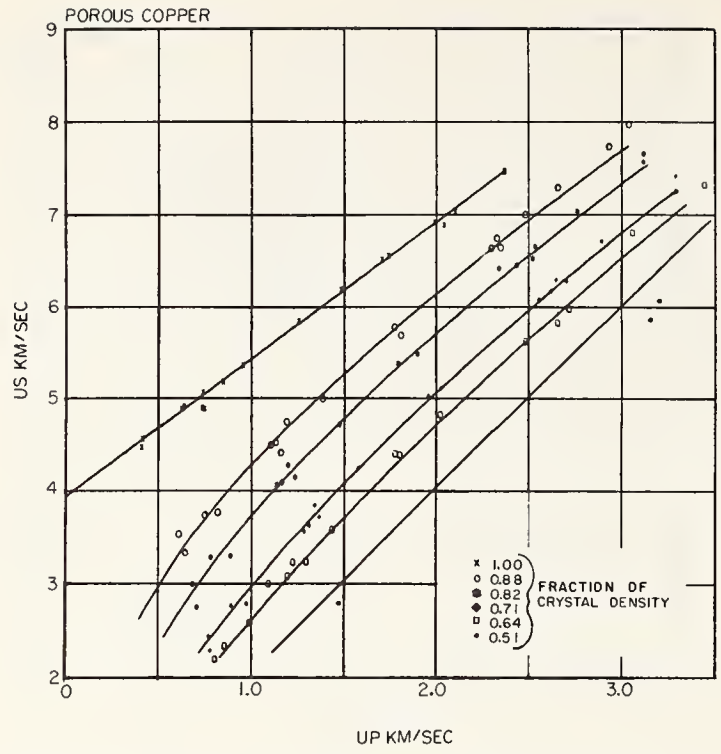

FIGURE 12. *Shock velocity-particle velocity data for porous Cu.*

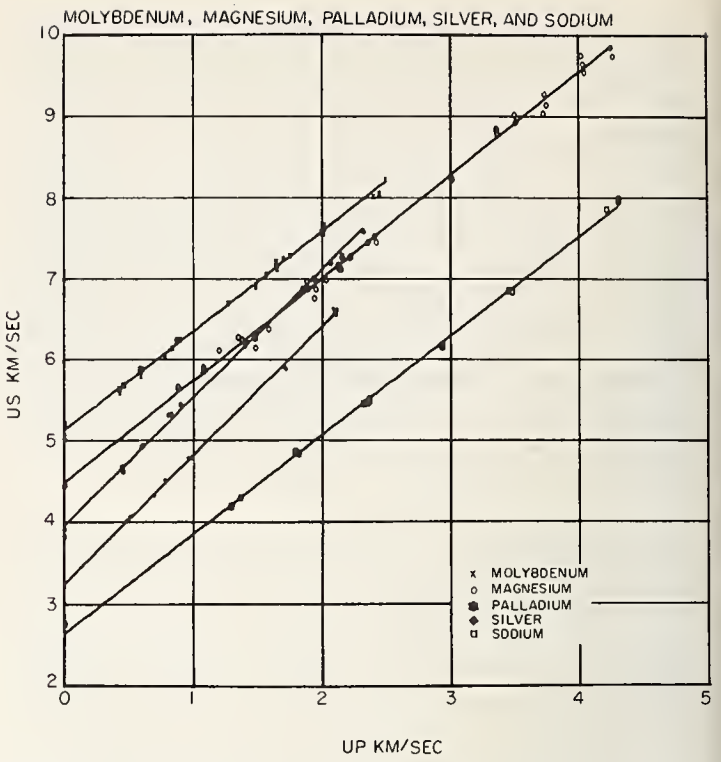

FIGURE 14. *Hugoniot* $u_s - u_p$ *data for* Mo, Mg, Pd, Ag, *and* Na.

Where possible, bulk sound speeds derived from both compressibility and ultrasonic measurements have been included, although these have not been used in the least square fits of the Hugoniot data.

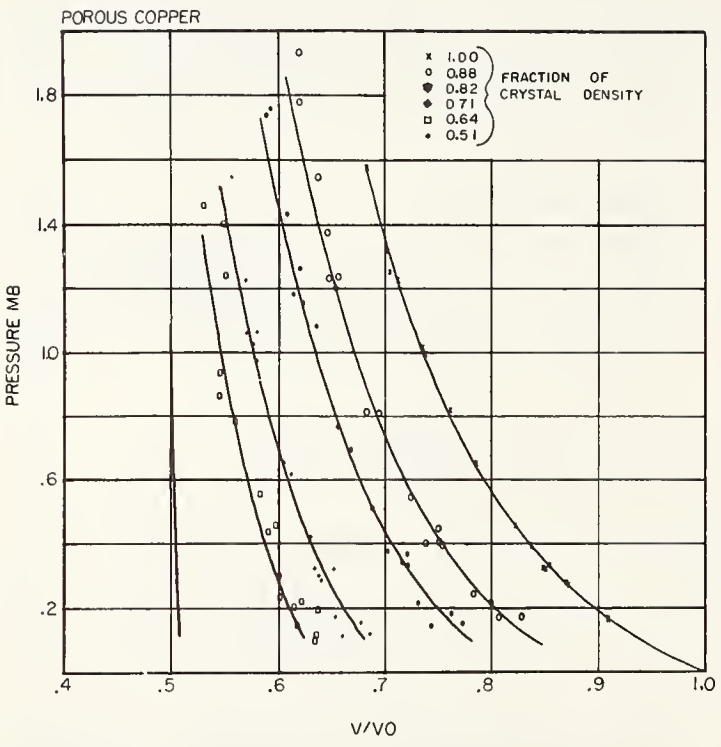

FIGURE 13. *Pressure versus relative volume data for porous Cu.*

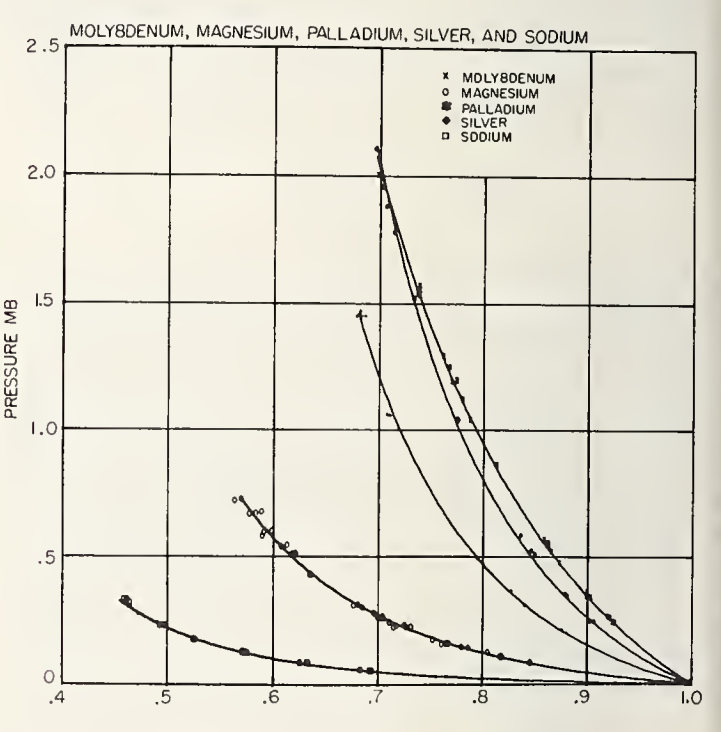

FIGURE 15. *Hugoniot* $P - V/V_0$ *data for* Mo, Mg, Pd, Ag, *and* Na.

The curves span a very large region in this plane. Although there is some scatter in the data, it is evident that the compression curves are well determined.

density material, and P_H is the pressure on the crystal density Hugoniot at the volume V. This Hugoniot can be transformed to the $u_s - u_p$ plane through the equations

$$u_s = V_0^* [P/(V_0^* - V)]^{1/2} \tag{8}$$

$$u_p = [P(V_0^* - V)]^{1/2}. \tag{9}$$

In figures 10 to 13 the experimental $u_s - u_p$ and $P - V/V_0$ data are given for crystal density and porous 2024 Al and Cu. The crystal data is the shock velocity-particle velocity data fitted with the linear relation listed in table 2. The other Hugoniots were

calculated from eq (7) assuming $\rho\gamma$ constant and using the average initial volume of each group of data points as the Hugoniot centering point. The agreement with the data is quite good, a further indication that this simple volume dependence of the Grüneisen parameter is adequate. Much of the scatter in the data probably arises from the difficulty of measuring initial densities accurately.

3. Indirect Measurement of the Equation of State

Once the Hugoniot $u_s - u_p$ curves and the Grüneisen parameters have been determined for the primary standards as outlined in section 2, it is possible to use these materials to investigate the equation of state of other materials by use of the impedance match technique [4]. Although a large number of materials have been studied in this way, we have selected only a few substances which are under particular consideration as static high-pressure standards. These include five metals, Ag, Na, Mg, Pd and Mo, and one oxide, MgO.

The $u_s - u_p$ and $P - V/V_0$ Hugoniot data for the five metallic elements are presented in figures 14 and 15. There is evidently considerable scatter in the data, and the possibility of phase transformations along the Hugoniots is certainly not precluded. However, the volume changes at such transformations are undoubtedly quite small, and since velocity measurements are essentially differential $P-V$ measurements, as seen by eqs (8) and (9), the resulting compression curves should be quite accurate.

The situation with periclase is not so favorable. The Hugoniot $u_s - u_p$ and P-V/V_0 data for crystal MgO and three lower density ceramics are presented in figures 16 and 17. The linear least square fit of the crystal data extrapolates at zero pressure to 6.6 km/s, a value considerably below the currently accepted bulk sound speed of 6.73 km/s. The discrepancy is in the wrong direction to be explained by rigidity effects. This discrepancy is larger than can be explained by the rather large scatter in the experimental data. A possible explanation is that MgO transforms to the CsCl structure somewhere on the Hugoniot below about 200 kbar. Since the Hugoniot data appear to be characteristic of the same phase, a straightforward linear Hugoniot fit, together with the thermodynamic value of the Grüneisen parameter, has been used to calculate the Hugoniots of the porous ceramics by the method of section 2.4. The results are gratifying, and again give additional confidence to the assumption of a constant value for the product $(\rho\gamma)$. The experimental values of $(\partial E/\partial P)_V$ for periclase, also calculated by the methods of section 2.4, are plotted in figure 18. Although attendant with the usual large scatter found with this sort of experiment, it is obvious that a constant value of $(\partial E/\partial P)_V$ is again consistent with the data.

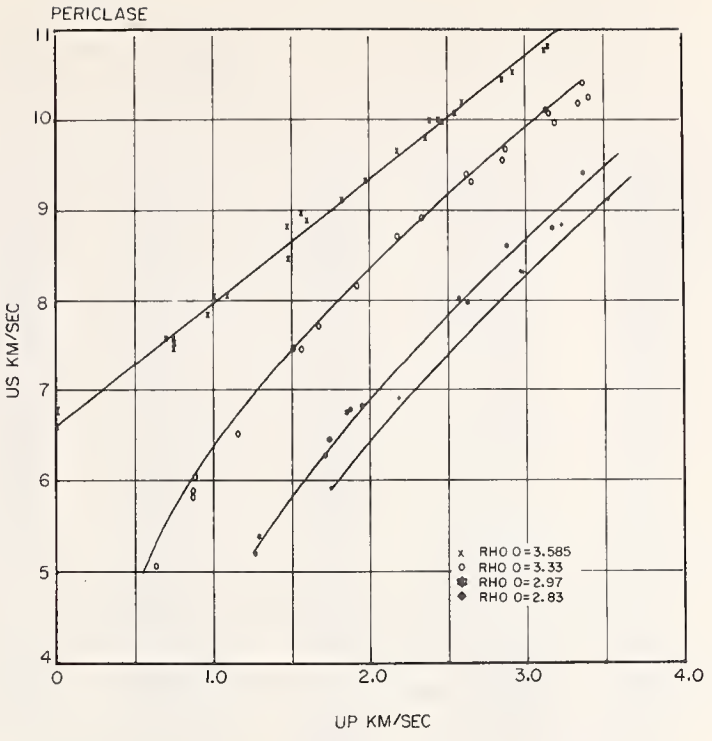

FIGURE 16. *Hugoniot* $u_s - u_p$ *data for* MgO.

The crystal density material ($\rho_0 = 3.585$) has been fitted by the method of least squares to a linear $u_s - u_p$ relation. The resulting curve extrapolates considerably below the bulk sound speed, indicating that the material has possibly transformed to a different phase at these pressures. The curves through the data points for the lower density materials have been calculated from this fit, using a thermodynamic Grüneisen parameter with $(\partial E/\partial P)_V = 0.211$. The agreement is seen to be good.

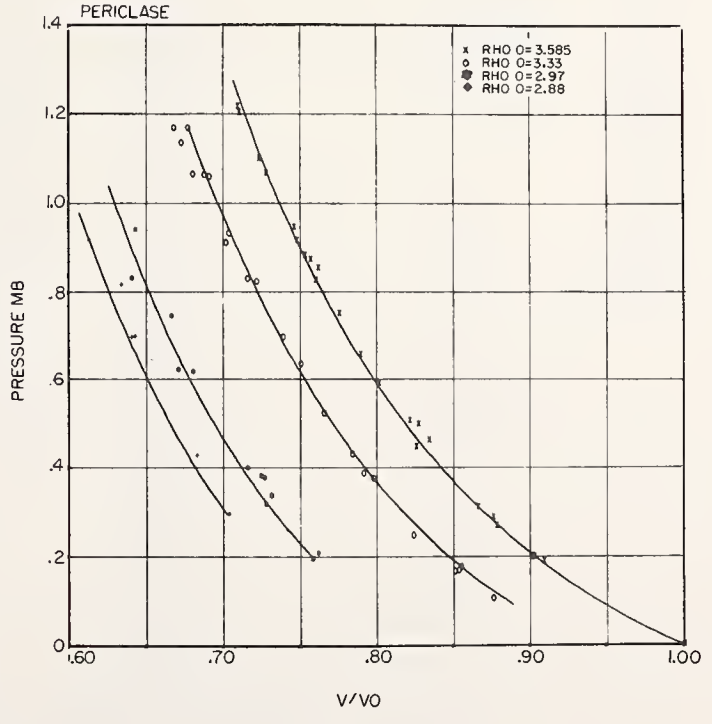

FIGURE 17. *Hugoniot* $P - V/V_0$ *data for* MgO.

The solid curves are transformations of the calculated $u_s - u_p$ curves from figure 16.

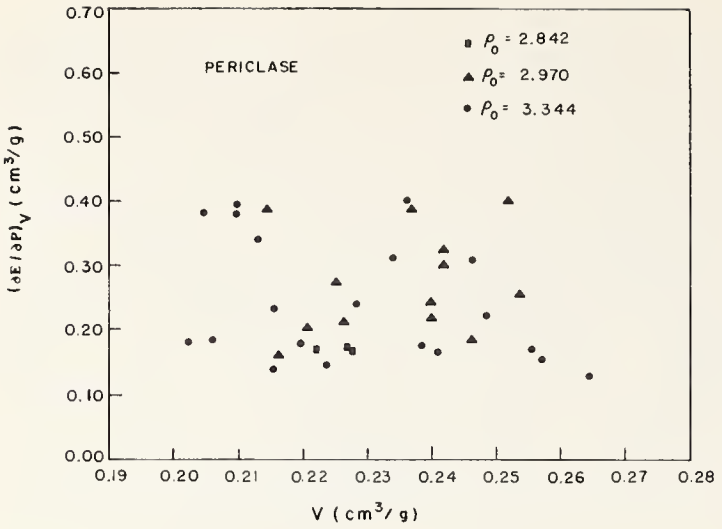

FIGURE 18. *Experimental values for* $(\partial E/\partial P)_V$ *versus volume determined from shock wave studies on porous* MgO.
The data points were computed by the same method as used in figures 8 and 9.

4. Transformation of Hugoniot Data to Isothermal Compression Data

As mentioned earlier, the extension of the Hugoniot data to regions off the Hugoniot represents the major shortcoming in using dynamically established standards in static experimental work. However, it is nevertheless possible to approximate the room temperature isotherms from the Hugoniot data under certain assumptions. For such calculations it is most convenient to work through the general energy-pressure equation (eq (4)). This equation states that the pressure and energy at any particular volume can be related to these quantities on the Hugoniot through some average value of the Grüneisen parameter γ. In view of the experimental evidence for porous Cu, 2024 Al, and MgO, as well as theoretical considerations, γ may be taken to be independent of pressure and a function of volume alone; the relationship $(\partial E/\partial P)_V$ = constant appears to be satisfactory in the absence of a more compelling choice. More complicated volume dependencies of γ lead to only slightly differing results for most materials. Calculation of isotherms requires an arbitrary choice for the specific heat as well, since data are unavailable in the region of interest. We have chosen to use one of the simplest forms of the Debye theory, characterized by a single Debye theta, $\Theta(V)$, which is a function only of volume [7]. This form for the specific heat is consistent with the assumption that the Grüneisen parameter depends only on the volume, since the specific heat obtained in this manner is a function only of entropy. In these calculations, $\Theta(V)$ has been chosen so that the Debye theory will give the correct room-temperature, zero-pressure value for the specific heat. With this assumption, the thermal energy, $E_T = E - E_{293}$ (where E_{293} is the energy of the solid at 293 K and the same volume) can be calculated. In turn, this energy and the corresponding thermal pressure, $P_T = E_T\gamma/V$, can then be removed from the Hugoniot curve to yield the room temperature isotherm.

The thermodynamic and Hugoniot data used to perform these calculations are listed in tables 1 and 2 respectively. The resulting P-ρ isotherms are tabulated in table 3, and the P-V/V_0 isotherms are

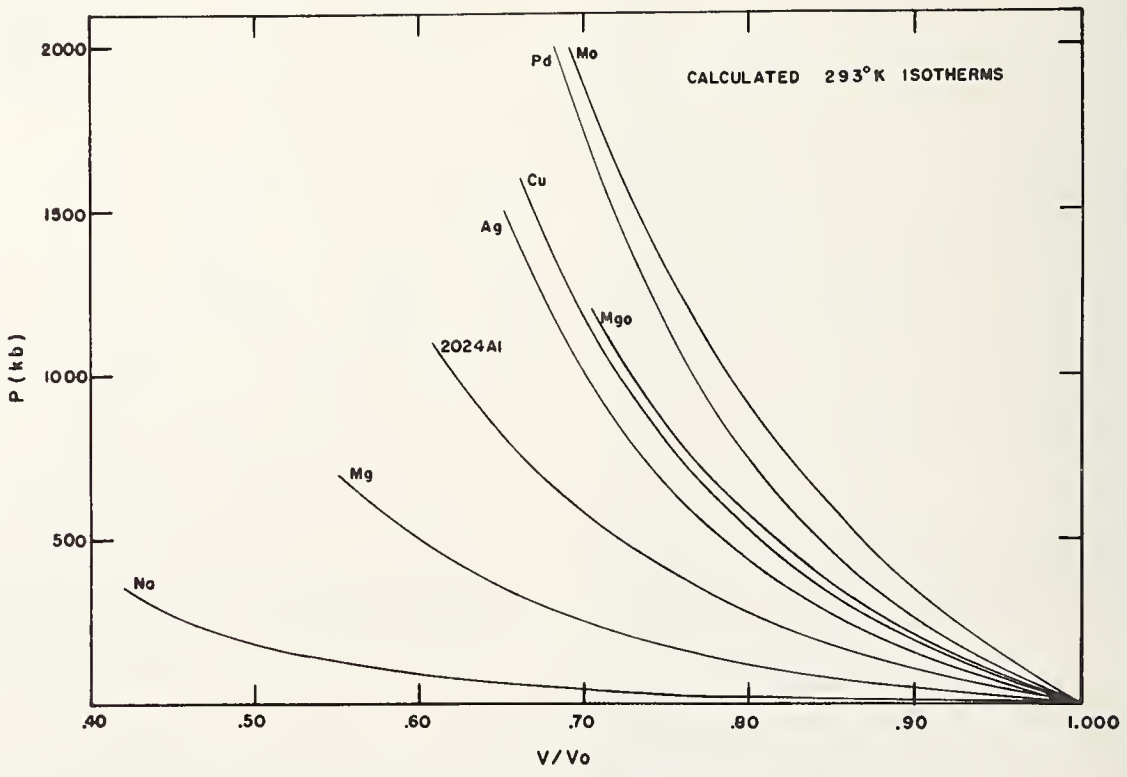

FIGURE 19. *Calculated 293 K* $P - V/V_0$ *isotherms for various materials.*

Pressure (Mb)	Calculated Density on 293 °K Isotherm							
	2024 Aluminum	Copper	Molybdenum	Silver	Palladium	Sodium	Magnesium	MgO
0.000	2.785	8.930	10.206	10.490	11.991	.968	1.740	3.585
.005	2.803	8.963	10.225	10.539	12.024	1.037	1.765	3.597
.010	2.821	8.995	10.244	10.587	12.056	1.096	1.789	3.608
.015	2.838	9.027	10.263	10.635	12.088	1.147	1.812	3.620
.020	2.855	9.059	10.282	10.681	12.119	1.193	1.834	3.631
.025	2.872	9.090	10.301	10.726	12.150	1.235	1.856	3.642
.030	2.888	9.120	10.319	10.771	12.181	1.274	1.876	3.653
.035	2.904	9.151	10.338	10.815	12.211	1.310	1.896	3.664
.040	2.920	9.180	10.356	10.858	12.242	1.344	1.916	3.675
.045	2.935	9.210	10.374	10.901	12.271	1.376	1.935	3.685
.050	2.950	9.239	10.393	10.942	12.301	1.407	1.954	3.696
.055	2.965	9.268	10.411	10.983	12.330	1.436	1.972	3.707
.060	2.980	9.296	10.429	11.024	12.359	1.464	1.989	3.717
.065	2.995	9.324	10.447	11.064	12.388	1.491	2.007	3.727
.070	3.009	9.352	10.465	11.103	12.416	1.517	2.023	3.737
.075	3.023	9.380	10.482	11.142	12.444	1.541	2.040	3.748
.080	3.037	9.407	10.500	11.180	12.472	1.565	2.056	3.758
.085	3.051	9.434	10.518	11.217	12.500	1.588	2.072	3.768
.090	3.064	9.460	10.535	11.255	12.527	1.611	2.088	3.777
.095	3.078	9.487	10.553	11.291	12.554	1.632	2.103	3.787
.100	3.091	9.513	10.570	11.327	12.581	1.653	2.118	3.797
.105	3.104	9.538	10.587	11.363	12.608	1.674	2.133	3.806
.110	3.117	9.564	10.605	11.398	12.634	1.693	2.147	3.816
.115	3.130	9.589	10.622	11.433	12.660	1.713	2.161	3.825
.120	3.142	9.614	10.639	11.468	12.686	1.731	2.176	3.835
.125	3.155	9.639	10.656	11.502	12.712	1.750	2.189	3.844
.130	3.167	9.664	10.673	11.536	12.737	1.768	2.203	3.853
.135	3.179	9.688	10.690	11.569	12.763	1.785	2.216	3.863
.140	3.191	9.712	10.706	11.602	12.788	1.802	2.230	3.872
.145	3.203	9.736	10.723	11.634	12.813	1.819	2.243	3.881
.150	3.215	9.760	10.740	11.667	12.837	1.835	2.256	3.890
.200	3.328	9.987	10.902	11.972	13.075	1.980	2.376	3.976
.250	3.431	10.198	11.059	12.251	13.297	2.102	2.483	4.057
.300	3.527	10.394	11.210	12.508	13.506	2.206	2.581	4.133
.350	3.616	10.579	11.356	12.747	13.703	2.298	2.671	4.205
.400	3.701	10.754	11.497	12.972	13.891		2.754	4.273
.450	3.781	10.920	11.635	13.183	14.069		2.832	4.339
.500	3.858	11.079	11.768	13.383	14.240		2.904	4.401
.550	3.931	11.230	11.898	13.573	14.403		2.973	4.461
.600	4.001	11.375	12.025	13.754	14.561		3.038	4.519
.650	4.068	11.514	12.149	13.927	14.712		3.100	4.575
.700	4.132	11.648	12.270	14.093	14.858		3.158	4.629
.750	4.195	11.777	12.388	14.252	14.999			4.681
.800	4.255	11.902	12.504	14.405	15.135			4.731
.850	4.313	12.022	12.617	14.552	15.268			4.780
.900	4.369	12.139	12.728	14.694	15.396			4.828
.950	4.424	12.252	12.837	14.831	15.520			4.874
1.000	4.477	12.362	12.944	14.963	15.642			4.919
1.050	4.528	12.469	13.050	15.091	15.759			4.963
1.100	4.578	12.573	13.153	15.216	15.874			5.005
1.150		12.674	13.255	15.336	15.986			5.047
1.200		12.773	13.355	15.453	16.095			5.088
1.250		12.869	13.453	15.567	16.202			
1.300		12.962	13.550	15.677	16.306			
1.350		13.054	13.645	15.785	16.407			
1.400		13.143	13.739	15.890	16.507			
1.450		13.231	13.832	15.992	16.604			
1.500		13.316	13.924	16.091	16.699			
1.550		13.399	14.014		16.792			
1.600		13.481	14.103		16.884			
1.650			14.190		16.973			
1.700			14.277		17.061			
1.750			14.363		17.147			
1.800			14.447		17.232			
1.850			14.531		17.315			
1.900			14.613		17.396			
1.950			14.695		17.476			
2.000			14.776		17.555			

TABLE 3. *Calculated 293 K isotherms*

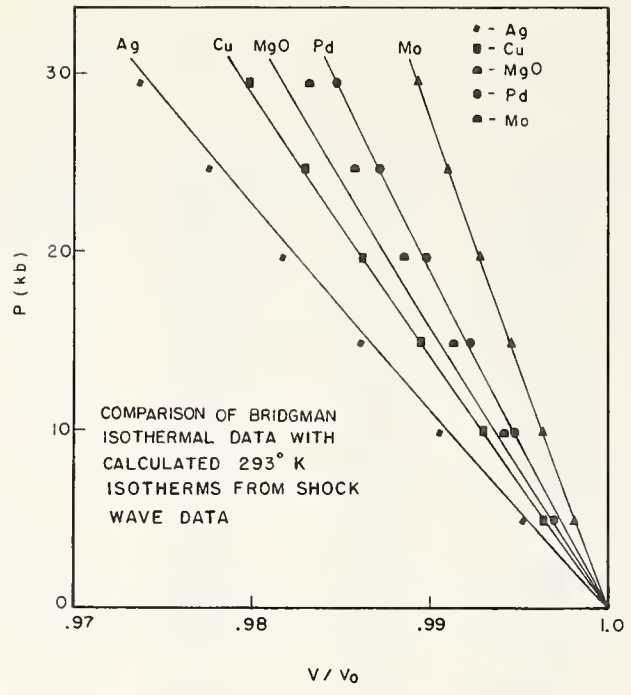

FIGURE 20. *Comparison of Bridgman isothermal data with calculated 293 K isotherms from shock wave data.*

The agreement to 30 kbar, with the exception of the data for MgO, is acceptable. The Bridgman data are from reference [9]. The solid lines are the lower ends of the calculated 293 K isotherms from figure 19.

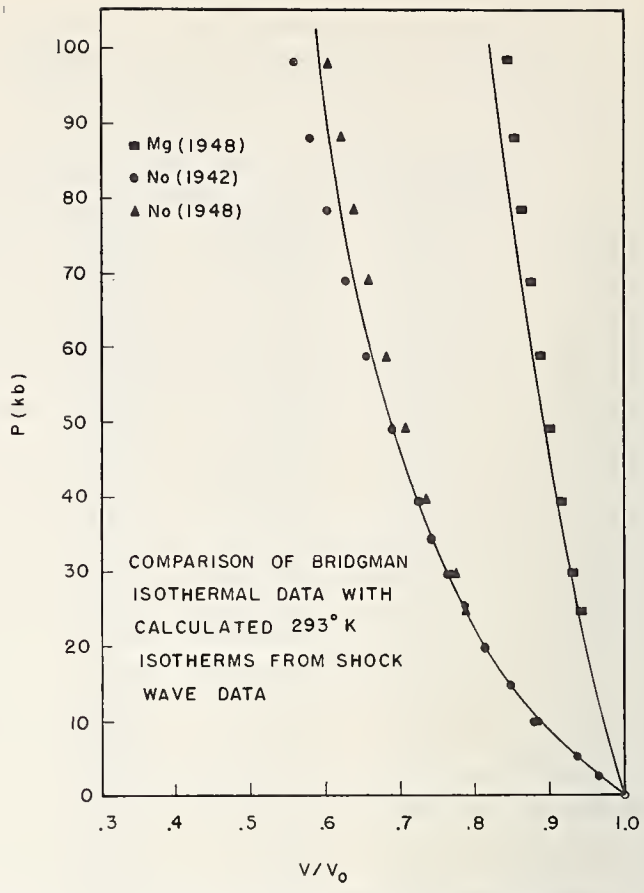

FIGURE 21. *Comparison of Bridgman isothermal data with calculated 293 K isotherms from shock wave data.*

The 1948 Bridgman data (ref. [10]) would indicate consistently lower compressibilities than the earlier 1942 (ref. [11]) work. The solid lines are the calculated 293 K isotherms from figure 19.

plotted in figure 19. These isotherms have been calculated to pressures only slightly below the maximum pressures reached on the Hugoniots, and therefore represent small extensions of the data. They should therefore be used with caution in the very high pressure ranges.

The calculated isotherms are compared with the work of Bridgman [8, 9, 10] in figures 20 and 21 for most of the materials included here. The agreement, at least to pressures of 30 kbar, is in general quite good. Above about 50 kbar there is considerable disagreement for both Na and Mg, with the 1948 Bridgman data being consistently too high in pressure. The most serious disagreement is with MgO. In view of the difficulties with the sound speed and the likelihood of a phase change below 200 kbar in this material, the Bridgman isotherm is probably more correct in this low-pressure region. It may be remarked that if the Hugoniot intercept is made to agree with the ultrasonic value of 6.73 km/s, then the Bridgman isotherm and our calculated shock wave isotherm agree very nicely as well.

5. References

[1] McQueen, R. G., Laboratory techniques for very high pressures and the behavior of metals under dynamic loading. Metallurigical Soc. Confs., Vol. 22, K. A. Gschneider, Jr., M. T. Hepworth, and N. A. D. Parlee, eds. (Gordon and Breach Science Publishers, New York, 1964).

[2] Rice, M. H., McQueen, R. G., and Walsh, J. M., Solid State Physics, Vol. 6, pp. 1–63 (Academic Press, New York, 1958).

[3] McQueen, R. G., and Marsh, S. P., J. Appl. Phys. **31**, 1253 (1960).

[4] Walsh, J. M., and Christian, R. H., Phys. Rev. **97**, 1544 (1955).

[5] Shreffler, R. G., and Deal, W. E., J. Appl. Phys. **24**, 44 (1953).

[6] Taylor, J. W., private communication.

[7] Ziman, J. M., Electrons and Phonons, p. 56 (Claredon Press, Oxford, 1960).

[8] Bridgman, P. W., Proc. Am. Acad. Arts Sci. **77**, 189 (1949).

[9] Bridgman, P. W., Proc. Am. Acad. Arts Sci. **76**, 55 (1948).

[10] Bridgman, P. W., Proc. Am. Acad. Arts Sci. **74**, 425 (1942).

[11] Hampel, C. A., ed., Rare Metals Handbook, 2d ed., pp. 689, 695 (Reinhold Publ. Corp., London, 1961).

[12] Clark, S. P., ed., Handbook of Physical Constants (The Geological Society of America, New York, 1966).

[13] JANAF Thermochemical Tables (The Dow Chemical Company, Midland, Michigan, June 1966).

[14] Marsh, S. P., unpublished data.

[15] Hearman, R. F. S., Phil. Mag. Suppl. Vol. **5**, 323 (1956).

[16] Overton, W. C., Jr., and Gaffney, J., Phys. Rev. **98**, 969 (1955).

[17] Lazarus, D., Phys. Rev. **76**, 545 (1949).

[18] Neighbors, J. R., and Alers, G. A., Phys. Rev. **111**, 707 (1958).

[19] Rohl, H., Ann. Phys. **16**, 887 (1933).

[20] Bolef, D. I., and de Klerk, J., J. Appl. Phys. **33**, 2311 (1962).

[21] Chung, D. H., Swica, J. J., and Crandall, W. B., J. Am. Ceram. Soc. **46**, 452 (1963).

[22] Susse, C., J. Rech. Centre National de Rech. Sci. **54**, 23 (1961).

[23] Schrieber, E., and Anderson, O. L., J. Geophys. Res. **73**, 2837 (1968).

[24] Goens and Schmidt, Physik Z. **37**, 385 (1936).

[25] Daniels, W. B., Phys. Rev. **119**, 1246 (1960).

Chairman: C. W. BECKETT
National Bureau of Standards
Washington, D.C. 20234

Effect of Pressure on the Lattice Parameters of Lead Chalcogenides and Nickel Arsenide-Type Compounds

S. Minomura, H. Nagasaki, and I. Wakabayashi

Institute for Solid State Physics, University of Tokyo, Tokyo, Japan

1. Introduction

There has been considerable interest on a pressure scale in lead chalcogenides and nickel arsenide-type compounds. Lead chalcogenides exhibit the first-order transitions at 24,680 (PbS), 43,320 (PbSe), and 41,200 (PbTe) kg/cm^2 in the Bridgman's *P-V* data [1],[1] accompanied by the extremely sharp rise in electrical resistance [2]. Nickel arsenide-type compounds exhibit the large negative pressure dependence of magnetic transition temperatures in the rate of −12.3(MnAs) [3], −3.3(MnSb) [3, 4], −6(CrTe) [5], and −6(NiS) [6] degree/kbar, etc.

Bassett, Takahashi, and Stock [7] have observed the x-ray powder patterns of high-pressure polymorphs in lead chalcogenides, using diamond anvils, which have a correspondence with the SnS-type patterns, but are not yet identified completely at present. Lynch [8] has measured the lattice parameters of MnSb as function of pressure up to 150 kbar, using diamond x-ray cell and discussed the negative pressure dependence of Curie temperature in the relative changes of three shortest Mn-Mn distances; $c/2$, a, and $(c^2/4+a^2)^{1/2}$.

In this experiment the lattice parameters have been measured in two lead chalcogenides (PbS and PbTe) up to 90 kbar and in four nickel arsenide-type compounds (MnSb, MnTe, CrSb, and CrTe) up to 170 kbar.

2. Experimentals

Table 1 summarizes the materials, sources, and atmospheric lattice parameters. The materials were diluted in 5 to 13 times of weight by amorphous boron powder for reduction of x-ray absorption. The x-ray powder photographs were taken at quasi-hydrostatic pressure and at room temperature, using a Drickamer-type high pressure cell [9]. The x-ray diffraction angles allowed about 20 degrees using Mo target at the maximum pressure of 170 kbar. Pressures were determined by markers of NaCl, which was scaled by Bridgman's *P-V* data [10] and Drickamer's x-ray data [11]. The lattice parameters calculated by least square method.

3. Results and Discussions

3.1. Lead Chalcogenides

The normal forms of lead chalcogenides have NaCl-type structure. The x-ray powder patterns which have a correspondence with the SnS-type patterns were observed in PbS above 25 kbar and in PbTe above 45 kbar. Tables 2 and 3 show the observed and calculated *d*-spacings of the orthorhombic patterns in PbS at 45 kbar and in PbTe at

TABLE 1. *Materials, sources, and atmospheric lattice parameters*

Materials	*Sources*	*Structures*	*a*	*c*	*c/a*
			(Å)	(Å)	
PbS	Kanto Chem. Co.	NaCl	5.935	.....	.....
PbTe	Dr. Y. Sato of Electrical Communication Lab.	NaCl	6.439	.....	.....
MnSb	Dr. T. Kaneko of Tohoku Univ.	hex.	4.13	5.78	1.40
MnTe	Dr. S. Anzai Keio Univ.	hex.	4.15	6.71	1.62
CrSb	Dr. T. Kaneko of Tohoku Univ.	hex.	4.11	5.44	1.32
CrTe	Dr. T. Kaneko of Tohoku Univ.	hex.	3.98	6.21	1.57

[1] Figures in brackets indicate the literature references at the end of this paper.

Paper presented at the Symposium on Accurate Characterization of the High-Pressure Environment, held at the National Bureau of Standards, Gaithersburg, Md., October 14–18, 1968.

TABLE 2. *Observed and calculated* d *spacings for orthorhombic phase of* PbS *at 45 kbar and relative intensities of* SnS*-type compounds*

$d_{obs.}$	*hkl*	$d_{calc.}$	I/I_1(SnS)	I/I_1(GeS)
(Å)		(Å)		
3.35 *vs*	120	3.39	10	80
3.18 *s*	021	3.17	15	40
2.84 *vs*	040	2.85	100	100
2.53 *s*	(boron ?)			
2.30 *s*	131	2.32	15	50
2.00 *s*	150	2.01	10	10
1.87 *w*	230	1.88	—	50
1.79 *w*	151	1.78	5	50

TABLE 3. *Observed and calculated* d*-spacings for orthorhombic phase of* PbTe *at 80 kbar and relative intensities of* SnS*-type compounds*

$d_{obs.}$	*hkl*	$d_{calc.}$	I/I_1(SnS)	I/I_1(GeS)
(Å)		(Å)		
3.69 *m*	120	3.68	10	80
3.38 *s*	021	3.37	15	40
2.99 *s*	040	2.97	100	100
2.43 *s*	131	2.43	15	50
2.31 *m*	210	2.30	1	30
2.15 *w*	141	2.14	10	40
2.01 *m*	230	2.02	—	50
1.91 *w*	151	1.91	5	50

80 kbar, where the smoothed data of lattice parameters were used for the calculation, and the relative intensities of SnS and GeS. The other calculated patterns, such as 101 and 111 lines etc., were not detected for our instruments, because of their low resolution. However, assuming the SnS-type structure as the high-pressure polymorph in lead chalcogenides throughout this paper, the diffraction patterns were indexed to orthorhombic set of indices.

Figure 1 shows the unit cells of NaCl-type and orthorhombic structures. The orthorhombic lattice parameters were calculated from 120, 021, and 040 lines. Figures 2 and 3 are a plot of lattice parameters versus pressure in PbS and PbTe. Tables 4 and 5 summarize the smoothed date of a/a_0, b/b_0, c/c_0, V/V_0, and P in the NaCl-type and orthorhombic structures. Figures 4 and 5 are a plot of V/V_0 versus pressure. The crosses are Bridgman's data. The $P-V$ data suggest the first-order phase transition from the NaCl-type to the orthorhombic structures which accompanies the volume discontinuity of about 3 percent in PbS and about 2 percent in PbTe. The c axes are slightly more compressible than the a and b axes in the orthorhombic phase.

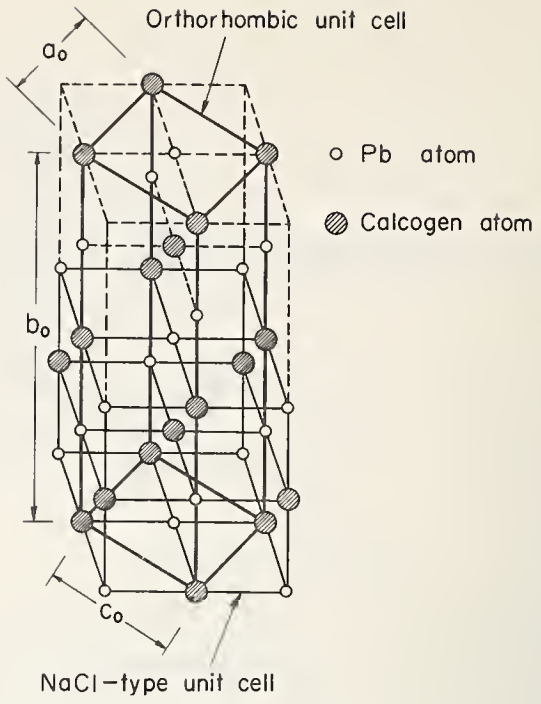

FIGURE 1. NaCl*-type and orthorhombic unit cells.*

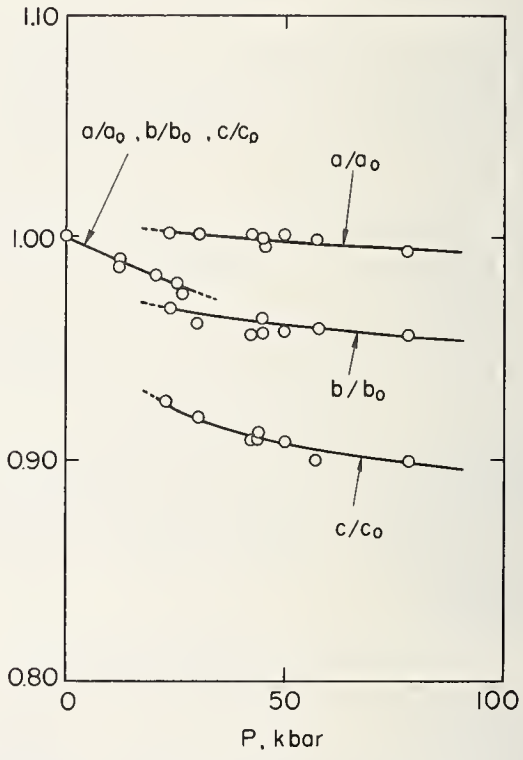

FIGURE 2. *Lattice parameters versus* P *in* PbS.

3.2. Nickel Arsenide-Type Compounds

Table 6 summarizes the pressure dependence of magnetic transition temperatures and the volume magnetostriction given by the thermal dilatation data at the atmospheric pressure in MnSb, MnTe,

TABLE 4. *Lattice parameters and compressibility of* PbS

p	a/a_0	b/b_0	c/c_0	V/V_0
NaCl-type structure				
kbar				
0	1.000	1.000	1.000	1.000
10	0.992	0.992	0.992	0.973
20	0.983	0.983	0.983	0.950
Orthorhombic structure				
30	1.014	0.966	0.919	0.902
40	1.009	.962	.914	.887
50	1.005	.960	.905	.873
60	1.000	.958	.902	.864
70	0.998	.956	.900	.858

*NaCl-type structure is also described in terms of orthorhombic axes.

TABLE 5. *Lattice parameters and compressibility of* PbTe

p	a/a_0	b/b_0	c/c_0	V/V_0
NaCl-type structure				
kbar				
0	1.000	1.000	1.000	1.000
10	0.992	0.992	0.992	0.978
20	.986	.986	.986	.956
30	.978	.978	.978	.938
40	.972	.972	.972	.920
Orthorhombic structure				
50	1.030	0.931	0.926	0.889
60	1.029	.927	.917	.874
70	1.028	.922	.902	.859
80	1.027	.919	.897	.844
90	1.026	.915	.888	.832

*NaCl-type structure is also described in terms of orthorhombic axes.

TABLE 6. *The pressure dependence of magnetic transition temperatures and the volume magnetostriction at the atmospheric pressure*

Compounds	$T_{C,N}$	$\partial T_{C,N}/\partial P$	Volume magnetostriction	
			Δa	Δc
	(K)	(K/bar)	(percent)	(percent)
MnSb	586(T_C)	− 3.3[3,4]	+ 0.3[12]	0
MnTe	307(T_N)	+ 2.6[13]	0	− 0.8[14]
CrSb	713(T_N)	—	+ 1.2[15]	− 2.9[15]
CrTe	339(T_C)	− 6[5]	+ 0.16[16]	+ 0.14[16]

CrSb, and CrTe. Figure 6 shows the unit cell of nickel arsenide-type compounds. The hexagonal lattice parameters were calculated from the following lines: 101, 102, 110, 103, and in some cases 202, 004, 211, 212, 114, 213, in MnSb; 101, 102, 110, 201, and in some cases 202, 203 in MnTe; 110, 102, 101, and in some cases 103 in CrSb and CrTe.

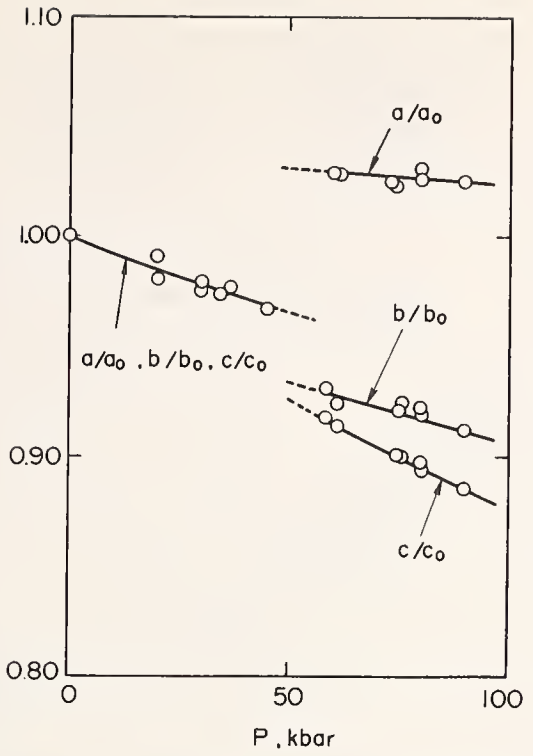

FIGURE 3. *Lattice parameters versus* P *in* PbTe.

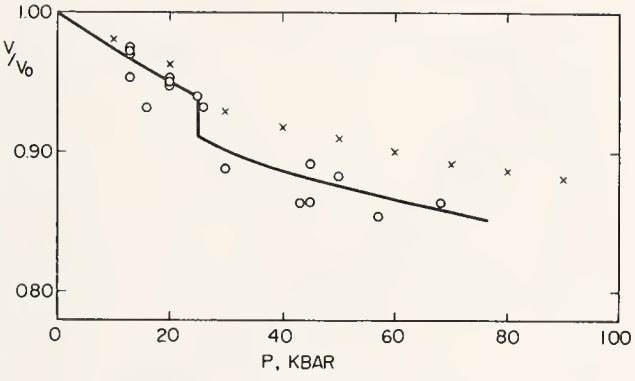

FIGURE 4. V/V_0 *versus* P *in* PbS.

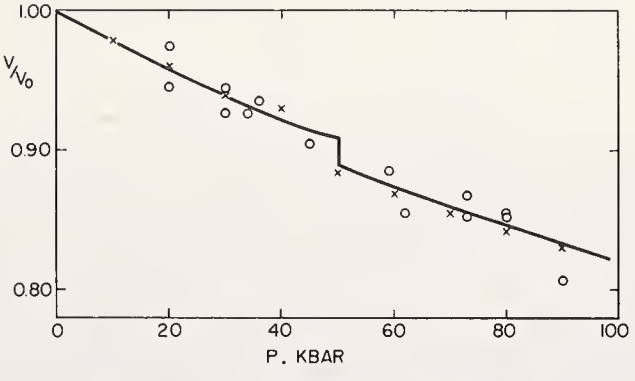

FIGURE 5. V/V_0 *versus* P *in* PbTe.

Figures 7–10 are a plot of lattice parameters versus pressure. MnSb exhibits the Curie temperature at 65 kbar decreases up to the room temperature. The small but measurable irregularity in the

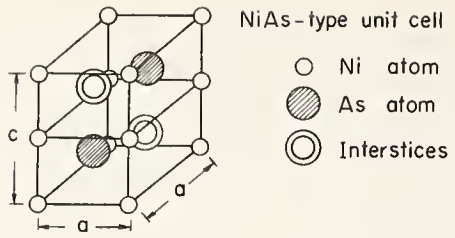

FIGURE 6. NiAs-*type unit cell.*

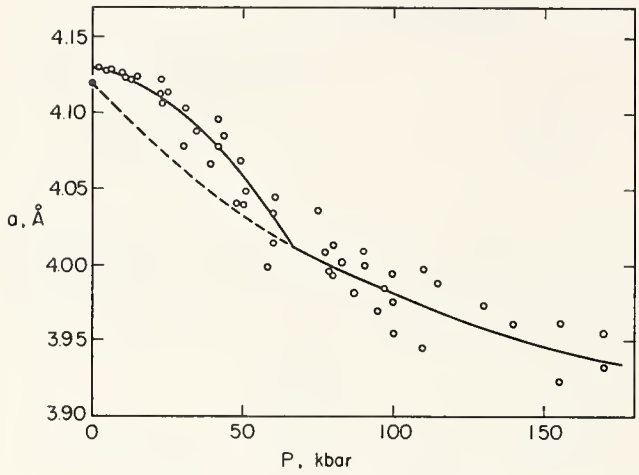

FIGURE 7(a). a *versus* P *in* MnSb.

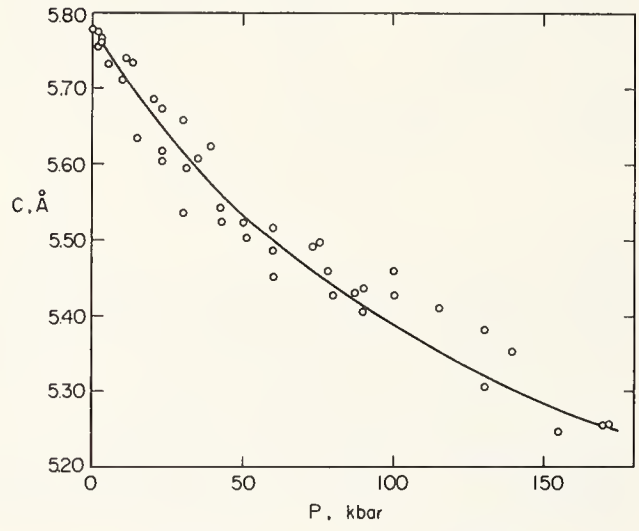

FIGURE 7(b). c *versus* P *in* MnSb.

a-P curve is observed at about 65 kbar, as shown in figure 7(a). The distortion in the *a* axis below 65 kbar from the dotted curve which is drawn by the extrapolation from the curve above 65 kbar is considered as the magnetostriction. CrSb exhibits the sharp rise in *c* axis and the sharp drop in *a* axis at about 80 kbar, which is not yet established, but may suggest the first-order or second-order phase transitions. The experiment on the pressure dependence of Néel temperature in CrSb is in progress.

Tables 7 to 10 summarize the smoothed data of a/a_0, c/c_0, $(c/a)/(c/a)_0$, and V/V_0, and P. The lattice parameters are expressed by the following function of pressure:

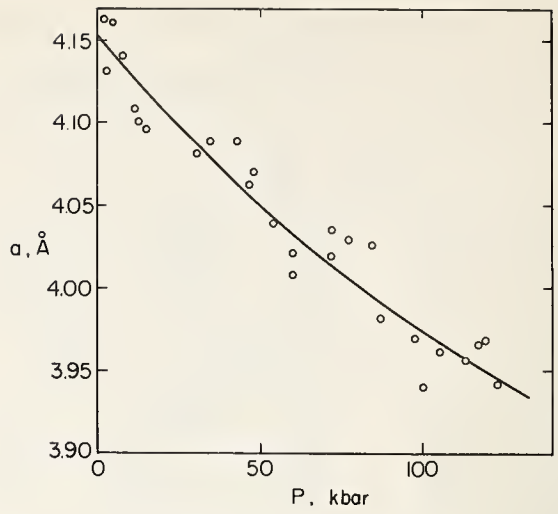

FIGURE 8(a). a *versus* P *in* MnTe.

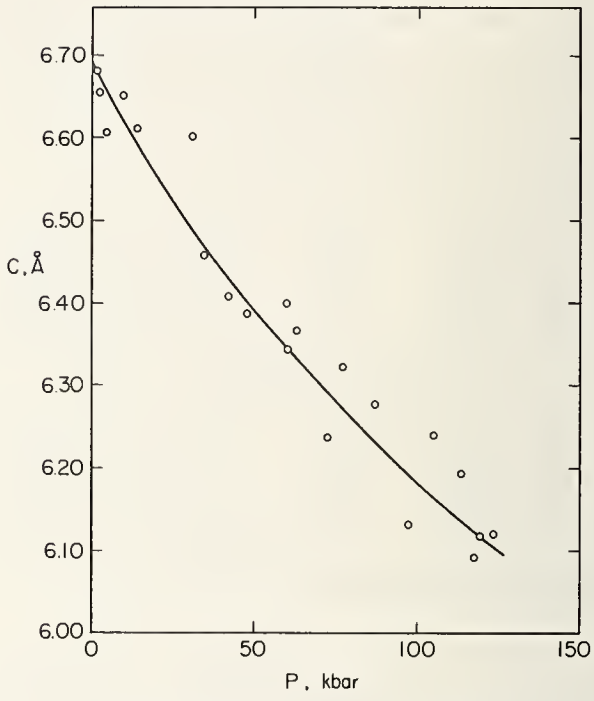

FIGURE 8(b). c *versus* P *in* MnTe.

MsSb,

$-\Delta a/a_0 = 1.32 \times 10^{-4}P + 4.64 \times 10^{-6}P^2$ (below 65 kbar),

$-\Delta a/a_0 = 2.7 \times 10^{-3} + 4.64 \times 10^{-4}P - 1.21 \times 10^{-6}P^2$ (above 65 kbar),

$-\Delta c/c_0 = 9.42 \times 10^{-4}P - 2.50 \times 10^{-6}P^2$;

MnTe,

$-\Delta a/a_0 = 5.52 \times 10^{-4}P - 1.18 \times 10^{-6}P^2$,

$-\Delta c/c_0 = 10.6 \times 10^{-4}P - 2.79 \times 10^{-6}P^2$;

CrSb,

$-\Delta a/a_0 = 3.9 \times 10^{-4}P - 1.7 \times 10^{-6}P^2$,

$-\Delta c/c_0 = 5.8 \times 10^{-4}P - 1.0 \times 10^{-6}P^2$;

CrTe,

$-\Delta a/a_0 = 1.6 \times 10^{-3} + 3.0 \times 10^{-4}P$,

$-\Delta c/c_0 = 1.4 \times 10^{-3} + 8.0 \times 10^{-4}P$.

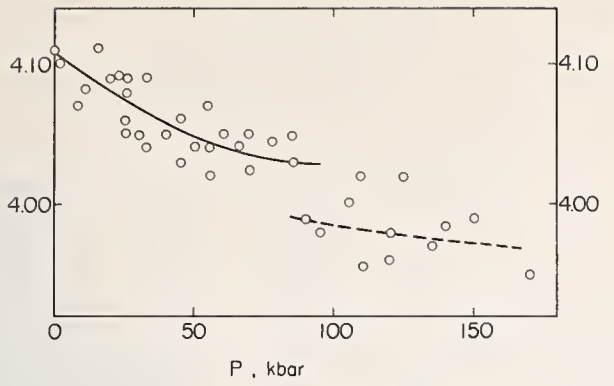

FIGURE 9(a). a *versus* P *in* CrSb.

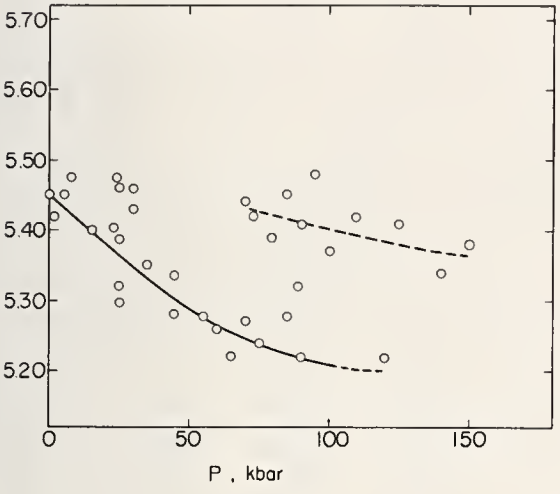

FIGURE 9(b). c *versus* P *in* CrSb.

TABLE 7. *Smoothed data of* a/a_0, c/c_0, $(c/a)/(c/a)_0$, *and* V/V_0 *in* MnSb

P	a/a_0	c/c_0	$(c/a)/(c/a)_0$	V/V_0
kbar				
0	1.000	1.000	1.000	1.000
10	0.998	0.989	0.992	0.985
20	.995	.980	.984	.971
30	.992	.971	.979	.955
40	.987	.964	.976	.940
50	.982	.957	.975	.923
60	.976	.951	.975	.905
65	.972	.949	.976	.895
70	.970	.946	.975	.891
80	.968	.941	.972	.882
90	.966	.937	.970	.873
100	.964	.932	.967	.866
110	.962	.928	.965	.859
120	.960	.925	.964	.852
130	.958	.921	.962	.846
140	.957	.918	.959	.840
150	.955	.914	.957	.834
160	.954	.911	.956	.829
170	.953	.908	.954	.825

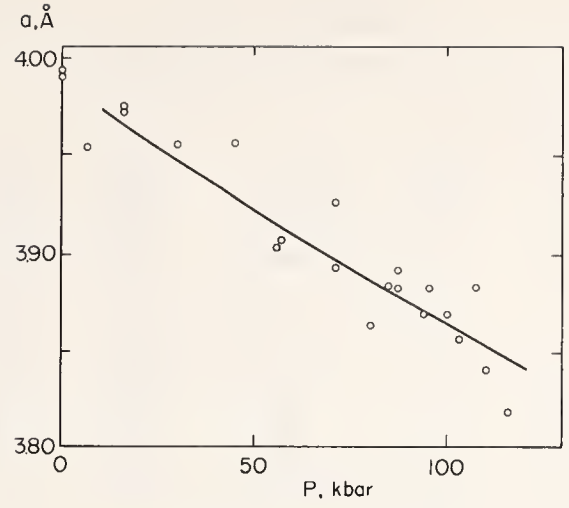

FIGURE 10(a). a *versus* P *in* CrTe.

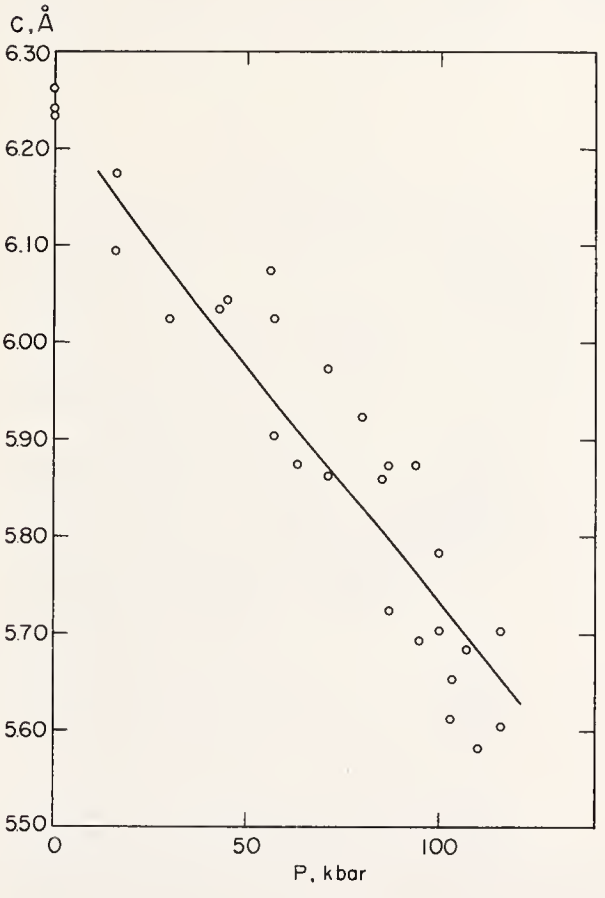

FIGURE 10(b). c *versus* P *in* CrTe.

Figure 11 shows the smoothed data of c/a ratio versus pressure. Empirical exchange interaction curves relating magnetic transition temperatures to interatomic distances have been frequently discussed in nickel arsenide-type compounds. However, the pressure dependence of magnetic transition temperatures may not be quantitatively understood by the relative change in the neighboring atomic distances ($c/2$ or a) and the bonding angles of nearest neighboring atoms (c/a).

TABLE 8. *Smoothed data of* a/a_0, c/c_0, $(c/a)/(c/a)_0$, *and* V/V_0 *in* MnTe

P	a/a_0	c/c_0	$(c/a)/(c/a)_0$	V/V_0
kbar				
0	1.000	1.000	1.000	1.000
10	0.996	0.988	0.994	0.977
20	.989	.978	.988	.956
30	.984	.969	.985	.938
40	.980	.962	.982	.924
50	.975	.955	.979	.907
60	.971	.947	.975	.893
70	.967	.942	.972	.881
80	.964	.935	.970	.868
90	.960	.929	.967	.856
100	.957	.922	.964	.844
110	.954	.917	.962	.835
120	.951	.913	.960	.826
130	.948	.909	.958	.816

TABLE 9. *Smoothed data of* a/a_0, c/c_0, $(c/a)/(c/a)_0$, *and* V/V_0 *in* CrSb.

P	a/a_0	c/c_0	$(c/a)/(c/a)_0$	V/V_0
kbar				
0	1.000	1.000	1.000	1.000
10	0.996	0.994	0.998	0.986
20	.993	.989	.996	.976
30	.990	.983	.993	.964
40	.988	.977	.989	.954
50	.985	.972	.987	.944
60	.983	.968	.985	.935
70	.982	.965	.983	.930
80	.981	.961	.980	.925
90	.980	.959	.979	.921
100	.980	.958	.977	.920

TABLE 10. *Smoothed data of* a/a_0, c/c_0, $(c/a)/(c/a)_0$, *and* V/V_0 *in* CrTe.

P	a/a_0	c/c_0	$(c/a)/(c/a)_0$	V/V_0
kbar				
0	1.000	1.000	1.000	1.000
10	0.999	0.995	0.996	0.993
20	.995	.987	.992	.977
30	.992	.979	.987	.963
40	.989	.969	.980	.948
50	.985	.963	.978	.934
60	.982	.953	.971	.919
70	.980	.947	.966	.910
80	.977	.939	.961	.897
90	.974	.931	.956	.883
100	.971	.923	.951	.870

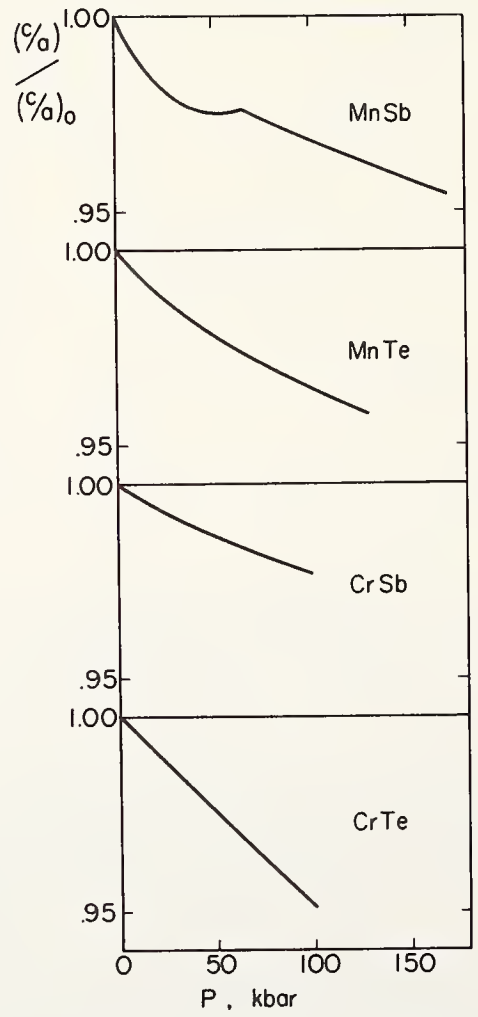

FIGURE 11. $(c/a)/(c/a)_0$ *versus* P.

According to the molecular magnetic field approximation [17], the internal energy E of magnetic substances includes the elastic energy E_{el} and the magnetic exchange interaction energy E'_{ex}

$$E = E_{el} + E_{ex'} \tag{1}$$

where

$$E_{el} = (\Delta V)^2/2kV \tag{2}$$

and

$$E_{ex} = -\frac{1}{2}\gamma\sigma^2 = -\frac{3k}{2}T_{C,N} = \text{const} \cdot -2J_{ex}S_1 \cdot S_2 \tag{3}$$

ΔV is the volume magnetostriction, k the compressibility, γ the coefficient of molecular field, σ the intrinsic magnetization per unit mass at absolute zero temperature, $T_{C,N}$ the Curie or Néel temperatures, and J_{ex} the exchange integral between spin S_1 and spin S_2. The differentiation of eq (3) as

regards P,

$$\frac{1}{T_{C,N}}\frac{\partial T_{C,N}}{\partial P}=\frac{1}{J_{ex}}\frac{\partial J_{ex}}{\partial P}+\frac{2}{\sigma}\frac{\partial \sigma}{\partial P}. \tag{4}$$

$\partial E/\partial V=0$ leads using eqs (1), (2), and (3),

$$\frac{\Delta V}{V_0}=-\frac{3k}{2V_0}\frac{\partial T_{C,N}}{\partial P}. \tag{5}$$

When the volume magnetostriction is only in a axis, eq (5) is replaced by

$$\frac{\Delta V}{V_0}=2\frac{\Delta a}{a_0}. \tag{6}$$

Figure 12 is a plot of the magnetostriction in a axis of MnSb versus pressure. The pressure dependence of Curie temperature reported by Samara and Giardini is expressed by the function of P with the critical pressure $P_c=150$ kbar and the constant $\alpha=1.52$.,

$$T_C=T_C^0\left(1+\alpha\frac{P}{P_C}\right)\left(1-\frac{P}{P_C}\right)^2,$$

where

$$J_{ex}=J_0\left(1+\alpha\frac{P}{P_C}\right),$$

and

$$\sigma=\sigma_0\left(1-\frac{P}{P_C}\right). \tag{7}$$

Equation (7) leads the initial pressure dependence of J_0 and σ_0,

$$\frac{1}{J_0}\frac{\partial J_0}{\partial P}=\frac{\alpha}{P_C}=10\times10^{-6}\ \text{bar}^{-1}$$

$$\frac{1}{\sigma_0}\frac{\partial \sigma_0}{\partial P}=-\frac{1}{P_C}=-6.7\times10^{-6}\ \text{bar}^{-1}$$

These values coincide within experimental errors with the data reported by Hirone et al. [4]. The negative pressure dependence of magnetic transition temperature is due to the negative change in intrinsic magnetization, which may be caused by the relative change in band structure or redistribution of electrons between the spin orientations.

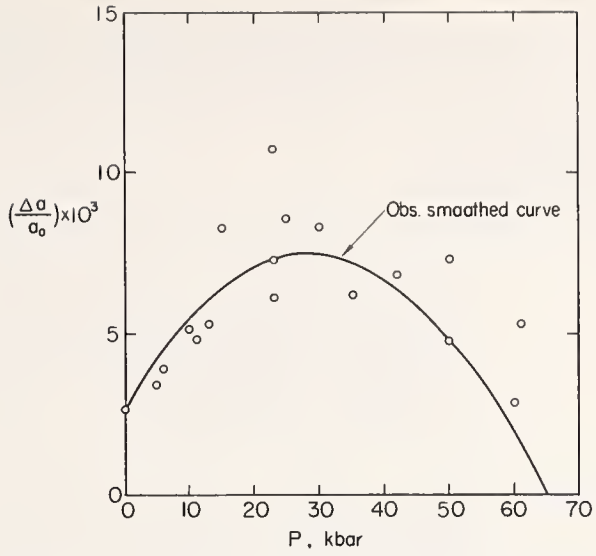

FIGURE 12. *Magnetostriction of* a *versus* P *in* MnSb.

4. References

[1] Bridgman, P. W., Phys. Rev. **57**, 237 (1940); Proc. Am. Acad. Arts Sci. **74**, 21 (1940); ibid. **76**, 55 (1948).
[2] Samara, G. A., and Drickamer, H. G., J. Chem. Phys. **37**, 1159 (1962).
[3] Samara, G. A., and Giardini, A. A., Physics of Solids at High Pressures, ed. C. T. Tomizuka and R. M. Emrick, Academic Press (1965), p. 308.
[4] Hirone, T., Kaneko, T., and Kondo, K., ibid. p. 298.
[5] Grazhdankina, N. P., Gaidukov, L. G., Rodionov, K. P., Oleinik, M. I., and Shchipanov, V. A., Soviet Physics—JETP **13**, 297 (1961).
[6] Anzai, S., and Ozawa, K., J. Phys. Soc. Japan **24**, 271 (1968).
[7] Bassett, W. A., Takahashi, T., and Stock, P. W., Rev. Sci. Instr. **38**, 37 (1967); T. Takahashi, private communication.
[8] Lynch, R. W., J. Chem. Phys. **47**, 5180 (1967).
[9] Perez-Albuerne, E. A., Foresgren, K. F., and Drickamer, H. G., Rev. Sci. Instr. **35**, 29 (1964).
[10] Bridgman, P. W., Proc. Am. Acad. Arts Sci. **76**, 1 (1945).
[11] Perez-Albuerne, E. A., and Drickamer, H. G., J. Chem. Phys. **43**, 1381 (1965).
[12] Willis, B. T. M., and Rooksby, H. P., Proc. Phys. Soc. (London) **67**, 290 (1954).
[13] Ozawa, K., Anzai, S., and Hamaguchi, Y., Phys. Letters **20**, 132 (1966).
[14] Greenwald, S., Acta Cryst. **6**, 396 (1953).
[15] Willis, B. T. M., Acta Cryst. **6**, 425 (1953).
[16] Ido, H., Suzuki, K., and Kaneko, T., private communication.
[17] Kittel, C., Introduction to Solid Physics, John Wiley & Sons, Inc. (1956), pp. 402–408.

DISCUSSION

W. A. Bassett (*University of Rochester, Rochester, New York*): We have calculated the intensities for the diffraction pattern produced by lead and sulfur in the SnS structure using the SnS lattice parameters (see accompanying table). These intensities differ significantly from those for tin and sulfur in the SnS structure. We feel that these differences should be taken into consideration in identifying the structure and in determining the lattice parameters.

In table 2 you do not report a reflection having the index (110), yet the calculated intensity is $I/I_1=49$ and should be observable. Your reflection $d=2.84$ Å is indexable as (111) and (130) as well as (040). Of these, the (111) should contribute the most to the

intensity. The reflection $d = 2.00$ Å may be indexable as a combination of (141), (002), and (150). Of these the (141) would contribute the most to the intensity. The reflection $d = 1.87$ Å may be indexed as a combination of (211) and (230) of which (211) contributes the most intensity.

Table of calculated intensities for PbS *in the* SnS *structure*

Wavelength = 0.70926 Å

$a = 4.34$ Å, $b = 11.20$ Å, $c = 3.99$ Å
Pb: $x = 0.1150$, $y = 0.1180$, $z = 0.2500$
S: $x = 0.5220$, $y = 0.1500$, $z = 0.7500$

d	hkl	I/I_1
4.047	110	49
3.430	120	67
3.250	021	100
2.937	101	53
2.841	111	86
2.830	130	9
2.800	040	64
2.308	131	51
2.130	210	25
2.027	141	39
1.995	002	28
1.991	150	17
1.879	211	35
1.876	230	23
1.789	112	13
1.781	151	19
1.725	122	23
1.715	160	11
1.698	231	17

AUTHORS' CLOSURE

We have compared the intensities of the high-pressure phase of PbS with those of GeS and SnS obtained at atmospheric pressure. But this must be done only occasionally as you suggested. We also think that the intensities of the high-pressure phase of PbS should be compared with the computed values for SnS-type PbS in order to identify the structure of the high-pressure phase of PbS. The relative intensities at high pressures, however, have been found to change to a considerable extent without phase transitions. This may be due perhaps to some strains etc. Therefore, the computed values at atmospheric pressure are thought to be not necessarily directly applicable to the pressure measurements.

We have used MoK_α-radiation and $d = 4.047$ Å corresponds to $\theta = 5.03°$. This angle is the limit where the direct beam disturbs x-ray patterns, so we could not detect the diffracted beam at this angle.

In our study, we have calculated the lattice parameters and the compressibilities of high-pressure phases of PbS and PbTe assuming that their phases have SnS-type structures, although the problem of identification of these structures at high pressures has not been solved yet.

The Compressibility and Thermal Expansion of LiF to 60 kbar and 600 °C as Determined by X-Ray Diffraction: Report of Progress*

L. C. Carrison** and C. B. Sclar***

Battelle Memorial Institute, Columbus Laboratories, 505 King Avenue, Columbus, Ohio 43201

Measurements were made of the compressibility of LiF to 60 kbars over the temperature range 25 °C to 600 °C by high-pressure high-temperature x-ray powder diffraction methods. Pressures were determined by using NaCl as an internal calibrant. These results also provide data on the thermal expansion of LiF between 25 and 600 °C at pressures of 38 and 57 kbar. This paper demonstrates the feasibility of determining the unit-cell volume of crystalline solids under concomitant high pressure and high temperature by *in situ* x-ray methods.

1. Introduction

An important area of crystal physics which has been relatively unexplored because of the limitations of existing experimental apparatus is that of the compressibility and thermal expansion of crystalline solids at high temperature and high pressure, respectively. The recent development of a high-pressure, high-temperature x-ray powder diffraction apparatus by Freud and Sclar [1, 2][1] provides a means of determining the unit-cell volume of crystalline solids at concomitant high pressure and high temperature to at least 100 kbar and 1000 °C. This paper presents the results obtained to date on a study which demonstrates the feasibility of this experimental approach.

The authors respectfully acknowledge the interest and support of Dr. J. N. Plendl and Mr. L. C. Mansur of Air Force Cambridge Research Laboratories during the course of this program.

2. Experimental Approach

2.1. High-Pressure High-Temperature X-Ray Diffraction Apparatus

The apparatus used in this study is a modified miniaturized "belt" apparatus which belongs to the family of internally heated compressible-gasket solid-media devices. The unique feature of this device is that the die-support ring assembly is fabricated in two parts which mate along a plane normal to the piston axis. This split-die design permits entry of filtered MoKα radiation into the high-pressure volume and egress of both the diffracted rays and the undeviated beam through suitable grooves and fan-shaped slots ground in the mating surfaces. The high-pressure x-ray windows are either a beryllium ring with a wedge-shaped cross-section or epoxy resin stops at the bore of the die.

The high-pressure medium is either "amorphous" boron or boron nitride, and the sample is in the form of a thin cylinder which is coaxial with the pistons and normal to the x-ray beam. The extrudable gaskets between the pistons and the die are made of pyrophyllite as they are in conventional devices inasmuch as they are not part of the x-ray path. High sample temperatures are attained by resistance heating of carbon rods adjacent to the sample. Temperatures are determined with a thermocouple in contact with the sample. The apparatus is portable and is used in conjunction with a conventional x-ray source.

The diffracted rays are recorded on the cylindrical film of a Debye-Scherrer camera 114.6 mm in diameter. In this study, lattice parameters were determined with a precision of about ± 0.2 percent. The diffraction lines used for this purpose were as follows: for NaCl (200), (220), (222), (400), (420), (422); for LiF (111), (200), (220), (311), (222). A photograph and a schematic drawing of the apparatus are shown in figures 1 and 2, respectively.

2.2. Calibration of High-Pressure Apparatus

The high-pressure apparatus was calibrated by means of the established fixed points on the room-temperature electrical-resistance absolute pressure scale, viz., Bi I $\rightarrow$ II transition at 25 kbar and Bi III $\rightarrow$ V transition at 75 kbar. However, in a miniaturized compressible-gasket apparatus like the "belt," it is recognized that the internal sample pressure may not be the same for successive experiments at a constant ram force. Furthermore, the electrical-resistance scale is a room-temperature scale, and it is not possible to predict the effect of elevated temperature on the internal sample pressure. Consequently, an internal pressure calibrant is needed if one is to know the sample pressure accurately at high pressure and high temperature. Such an internal calibrant is available in NaCl through the use of the semi-theoretical equation of

*Supported by Air Force Cambridge Research Laboratories under Contract No. F19628-68-C-0123.

**Present address: General Electric Co., Worthington, Ohio 43085.

***Present address: Department of Geological Sciences, Lehigh University, Bethlehem, Pa. 18018.

[1] Figures in brackets indicate the literature references at the end of this paper.

Paper presented at the Symposium on Accurate Characterization of the High-Pressure Environment, held at the National Bureau of Standards, Gaithersburg, Md., October 14–18, 1968.

385-762 O - 71 - 12

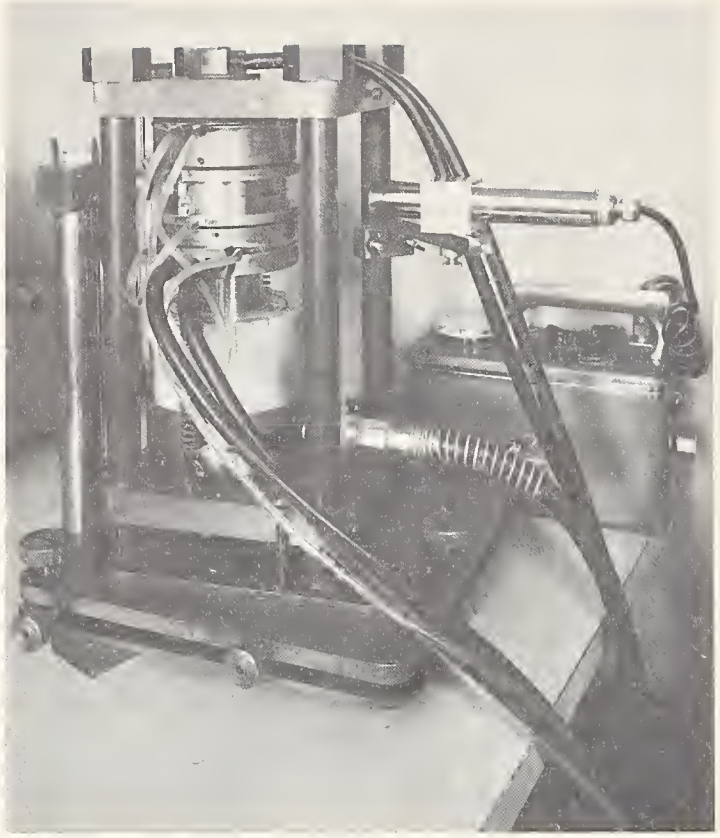

FIGURE 1. *Photograph of high-pressure high-temperature x-ray powder diffraction apparatus.*

The scale is in centimeters.

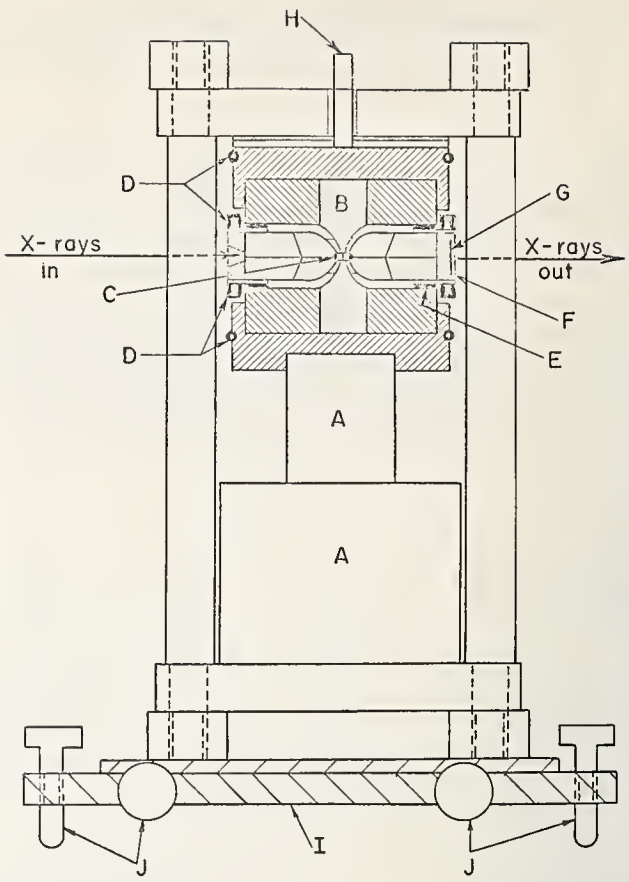

FIGURE 2. *Schematic drawing of high-pressure high-temperature x-ray powder diffraction apparatus.*

A = hydraulic ram, *B* = tungsten carbide pistons, *C* = steel die and high-pressure volume, *D* = water cooling tubes, *E* = rubber shim for positioning, *F* = Debye-Scherrer Camera, *G* = x-ray film, *H* = electrical power lead, *I* = press positioning table, *J* = adjusting screws for table.

state for sodium chloride proposed by Decker [3].

As a means of exploring the reproducibility of internal sample pressure as a function of applied load and to obtain information on the magnitude of the errors involved, a series of calibration experiments was carried out. The results are summarized in figure 3. Each line in this figure represents for an individual run the change in internal sample pressure, as revealed by the lattice parameter of sodium chloride (Decker scale), for a given internal geometry with increasing applied load. Although a fairly good linear relationship exists between a_0 and applied load, if reproducibility has been achieved all the lines for a common geometry would have overlapped. Obviously, this is not the case, and the spread in the line positions shows the magnitude of the nonreproducibility of internal sample pressure. As a result of these experiments, it was concluded that an internal calibrant, namely, sodium chloride, would have to be used with each run. All the data reported in this paper are based on pressures determined by the lattice parameter of sodium chloride as related to the Decker equation of state.

A second type of calibration experiment was run at elevated temperature to determine for a constant applied load the variation in internal sample pressure as a function of thermal cycling. The results are presented in figure 4, in which the numbered points represent sequential runs at which the lattice parameter of NaCl was determined. These results show that it is not possible to thermally cycle from room temperature to an elevated temperature and back at constant applied load without significant changes in the internal pressure. There appears to be a cumulative loss in internal pressure with an increasing number of thermal cycles at constant load providing that each successive run is carried out at a higher temperature. In any event, it is clear that an internal pressure calibrant must be used to determine sample pressure if the run is cycled thermally.

3. Experimental Results on Lithium Fluoride

3.1. Compressibility

Data on the isothermal compressibility of LiF were obtained to 60 kbar at temperatures of 25, 200, 400, and 600 °C. The lattice parameters (a_0) used for NaCl and LiF at 1 atm and 25 °C in calculating $\Delta a/a_0$ were 5.6402 Å and 4.0270 Å, respectively. X-ray diffraction patterns were obtained of LiF-NaCl mixtures at high-pressure and elevated temperature

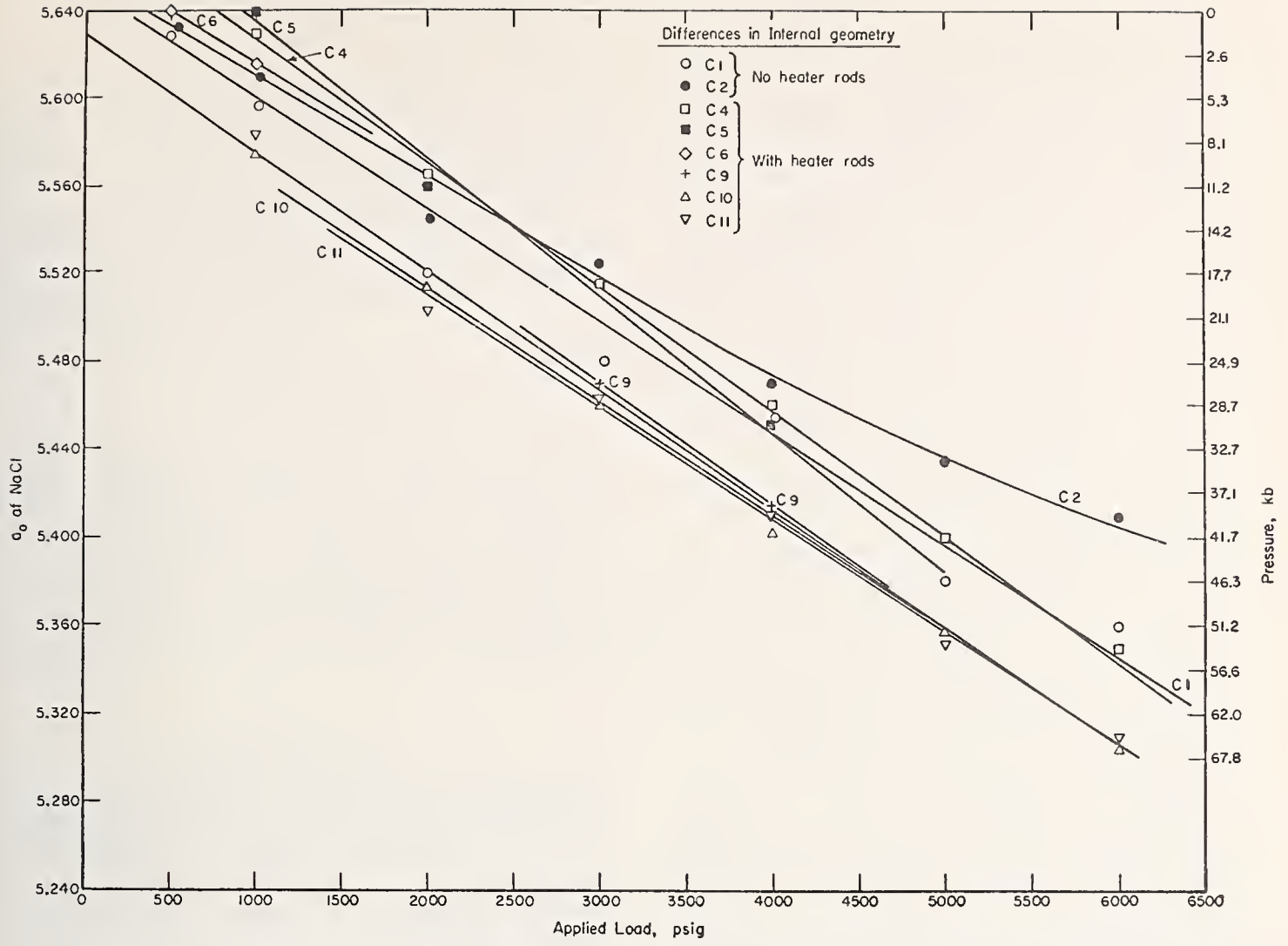

FIGURE 3. *Graph showing the lattice parameter of* NaCl *versus applied load at 25 °C for a number of individual runs.*

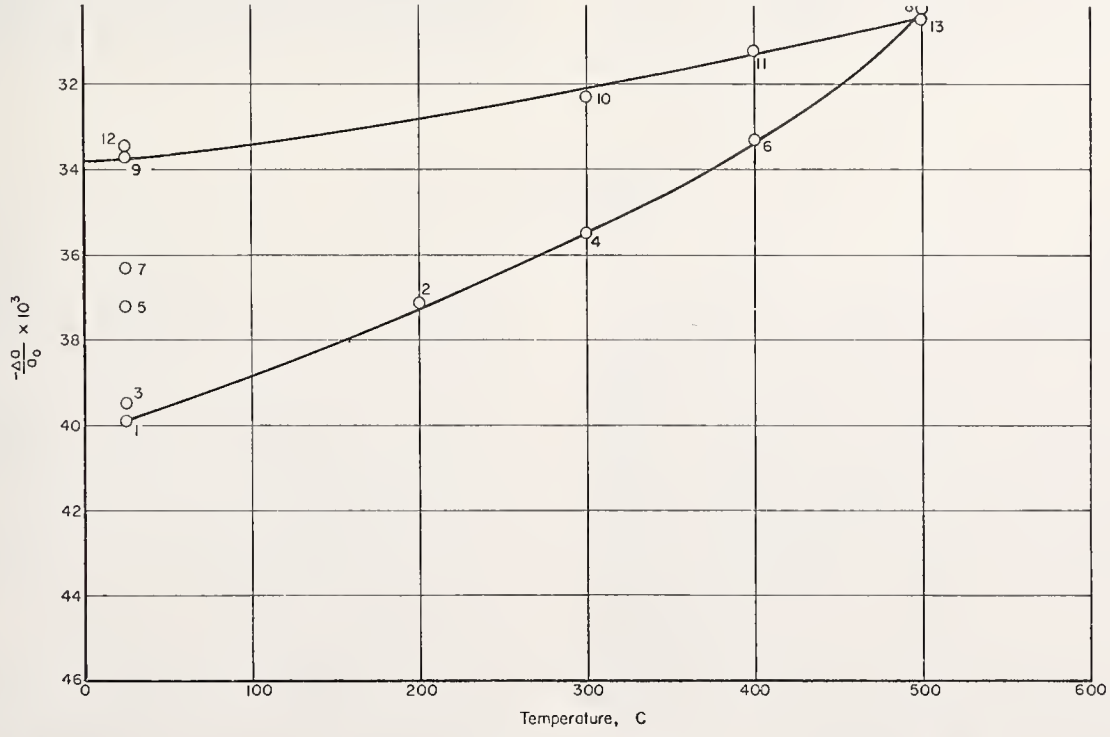

FIGURE 4. *Graph showing variation in lattice parameters of* NaCl *for an individual experiment in which the sample was thermally cycled at a constant applied load of 4000 psig.*

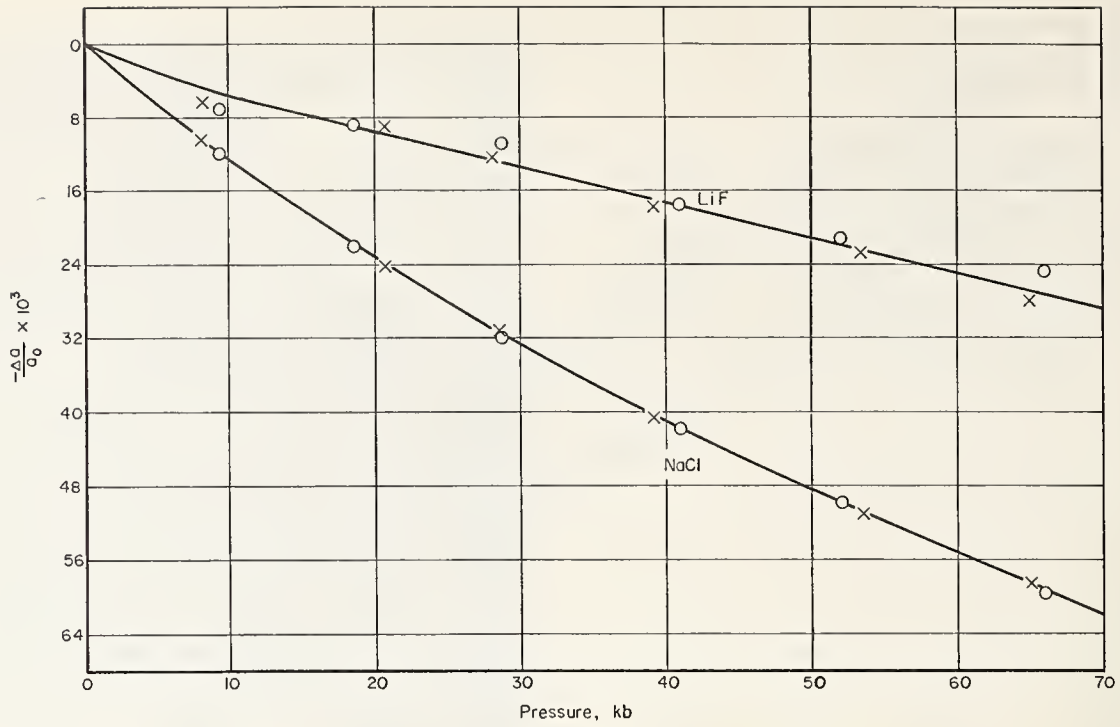

FIGURE 5. $\Delta a/a_0$ *versus pressure for* LiF *at 25 °C using* NaCl *to determine pressure.*

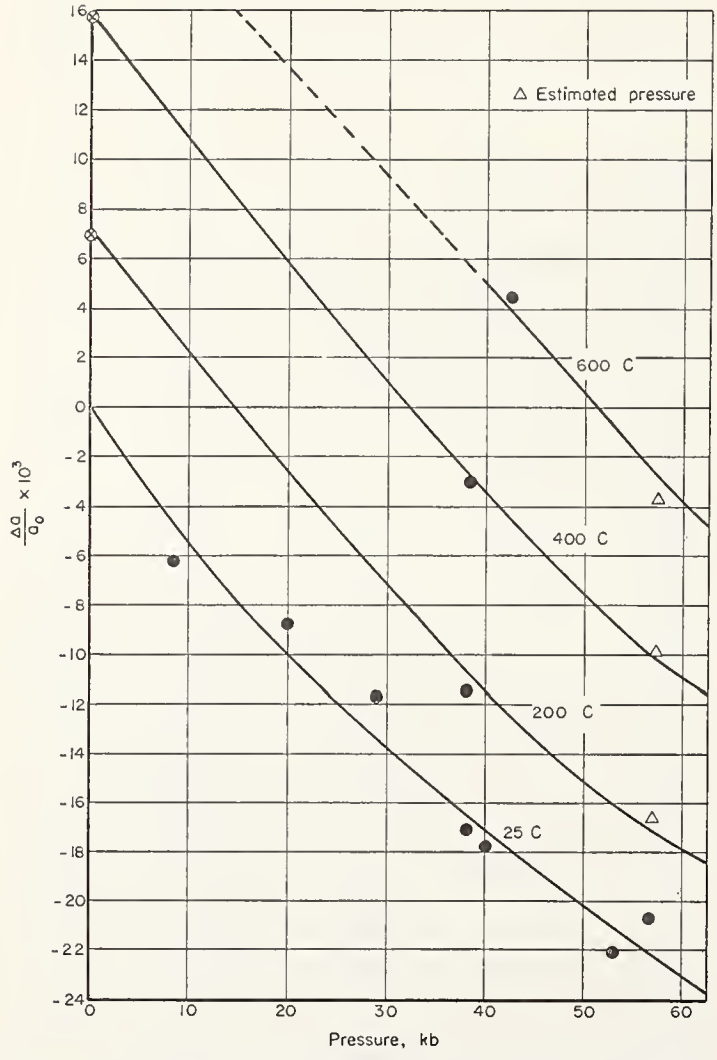

FIGURE 6. $\Delta a/a_0$ *versus pressure for* LiF *at 25, 200, 400, and 600 °C.*

using Zr-filtered MoKα radiation ($\lambda = 0.7107$ Å).

Figure 5 is a plot of the data for LiF and for admixed NaCl used an as internal calibrant carried out in duplicate experiments at 25 °C. These results agree with earlier data published by Bridgman [4] and by Pagannone and Drickamer [5] within 0.2 percent. Figure 6 shows $\Delta a/a_0$ versus pressure for LiF at elevated temperatures; thermal expansion data at room pressure are those given in [6]. The numerical data on which these graphs are based are given in table 1.

TABLE 1. $\Delta a/a_0$ *versus pressure for* LiF

Pressure	Temperature, °C			
	25	200	400	600
kbar				
0	0.000	*+0.0070	*+0.0158	.....
8.5	−0.0062	.....	.....	.....
20	−0.0087	.....	.....	.....
29	−0.0116	.....	.....	.....
38	−0.0171	−0.0114	−0.0030	.....
40	−0.0177	.....	.....	.....
42	.....	.....	.....	+0.0045
53	−0.0220	.....	.....	.....
57	−0.0206	**−0.0166	**−0.0099	**−0.0037
65	−0.0264	.....	.....	.....

*From reference [6].
**Estimated pressure; unable to measure lattice parameter of NaCl accurately because lines were weak.

3.2. Thermal Expansion Under Pressure

Data on the thermal expansion of LiF at 38 and 57 kbar are presented graphically in figure 7. For comparison, the thermal expansion of LiF at room pressure, based on data in the literature, is also shown. The results show that the coefficient of thermal expansion of LiF is essentially the same at 38 kbar up to 600 °C as it is at room pressure. On the other hand, the coefficient of thermal expansion appears to show a slight decrease at 57 kbar in the same temperature range.

4. Conclusions

Despite the experimental difficulties and the limited accuracy of the results relative to room-pressure measurements, useful data on the compressibility and thermal expansion of crystalline solids at high pressure and high temperature may be obtained by *in situ* x-ray diffraction methods. An internal calibrant, such as NaCl, is necessary, however, in order to determine the pressure accurately.

5. References

[1] Freud, P. J., and Sclar, C. B., Apparatus for high-pressure high-temperature x-ray powder diffraction studies to 100 kbar and 1000 °C (abstract), Abstracts for 1967, Geol. Soc. Am. Spec. Paper 115 (1968).

[2] Freud, P. J., and Sclar, C. B., Apparatus for high-pressure high-temperature x-ray powder diffraction studies, Rev. Sci. Instr. **40**, 434–437 (1969).

[3] Decker, D. L., Equation of state of NaCl and its use as a pressure gauge in high-pressure research, J. Appl. Phys. **36**, 157–161 (1965).

[4] Bridgman, P. W., Linear compressions to 30,000 kg/cm², including relatively incompressible substances, Proc. Am. Acad. Arts Sci. **77**, 189–234 (1949).

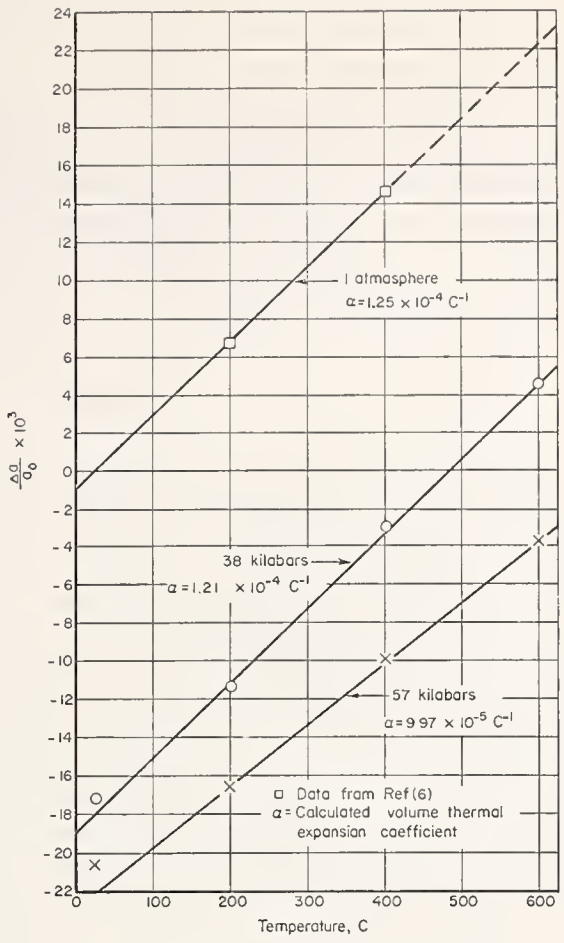

FIGURE 7. $\Delta a/a_0$ *versus temperature for* LiF *at room pressure. 38 kbar and 57 kbar.*

[5] Pagannone, M., and Drickamer, H. G., Effect of high pressure on the compressibilities of NaI, LiF, and NaF, J. Chem. Phys. **43**, 2266–2268 (1965).

[6] Handbook of Physical Constants, ed. S. P. Clark, Geol. Soc. Am., Memoir 97 (1966) (unpublished data of H. A. McKinstry).

DISCUSSION

J. D. Barnett *(Brigham Young University, Provo, Utah)*: The vertical dispersion of your points appears to me to be simply a result of not having the sample in the appropriate spot within the high-pressure volume. With a camera of only five-centimeter radius it is necessary, in order to obtain an accurate calibration by use of sodium chloride, to have the sample location fixed within about five-thousandths of an inch. I question whether you can do this repeatedly and maintain the position, at pressure in a sample that is several millimeters across, particularly in view of the motion due to the distortion of the pyrophyllite. A displacement of your sample five-thousandths of an inch towards the film will account for the spread that you are getting.

In a study we have made of lithium fluoride, using something like 50 x-ray patterns rather than the 8 or 10 that you used, our data differ only slightly from your average values. If you take the median of your points, and assume that your sample was misalined to fit the average of the scattered points, all of your compression data on lithium fluoride are shifted. The resultant lattice spacing of lithium fluoride is thus inaccurate, since it shifts the curves on your graph in different directions in different experiments. This is one of the disadvantages of the small camera, since precise x-ray work requires that sample-to-film distance be controlled very accurately.

I believe that you could correct your data by "calibrating" the x-ray patterns, using your measured lattice parameters at zero pressure as a reference in each run. That would, in effect, determine the position of the sample within the apparatus.

AUTHORS' CLOSURE

I believe that Dr. Barnett has a valid point on the matter of the effect of position of the sample on the indicated pressure. In checking position of samples after completion of the runs, however, we find that the shifts from center after pressurization are less than one-tenth of a millimeter (0.004 in). I don't know how much less, because it is very difficult to make this measurement accurately.

It is also important to note that the cylindrical sample is only 0.3 mm in diameter. As I indicated in my opening remarks, the data that we have presented are fragmentary and preliminary, and are only illustrative. There are a number of factors that can be responsible for the scatter shown, and the problem is one of resolving the magnitude of contribution from the different factors.

Ultrasonic and Static Equation of State for Cesium Halides*

G. R. Barsch

Materials Research Laboratory and Department of Physics, The Pennsylvania State University, University Park, Pa. 16802

and

Z. P. Chang

Materials Research Laboratory, The Pennsylvania State University, University Park, Pa. 16802

1. Introduction

In spite of several promising attempts, the problems of accurate pressure measurement and of an accurate pressure scale above 30 kbar are not yet completely and satisfactorily solved. The present paper is concerned with the equation of state of solids as one of several possible approaches to this problem. If the equation of state, i.e., the relation between pressure and volume, is known for a standard, it is possible to calculate the pressure from the dimensional changes of a gage specimen subjected to hydrostatic compression that can be measured by x-ray or by optical methods.

At present, theoretical equations of state will contain a high degree of uncertainty because of the many simplifying assumptions which are necessary, even for the simplest solids, to make the calculations feasible. Therefore it seems more promising at present to utilize empirical equations of state for the task of pressure calibration and measurement.

Naturally those empirical equations of state are less useful for setting up a pressure scale which presume the availability of a pressure scale, such as direct volumetric data obtained from x-ray methods. The remaining two methods utilizing shock wave and ultrasonic data should be regarded as mutually complementary.

While the former has the advantage of being based on direct measurements at very high pressures, it suffers from uncertainties that arise in the conversion from the shock-Hugoniot to pure isothermal conditions and from the fact that the presence and effect of nonhydrostatic stress in shock loading is not fully understood. On the other hand, an equation of state based on ultrasonic data of the elastic constants and their pressure derivatives is free from arbitrary assumptions, but is confined to comparatively low pressure. As has been shown by Anderson [1],[1] however, the ultrasonic equation of state is valid over a larger pressure range than that required in the ultrasonic measurements. It is this fact which makes it possible to use the ultrasonic equation of state as a pressure standard for high pressure, because it is based on measurements at low pressure in a range where the pressure scale is already established more reliably. It has been shown by Anderson [1] that the pressure-versus-volume compression curves of 14 materials calculated from Murnaghan's equation of state [2] by using the bulk modulus and its first pressure derivative measured ultrasonically below 10 kbar agree with directly measured data up to 100 or 200 kbar, and in the case of very incompressible substances even up to 1 Mbar. With increasing pressure, increasing discrepancies between the two sets of data occur which may be attributed to one or several of the following causes.

First, Murnaghan's equation of state is based on integration of a linear relation between bulk modulus and pressure and contains only two empirical[2] parameters, the zero pressure values of the bulk modulus and its first pressure derivative. One must expect, however, that the pressure dependence of the bulk modulus becomes nonlinear at sufficiently high pressures and that more than two parameters corresponding to the higher pressure derivatives of the bulk of modulus are necessary for the characterization of the equation of state over a wider range of pressure. The second possible cause of the discrepancy consists of experimental errors, statistical or systematic, of the ultrasonic or of the directly measured compression data.

The improvements that can be obtained by using a three-parameter equation of state have also been investigated by Anderson [3] on the basis of an equation of state proposed by Keane [4]. A very good fit of the directly measured compression curves of all five materials considered can be obtained in this manner up to the highest pressures measured if two parameters—the initial bulk modulus and its first pressure derivative—are determined from ultrasonic data, and the third parameter—the

*This work was supported by the U.S. Atomic Energy Commission.

[1] Figures in brackets indicate the literature references at the end of this paper.

Paper presented at the Symposium on Accurate Characterization of the High-Pressure Environment, held at the National Bureau of Standards, Gaithersburg, Md., October 14–18, 1968.

[2] One must distinguish between empirical parameters (which can be determined from experimental data other than high pressure measurements) and adjustable parameters (which are determined by fitting directly measured pressure vs volume compression curves to some phenomenological or theoretical equation of state). In this paper empirical parameters will be considered only.

limiting value of the bulk modulus at infinite pressure—is adjusted to fit the empirical compression data. As emphasized by Anderson [3], the usefulness of this approach consists of combining the merits of the low-pressure ultrasonic data and the shock wave data which are more reliable at high pressure so that the resulting equation of state can be used for predictions beyond the pressure range of the shock wave data. The question that remains unanswered in this approach is whether the third parameter is compatible with the second pressure derivative of the bulk modulus or whether it provides only an approximate fit of the empirical data at high pressure which may be sufficiently accurate, though, for interpolating and extrapolating the data at high pressure. Since for the five materials considered by Anderson [3] the second pressure derivatives of the bulk modulus have not yet been determined ultrasonically this point must await future clarification.

For the cesium halides CsCl, CsBr, and CsI the second pressure derivatives of the elastic constants have been measured recently by an ultrasonic method [5], so that for these materials the second pressure derivatives of the bulk modulus are available in addition to the bulk modulus and its first pressure derivative. This provides the opportunity of investigating the consequences and improvements which can be attained with a purely ultrasonic three-parameter equation of state. For CsI the previous measurements have been repeated with increased accuracy and extended as a function of temperature. On the basis of the resulting ultrasonic equation of state, it is possible to use CsI as a pressure standard over a wide range of pressure and temperature.

To this end a special mathematical representation must be adopted for the equation of state. Possible forms with three parameters are, for example, (1) a truncated Taylor expansion of the volume with respect to pressure up to and including third order terms in pressure, (2) a generalized form of Murnaghan's equation based on integration of a quadratic expression for the pressure dependence of the bulk modulus [46], (3) the second-order approximation of Birch's equation of state [6–8], (4) Keane's equation of state [3, 4], (5) a semi-theoretical equation of state based on a special model for the interatomic forces containing empirical parameters. All these forms may be designed to agree in the bulk modulus and its first two pressure derivatives, but they will differ in the higher than second-order pressure derivatives of the bulk modulus, or equivalently, in the quality of approximation to the true equation of state.

It is well known, for example, that the Taylor expansion (1) is so slowly convergent that it is insufficient for the description of empirical compression curves even over a moderate range of pressure [7, 1]. Therefore, this form need not be considered in the present paper. Objections have also been raised against the quadratic expression for the pressure dependence of the bulk modulus [7, 3], because a negative second pressure derivative of the bulk modulus which is demanded by shock wave data implies that the bulk modulus decreases with pressure after passing through a maximum, which is unlikely on physical grounds. In this paper additional evidence against the use of the corresponding form (2) for the equation of state will be presented. The quality of the remaining equations can be verified by comparison of the compression curves calculated from ultrasonic data with direct experimental data, in connection with a careful error analysis. In addition, theoretical considerations on the rate of convergence of any form based on a truncated Taylor expansion permit an evaluation. It is therefore the purpose of this paper to compare several representations of the three-parameter ultrasonic equation of state with static experimental data of Bridgman [9, 10] and of Perez-Albuerne and Drickamer [11, 12] that were obtained with a free-piston apparatus and with a high-pressure x-ray camera, respectively. A complete error analysis will also be carried out. In addition, the convergence of the equations of Murnaghan, Birch, and Keane will be checked by comparison with a lattice theoretical equation with empirical parameters which are determined from the bulk modulus and its first two pressure derivatives.

While the present paper was inspired by the observation of Anderson [1, 3] that the ultrasonic equation of state is valid over a considerably larger pressure range than the ultrasonic measurements themselves, it extends the previous work of Anderson insofar as (1) the second pressure derivative of the bulk modulus is included from ultrasonic measurements and a purely ultrasonic three-parameter equation of state is used, (2) several alternative expressions for three-parameter equations of state are critically compared and finally Birch's equation of state in second-order approximation is used, (3) the effect of the omission of higher order terms is estimated, (4) a careful analysis of the effect of the errors of all input data is performed, and (5) the variation with temperature is taken into account.

The credit and priority for having proposed a pressure standard on the basis of the equation of state of an alkali halide, NaCl, belongs to Decker [13, 14]. However, only one of his three empirical parameters, namely the zero pressure value of the bulk modulus, is obtained from ultrasonic measurements. The remaining parameters are determined from the lattice constant and the thermal expansion as a function of temperature. Decker's equation of state does not agree with the ultrasonic value for the first pressure derivative of the bulk modulus and, strangely enough, Decker dismisses the ultrasonic value for the pressure coefficient of the bulk modulus of Bartels and Schuele [15] as inaccurate because it differs from his theoretical

equation of state [14]. Instead, it is just as likely that Decker's equation of state is in error because of the uncertainty in the empirical parameters and/or because of the special assumptions about the interatomic forces which are implicit in this equation of state. This point will be discussed below in section 3.2.

Since the bulk modulus and its pressure derivatives completely characterize the equation of state for constant temperature, it is an undisputable requirement that any theoretical equation of state must agree with these experimental data. In view of our very limited knowledge on the interatomic forces in solids, the most natural way in meeting this requirement is to use a model potential with adjustable parameters which are fitted to the experimental values of the bulk modulus and its pressure derivatives. It will be shown below in section 3.2 that in the pressure range of interest the Birch equation of state [6–8], which is an empirical equation of state based on a rapidly converging Taylor expansion of the interatomic potential, is within the limits of experimental error indistinguishable from such a semitheoretical equation of state. For this reason the ultrasonic equation of state proposed in this paper will be based on Birch's equation of state.

Objections have also been raised against the use of NaCl as a pressure standard because a phase transition to the CsCl structure occurs at high pressure [16]. Although the magnitude of the transition pressure is still controversial and may be as high as 300 kbar [17, 18], it seems more advantageous to use alternative materials for which no high-pressure transition is known. Therefore the three cesium halides, CsCl, CsBr, and CsI, were selected. Of these materials, CsCl has the disadvantage that its use as a high-pressure standard is restricted in temperature to the range below 470 °C because of the phase transition to the NaCl structure [19–21]. In spite of this limitation a detailed discussion of CsCl will be presented in this paper because, of the three cesium halides considered, CsCl is the only one for which equation of state data from direct measurements are available above 100 kbar [11, 12] which allow a more critical comparison of the ultrasonic and the directly measured equation of state than Bridgman's compression data below 100 kbar [9, 10].

Another advantage of the three cesium halides is that they are the most highly compressible of all alkali halides which made it possible to determine the second pressure derivatives of the bulk modulus from ultrasonic measurements below 10 kbar [5] and to propose a purely ultrasonic three-parameter equation of state. The high compressibility is also advantageous since it corresponds to a high sensitivity of the pressure measurement with respect to the dimensional changes of the crystal.

TABLE 1. *Bulk modulus* B_0, *first pressure derivative* $B_0^{(1)}$, *and second pressure derivative* $B_0^{(2)}$ *of* CsCl *and* CsBr *at 300 °K from ultrasonic measurements*

(calculated from the experimental values underlying the results reported in ref. [5])

	CsCl	CsBr
$B_0 = B^T$ (kbar)	167.4 ±0.9	143.4 ±.8
$B_0^{(1)} = \left(\frac{\partial B^T}{\partial p}\right)_T$	5.98 ±.09	5.95 ±.08
$B_0^{(2)} = \left(\frac{\partial^2 B^S}{\partial p^2}\right)_T$ (kbar)$^{-1}$	−0.042 ±.04	−0.050 ±.004

2. Dependence of Bulk Modulus on Pressure and Temperature

The pressure dependence of the elastic constants of one or of several of the cesium halides CsCl, CsBr, CsI has been measured by several authors [22–24, 5], but only in one case was the precision sufficiently high so that not only the first, but the second pressure derivatives also could be determined [5]. These data will be used in the present paper.

The isothermal bulk modulus and its first isothermal pressure derivative have been calculated for CsCl and CsBr from revised data for the adiabatic bulk modulus and its isothermal pressure derivative of reference [5] by using the thermal data tabulated in reference [25] and the conversion formulae of Overton [26]. The results are listed in table 1 together with the isothermal second pressure derivative of the adiabatic bulk modulus corresponding to the unproccessed ultrasonic data. These second pressure derivatives were not converted to the purely isothermal quantities since this would require the value of the temperature derivative of the first pressure derivative of the adiabatic bulk modulus, which was not available for the data of reference [5]. It will be shown below that for CsI the difference between the intermediate isothermal-adiabatic and the pure isothermal derivative is not much larger than the experimental error. For the comparison of the ultrasonic equation of state with direct experimental data it is therefore sufficient to use the unconverted intermediate second pressure derivatives listed in table 1, the more so since in the pressure range to be considered the contribution from this term is small.

The experimental error shown in table 1 was calculated from a careful statistical analysis of the raw data underlying the values reported in reference [5]. This was done by fitting the pressure dependence of the bulk modulus to a parabola and taking into

account that the bulk modulus is a linear combination of two elastic constants, $B=(1/3)(c_{11}+2c_{12})$, which were determined from four independent series of measurements for the three elastic constants c_{11}, c_{12}, and c_{44}. The method used is described in chapter 6 of ref. [27]. The errors shown in table 1 correspond to the standard error arising from the statistical mean square deviation plus an estimate for all other errors which are represented primarily by the uncertainty in the pressure reading. The pressure was measured by means of a manganin cell in connection with a resistance calibration curve provided by the Harwood Engineering Co., Walpole, Mass., and stated to be as accurate as 10^{-4}. The resistance was measured with an ac bridge in connection with a Foxboro automatic recorder with an accuracy of 2 percent. This was the weakest link in the chain of accuracy limiting factors. Part of this error appears in the statistical error, and the remaining possible systematic error has been estimated as 1 percent and is included in the total error shown in table 1. Also included in the error shown is the uncertainty arising in the conversion from the adiabatic and intermediate ultrasonic data to the purely isothermal data, which was calculated from a liberal estimate of the uncertainty of the thermal data used in the conversion.

Very recently, for CsI we have repeated the ultrasonic measurements of the pressure dependence of the elastic constants. The objective was, first, to attain higher accuracy by measuring the resistance change of the manganin pressure cell with a Carey-Foster bridge. Moreover, the measurements were carried out at four different temperatures up to 250 °C. It was possible to determine the temperature derivative of the pressure coefficient of the bulk modulus and to convert the second pressure derivative of the bulk modulus from the intermediate to the purely isothermal value. The ultrasonic values of the bulk modulus and its derivatives with respect to temperature and pressure are shown in table 2 together with the converted purely isothermal values. The first and second temperature derivatives of the adiabatic bulk modulus were taken from reference [28]. Details of the measured elastic constant data and the conversion formulae not contained in Overton's paper [26] will be published elsewhere.[3] The data of table 2 agree within experimental error with those of reference [5], but they are more accurate than these previous values. The errors shown in table 2 were calculated in the same manner as those in table 1, and for the possible systematic error of the pressure measurement a value of 0.5 percent has been assumed. For the thermal quantities which are required for the conversion from the adiabatic to isothermal conditions, smaller errors have also been assumed. With the increased accuracy of the pressure measurement, the effect of these errors becomes now comparable to the error of the ultrasonic data. For the pressure coefficient of the bulk modulus, for example, the error is increased by as much as 33 percent due to the conversion from the intermediate to the purely isothermal value. Since this error turns out to be one of the main accuracy-limiting factor for the equation of state, the thermal data that were used in addition to the data of table 2 for the conversion are listed in table 3, together with their estimated errors. Since the formula for the conversion of the second pressure derivative is so lengthy and de-

[3] The formula for converting the isothermal second pressure derivative of the adiabatic bulk modulus to the isothermal pressure derivative of the isothermal bulk modulus has been published recently by Yu [47].

TABLE 2. *First and second derivatives of the adiabatic and isothermal bulk modulus with respect to temperature and pressure for* CsI *at 25 °C*

	B^S	B^T
B (kbar)	126.2 ±0.2	118.9 ±0.5
$\left(\frac{\partial B}{\partial T}\right)_p$ (kbar/°C)	[1] −0.0667 [2] ±.0034	−0.1028 [3] ±.0060
$\left(\frac{\partial^2 B}{\partial T^2}\right)_p$ (kbar/(°C)^2)	[1] -5.0×10^{-5}	-1.3×10^{-4}
$\left(\frac{\partial B}{\partial p}\right)_T$	5.70 ±.06	5.93 [3] ±.08
$\left(\frac{\partial^2 B}{\partial p^2}\right)$ (kbar)$^{-1}$	−0.061 ±.004	−0.073 [4] ±.008
$\left(\frac{\partial^2 B}{\partial p \partial T}\right)$ (°C)$^{-1}$	1.4×10^{-3}	2.6×10^{-3}

[1] From reference [28].
[2] Estimated error: 5 percent.
[3] From error of data listed in table 3.
[4] Estimated error: twice the value of $\Delta(\partial^2 B^S/\partial p^2)_T$.

TABLE 3. *Density* ρ_0, *linear thermal expansion coefficient* α *with temperature derivative* $(\partial\alpha/\partial T)$, *and specific heat* c_p *with temperature derivative* $(\partial c_p/\partial T)_p$ *and estimated errors for* CsI *at 25 °C*

ρ_o (g cm^{-3})	4.525 ±0.3%	Ref. [29]
α (10^{-5}(°C)$^{-1}$)	4.05 ±2%	Ref. [30]
$(\partial\alpha/\partial T)_p$ (10^{-8}(°C)$^{-2}$)	6.6 ±3%	Ref. [30]
c_p (Jg^{-1}(°C)$^{-1}$)	0.200 ±1%	Ref. [31]
$(\partial c_p/\partial T)_p$ (10^{-3}Jg^{-1}(°C)$^{-2}$)	0.043 ±3%	Ref. [31]

pends on a large number of variables, no rigorous error analysis has been carried out, and an estimate will be used in this case. It is assumed that the error of $(\partial^2 B^T/\partial p^2)_T$ is twice as large as the error of $(\partial^2 B^S/\partial p^2)_T$.

Since the temperature dependence of the bulk modulus is nonlinear, and since there is no theoretical evidence that the pressure coefficient of the bulk modulus depends linearly on temperature, the data of table 2 will not be used for calculating the high-pressure equation of state as a function of temperature. Instead, the bulk modulus and its first two pressure derivatives will be calculated from the formula

$$B_0(T)=B_0^R+\left(\frac{\partial B}{\partial T}\right)^R(t-t_R)+\frac{1}{2}\left(\frac{\partial^2 B}{\partial T^2}\right)^R(t-t_R)^2 \tag{2.1}$$

with the superscript R referring to the reference temperature t_R. Further it is [6, 32]:

$$B_0^{(1)}=-\frac{C}{9B_0} \tag{2.2}$$

$$B_0B_0^{(2)}=\frac{1}{9}-[1+B_0^{(1)}]B_0^{(1)}+\frac{D}{27B_0} \tag{2.3}$$

where C and D are linear combinations of the third- and fourth-order elastic constants, respectively. Their room temperature values are listed in table 4 together with their first temperature derivatives. Since at high temperatures (above the Debye temperature) the temperature dependence of the higher order elastic constants is linear in the first-order approximation of the quasiharmonic approximation [33, 34], the experimental data taken at different temperatures were interpolated linearly,

$$C=C_R+\left(\frac{\partial C}{\partial T}\right)^R(t-t_R) \tag{2.4}$$

$$D=D_R+\left(\frac{\partial D}{\partial T}\right)^R(t-t_R). \tag{2.5}$$

For the temperature dependence of the high-pressure equation of state, the bulk modulus and its first two pressure derivatives will be calculated in section 4 as a function of temperature according to eqs (2.1) to (2.5) with the coefficients B_0, $(\partial B/\partial T)$, $(\partial^2 B/\partial T^2)$, C, $(\partial C/\partial T)$, D, and $(\partial D/\partial T)$ listed in tables 2 and 4 for the isothermal case.

TABLE 4. *Linear combinations* $C=c_{111}+6c_{112}+2c_{123}$ *and* $D=c_{1111}+8c_{1112}+6c_{1122}+12c_{1123}$ *of the intermediate and of the isothermal third- and fourth-order elastic constants, and their temperature derivatives for* CsI *at 25 °C*

	Intermediate	Isothermal
C (kbar)	-6.13×10^3	-6.32×10^3
$\left(\frac{\partial C}{\partial T}\right)_P$ (kbar/°C)	3.6	2.6
D (kbar)	1.02×10^5	1.03×10^5
$\left(\frac{\partial D}{\partial T}\right)_p$ (kbar/°C)	−11.0	−16.0

3. Evaluation of Several Three-Parameter Equations of State

3.1. Phenomenological Equations of State

A variety of mathematical expressions have been proposed for the description of the equation of state of solids at high pressure, i.e., for the relation between pressure and volume for specified thermodynamic conditions. Most of these are based on some truncated Taylor expansion and can therefore be expressed in terms of an arbitrary number of parameters, corresponding to the order of the approximation. Which one of these expressions for a given number of parameters is best suited for an accurate representation of experimental (or theoretical) data over a specified pressure range depends on the rate of convergence of the underlying Taylor expansion and can only be determined *a posteriori*, i.e., by comparing this approximate phenomenological equation of state with experimental or rigorous theoretical data. Such a comparison will be made in sections 3.2 and 3.3 by using the equations presented subsequently and in section 3.2.

For convenience, isothermal conditions will be assumed and all quantities will be given in dimensionless form. All parameters occurring in the explicit expressions for the equation of state are therefore dimensionless quantities also, which depend only on the temperature and the material considered. Let

$$R=V/V_0 \tag{3.1}$$

and

$$\pi=p/B_0 \tag{3.2}$$

denote the compression ratio of the volume V and the pressure p in units of the bulk modulus B_0, respectively, with the index 0 always referring to zero pressure.

The classical expression for the equation of state consists of a truncated Taylor series of the volume with respect to pressure (see, e.g., [1]):

$$R_N(\pi)=\sum_{i=0}^{N} t_i\pi^i. \tag{3.3}$$

From the definition of the bulk modulus at arbitrary pressure,

$$B=-V\left(\frac{\partial p}{\partial V}\right)=-B_0\left(\frac{\partial \pi}{\partial \ln R}\right) \tag{3.4}$$

and its Taylor expansion with respect to pressure (written here for later reference in the Nth order approximation),

$$B_N(p)=\sum_{i=0}^{N}\frac{1}{i!}B_0^{(i)}p^i \tag{3.5}$$

the expansion coefficients t_i can be expressed in terms of the zero pressure values of the bulk modulus and its pressure derivatives $B_0^{(i)}$. The first four expansion coefficients are [1]

$$\begin{aligned}
t_0&=1,\\
t_1&=-1,\\
t_2&=(1/2)\,(B_0^{(1)}+1),\\
t_3&=(1/6)\,[1+3B_0^{(1)}+2(B_0^{(1)})^2-B_0B_0^{(2)}],\\
t_4&=(1/24)\,[1+6B_0^{(1)}+11(B_0^{(1)})^2+6(B_0^{(1)})^3\\
&\quad -2(2+3B_0^{(1)})B_0B_0^{(2)}+B_0^2B_0^{(3)}]\cdot
\end{aligned} \tag{3.6}$$

It has long been recognized that (3.3) is very slowly convergent and therefore useful only for small pressures, $\pi \ll 1$ [1, 7, 9]. If this form with a given number of terms is used as an empirical equation, then the coefficients that are obtained by fitting the experimental compression data depend for larger pressures, e.g., $\pi<1$, on the pressure range of the experiments and must be extrapolated to zero pressure [1, 7, 24].

These disadvantages are avoided in the equation of state proposed by Birch [6–8],

$$\pi_N(R)=\frac{3}{2}R^{-5/3}\sum_{i=1}^{N} b_i(R^{-2/3}-1)^i \tag{3.7}$$

which is based on the Taylor expansion of the strain energy with respect to the Eulerian strain components.

Again the expansion coefficients can be expressed in terms of the pressure derivatives of the bulk modulus. The first four coefficients are

$$\begin{aligned}
b_1&=1,\\
b_2&=(3/4)\,(B_0^{(1)}-4),\\
b_3&=(1/24)\,[143+9(B_0^{(1)}-7)B_0^{(1)}+9B_0B_0^{(2)}]\\
b_4&=(1/192)[-1888+1122B_0^{(1)}-288(B_0^{(1)})^2\\
&\quad +27(B_0^{(1)})^3+36(3B_0^{(1)}-8)B_0B_0^{(2)}+27B_0^2B_0^{(3)}].
\end{aligned} \tag{3.8}$$

The advantage of (3.7) is that it is much more rapidly convergent than (3.3), and that even in the pressure range as large as $\pi \leqslant 0.5$ the approximation with only two terms corresponding to $N=2$ is sufficiently accurate for many practical purposes such as arise, e.g., in geophysics.

Another approach to the equation of state is due to Murnaghan and consists of integrating the Taylor expansion of the bulk modulus (3.4) under the assumption that the linear approximation in (3.5) corresponding to $N=1$ is sufficient [2]. The resulting "first-order Murnaghan equation of state" is [2, 11]

$$R_1=(1+m\pi)^{-1/m} \tag{3.9a}$$

or

$$\pi_1=m^{-1}(R^{-m}-1). \tag{3.9b}$$

Correspondingly, one obtains by integrating (3.4) in connection with (3.5) for $N=2$ the "second-order Murnaghan equation of state" [46]:

$$R_2=\{[2+(n+1)m\pi]/[2-(n-1)m\pi]\}^{-1/nm} \tag{3.10a}$$

or

$$\pi_2=2m^{-1}[R^{-nm}-1]\,[(n-1)R^{-nm}+(n+1)]^{-1}. \tag{3.10b}$$

The parameters occurring are

$$m=B_0^{(1)},\qquad n=[1-(2B_0B_0^{(2)})/(B_0^{(1)})^2]^{1/2}. \tag{3.11}$$

For $B_0^{(2)}=0$ it is $n=1$, and the second-order Murnaghan equation (3.10) reduces to the first-order form (3.9).

The three types of equations considered so far are based on different kinds of Taylor expansions and can be used with any desired number of parameters. In this paper only the two- and three-parameter forms of Birch's and Murnaghan's equations will be considered.

Another three-parameter equation of state has been proposed by Keane [4] and recently been discussed by Anderson [3]. This equation is not based on any Taylor expansion, but on the assumption that the bulk modulus is a monotonously increasing function of pressure, and its pressure coefficient a monotonously decreasing function of pressure, according to

$$\left(\frac{\partial B}{\partial p}\right)=\frac{(B_0^{(1)}-B_\infty^{(1)})B_0}{B(p)}+B_\infty^{(1)}. \qquad (3.12)$$

$B_\infty^{(1)}$ is the limiting value of the pressure coefficient of the bulk modulus for infinite pressure. Kean's equation of state is obtained by twofold integration of (3.12) in connection with (3.4) [3, 4]:

$$\pi_K=(B_0^{(1)}/B_\infty^{(1)})^2)\,[R^{-B_\infty^{(1)}}-1] + [(B_0^{(1)}/B_\infty^{(1)})-1]\ln R. \qquad (3.13)$$

By comparing the Taylor expansion of (3.13) with (3.3) and (3.6) the third parameter, $B_\infty^{(1)}$ can be expressed in terms of the second pressure derivative of the bulk modulus as follows:

$$B_\infty^{(1)}=B_0^{(1)}+(B_0B_0^{(2)}/B_0^{(1)}). \qquad (3.14)$$

The two assumptions of Keane ($B(p)$ monotonously increasing with p, $(\partial B/\partial p)$ monotonously decreasing with p) lead to the following condition for the bulk modulus and its first two pressure derivatives:

$$-(B_0^{(1)})^2<B_0B_0^{(2)}<0. \qquad (3.15)$$

Both inequalities are fulfilled for the experimental data of CsCl, CsBr, and CsI listed in tables 1 and 2 so that it is consistent to use, for these materials, Keane's expression (3.13) for the representation of the equation of state.

3.2. A Lattice Theoretical Equation of State and Comparison With the Phenomenological Equations of Section 3.1

An ionic crystal, such as one of the alkali halides, seems ideally suited for deriving a theoretical equation of state because the interatomic forces can be described quite adequately and successfully in terms of Coulomb and van der Waals attraction, and in terms of a Born-Mayer type repulsive potential with empirical or adjustable parameters. In view of the considerable success of the classical theory of ionic crystals, it is not surprising that this approach has been used also for the equation of state of alkali halides [12–14, 35]. It should be remembered, however, that these equations of state are semi-empirical, and that their accuracy is limited by the accuracy of the empirical quantities that were used for the determination of the parameters in the repulsive potential. Since these parameters are determined from experimental data measured at low pressure one must expect that the effect of their errors increases with increasing pressure. Thus from this point of view there would be no advantage in using a lattice "theoretical" equation of state instead of a phenomenological equation as discussed in section 3.1, provided the phenomenological equation selected converges sufficiently fast and differs in the pressure range considered from the lattice theoretical equation with the same number of parameters by an amount smaller than the effect of the experimental error of the input data.

Another limitation of the kind of lattice theoretical equation of state considered is that it is based on several simplifying assumptions and that their effect on the results is not easy to determine and would require a much higher theoretical effort. First, it has been noted that the inverse power law for the van der Waals potential should be screened at smaller interatomic separations due to the interpenetration of the electronic shells [36]. Also, the use of an exponential law for the repulsive interaction is only an approximation because the radial dependence of the electronic wave functions corresponds to a series of terms consisting of products of polynomials and exponential functions and is reflected in the radial dependence of the cohesive energy [37, 38]. More specific approximations of dubious justification made in previous lattice theoretical equations of state consist of the use of an inverse power potential for the repulsive interaction and neglect of second nearest neighbor effects [35], or of the evaluation of the repulsive parameters for the second nearest neighbor interaction from the electronic polarizabilities [13]. The equation of state of Decker is further based on the Debye-Grueneisen approximation, and the Grueneisen constant and its first pressure derivative are determined jointly with the first nearest neighbor repulsive parameters from empirical data of the thermal expansion as a function of temperature [13].

In view of the considerable difficulties encountered in deriving a sufficiently reliable lattice theoretical equation of state, the question arises whether an empirical ultrasonic equation of state based on any of the phenomenological equations discussed in section 3.1 agrees within the uncertainty limit caused by the experimental error of the empirical parameters with the corresponding lattice theoretical equation of state. In order to explore this possibility, a simple lattice theoretical equation of state with four empirical parameters was compared with the phenomenological equations discussed in section 3.1. This equation of state is based on the expression

$$\phi=-\frac{\alpha e^2}{r}-\frac{C}{r^6}-\frac{D}{r^8}+A_1e^{-\frac{r}{\rho_1}}+A_2e^{-\frac{(2/\sqrt{3})r}{\rho_2}} \qquad (3.16)$$

for the lattice energy per ion pair where the symbols have the usual meaning [39], and the effect of thermal motion has been neglected. This expression contains the usual Coulomb and van der Waals terms, and first and second nearest neighbor repulsive interaction. In general, two exponential terms

are required for the second nearest neighbor interaction, but these two reduce to one if it is assumed that the same constant ρ_2 describes both cation-cation and anion-anion interaction. The van der Waals constants C, D were taken from references [40] and [41], respectively, and the repulsive constants A_1, A_2, ρ_1, ρ_2 were determined from the zero pressure values of the lattice constant, and of the bulk modulus and its first two pressure derivatives.

The equation of state based on (3.16) according to

$$p=-\frac{\partial\phi}{\partial v_c}=-\frac{1}{2r^2}\frac{\partial\phi}{\partial r} \tag{3.17}$$

was compared with (a) Murnaghan's first-order equation (3.9); (b) Birch's equation (3.7) in first-order approximation; (c) Murnaghan's second-order equation (3.10); (d) Birch's equation (3.10) in second-order approximation; and (e) Keane's equation (3.13). The same ultrasonic values for the bulk modulus and its first two pressure derivatives were used for these phenomenological equations so that the difference $\Delta p = p_{\text{lattice}} - p_{\text{phen.}}$ between the lattice theoretical equation of state based on (3.16) and the phenomenological equations (a) to (d) arises from differences in the second and higher pressure coefficients of the bulk modulus (cases (a) and (b)), or from differences in the third and higher order pressure derivatives of the bulk modulus (cases (c) to (e)). This difference Δp is therefore an indication of the quality of the different phenomenological equations in approximating the lattice theoretical equation based on (3.16), and a measure of the rate of convergence of the various Taylor-expansions underlying the phenomenological equations (a) to (e). Although the exact or true potential energy of the lattice will be given only approximately by (3.16) and the thermal energy has been neglected, one may expect that the difference between the two values of Δp referred to (3.16) and to the volume dependence of the true free energy is a higher order quantity, so that for ionic crystals the difference Δp based on (3.16) may be considered as a fair estimate of the deviation of the phenomenological equations from the true equation of state.

The difference $|\Delta p|$ is plotted for CsI in figure 1 for the five cases (a) to (e) as a function of pressure. The ultrasonic data of table 2 were used in connection with the room temperature value of the lattice constant from reference [30]. For CsCl and CsBr curves very similar to those of figure 1 were obtained. It is apparent that in the entire pressure range up to 500 kbar the quality of the second-order Birch equation in approximating the lattice theoretical equation is one order of magnitude better than Keane's equation, and about two orders of magnitude better than the second order Murnaghan equation. As all three equations contain the same number of three empirical parameters, this drastic

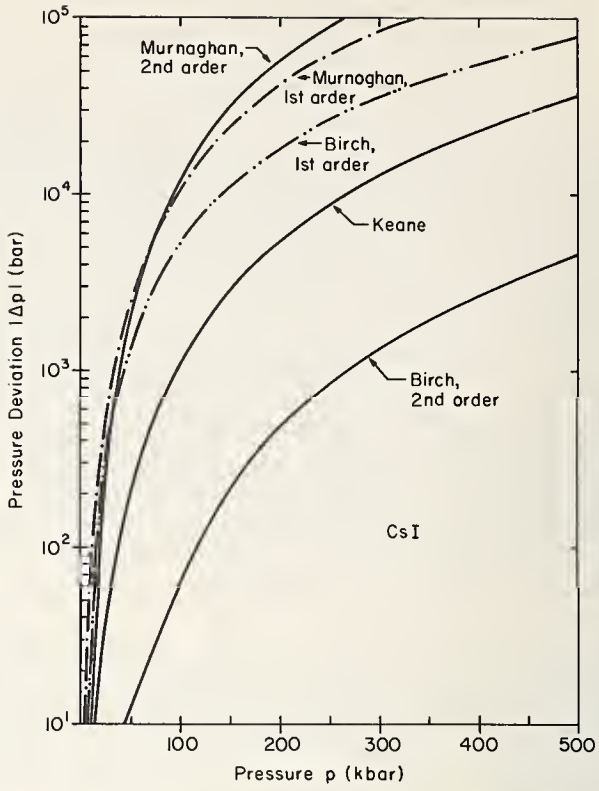

FIGURE 1. *Pressure difference between phenomenological and lattice theoretical equation of state versus pressure for* CsI.

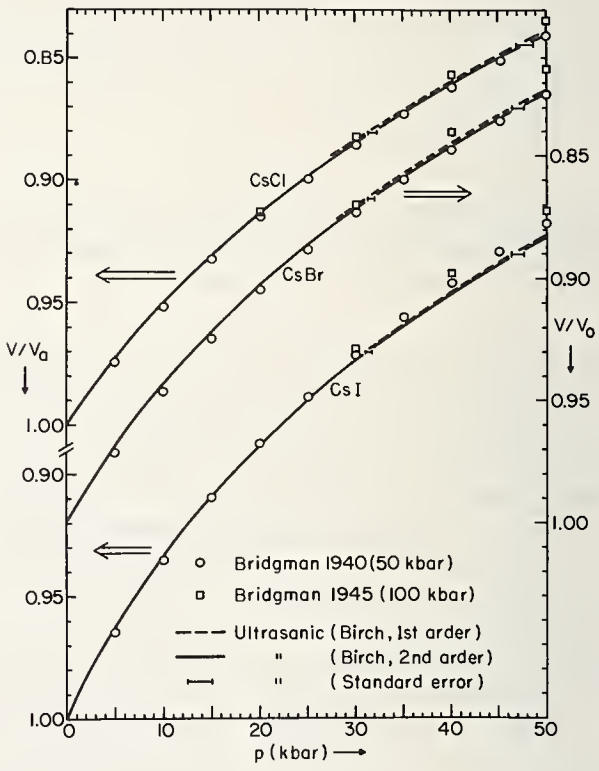

FIGURE 2. *Comparison of compression data for* CsCl, CsBr, *and* CsI *by Bridgman [9, 10] with ultrasonic Birch equation of state in first- and second-order approximation.*

superiority of Birch's equation is quite surprising. The first-order Birch equation also can be seen to be superior to the first-order Murnaghan equation, but the difference is not quite as pronounced. As expected, the two three-parameter equations accord-

ing to Birch and to Keane are superior to any of the two-parameter (first-order) equations of Murnaghan and Birch, but interestingly enough the second-order Murnaghan equation gives above 80 kbar larger deviations than the first-order Murnaghan equation and shows, in fact, the largest deviation from the lattice theoretical equation of all cases considered.

These results suggest the superiority of the second-order Birch equation over all other phenomenological equations considered containing an equal or smaller number of parameters.

The absolute magnitude of the discrepancy ranges for the second-order Birch equation from 65 bars (or 0.065 percent) at 100 kbar to 4.6 kbar (or 0.9 percent) at 500 kbar. It will be shown below in section 4 that this discrepancy is considerably smaller than the errors that may be expected from the error of the ultrasonic input data and from the measurement of the lattice constant. Thus in the pressure range up to 500 kbar it seems sufficient to use a second-order (three-parameter) Birch equation instead of a lattice theoretical equation with an equal number of empirical parameters.

3.3. Comparison of Ultrasonic Equations of State With Piezometric Data

In this section phenomenological equations of state discussed in section 3.1 will be calculated from the ultrasonic data of tables 1 and 2, and compared with direct piezometric data of Bridgman [9, 10] and Perez-Albuerne and Drickamer [11, 12]. The purpose is first, to determine whether the ultrasonic and the piezometric data are compatible within experimental error; second, to check whether the contribution from the second pressure derivative of the bulk modulus is noticeable in the pressure range considered and improves the agreement with the piezometric data; and third, to provide further support for the above conclusions concerning the superiority of the Birch equation of state as compared with Murnaghan's equation.

From the comparison of the ultrasonic equation of state (based on the first- and second-order Birch equation) with Bridgman's piezometric data in figure 2, one may make the following observations. First, the effect of the second pressure derivative of the bulk modulus is noticeable in the pressure range below 50 kbar, but is within the limit of error of the ultrasonic data, calculated from the errors shown in tables 1 and 2 by means of the Gaussian error propagation law. Second, the agreement between ultrasonic and piezometric data is improved by including the second pressure derivative $B_0^{(2)}$ for Bridgman's data of 1940 [9] for CsCl and CsBr, but worsened in all other cases. Third, for CsCl and CsBr Bridgman's data of 1940 [9] agree well above about 15 kbar (within experimental error) with the ultrasonic data, but below that pressure and in all other cases, differences which are outside the range of error of the ultrasonic data occur.

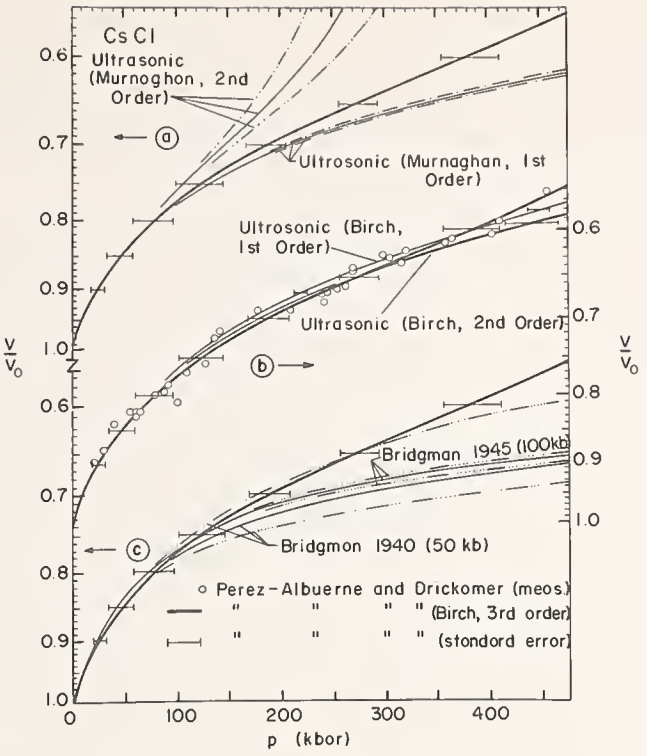

FIGURE 3. *Comparison of compression data for* CsCl *by Perez-Albuerne and Drickamer* [*11, 12*] *with* (*a*) *ultrasonic Murnaghan equation of state in first- and second-order approximation,* (*b*) *ultrasonic Birch equation of state in first- and second-order approximation, and* (*c*) *extrapolated compression data by Bridgman* [*9, 10*].

One must conclude then that Bridgman's earlier data of 1940 are more accurate than his later data of 1945 [10], and that the results for the less compressible materials CsCl and CsBr are more accurate than for the more compressible CsI.

In figures 3a and 3b the ultrasonic equation of state as based on the first- and second-order approximations of the equations of Murnaghan and of Birch, respectively, are for CsCl compared with the data obtained by Perez-Albuerne and Drickamer [11] with a high-pressure x-ray camera. The error of the ultrasonic data is indicated by the broken curves in figure 3a, and by a few selected error bars on figure 3b. The x-ray data were fitted to a third-order Birch equation (four parameters) and are plotted as the full curve. In figure 3b the individual data are plotted also in order to show the large scatter present. The error was calculated from the standard deviation according to the method described in reference [27], section 6.25, and is shown as error bars.

It is apparent from figure 2a that the ultrasonic data agree well with the x-ray data up to about 225 kbar in the first-order Murnaghan approximation, but only up to about 150 kbar in the second-order Murnaghan approximation. Thus the inclusion of the second pressure derivative $B_0^{(2)}$ actually deteriorates the agreement between the two sets of data. Since the second-order Murnaghan equation shows an in-

flection point near 150 kbar, which is unlikely on physical grounds, one has to discard the second-order Murnaghan equation as inappropriate. This confirms the conclusion arrived at before on the basis of figure 1, and substantiates similar expectations expressed earlier by Anderson [3].

Figure 3b shows that the difference between the Birch equations in first- and second-order approximation is much smaller than that for the Murnaghan equations, and that both the first- and the second-order equations are in substantial agreement with he x-ray data. Surprisingly enough, the first-order ultrasonic Birch equation agrees within experimental error with the x-ray data, but the second-order ultrasonic Birch equation deviates markedly above about 400 kbar from the x-ray data. Since the effect of a possible systematic error in the pressure scale used in the ultrasonic measurements is included in the error of the ultrasonic data, and since the error indicated for the x-ray data is based on the mean square deviation only, one is compelled to suspect the presence of a systematic error in the x-ray measurements which becomes excessively large above about 400 kbar. This conjecture is substantiated by the fact that the least square fit of the x-ray data to a third-order Birch equation exhibits an inflection point near 300 kbar, which is unlikely on physical grounds. Although any discussion of a possible source for such a possible error is purely speculative, one may expect the pressure scale used in the x-ray measurements to be a very likely cause. This pressure scale is based on the equation of state of Ag and Mo that were obtained from the conversion of shock wave data.

A feature worth noting is that the total error of the ultrasonic data is smaller than the purely statistical error of the x-ray data in the entire pressure range considered.

Since significant differences were found for the cesium halides between the ultrasonic data and Bridgman's volumetric data, it was deemed worthwhile to compare Bridgman's data with the x-ray data. To this end Bridgman's data were fitted to a third-order Birch equation and then extrapolated over the pressure range covered in the x-ray measurements. The results are compared in figure 3c with the x-ray data. Also shown are the error limits of Bridgman's data based on the mean square deviation. It is apparent that Bridgman's data of 1945 [10] are much more precise, but of so low accuracy, that they differ from the x-ray data above about 180 kbar. On the other hand, Bridgman's data of 1940 [9] show a very large statistical error when fitted to a third-order Birch equation, so that the agreement with the x-ray data within the joint experimental error is extended to as high pressures as about 380 kbar. Since both curves of Bridgman fall quite close to each other, it is still safe to conclude that the agreement between Bridgman's data and the x-ray data is quite poor. The fair agreement found between the x-ray data and the ultrasonic data must therefore be taken as evidence in favor of both these sets of data, and against the reliability of Bridgman's data. The observation that Bridgman's data are of rather limited accuracy only has been made by several authors who also discuss possible causes of error [42–44].

4. Ultrasonic Equation of State in Second-Order Birch Equation

From the discussion of the preceding section it seems justified to propose an ultrasonic equation of state for use as a high-pressure standard. For this purpose CsI has been selected, and an equation of state calculated from the ultrasonic data of tables 2 and 4 on the basis of the second-order Birch equation. The results are expressed in terms of the lattice parameter and are listed in table 5 and plotted in figure 4. The absolute values of the lattice parameter at zero pressure were taken from the thermal expansion data of references [30],

$$a = 4.549 + 1.767 \times 10^{-4} t + 1.528 \times 10^{-7} t^2 \qquad (4.1)$$

with a in angstrom units and t in degrees Celsius. The relative compression $a(T, p)/a(T, o)$ is, however, independent of these data (except for the thermodynamic conversion from the mixed ultrasonic to the pure isothermal data).

Since for practical applications the reliability of these results is of crucial importance a detailed error analysis has been carried out at room temperature.

The pressure is according to (3.2), (3.7), and (3.8) in second-order Birch approximation a function of the bulk modulus B_0, of its first two pressure derivatives $B_0^{(1)}$ and $B_0^{(2)}$, and via the temperature dependence of these quantities, a function of temperature. If instead of the volume compression

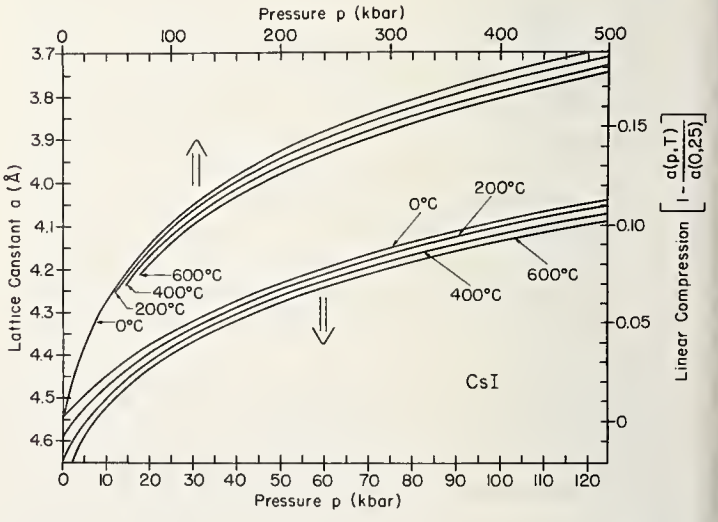

FIGURE 4. *Equation of state of* CsI, *calculated in second-order Birch approximation from ultrasonic data of tables 2 and 3.*

TABLE 5. *Pressure according to ultrasonic equation of state for* CsI *as a function of the lattice constant* a *and temperature.*

$\frac{a(p, T)}{a(0, 25)}$	a	0 °C	25 °C	100 °C	200 °C	300 °C	400 °C	500 °C	600 °C
1.030	4.691								0.54
1.025	4.668							0.30	1.26
1.020	4.645							1.23	2.12
1.015	4.622						1.10	2.29	3.13
1.010	4.600					0.98	2.36	3.50	4.31
1.005	4.577				0.95	2.43	3.77	4.89	5.66
1.000	4.554		0.00	1.11	2.60	4.05	5.36	6.45	7.21
0.995	4.531	1.52	1.87	2.96	4.43	5.85	7.14	8.21	8.97
0.990	4.508	3.58	3.92	4.99	6.44	7.84	9.12	10.19	10.96
0.985	4.486	5.83	6.17	7.22	8.65	10.05	11.33	12.41	13.20
0.980	4.463	3.29	8.63	9.67	11.09	12.48	13.77	14.88	15.71
0.975	4.440	10.98	11.31	12.35	13.77	15.17	16.48	17.62	18.52
0.970	4.417	13.91	14.25	15.29	16.70	18.12	19.47	20.7	21.6
0.965	4.395	17.11	17.45	18.49	19.92	21.4	22.8	24.0	25.1
0.960	4.372	20.6	20.9	22.0	23.4	24.9	26.4	27.8	29.0
0.955	4.349	24.4	24.8	25.8	27.3	28.9	30.4	31.9	33.2
0.950	4.326	28.5	28.9	30.0	31.5	33.1	34.8	36.4	37.9
0.945	4.304	33.0	33.4	34.6	36.1	37.8	39.6	41.4	43.1
0.940	4.281	37.9	38.3	39.5	41.1	43.0	44.9	46.9	48.8
0.935	4.258	43.3	43.7	44.9	46.6	48.6	50.7	52.9	55.0
0.930	4.235	49.0	49.5	50.8	52.6	54.7	57.0	59.5	61.9
0.925	4.212	55.3	55.8	57.3	59.1	61.4	64.0	66.7	69.4
0.920	4.190	62.1	62.7	64.2	66.2	68.7	71.5	74.5	77.6
0.915	4.167	69.5	70.2	71.8	73.9	76.7	79.8	83.1	86.5
0.910	4.144	77.6	78.3	80.1	82.4	85.4	88.8	92.5	96.3
0.905	4.121	86.3	87.1	89.1	91.5	94.8	98.6	103.	107.
0.900	4.099	95.7	96.7	98.9	101.	105.	109.	114.	119.
0.895	4.076	106.	107.	110.	112.	116.	121.	126.	131.
0.890	4.053	117.	118.	121.	124.	129.	134.	139.	145.
0.885	4.030	129.	131.	134.	137.	142.	148.	154.	160.
0.880	4.008	142.	144.	147.	151.	156.	163.	169.	176.
0.875	3.985	156.	158.	162.	166.	172.	179.	186.	194.
0.870	3.962	172.	174.	178.	182.	189.	197.	205.	213.
0.865	3.939	188.	191.	196.	200.	208.	216.	225.	234.
0.860	3.917	207.	210.	215.	220.	228.	237.	247.	256.
0.855	3.894	226.	230.	236.	241.	250.	260.	270.	280.
0.850	3.871	247.	251.	258.	264.	273.	285.	296.	307.
0.845	3.848	270.	275.	283.	289.	299.	311.	324.	335.
0.840	3.825	295.	301.	309.	316.	327.	341.	354.	366.
0.835	3.803	323.	329.	338.	345.	358.	372.	387.	399.
0.830	3.780	352.	359.	369.	377.	391.	407.	422.	435.
0.825	3.757	384.	392.	404.	412.	427.	444.	461.	474.
0.820	3.734	419.	427.	441.	449.	466.	485.	503.	516.
0.815	3.712	456.	466.	481.	490.	509.	529.	548.	561.
0.810	3.689	497.	508.	525.	535.	555.	577.	597.	610.

385-762 O - 71 - 13

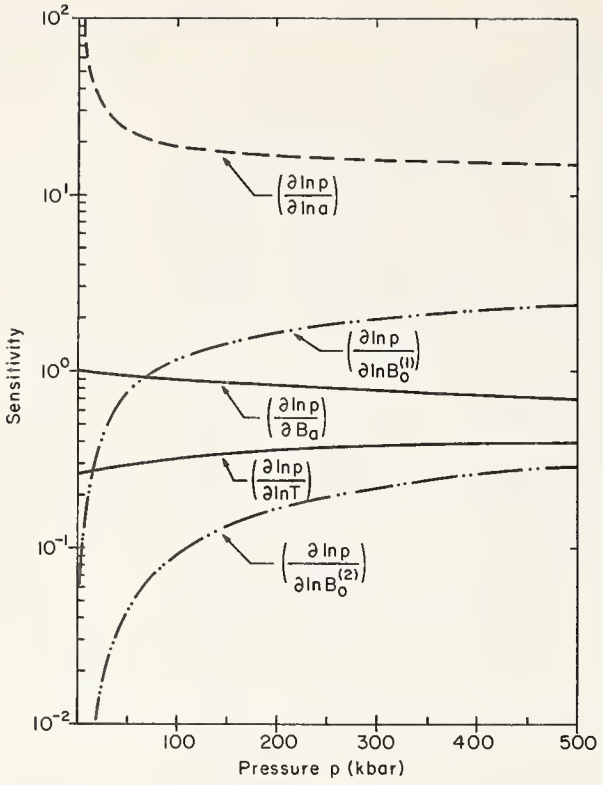

FIGURE 5. *Sensitivity of equation of state of* CsI *with respect to changes of the bulk modulus* B_0, *its first two pressure derivatives* $B_0^{(1)}$ *and* $B_0^{(2)}$, *temperature* T, *and lattice parameter* a, *at 25 °C in second-order Birch equation.*

ratio R according to (3.1) the linear compression ratio

$$L=\frac{a(p, T)}{a(o, T)} \tag{4.2}$$

is used as independent variable according to

$$R=L^3 \tag{4.3}$$

then the functional dependence of the pressure on all variables is of the form

$$p=p(B_0(T), B_0^{(1)}(T), B_0^{(2)}(T), L) \tag{4.4}$$

The pressure as calculated from the ultrasonic equation of state will therefore be subject to the errors $\Delta B_0(T)$, $\Delta B_0^{(1)}(T)$, $\Delta B_0^{(2)}(T)$ of the ultrasonically determined input data at a given temperature, which will be taken as 25 °C. These errors limit, therefore, the accuracy of the pressure scale based on the ultrasonic equation of state. In addition to these errors in the pressure scale, the actual pressure measurement will be limited in accuracy because of insufficient control and characterization of the temperature, corresponding to an error ΔT, and because of an error Δa in the measurement of the lattice constants. The relative error in pressure due to each of these errors considered separately is given by

$$\frac{\Delta p}{p}=S_x\cdot\frac{\Delta x}{x}, \tag{4.5}$$

where the factor

$$S_x=\frac{\partial \ln p}{\partial \ln x}. \tag{4.6}$$

represents the sensitivity and x denotes any of the five variables B_0, $B_0^{(1)}$, $B_0^{(2)}$, T, and a. The sensitivity was calculated according to (4.6) from the data of tables 2 to 4 for CsI and is plotted in figure 5 as a function of pressure for these five variables. The sensitivity with respect to errors in the bulk modulus B_0 and the lattice constant decreases with pressure, while that with respect to all other variables increases with pressure. At pressures above 65 kbar the sensitivity increases in the sequence $B_0^{(2)}$, T, B_0, $B_0^{(1)}$, a.

Of greater practical interest is the actual uncertainty in pressure Δp which occurs for any given error Δx of the five independent variables. These errors were also calculated for CsI as a function of pressure from the values for ΔB_0, $\Delta B_0^{(1)}$ and $\Delta B_0^{(2)}$ given in table 2 for the purely isothermal quantities, and by assuming a temperature error of $\Delta T=1$ °C. For the lattice constant an error of $\Delta a/a=10^{-3}$ was assumed which corresponds to the best accuracy attainable at present with high-pressure x-ray cameras [45]. The results are plotted in figure 6 which contains also the total error according to the Gaussian error propagation law.

It is apparent that below 100 kbar the accuracy limiting factor is the measurement of the lattice constant, and between 100 and 150 kbar it is the first pressure derivative of the bulk modulus, and above 150 kbar it is the second pressure derivative of the bulk modulus. The contributions from the errors of all other variables are in the pressure range up to 500 kbar much smaller than the larger of the two contributions arising from the lattice constant and the first and second pressure derivatives of the bulk modulus, and may therefore be ignored for all practical purposes.

The total accuracy of the ultrasonic equation of state if it is used in connection with x-ray measurements of the lattice constant at high pressure ranges from 600 bars at 10 kbar (6 percent) over 3 kbar at 100 kbar (3 percent) to 33 kbar at 500 kbar (7 percent). In the pressure range from 25 kbar to 150 kbar the total error in pressure is always smaller than 3.5 percent. In this pressure range the ultrasonic equation of state of CsI should therefore be useful as an auxiliary pressure standard.

A similar error analysis can be carried out for temperatures above room temperature. Since the ultrasonic measurements were carried out up to 250 °C one should expect that the accuracy of the equation of state of CsI proposed here will be approximately the same. The values above 250 °C are calculated by extrapolation of the third- and fourth-order elastic constants and are based on a linear approximation for their temperature dependence. Above 250 °C the accuracy will therefore be lower than at room temperature.

Strictly speaking, the accuracy plotted in figure 6 refers to the sample of CsI only, which was used for the ultrasonic measurements. Since it is known that the elastic constants and therefore the bulk modulus depend somewhat on the concentration of impurities, dislocations, and crystal imperfections, one may have to consider the possibility that an additional uncertainty is introduced by this effect. One should expect, however, that this effect is more pronounced for the bulk modulus and its second pressure derivative than for its first pressure derivative, because the first pressure derivative is given by a ratio of third- and second-order elastic constants, so that this effect may partly cancel. Since the first pressure derivative is the accuracy limiting factor below 150 kbar and since the accuracy of this factor amounted to as much as 1.3 percent for the ultrasonic data used here, one may expect that this value should not be significantly increased by the effect of crystal imperfections.

If the accuracy of the first and second pressure derivatives of the bulk modulus could be increased by factors of three and four, respectively, so that the error would amount to about 0.4 and 2.7 percent, respectively, then the uncertainty in the lattice constant measurement would be the accuracy limiting factor up to 500 kbar. The total error at 500 kbar would amount to 6.8 kbar (1.4 percent) only. This increase in accuracy seems quite feasible at present and would require more accurate pressure measurement in the ultrasonic experiments, and more reliable measurements of the thermal expansion coefficient, of the specific heat, and of the temperature dependence of these quantities. It is through the temperature derivatives of the thermal expansion coefficient and of the specific heat that an additional error is introduced in the conversion from the ultrasonically measured isothermal pressure derivative of the adiabatic bulk modulus to the purely isothermal value. The potential benefit of this increased accuracy seems to justify the pursuit of this work as a future task.

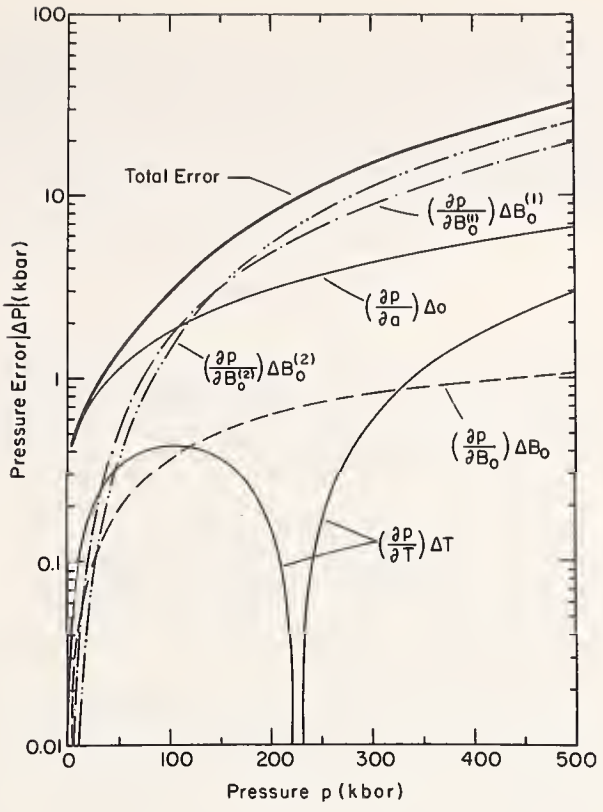

FIGURE 6. *Total error of pressure of equation of state of* CsI *and contributions from individual errors of material parameters* ($\Delta B_0 = 0.5$ kbar, $\Delta B_0^{(1)} = 0.08$, $\Delta B_0^{(2)} = 0.008$ (kbar)$^{-1}$), *of temperature* ($\Delta T = 1$ °C) *and of lattice parameter* ($\Delta a/a = 10^{-3}$) at 25 °C *in second-order Birch equation.*

5. Conclusions and Summary

A three-parameter equation of state based on ultrasonically measured values of the bulk modulus and its first two pressure derivatives has been proposed for CsCl and CsBr at room temperature, and for CsI between 0 °C and 600 °C. The phenomenological equation of state of Birch has been used in the second-order approximation and has been found to be superior to the equations of Murnaghan and Keane. The ultrasonic equation of state does not agree within the carefully established limits of experimental error with the piezometric data of Bridgman, but it does agree up to 400 kbar with data obtained from high-pressure x-ray measurements by Perz-Albuerne and Drickamer.

Even at these high pressures the accuracy of the ultrasonic equation of state is better than that of the x-ray data. Although at present the total accuracy of the ultrasonic equation of state is at high pressure limited by the error of the first and second pressure derivatives of the bulk modulus, it seems possible to improve this accuracy and to present an ultrasonic equation of state for cesium halides with high enough accuracy so that the predominant accuracy limiting factor will be the error in the x-ray measurement of the lattice parameter.

6. Acknowledgments

The authors would like to express their sincere appreciation to Prof. H. G. Drickamer for sending a table of the numerical results of his equation of state data for CsCl which were published in references [11] and [12] in graphical form. Thanks are also extended to Mrs. J. Schiff for most of the computer programming required for the numerical calculations.

NOTE ADDED IN PROOF:

The ultrasonic data reported in tables 1, 2, and 4 differ slightly from the numerical values presented at the Symposium in 1968. This change is due to the fact that the earlier data were based on an approximation used in the processing of the ultrasonic data which was later found to be unjustified. While the resulting changes in the room temperature data for the ultrasonic equation

of state shown in figures 2 and 3 are insignificant a more pronounced change accrued for the ultrasonic equation of state data at high temperatures, which are reported in table 5 and figure 4. Whereas for the earlier data the isotherms were found to intersect at high pressures, the revised data lead to an equation of state with isotherms which are quite evenly spaced apart, and which do not exhibit the unusual behavior of negative thermal expansion at high pressure.

7. References

[1] Anderson, O. L., J. Phys. Chem. Sol. **27**, 547 (1966).
[2] Murnaghan, F., Proc. Natl. Acad. Sci. **30**, 244 (1944).
[3] Anderson, O. L., Phys. Earth Planet. Interiors **1**, 169 (1968).
[4] Keane, A., Austral. J. Phys. **7**, 3 (1954).
[5] Chang, Z. P., and Barsch, G. R., Phys. Rev. Let. **19**, 1381 (1967).
[6] Birch, F., Phys. Rev. **71**, 809 (1947).
[7] Birch, F., J. Geophys. Res. **57**, 227 (1952).
[8] Knopoff, L., J. Geophys. Res. **68**, 2929 (1963).
[9] Bridgman, P. W., Proc. Am. Acad. **74**, 21 (1940).
[10] Bridgman, P. W., Proc. Am. Acad. **76**, 1 (1945).
[11] Perez-Albuerne, E. A., and Drickamer, H. G., J. Chem. Phys. **43**, 1381 (1965).
[12] Drickamer, H. G., Lynch, R. W., Clendenen, R. L., and Perez-Albuerne, E. A., Sol. State Phys. **19**, 135 (1966).
[13] Decker, D. L., J. Appl. Phys. **36**, 157 (1965).
[14] Decker, D. L., J. Appl. Phys. **37**, 5012 (1966).
[15] Bartels, R. A., and Schuele, D. E., J. Phys. Chem. Sol. **26**, 537 (1965).
[16] Larson, D. B., Keeler, R. N., Kusubov, A., and Hord, B. L., J. Phys. Chem. Sol. **27**, 476 (1966).
[17] Jamieson, J. C., in Physics of Solids under Pressure, C. T. Tomizuka and R. M. Emrick, eds. (Academic Press, Inc., New York, 1965) pp. 444–455.
[18] Bassett, W. A., Takahashi, T., Mao, H. K., and Weaver, J. S., J. Appl. Phys. **39**, 319–325 (1968).
[19] Menary, J. W., Ubbelohde, A. R., Woodward, F. R. S. and I., Proc. Roy. Soc. **A208**, 158 (1951).
[20] Hoodless, I. M., and Morrison, J. A., J. Phys. Chem. **66**, 557 (1962).
[21] Rao, K. J., Rao, G. V. S., and Rao, C. N. R., Trans. Faraday Soc. **63**, 1013 (1967).
[22] Koliwad, K. M., and Ruoff, A.L., Bull. Am. Phys. Soc. **10**, 1113 (1965).
[23] Reddy, P. J., and Ruoff, A.L., in Physics of Solids at High Pressures, C. T. Tomizuka and R. M. Emrick, eds. (Academic Press, New York, 1965), p. 510.
[24] Chang, Z. P., Barsch, G. R., and Miller, D. L., Phys. Stat. Sol. **23**, 577 (1967).
[25] Barsch, G. R., and Chang, Z. P., Phys. Stat. Sol. **19**, 139 (1967).
[26] Overton, W. C., Jr., J. Chem. Phys. **37**, 116 (1962).
[27] Smart, W. M., Combination of Observations (Cambridge Univ. Press, Cambridge, 1958).
[28] Slage, O. D., and McKinstry, H. A., J. Appl. Phys. **38**, 451 (1967).
[29] Standard X-ray Diffraction Powder Patterns, NBS Circular 539, Vols. 1 to 7, National Bureau of Standards, Washington, D.C., 1953–1957.
[30] Johnson, J. W., Agron, P. A., and Bredig, M. A., J. Am. Chem. Soc. **77**, 2734 (1955).
[31] Landolt-Börnstein, 6th Ed., Vol. 2, Part 4, Springer-Verlag, Berlin (1961).
[32] Barsch, G. R., and Chang, Z. P., J. Appl. Phys. **39**, 3276 (1968).
[33] Nranyan, A. A., Sov. Phys.-Sol. State **5**, 129; 1361 (1964).
[34] Ghate, P. B., Phys. Rev. **139**, A1666 (1965).
[35] Arenstein, M., Hatcher, R. D., and Neuberger, J., Phys. Rev. **132**, 73 (1963).
[36] Pavlovski, M. N., Vashchenko, V. Ya., and Simakov, G. V., Sov. Phys.-Sol. State **7**, 972 (1965).
[37] Löwdin, P. O., Adv. Phys. **5**, 1 (1956).
[38] Fröman, A., and Löwdin, P. O., J. Phys. Chem. Sol. **23**, 75 (1962).
[39] Tosi, M. P., Sol. State Phys. **16**, 1 (1964).
[40] Chandra, M., Proc. Phys. Soc. **91**, 257 (1967).
[41] Mayer, J. E., J. Chem. Phys. **1**, 270 (1933).
[42] Jeffery, R. N., Barnett, J. D., Vanfleet, H. B., and Hall, H. T., J. Appl. Phys. **37**, 3172 (1966).
[43] Rotter, C. A., and Smith, C. S., J. Phys. Chem. Sol. **27**, 267 (1966).
[45] McWhan, D. B., Accuracy of High-Pressure X-ray Diffraction Measurements, 1964 Symp. on High-Pressure Technology, ed. E. C. Lloyd and A. H. Giardini, publ. by ASME (1965).
[46] Rose, M. F., Phys. Stat. Sol. **21**, 235 (1967).
[47] Yu, J. S., Appl. Sci. Res. **19**, 220 (1968).

DISCUSSION

D. J. Pastine (*U.S. Naval Ordnance Laboratory, White Oak, Maryland*): While it is apparently true that the Murnaghan and Birch equations-of-state may converge rapidly, this depends upon the second and higher derivatives of bulk modulus with respect to pressure. However, the values of the second derivatives are not well known, and the values of the higher order derivatives are not known at all. The second derivative may also be obtained from shock data, and this might be advantageous in cases where the values are difficult to obtain otherwise.

In obtaining your results from ultrasonic data, are you comparing isotherms with isotherms?

AUTHORS' CLOSURE

The reason we chose to work with the cesium halides was because these substances are very compressible, and the plot of the elastic constants versus pressure shows sufficient curvature to permit the second derivatives to be readily determined at pressures below 10 kilobars. It would be more difficult to pick up the second derivative ultrasonically below 10 kilobars with equal accuracy for less compressible materials. But if we have a pressure scale based on cesium halides, then we could use an iterative procedure based on ultrasonic measurements at higher pressures, say up to 50 kilobars, and use the second pressure derivatives obtained to calculate another equation-of-state for less compressible materials up to one or two megabars.

All we have shown here concerning convergence

is that the deviation of the second order Birch equation from an exact lattice theoretical equation based on a model potential, which includes first and second nearest neighbors, is small in the pressure range of interest. We have not included thermal motion, which was justified in our case because the pressure dependence arises mainly from the cohesive contribution, and because the thermal equation-of-state is based on so many other assumptions.

On the matter of reducing our ultrasonic data, I should have made the point that all these data were first converted to isothermal conditions. For the first pressure derivatives, for example, we must know the pressure derivative of the Grüneisen constant, which we have calculated from thermal data by means of thermodynamic identities.

Calculation of the *P-V* Relation for Sodium Chloride up to 300 Kilobars at 25°C

J. Scott Weaver, Taro Takahashi, and William A. Bassett

Department of Geological Sciences and Space Science Center, University of Rochester, Rochester, N.Y. 14627

The *P-V* relation for the Bl phase of NaCl was calculated up to 300 kilobars at 25 °C by means of the Hildebrand and Mie-Grüniesen equations. The effect of (1) the uncertainty in the parameters used, (2) the functional form for the temperature-dependent part of internal energy, (3) the anharmonic contribution, and (4) the second nearest neighbor repulsion on the calculated *P-V* relation is discussed. It was found that the calculated *P-V* relation for NaCl is sensitive to the value chosen for Bt_0, and that the effect of (2), (3), and (4) on the calculated *P-V* relation is small. The precision for the present calculation has been estimated to be ±2.5 percent. The calculated *P-V* relation is in agreement within experimental uncertainties with the fixed points on the absolute pressure scale, with that determined by Bridgman up to 100 kilobars, and that obtained by Fritz from shock wave data up to 260 kilobars. Simultaneous determinations of the effect of pressure on the volumes of NaCl and MgO were made by x-ray diffraction on an intimate mixture of these two materials. It was found that the pressure values calculated from the volume of NaCl using the calculated *P-V* relation are in agreement with those calculated from the volume of MgO using the *P-V* relation calculated from the values of Bt_0 and Bt_0' with the Murnaghan equation. This agreement verifies not only the calculated *P-V* relation for NaCl, but also establishes the validity of the internal standard method for pressure determination.

1. List of Notation

The subscript zero denoted quantities evaluated at $P=0$, $V=V_0$. For example: V_0; B_{t0}''; etc.

The other notations used and not defined in the text are:

$A=(\partial \ln \gamma/\partial \ln V)_T$
$B_s=-(\partial P/\partial \ln V)_s$ the adiabatic bulk modulus
$B_s'=(\partial B_s/\partial P)_T$
$B_s''=(\partial B_s'/\partial P)_T$
$B_t=-(\partial P/\partial \ln V)_T$
$B_t'=(\partial B_t/\partial P)_T$
$B_t''=(\partial B_t'/\partial P)_T$
$B^*=-V(\partial P^*/\partial V)_T$
$C_r=$ dipole-dipole van der Waals coefficient.
$C_v=$ specific heat at constant volume.
$D_r=$ dipole-quadrupole van der Waals coefficient.
$e=$ electron charge or Naperian base.
$E^*(V, T)=$ temperature dependent part of the internal energy.
$P=$ pressure.
$P^*=-(\partial E^*/\partial V)_T+T(\partial P/\partial T)_V$
$P_{M=\frac{1}{6}}\alpha_r e^2/r_0^4$
$P_6=c_r/r_0^9$
$P_8=\frac{4}{3}Dr/r_0^{11}$
$P_R=br_0/3\rho$
$r=$ nearest neighbor distance
$S=$ entropy
$T=$ temperature (K)
$U(V, T)=$ internal energy
$V=$ molar volume
$x=V/V_0$
$\alpha=(\partial \ln V/\partial T)_P$ isobaric thermal expansion coefficient
$\alpha_r=$ Madelung constant
$\gamma=T\alpha B_t V/C_v$ thermodynamic Grüneisen parameter
$\delta_s=-(\alpha B_s)^{-1}(\partial B_s/\partial T)_P$
$\delta_t=-(\alpha B_t)^{-1}(\partial B_t/\partial T)_P$
$\epsilon=(\partial \ln \alpha/\partial \ln V)_T$
$\theta=$ Debye characteristic temperature
$\rho=$ interaction length in the repulsion energy
$\phi=$ lattice energy

Paper presented at the Symposium on Accurate Characterization of the High-Pressure Environment, held at the National Bureau of Standards, Gaithersburg, Md., October 14–18, 1968.

2. Introduction

In the internal standard method of pressure determination in high pressure x-ray diffraction studies, the pressure is inferred from the molar volume of a standard substance mixed with the material being studied. Hence the pressure-volume ($P-V$) relation of the standard must be accurately known over the pressure range of interest. However, due to the lack of direct and accurate means of determining the $P-V$ relation at pressures above 60 kbar, desirable experimental data are not available in the pressure range. One experimental approach to the determination of the $P-V$ relation is the study of the propagation of a shock wave through a material. Such studies yield values for both pressures and volume along a non-adiabatic, non-isothermal path known as the Hugoniot from which the required isothermal $P-V$ relation may be calculated. In the conversion of the Hugoniot to an isotherm, the results depend critically on the assumptions made about the form of the equation of state. Another approach involves calculation of the $P-V$ relation from a suitable approximation to the equation of state whose parameters are fixed on the basis of the properties of the material determined at low pressures. In such an approach, however, large errors in a calculated $P-V$ relation can result from small

errors in the values of the various low-pressure parameters or from inadequacy in the form of the equation of state used. Hence, neither of these approaches is free from objection.

This paper presents a discussion of the $P-V$ relation of the B1 phase of NaCl for pressures up to 300 kbar at 25 °C. The approach taken here is an attempt to calculate the $P-V$ relation from low-pressure properties, and then to compare the resulting $P-V$ relation with the results of shock-wave propagation studies. An additional test of validity of the calculated $P-V$ relation and the internal standard method is obtained from simultaneous determinations of the molar volumes of NaCl and MgO. The results of a study of the sensitivity of the calculated $P-V$ relation for NaCl to the form of the equation and to the value of the low-pressure properties for NaCl are used to estimate the precision of the $P-V$ relation.

NaCl offers a number of advantages as a substance for use as an internal standard. Properties contributing to its usefulness include:

(1) The small bulk modulus of NaCl (237.4 kbar at 25 °C) yields good sensitivity since a given change in pressure results in a relatively large change in volume.

(2) The isometric structure of NaCl yields an x-ray diffraction pattern containing relatively few lines, thus minimizing interference with the sample pattern. In addition, each NaCl reflection yields a value for the molar volume.

(3) The low yielding strength of NaCl aids in producing a more hydrostatic pressure environment than other solid media having higher yielding strength. In addition, NaCl has a low absorption coefficient for a wide range of the electromagnetic radiations including x-rays, visible, and infrared.

(4) NaCl has been the subject of a great number of theoretical and experimental studies, so that most of the properties necessary for calculation of the $P-V$ relation are available from the literature.

3. Previous Studies

Figure 1 shows the results of calculations of the $P-V$ relation for NaCl at 25 °C by Decker (1965, 1966), who used the vibrational Mie-Grüneisen equation, and by Perez-Albuerne and Drickamer (1965), who used the thermal Hildebrand equation. These are compared with the shock Hugoniot data obtained by Christian (1957) and with five points along a 25 °C isotherm calculated by Fritz (1967) from shock wave data. The discrepancy between the calculated $P-V$ relations and the experimental data appears to be due to the values of Bt_0 chosen by Decker and by Perez-Albuerne and Drickamer.

A family of isothermal $P-V$ relations may be obtained from the expansion of Bt as a Tayler series in P:

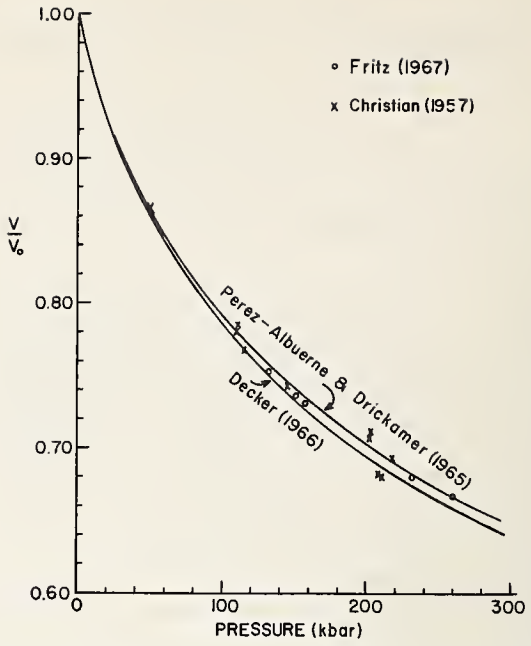

FIGURE 1. *Comparison of the* P–V *relations for* NaCl *calculated by Perez-Albuerne and Drickamer (1965) using the thermal Hildebrand equation and by Decker (1966) using the vibrational Mie-Gruneisen equation, with the Hugoniot data obtained by Christian (1957) and with five points along a 25 °C isotherm calculated from Hugoniot data by Fritz (1967).*

The last of these has been superseded by more recent work (Fritz et al., this volume) and may be disregarded.

$$Bt=-(\partial P/\partial \ln V)_T=B_0+B_0'P+\tfrac{1}{2}B_0''P^2+\ldots\ldots \quad (1)$$

Neglecting P^2 and higher terms, eq (1) leads to the Murnaghan equation (Anderson, 1965; Murnaghan, 1944):

$$P=(Bt_0/Bt_0')\,[(V/V_0)^{-Bt_0'}-1]. \quad (2)$$

If the P^2 term is retained, eq (1) leads to an equation of the form:

$$P=(2Bt_0/Bt_0')\,[(V/V_0)^{-qBt_0'}-1]\,[1+q-(1-q)\,(V/V_0)^{-qBt_0'}]^{-1} \quad (3)$$

where $q=[1-2Bt_0Bt_0''/(Bt_0')^2]^{1/2}$. Rose (1967) has derived a similar equation.

Another family of $P-V$ relations may be obtained from finite strain theory (Birch, 1938, 1952), by noting that the free energy is a function of strain, ϵ, where $2\epsilon=y=[(V/V_0)^{-2/3}-1]$:

$$P=(3/2)Bt_0y(1+y)^{5/2}(1-\xi y+\eta y^2+\ldots\ldots) \quad (4)$$

where

$$\xi=-(3/4)\,(Bt_0'-4) \text{ and } \eta=(3/8)\,[Bt_0Bt_0''+(Bt_0')^2-7Bt_0'+143/9].$$

The values of Bt_0 and Bt_0' for NaCl used to evaluate these relations are given in table 2. The value of Bt_0'' for NaCl is not known at present. However, the values for Bs_0, Bs_0', and Bs_0'' for CsCl, CsBr, and CsI determined by Chang and Barsch (1968) yield a relation, $Bs_0Bs_0'' \approx -Bs_0'$ for these three compounds. Hence the effect of Bt_0'' was investigated by calculating pressure values for the two cases: (1) $Bt_0''=0$ and (2) $Bt_0''=-Bt_0'/Bt_0$. The calculated $P-V$ relations for NaCl are shown in figure 2. It is seen that none of these $P-V$ relations agrees with the shock compression results of Fritz (1967). In particular, pressure calculated from Murnaghan equation is far greater than Fritz's values. This suggests that Bt_0'' is a negative number and that the effect of Bt_0'' can not be neglected for $V/V_0 \leq 0.8$. The Rose equation (1967) appears to be in better agreement with the shock data for $Bt_0''=-Bt_0'/Bt_0$. However, use of this equation with $Bt_0'' < 0$ leads to a physically unreasonable condition at high pressures. For example, if $Bt_0''=-Bt_0'/Bt_0$, Bt increases to a maximum at $P=Bt_0$, and thereafter, it decreases and becomes negative for $P > Bt_0\,[1+(1+2/Bt_0')^{1/2}]$. A negative value of Bt violates the First Law of Thermodynamics, while a negative value of Bt' seems unlikely for a single-component system in the absence of any phase transformation.

Four $P-V$ relations calculated with the Birch equation are shown in figure 2. The curve *Birch 1* was calculated assuming that $\xi=\eta=0$. The effect of the ξ term is shown by *Birch 2*, which was calculated with $\eta=0$ and $\xi=-1.013$ (or $Bt_0'=5.35$). The effect of η and the value of Bt_0'' is shown by *Birch 3a* in which $\eta=2.65$ and $Bt_0''=0$, and by *Birch 3a* in which $\eta=0.64$ and $Bt_0''=-Bt_0'/Bt_0$. From figure 2 it can be seen that both the ξ and η terms exercise a significant effect on the calculated pressure. Thus, eqs (2), (3), and (4) failed to describe adequately the $P-V$ relation of NaCl up to 300 kbar from the parameters determined at low pressures. On the other hand, with the refined experimental values for Bt_0, the Hildebrand and Mie-Grüneisen equations appear to be capable of accounting the compression of NaCl in the pressure range of present interest.

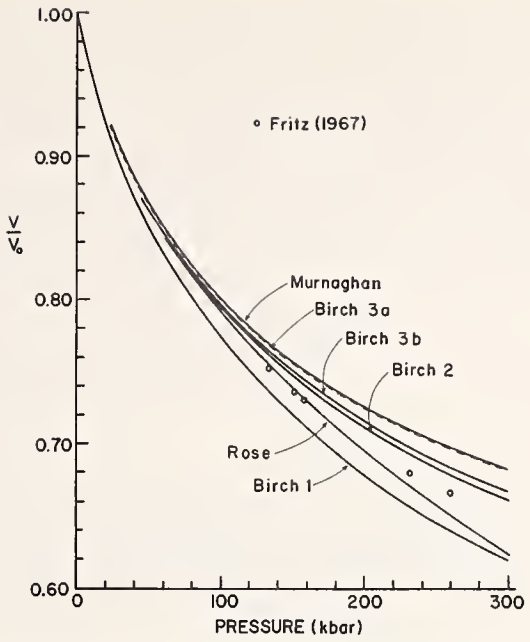

FIGURE 2. *Various* P–V *relations for* NaCl *calculated by means of the Murnaghan, Rose, and Birch equations.*

The values for the parameters used are: $Bt_0=237.4$ kbar, $B_{t_0}'=5.35$, and $B_{t_0}''=0.00$ or -0.0225 kbar^{-1}. The equations shown are: *Murnaghan*, eq (2); *Rose*, eq (3); *Birch 1*, eq (4) with $\xi=\eta=0$; *Birch 2*, eq (4) with $\xi=-1.013$, $\eta=0$; *Birch 3a*, eq (4) with $\xi=-1.013$, $\eta=2.648$ ($B_{t_0}''=0$); *Birch 3b*, eq (4) with $\xi=-1.013$, $\eta=0.642$ ($B_{t_0}''=-0.0225$ kbar^{-1}). Five points along a 25 °C isotherm calculated by Fritz (1967) from Hugoniot data are shown for comparison. These points have been superseded by more recent work (Fritz et al., this volume) and may be disregarded.

4. Calculation of the $P-V$ Relation

The internal energy of a solid may be written in the form

$$U(V, T)=\phi(V)+E^*(V, T).$$

In the vibrational formulation of the equation of state,

TABLE 1. *Definition of the models of solid used for the calculation of the* P – V *relation for* NaCl.

E^* is the energy due to the lattice vibrations; P^* the pressure resulting from the lattice vibrations; and B^* the contribution of the lattice vibrations to bulk modulus.

Model	E^*	P^*	B^*	Remarks
I	constant	0	0	Thermal formulation at 0° K.
II	$(9/4)R\theta$	$(9/4)\gamma R\theta/V$	$(1+\gamma-A)P^*$	Vibrational formulation at 0° K.
III	$6RTDe(\theta/T)+(9/4)R\theta$	$\gamma E^*/V$	$-(A-1)-(\gamma E^*/V)-(\gamma^2/V)(TCv-E^*)$	Vibrational Mie-Grüneisen
IV	$6RTDe(\theta/T)$	$\gamma E^*/V$	$-(\gamma E^*/V)-(\gamma^2/V)(TCv-E^*)$	Thermal Mie-Grüneisen
V	(**)	$T\alpha_0Bt_0(\gamma/\gamma_0)(V_0/V)$	$-(A-1)P^*$	Vibrational Hildebrand
VI	(**)	$T\alpha_0Bt_0$	0	Thermal Hildebrand

$De(\theta/T)=3(T/\theta)^3\int_0^{\theta/T}[u^3/(e^u-1)]du$ . . . . . Debye function. θ = Debye temperature.

*For these two cases, E^* should be a function of temperature alone. However, it is not necessary to know the functional form of E^*, since it is not used in the calculation.

ϕ is the potential energy due to the static lattice while E^* is the energy due to the lattice vibrations including the zero point vibrations. On the other hand, in the thermal formulation, the energy due to the zero point vibrations is included in ϕ, and hence E^* is taken to be the thermal energy. A relation for the pressure is found by combination of the expressions for the internal energy with the thermodynamic identity:

$$P = -(\partial U/\partial V)_T + T(\partial P/\partial T)_V,$$

and then

$$P = -d\phi/dV + P^*,$$

where P^* is the pressure resulting from the lattice vibrations. For NaCl, P^* is less than 10 kbar so that the lattice energy ϕ predominates at high pressure. The isothermal bulk modulus then assumes the form:

$$B_t = V(d^2\phi/dV^2) + B^*,$$

where B^* is a contribution of the lattice vibrations to the bulk modulus.

Since the elastic constants of NaCl determined by Slagle and McKinstry (1967) closely obey the Cauchy relation ($C_{12} = C_{44}$), a central-force model for ϕ is reasonable. For an ionic solid, the principal terms in the attractive part of ϕ result from the Coulomb and van der Waals (dipole-dipole and dipole-quadrupole) interactions. Since a unique form for the repulsive part of ϕ is not available, the Born-Mayer exponential form between the nearest neighbors containing two adjustable parameters was adopted. Thus, the adopted form for ϕ in terms of the nearest neighbor distance, r, becomes:

$$\phi = -\alpha_r e^2/r - C_r/r^6 - D_r/r^8 + be^{-r/\rho}$$

and hence

$$P = -P_M x^{-4/3} - P_6 x^{-3} - P_8 x^{-11/3} + P_R x^{-2/3} \exp(-r_0 x^{1/3}/\rho) + P^*$$

and

$$B_t = -(4/3)P_M x^{-4/3} - 3P_6 x^{-3} - (11/3)P_8 x^{-11/3} + (1/3)P_R x^{-2/3}(2 + r_0 x/\rho) \cdot \exp(-r_0 x^{1/3}/\rho) + B^*$$

$$x = V/V_0,$$

where a new set of parameters, P_M, P_6, P_8, P_R, with the dimensions of pressure have been introduced for convenience. The quantities characterizing the repulsion (b and ρ; or P_R and r_0/ρ) can be determined by two boundary conditions: that the expressions for P and Bt yield the correct values of 0 and Bt_0 respectively when $V = V_0$ (or $x = 1$).

A number of approximate forms for the temperature dependent part of the internal energy E^* are possible. The $P-V$ relation was calculated for six different choices for the form of E^* in order to test the sensitivity of the final results to the choice of a model for the vibrational energy. The models selected are shown in table 1. Models I and II are extreme cases in which the thermal contribution to E^* is ignored. Hence these models are appropriate for calculation of the 0 K isotherm only.

Models III and IV are based on the Mie-Grüneisen approximation to the vibrational and thermal formulations of the equation of state. The Mie-Grüneisen approximation may be derived if E^* has the functional form $T \cdot Q(\theta/T)$, where θ is a purely volume-dependent characteristic temperature, and therefore, $-d \ln \theta/d \ln V$ is equal to the thermodynamic Grüneisen parameter, γ. In the present study, the Debye functional form was adopted for E^*, since the specific heat values calculated for NaCl using this form agree closely with experimental values. The Grüneisen parameter γ was assumed to obey a power law in the volume of the form:

$$\gamma = \gamma_0 (V/V_0)^A$$

where the value of A was obtained from the thermodynamically exact relation derived by Bassett et al. (1967):

$$A = (\partial \ln \gamma/\partial \ln V)_T = 1 + (1 + \gamma \cdot \alpha \cdot T)\delta_s - Bs' + \gamma + T(\partial\gamma/\partial T)_V.$$

The term $T(\partial\gamma/\partial T)_V$ is zero from the assumptions inherent the Mie-Grüneisen approximation. The power law form for γ leads to a relation for the Debye temperature as a function of compression:

$$\theta = \theta_0 \cdot \exp\{\gamma_0 A^{-1}[1 - (V/V_0)^A]\}$$

where the subscript "0" denotes the values evaluated at zero pressure. Fumi and Tosi (1962) have shown that the assumptions leading to the vibrational formulation of the Gruneisen approximation are valid for temperatures somewhat less than the Debye temperature or greater, and that the thermal formulation is not appropriate in a temperature region near the Debye temperature. Therefore, Model IV is less satisfactory than Model III.

The Hildebrand approximation, on which Models V and VI are based, results from the assumption that E^* is a function of the temperature only, so that $P^* = T(\partial P/\partial T)_V = T \cdot \alpha \cdot Bt$. This implies that Cv is a function of temperature only, and therefore Cv is constant in a isothermal condition, and the relationship below holds:

$$P^* = P_0^*(\gamma/\gamma_0)/(V/V_0),$$

TABLE 2. *Physical parameters for* NaCl *used for the calculation of the* $P-V$ *relationship at* 25 °C

Parameters	Values	References
(A) *Experimentally Determined Parameters*		
a_0	5.6403 Å	Clark (1967).
Bs_0'	250.0 ± 1.8 kbar	Slagle and McKinstry (1967), 250.8 ± 1.8 kbar; Haussuhl (1960), 250.0 ± 1.3 *kbar*.
$-(\partial Bs/\partial T)_P$	0.109 ± 0.007 kbar °C^{-1}	Slagle and McKinstry (1967), 0.103; Bartels and Schuele (1965), 0.108; Haussuhl (1960), 0.117 ± 007 kbar °C^{-1}.
	5.27 ± 0.25	Bartels and Schuele (1965).
α_0	$(11.85 \pm 0.20)10^{-5}$ °C^{-1}	Slagle and McKinstry (1967), 11.48; Collins and White (1964), 11.85; Enck cited in Decker (1965), 12.00×10^{-5} °C^{-1}.
ϵ_0	$10. \pm 1$	Slagle and McKinstry (1967), 9.03; Collins and White (1964), 11.07.
θ_0	290 ± 12 K	Yates and Panter (1962).
α_r	1.74756	Tosi (1964).
C_r	$(180 \pm 36)10^{-60}$ erg cm^6	Mayer (1933).
D_r	$(180 \pm 90)10^{-76}$ erg cm^8	Mayer (1933).
(B) *Parameters Derived From the Values Listed Above*		
V_0	27.012 cm^3 mole^{-1}	
P_M	106.214 kbar	
P_6	15.95 ± 3.19 kbar	
P_8	2.64 ± 1.32 kbar	
Cv_0	0.4760 ± 0.0018 kbar cm^3 deg^{-1} mole^{-1}	
γ_0	1.597 ± 0.030	
Bt_0	237.4 ± 1.7 kbar	
Bt_0'	5.35 ± 0.30	
δs_0	3.67 ± 0.25	
A	1.20 ± 0.36	
(C) *Equations Used for Deriving the Values in* (B)		
$Cv_0 = 6R \cdot 3(T/\theta_0)^3 \int_0^{\theta_0/T} [u^4 e^u/(e^u-1)^2]du$		
$\gamma_0(1+\gamma_0\alpha_0 T) = \alpha_0 Bs_0 V_0/Cv_0$		
$\delta s_0 = -(\partial Bs/\partial T)_P/\alpha_0 Bs_0$		Anderson (1967).
$A = 1 + (1+\gamma_0\alpha_0 T)\delta s_0 - Bs_0' + \gamma_0$		Bassett et al. (1967).
$Bt_0' = (1+\gamma_0\alpha_0 T)^{-1}[Bs_0' + \gamma_0\alpha_0 T(\delta t_0 + A)]$		Bassett et al. (1967).
$\delta t_0 = \delta s_0 + (1+\gamma_0\alpha_0 T)[\gamma_0 + \gamma_0\alpha_0 T(\epsilon_0 + A)]$		Bassett et al. (1967).

where the subscript "0" indicates the quantities evaluated at zero pressure. According to Fumi and Tosi (1962), the vibrational Hildebrand approximation is appropriate for temperatures exceeding a temperature somewhat greater than the Debye temperature, whereas the thermal formulation is less satisfactory at temperatures near the Debye temperature. Model V is the vibrational formulation of the Hildebrand approximation, and Model VI is based on a simple case of the thermal Hildebrand approximation, in which P^* is assumed to be constant. In this latter case, the Gruneisen parameter is proportional to volume, or equivalently, the bulk modulus is a function of the volume only. This is the model used by Perez-Albuerne and Drickamer (1965), and should be inferior to Model V.

The values adopted for the various parameters of NaCl are listed in table 2. The values shown in table 2a were adopted from the literature, while the values in table 2b were calculated from the values in table 2a using the relations indicated. Since the isothermal bulk modulus at zero pressure, Bt_0, is used as a boundary condition, the calculated $P-V$ relation is quite sensitive to the values chosen. In the present study, the value of Bt_0 was calculated from the value of adiabatic bulk modulus, Bs_0, determined by Slagle and McKinstry (1967) by means of the pulse superposition technique. Their value was selected rather than a smaller value found by Bartels and Schuele (1965) in view of the high precision expected from the pulse superposition technique and the agreement with the value obtained by Haussuhl (1960). Since there was no compelling reason to select one value of $-(\partial Bs/\partial T)_P$ over another, the arithmetic mean of these values listed was adopted with an uncertainty calculated by assuming that the values are independent measurements of the same quality. Similarly, an intermediate value was chosen for α_0.

The P—V relations calculated using the six models are compared in figure 3, which also shows the results of Decker's revised calculation (1968) of the Mie-Gruneisen equation and five points along a 25 °C isotherm calculated from shock data by Fritz (1967). Models I and II are seen to be inconsistent with the results of experiments and with other models. Such a discrepancy is expected due to the lack of a temperature-dependent term in the internal energy. The other four models yield a range of pressures of only 4 kbar at 280 kbar, showing that the calculated pressures are not sensitive to the exact form chosen for the temperature-dependent part of the internal energy. However, Models IV and VI, which are the thermal formulations of the Mie-Grüneisen and Hildebrand approximations respectively, are probably inferior to Models III and V, the vibrational formulations, as already discussed in the previous page. The close correspondence between pressures calculated on the basis of either of Models III or V and Decker's 1968 recalculation

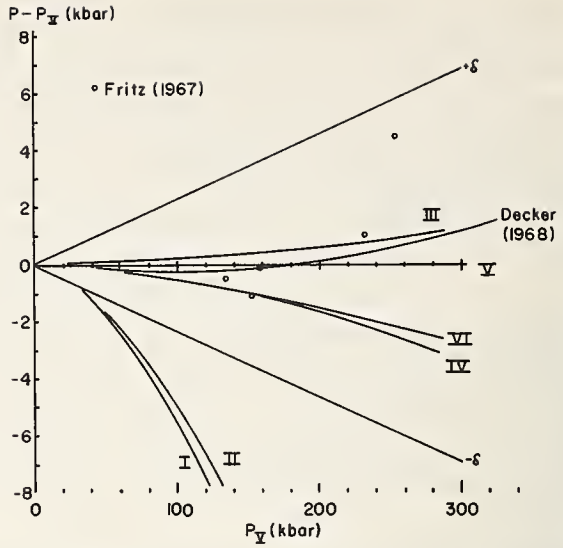

FIGURE 3. *Effect of the form of the temperature dependent part of the internal energy on the* P–V *relation for* NaCl.

Curves I–VI correspond to different choices for E^* (see table 1). Decker's (1968) revised calculations are included to illustrate the effect of the second nearest neighbor repulsion. The calculated P–V relations are compared with five points along a 25 °C isotherm calculated by Fritz (1967) from Hugoniot data. These points have been superseded by more recent work (Fritz et al., this volume) and may be disregarded. The uncertainty in the pressure values for Model V (P_V) resulting from the uncertainties in the parameters used in the calculation is shown by curves $+\delta$ and $-\delta$.

TABLE 3. *The sensitivity of the pressure values calculated with the Mie-Gruneisen equation (Model VI) to the uncertainties in the parameters at a compression of* $V/V_0 = 0.650$ *(~ 300 kbar).*

In order to show the direction of the change in the pressure values, only the positive values for the designated uncertainties were considered. The sensitivity for the Hildebrand equation (Model V) is similar to that for the Mie-Gruneisen equation shown here.

Parameter (x)	Uncertainty ($\delta x/x$)	Effect on P ($\delta P/P$)	Sensitivity $(\delta P/P)/(\delta x/x)$
	(*Percent*)	(*Percent*)	
Bt_0	0.6	+1.1	+1.9
γ	1.9	−0.2	−0.1
A	34	+1.8	+0.05
θ	4.1	−0.01	−0.003
C_r	20	−0.5	−0.03
D_r	50	−0.2	−0.004

indicates that the effect of the second-nearest neighbor interaction which was included in his calculation is negligibly small.

The total uncertainty in the calculated P was estimated to be ± 2.5 percent on the basis that the uncertainties in the individual parameters are independent and Gaussian. If the change in P resulting from the uncertainty in the ith parameter is δP_i, then the total uncertainty in P can be calculated by:

$$\delta P = \sum_i [(\delta P_i)^2]^{1/2}.$$

As can be seen from table 3, the main sources of the uncertainty in P are the uncertainties on Bt_0 and A. The total uncertainty thus calculated is shown with two curves labelled $+\delta$ and $-\delta$ in figure 2, and is sufficiently large, so that the two models are indistinguishable. Hence it does not appear reasonable to use the shock experiment data for selecting one of these models over another.

The sensitivity of Models III and V to the uncertainties in the parameters used was examined by recalculating the repulsion parameters and the $P-V$ relation with each parameter individually veried to the uncertainty limit given in table 2. The change in pressure divided by the uncertainty in the parameter provides a measure of the sensitivity of the $P-V$ relation to the value adopted for the parameter. The results are presented in table 3 for $V/V_0=0.650$. The calculated pressure is insensitive to the values of all the parameters except Bt_0. The sensitivity of P to the Bt_0 value is due to the use of this parameter as a boundary condition, and hence, a change in this value is not compensated by a change in the repulsion parameters.

5. Internal Consistency of Calculation

Thomsen and Anderson (1968) have pointed out that once a functional form for the lattice energy ϕ has been chosen, then the vibrational spectrum and hence γ are determined. Therefore, in principle, ϕ and γ cannot be chosen independently as was done in the present study. However, in practice, this inconsistency in ϕ and γ probably does not affect the results of calculations significantly. Using the same values for the parameters for NaCl as used in this work, they have calculated $\gamma_0=1.526$ and $A=0.40$ by means of a relationship derived by them on the basis of the lattice dynamic treatment given by Leibfried and Ludwig (1961). Their value for γ_0 is consistent with the value of 1.597 ± 0.030 obtained on the basis of the exact thermodynamic relation. On the other hand, their value for A differs from the value of 1.20 ± 0.36 which was obtained in the present work on the basis of the thermodynamically exact treatment of the experimental data. The discrepancy between these two values for A may be attributed to (1) failure of the fourth-order anharmonic theory used by Thomsen and Anderson (1968), or (2) failure of the lattice energy form adopted in the present work. It is also possible that this discrepancy may disappear when an allowance is made for the uncertainties in the values of the parameters used, since the discrepancy corresponds to only twice the uncertainty estimated for A in the present work. If the value for A obtained by Thomsen and Anderson were adopted, it would yield calculated pressure values about 3.5 percent smaller than the results presented here.

The internal consistency of the present calculation can also be examined by a comparison of the calculated value for Bt_0' and the experimental value. This test is valid, since the experimental value for Bs_0' was only used for calculating the value for A and was not used as a boundary condition. The vibrational formulation of the Hildebrand approximation (Model V) yields a value of 4.90 for Bt_0', whereas the experimental value obtained Bartels and Schuele (1965) is 5.35 ± 0.30, and that by Chang (1965) 5.18 ± 0.09. Since the uncertainty in the volume determination by the x-ray diffraction technique is 0.3 percent, the error in the $P-V$ relation for NaCl resulting from the discrepancy in the calculated and experimental Bt_0' is not significant in comparison with the uncertainty in the volume determination. However, more work is required before this discrepancy is resolved.

6. Comparison Between the P–V Relations for NaCl and MgO

The calculated $P-V$ relation for NaCl may be verified by a comparison of the effect of pressure on the volume of NaCl with that of a material of a known $P-V$ relation. For this purpose, the effect of pressure on the molar volumes of NaCl and MgO was obtained by simultaneous determinations of their volumes by means of the x-ray diffraction method. An agreement in the pressures calculated from the volumes of NaCl and MgO would not only verify the calculated $P-V$ relationship for NaCl, but would also indicate the validity of the internal standard method for the determination of pressure by means of NaCl and the diamond-anvil type x-ray camera.

6.1. Techniques

The measurements reported in this paper were made by means of the diamond-anvil x-ray diffraction camera described by Bassett et al (1967). In this device, an intimate mixture of powders of MgO (ground synthetic single crystal prepared by J. Swica, Ritter-Pfalder Co.) and NaCl (Baker analytical reagent) having particle sizes less than 1 μm was placed between two flat, parallel faces of diamond anvils. One anvil face is approximately 0.3 mm in diameter, and the other is 1.8 mm in diameter. The diamond anvils mounted on the ends of pistons are driven together by a simple screw device. An x-ray beam of filtered molybdenum radiation, 0.07 mm in diameter, is directed through one of the diamonds along the axis of compression to impinge upon the portion of the sample at the center of the area while the sample is under pressure. The x-rays diffracted by the sample emerge through the other diamond and are recorded on a cylindrical film, of which the center of curvature coincides exactly with the sample as in the case of Debye-Scherrer geometry. The x-ray diffraction

TABLE 4. *The results of simultaneous determinations of the effect of pressure on the molar volume of* MgO *and* NaCl *at 25 °C*

P_{MgO} indicates the pressure values obtained on the basis of the P–V relation for MgO calculated from the Murnaghan equation using $Bt_0=1599$ kbar and $Bt_0'=4.52$ (Anderson and Andreatch, 1966). P_{NaCl} indicates the pressure values obtained on the basis of the P–V relation for NaCl according to Model V. The precision for the determination of V/V_0 is ±0.3 percent. Uncertainty in pressure represents that resulting from the uncertainty in V/V_0.

Run No.	MgO		NaCl		$P_{MgO}-P_{NaCl}$
	V/V_0	P_{MgO}	V/V_0	P_{NaCl}	
		kbar		*kbar*	
9 UP 23.....	0.983	28±5	0.911	28±1	0±5
7 UP 28.....	.940	115±6	.764	122±2	−7±6
9 UP 20.....	.928	142±7	.735	154±3	−12±8
9 UP 22.....	.907	196±7	.700	199±3	−3±8
9 UP 18.....	.902	211±8	.692	211±3	0±9
12 UP 3.....	.895	232±8	.679	232±3	0±9
9 UP 19.....	.888	251±8	.671	246±4	5±9
9 UP 21.....	.887	254±8	.676	238±4	16±9
12 UP 5.....	.884	265±9	.662	262±4	3±10
12 UP 4.....	.883	266±9	.664	259±4	7±10
Root Mean Square.....					±7.4

patterns consist of the lines produced by NaCl and MgO both compressed together in the diamond-anvil cell. In addition, the film is marked by the diffraction pattern of a piece of polycrystalline NaCl mounted on the outside surface for the diamond facing the film. This provides a means of determining sample-to-film distance and of correcting for changes in film and instrument dimensions. These corrections are small compared with the scatter of data points.

The diamond-anvil press operates on the Bridgman anvil principle. As a result, pressure in the sample ranges from 1 bar at the edge to a maximum near the center of the anvil faces. The material at the center of the anvil area constitutes the most desirable sample for lattice parameter determinations by x-ray diffraction for three reasons. First, the pressure is highest there. Second, the pressure gradient is smallest, allowing a minimum of pressure range in the x-ray beam. Third, the shearing is least where the pressure gradient is smallest. One way to take advantage of these features of the Bridgman anvil geometry is to direct a narrow x-ray beam through the sample center normal to the anvil faces. In practice, some degree of line broadening due to pressure gradient within the x-ray beam is inevitable.

In the present investigation, the part of the diffraction pattern produced by the portion of the sample at maximum pressure was used. In practice, the outermost part of each broadened line, i.e., the part of the line with the highest 2θ hence the smallest d-value, was measured and then corrected for the line breadth due to causes other than pressure gradient. This correction consists of subtracting the 1-bar line breadth from the outer-edge to outer-edge distance. Lattice parameters calculated from measurements made in this way show less scatter than those based on measurements made from center to center distances of the broadened lines. It is believed that shearing of the sample within a high pressure gradient environment produces preferred orientation within the sample leading to a scatter of data.

A standard Norelco Comparator was used to measure the distance between the diffraction lines. An analysis of the measurements shows that the comparator yields results with a precision of 25 μm. Therefore, a precision of ±0.1 percent has been assigned to the lattice parameter determinations based on the precision of the comparator technique and on the agreement between the values derived from the (200) and (220) diffraction lines. The resulting precision in V/V_0 is thus ±0.3 percent. The results of the present determinations are tabulated in table 4.

6.2. Results of the Simultaneous Measurements of the Volumes of NaCl and MgO

A direct comparison between the effect of pressure on the volume of NaCl and of MgO by means of the x-ray diffraction method using an intimate mixture of the powdered sample of NaCl and MgO should provide a test for (1) the reliability of the calculated P–V relation for NaCl, and (2) the adequacy of the NaCl internal standard method for pressure determinations.

The P–V relation for MgO calculated from the Murnaghan equation, eq (2), using the two parameters $Bt_0=1599$ kbar and $Bt_0'=4.52$ determined by Anderson and Andreatch (1966) for single-crystal MgO at 23 °C was adopted for the present study. The single-crystal values were chosen over the values for polycrystalline samples in view of the fact that the elastic properties of polycrystalline MgO may be sensitive to the chemical additives used for sample preparation as pointed out by Schreiber and Anderson (1968). In comparison with the P–V relation calculated with the Murnaghan equation, the Rose equation, eq (3), with

$$Bt_0Bt_0''=-Bt_0'$$

yields pressure values about 2 percent smaller, and the Birch equation, eq (4), yields pressure values between the Murnaghan and Rose equations. Since

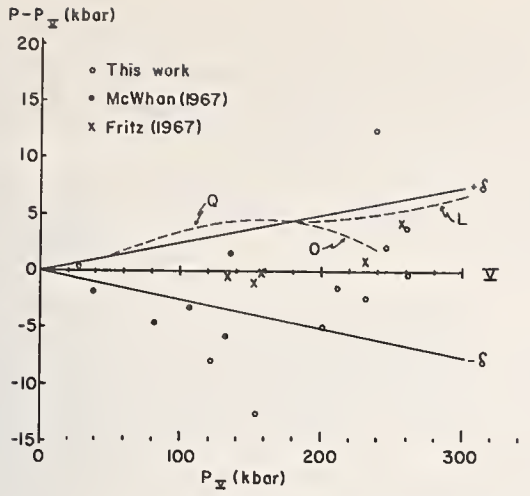

FIGURE 4. *Comparison of pressures calculated from Model V for* NaCl *with those from the Murnaghan equation for* MgO *using the values of* V/V_0 *obtained by simultaneous determinations of the volumes of* NaCl *and* MgO.

Open circles are experimental points obtained in this study, and the solid circles are the data obtained by McWhan (1966). Uncertainty in Model V is shown by $+\delta$ and $-\delta$. The 22 °C isotherm calculated for NaCl from shock-wave data by Fritz et al. (this volume)—curves "*Q*" and "*L*"—has been added for completeness but is not discussed in the text.

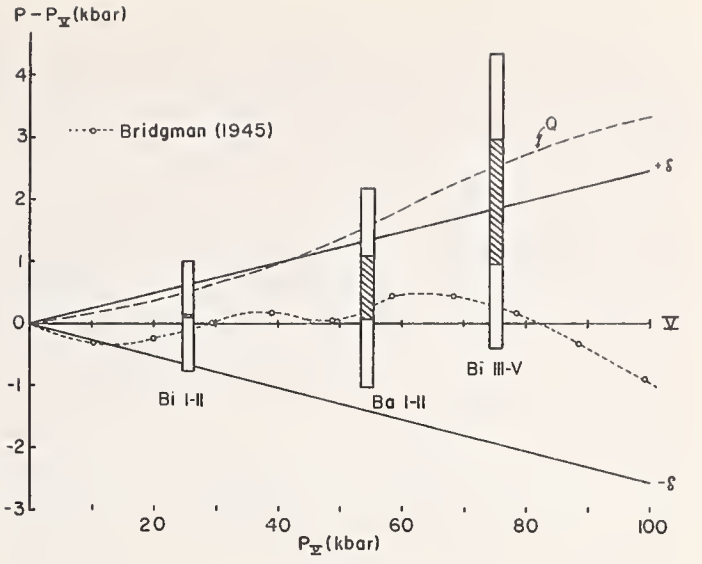

FIGURE 5. *Comparison of pressures calculated for Model V with those from the volumetric determinations by Bridgman (1945), and with those for three fixed points on the absolute pressure scale.*

The pressures corresponding to the phase transformations in Bi and Ba are listed in table 5. The values of P_V (pressure calculated from V/V_0 on the basis of Model V for NaCl) were calculated from the NaCl volumes at the pressure of each phase transformation measured by Jeffery et al. (1967). The cross-hatched portion of the error flags indicates the uncertainty in the determination of the fixed points, while the clear portion indicates the uncertainty due to the uncertainty in the measurement of V/V_0 for NaCl. Curve "*Q*" has been added to show the 22 °C isotherm for NaCl calculated from Hugoniot data (Fritz et al., this volume) which has become available since the writing of the text.

the uncertainty in the determination of V/V_0 leads to uncertainties ranging from ±5 kbar at $V/V_0=1$ to ±9 kbar at $V/V_0=0.87$ (~ 310 kbar), there is no compelling reason to choose one of these equations over another.

The values for P_{MgO} listed in table 4 were obtained from the experimental values for V/V_0 using the P–V relation for MgO. Thus, P_{MgO} is the pressure to which the MgO grains in the NaCl–MgO mixture are subjected. Similarly, the values for P_{NaCl} were obtained from the V/V_0 values using the P–V relation for NaCl according to Model V. Figure 4 compares the values for these two pressures. The results obtained by McWhan (1967) are also shown in figure 4. The mean difference between P_{NaCl} and P_{MgO} has been calculated to be −0.3 kbar from the data of McWhan and the present study, and the root mean square difference is ±6.4 kbar. In view of the uncertainty in the pressure values resulting from that in the V/V_0 measurements, it is concluded that P_{NaCl} is consistent with P_{MgO}.

Reliability of the internal standard method for the determination of pressure in a high-pressure x-ray diffraction device has been questioned, since heterogeneous pressure distribution must exist in a mechanical mixture of two or more materials having different bulk moduli and other properties. If such a heterogeneous pressure distribution exists in the sample, the pressure indicated by the NaCl volume should not be the same as the pressure exerted on a material mixed with NaCl. Since MgO has about seven times as large zero pressure bulk modulus as NaCl and has a far greater shear strength than NaCl, a comparison of the pressure values obtained from the NaCl volume (P_{NaCl}) with those from the MgO volume (P_{MgO}) should provide a test for the internal standard method for pressure determination. As shown in table 4, the root mean square value for ($P_{MgO}-P_{NaCl}$) is ±7.4 kbar, and is well within the experimental uncertainty in the pressure values obtained from the MgO volume. Therefore, the internal standard method appears to be valid.

7. Comparison Between the NaCl Pressure Scale and the Fixed Points

Jeffery et al. (1966) have determined the molar volume of NaCl at pressures corresponding to several of the phase transformations which have been used as fixed points in the 0 to 100 kbar pressure range. These data permit a direct comparison between Model V NaCl scale and the fixed points. Table 5 shows the mean value of V/V_0 obtained from the experiments with increasing and decreasing pressure, the corresponding pressure from Model V, the literature value of the pressure at the phase transformation, and differences in the two pressures. The differences are also graphically shown in figure 5. It can be seen that the difference is small compared to experimental uncertainties in the case of Bi I-II and Ba I-II transformations, and is comparable with the experimental uncertainty in the case of Bi III–V. Figure 5 also shows the volumetric data obtained by Bridgman (1945) which are in agreement with Model V within experimental uncertainty.

In the case of Bi III-V, the discrepancy between the pressure value obtained by Haygarth et al. (1968) by means of the direct single-stage piston-cylinder method and that calculated from the V/V_0 data of Jeffery et al. (1966) using the Model V $P-V$ relation for NaCl may be attributed to the following causes: (1) The Model V $P-V$ relation for NaCl may be in error. However, this is not likely because Model V is in good agreement with the experimental data of Bridgman (1945) up to 100 kbar, and is consistent with the Bt_0 value obtained by the high-precision ultrasonic method; (2) The V/V_0 for NaCl at the phase transformation pressures determined by Jeffery et al. (1966) may be in error because of a heterogeneous pressure distribution in a mixture of NaCl and sample. Because of such an inhomogeniety in pressure distribution, the errors in the measurements may be non-Gaussian, and hence the arithmetic mean of the determinations for V/V_0 of NaCl made during increasing and decreasing pressure might not represent a true value at the transformation; (3) The pressure value determined by Haygarth et al. (1968) may be in error. This may be tested if the compression of NaCl was determined up to 80 kbar at 25 °C by means of the same experimental apparatus as used for their study of Bi III-V. If the compression values for NaCl thus obtained agree with those of Bridgman (1945), which is in turn in agreement with Model V of this study, the discrepancy between the pressure values obtained by Haygarth et al. and by the present study for Bi III-V could be due to the cause (2). On the other hand, if the compression values for NaCl are different from Bridgman's in such a way that the value of Haygarth et al. becomes in agreement with Jeffery et al., then the $P-V$ relation determined by Bridgman and that calculated in this study would be in error. Future studies would hopefully dissolve the discrepancy between the existing results.

8. Summary and Conclusions

On the basis of the discussion presented above, the following conclusions may be made:

(1) The thermal and vibrational formulations of the Hildebrand and Mie-Grüneisen approximations yield the pressure values to within ±1 percent for a given V/V_0 value for NaCl up to 300 kbar at 25 °C. Hence in the harmonic approximation, the $P-V$ relations are insensitive to the specific form chosen for the temperature dependent part of the vibrational energy.

(2) Effect on the pressure values of the anharmonic part of the internal energy is probably small, since the specific form chosen for the potential energy yields the correct value for γ_0. Yet, complete internal consistency is not found as shown by the failure of the theory to yield correct values for A and Bt_0'. However, the effect of these terms on the calculated pressure is small.

TABLE 5. *Comparison between the pressure values calculated from the* P–V *relation for* NaCl *using the* V/V_0 *values obtained by Jeffery et al. (1966) for the phase transformations in* Bi *and* Ba

Phase transformation	[1] NaCl V/V_0	P_{NaCl} Model V	P Direct methods	$P-P_{NaCl}$
		kbar	*kbar*	*kbar*
Bi I–II.....	0.917±0.002	25.4±0.8	[2] 25.5±0.1	0.1
Ba I–II.....	0.855±0.002	54.4±1.1	[3] 55.0±0.5	0.6
Bi III–V.....	0.821±0.002	75.5±1.4	[4] 77.5±1.0	2.0
			[5] 78.2	? 7

[1] Jeffery et al. (1966).
[2] Heydemann (1967).
[3] Haygarth et al. (1967).
[4] Haygarth et al. (1968), extrapolated from high temperature.
[5] Haygarth et al. (1968), 22 °C direct measurement.

(3) The close agreement of the $P-V$ relations obtained in this study with Decker's (1968) revised calculation suggests that the effect of the second nearest neighbor repulsion is small.

(4) The calculated pressures are insensitive to the values of the various parameters used with an exception of Bt_0. Thus a pressure scale based on the relations presented in this study will not require significant revision as more precise values for the parameters become available.

(5) The estimated precision of ±2.5 percent in the calculated pressure is of the same order as the uncertainty in pressure resulting from the uncertainty in the measured value of V/V_0 for NaCl.

(6) The $P-V$ relation based on Models III–VI is in agreement with the fixed points on the absolute pressure scale; with Bridgman's volumetric studies on NaCl to 100 kbar; with the results derived from shock-wave measurements to 260 kbar; and with the $P-V$ relation for MgO which are based on the Murnaghan, Rose, or Birch equations with the parameters determined by means of ultrasonic methods.

(7) The internal standard method for determining pressure using NaCl appears to be valid as shown by the consistency of the pressure values obtained from the compression V/V_0 values for NaCl and MgO.

(8) A NaCl pressure scale based on Model V has been adopted for the experimental studies at the University of Rochester. Model V (the vibrational Hildebrand equation) was selected because the vibrational formulation may be expected to be superior to the thermal formulation, and because, in practice, the Hildebrand equation is easier for calculation. The relation can be conveniently

expressed as:

$$P = 8.4x^{0.2} - 106.2x^{-4/3} - 15.95x^{-3} - 2.64x^{-11/3} + x^{-2/2} \cdot \exp\,(14.050 - 9.292x^{1/3}) \text{ kbar at 25 °C.}$$

On this pressure scale, the B1–B2 phase transformation in NaCl reported by Bassett et al. (1968) occurs at a pressure of

$$301 \pm 4 \text{ kbar } (V/V_0 = 0.643 \pm 0.002)$$

with an additional uncertainty of ±8 kbar due to the uncertainty in the pressure scale.

(9) Significant improvement in the precision of the calculated P–V relation will require improvement in the values of Bt_0 and A. Although the P–V relation is insensitive to the latter, the large uncertainty in this parameter yields a large uncertainty in the pressure. However, a reduction of this uncertainty may be difficult since A depends on the difference between δs and Bs'.

9. Acknowledgments

We are grateful to Leon Thomsen and Orson L. Anderson of the Lamont Geological Observatory, Columbia University, for providing us with their manuscript in advance to its publication; to Daniel L. Decker of the Brigham Young University for providing the results of his revised calculations for the P–V relation of NaCl; and to J. N. Fritz of the Los Alamos Scientific Laboratories for his unpublished data for the compression of NaCl. The present research program has been supported by the National Science Foundation through grants GP–5304 and GA–1430.

10. References

Anderson, O. L., The use of ultrasonic measurements under modest pressure to estimate compression at high pressure, J. Phys. Chem. Solids **27**, 547–565 (1966).

Anderson, O. L., Equation for thermal expansivity in planetary interiors, J. Geophys. Res. **72**, 3661–3668 (1967).

Anderson, O. L., and Andreatch, P. Jr., Pressure derivatives of elastic constants of single crystal magnesium oxide at 23 deg. and −195.8 deg. C., J. Am. Ceram. Soc. **49**, 404–409 (1966).

Bartels, R. A., and Schuele, D. E., Pressure derivatives of the elastic constants of sodium chloride and potassium chloride at 295 deg. K and 195 deg. K., J. Phys. Chem. Solids **26**, 537–550 (1965).

Bassett, W. A., Takahashi, T., and Stook, P. W., X-ray diffraction and optical observations on crystalline solids up to 300 kbar, Rev. Sci. Instr. **38**, 37–42 (1967).

Bassett, W. A., Takahashi, T., Mao, K. K., and Weaver, J. S., Pressure-induced phase transformation in NaCl, J. Appl. Phys. **39**, 319–325 (1968).

Birch, F., The effect of pressure upon the elastic parameters of isotropic solids according to Murnaghan's theory of finite strain, J. Appl. Phys. **9**, 279–288 (1938).

Birch, F., Elasticity and constitution of the earth's interior, J. Geophys. Res. **57**, 227–286 (1952).

Bridgman, P. W., The compression of twenty-one halogen compounds and eleven other simple substances to 100,000 kg/cm², Proc. Am. Acad. Arts Sci. **76**, 1–24 (1945).

Chang, Z. P., Third order elastic constants of sodium chloride and potassium chloride single crystals, Phys. Rev. **A140**, 1788–1799 (1965).

Chang, Z. P., and Barsch, G. R., Nonlinear pressure dependence of elastic constants and fourth-order elastic constants of cesium halides, Phys. Rev. Letters **19**, 1381–1382 (1967).

Christian, R. H., The equation of state of alkali halides at high pressure, Univ. Calif. Radiation Lab. Report 4900, 1–89 (1957).

Collins, J. G., and White, G. K., in C. J. Gorter, ed., Progress in Low Temperature Physics, Vol. **4**, 450–479 (North Holland Publishing, Amsterdam, 1964).

Decker, D. L., Equation of state of NaCl and its use as a pressure gauge in high-pressure research, J. Appl. Phys. **36**, 157–161 (1965).

Decker, D. L., Equation of state of sodium chloride, J. Appl. Phys. **37**, 5012–5014 (1966).

Decker, D. L., Personal communication (1968).

Fritz, J., Personal communication (1967). *See also:* McQueen (1967).

Fumi, F. G., and Tosi, M. P., On the Mie-Gruneisen and Hildebrand approximations to the equation of state of cubic solids, J. Phys. Chem. Solids **23**, 395–404 (1962).

Haussuhl, S., Thermo-elastische Konstanten der Alkalihalogenide vom NaCl–Typ, Zeit. Physik **159**, 223–229 (1960).

Haygarth, J. C., Getting, I. C., and Kennedy, G. C., Determination of the pressure of the Barium I–II transition with single-stage piston-cylinder apparatus, J. Appl. Phys. **38**, 4557–4564 (1967).

Haygarth, J. C., Ludemann, H. D., Getting, I. C., and Kennedy, G. C., The upper bismuth pressure calibration point, presented at this Symposium.

Heydemann, P. L. M., The Bi I–II transition pressure measured with a dead weight piston gauge, J. Appl. Phys. **38**, 2640–2644 (1967).

Jeffery, R. N., Barnett, J. D., Vanfleet, H. B., and Hall, H. T., Pressure calibration to 100 kbar based on the compression of NaCl, J. Appl. Phys. **37**, 3172–3180 (1966).

Leibfried, G., and Ludwig, W., Theory of anharmonic effects in crystals, Solid State Physics **12** (Academic Press, New York, 1961).

Mayer, J. E., Van der Waals potential in the alkali halides, J. Chem. Phys. **1**, 270 (1933).

McQueen, R. G., Jamieson, J. C., and Marsh, S. P., Shock wave compression and x-ray studies of titanium dioxide, Science **155**, 1401–1404 (1967).

McWhan, D. B., Linear compression of α-quartz to 150 kbar, J. Appl. Phys. **38**, 347–352 (1967).

Murnaghan, F. D., The compressibility of media under extreme pressures, Proc. Nat. Acad. Sci. **30**, 244–247 (1944).

Perez-Albuerne, E. A., and Drickamer, H. G., Effect of high pressures on the compressibilities of seven crystals having the NaCl or CsCl structure, J. Chem, Phys. **43**, 1381–1387 (1965).

Robie, R. A., et al., in S. P. Clark, ed., Handbook of Physical Constants, Geol. Soc. Am. Mem. **97**, New York (1966).

Rose, M. F., Higher order elastic constants and the equation of state of F. C. C. metals, Phys. Stat. Solid **21**, 235 (1967).

Schreiber, E., and Anderson, O. L., Revised data on polycrystalline magnesium oxide, J. Geophys. Res. **73**, 2837–2838 (1968).

Slagle, O. D., and McKinstry, H. A., Temperature dependence of the elastic constants of the alkali halides. I. NaCl, KCl, and KBr, J. Appl. Phys. **38**, 437–446 (1967).

Thomsen, L., and Anderson, O. L., Consistency in the high-temperature equation of state of solids (in press) J. Geophys. Res.

Tosi, M. P., Cohesion of ionic solids in the Born model, in F. Seitz and D. Turnbull, eds., Solid State Physics **16**, 1–120 (Academic Press, New York, 1964).

Yates, B., and Panter, C. H., Thermal expansion of alkali halides at low temperatures, Proc. Phys. Soc. (London) **80**, 373–382 (1962).

385-762 O - 71 - 14

The Hugoniot Equation of State of Sodium Chloride in the Sodium Chloride Structure*

J. N. Fritz, S. P. Marsh, W. J. Carter, and R. G. McQueen

University of California, Los Alamos Scientific Laboratory, Los Alamos, New Mexico 87544

The Hugoniot equation of state of NaCl has been obtained by measuring the shock velocity through NaCl on copper and 2024 aluminum base plates. Shock velocities through the base plates and standard impedance-matching were used to obtain the Hugoniot curves for both single-crystal (in various orientations) and pressed-powder samples. The smooth behavior of the resulting shock locus up to 230 kbar indicates that NaCl exists in the sodium chloride structure up to this pressure. In the shock-particle velocity plane the best linear fit to the data reported here is u_s (km/s) $= (3.528 \pm .012) + (1.343 \pm .009) u_p$. A quadratic fit, which gives a large weight to the measured bulk sound speed in NaCl, is $u_s = 3.403 + 1.5422\, u_p - 0.07345\, u_p^2$. Isotherms at 293 K, using different forms for the Grüneisen parameter and a simple Debye model for the specific heat, are calculated from the Hugoniots and are presented here. They should prove useful when NaCl is used as an internal standard in high-pressure x-ray devices.

1. Introduction

Since Jamieson [1][1] first used NaCl as an internal pressure standard in his high-pressure x-ray apparatus, it has been a serious candidate for a pressure standard in high-pressure x-ray work. Decker [2] has advocated the use of NaCl as a standard. His proposal was based on a Born-Mayer equation of state. Parameters were fixed by the initial density and sound speed of NaCl at zero pressure and he achieved a prediction of the curvature of the P–V isotherm, which can be converted in terms of variables familiar to workers in the dynamic-pressure field to a prediction of the slope of the shock velocity versus particle velocity Hugoniot. His results were supported by the then existing shock-wave data. An increase of 1.3 percent in the value of the sound speed he used in his work would bring his isotherm into agreement with the result of the present report.

Objections have been raised [3, 4, 5] to using NaCl as a standard because of the possibility of the transition to the CsCl structure at a pressure as low as 20 kbar. Such a low-pressure transition would unacceptably complicate the use of NaCl as a continuous pressure standard. Others [6, 7, 8, 9] have found no evidence for a transition as low in pressure as this. From the work of Jamieson [9, 10] on the solution salts, $Na_xK_{1-x}Cl$, one can conclude that the B1 to B2 transition must be considerably above 130 kbar in the pure end member, NaCl. Finally, Bassett et al. [11] have found and reversed the B1 to B2 transition in NaCl at approximately 300 kbar at room temperature. It would seem that whatever the remaining phenomena are at 20 kbar, it does not involve the B1 to B2 transition, and that NaCl will remain in the B1 structure to high and useful pressures.

Perez-Albuerne and Drickamer [8] have compared NaCl by x-ray techniques with Ag and Mo. If the compression curves of Ag and Mo are known, this would determine a NaCl isotherm. Using older shock wave data [12], results were obtained which, because of the individual scatter in a data point, were used only to verify the calculation of an isotherm from a particular form of a Born-Mayer treatment. Their calculated isotherm is in agreement with the isotherm we report as well as that of Bridgman [6].

Direct shock-particle velocity data on NaCl could not be obtained because of the impracticality of fabricating the assemblies required for our shock-wave techniques. Hence we have employed the shock-wave impedance match technique using 2024 aluminum base plates as the standard. In this way, NaCl becomes a secondary standard, dependent on the Hugoniot and extended equation of state of 2024 aluminum. If the 2024 aluminum Hugoniot is accepted as known, a shock-locus for NaCl is obtained that is felt to be accurate to 1 percent in pressure. Subsequent modifications, if any, of the primary standard may be easily translated to a new Hugoniot locus for NaCl. As always, the largest uncertainty in an isothermal curve derived from shock-wave data is related to the choice of the Grüneisen gamma used to reduce the Hugoniot to an isotherm. Several functions of volume have been used for $\gamma(V)$ and the resultant isotherms reported.

2. Experimental Methods and Results

The impedance matching technique used for obtaining the shock locus for NaCl has already been adequately described [12]. Single crystals in the (100), (110), and (111) orientations as well as some pressed powder samples were shock-loaded on base plates of 2024 aluminum, copper, and 921–T aluminum. The data taken on 921–T aluminum base plates have been discarded for reasons described

*Work done under the auspices of the U.S. Atomic Energy Commission.

[1] Figures in brackets indicate the literature references at the end of this paper.

Paper presented at the Symposium on Accurate Characterization of the High-Pressure Environment, held at the National Bureau of Standards, Gaithersburg, Md., October 14–18, 1968.

TABLE 1. NaCl *Hugoniot data in the B1 phase*

u_s	u_s std.	u_p	P	ρ
km/s	*km/s*	*km/s*	*kbar*	*g/cm³*
100 orientation				
4.03	5.67	0.33	29	2.358
4.10	5.75	0.40	35	2.397
4.12	5.79	0.44	39	2.423
4.31	5.94	0.58	54	2.502
4.36	5.96	0.60	57	2.510
4.59	6.17	0.79	78	2.613
4.59	6.19	0.81	80	2.625
4.95	6.45	1.03	111	2.735
4.89	6.45	1.04	110	2.748
4.99	4.96*	1.07	116	2.755
4.99	6.50	1.09	117	2.766
4.99	6.54	1.12	121	2.789
5.01	6.55	1.13	122	2.793
5.51	6.92	1.44	172	2.932
5.43	6.91	1.44	170	2.949
5.47	6.92	1.45	171	2.942
5.47**	6.92	1.45	171	2.941
5.59	5.41*	1.53	184	2.977
5.67	7.07	1.57	193	2.992
5.84	5.58*	1.70	215	3.052
5.94	7.36	1.82	234	3.121
5.96	7.37	1.84	237	3.129
6.12	7.47	1.92	254	3.151
6.12	7.47	1.92	254	3.152
6.15	7.51	1.95	259	3.166
6.15	7.51	1.95	259	3.167
6.13	7.52	1.96	260	3.185
6.20	7.54	1.97	264	3.170
111 Orientation				
4.08	5.75	0.40	35	2.399
4.32	5.96	0.60	56	2.515
4.31	6.00	0.63	59	2.538
4.59	6.19	0.81	80	2.626
4.59	6.20	0.82	81	2.632
4.96	6.44	1.03	110	2.729
4.98	4.96*	1.07	115	2.757
5.01	6.50	1.08	117	2.760
4.99	6.50	1.08	117	2.765
4.99	6.53	1.11	119	2.780
5.03	6.55	1.13	123	2.787
5.02	6.56	1.13	123	2.795
5.45	6.92	1.45	171	2.947
5.47	6.92	1.45	171	2.944
5.57	5.41*	1.53	184	2.981

*Copper base plates. The rest are 2024 aluminum.
**This sample had a (110) orientation.

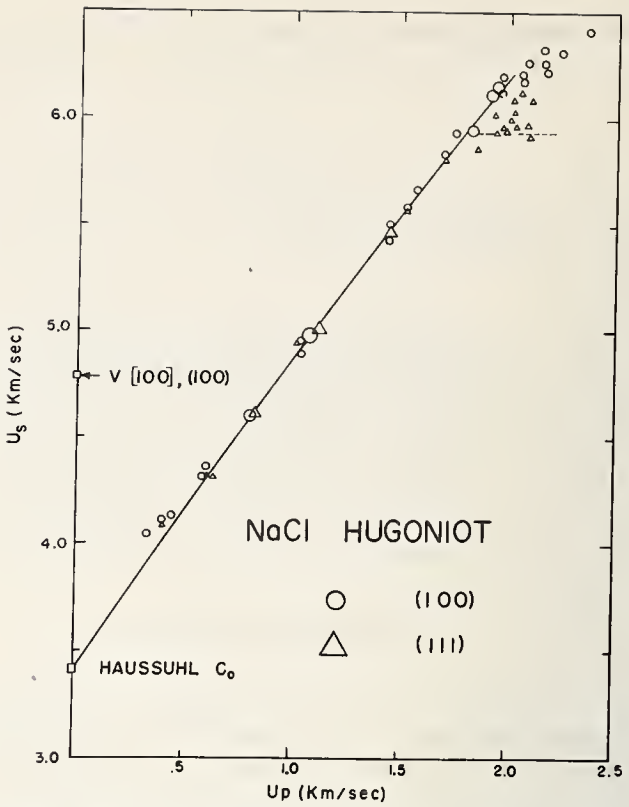

FIGURE 1. *The shock velocity-particle velocity Hugoniot of* NaCl. The elastic wave velocities were obtained from data in reference (14). The larger symbols indicate multiple data points.

elsewhere [13]. In this report only those data whose final shocked state is believed to remain in the B1 structure are reported. The majority of the data were taken on 2024 aluminum with a few points taken on copper base plates as a consistency check. The data necessary for impedance calculations for the primary standards are:

2024 Aluminum: $\rho_0 = 2.785$ g/cm³,
$u_s = 5.328 + 1.338 u_p$ km/s
$(\partial E/\partial P)_V = 0.19$ cm³/g

Copper: $\rho_0 = 8.93$ g/cm³,
$u_s = 3.940 + 1.489 u_p$ km/s
$(\partial E/\partial P)_V = 0.057$ cm³/g

A constant $(\partial E/\partial P)_V$ was used to generate the release isentropes necessary for the impedance match calculations. The data are reported in table 1 and illustrated in figure 1. In addition to the tabulated data, data points showing the onset of the B1 to B2 (presumably) phase transition are included in the figure for both (100) and (111) orientations.

Both linear and quadratic terms in u_p were used to fit these data. In the absence of other information, there would be no point in going to an order higher than linear to fit the data; however, consideration must be given to the measured sound speeds in NaCl. In fact, the c_0 coefficient in our quadratic fit was forced to agree with the sound speed ob-

tained from Haussuhl's [14] measurement of the elastic constants of single-crystal NaCl. The least squares analysis of the data gives r.m.s. deviation of $\Delta u_s = \pm 0.056$ km/s or less over the range of the data. Within the range of the data, the quadratic and linear fits agree to within this Δu_s except for the lowest four data points. The low shock pressures for these four points (< 40 kbar) were produced by relatively complicated driver arrangements that depend on impedance mismatches. It is not impossible that overtaking waves could influence these measurements. The shock velocities at these pressures are notably below some of the single crystal longitudinal velocities. Premature closure of flash gaps could give rise to the sort of discrepancy we see here, but since a low-pressure cannon shot has indicated that the Hugoniot elastic limit of NaCl is only about 2/3 of a kilobar, there is not sufficient motion imparted to a shim to close any flash gaps used here. Gap closure corrections are more critical in this pressure regime and conceivably could cause errors in shock wave velocity, even of the size to explain these low pressure shots. In any event, forcing the Hugoniot through the sound speed prevents these points from appreciably influencing the fit to the data. The large bulk of the data at higher pressure with its linearity fixes the next two terms of the series. Some evidence that these lower points influence the slope in the right direction is afforded by Bartels and Schuele's [15] measurement of $(\partial B_S/\partial P)_T = 5.27$.

From the thermodynamic identities

$$s_0 = [1 + (\partial B_S/\partial P)_S]/4$$

and

$$(\partial B_S/\partial P)_S = (\partial B_S/\partial P)_T + \gamma (T/B_S)(\partial B_S/\partial T)_P$$

and Haussuhl's [14] value for $(\partial B_S/\partial T)_P$ of -0.000117 Mbar/°K, we obtain $s_0 = 1.513$. This is in satisfactory agreement with our fitted slope of 1.542. Although a linear fit represents the shock-wave data adequately, emphasis should be placed on the ultrasonic measurements in the low pressure region. The quadratic fit

$$u_s = 3.403 + 1.5422 u_p - 0.07345 u_p^2 \text{ (km/s)} \qquad (1)$$

represents the ultrasonic data in the low pressure region and the shock-wave data in the high-pressure region. The number of significant figures quoted in the above equation gives the exact form of the Hugoniot used in a subsequent reduction to an isotherm. The r.m.s. spread in u_s about the fitted values is ± 0.05 km/s. Our data for NaCl in the B1 phase are in agreement with the data of Larson, et al. [3], to within the quoted error. Unpublished data of Hauver and Melani [16] are in agreement with ours in the vicinity of $u_p = 1$ km/s and are 0.07 km/s higher than ours near $u_p = 2$ km/s. However, their data were based on the old 2024 aluminum standard.

TABLE 2. *Thermodynamic parameters for* NaCl

Quantity	Value	Reference
M	58.443 g/mole	[17]
N	6.02252×10^{23}	
a_0	5.6393 Å at 22 °C	[19]
$\beta = \frac{1}{V}\left(\frac{\partial V}{\partial T}\right)_P$	1.195×10^{-4}/K at 20 °C	[19]
B_s	0.2505 Mbar at 22 °C	[14]
C_p	12.05 cal/mole−K at 20 °C	[20, 21]

Derived Values at 293 K

$\rho = 2.1645$ g/cm^3
$B_s = 0.2507$ Mbar
$C_p = 0.8627 \times 10^7$ ergs/g−K
$c_0 = 3.403 \times 10^5$ cm/s
$\gamma = \beta c_0^2/C_p = 1.6044$
$\gamma\beta T = 0.0562$
$Cv = 0.8168 \times 10^7$ ergs/g−K
$B_T = 0.2374$ Mbar
$K_T = 4.213$ Mbar^{-1}
$(\partial P/\partial T)_V = 0.0284$ kbar/K
$(\partial E/\partial P)_V = 0.2880$ cm^3
$3nk = 0.8535 \times 10^7$ ergs/g−K
$C_V/3nk = 0.9570$
$\theta_D/T = 0.9420$
$\theta_D = 276$ K

Revision of the necessary impedance match calculations will bring the results into better agreement.

3. Reduction of the Hugoniot to a 293 K Isotherm

Details of this calculation have been discussed earlier [13]. The auxiliary information needed for this reduction is given in table 2. Original references should be consulted for the accuracy of these numbers. The table gives the exact input used in our calculations. The particular numerical code used integrates the equation

$$dT_H = -T_H \frac{\gamma dV}{V} + \frac{(V_0 - V)dP_H + P_H dV}{2C_V} \qquad (2)$$

for the temperature along the Hugoniot. A Debye expression,

$$E_T = 3nkT D_3(\theta(V)/T) \qquad (3)$$

$$D_3(x) = \frac{3}{x^2}\int_0^x \frac{z^3 dz}{e^z - 1} \qquad (4)$$

$$\gamma = -d \ln \theta / d \ln V \qquad (5)$$

TABLE 3. *The* $(\partial E/\partial P)_V$ *constant, 293 °K* NaCl *isotherm and its antecedent Hugoniot*

P	Hugoniot ρ_H	T_H	Isotherm ρ	V/V_0	a/a_0	P	Hugoniot ρ_H	T_H	Isotherm ρ	V/V_0	a/a_0
kbar	*g/cm³*	*K*	*g/cm³*			125	2.793	618	2.828	.7654	.9147
0	2.1645	293	2.1645	1.0000	1.0000	130	2.810	637	2.847	.7603	.9127
5	2.206	302	2.208	.9803	.9934	135	2.827	657	2.865	.7555	.9108
10	2.245	311	2.248	.9629	.9875	140	2.843	678	2.883	.7508	.9089
15	2.281	319	2.286	.9469	.9820	145	2.859	699	2.901	.7461	.9070
20	2.314	328	2.321	.9326	.9770	150	2.875	721	2.918	.7418	.9052
25	2.347	336	2.355	.9191	.9723	155	2.891	743	2.935	.7375	.9035
30	2.377	345	2.386	.9072	.9680	160	2.906	765	2.952	.7332	.9017
35	2.406	355	2.417	.8955	.9639	165	2.921	788	2.969	.7290	.9000
40	2.434	365	2.446	.8849	.9601	170	2.936	811	2.986	.7249	.8983
45	2.461	375	2.473	.8753	.9566	175	2.951	835	3.002	.7210	.8967
50	2.486	386	2.500	.8658	.9531	180	2.965	859	3.019	.7170	.8950
55	2.511	398	2.526	.8569	.9498	185	2.980	884	3.035	.7132	.8934
60	2.535	410	2.552	.8482	.9466	190	2.994	909	3.051	.7094	.8919
65	2.558	423	2.576	.8403	.9436	195	3.008	934	3.067	.7057	.8903
70	2.581	436	2.600	.8325	.9407	200	3.022	960	3.082	.7023	.8889
75	2.602	450	2.623	.8252	.9380	205	3.035	986	3.098	.6987	.8873
80	2.624	464	2.645	.8183	.9354	210	3.049	1013	3.113	.6953	.8859
85	2.644	479	2.667	.8116	.9328	215	3.062	1040	3.129	.6918	.8844
90	2.664	494	2.689	.8049	.9302	220	3.075	1067	3.144	.6885	.8830
95	2.684	510	2.710	.7987	.9278	225	3.089	1094	3.159	.6852	.8816
100	2.703	527	2.731	.7926	.9254	230	3.102	1123	3.174	.6819	.8802
105	2.722	544	2.751	.7868	.9232	235	3.114	1151	3.189	.6787	.8788
110	2.740	562	2.771	.7811	.9210	240	3.127	1180	3.204	.6756	.8774
115	2.758	580	2.790	.7758	.9189	245	3.140	1209	3.218	.6726	.8762
120	2.776	599	2.809	.7706	.9168	250	3.152	1238	3.233	.6695	.8748

is used for the thermal part of the energy.

With a γ that depends only on volume, the appropriate fractional thermal energy and corresponding thermal pressure may be subtracted from the Hugoniot to yield the desired isotherm. The choice of Debye theta at zero pressure and 293 K was dictated by the value of C_V at these conditions, since this is the important quantity in the integration of (2). Since the numerical value for $E(P=0, T=273\ \mathrm{K})-E(0, 0)$ predicted by this model ($+1.76\times10^9$ ergs/g) agrees with the value obtained by fitting $C_P(T)$ ($\Delta E=1.77\times10^9$, JANAF Tables [21]) we have some evidence that we have an overall fit for $C_V(T)$ at the lower T region as well.

Probably the largest uncertainty in transforming a Hugoniot to an isotherm comes from ignorance about the way the Gruneisen gamma behaves at high pressures and temperatures. In the few cases where its high-pressure behavior has been measured, the assumption that $(\partial E/\partial P)_V$ is constant has been adequate to represent the data within the experimental precision, but other forms for $\gamma(V)$ are not excluded. We have used this assumption to calculate our "base room temperature isotherm." The results, finely spaced for more convenient usage, are given in table 3.

It is of interest to see what effect varying the parameters that went into the calculation will have on the calculated isotherm. The equation

$$\gamma(V)=\frac{t-2}{3}-\frac{1}{2}\frac{d\ \ln\{d[P_K(V)V^{2t/3}]/dV\}}{d\ \ln V} \qquad (6)$$

is a generalization of the Slater, Dugdale-MacDonald, and Free Volume relations between $\gamma(V)$ and $P_K(V)$ which has been used by Grover et al. [22] in their comparison of static and dynamic high-pressure data on the alkali metals. Values of t of 0, 1, and 2 correspond to the above theories, but the value of t can be chosen to give the proper thermodynamic value of γ at the Hugoniot centering point. Further, if the expression for $\gamma(V)$ obtained from differences between the Hugoniot curve and the zero Kelvin curve is equated with the above

expression for γ, the Hugoniot centering point is taken to be at zero pressure and temperature, and a linear u_s-u_p Hugoniot is used, an integro-differential equation for $P_K(V)$ is obtained. When solved this gives not only $P_K(V)$, but also a $\gamma(\eta)$, where $\eta = 1 - \rho_0 V$, that parametrically depends only on t and the slope, s, of the u_s-u_p Hugoniot. At zero compression, this reduces to the relation

$$\gamma_0 = 2s - (t+2)/3 \qquad (7)$$

between γ_0, t, and s. A linear u_s-u_p Hugoniot for NaCl that passes through most of the shock-wave data and the measured sound speed has $s = 1.429$. With the correct γ_0, (7) yields $t = 1.761$. The $\gamma(\eta)$ obtained in this fashion will not significantly differ from one where the precise experimental Hugoniot is used as input and where the difference between the temperature of the Hugoniot centering point and zero temperature is taken into account. The resulting $\gamma(\eta)$, as well as others, are shown in figure 2. This $\gamma(\eta)$ may be accurately represented by a polynominal in η for $0 < \eta < 0.5$.

$$\gamma = 1.6044 - 0.9955\,\eta + 1.4961\,\eta^2 - 1.9284\,\eta^3 \qquad (8)$$

This representation, along with the more precise Hugoniot fit, was then used in the numerical code that calculates the isotherm. The resultant curve, labelled (1), is shown in figure 3. An ionic solid may not be the best place to use such a theory for $\gamma(\eta)$, but it does offer an alternate $\gamma(\eta)$ behavior to compare with the base isotherm.

Another $\gamma(\eta)$ behavior is offered by Decker [2]. A term linear in the change in lattice parameter was added to γ_0 to give the best fit to high-temperature (i.e., a slight increase in volume) thermal expansion data. This should give the right initial slope of $\gamma(\eta)$ but as Decker says, it is uncertain whether this volume dependence remains accurate to the large volume changes obtained in the shock wave data. This $\gamma(\eta)$ is given by

$$\gamma = 1.6044 + 2.55\ ((1-\eta)^{1/3} - 1). \qquad (9)$$

Decker actually used the value $\gamma_0 = 1.59$. A poly-

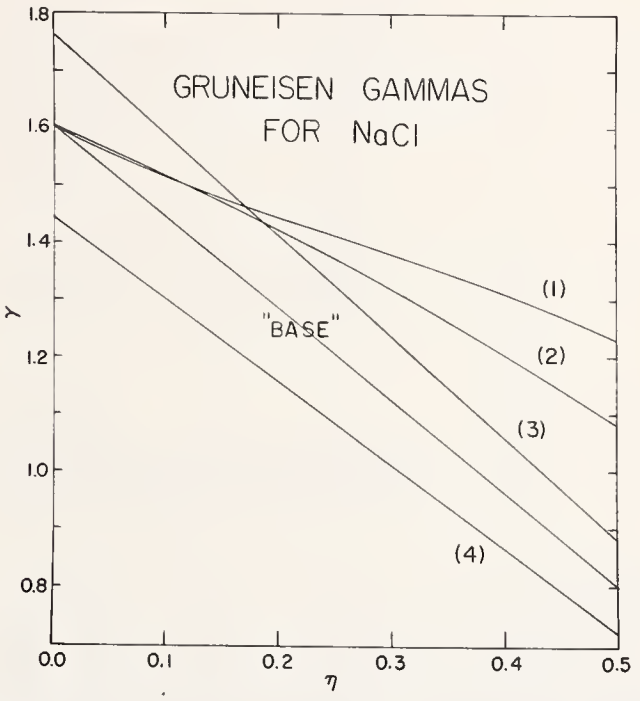

FIGURE 2. *The various functions used for the Grüneisen parameter.*

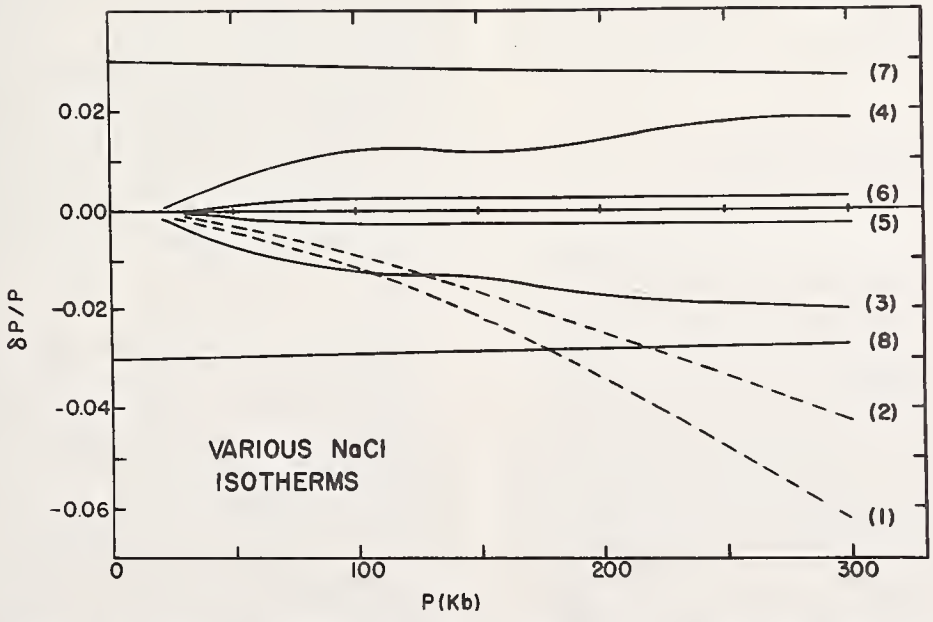

FIGURE 3. *Pressure variations in the base isotherm due to various changes in the input data.*

In this figure we show the fractional change in pressure from the base isotherm,

$$\delta P/P = P(\text{new parameters})/P\,(\text{base}) - 1,$$

at a given density. The actual abcissa is the pressure of the base isotherm at this density.

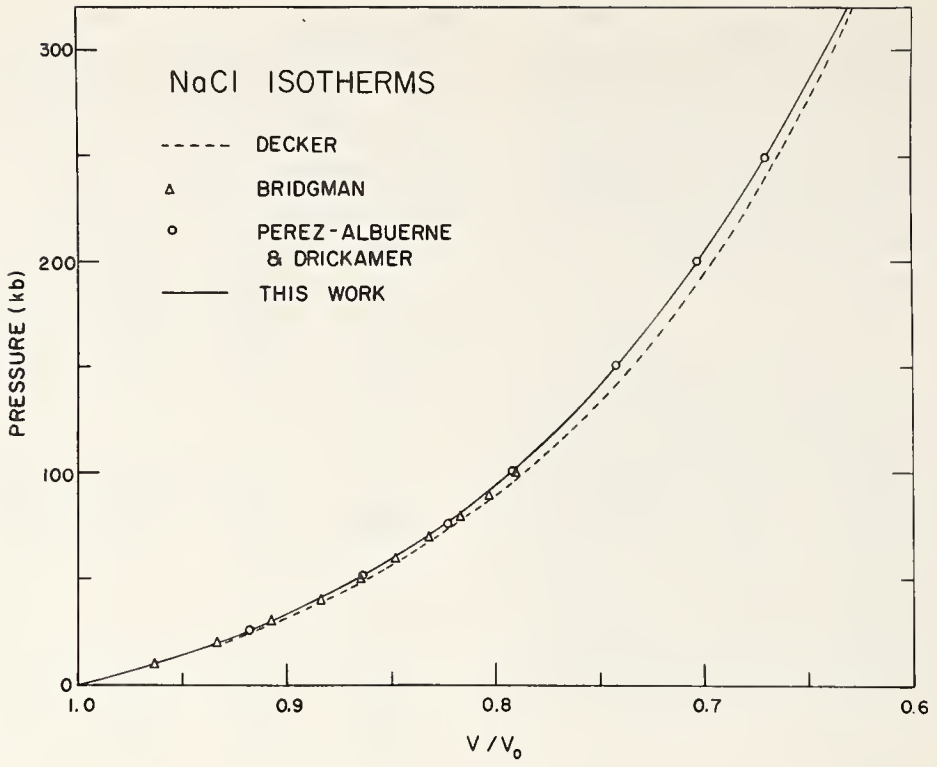

FIGURE 4. NaCl *isotherms.*

The solid line shows the isotherm calculated from the quadratic fit to the Hugoniot in the $u_s - u_s$ plane. The isotherm from the linear fit is parallel to Decker's isotherm and roughly maintains a constant pressure offset from Decker's isotherm from 200 to 320 kbar.

nominal fit to (9) was used to calculate isotherm (2) in figure 3.

Isotherms (3) and (4) show the effect of varying γ_0 by plus and minus 10%. For these isotherms $(\partial E/\partial P)_V$ was kept constant. Isotherms (5) and (6) show the effect of scaling C_V by plus and minus 10%. This was done by changing the value of 3nk in the calculations. Isotherms (7) and (8) were obtained by adding and subtracting, respectively, 0.05 km/s to c_0 in the input Hugoniot.

4. Comparison With Other Isothermal Data and Discussion

The "base isotherm" is shown in figure 4 along with Decker's, that calculated by Perez-Albuerne and Drickamer, and Bridgman's data. The agreement between our isotherm and that of Perez-Albuerne and Drickamer's is well within the experimental error of both methods. The latter isotherm is slightly lower (1 to 2 kbar) than ours in the pressure range from 40 to 100 kbar. Bridgman's isotherm is still lower by again this pressure difference in this region. The lower portion of our isotherm is chiefly determined by using Haussühl's sound speed. The initial slope of the $u_s - u_p$ Hugoniot could be changed from 1.542 to 1.512 to agree with Bartels and Schuele, but this would decrease the computed isotherm by only ¼ kbar at 40 kbar. At 60 kbar, the shock-wave measurements are slightly above the fit used. Above this, where the shock-wave measurements should be relatively free of elastic-plastic flow effects because of the low Hugoniot elastic limit of NaCl, the fit and the data are consistent. Decker's isotherm falls below ours, with the spread in pressure being about 5 kbar at 100 kbar, 12 kbar at 200 kbar, and remaining approximately the same thereafter. As he noted, Decker's isotherm is most sensitive to the value of the bulk modulus used. A choice of bulk modulus equivalent to the sound speed we have used would bring the two isotherms into essential agreement. It is perhaps worthwhile to emphasize at this point that at and above 80 kbar, and to a lesser extent at 60 kbar, our isotherm does not particularly depend on the precise value of the bulk modulus used, because the shock-wave data then determines the Hugoniot used to calculate the isotherms.

Jeffrey et al. [23] have given the pressures of various phase transitions by determining a/a_0 of NaCl used as an internal standard. Using their values of a/a_0 and Decker's pressure scale they obtain 24.8 ± 0.8 kbar for the Bi I–II transition, 53.3 ± 1.2 kbar for the Ba I–II transition, and 73.8 ± 1.3 kbar for the Bi III–V transition. Using our isotherm and their a/a_0 values, these numbers become 25.8 ± 8, 56.3 ± 1.2, and 78.2 ± 1.3. Bridgman's volume scale as reported by Jeffrey et al., has 25.4, 58.8, and 88 kbar for these transitions. McWhan [24] also measured the Bi III–V transition with NaCl as an internal standard. He took his values on the increasing pressure cycle, whereas

Jeffrey et al. averaged increasing and decreasing pressure readings. McWhan's $V/V_0 = 0.816 \pm .006$ corresponds to 81.7 ± 4.5 kbar on our isotherm. The Birch-Murnaghan equation and the input parameters as used by McWhan for his pressure value is consistent with our isotherm up to a pressure of 100 kbar. Beyond that, the Birch-Murnaghan value for the pressure increases more rapidly than our isotherm by 6 kbar at 150 kbar and 13 kbar at 200 kbar.

The highest measured pressure on our Hugoniot for the B1 phase is 264 kbar. The offset down to the isotherm is about 16 kbar at this volume. Our isotherm above 250 kbar is then a consequence of an extrapolation of the Hugoniot data. The downward curvature of the quadratic $u_s - u_p$ fit is a relic of trying to fit the ultrasonic data and shock data smoothly together in the lower pressure region and probably should not be there. Both the data alone and calculations of a $u_s - u_p$ curve from a Born-Mayer form for the interaction potential indicate a linear behavior in this region. Accordingly we have listed in table 4 the isotherm above 200 kbar that obtains from the best linear fit to our data. In this calculation we have again used constant $(\partial E/\partial P)_V$. From 200 to 230 kbar this is essentially identical to the isotherm resulting from the quadratic fit. Above 230 kbar it becomes stiffer.

A clear indication of a phase transition is exhibited by the higher pressure data points plotted in figure 1. Although (111) and (100) oriented crystals have indistinguishable Hugoniots at lower pressures, they clearly separate in the region where the phase transition occurs. Since a uniaxial compression of 50 percent in the (111) direction produces the B2 structure from the B1 structure, one can expect that a shock wave in this direction will see a lower energy barrier in the way of this transition. Indeed, the (111) data are lower. If a shock wave is not complicated by relaxation effects and deviatoric stresses, a phase transition with a sufficient ΔV and an appropriate slope in the P–T plane appears as a horizontal plateau in the u_s-u_p plane. This is because the flash gaps measure the shock velocity of the first wave in a two-wave structure, which remains constant as we increase the driving pressure, and the particle velocity, measured indirectly by measuring the shock velocity of the standard, is increasing with the driving pressure. Time-dependent effects clearly influence the NaCl data in this region, but the onset of a phase transition is beyond question. At these pressures, even though a considerable time may be required for a phase transition to go to completion, any part of the ΔV of the reaction manifests itself immediately as a shock velocity less than would be expected from a smooth continuation of the initial phase. A plateau has been drawn somewhat arbitrarily through the (111) data. Although the data scatter upwards from this line, the clustering toward the bottom is sufficiently sharp to give some credence to the plateau as drawn.

TABLE 4. *The* NaCl *isotherm above 200 kbar using the linear* u_s-u_p *fit*

P	Hugoniot ρ_H	T_H	Isotherm ρ	V/V_0	a/a_0
kbar	*g/cm³*	*K*	*g/cm³*		
200	3.023	950	3.081	0.7025	0.8890
205	3.036	977	3.096	.6991	.8875
210	3.050	1004	3.111	.6958	.8861
215	3.063	1031	3.126	.6924	.8847
220	3.075	1059	3.140	.6893	.8834
225	3.088	1087	3.154	.6863	.8821
230	3.100	1116	3.168	.6832	.8808
235	3.113	1145	3.182	.6802	.8795
240	3.125	1174	3.196	.6773	.8782
245	3.137	1204	3.210	.6743	.8769
250	3.148	1234	3.223	.6716	.8757
255	3.160	1264	3.236	.6689	.8745
260	3.171	1295	3.249	.6662	.8734
265	3.183	1326	3.262	.6635	.8722
270	3.194	1357	3.275	.6609	.8711
275	3.205	1389	3.288	.6583	.8699
280	3.216	1421	3.300	.6559	.8689
285	3.227	1454	3.313	.6533	.8677
290	3.238	1487	3.325	.6510	.8667
295	3.248	1520	3.337	.6486	.8656
300	3.259	1553	3.349	.6463	.8646
305	3.269	1587	3.361	.6440	.8636
310	3.279	1621	3.373	.6417	.8625
315	3.289	1656	3.384	.6396	.8616
320	3.299	1690	3.396	.6374	.8606

The behavior of the (100) data is different; it tends to drift slowly upward in a manner which one might expect from a reaction whose relaxation time is comparable to the time it takes a shock wave to traverse the sample. The (111) plateau intersects both the linear and quadratic fits to the B1 phase at $u_s = 5.94$ and $u_p = 1.80$ km/s. The pressure on the Hugoniot is 231 kbar, the density is 3.105 g/cm³ and the temperature is between 1120 and 1130 K. This number should provide an upper bound to the actual transition pressure.

Bassett, et al. [11], have observed the B1–B2 transition at a $V/V_0 = 0.643 \pm 0.002$. Using our isotherm from the extrapolated linear Hugoniot, we find the pressure of this transition as 307 ± 5 kbar. The extrapolation of the quadratic fit would have yielded 295 ± 5 kbar. This should set the upper limit of pressure for the use of NaCl in the B1 phase as an internal pressure standard at room temperature.

5. Acknowledgments

The authors would like to thank G. E. Hauver and A. Melani for the opportunity to look at their un-

published data and D. L. Decker for sending us his tabulated pressure-volume isotherms.

6. References

[1] Jamieson, J. C., Science **139**, 1291 (1963).
[2] Decker, D. L., J. Appl. Phys. **36**, 157 (1965).
[3] Larson, D. B., Keeler, R. N., Kusubov, A., and Hord, B. L., J. Phys. Chem. Solids **27**, 476 (1966).
[4] Evdokimova, V. V., and Vereshchagin, L. F., J. Exp. Theor. Phys. **43**, 1208 (1962); **16**, 855 (1963).
[5] Pistorius, C. W. F. T., J. Phys. Chem. Solids **25**, 1477 (1964).
[6] Bridgman, P. W., Proc. Am. Acad. Arts Sci. **76**, 1 (1945).
[7] Johnson, Q. Science **153**, 419 (1966).
[8] Perez-Albuerne, E. A., and Drickamer, H. G., J. Chem. Phys. **43**, 1381 (1965).
[9] Jamieson, J. C., Physics of Solids at High Pressures, pp. 444–459, C. T. Tomizuka and R. M. Emrick, eds. (Academic Press, New York, 1965).
[10] Jamieson, J. C. private communciation.
[11] Bassett, W. A., Takahashi, T., Mao, H. and Weaver, J. S. J. Appl. Phys. **39**, 319 (1968).
[12] Rice, M. H., McQueen, R. G., and Walsh, J. M., Solid State Phys. **6**, 1 (1958).
[13] Carter, W. J., Marsh, S. P., Fritz, J. N., and McQueen, R. G., The equation of state of selected materials for high-pressure references, NBS Symp. on the Accurate Characterization of the High Pressure Environment, Washington, 1968.
[14] Haussühl, S., Zeit. Physik **159**, 223 (1960).
[15] Bartels, R. A., and Schuele, D. E., J. Phys. Chem. Solids **26**, 537 (1965).
[16] Hauver, G. E., and Melani, A., private communication.
[17] Johnson, W. H., Jr., and Nier, A. O., Handbook of Physics, E. U. Condon and H. Odishaw, eds., pp. 9–65, 2d ed. (McGraw-Hill, New York, 1967).
[18] National Bureau of Standards Circular 539, **2**, 41 (1965).
[19] Rubin, T., Johnston, H. L., and Altman, H. W., J. Chem. Phys. **65**, 65 (1961).
[20] Barron, T. H. K., Leadbetter, A. J., and Morrison, J. A., Proc. Roy. Soc. **A279**, 62 (1964).
[21] JANAF Thermochemical Tables, The Dow Chemical Company, Midland, Michigan (June 1966).
[22] Grover, R., Keeler, R. N., Rogers, F. J., and Kennedy, G. C., On the compressibility of the alkali metals, J. Phys. Chem. Solids (to be published).
[23] Jeffery, R. N., Barnett, J. D., VanFleet, H. B., and Hall, H. T., J. Appl. Phys. **37**, 3172 (1966).
[24] McWhan, D. B., J. Appl. Phys. **38**, 347 (1967).

DISCUSSION

D. J. Pastine (*U.S. Naval Ordnance Laboratory, White Oak, Maryland*): In combining the effects of the possible deviation of the several parameters, illustrated in figure 3, should all the effects be added if all the deviations in the initial conditions were made at the same time?

D. Decker (*Brigham Young University, Provo, Utah*): In our work, I varied all the parameters by the maximum amount, but found that the total error was less than the sum of the possible individual errors. The value of B_0' in the new calculations that we have made is 4.93, which differs a little from yours. Also, there are at least five ultrasonic measurements giving values for B_0' ranging between 6.05 and 3.31 so that presently it appears that ultrasonic data cannot be used to refine the equation of state.

D. B. McWhan (*Bell Telephone Laboratories, Murray Hill, New Jersey*): I would say that the results and outlook concerning calculation of the NaCl isotherm is encouraging. A couple of years ago in some work on quartz, I looked at the volume of sodium chloride at the bismuth transition. At that time the Decker equation gave values below those of the present shock data, and the Birch equation gave values above. Since then the starting parameters for both theories seem to have come into question, and when one modifies B_0, as Decker has done, then the values fall right on the shock data. If one does the same thing with B_0' with the Birch equation, it will also agree with the shock data. Thus there are three independent results that are in agreement at least up to about 150 kilobars.

I would like to note that, as I mentioned, we determine the volume of sodium chloride at the bismuth transition only on the upstroke, and obtained a value of about 0.816. The Hall group got a value of 0.818. I think this is remarkably good agreement for two completely different pieces of equipment, in independent experiments.

J. S. Weaver (*Department of Geological Sciences, University of Rochester, Rochester, New York*): In our work, the deviations are given in our table 3, of our paper given earlier in this Session, listing the sensitivity of the calculated pressure values to these deviations. If one parameter is increased the pressure may increase or decrease. Our 2½ percent is obtained by squaring the individual deviations, summing them, and then taking the square root. This assumes that the parameter variations are independent and gaussian.

I think that the explanation of your better agreement with other values of B_0' is related to taking account of the second-nearest-neighbor effect.

AUTHORS' CLOSURE

In reply to Dr. Pastine: The effects of possible deviation of the parameters involved in the calculation may be added but the total effect is small. We should point out that, in contrast to Decker's calculation, the only assumed parameter that we are varying which has any significant effect on the resulting isotherm is the Grüneisen parameter. Whether or not one decides to include the uncertainty in the specific heat, the only other bit of information one needs to convert a Hugoniot to an isotherm, makes no practical change in the final result.

Consistency in the High-Temperature Equation of State of Solids*

Leon Thomsen and Orson L. Anderson

Lamont Geological Observatory of Columbia University, Palisades, New York 10964

Four equations of state for solids are examined theoretically for mutual consistency in the high-temperature regime. It is found that neither the Birch-Murnaghan nor the Murnaghan equation can be shown to be consistent with either the Mie-Grüneisen or the Hildebrand equation. An expression is derived for the volume dependence of the Grüneisen parameter $\gamma(\rho)$. A recent theoretical treatment of NaCl, proposed for use as a pressure standard, is neither internally consistent, nor is it sufficiently precise for such a purpose.

1. Introduction

In current use there appear several different equations of state for solids which differ in their derivations, in the quantities which they exhibit explicitly, and in the quantities which they leave as experimental parameters. It is the purpose of this paper to discuss together some of these equations, and to show to what extent their separate derivations are mutually consistent. Such consistency becomes important when two of these equations are used together in interpreting experimental data. For example, one method [cf. Takeuchi and Kanamori, 1966] of reducing shock-wave data employs the Mie-Grüneisen equation to account for thermal effects in transforming the Hugoniot into an isotherm, which is then compared with the Birch-Murnaghan equation. Clearly, if this calculation is to have meaning, assumptions made in any one part of it must not be violated in another part. As another example, when a high-pressure experiment is calibrated using the equation of state of NaCl provided by Decker [1965], the resulting data are constrained by the assumptions of the Mie-Grüneisen equation of state, as used by Decker. If these data are then compared and extrapolated with the Birch-Murnaghan equation of state, the problem of consistency again must be faced.

Many equations of state can be classified into one of two broad classes: 'isothermal' equations which are concerned primarily with effects of compression at constant temperature, and 'thermal' equations which treat strictly thermal effects more precisely.

In this paper, we first give brief accounts of the derivations of some of these equations of state. Second, we develop a simple framework in which they can all be considered together. Next, we show how the same reasoning which was used in the isothermal case leads to an expression for $\gamma(\rho)$. Then we consider the restrictions imposed upon the isothermal equations by the thermal equations. Turning finally to recent work on NaCl, we find that internal consistency in the Mie-Grüneisen equation generates in this special case a $\gamma(\rho)$ from the microscopic lattice potential energy.

2. Isothermal Equations of State

Prominent among this class is the Birch-Murnaghan equation

$$P(\rho, T)=\tfrac{3}{2}K_0(T)(y^{7/3}-y^{5/3})[1-\xi(T)(y^{2/3}-1)] \quad (1)$$

where

$$y(\rho, T)=\frac{\rho}{\rho_0(T)}. \quad (1a)$$

Here P is pressure, ρ density, T temperature, K the isothermal bulk modulus $\rho(\partial P/\partial\rho)_T$, and the subscript $_0$ refers to zero pressure. ξ is related to experimental quantities by

$$\xi(T)=-\tfrac{3}{4}[K_0'(T)-4] \quad (2)$$

where K_0' is $(\partial K/\partial P)_T$ as $P\to 0$. The B–M equation is derived [Murnaghan, 1937; Birch, 1938, 1947, 1952] from the theory of finite strain, in which it is proved that the strain is given by

$$\epsilon=\frac{-1}{2}(y^{2/3}-1)=\epsilon(\rho, T) \quad (3)$$

and it is assumed that a Taylor expansion, in the strain, of the Helmholtz free energy may be terminated at the cubic terms. It should be noted that the uniqueness of this definition of strain has been questioned by Knopoff [1963].

Leaving such questions aside, in the present case of homogeneous isotropic compression, the free energy is assumed to be

$$F(\rho, T)=\frac{9}{2}\frac{K_0(T)}{\rho_0(T)}\epsilon^2+6\frac{K_0(T)}{\rho_0(T)}\xi(T)\epsilon^3. \quad (4)$$

The B–M equation then follows from

$$P=-\left(\frac{\partial F}{\partial V}\right)_T \quad (5)$$

where $V=1/\rho$ is the specific volume. We will return

*Lamont Geological Observatory Contribution No. 1563.

Paper presented at the Symposium on Accurate Characterization of the High-Pressure Environment, held at the National Bureau of Standards, Gaithersburg, Md., October 14–18, 1968.

to the discussion of this equation shortly.

Another important member of this class is the equation of Murnaghan [1944]

$$P(\rho, T) = \frac{K_0(T)}{K_0'(T)} (y^{\beta T} - 1) \tag{6}$$

where $\beta_T = K_0'(T)$. This follows from the assumption

$$K(P, T) = K_0(T) + K_0'(T)P$$

and is, experimentally, nearly indistinguishable from (1) over a considerable range of compression. This fact may be understood on the basis of the uniqueness of the Taylor expansion. Any two functions $f_1(y)$ and $f_2(y)$ that are constructed so as to satisfy the same boundary conditions

$$\left.\frac{d^n f_1}{dy^n}\right|_{y_0} = \left.\frac{d^n f_2}{dy^n}\right|_{y_0}$$

for $n = 0, 1 \ldots M$ will have the same Taylor expansion about y_0, through terms in y^M, and will differ only in the higher-order terms. The B–M and the Murnaghan equations represent two such functions, with $y_0 = 1$, and T not entering the problem. They are both four-parameter equations for the free energy F, with one of these parameters explicitly set to zero, leaving only ρ_0, K_0, and K_0' apparent. Since the $M + 1 = 4$ term of the expansion in which they first begin to differ is

$$81 \frac{K_0}{\rho_0} \left[K_0 K_0'' + K_0'^2 - 7K_0' + \frac{143}{9} \right] \frac{\epsilon^4}{4!} \tag{7}$$

it is clear that the B–M assumption on K'' is

$$K_0'' = \frac{1}{K_0} \left(7K_0' - K_0'^2 - \frac{143}{9} \right). \tag{8}$$

The Murnaghan equation, of course, assumes

$$K_0'' = 0. \tag{9}$$

For a typical oxide, $K_0' = 4$, $K_0 = 1{,}000$ kbar, and the RHS of (8) is 3.9×10^{-3} kbar^{-1}. This number is sufficiently close to zero to insure that the two forms agree closely over a wide range of y.

It is of interest to note that the RHS of (8) is not zero for any real K_0', and reaches its extremum at $K_0' = 3.5$. It seems to be a remarkable coincidence that solids should have values of K_0' so close to this extremum value. An examination of the derivation of eq (8) shows that this number, 7/2, has its ultimate source in the fact that the number of dimensions in physical space is 3. We find it very interesting that typical values of K_0' are close to 3.5 and not some other number, like 10. In any case, this situation helps explain why it is that the series (4) is so quickly convergent.

3. Thermal Equations of State

This class is most often motivated by considerations of the theory of lattice dynamics. In this theory, the lattice potential energy is expanded in a Taylor series about the equilibrium lattice configuration. Most, if not all, observed phenomena are explainable in principle if the series is terminated at the fourth-order terms:

$$\Phi = \Phi_0 + \Phi_1 + \Phi_2 + \Phi_3 + \Phi_4 \tag{10}$$

where

$$\Phi_k = \frac{1}{K!} \sum \Phi \overset{\mathbf{m}}{\underset{i}{\mu}} \ldots \overset{\mathbf{n}}{\underset{j}{\nu}} \underbrace{q\overset{\mathbf{m}}{\underset{i}{\mu}} \ldots q\overset{\mathbf{n}}{\underset{j}{\nu}}}_{k \text{ terms}}$$

and $\Phi \overset{\mathbf{m}}{\underset{i}{\mu}} \ldots \overset{\mathbf{n}}{\underset{j}{\nu}}$ is the kth order coupling parameter, and $q\overset{\mathbf{m}}{\underset{i}{\mu}}$ is the ith component of the displacement from equilibrium of the atom in the μth position of the unit cell which is located by the lattice vector $\mathbf{m}$. The temperature is introduced with the assumption of thermal equilibrium, and the free energy can then be written down. It is

$$F(\rho, T) = \Phi_0(\rho) + \sum_{\mathbf{k}, \lambda} [\tfrac{1}{2}\hbar\omega(\mathbf{k}, \lambda) + kT \ln (1 - e^{-\hbar\omega(\mathbf{k}, \lambda)/kT})] + F_3(T) + F_4(T) \tag{11}$$

Here, Φ_0 is the energy of assembling the (static) lattice to its equilibrium configuration; $\omega(\mathbf{k}, \lambda)$ is a vibrational eigenfrequency, a function of the wave vector $\mathbf{k}$ and the polarization; F_3 and F_4 are complicated functions of temperature only, which are given explicitly by Leibfried and Ludwig [1961]. At high temperature, the energy enters the classical regime, and the equations simplify. We will content ourselves here with this restriction to temperatures greater then Θ_D, the Debye temperature.

$$F = \Phi_0 + kT \sum \ln \frac{\hbar\omega(\mathbf{k}, \lambda)}{kT} - \frac{k^2T^2}{16Ns} \sum_{\substack{\mathbf{k} \\ \lambda}} \sum_{\substack{\mathbf{k}' \\ \lambda}} \sum_{\substack{\mathbf{k}'' \\ \lambda}} \frac{\left| \Phi \overset{\mathbf{k}\mathbf{k}'\mathbf{k}''}{\underset{\lambda\lambda\,\lambda}{}} \right|^2}{(\omega\omega'\omega'')^2} \times \left(\frac{2\omega - \omega''}{\omega + \omega' - \omega''} + \frac{\omega}{\omega + \omega' + \omega''} \right) + \frac{k^2T^2}{8Ns} \sum_{\substack{\mathbf{k} \\ \lambda}} \sum_{\substack{\mathbf{k}' \\ \lambda'}} \frac{\left| \bar{\Phi} \overset{\mathbf{k}\mathbf{k}}{\underset{\lambda\lambda'}{}} \right|}{(\omega\omega')^2} \tag{12}$$

This equation is the high-temperature form of equations 10.2 and 10.4 of Leibfried and Ludwig [1961]. N is the number of elementary cells; s is the number of atoms in a cell. $\Phi^{\mathbf{kk'k''}}_{\lambda\lambda'\lambda''}$ and $\Phi^{4\,\mathbf{kk'}}_{\lambda\lambda'}$ describe, respectively, the third- and fourth-order derivatives of the lattice potential energy, and are defined precisely by Leibfried and Ludwig. The frequencies ω depend on the lattice configuration through $\mathbf{k}$; insofar as this configuration can be described by the single parameter ρ, we can say that $\omega = \omega(\rho)$. However, the frequencies appearing in F_3 and F_4 of eqs (11) and (12) must be evaluated at a fixed density because of the presence of $\left|\Phi^{\mathbf{kk'k''}}_{\lambda\lambda'\lambda''}\right|^2$ and $\Phi^{4\,\mathbf{kk'}}_{\lambda\lambda'}$.

This situation can be briefly summarized by the statement that the anharmonic high T approximation is

$$F(\rho, T) = A(T) + B(\rho) + C(\rho)T + D(\rho)T^2. \tag{13}$$

In the *harmonic* approximation, Φ_3 and Φ_4 are zero, implying that $B(\rho)$ is quadratic in the strain, $C(\rho)$ is constant, and $D(\rho)$ is zero. In the *fourth-order anharmonic* approximation (which we shall call the anharmonic approximation) Φ_3 and Φ_4 are nonzero, but the next terms (Φ_5 and Φ_6) *are* zero, implying that $B(\rho)$ is quartic, $C(\rho)$ is quadratic, and $D(\rho) = D$ is constant.

The anharmonic equation of state is, from (5),

$$P(\rho, T) = -\frac{d\Phi_0}{dV} - \frac{1}{V}\sum_i \frac{d\ln\omega_i}{d\ln V}\hbar\omega_i\left[\frac{1}{2} + \frac{1}{e^{\hbar\omega/kT}-1}\right] \tag{14}$$

$$= -\frac{d\Phi_0}{dV} + \frac{1}{V}\sum_i \gamma_i\epsilon_i \tag{14a}$$

where

$$\gamma_i \equiv \frac{d\ln\omega_i}{d\ln\rho}$$

and

$$\epsilon_i = \hbar\omega_i\left[\frac{1}{2} + \frac{1}{e^{\hbar\omega i/kT}-1}\right]$$

are the Grüneisen parameter and the energy, respectively, of the ith normal mode of vibration.

The *further* assumption that all the γ_i are equal leads to the Mie-Grüneisen equation [Grüneisen, 1926].

$$P(\rho, T) = -\frac{d\Phi_0}{dV} + \gamma\frac{E_{\text{vib}}}{V} \tag{14b}$$

where $E_{\text{vib}} = \Sigma\epsilon_i$.

The alternative assumption that E_{vib} is a function of T only yields the Hildebrand equation [Hildebrand, 1931]

$$P(\rho, T) = -\frac{d\Phi_0}{dV} + \alpha KT \tag{14c}$$

where $\alpha = -1/\rho(\partial\rho/\partial T)_P$ is the thermal expansivity. These two equations were discussed by Fumi and Tosi [1962]. At high temperatures they converge together, as the first assumption becomes irrelevant, the second is automatically fulfilled, and the pressure becomes

$$P(\rho, T) = -\frac{d\Phi_0}{dV} + \frac{\gamma}{V}3NskT$$

$$= B'(\rho) + C'(\rho)T \tag{14d}$$

where $\gamma(\rho) = (1/3Ns)\Sigma\gamma_i$ and $C'(\rho) = \alpha K$. This equation is equivalent to

$$\left(\frac{\partial^2 P}{\partial T^2}\right)_\rho = \left(\frac{\partial \alpha K}{\partial T}\right)_\rho = 0, \tag{15}$$

and this is a simple statement of the anharmonic high T approximation.

4. A Coherent Framework

In the present context, it is clear that the difference between the isothermal $B-M$ equation (1) and the thermal equations (13) is merely one of viewpoint. We may expand $F(\rho, T)$ about a point ρ_0, θ corresponding to zero pressure and some finite temperature θ in many equivalent ways. If $t = T - \theta$

$$F(\rho, T) = [F_{00} + \dot{F}_{00}t + \ddot{F}_{00}\frac{t^2}{2} + \ldots] + g(t)$$

$$+ [F^*_{00} + \dot{F}^*_{00}t + \ddot{F}^*_{00}\frac{t^2}{2} + \ldots]\epsilon$$

$$+ [F^{**}_{00} + \dot{F}^{**}_{00}t + \ddot{F}^{**}_{00}\frac{t^2}{2} + \ldots]\frac{\epsilon^2}{2}$$

$$+ [F^{***}_{00} + \dot{F}^{***}_{00}t + \ddot{F}^{***}_{00}\frac{t^2}{2} + \ldots]\frac{\epsilon^3}{6}$$

$$+ \ldots \tag{16a}$$

$$= [F_{00} + F^*_{00}\epsilon + F^{**}_{00}\frac{\epsilon^2}{2} + F^{***}_{00}\frac{\epsilon^3}{6} + \ldots]$$

$$+ [\dot{F}_{00} + \dot{F}^*_{00}\epsilon + \dot{F}^{**}_{00}\frac{\epsilon^2}{2} + \dot{F}^{***}_{00}\frac{\epsilon^3}{6} + \ldots]t$$

$$+ [\ddot{F}_{00} + \ddot{F}^*_{00}\epsilon + \ddot{F}^{**}_{00}\frac{\epsilon^2}{2} + \ddot{F}^{***}_{00}\frac{\epsilon^3}{6}$$

$$+ \ldots]\frac{t^2}{2} + \ldots + g(t) \tag{16b}$$

where the symbol $\cdot$ means $(\partial/\partial t)_\epsilon$, the superscript * means $(\partial/\partial\epsilon)_t$, and the subscript $_{00}$ indicates evaluation at $P=\epsilon=0$, $t=0$. The function $g(t)$ contains the nonpolynomial terms in t that are necessary to obtain the correct specific heat. The viewpoint in (16a) is clearly that of the B–M equation; the coefficient of ϵ will vanish when the boundary conditions at $P=0$ are invoked, and the part independent of ϵ is one to which our attention need not be explicitly directed in the derivation of an isothermal equation of state.

But the viewpoint in (16b) is not that of the anharmonic theory. This is because the strains, as defined, are functions of T as well as ρ, and thus the coefficients of the various powers of t are not of the proper form. What is needed is a recognition of the fact that the free energy depends on the *total* strain from a *fixed* initial state. This strain, containing both isobaric and isothermal compression is clearly

$$e \equiv -\frac{1}{2}\,(x^{2/3}-1) \tag{17}$$

where $x \equiv \rho/\rho_{00}$ and ρ_{00} is the density at $P=0$, $t=0$. Then we can expand F in terms of e and t in an equally valid and more instructive manner:

$$\begin{aligned} F(\rho,T) &= [F_{00}+\dot{F}_{00}t+\ddot{F}_{00}\frac{t^2}{2}+\ldots]+g(t) \\ &\quad +[F^{\dagger}_{00}+\dot{F}^{\dagger}_{00}t+\ldots]e \\ &\quad +[F^{\dagger\dagger}_{00}+\dot{F}^{\dagger\dagger}_{00}t+\ldots]\frac{e^2}{2} \\ &\quad +[F^{\dagger\dagger\dagger}_{00}+\ldots]\frac{e^3}{6} \\ &\quad +[F^{\dagger\dagger\dagger\dagger}_{00}+\ldots]\frac{e^4}{24} \qquad (18a) \\ &= [F_{00}+F^{\dagger}_{00}e+F^{\dagger\dagger}_{00}\frac{e^2}{2}+F^{\dagger\dagger\dagger}_{00}\frac{e^3}{6} \\ &\quad +F^{\dagger\dagger\dagger\dagger}_{00}\frac{e^4}{24}+\ldots]+[\dot{F}_{00}+\dot{F}^{\dagger}_{00}e \\ &\quad +\dot{F}^{\dagger\dagger}_{00}\frac{e^2}{2}+\ldots]t+[\ddot{F}_{00}+\ldots]\frac{t^2}{2} \qquad (18b) \\ &\quad +\ldots+g(t) \end{aligned}$$

where the symbol $\cdot$ means $(\partial/\partial t)_\rho$, the superscript $\dagger$ means $(\partial/\partial e)_t$, and the subscript $_{00}$ indicates evaluation at $t=0$, $e=0$. The anharmonic theory is invoked to give the nonpolynomial term in t; from (12) it is clearly

$$g(t) = -3Nsk\left[(t+\theta)\ln\left(1+\frac{t}{\theta}\right)-t\right]. \tag{19a}$$

The expansions in (18) were truncated in accordance with the approximations of the fourth-order anharmonic theory, as noted above.

It is clearly possible to derive (18) from (16) by expanding ϵ in terms of e and t. But the degree of the expansion will be necessarily different for each term. In other words, each $\gamma(\rho, T)$ appearing in (1) must be handled differently. We may conclude that the B–M equation, in the form of (1) and (4), is not consistent with the anharmonic theory, or with its results, equations 14. However, in the modified form implied by equation 17, it clearly is consistent, except for the term in e^4. This term will contribute to K at high pressure and to $(\partial K/\partial T)_p$ at zero pressure.

The coefficients in (18) are defined experimentally by

$$\begin{aligned} &F_{00}=0 \\ &\dot{F}_{00}=0 \\ &F^{\dagger}_{00}=0 \\ &F^{\dagger\dagger}_{00}=9\frac{K_{00}}{\rho_{00}} \\ &F^{\dagger\dagger\dagger}_{00}=-27\frac{K_{00}}{\rho_{00}}\,(K'_{00}-4) \\ &F^{\dagger\dagger\dagger\dagger}_{00}=-27\frac{K_{00}}{\rho_{00}}\left(K''_{00}K_{00}+K'^{2}_{00}-\frac{1}{9}\right) \qquad (19b) \\ &\dot{F}^{\dagger}_{00}=-3\frac{\alpha_{00}K_{00}}{\rho_{00}} \\ &\dot{F}^{\dagger\dagger}_{00}=-9\frac{\alpha_{00}K_{00}}{\rho_{00}}\left[\delta_{00}-K'_{00}+\frac{5}{3}\right] \\ &\ddot{F}_{00}=\frac{1}{\theta}\,[3\,Nsk-C_{v00}] \end{aligned}$$

Some of the quantities needed in the next (sixth-order) approximation are

$$\dot{F}^{\dagger\dagger\dagger}=-27\frac{\alpha_{00}K_{00}}{\rho_{00}}\,[\zeta_{00}-(\delta_{00}-3)\,(K'_{00}-4)]$$

$$\dot{F}^{\dagger}_{00}=-\frac{3}{\rho_{00}}\left(\frac{\partial\alpha K}{\partial T}\right)_\rho=-3\frac{\alpha^2_{00}K_{00}}{\rho_{00}}\,[K'_{00}-2\delta_{00}+\beta_{00}] \tag{19c}$$

$$\dot{F}_{00}\dagger\dagger\dagger = -18\,\frac{\alpha_{00}^2 K_{00}}{\rho_{00}}\left[(K'_{00}-4)\left(\delta_{00}+\frac{1}{2}\beta_{00}-\frac{8}{3}\right)\right.$$

$$\left.+\frac{7}{3}\left(\delta_{00}-\frac{1}{2}\beta_{00}\right)-\zeta_{00}-\frac{1}{2\alpha_{00}^2 K_{00}}\left(\frac{\partial^2 K}{\partial T^2}\right)_P-\frac{49}{18}\right]$$

where the derivatives are evaluated, of course, at the 00 point. δ is the anharmonic parameter

$$\delta \equiv \frac{-1}{\alpha K}\left(\frac{\partial K}{\partial T}\right)_P$$

and

$$\beta \equiv \frac{1}{\alpha^2}\left(\frac{\partial \alpha}{\partial T}\right)_P$$

$$\zeta \equiv \frac{1}{\alpha}\frac{\partial^2 K(P,T)}{\partial P \partial T}$$

are introduced here to simplify the notation.

These coefficients are complicated for two reasons: the pressure is a volume derivative of the free energy rather than a strain derivative; and the values of K and α are such that in the laboratory we always measure $(\partial/\partial T)_P$ instead of $(\partial/\partial T)_\rho$. It is of interest to note that because of the sums in the last three equations of (19c), knowledge of $(\partial^2 K)/\partial T^2)_P$ is of limited usefulness without similar knowledge of $K(\partial\alpha/\partial T)_P$. Both these terms are needed if the anharmonic theory is applied as in this context.

The fourth-order anharmonic high T approximation is that terms in $\dot{F}_{00}\dagger\dagger\dagger$, $\ddot{F}_{00}\dagger$, $\ddot{F}_{00}\dagger\dagger$, etc., are small compared to all other terms. For example,

$$\left|\ddot{F}_{00}\dagger\frac{t^2}{2}e\right| << |\dot{F}_{00}\dagger te| \tag{20}$$

or

$$\left|(K'_{00}-2\delta_{00}+\beta_{00})\frac{\alpha_{00}t}{2}\right| << 1$$

is actually an approximate statement of eq (15), evaluated at the 00 point. Of course, this will be true for small enough values of t, and despite the large uncertainties in $(\partial\alpha/\partial T)_P$, it seems that this inequality will hold perhaps to $t \sim 1{,}000°$.

However, (20) is not sufficient to insure the adequacy of the anharmonic high T approximation. It must be shown that each term neglected is much smaller than *each* term retained, requiring, for example,

$$\left|\ddot{F}_{00}\dagger e\frac{t^2}{2}\right| << \left|F_{00}\dagger\dagger t\frac{e^2}{2}\right| \tag{21a}$$

or

$$|(K'_{00}-\delta_{00}+\beta_{00})\alpha_{00}t| << \left|3\left(K_{00}-\delta_{00}-\frac{5}{3}\right)e\right|. \tag{21b}$$

This inequality is not demonstrable, in general, except for very small values of e.

5. Thermal Equations From the Isothermal Viewpoint

The expansion in (18) gives new insight into the quantities appearing in the thermal equations (14). The equation of state which follows from (18) via (5) is, in the anharmonic high T approximation,

$$P(\rho,T)=\frac{3}{2}K_{00}(x^{7/3}-x^{5/3})[1-\xi(\theta)(x^{2/3}-1)$$

$$-\frac{1}{3V_{00}}x^{5/3}F\dagger\dagger\dagger\dagger_{00}\frac{e^3}{3!} \tag{22}$$

$$+\alpha_{00}K_{00}x^{5/3}\left[1+3e\left(\delta_{00}-K'+\frac{5}{3}\right)\right]t.$$

Comparison with (14d) gives an expression for the Grüneisen parameter, as a function of density:

$$\gamma(e)=\gamma_{00}(1-2e)\left\{1+3e\left[\delta_{00}-K'_{00}+\frac{5}{3}\right]\right\} \tag{23}$$

where $\gamma_{00}=(V\alpha K)_{00}/3sR$. This expression for γ contains *no* assumptions beyond those already implicit in the Mie-Grüneisen equation (14d), except that the strain as defined in (17) is the appropriate measure of the displacements in (10). In particular, all questions concerning the number and weighting of mode gammas have been avoided; the answers are contained within the measured values of α_{00}, etc. Whenever some other expression for $\gamma(\rho)$, for example, that of Dugdale and MacDonald [1953], is used, it must converge to (23) in the high-temperature regime. To the extent that it does not so converge, one may conclude that the additional assumptions it contains are not verified.

Different materials exhibit a large variety of behavior of $\gamma(\rho)$. Some of the possibilities are illustrated in figure 1 for several minerals of possible importance in the earth. It is seen that for some materials γ decreases rapidly, and goes through zero at compressions found in the lower mantle. This is remarkable behavior, and raises well-known problems with the thermal expansivity and the sign of the temperature changes accompanying adiabatic compression. The present work adds to our belief that such problems are real and must be seriously faced.

6. Thermal Restrictions on Isothermal Equations

While the demonstration of (20) and (21) is sufficient to establish the adequacy of the anharmonic high T approximation, it is for some purposes more convenient to consider the exact statement of the

approximation

$$\left(\frac{\partial^2 P}{\partial T^2}\right)_\rho = 0. \tag{15}$$

In this section, we consider (15) as a property of thermal equations in the anharmonic high T approximation that must be possessed by isothermal equations used in the same context. We discuss the conditions necessary for the inclusion of (15) in two generalized isothermal forms of the equations of state. Consider the form

$$P(\rho, T) = \sum_{i=1}^{M} c_i(T) y^{n_i} \tag{24}$$

of which (1) is an example. The c_i here are experimental quantities fixed by the boundary conditions at $y=1$. The n_i are independent of T, and the only restriction on M is that it be finite. If such an equation is to meet the anharmonic high T condition (15), it must be that

$$\sum_i [c_i + (2\alpha_0 c_i + \alpha_0 c_i) n_i + c_i \alpha_0^2 n_i^2] y^{n_i} = 0. \tag{25}$$

Since the y^{n_i} are linearly independent, each bracket must equal zero independently, giving M algebraic equations which can be solved explicitly for the n_i in terms of c_i, α_0, and their derivatives. It is obvious that any rational n_i (e.g., $n_1 = 5/3$) can only meet this condition approximately, at least in macroscopic physics. This approximation is separate from, and additional to, the approximation in (21). But it is not possible, under present limitations, to state whether or not it is serious.

However, it is of interest to know whether the condition (15) can be met *exactly* by *any* equation of state. Consider the form

$$P(\rho, T) = K_0(T) f(y) \tag{26}$$

of which the Murnaghan equation (6) is an example (provided K_0' is independent of T). The second-order B–M eauation (with $\xi = 0$) is another example. Some of the properties of this form are discussed by Birch [1968]. The *only* equation of the form (26) which meets the anharmonic high T condition is

$$P(\rho, T) = \frac{K_0}{n_1 - n_2}(y^{n_1} - y^{n_2}) \tag{27}$$

where

$$n_1 \equiv \frac{K_0'}{2}[1 + \sqrt{1 - R_0(T)}]$$

$$n_2 \equiv \frac{K_0'}{2}[1 - \sqrt{1 - R_0(T)}]$$

with

$$R_0(T) \equiv \frac{4}{\alpha_0^2 K_0 (K_0')^2} \frac{d^2 K_0}{dT^2}.$$

The Murnaghan equation (6) is a special case of (27) corresponding to $R_0(T) = 0$. Therefore, one may use the M–G equation in conjunction with the Murnaghan equation only after demonstrating that $R_0 \ll 1$.

The demonstration is not generally possible. Soga and Anderson [1967] measured K_S at zero pres-

TABLE 1. *Mineral parameters*

Parameter	Polycrystal Al_2O_3	Single crystal MgO	Polycrystal Mg_2SiO_4
δ_{00}	*5.06	*3.54	†4.88
K'_{00}	†3.99	‡4.52	‡4.9
$\delta_{00} - K'_{00} + 1$	2.07	0.02	0.98
β_{00}	*2.24	*2.85	†3.49
γ_{00}	1.27	1.46	0.77
θ	1042 K	946 K	650 K

*Soga and Anderson [1966].
†Soga and Anderson [1967].
‡Anderson and Liebermann [1967].

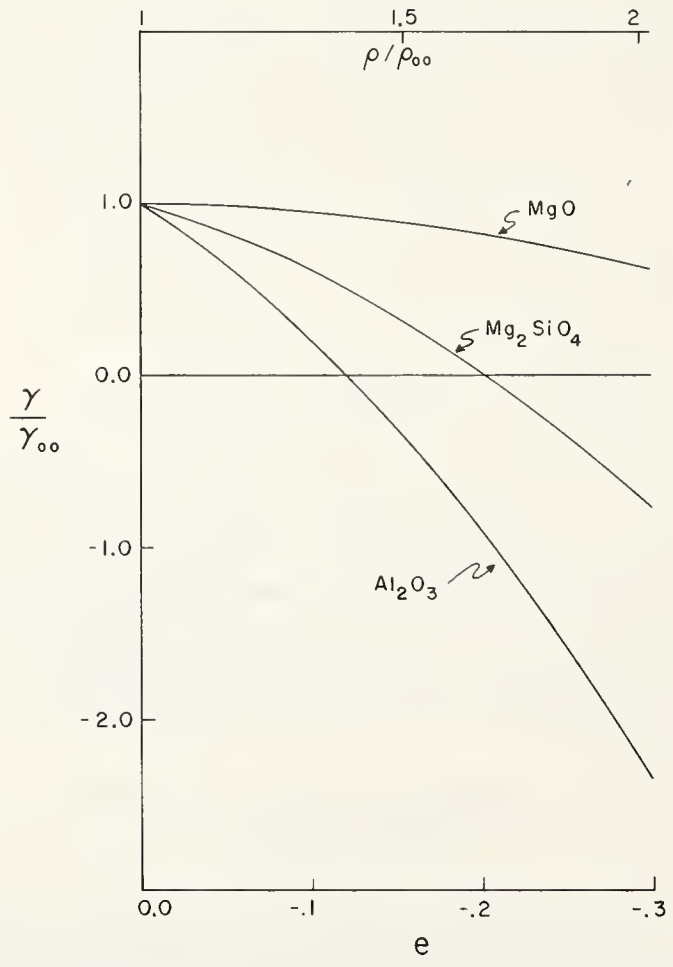

FIGURE 1. *Grüneisen parameter as a function of strain, from eq (27), using the mineral parameters of table 1.*

sure and high temperature for the polycrystalline oxides MgO, Al_2O_3, and Mg_2SiO_4. This can be converted from the adiabatic modulus to the isothermal modulus using

$$K=K_S/(1+T\alpha\gamma).$$

It is then found that the curvature d^2K_0/dT^2 is so small as to be unmeasurable, being equal to zero within a fourth of a standard deviation for all materials. However, if the standard deviation of d^2K_0/dT^2 from its mean is taken as an upper bound for d^2K_0/dT^2, then the quantity R_0 may, because of the factor $1/K_0\alpha_0^2$, be quite large, and one therefore cannot conclude that $R_0 \ll 1$. Much more precise measurements of the temperature dependence of K_0 will be needed before it can be shown that $R_0 \ll 1$.

7. Internal Consistency in the Q–H Approximation

In applying the Mie-Grüneisen equation of state, various assumptions are necessary, and it is important that these be made in a self-consistent way. In particular, we wish to discuss here the relations between γ and Φ_0.

When the atomic interaction is unknown, then both γ and Φ_0 may be chosen independently. But where the interaction is known, both γ and Φ_0 are thereby determined. For example, Decker [1965] in determining a numerical equation of state for NaCl assumes an interaction with Coulombic, dipole-dipole, dipole-quadripole, and exponential repulsion terms. Since all these are central forces, he obtains an expression for Φ_0 (which he denotes by Φ) which involves only the lattice parameter r. He then assumes

$$\gamma=\gamma_0+\lambda\frac{r-r_0}{r_0}$$

for the volume dependence of γ, where

$$\gamma_0=\left(\frac{\alpha K}{\rho C_P}\right)_{P=0}=1.59\pm.16$$

and $r_0=R(P=0)$. λ is empirically chosen to be 2.55.

However, γ is the logarithmic derivative of $\overline{\omega^2}$, and $\overline{\omega^2}$ is determined by the atomic interaction. From Leibfried and Ludwig [1961]

$$\overline{\omega^2}=\frac{1}{3sN}\sum_{\mathbf{k},\lambda}\omega^2(\mathbf{k},\lambda)=\frac{1}{3s}\sum_{\mu,i}\frac{1}{M_\mu}\Phi^{0\,0}_{\mu\mu\,i\,i}$$

$$=\frac{-1}{3s}\sum_{\mu,i}\frac{1}{M_\mu}\sum{}'\,\Phi^{\mathbf{h}0}_{\nu\mu\,i\,i} \qquad (28)$$

where Σ' indicates summation over all lattice points except $\mathbf{h}=0$, $\nu=\mu$. M_μ is the mass of atom μ.

Where the interaction depends only on the distance $R^{\mathbf{h}}_{\mu\nu}$ between atoms, the potential is

$$\Phi=\tfrac{1}{2}\Sigma\phi_{\mu\nu}(R^{\mathbf{h}}_{\mu\nu})$$

and (28) becomes

$$\overline{\omega^2}=-\frac{1}{3s}\sum{}'\frac{1}{M_\nu}\nabla^2\phi_{\mu\nu}(R^{\mathbf{h}}_{\mu\nu}) \qquad (29)$$

where ∇^2 is the Laplacian operator. Grüneisen's parameter is

$$\gamma=\frac{1}{18s\overline{\omega^2}}\sum{}'\frac{1}{M_\nu}R^{\mathbf{h}}_{\mu\nu}\frac{\partial}{\partial R^{\mathbf{h}}_{\mu\nu}}\nabla^2\phi_{\mu\nu}. \qquad (30)$$

Where the interaction $\phi_{\mu\nu}$ is specified, it is easy to compute these functions. For the potential used by Decker [1965]

$$\overline{\omega^2}=-\frac{C^*}{6r^8}-\frac{D^*}{6r^{10}}$$
$$+\frac{b}{\rho^2}\left(\frac{M_++M_-}{M_+M_-}\right)\left(1-2\frac{\rho}{r}\right)e^{-r/\rho}$$
$$+\frac{2b_+}{\rho_+^2M_+}\left(1-2\frac{\rho_+}{r}\right)e^{-r\sqrt{2}/\rho_+}$$
$$+\frac{2b_-}{\rho_-^2M_-}\left(1-2\frac{\rho_-}{r}\right)e^{-r\sqrt{2}/\rho_-} \qquad (31)$$

and

$$\gamma=\frac{-1}{36\overline{\omega^2}}\left[\frac{8C^*}{r^8}+\frac{10D^*}{r^{10}}+\frac{6b}{\rho^2}\frac{M_++M_-}{M_+M_-}\left(2+2\frac{\rho}{r}-\frac{r}{\rho}\right)e^{-r/\rho}\right.$$
$$+\frac{b_+12}{\rho_+^2M_+}\left(2+2\frac{\rho_+}{r\sqrt{2}}-\frac{r\sqrt{2}}{\rho_+}\right)e^{-r\sqrt{2}/\rho_+}$$
$$\left.+\frac{b_-12}{\rho_-^2M_-}\left(2+2\frac{\rho_-}{r\sqrt{2}}-\frac{r\sqrt{2}}{\rho_-}\right)e^{-r\sqrt{2}/\rho_-}\right]. \qquad (32)$$

Here

$$C^*=30\left[\left(\frac{c_{--}}{M_-}+\frac{c_{++}}{M_+}\right)S''_8+c_{+-}\left(\frac{1}{M_+}+\frac{1}{M_-}\right)S'_8\right]$$

$$D^*=56\left[\left(\frac{d_{--}}{M_-}+\frac{d_{++}}{M_+}\right)S''_{10}+d_{+-}\left(\frac{1}{M_-}+\frac{1}{M_+}\right)S'_{10}\right]$$

and the c's, the d's, and the S's are defined by Mayer [1933]. Using the values for the constants found in Decker [1965] and in his reference, Mayer [1933], γ can be calculated numerically, and is shown in

385-762 O - 71 - 15

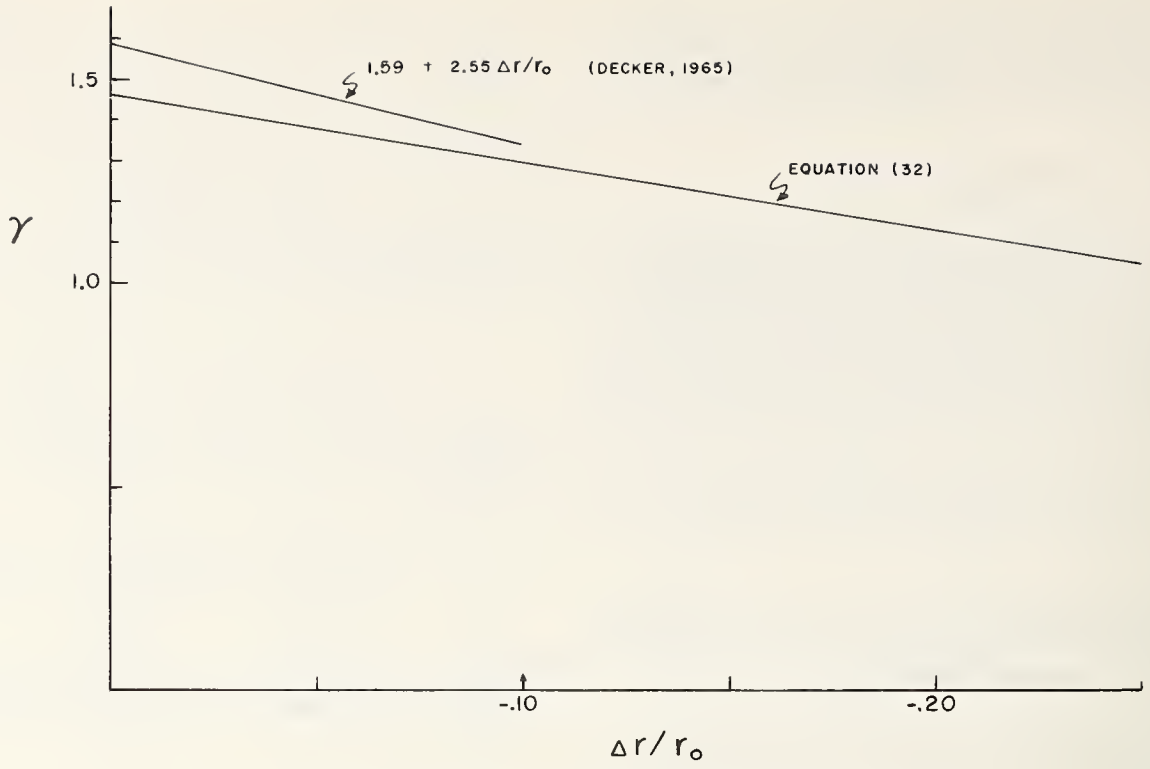

FIGURE 2. *Grüneisen parameter for the* NaCl *model of Decker [1965].*

figure 2. Also shown is the linear relation of Decker, and an arrow marking the maximum compression considered by him.

It is seen that, in the low-compression range, γ is nearly linear with $\Delta r/r_0$, with an initial value of 1.46, and an average slope of 1.70. It is nearly equivalent to a power law $\gamma/\gamma_0=(V/V_0)^q$ with exponent $q\approx 0.4$. Decker remarks that, for such behavior of γ, "the fit to the experimental thermal expansion became quite poor."

Decker's idea was that the equation of state of NaCl was sufficiently well understood theoretically that salt might be used as a pressure gauge in experiments on other materials. On the basis of the present remarks, it appears that the fourth-order anharmonic approximation, as used by Decker, is not sufficient to accurately describe the behavior of NaCl. The application of the sixth-order anharmonic treatment, straightforward in this case, might be expected to yield better agreement.

However, a feature of the central force assumption implies that even this will not be sufficient, unless an atomic interaction which includes non-central forces is used. Leibfried and Ludwig show that, for central forces in cubic crystals, the inequalities

$$c_{12} < c_{44} \tag{33a}$$

and

$$\left(\frac{dc_{12}}{dT}\right)_V < \left(\frac{dc_{44}}{dT}\right)_V \tag{33b}$$

are implied for the adiabatic elastic constants c_{ij}. If these are not satisfied by the data, then non-central forces must be involved. Such is the case for NaCl [Barsch and Chang, 1964]. It thus appears that a theoretical basis for accurately describing the properties of NaCl must include non-central forces.

8. Summary

The conclusions reached here are of three sorts; those relating to mutual consistency, those relating to internal consistency, and those relating to adequacy of approximation. Of the first sort:

1. Because, in eq (1), each $\gamma(T)$ must be treated differently, we conclude that the Birch-Murnaghan equation, in the form (1) and (4), is not consistent with lattice dynamics in the anharmonic high T approximation, nor with its results, the Mie-Grüneisen and Hildebrand equations.

2. However, with the modification implied by eq (17), the B–M equation becomes identical to the anharmonic high T equations, provided only that the term of (18) in e^4 can be shown to be negligible. The demonstration of this negligibility is beyond present experimental techniques.

3. The Murnaghan equation is consistent with the anharmonic high T equations, provided only that $R_0(T)$, eq (25), can be shown to be negligible compared to unity. The demonstration of this negligibility is beyond present experimental techniques.

4. Where two equations cannot be definitely proven consistent, they should not be used in the same calculation.

Of the second sort:

5. The Grüneisen parameter $\gamma(e)$ is defined in terms of boundary conditions by the expression in (23). Any other assumption on $\gamma(\rho)$, such as that of Slater [1939] or of Dugdale and MacDonald [1953], must converge to this at high temperature.

6. Once an assumption has been made concerning the interaction between atoms in a crystal, then the lattice dynamics is completely determined, and only the degree of approximation remains to be chosen. In particular, in the fourth-order approximation, when the interaction is assumed, ϕ_0, ω_i^2, and $\bar{\gamma}$ are all determined.

Of the third sort:

7. The data of NaCl are such as to require non central forces for an adequate theoretical explanation.

9. Acknowledgments

We appreciate helpful criticism from Francis Birch, and access to the unreduced data of Naohiro Soga. We thank the Journal of Geophysical Research for granting permission to reproduce substantial portions of Thomsen and Anderson [1969] in this review article.

This research was supported by the National Aeronautics and Space Administration under contract NSG–445, and by the National Science Foundation under grant GA–1208, and by the Air Force Office of Scientific Research under contract F44620–68–C–0079.

10. References

Alder, B. J., Is the mantle soluble in the core, J. Geophys. Res., **71**, No. 20, 4973 (1966).

Anderson, D. L., and Toksöz, M. N., Spherical waves on a spheroidal earth, J. Geophys. Res. **68**, No. 11, 3483 (1963).

Anderson, O. L., and Liebermann, R. C., Elastic constants of oxide compounds used to estimate the properties of the earth's interior, in Proc. NATO Advanced Study Institute: on the Application of Modern Physics to the Earth and Planetary Interiors, March 29–April 4, 1967, Newcastle upon Tyne, John Wiley & Sons, 1969.

Anderson, O. L., Schreiber, F., Liebermann, R. C., and Soga, N., Some elastic constant data on minerals relevant to geophysics, Rev. of Geophys., **6**, No. 4, 491 (1968).

Barsch, G. R., and Chang, Z. P., Pressure derivatives of the elastic constants for cubic symmetry—II. Numerical results, Phys. Stat. Sol. **19**, 139 (1967).

Birch, F., The effect of pressure upon the elastic parameters of isotropic solids, J. Appl. Phys. **9**, No. 4, 279 (1938).

Birch, F., Finite elastic strain of cubic crystals, Phys. Rev. **71**, 809 (1947).

Birch, F., Elasticity and constitution of the earth's interior, J. Geophys. Res. **57**, No. 2, 227 (1952).

Birch, F., Thermal expansion at high pressures, J. Geophys. Res. **73**, No. 2, 817 (1968).

Decker, D. L., Equation of state of NaCl, J. Appl. Phys. **36**, No. 1, 157 (1965).

Dugdale, J. S., and MacDonald, D. K. C., The thermal expansion of solids, Phys. Rev. **89**, No. 4, 832 (1953).

Fumi, F. G., and Tosi, M. P., On the Mie-Grüneisen and Hildebrand approximations, J. Phys. Chem. Solids **23**, 395 (1962).

Grüneisen, F., Zustand des festen Körpers, in Handbuch der Physik **10**, No. 22 (Springr-Verlag, Berlin, 1926). Also, in translation, NASA Republication RE 2–18–59W.

Hildebrand, J. H., Gitterenergien vom thermodynamischem Standpunkt aus, Z. Physik **67**, 127 (1931).

Johnson, L. P., Array measurements of *P* velocities in the upper mantle, J. Geophys. Res. **72**, No. 24, 6309 (1967).

Leibfried, G., and Ludwig, W., Theory of anharmonic effects in crystals, Solid State Physics **12** (Academic Press, New York, 1961).

McQueen, R. G., Marsh, S. P., and Fritz, J. N., The Hugoniot equation of state of twelve rocks, J. Geophys. Res. **72**, No. 20, 4999 (1967).

MacDonald, G. J. F., Radioactivity of the earth, J. Geophys. Res. **69**, No. 4, 2933 (1964).

Mayer, J. E., Van der Waals potential in the alkali halides, J. Chem. Phys. **1**, 270 (1933).

Murnaghan, F. D., Finite deformations of an elastic solid, Am J. Math. **59**, 235 (1937).

Murnaghan, F. D., The compressibility of media under extreme pressures, Proc. Natl. Acad. Sci. **30**, 244 (1944).

Schreiber, F., and Anderson, O. L., Pressure derivatives of the sound velocities of polycrystalline forsterite, with 6% porosity, J. Geophys. Res. **72**, No. 2, 762 (1967).

Slater, J. C., Introduction to Chemical Physics (McGraw-Hill, New York, 1939).

Soga, N., and Anderson, O. L., High-temperature elastic properties of polycrystalline MgO and Al_2O_3, J. Am. Ceram. Soc. **49**, No. 7, 355 (1966).

Soga, N., and Anderson, O. L., High-temperature elasticity and expansivity of forsterite and steatite, J. Am. Ceram. Soc. **50**, No. 5, 239 (1967).

Takeuchi, H., and Kanamori, H., Equations of state of matter from shock-wave experiments, J. Geophys. Res. **71**, No. 16, 3985 (1966).

Thomsen, L., and Anderson, O. L., On the high-temperature equation of state of solids, J. Geophys. Res. **74**, No. 4, 981 (1969).

Chairman: F. R. Boyd, Jr.
Geophysical Laboratory
Carnegie Institution of Washington

The Solid-Liquid Phase Line in Cu*

R. G. McQueen, W. J. Carter, J. N. Fritz, and S. P. Marsh

University of California, Los Alamos Scientific Laboratory, Los Alamos, New Mexico 87544

1. Introduction

It is well known that the increase in temperature due to shock loading is great enough to melt many solids with the shock strengths presently attainable in the laboratory. Using Hugoniot data and zero-pressure data it is possible to calculate with some confidence the shock strength required to melt a material on the pressure release wave. In a previous paper, [1],[1] these calculations ignored details of the true location of the melting phase line, since no information was available for this at high pressure, and in effect actually forced the phase line to be located at a fixed volume in the P–V plane. However, these calculations did conserve energy around the path determined by the Hugoniot, the pressure release isentrope and the zero pressure isobar. Subsequent measurements of the residual temperature of shock loaded Cu by J. Taylor [2] gave substantial agreement with these calculations. However gratifying these experiments were, the question of where the melting phase line at high pressure was located remained unanswered.

Aside from the basic interest in melting phenomena, the location of the phase line and the effect that melting might have on materials such as Cu when used as a shock-wave standard indicated that additional work should be done on this problem.

2. Experimental Program

Direct measurements to determine the location of the melting phase line at high temperatures and pressures appear to be either impossible or at best quite difficult. If the thermodynamics of the transition were of the correct type, a small break might be observed in the Hugoniot where melting first begins. However, as for most normally melting materials, the discontinuities that exist in the temperature-volume isobars appear only as a change in slope in the energy-volume isobars. Since it is the latter variables that are observed in shock-wave studies, it is not surprising that Hugoniot data, even in the sensitive $u_s - u_p$ plots, go smoothly through regions where melting is believed to occur. An alternative approach is to calculate the phase line from known zero-pressure data and the equation of state loci of the solid and liquid phases. Good equations of state exist for many solids and for some liquids but not for both phases of the same material. We have made an effort to obtain the Hugoniot equation of state for materials in the liquid phase that are normally solid. This was done by either preheating samples in electric furnaces or by preshocking the material under investigation by a shock strong enough to cause melting. Both techniques not only entertain additional experimental difficulties but also suffer from unfavorable precision requirements. An alternative approach is to measure the Hugoniot of a material at low initial density.

It is well known that shock-loading porous materials cause the internal energy at a given shock pressure to be substantially greater than that ob-

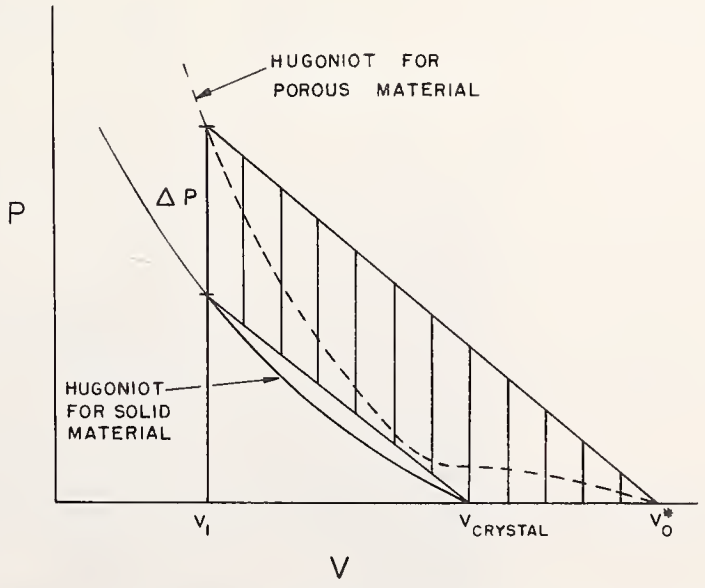

FIGURE 1. *Pressure versus volume schematic to illustrate how the use of porous materials increases the internal energy on shock loading.*

The area designated by the vertical lines represents the increase in internal energy due to shock loading at a low initial density.

*Work done under the auspices of the U.S. Atomic Energy Commission.
[1] Figures in brackets indicate the literature references at the end of this paper.

Paper presented at the Symposium on Accurate Characterization of the High-Pressure Environment, held at the National Bureau of Standards, Gaithersburg, Md., October 14–18, 1968.

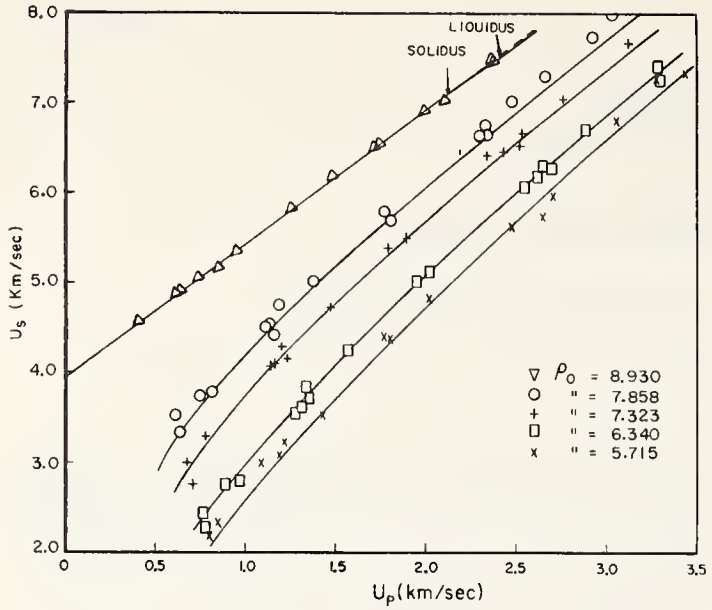

FIGURE 2. *Shock velocity-particle velocity data on* Cu *with various initial densities.*

The curve through the density 8.93 g/cm³ data has been drawn on the basis of the melted phase calculations. The onset and completion of melting in the crystal density Hugoniot are indicated. All other curves were obtained from the $\rho_0 = 7.323$ g/cm³ liquid Hugoniot and a $\gamma_0 = 2.6$.

tained on nonporous materials. The greater the porosity the greater will be the shock heating. This effect is demonstrated schematically in figure 1. In the past, experiments using porous specimens were used to obtain the high-pressure Grüneisen parameter or to check values of the Grüneisen function being used in equation-of-state calculations. If the porosity is large enough and the extra energy is sufficient to cause the high-pressure state to be in the liquid phase, one can use these data in an attempt to establish the Hugoniot of the material centered in the liquid state at a relatively high tem-

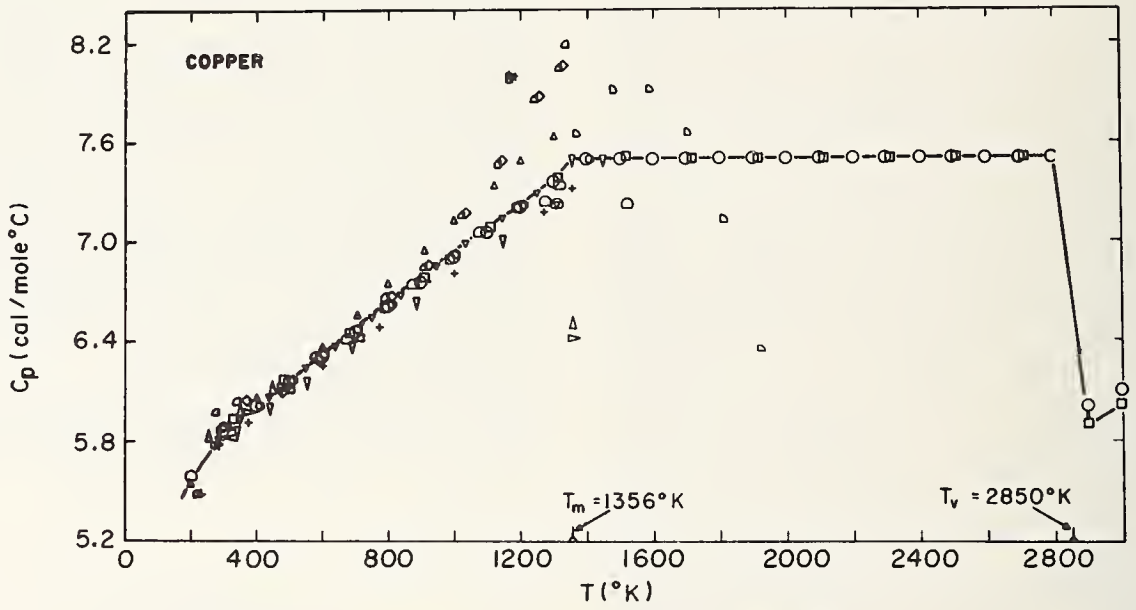

FIGURE 3. *Specific heat as a function of temperature for* Cu.

These data are from the compilation of ref. [4] and were obtained from the following original data sources:

Metals Handbook (American Society for Metals, Novelty, Ohio, 1961), 8th rev. ed.
Stull, D. R., and Sinke, G. C., Thermodynamic Properties of the Elements (American Chemical Society, Washington, 1956).
Stull, D. R., and Sinke, G. C., The Thermodynamic Properties of the Elements in Their Standard States (Dow Chemical Co., Midland, Mich., 1955).
Smithsonian Physical Tables. ed. W. E. Forsythe (Smithsonian Institution, Washington, 1956), 9th rev. ed.
Metals Reference Book, ed. C. J. Smithells (interscience, New York, 1955). Vol. II, 2d ed.
Rare Metals Handbook, ed. C. A. Hampel (Reinhold, New York, 1961), 2d ed.
Hultgren, R., Specific Heat of Metals and Alloys, AFOSR Tech. Note 4 (June, 1960).
Handbook of Chemistry, ed. N. A. Lange (McGraw-Hill, New York, 1961), 10th ed.
Handbook of Chemistry and Physics (Chemical Rubber Publ. Co., Cleveland, 1949), 31st ed.
Materials in Design Engineering, 50(5)141, Mid-October Issues, 1959. Kubaschewski, O., and Evans, E. L., Metallurgical Thermochemistry (Pergamon, Oxford, 1958), 3d ed.
Mechanical Properties of Metals and Alloys, National Bureau of Standards Circular C447 (Washington, 1943).
Engineering Materials Handbook, ed. C. L. Mantell (McGraw-Hill, New York, 1958).
Lucks, C. F., and Deem, H. W., Thermal Properties of Thirteen Metals, ASTM Special Tech. Publ. 227 (1958).
Butts, Allison, Copper; The Metal and Its Alloys (Reinhold, New York, 1954).
Fieldhouse, I. B., Hedge, J. C., Lang, J. I., and Waterman, T. E., Measurements of Thermal Properties I, WADC Tech. Rept. 55–495 (1956).
Fieldhouse, I. B., Hedge, J. C., Lang, J. I., and Waterman, T. E., Measurements of Thermal Properties II, WADC Tech. Rept. 55–495 (1956).
Seibel, R. D., and Mason, G. L., Thermal Properties of High Temperature Materials, WADC Tech. Rept. 57–468 (1958).
Lucks, C. F., and Deem, H. W., Thermal Conductivities, Heat Capacities, and Linear Thermal Expansion of Five Materials, WADC Tech. Rept. 55–496 (1955).
Makin, S. M., Standring, J., and Hunter, P. M., Determination of the Coefficients of Linear Thermal Expansion at *T*°C, R and DB(C)TT–45 (1953).
Bell, I. P., Fast Reactor-Physical Properties of Materials of Construction, Culcheth Laboratory FRDC/P–112 (Lancashire, England, 1955).
Johnson, V. J., A Compilation of Thermophysical Properties of Cryogenic Materials, WADC Progress Rept. 6 (1958).
Goldsmith, A., Waterman, T. E., and Hirschhorn, H. J., Thermophysical Properties of Solid Materials, Vol 1, WADC Tech. Rept. 58–376 (August, 1960).

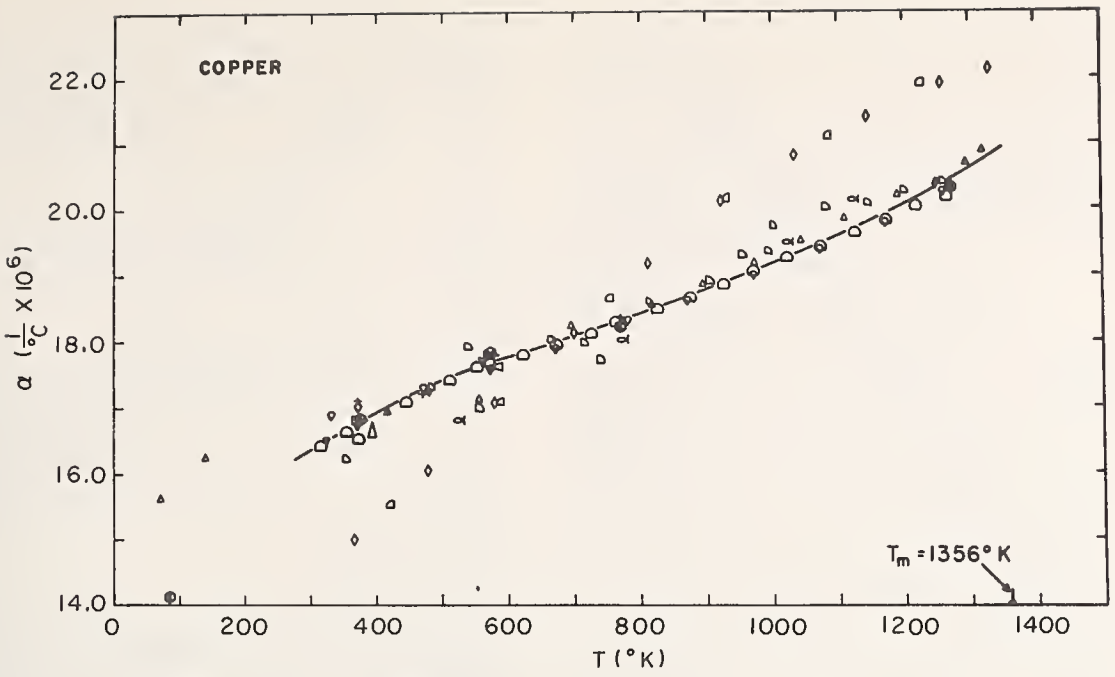

FIGURE 4. *Linear thermal expansion coefficients as a function of temperature.*

See ref. [4] for identification of the symbols.

perature. For the present application we have examined the shock-wave data on Cu measured in this laboratory. These data were obtained using the flash-gap impedance match technique with deoxidized Cu as a standard [3] and are summarized in figure 2. In addition to the shock-wave data it is necessary to know the thermodynamic equation of state along the $P=0$ isotherm. For this a compilation of specific heat data, figure 3, and thermal expansion data, figure 4, were used to determine the internal energy, E, and temperature, T, versus volume, V, given in figure 5 (see ref. [4]).

Hugoniot data were obtained for Cu at average initial densities of 8.93, 7.858, 7.323, 6.340, and 5.717 g/cm³. It is seen from figure 5 that the density 7.323 g/cm³ corresponds to a liquid density at $T=2370$ K, which is more or less in the center of the liquid phase region. It was this set of Hugoniot data that was used to determine the liquid Hugoniot equation of state centered at $T=2370$ K.

These data were fitted with a smooth curve in the u_s-u_p plane. Selected points on this curve were then recentered at this density and an initial internal energy corresponding to that volume as given in figure 5. The transformation is effected through the Hugoniot energy equation centered at $P_0=0$,

$$E=E_0+P(V_0-V)/2 \tag{1}$$

and the usual assumption that

$$\rho\gamma=\partial P/\partial E)_V \tag{2}$$

is a function of volume only. At a given volume, V, or density, ρ, the pressure increase, ΔP, due to

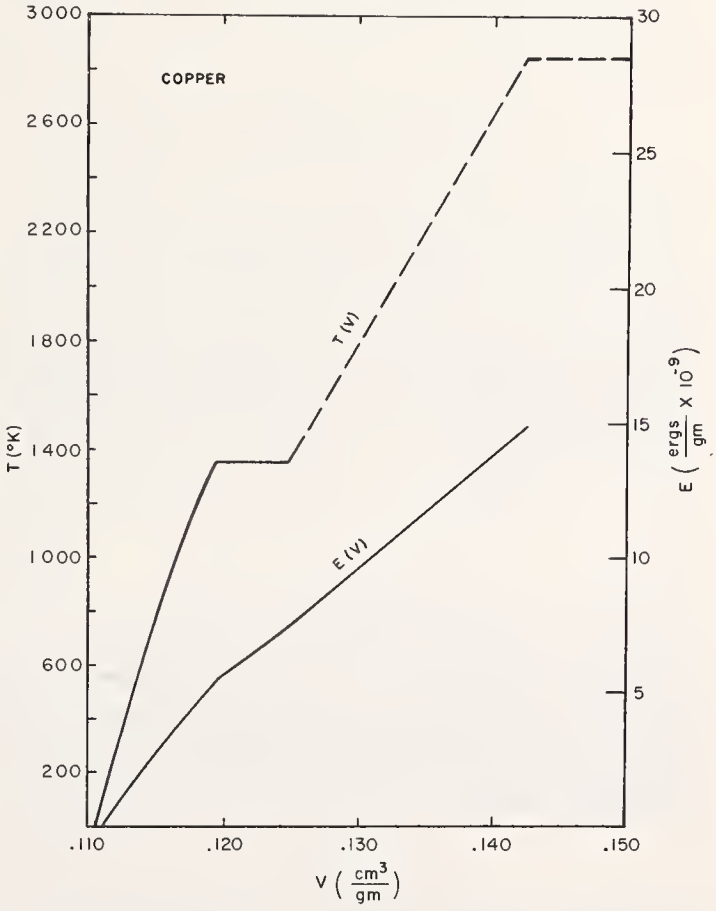

FIGURE 5. *Energy and temperature as functions of volume for* Cu.

These curves are required to establish initial conditions for the calculations were derived from the data presented in figures 3 and 4.

the assumed increase in initial thermal energy, ΔE_0, is given by

$$\Delta P=\rho\gamma\Delta E_0/(1-\rho\gamma(V_0-V)/2). \tag{3}$$

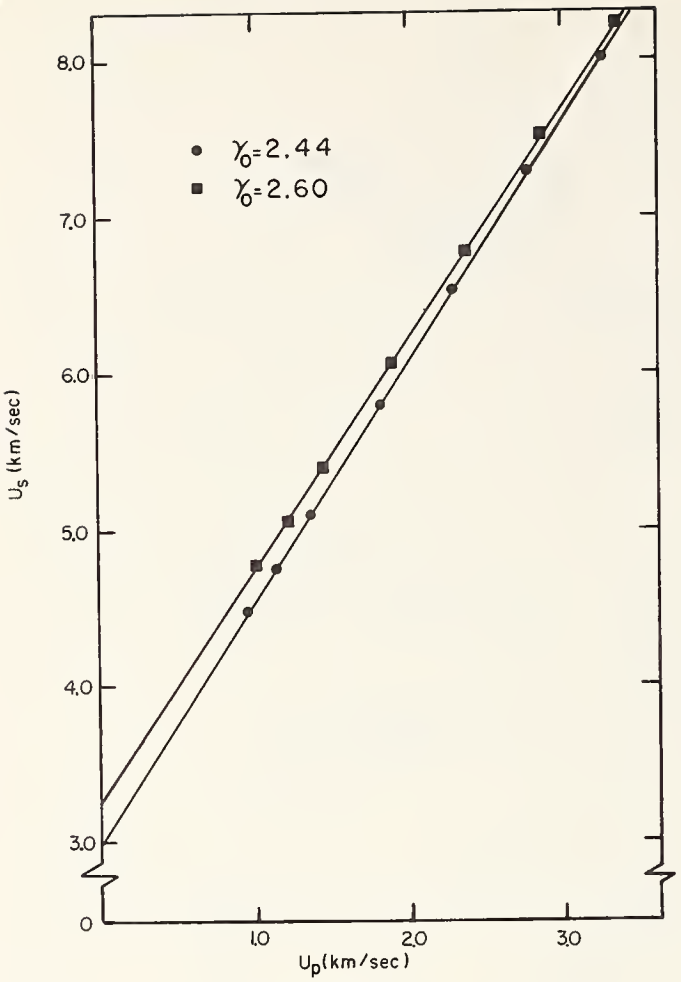

FIGURE 6. *Two* $u_s - u_p$ *transforms of the* $\rho_0 = 7.323$ *g/cm*^{3} *data centered at* T = 2370 °K *using* $\gamma_0 = 2.44$ *and* $\gamma_0 = 2.6$

In the present study $\rho\gamma$ was assumed to be constant. This gives the $P-V$ Hugoniot centered at the high-temperature point which can be transformed to the $u_s - u_p$ Hugoniot through the usual Hugoniot equations

$$u_s = V_0[(P-P_0)/V_0 - V)]^{1/2} \tag{4}$$

and

$$u_p = [(P-P_0)\ (V_0 - V)]^{1/2}. \tag{5}$$

The $u_s - u_p$ Hugoniots so determined were found to be quite linear in the region covered by the data. Two Hugoniots obtained by this technique using two values for $\rho\gamma$ are given in figure 6. The Hugoniot fits obtained from these curves are listed in table 1, where

$$u_s = c_0 + s u_p. \tag{6}$$

Although both sets fit the data adequately, it is apparent that the zero pressure sound velocities and slopes are very dependent upon the value of γ_0 used.

The value $\gamma_0 = 2.44$ comes from the room-temperature thermodynamic $\gamma = 2.0$ and the assumption that $(\rho\gamma)_{290\ K} = (\rho\gamma)_{2370\ K}$. This relationship has been shown to be reasonably compatible with the crystal density Hugoniot and the one centered at

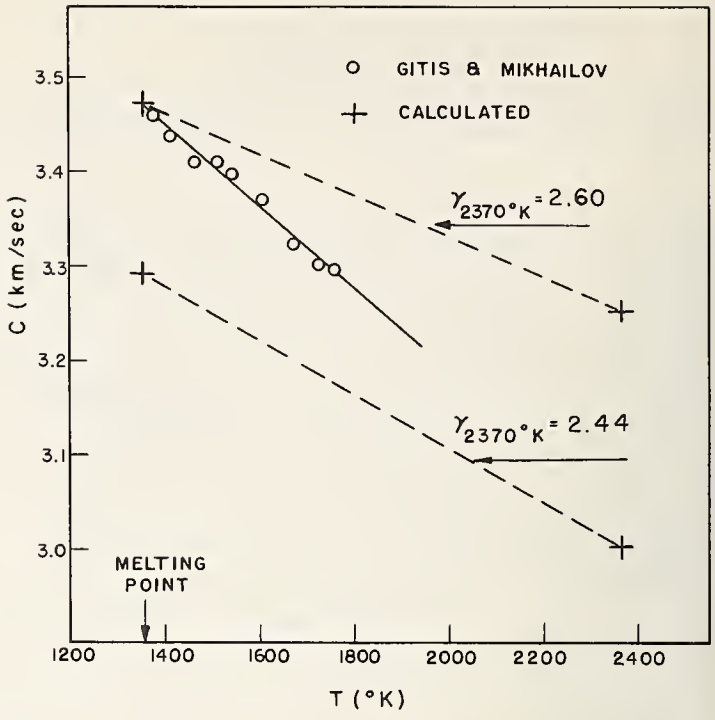

FIGURE 7. *Sound velocity versus temperature for liquid* Cu.

The dots, ○, are the data for Cu as reported by Gitis and Mikhailov [5]. The two +'s at $T = 2370$ °K are the Hugoniot intercepts listed in table 1. The two +'s at $T = 1356$ °K were calculated from the equation of state listed in table 1.

TABLE I.

ρ_0	γ_0	c_0	s
(*g/cm*^{3})		(*km/s*)	
7.323	2.6	3.25	1.49
7.323	2.44	3.00	1.54

$\rho_0 = 7.32$. However, close examination shows that when this approximation is used the calculated Hugoniot for $\rho_0 = 7.32$ does not give as precise agreement with the porous shock data as might be desired. This is most noticeable in the lower and upper pressure regions. Of course, there is no reason to believe that such a simple relationship ($\rho\gamma$=constant) should hold across a melting phase boundary. This value of γ does give a zero pressure intercept in the $u_s - u_p$ plane that is in good agreement with the sound velocity at $T = 2370$ K extrapolated from the data presented by Gitas and Mikhailov [5], but the calculated sound velocity using this γ and the Hugoniot fit is too low in the vicinity of the melting point (see fig. 7).

The sound velocity, c, at any pressure P, and volume, V, are computed from the Hugoniot and Grüneisen function through the relationship

$$c^2 = -V^2 \frac{dP_H}{dV}\left[1 - \rho\gamma(V_0 - V)/2\right] + V^2\rho\gamma(P - P_H)/2. \tag{7}$$

Equation (7) can be obtained by considering a small isentropic expansion at the point (P, V) and equating the ratio of the pressure and energy differences with the Grüneisen parameter. If eq (6) is used to define the Hugoniot then

$$P_H = \frac{c_0^2(V_0 - V)}{[V_0 - s(V_0 - V)]^2} \tag{8}$$

and

$$\frac{dP_h}{dV} = -c_0^2 \frac{[V_0 + s(V_0 - V)]}{[V_0 - s(V_0 - V)]^3}$$

which when substituted in eq (7) gives

$$(\rho c)^2 = c_0^2[V_0 + (s - \gamma_0)(V_0 - V)]/[V_0 - s(V_0 - V)]^3 + (\rho\gamma)P. \tag{10}$$

Using the equation of state for $\gamma = 2.6$ in table 1 and evaluating eq (10) at the melting volume yields a value of $c = 3.47$ km/s, which is in substantial agreement with the Russian data in the temperature region. If one believes that the temperatures at 7.32 g/cm³ and 8.01 g/cm³ are 2370 K and 1356 K respectively as read from the graph in figure 5, then sound velocity/temperature gradients of 0.22 m/s K and 0.29 m/s K are obtained in this temperature range. These slopes are about a factor of two less than the value quoted by Gitis and Mikhailov. There is no γ compatible with their slope of 0.46 m/s K. Some error is undoubtedly associated with the data in figure 5 but the thermal expansion data is certainly not so poor as to explain the discrepancy. The sound velocity measurements probably entertain larger errors than are quoted in the paper.

3. Calculated Phase Line

The P, V, E equation of state given by the Hugoniot and the Grüneisen function can be extended to a complete thermal equation of state through use of the thermodynamic identity

$$dS = C_V \frac{dT}{T} + C_V(\rho\gamma)dV \tag{11}$$

where C_V is heat capacity at constant volume. Thus the Gibbs free energy

$$G = E + PV - TS \tag{12}$$

can be computed for both the solid and liquid phases. The solid and liquid phases are coupled at the phase line through the requirement that

$$G_{\text{solid}} = G_{\text{liquid}}. \tag{13}$$

Since the difference in internal energies, ΔE_{L-S}, and the densities of the two phases at the melting point have been measured, it is necessary that the two equations of state also satisfy these conditions. This was done by slight adjustments of the values of C_V used for each phase so that a correct value for the average value of the thermal expansion was obtained. The correct initial internal energies are thus determined which are also required to be compatible with the data given in figure 5. Once this has been done, the phase line at higher pressures is located by satisfying eq. (13).

The results of one calculation are given in figure 8. Because of the thought that ordinary melting is determined by simple order-disorder arrangements which are reflected by a change in entropy, it was decided to see how these phase boundaries compared with lines of constant entropy. Hence we have plotted the two isentropes originating at the phase boundaries at $P = 0$. It can be seen that the two sets of curves are very similar, especially for the liquid boundary. This tells us immediately that the equation of state currently being used in impedance match solutions gives satisfactory solutions even in the high-pressure melted regime. $P - u_p$ plots demonstrating this are given in figure 9, where release isentropes currently being used are compared with those calculated with the postulated liquid equation of state. For assumed $\rho_0 u_s$ lines drawn on the graph there is less than one tenth percent disagreement in the region of interest, well within present experimental accuracy.

The standard room temperature Hugoniot intersects the phase line at a pressure of 1.33 Mbar. On the basis of equilibrium thermodynamics, we have computed the Hugoniot locus through the mixed phase region and into the liquid state. These results are also given in figure 8 and in the $u_s - u_p$ plane in figure 2. The points where the Hugoniot crosses the mixed-phase region are indicated in the graph. It is only by sighting down the curve that these can be detected. This indicates that it will probably be very difficult to establish the melting point on the Hugoniot by detecting kinks in the experimental data.

These results are comforting in that it suggests that hydrodynamic calculations used to study the effects of underground nuclear explosions can give meaningful results without a detailed description of the liquid equation of state. Moreover, since the very low initial-density porous Hugoniot data can be calculated relatively well, it appears that a detailed description of the vapor phase is also not required.

4. Comparison of the Phase Line With the Kraut-Kennedy Relation

Two papers have appeared recently in the literature [6, 7] in which it is reported that, for a wide range of materials, the melting temperature, T_m, varies linearly with the room-temperature isothermal

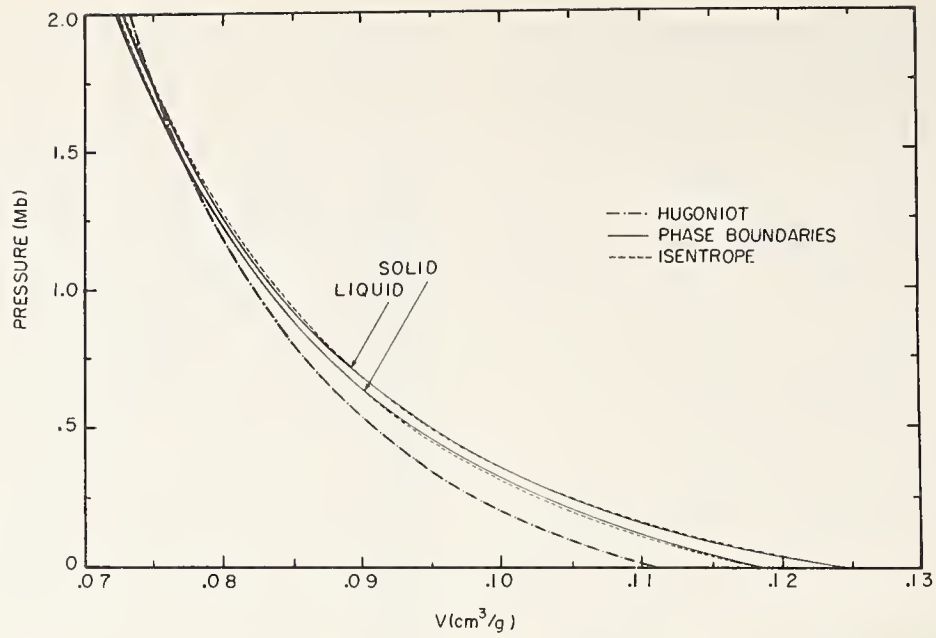

FIGURE 8. *Pressure-volume plots of the two calculated phase line boundaries, the isentropes originating at the melting boundary at* $P=0$, *and the crystal density Hugoniot.*

It can be seen that the phase-line boundaries predict a smaller volume change at high pressure for the transition than is indicated by volume separation of the two isentropes. In some calculations the volume change for the phase change approached zero, a situation that could be construed as the approach to a critical point. In all these calculations the results are suspect in the one Mbar region and above, since the liquid Hugoniot used for the calculations has been extrapolated far beyond the original data.

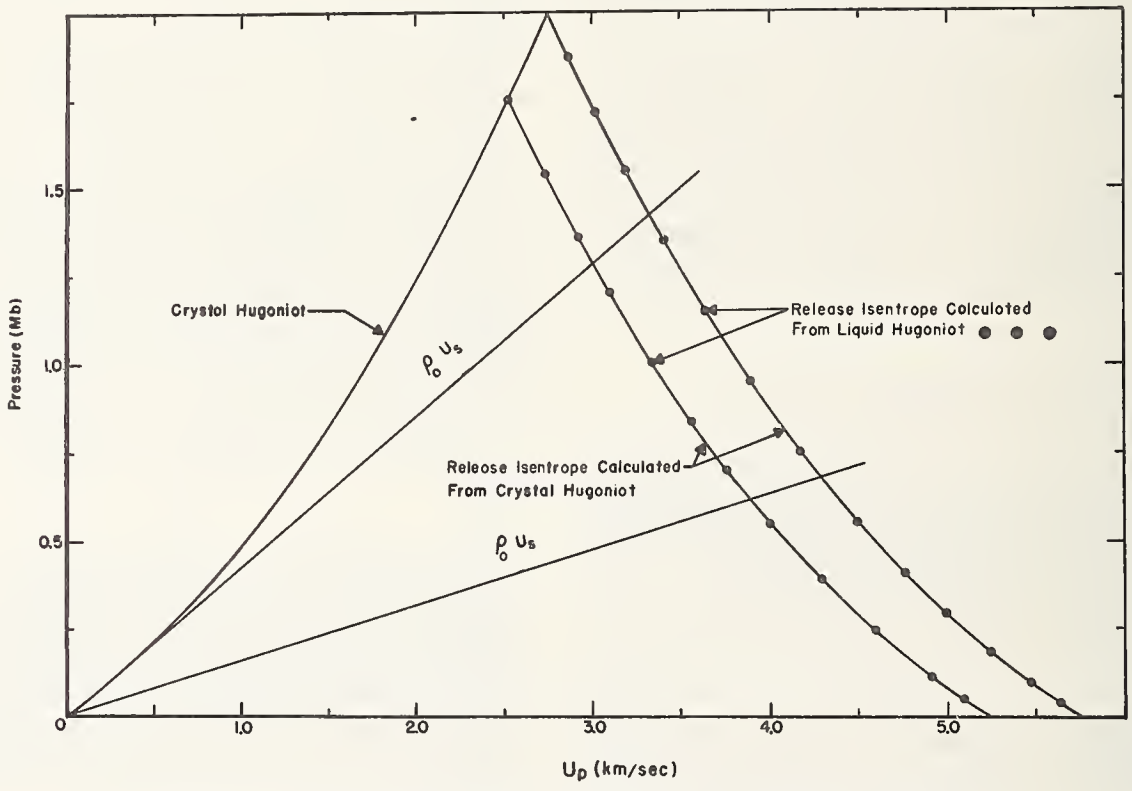

FIGURE 9. *Pressure-particle velocity curves from 1.75 Mbar and 2.0 Mbar.*
The solid curves were calculated from the crystal density Hugoniot and are currently being used in impedance-match solutions. The dots are selected points on the release isentrope and were calculated from the liquid equation of state. It is apparent that the current solutions are adequate.

volume compression $(\Delta V/V_0)_{RT}=(V_0-V)/V_0$, as

$$T_m=T_m^0\,[1+\alpha(\Delta V/V_0)_{RT}]. \tag{14}$$

Although the physical significance of the phenomena is obscure, their results are impressive and worth further investigation, especially with respect to possible uniqueness of the room temperature isotherm in predicting phase lines. We have already noted the simultaneity of the phase line with the boundary isentropes, and while the agreement is close, it is not exact. In general the volume change

for the transition decreases more rapidly than the volume separation of the two isentropes. In the temperature-volume plane this disagreement is considerably magnified. This can be seen in figure 10 where the temperature and compression, $\Delta V/V_{PL}$, along the phase line is compared with the temperature vs. compression along the two isentropes. The Kraut-Kennedy relationship is also compared in this plot. To obtain this plot we calculated the room temperature isotherm in the usual manner from the crystal density Hugoniot. The temperature-compression points were then tabulated from the isotherm and phase line at fixed pressure points. It can be noted that although these points are fairly linear they do bend downward at large compressions while the plotted isentropes are concave upward. The Kraut-Kennedy curve is more linear but suffers from the fact that the α coefficient is not a priori predictable. Similar P–T plots are given in figure 11.

5. Comparison of Shapes of the Melting Phase Lines with Compressibility Data

In an earlier paper [1] we compared the pressure-temperature data along the melting phase line with calculated pressure-temperature curves along isentropes. For the few selected cases the slopes of the isentropes, $dP/dT|_S$, were comparable but smaller than those of the phase lines. In light of the recent developments we have attempted to make a more extensive study of existing data.

By considering the total differentials of the phase line and the isentropes at the $P=0$ melting point the relationship

$$\frac{\left.\frac{dP}{dV}\right|_{PL}-\left.\frac{dP}{dV}\right|_{S}}{\left.\frac{dP}{dT}\right|_{PL}\left.\frac{dP}{dT}\right|_{S}}=\left[\left.\frac{dP}{dV}\right|_{PL}-\left.\frac{dP}{dV}\right|_{S}\right]\frac{1}{\rho\gamma C_v} \qquad (15)$$

between the slopes along the phase line (designated by PL) and isentropes (designated by S) can be obtained. Examination of eq (15) shows that if the $P-V$ slopes are the same then the initial $P-T$ slopes will also be identical. If the pressure-volume derivatives are not the same, considerably larger discrepancies will be found for the pressure-temperature derivatives. For this study it was decided to compare both pressure-temperature and pressure-volume derivatives.

With $dS=0$, eq (11) gives

$$\left.\frac{dP}{dV}\right|_S \Big/ \left.\frac{dP}{dT}\right|_S = T_m(\rho\gamma). \qquad (16)$$

Equation (15) can then be written as

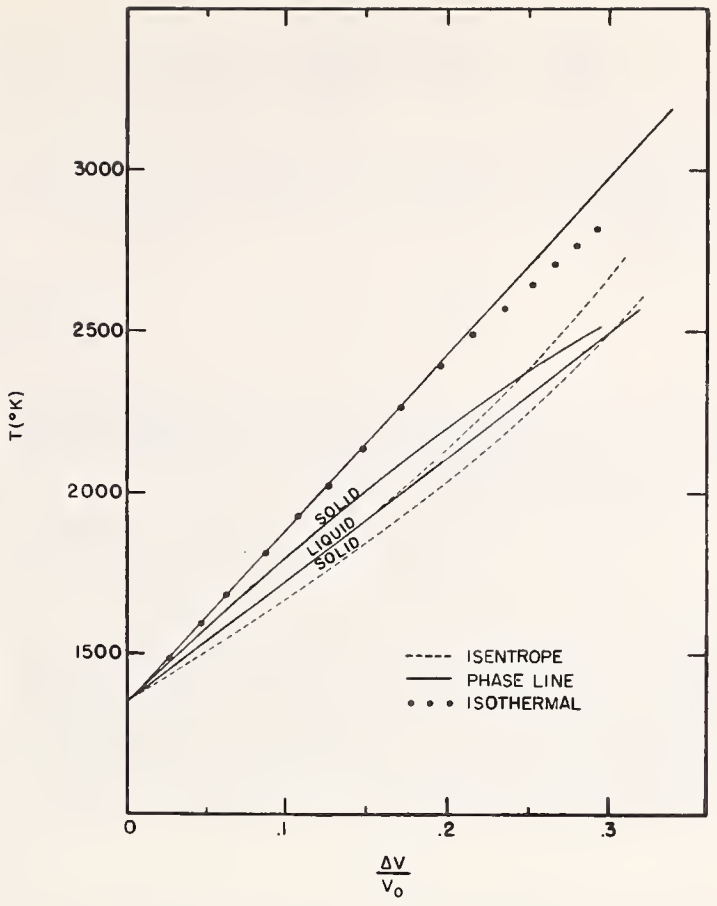

FIGURE 10. *Temperature versus* $\Delta V/V_0$.
The dots represent points calculated from the room temperature isotherm and phase line after Kraut and Kennedy. The solid line is simply a linear fit of the low pressure region. The other two solid lines represent the actual compression along the phase boundaries as given by the calculations. The dashed lines are similar quantities obtained from the isentropes plotted in figure 8. The initial agreement between the phase line and isentrope along the liquid boundary is quite good but becomes rather poor at higher temperatures, a manifestation of the more rapid decrease in the size of the volume change on the actual phase line.

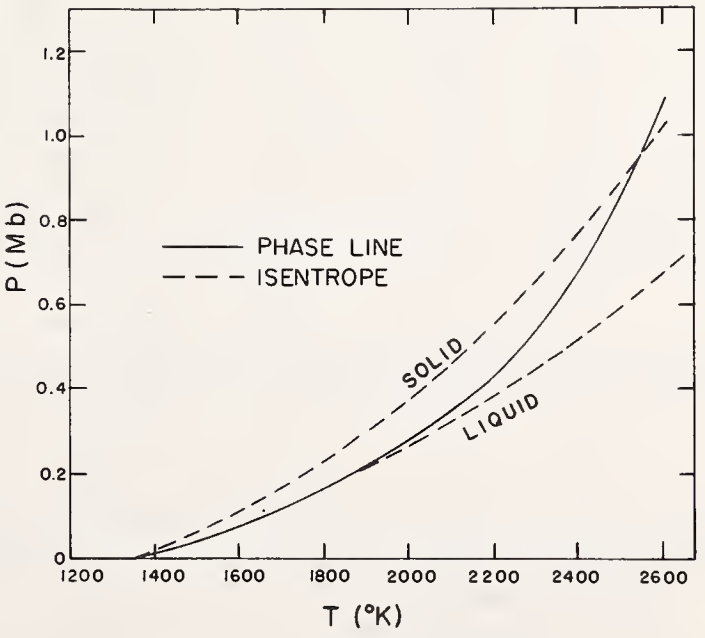

FIGURE 11. *Pressure versus temperature.*
The solid line represents the calculated phase line and the dashed lines the pressure-temperature loci along the two isentropes. As before the agreement between the phase line and the calculated liquid isentrope is good initially. The phase line crosses the solid isentrope at about one Mbar, indicating that although the isentropes do not give the exact location of the phase line they indicate, in this case, that melting does occur at nearly constant entropy.

$$\left.\frac{dP}{dV}\right|_{PL} = \left.\frac{dP}{dT}\right|_{PL} \frac{\left\{\left.\frac{dP}{dT}\right|_S + TC_V(\rho\gamma)^2\right\}}{dP/dT|_{PL} - (\rho\gamma)C_V} \tag{17}$$

to find the $P-V$ slopes of the phase line in terms of other thermodynamic quantities. The quantity $dP/dV|_S$ was computed from eq (10) and the relationship

$$\left.\frac{dP}{dV}\right|_S = -(\rho c)^2. \tag{18}$$

All quantities are computed at $P=0$ at the melting point. The product $\rho\gamma=$ constant, was determined from room temperature quantities. Results of these calculations are listed in table 2.

From these data it can be seen that the initial P–V slopes of the isentropes at the phase boundary are in general smaller than the P–V slopes of the phase lines by several percent. This results in the isentropic slope, $dP/dT|s$, being larger than the slope of the phase line. The agreement is better when phase lines are compared with the room-temperature isentropic compressions. The room temperature isothermal compressions will be slightly larger and the zero-Kelvin compressions slightly smaller than the latter. It would be fortunate if the agreement were better so that these results could be extrapolated to other materials with greater confidence. However, one must keep in mind that many of the quantities listed in these tables are of a very dubious quality, and perhaps the agreement, both good and bad, is fortuitous.

As was noted in the Kraut-Kennedy paper, their law is an approximation of the equation

$$T_M = T_M^\circ \exp\left[\alpha\Delta V/V_0\right]. \tag{19}$$

This of course is the equation for the temperature along an isentrope. Equation (11) when integrated along the isentrope gives

$$T = T_0 \exp\left[-(\rho\gamma)\Delta V\right] \tag{20}$$

where the compression is taken along the isentrope. From the table it can be seen that eq (20) will give very nearly the correct initial slope of the phase line, better in general than that obtained when using the isothermal compression at the phase line.

TABLE 2.

Material	ρ_0 g/cm^3	c_0 km/sec	s	γ_0	C_P (a) ergs/g°K	T_M °K	ρ_M g/cm^3	c_{MP} km/sec	$dP/dT\|_S$ kb/°K	$dP/dT\|_{PL}$ kb/°K	c_{PL}* km/sec	c_{PL}/c_{MP}	c_{PL}/c_0
Li	0.53	4.65	1.13	0.81	32.80×10^6	453	0.512	4.51	.28	.300[b]	4.32	0.96	.93
Na	0.968	2.63	1.22	1.17	12.40	371	0.951	2.59	.14	.120[b]	2.62	1.01	1.00
K	0.86	1.97	1.18	1.23	7.53	337	0.851	1.96	.078	.078[b]	1.96	1.00	1.00
Rb	1.53	1.13	1.27	1.06	3.35	312	1.51	1.12	.057	.069[b]	1.11	0.99	.98
Cs	1.826	0.70	1.57	0.54	2.18	303	1.844	0.713	.058	.040[f]	.719	1.01	1.03
Cu	8.93	3.94	1.49	2.00	3.70	1356	8.368	3.71	.40	.280[c]	3.87	1.04	.98
Ag	10.49	3.23	1.60	2.50	2.34	1234	9.658	3.00	.26	.210[c]	3.12	1.04	.97
Au	19.32	2.99	1.56	2.97	1.30	1336	18.28	2.89	.37	.160[c]	3.53	1.22	1.18
Mg	1.74	4.49	1.26	1.43	10.00	923	1.640	4.28	.21	.148[f]	4.42	1.03	.98
Zn	7.14	3.01	1.58	2.45	3.69	693	6.98	2.95	.35	.225[f]	3.15	1.07	1.05
Cd	8.64	2.43	1.68	2.32	2.30	594	8.419	2.36	.33	.160[f]	2.60	1.10	1.07
Hg	13.54	1.49	2.05	1.96	1.39	234	14.148	1.64	.09	.183[d]	1.80	1.10	1.21
Al	2.706	5.17	1.47	2.0	8.63	933	2.540	4.88	.30	.17 [e]	5.28	1.08	1.02
In	7.279	2.42	1.54	1.97	2.43	430	7.190	2.39	.48	.240[e]	2.49	1.04	1.03
Tl	11.85	1.86	1.52	2.25	1.30	576	11.66	1.84	.30	.160[e]	1.95	1.06	1.05
Sn	7.287	2.61	1.49	2.11	2.27	505	7.176	2.57	.44	.300[f]	2.63	1.02	1.01
Pb	11.34	2.05	1.46	2.77	1.30	601	10.984	2.02	.26	.120[f]	2.28	1.13	1.11
Nb	8.59	4.44	1.21	1.47	2.65	2693	8.047	4.25	.34	.200[f]	4.43	1.04	1.00
Ta	16.65	3.41	1.20	1.60	1.37	3270	15.39	3.26	.29	.200[f]	3.37	1.03	.99
Pd	11.99	3.95	1.59	2.26	2.33	1823	11.244	3.70	.35	.25[f]	3.88	1.05	.98
Pt	21.42	3.60	1.54	2.40	1.27	2043	20.174	3.42	.45	.240[f]	3.70	1.08	1.03

* $c_{PL} = V(-dP/dV_{PL})^{1/2}$

a. Rare Metals Handbook, 2nd Ed., C. A. Hampel, ed., Reinhold Publishing Corp., London (1961).

b. H. D. Luedemann and G. C. Kennedy, J. Geophys. Res. 73, 2795 (1968).

c. L. H. Cohen, W. Klement, Jr., and G. C. Kennedy, Phys. Rev. 145, 519 (1966).

d. A. V. Grosse, J. Inorg. Nuc. Chem. 27, 773 (1965).

e. A. Jayaraman, W. Klement, Jr., R. C. Newton and G. C. Kennedy, J. Phys. Chem. Solids 24, 7 (1963).

f. Metals Reference Book, Vol. 2, 2nd Ed., C. J. Smithells, ed., Interscience Publishers Inc., New York (1955).

6. References

[1] McQueen, R. G., and Marsh, S. P., J. Appl. Phys. **31**, 1253 (1960).
[2] Taylor, J. W., J. Appl. Phys. **34**, 2727 (1963).
[3] McQueen, R. G., Marsh, S. P., Carter, W. J., Fritz, J. N., and Taylor, J. W., High Velocity Impact Phenomena, ed. E. V. Cohen (Academic Press, Inc., New York), in press.
[4] Carter, W. J., Thermodynamic Properties of Seven Metals at Zero Pressure, LAMS-2640 (1961).
[5] Gitis, M. B., and Mikhailov, I. G., Akusticheskii Zhurnal **11**, 434 (1965); Soviet Physics-Acoustics **11**, 372 (1966).
[6] Kraut, E. A., and Kennedy, G. C., Phys. Rev. Letters **16**, 608 (1966).
[7] Kraut, E. A., and Kennedy, G. C., Phys. Rev. **151**, 668 (1966).

DISCUSSION

M. van Thiel (*Lawrence Radiation Laboratory, University of California, Livermore, California*): The graph of figure 10 indicates that the mixed phase region increases with increasing temperature. Would you comment on the significance of this? Also, in figure 10, would you explain the meaning of ΔV?

J. O. Erkman (*U.S. Naval Ordnance Laboratory, White Oak, Maryland*): In experiments with porous material, to what degree do you have a steady shock? How much error is introduced from this source?

R. Grover (*Lawrence Radiation Laboratory, University of California, Livermore, California*): Is the value of ΔS and ΔV at transition, and the agreement between the isentrope and the melting line, particularly sensitive to the assumption of a constant value for $\rho\gamma$? I have tried to estimate the changes in gamma on melting, and find values between, say, 10 percent and 20 percent.

F. R. Boyd, Jr. (*Geophysical Laboratory, Carnegie Institution of Washington, Washington, D.C.*): You mentioned the fact that there was no substance for which there is a Hugoniot for both the solid and the liquid. Since there is a Hugoniot for liquid mercury, would it not be a practical and significant experiment to freeze mercury and shock it?

AUTHORS' CLOSURE

In reply to van Thiel: It is difficult to judge the size of the mixed phase region from figure 10. From figure 8, however, it can be seen that the mixed phase region decreases with increasing pressure, or equivalently with increasing temperature. Of course, if the phase line is indeed an isentrope, then from the Clapeyron equation it must be this ΔV that is causing the curvature of the phase line seen in figures 10 and 11.

In reply to Erkman: We assume that we have a steady shock front. This is a bothersome problem, particularly at very low pressures, and we do not know to what extent we fail to realize this condition, nor how much error is introduced. However, at sufficiently high pressures, far above that required for void collapse, steady state flow should be attained. Much more work remains to be done on the shock properties of porous materials.

Replying to Grover: Isentropes are not extremely sensitive to the functional form of $\gamma(v)$, or even to the value of γ. However, the position of the phase line is somewhat more sensitive to $\gamma(v)$, since γ is an important thermodynamic parameter distinguishing the two phases and is needed to calculate the locus $\Delta G=0$. Here, the functional form of γ is much more important, and the assumption of constant $\rho\gamma$ may not be valid. Ten percent is about the increase in gamma from the solid to the liquid which we predict by this model, in good agreement with Grover's estimate.

Dr. Boyd's suggestion for shocking frozen mercury could, I think, be quite easily done, and would be a most interesting experiment.

Shear Strength Effects on Phase Transition "Pressures" Determined From Shock-Compression Experiments*

O. E. Jones and R. A. Graham

Sandia Laboratories, Albuquerque, New Mexico 87115

Plane-wave shock compression experiments provide an independent, and often unique, method for establishing pressures at which phase transitions occur in solids. The transition stress which is measured in a shock experiment consists of two components: a mean isotropic pressure, and a deviatoric shear stress which is related to the yield strength, i.e., the Hugoniot elastic limit (HEL), of the solid when subjected to shock compression. The effects of the nonzero shear strength of a solid on the measured shock transition stress are discussed, and methods outlined for calculating the isotropic pressure component needed for comparison with hydrostatic results. Comparison requires that the compression to initiate the transition be independent of shear distortion. The shock propagation characteristics of a solid which are necessary for establishing a reliable equilibrium transition pressure are considered. Existing HEL data are collected in an Appendix and permit the importance of shear strength to be assessed for various materials. Shock compression data for phase transitions in Bi, Fe, Ge, CdS, and InSb are analyzed and shear strength corrections applied to obtain transition pressures.

1. Introduction

Discovery in shock compression experiments of the "130 kbar" polymorphic transition in iron by Bancroft et al. [1][1] in 1956, the observation of a shock-induced transition in bismuth [2], and the subsequent identification of the iron transition in static high-pressure experiments [3–8] have resulted in interest in shock compression as a method for establishing transition pressures. However, because solids have nonzero shear strengths, shock compression is not isotropic; if this shear strength is a substantial fraction of the transition stress, corrections to the shock measurements are required to obtain values comparable to hydrostatic values. Although it was recognized early [1, 9] that the finite shear strength of a solid gives rise to an elastic wavefront, whose amplitude is termed the Hugoniot elastic limit (HEL), shock transition stresses have frequently been directly compared to hydrostatic values and have not been corrected for shear strength effects. More recent development of techniques capable of examining the elastic wavefront in detail have yielded considerable HEL data which can now be used to calculate isotropic pressures from measured shock transition stresses, provided that equilibrium conditions are achieved.

After accounting for the contribution of the shear strength of the solid to the shock transition stress, the resulting value must be further corrected to isothermal conditions for comparison with hydrostatic results. In most cases, the temperature correction is smaller than that for the shear strength. In this paper, primary attention will be focused on shear strength effects.

*This work was supported by the U.S. Atomic Energy Commission.

[1] Figures in brackets indicate the literature references at the end of this paper.

Paper presented at the Symposium on Accurate Characterization of the High-Pressure Environment, held at the National Bureau of Standards, Gaithersburg, Md., October 14–18, 1968.

The object of this paper is to survey effects of the finite shear strength of a solid on the stress component measured in a shock-compression experiment [10] and to discuss how, in an idealized situation, this value may be corrected for comparison with hydrostatic values [11]. Deviations from this idealized behavior are examined, and an extensive collection of Hugoniot elastic limit references is reported and summarized in an Appendix. Then, several representative phase transitions, for which relatively complete data are available, are discussed and finite shear strength corrections are made. The compressions at which the shock and hydrostatic transitions occur are evaluated to assess the effects of shear on the transition pressures.

2. Stress Configuration Under Shock-Wave Compression

2.1. Uniaxial Strain [10]

Although all static very-high-pressure experiments involve some shear stress components, the idealized experiment involves only isotropic pressure, regardless of the pressure magnitude. On the other hand, plane-wave shock compression produces a precisely defined state of uniaxial strain in which shear stresses can be appreciable. Uniaxial strain is produced by simultaneously applying a uniform normal stress over the entire face of a homogeneous specimen in the form of a flat plate whose thickness is much less than its lateral dimensions. For a short period of time, before the arrival of unloading waves from the lateral edges, symmetry requires that each macroscopic volume element deform in the same manner as the adjacent volume element; thus, there is no net lateral deformation and compression occurs only in the direction of shock propagation.

This condition is illustrated in figure 1, where the principal strains $\epsilon_y = \epsilon_z$ in the plane of the plate

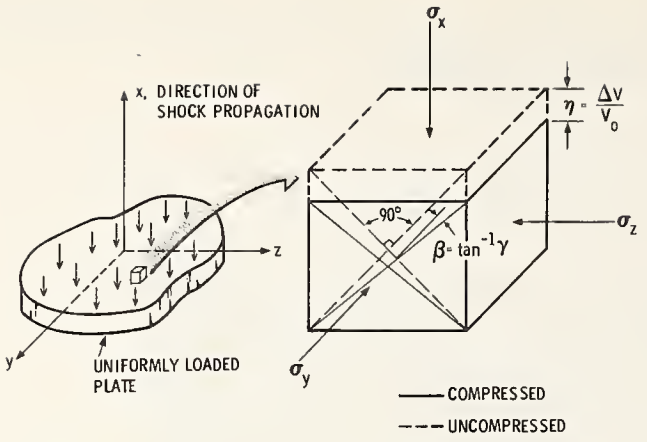

FIGURE 1. *Uniaxial strain compression of a volume element of an isotropic plate.*

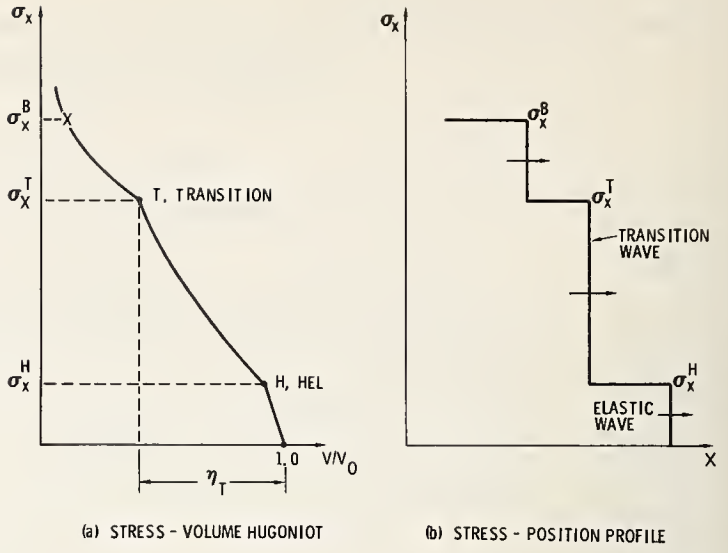

FIGURE 2. (a) *Hugoniot stress-volume curve for a solid exhibiting simple* yield and transition points. (b) *Corresponding multiple-wave stress-position profile for driving stress* σ_x^B.

are maintained equal to zero by the principal lateral stresses σ_y and σ_z. (For an isotropic material the lateral stresses are equal.) That uniaxial strain compression intrinsically involves shear strain is immediately evident from figure 1. The angular change θ in the original right angle between the face diagonals of the cube is equal to $\tan^{-1}\gamma$, where γ is the engineering shear strain. Because a solid has nonzero shear strength and can resist shear deformation the lateral stresses σ_y and σ_z will not be equal to the stress σ_x, and the stress state is anisotropic. In shock experiments, the stress component σ_x acting normal to the shock front is determined; except by inference, the lateral stress components are unknown.

Thus, because of this stress anisotropy, shear stresses are generated on planes inclined to the shock front. Their magnitude is limited by the shear strength of the solid. When the magnitude of the maximum shear stress exceeds some characteristic limiting value, the solid loses its resistance to shear deformation and yields in a manner which may be either plastic or brittle in character. In general, shear stresses are present in the yielded state above the yield point; however, in contrast to the elastic state, they undergo only small changes with increasing compression.

A representative stress-volume Hugoniot curve is shown in figure 2 for a solid which exhibits both a simple yield point and phase transition point. The yield point stress, obtained under shock conditions of uniaxial strain, is commonly termed the Hugoniot elastic limit (HEL). By "simple" we mean that rate effects are negligible and stress equilibrium is achieved. In this case shock wave propagation is steady, and the HEL and the transition stress have time-independent values. (Deviations from simple behavior will be discussed later.) In this case, the Hugoniot jump relations [10], expressing conservation of mass, momentum, and energy, describe points of the Hugoniot curve:

$$\eta \equiv \frac{\Delta V}{V_i} = \frac{u - u_i}{U - u_i}, \tag{1}$$

$$\sigma_x - \sigma_{xi} = \rho_i (U - u_i)(u - u_i), \tag{2}$$

$$E - E_i = \tfrac{1}{2}(\sigma_x + \sigma_{xi})(V_i - V), \tag{3}$$

where η is the compression, $V(=1/\rho)$ is specific volume, ρ is density, σ_x is the stress component acting normal to the shock front, U is laboratory shock velocity, u is particle velocity, and the subscript i denotes the state of the material ahead of the particular shock front under consideration.

2.2. Elastic-Plastic Behavior [12–14]

For an isotropic, plastically yielding solid, further insight into shock compression results from expressing the stress σ_x in terms of its spherical, of hydrostatic, component $\bar{P}$ and its deviatoric, or shear, component τ. By definition,

$$\bar{P} \equiv \tfrac{1}{3}(\sigma_x + \sigma_y + \sigma_z) = \sigma_x - \tfrac{2}{3}(\sigma_x - \sigma_y), \tag{4}$$

where, for an isotropic, homogeneous solid, $\sigma_y = \sigma_z$ by symmetry. The maximum resolved shear stress occurs at 45° to the plane of the shock front and is given by,

$$\tau = \frac{1}{2}(\sigma_x - \sigma_y). \tag{5}$$

Combining eqs (4) and (5),

$$\sigma_x = \bar{P} + \frac{4}{3}\tau, \tag{6}$$

$$\sigma_y = \bar{P} - \frac{2}{3}\tau. \tag{7}$$

Equations (6) and (7) are true regardless of the stress-strain relation for the solid.

For stresses below the HEL in figure 2, Hooke's law applies, and, for uniaxial strain ($\epsilon_y=\epsilon_z=0$), becomes,

$$\sigma_x=\left(K+\frac{4}{3}\mu\right)\eta, \qquad \text{for } \sigma_x \leq \sigma_x^H, \tag{8}$$

$$\sigma_y=\sigma_z=\left(K-\frac{2}{3}\mu\right)\eta, \qquad \text{for } \sigma_x \leq \sigma_x^H, \tag{9}$$

where K is the bulk modulus, μ is the shear modulus, and σ_x^H is HEL value of the stress σ_x. Equations (8) and (9) relate σ_x and σ_y:

$$\sigma_y=\sigma_z=\frac{\nu}{1-\nu}\sigma_x \qquad \text{for } \sigma_x \leq \sigma_x^H, \tag{10}$$

where ν is Poisson's ratio. For most isotropic solids $\nu \cong 1/3$; thus, for an isotropic material stressed below the HEL, the lateral stresses (cf. fig. 1) are about one-half the applied stress. The maximum resolved shear stress is obtained from eqs (5) and (10),

$$\tau=\frac{(1-2\nu)}{2(1-\nu)}\sigma_x=\mu\eta, \text{ for } \sigma_x \leq \sigma_x^H, \tag{11}$$

while the mean pressure $\bar{P}$ is, from eqs (6) and (11),

$$\bar{P}=\frac{(1+\nu)}{3(1-\nu)}\sigma_x, \text{ for } \sigma_x \leq \sigma_x^H, \tag{12a}$$

$$=K\eta \tag{12b}$$

which for $\nu=1/3$ is equal to about two-thirds of the applied stress σ_x. If the bulk modulus K is understood to be dependent on compression η, eq (12b) is also applicable for $\sigma_x > \sigma_x^H$.

Equation (11) shows that as σ_x and η increase, the maximum resolved shear stress τ increases. Because the shear strength of a solid is finite, the material will fail in shear at some critical value of stress σ_x^H corresponding to the HEL. This loss of shear resistance results in a sudden increase in the compressibility of the material and is responsible for the cusp at point H in figure 3. The stresses σ_x, $\bar{P}$, and τ are shown schematically in figure 3. Transformation of the material to the new phase at point T in figure 3 again results in an abrupt increase in the compressibility and a cusp in the Hugoniot curve at point T. The cusps at points H and T create concave downward regions in the Hugoniot curve, and result in the propagation of the multiple wave structure [10] shown schematically in figure 2.

For elastic-perfectly plastic behavior the shear stress above the HEL is idealized as having a constant value, independent of the stress amplitude, as shown in figure 3. This limiting shear stress τ^* is, from eq (11),

$$\tau^*=\frac{1}{2}\frac{(1-2\nu)}{(1-\nu)}\sigma_x^H. \tag{13}$$

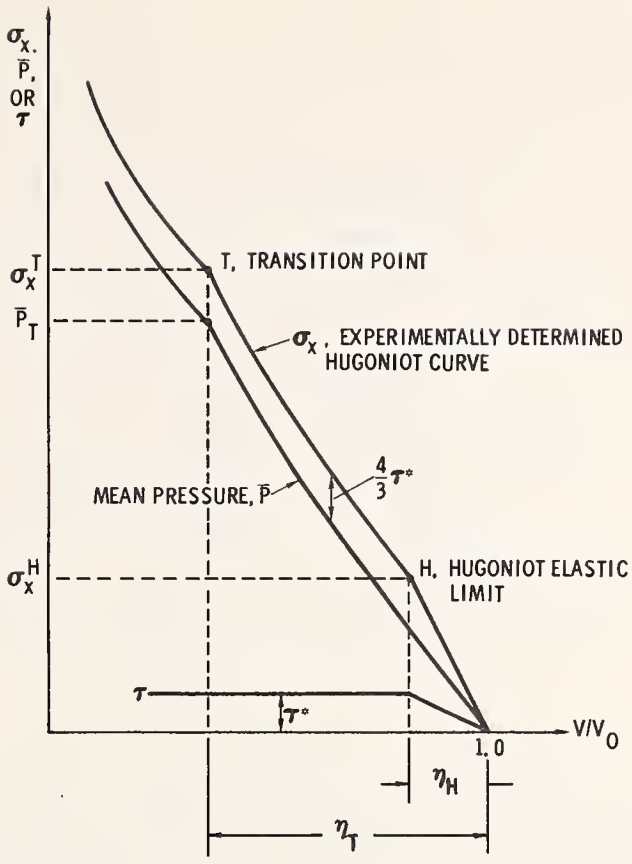

FIGURE 3. *Schematic diagram of the stress-volume behavior of a simple, elastic-perfectly plastic solid subjected to shock compression.*

It is likely that τ^* will increase somewhat with increasing compression as a result of work-hardening; however, for our purposes, we will ignore work-hardening as a higher order effect because its influence on σ_x (cf. eq (6) and fig. 3) will be small due to the dominance of the mean pressure $\bar{P}$. It has also been suggested that τ^* may increase with increasing $\bar{P}$. In the case of τ^* constant, the Hugoniot curve, as shown in figure 3, is parallel to the isotropic compression curve and offset above it by an amount $(4/3)\tau^*$ If the HEL is measured, then the mean pressure $\bar{P}$ can be calculated from the measured values of σ_x.

Early measurements by Fowles [14] and Lundergan et al. [15] demonstrated that an elastic-perfectly plastic model adequately described the shock compression of aluminum. More recent measurements [16–22] with improved time resolution show detectable rate effects in aluminum and other metals; but, it is observed that these effects do not cause significant departures from the final stress-volume states predicted by the elastic-perfectly plastic model.

Summarizing, in a simple (rate-independent) isotropic material exhibiting elastic-perfectly plastic behavior, a shock-induced phase transition occurs in the presence of shear stresses which cause a difference between the measured shock transition stress and the transition pressure determined hydro-

385-762 O - 71 - 16

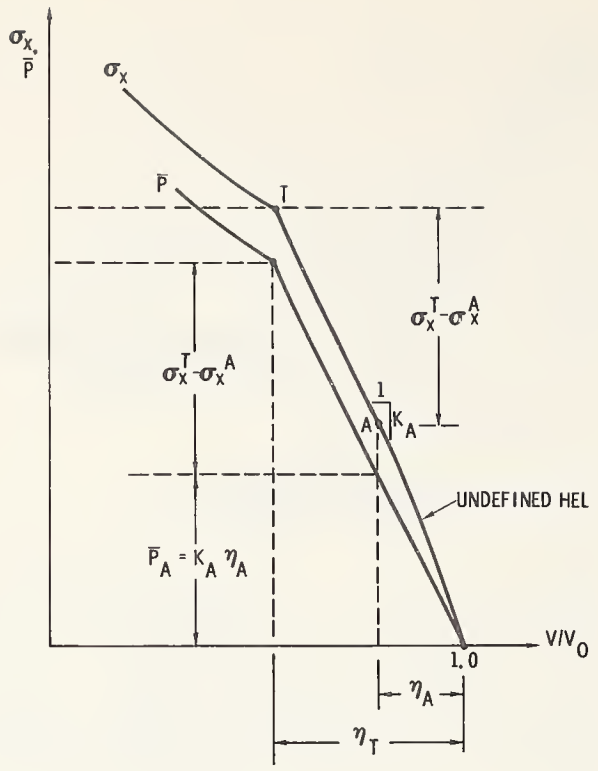

FIGURE 4. *Alternative procedure for determining the transition pressure for a simple solid which does not have a sharply defined HEL.*

statically. Because of these shear stresses, a transition pressure calculated from the shock transition stress is comparable to the hydrostatic transition pressure only if it can be assumed that the shear stress does not aid in initiating the transition. One way of testing this assumption is to experimentally determine whether a characteristic compression η_T will initiate the transition, independent of shear stress amplitude. If the assumption is justified, and if temperature effects are negligible, then the transition pressure which should be compared with hydrostatic results is $\bar{P}_T$, and not the shock transition stress σ_x^T. From eqs (6) and (13), and figure 3,

$$\bar{P}_T = \sigma_x^T - \frac{2}{3}\frac{(1-2\nu)}{(1-\nu)}\sigma_x^H = \sigma_x^T - \frac{4}{3}\frac{C_s^2}{C_l^2}\sigma_x^H, \quad (14a)$$

$$= K\eta_H + (\sigma_x^T - \sigma_x^H), \quad (14b)$$

where C_s and C_l are the ambient pressure shear wave and dilatational wave velocities, respectively, and η_H is the value of the compression corresponding to σ_x^H. For $\nu = 1/3$, the correction amounts to about one-third the value of the HEL. Only if the stress σ_x^T at which the shock-induced phase transition occurs is several order of magnitude greater than the HEL is it reasonable to neglect the correction in eq (14) and assume that σ_x^T is essentially an isotropic pressure. In any event the HEL must be measured *in addition to* the transition stress before the effects of shear strength can be accurately assessed.

For anisotropic solids, such as many single crystals, $\sigma_y \neq \sigma_z$ and the above development leading to eq (14a) is not applicable. However, if the material continues after yielding to withstand a limiting shear stress τ^*, then the offset between σ_x and $\bar{P}$ is constant, and the transition pressure $\bar{P}_T$ may be calculated from eq (14b) and from statically measured values of the bulk modulus K.

2.3. Deviations

It is reasonable to expect that all solids will exhibit significant nonequilibrium and strain-rate phenomena during some time interval (or, over some propagation distance) immediately following shock loading with the result that the transition stress and/or the HEL will not exhibit simple behavior. In these cases shock wave propagation is nonsteady and the Hugoniot equations (1)–(3) are not properly applicable. However, in the absence of any alternative theory, they are commonly used to reduce nonsteady shock data and obtain some kind of averaged value.

Experimentally there are two common ways of testing for nonsteady behavior of both transition waves and elastic waves. One method is to vary the shock propagation distance by changing the specimen thickness. In general, if the transition and HEL values depend on propagation distance, the values decrease with increasing distance and appear to asymptotically approach an equilibrium value. A second method is to vary the driving shock stress applied to the specimen and see if the jump properties of the shock front are affected. In general, smaller overstresses result in smaller deviations from simple behavior. In establishing a transition pressure from shock compression experiments, nonsteady behavior must be minimized; thus, the input driving stress should be only slightly above the transition stress and shock measurements should be performed only at propagation distances large enough to permit equilibrium conditions to be approached [23].

In some cases, even though the elastic wavefront is steady, the HEL may not be sharply defined, as shown in figure 4. In this event the transition pressure may be determined by an alternative procedure which is still based on the elastic-plastic concept of a constant offset between σ_x and $\bar{P}$. As shown in figure 4, a point A is chosen in the plastic state so that the slope of the Hugoniot curve passing through it defines the bulk modulus K. The transition pressure is then given by

$$\bar{P}_T = K_A\eta_A + (\sigma_x^T - \sigma_x^A), \quad (15)$$

where the subscript A denotes the point A on the Hugoniot curve.

A complication for brittle solids is that there are some indications that they cannot support shear stress following yielding ($\tau^* \cong 0$), so that the final

shock state lies on a Hugoniot curve corresponding to compression by an isotropic pressure and no HEL correction is required. As suggested in figure 5, the HEL for a brittle solid is, in general, dramatically large and can exceed a hundred kilobars. In addition the HEL is observed to increase substantially with increasing driving stress. Such behavior has been observed for quartz [24]. Whether or not the high-pressure states lie on an isotropic pressure curve can be deduced by comparing the Hugoniot curve with the statically determined hydrostat.

2.4. Shock Determinations of Transition Pressures

Although deviations from simple behavior, such as those discussed above, are of physical interest, their effects are highly undesirable if a fixed point transition pressure is to be obtained from shock-compression experiments. This is necessarily true of rate effects because of the inadequacy of present shock-wave theory for describing such phenomena. Thus, the most reliable transition pressures will be obtained for solids whose shock response most nearly approximates the simple, elastic-perfectly plastic behavior outlined earlier for both the HEL and the transition stress.

In general, a series of experimental measurements must be performed to establish whether the material will exhibit simple behavior, i.e., the HEL and the transition stress have time-independent values, for experimentally feasible specimen thickness (consistent with the uniaxial strain requirement) and driving stresses. Provided this is possible, the Hugoniot curve in figure 3 can be established and the transition pressure P_T calculated from eq (14) for the compression η_T. However, it remains to be demonstrated in each instance that the shock transition occurs at the same specific volume as the hydrostatic transition.

A temperature correction to the shock transition pressure $\bar{P}_T$ can be estimated [2] by assuming that the temperature at which the transition begins to occur can be approximated by the isentropic expression

$$\theta = \theta_0 \exp(\Gamma_0 \eta), \tag{16}$$

where θ_0 is the initial temperature and Γ_0 is the Grüneisen parameter at zero pressure. The change in the transition pressure due to this temperature rise is

$$\Delta \bar{P}_T = (dP/d\theta)\Delta\theta, \tag{17}$$

where $\Delta\theta = \theta - \theta_0$ is the temperature rise, and $dP/d\theta$ is the slope of the pressure-temperature phase line. If necessary, $dP/d\theta$ can be estimated from shock compression data taken in the mixed-phase region above the transition point [2, 25]. Because $\Delta\bar{P}_T$ is usually much smaller than P_T, a more sophisticated analysis is normally unwarranted.

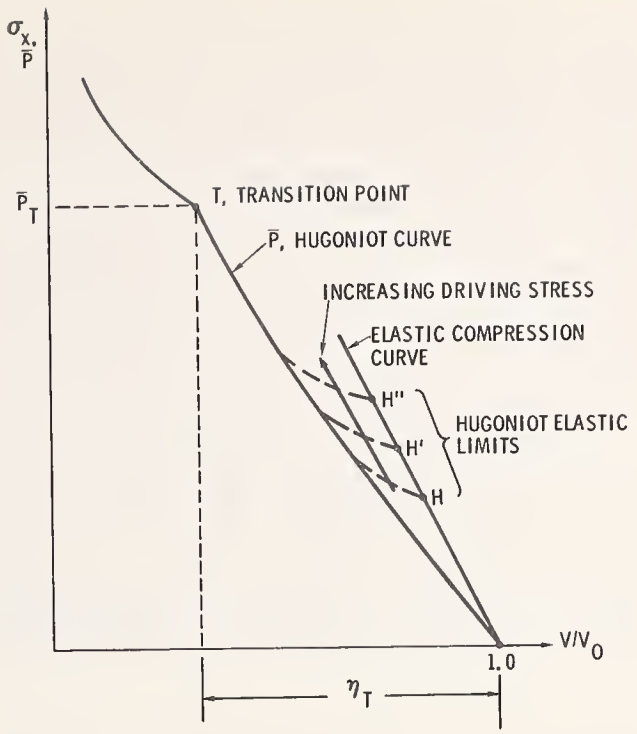

FIGURE 5. *Schematic diagram of the stress-volume behavior of a brittle solid subjected to shock compression.*

3. Survey of Hugoniot Elastic Limit Measurements

The considerations of the preceding sections show that a measured shock transition stress should not be directly compared with the corresponding hydrostatic pressure without first evaluating shear strength and temperature corrections. Consequently, shock compression studies should include simultaneous measurement of the HEL, as well as the transition stress.

Hugoniot elastic limit measurements often require different techniques than those employed for higher-stress shock measurements. This results from both the requirement to detect smaller amplitude disturbances as well as the requirement for better time-resolving capability to remove apparent ambiguities in observed behavior. These improved techniques are of recent development and far fewer HEL measurements have been reported than have strong shock measurements [26].

Table A of the Appendix is a survey of existing HEL measurements. Except for geological materials it is reasonably comprehensive, containing about 120 entries describing about 50 materials, and permits the importance of shear strength effects to be assessed for a variety of materials. The measurements are grouped according to the following material classes: (i) metals, (ii) brittle single crystals, and (iii) polycrystalline ceramics. Where appropriate, each entry describes the metallurgical condition of the material, a reported value for the HEL, remarks which include the prop-

agation distance (specimen thickness) and comments describing significant departures from steady behavior, the shock loading method employed, the measurement technique used, and the information source. Assignment of a unique HEL value to an elastic wavefront is often not obvious (cf. fig. 4); however, a representative value can generally be chosen, and this is given in the table. Although the table provides a reasonably complete summary of experimental results, individual references should be consulted for specific details. Private communications and abstracts have been used only for recent measurements of particular interest.

From table A it is immediately apparent that many materials exhibit time-dependent strain-rate effects in as much as their Hugoniot elastic limits decrease with increasing propagation distances. Stress relaxation immediately behind the elastic wavefront is further evidence of time-dependent behavior. Only at the larger propagation distances can a steady value for the HEL be expected. For example, for iron the HEL decreases by less than 10 percent for propagation distances exceeding about 25 mm [27].

For metals, it can be seen that the HEL seldom exceeds a few tens of kilobars; in contrast, for brittle single crystals and polycrystalline ceramics it commonly exceeds fifty kilobars and may be as high as several hundred. Most of the observed HEL values are large enough to warrant corrections to the transition stress measurements. Also, it is evident from table A that HEL values are strongly influenced by the structure-sensitive properties of the materials and, hence, are best measured directly for the material under consideration.

4. Comparison of Shock and Static Transition Pressures

In this section, several representative static and shock transitions, which have been relatively well characterized, will be compared. Bismuth is of

TABLE 1. *Comparison of several shock and static transitions*

Material condition	Bismuth [a]				Fe polycrystalline	Ge [k] [111] crystal	CdS [n]		InSb [q]	
	Cast	Pressed	Crystal							
			a-axis	c-axis			a-axis	c-axis	[100]	[111]
σ_x^T, kbar	25.6	25.4	24.6	25.6	[f] 129	136–142	28	32	20	17
$\bar{P}_T$, kbar	[b] 25.7	[b] 25.5	[c] 24.3	[c] 25.5	[g] 125	114–122	[o] 18	[o] 18	[r] 13	[r] 9
P static, kbar	[d] 25.48–25.50	.....	.....	.....	[h] 118	[l] 120–125	[p] 23		[s] 23	
					[i] 133					
η_T shock, percent	6.1	6.0	5.8	6.1	[f] 6.4	12–13	3.3	3.3	3.0	2.1
η_T static, percent	[e] 6.4	.....	.....	.....	[j] 6.1–6.6	[m] 12.5	[p] 4.8		[s] 4.6–5.3	

[a] Shock data from D. B. Larson, ref. [11].

[b] Calculated from eq (14a).

[c] Calculated from eq (14b) and the bulk modulus value given by A. A. Giardini et al., ref. [30].

[d] P. L. M. Heydemann, ref. [29].

[e] A. A. Giardini et al., ref. [30].

[f] T. R. Loree et al., ref. [23].

[g] Calculated from eq (14b) and the HEL data of J. W. Taylor et al., ref. [27] $\bar{P}_T$ has not been corrected for the effect of temperature, estimated to about plus 1 kbar.

[h] W. Stark et al., ref. [43].

[i] A. S. Balchan et al., ref. [3].

[j] Values computed from the lattice parameter measurements of H. K. Mao et al., ref. [8], at the transition pressures given in refs. [3] and [43].

[k] Shock data from R. A. Graham et al., ref. [34]. $\bar{P}_T$ has not been corrected for the effect of temperature, estimated to be about plus 1 kbar.

[l] S. Minomura et al., ref. [35].

[m] J. C. Jamieson, ref. [36].

[n] Shock data from J. D. Kennedy et al., ref. [37].

[o] Calculated from the observed η_T shock and the bulk modulus value given by G. A. Samara et al., ref. [38]. Temperature corrections are negligible.

[p] G. A. Samara et al., ref. [38].

[q] Shock data taken from refs. [40] and [41].

[r] Calculated from the observed η_T shock and the bulk modulus value given by R. E. Hanneman et al., ref. [42]. Temperature corrections are negligible.

[s] R. E. Hanneman et al., ref. [42].

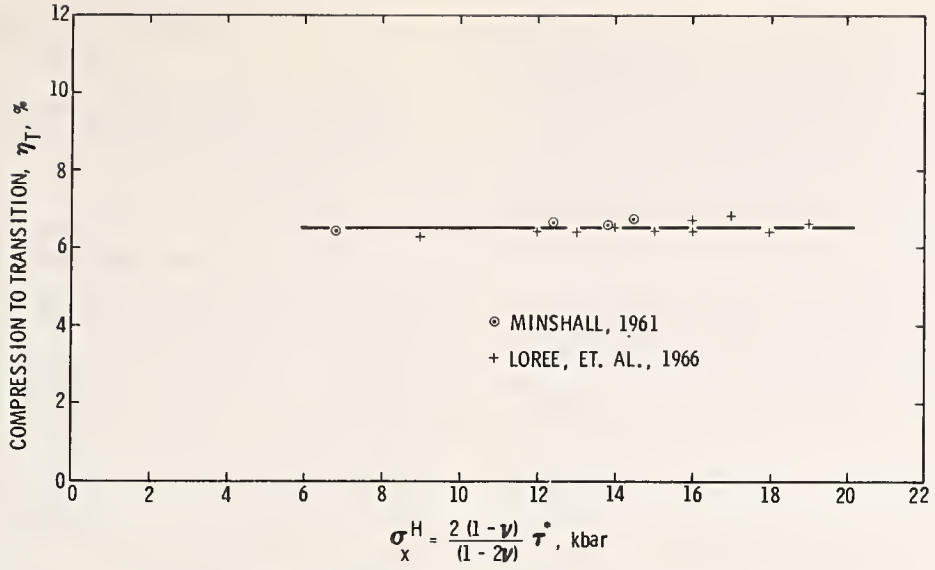

FIGURE 6. *Effect of shear stress on the shock compression* n_T *at which the iron transitions occurs.*

interest because it is used in static calibrations and differences between static and shock transition pressures have been reported [2]. Iron will be considered and a shear strength correction applied to the transition stress after analyzing experiments which examine the effect of shear on the transition. Germanium provides an interesting example of a phase transition in a solid with a large elastic limit. Finally, cadmium sulfide and indium antimonide will be considered since they apprently exhibit phase transitions in the range of elastic compression. Values associated with these transitions are summarized in table 1.

Temperature corrections calculated from eqs (16) and (17) show about a 1 kbar correction for all the shock transitions listed in table 1. Thus, only in the case of the Bi transition is the temperature correction comparable to the shear correction.

4.1. Bismuth

Duff and Minshall's shock measurements of the Bi I–II transition [2] were reported shortly after the discovery of the iron transition. This transition is now well established statically [28–30] and affords an excellent opportunity for a direct comparison of shock and static measurements. Duff and Minshall's measurements showed that the shock transition stress was higher than the hydrostatic value. They speculated that one source of the difference might be a shear strength effect which their detection method could not observe.

Recently, Larson [11] published an extensive investigation of the Bi I–II transition under shock-wave loading which appears to resolve the differences between static and shock values. The instrumentation which he employed had much better time resolution and better low pressure sensitivity than that employed in the earlier studies. Some of his results are compared to the corresponding hydrostatic values in table 1. The shock compression required to initiate the transition stress agrees with the static value [30] to within experimental error. A shear strength correction of -0.8 kbar was calculated [11] from the observed HEL values for polycrystalline material. The high compressibility of Bi and the large slope of its phase line combine to yield a substantial temperature correction of $+0.9$ kbar.

When these corrections are made, the calculated shock transition pressure $\bar{P}_T$ is in agreement with the static value to within experimental error. Further, the shear stresses present during shock compression do not significantly influence the transition. This latter observation is in agreement with the conclusion reached by Heydemann [29] in comparing his hydrostatic data to the static data of Kennedy et al. [28].

4.2. Iron

The "130 kbar" transition in iron has been widely used for pressure calibration. The measured HEL values (cf. table A) are large enough to warrant a shear strength correction to the transition stress. However, before making this correction, we will consider the evidence which indicates that the shock transition is not affected by shear stress.

Minshall [31] and Loree et al. [23], have reported experiments which permit the effect of shear on the transition to be quantitatively evaluated. The HEL of iron can be changed with heat treatment and/or small additions of carbon. In this manner, Minshall, and Loree et al. varied the HEL from 7 to 19 kbar and measured the characteristics of the shock transition. These data are shown in figure 6 where the compression to initiate the transition, η_T, is plotted for various HEL values. It is apparent that η_T is

unchanged even though the shear stress varies by a factor of three [32]. These data indicate that the shock transition is not influenced by shear stress and the shear strength correction to the observed transition stress can be applied according to eq (14a). This conclusion does not preclude the possibility that shear stresses might affect the kinetics of the transition.

For annealed Armco iron, Loree et al. [23] reported the iron transition stress to be 129 kbar at a volume compression η_T of 6.4 percent for a propagation distance (sample thickness) of 25.4 mm and minimum applied driving pressure. They did not simultaneously measure the HEL; however, the HEL of iron has been sufficiently characterized to permit a shear strength correction to be calculated. Basing the shear strength correction on the HEL value of 8.3 kbar measured by Taylor et al. [27] for 25.4-mm-thick annealed Armco iron specimens, the transition pressure $\bar{P}_T$ is calculated to be 125 kbar. Stress relaxation and other deviations from steady behavior should not introduce more uncertainty than ± 0.5 kbar.

The shock transition pressure and compression values are in general agreement with static results, although the range of static values given in the literature is substantial. It would be highly desirable to have values for the hydrostatic compression at the transition. This would be of interest because of the anomalously low values of the bulk modulus reported for shock compression of iron below the transition [27].

4.3. Germanium

Germanium has not been extensively investigated under shock compression but we consider its transition because it is an example of a transition in a material with a relatively large HEL. For shock propagation in the [111] direction, the transition stress σ_x^T has a value of about 139 kbar, and has been shown to correspond to a solid-solid transition from the diamond to the white tin crystal structure [34]. The HEL is about 44 kbar. The static transition occurs at about 120 kbar [35]; clearly shear strength effects cannot be ignored if the two values are to be compared. As can be seen from table 1, the transition occurs at very nearly the same compression for both shock and hydrostatic loading, which indicates it is insensitive to shear stress, in agreement with static observations [36]. The shock transition pressure $\bar{P}_T$ calculated from eq (14b) is between 114 and 122 kbar, which compares well with the static value of from 120 to 125 kbar. The effects of shock heating are estimated to affect the shock transition pressure by less than 1 kbar, an amount smaller than the experimental uncertainty.

4.4. Cadmium Sulfide and Indium Antimonide

The transitions in CdS and InSb occur at relatively low pressures and are especially interesting since they apparently occur below the HEL. Because of this, there is the possibility of an incorrect identification of the transition wave as an elastic wave or vice versa. Kennedy et al. [37] have considered this question and base their identification of the transition in CdS on the very large (~ 18 percent) volume change indicated between first and second wave. We have computed the shock transition pressure from the observed shock compression, η_T, and hydrostatic high-pressure bulk modulus values [38]. The shock transition pressure is significantly lower than the hydrostatically observed transition pressure [38]. Conversely, the hydrostatic compression η_T is larger than the shock compression [38]. Thus, the wurtzite-to-rocksalt transition in CdS, which is martensitic in character [39], is influenced by shear.

Similarly, InSb appears to exhibit an even greater sensitivity to shear. The shock values shown in table 1 were obtained by Kennedy [40, 41] in experiments identical to those used to study CdS, and are as yet unpublished. His identification of the transition wave is again based on the very large volume change (10 to 14 percent) between the first and second wave values. The shock transition pressure calculated from the observed compression and the static bulk modulus [42] is only about 60 percent of that observed statically. In addition, the compression observed under shock is roughly one-half that observed statically [42]. If the identification of the transition is correct, these values indicate an enormous influence of shear on this transition.

5. Summary

The transition stress measured in shock compression experiments consists of both pressure and shear components. If the shear strength of a solid is very small, it is reasonable to assume, as has been widely done, that the measured stress is essentially a transition pressure. However, for solids which have a large HEL and a phase transition occurring at relative low stress, such an assumption is not justified and a shear strength correction is required to determine the mean transition pressure. Precise characterization of phase transitions observed in shock experiments should include such corrections and, to do this studies of the HEL need to be undertaken at the same time the phase transition is being studied. The corrections are valid only if it can be demonstrated that the transition is not influenced by shear. Sensitivity of the transition to shear should be carefully evaluated before an observed shock transition is used as a static calibration point.

6. Acknowledgement

The authors express their appreciation to Drs. G. A. Samara and R. W. Rohde of Sandia Laboratory for their helpful discussions and critical comments.

7. References

[1] Bancroft, D., Peterson, E. L., and Minshall, S., J. Appl. Phys. **27,** 291 (1956).
[2] Duff, R. E., and Minshall, F. S., Phys. Rev. **108,** 1207 (1957).
[3] Balchan, A. S., and Drickamer, H. G., Rev. Sci. Instr. **32,** 308 (1961).
[4] Jamieson, J. C., and Lawson, A. W., J. Appl. Phys. **33,** 776 (1962).
[5] Clendenen, R. L., and Drickamer, H. G., J. Phys. Chem. Solids **25,** 865 (1964).
[6] Bundy, F. P., J. Appl. Phys. **36,** 616 (1965).
[7] Takahashi, T., and Bassett, W. A., Science **145,** 483 (1964).
[8] Mao, Ho-Kwang, Bassett, W. A., and Takahashi, T., J. Appl. Phys. **38,** 272 (1967).
[9] Minshall, S., J. Appl. Phys. **26,** 463 (1955).
[10] Previous summary discussions of shear strength effects and shock wave propagation have been given by Rice, M. H., McQueen, R. G., and Walsh, J. M., in Solid State Physics Vol. **VI,** ed, F. Seitz and D. Turnbull (Academic Press, New York, 1958).
Duvall, G. E., and Fowles, G. R., in High Pressure Physics and Chemistry, Vol. 2, ed. R. S. Bradley (Academic Press, New York, 1963).
Skidmore, I. C., Appl. Mat. Research **4,** 131 (1965).
Doran, D. G., and Linde, R. K., in Solid State Physics Vol. **19** ed. F. Seitz and D. Turnbull (Academic Press, New York, 1966).
[11] Larson, D. B., J. Appl. Phys. **38,** 1541 (1967).
[12] Wood, D. S., J. Appl. Mechanics **19,** 521 (1952).
[13] Morland, L. W., Phil. Trans. Roy. Soc. (London) **A251,** 341 (1959).
[14] Fowles, G. R., J. Appl. Phys. **32,** 1475 (1961).
[15] Lundergan, C. D., and Herrmann, W., J. Appl. Phys. **34,** 2046 (1963).
[16] Barker, L. M., Lundergan, C. D., and Herrmann, W., **35,** 1203 (1964).
[17] Butcher, B. M., and Canon, J. R., AIAA Journal **2,** 2174 (1964).
[18] Butcher, B. M., and Munson, D. E., in Proc. Fourth Symposium on Detonation, ACR–126, Office of Naval Research, U.S. Government Printing Office (1965).
[19] Butcher, B. M., and Karnes, C. H., J. Appl. Phys. **37,** 402 (1966).
[20] Munson, D. E., and Barker, L. M., J. Appl. Phys. **37,** 1652 (1966).
[21] Karnes, C. H., Proc. Symp. on the Mechanical Behavior of Materials under Dynamic Loads, San Antonio, Texas, Sept. 6–8 (1967), to be published.
[22] Graham, R. A., Anderson, D. H., and Holland, J. R., J. Appl. Phys. **38,** 223 (1967).
[23] Loree, T. R., Fowler, C. M., Zukas, E. G., and Minshall, F. S., J. Appl. Phys. **37,** 1918 (1966).
[24] Wackerle, J., J. Appl. Phys. **33,** 922 (1962).
[25] Graham, R. A., Jones, O. E., and Holland, J. R., J. Phys. Chem. Solids **27,** 1519 (1966).
[26] Van Thiel, M., Kusubov, A. S., and Mitchell, A. C., Compendium of Shock Wave Data, Lawrence Radiation Laboratory, University of California, UCRL 50108.
[27] Taylor, J. W., and Rice, M. H., J. Appl. Phys. **34,** 364 (1963).
[28] Kennedy, G. C., and LaMori, P. N., J. Geophys. Research **67,** 851 (1962).
[29] Heydemann, P. L. M., J. Appl. Phys. **38,** 2640 (1967) and errata **38,** 3424 (1967).
[30] Giardini, A. A., and Samara, G. A., J. Phys. Chem. Solids **26,** 1523 (1965).
[31] Minshall, F. S., in Response of Metals to High Velocity Deformation, ed. P. G. Shewmon and V. F. Zackay (Interscience, New York, 1961).
[32] The insensitivity of the iron transition to shear should not necessarily be extrapolated to other iron alloys. Significant shock-induced martensite to austenite transformation has been observed in martensitic 30 percent Ni-70 percent Fe at shock stresses as low as 20 kbar [33]. Martensitic transformations are observed to be sensitive to shear in static experiments; thus, shock transition stresses observed in martensitic iron alloys require independent verification of the effects of shear.
[33] Rohde, R. W., Holland, J. R., and Graham, R. A., accepted for publication, Trans. Met. Soc. AIME.
[34] Graham, R. A., Jones, O. E., and Holland, J. R., J. Phys. Chem. Solids **27,** 1519 (1966).
[35] Minomura, S., and Drickamer, H. G., J. Phys. Chem. Solids **23,** 451 (1962).
[36] Jamieson, J. C., Science **139,** 762 (1963).
[37] Kennedy, J. D., and Benedick, W. B., J. Phys. Chem. Solids **27,** 125 (1966).
[38] Samara, G. A., and Giardini, A. A., Phys. Rev. **140,** A388 (1965).
[39] Corll, J. A., Phys. Rev. **157,** 623 (1967).
[40] Kennedy, J. D., and Benedick, W. B., Bull. Am. Phys. Soc. **10,** 1112 (1965).
[41] Kennedy, J. D., private communication (1968).
[42] Hanneman, R. E., Banus, M. D., and Gatos, H. C., J. Phys. Chem. Solids **25,** 293 (1964).
[43] Stark, W., and Jura, G., ASME Publication 64–WA/PT–28 (1964).

8. Appendix—Table A. Summary of Hugoniot Elastic Limit Measurements

Material	Condition [a]	σ_{HEL}, kbar [b]	Remarks [c]	Technique [d]	Reference
METALS					
Iron Alloys					
Armco iron	annealed	7	25 mm	E–1	Bancroft et al. (1956)
Armco iron	AR, annealed	15–7	25–133 mm	E–1, 14	Minshall (1961)
Armco iron	normalized	8–7	20–51 mm+*	E–5	Jones et al. (1962)
Armco iron	annealed	11–7	6–51 mm+*	E–6	Taylor et al. (1963)
Armco iron	.....	10	25–60 mm+*	E–7	Ivanov et al. (1963)
Armco iron	annealed	12–6	6–40 mm+*	E–12	McQueen (1964)
Armco iron	.....	11–8	4–18 mm+	E–12	Peyre et al. (1965)
Ferrovac E iron	varied	12–6	12 mm*	E–5	Holland (1967)
Ferrovac E iron	annealed	10	13 mm*, temp 76–573 K	E–5	Rohde (1968a)
SAE 1018	normalized	13–10	20–51 mm+*	E–5	Jones et al. (1962)
SAE 1018	annealed-cold rolled	16–9	19 mm	E–5	Jones et al. (1964)
SAE 1018	varied	12	19 mm*	E–5	Jones et al. (1968)
SAE 1020	.....	10–12	127 mm	E–1	Minshall (1955)
SAE 1020	AR, annealed	15–11	50–127 mm	E–1	Minshall (1961)
SAE 1020	AR	10	51–76 mm	E–1	Costello (1957)
SAE 1040	.....	11	127 mm	E–1	Minshall (1955)
SAE 1040	AR, annealed	6–14	127 mm	E–1	Minshall (1961)
SAE 1055	AR, annealed	13–15	125–127 mm	E–1, 14	Minshall (1961)
SAE 1055	varied	8–15	25 mm	E–14	Loree et al. (1966)
1% carbon-iron	varied	12–17	25 mm	E–14	Loree et al. (1966)
1.5% carbon-iron	varied	16–19	25 mm	E–14	Loree et al. (1966)
2% carbon-iron	varied	15–21	25 mm	E–14	Loree et al. (1966)
SAE 4340	annealed	19–14	6–50 mm+*	G–5	Butcher et al. (1968a)
SAE 4340	annealed	23–21	3–6 mm	G–8	Graham et al. (1967b)
SAE 4340	RC–15	17	25 mm	E–14	Minshall (1961)
SAE 4340	RC–15	17–19	12 mm	G–2	Butcher et al. (1964)
SAE 4340	RC–30	16	23 mm	E–5	Jones et al. (1962)
SAE 4340	RC–32	16–20	12 mm	G–2	Butcher et al. (1964)
SAE 4340	RC–35	25	25 mm	E–14	Minshall (1961)
SAE 4340	RC–40	20–18	20–51 mm	E–5	Jones et al. (1962)
SAE 4340	RC–50	22	23 mm	E–5	Jones et al. (1962)
SAE 4340	RC–54	14–31	12 mm	G–2	Butcher et al. (1964)
Hampden tool steel	RC–20	14	19 mm	E–5	Jones et al. (1962)
Hampden tool steel	RC–62	~ 22	19 mmø	E–5	Jones et al. (1962)
Hampden tool steel	RC–66	> 24	19 mmø	E–5	Jones et al. (1962)
SAE 347 stainless steel	AR	6	127 mm	E–1,14	Minshall (1961)
3% silicon-iron crystal	.....	~ 7	13 mm*	G–6	Taylor (1968)
3.34% silicon-iron	annealed	10–9	6–25 mm+*	E–5	Mote (1968)
Invar, 36% nickel-64% iron	AR	13	wedge	E–10	Curran (1961)
Invar, 36% nickel-64% iron	annealed	5	13 mm	G–5	Graham et al. (1967a)
30% nickel-70% iron	annealed	5–3	10–13 mm	G–5	Graham et al. (1967a)
30% nickel-70% iron	martensitic	~ 20(ramp)	13 mmø	G–5	Graham et al. (1967a)
Russian steel 3	AR	13–6	20–120 mm+*	E–7	Ivanov et al. (1963)
Russian steel 30khGSA	annealed	17	60 mm+*	E–7	Ivanov et al. (1963)
Russian steel 30khGSA	hardened	18	60 mm+*	E–7	Ivanov et al. (1963)
Austenitic manganese steel	RB93	8	6 mm	E, G–5	Champion (1968)
304 stainless steel	RB77	6	6 mm	G–5	Butcher (1968b)
Vibrac	RC36	21	51–76 mm	E–1	Costello (1957)

8. Appendix—Table A. Summary of Hugoniot Elastic Limit Measurements—Continued

Material	Condition [a]	σ_{HEL}, kbar [b]	Remarks [c]	Technique [d]	Reference
Aluminum Alloys					
2024	T-4	5	wedge	E-10	Fowles (1961)
2024	annealed	1	wedge	E-10	Fowles (1961)
2024	.....	4	25 mm	E-5	Jones et al. (1962)
2024	.....	6	.....	E-6	McQueen (1964)
2024	T-4	.....	13 mm	G-6	Taylor (1968)
6061	T-6	6	13-25	G-1	Lundergan et al. (1963)
6061	T-6	5	6 mm	G-5	Halpin et al. (1963)
6061	T-6	5-7	25 mm	G-2	Barker et al (1964b)
6061	T-6	5	13 mm	G-4	Barker (1967)
6061	T-6	6	13-64 mm	G-2	Butcher et al. (1966)
1060	annealed	0.3-0.5	25 mm*	G-4, 5	Barker et al. (1966)
1060	annealed	0.6-0.2	6-24 mm+*	G-4	Karnes (1967)
Russian alloy D-1	annealed	2-1	40-120 mm+	E-7	Novikov et al. (1966)
Russian alloy D-16	annealed	3-2	30-80 mm+ temp 283-473 K	E-7	Novikov et al. (1966)
Russian alloy D-16	hardened	5	30 mm	E-7	Novikov et al. (1966)
French alloy AU4G	.....	8	.....	E-12	Peyre et al. (1965)
Other Metals					
Copper, crystal	[001]	2	5mm*	E-5	Mote (1968)
	[011]	1	5mm*	E-5	Mote (1968)
	[111]	1	5 mm* (relaxation suppressed by prestrain)	E-5	Mote (1968)
Copper, polycrystal	.....	~0.5 (ramp)	5 mmø	E-5	Mote (1968)
Copper	annealed	0.6-0.4	20-30 mm temp. 283-473 K	E-7	Novikov et al. (1966)
Copper	annealed	~0.4 (ramp)	13 mmø	G-6	Taylor (1968)
Copper	annealed	~0.5 (ramp)	ø	E-2, 3	Munson et al. (1966)
Copper	cold worked	.....	ø	G-6	Taylor (1968)
Lead	annealed	<0.2	.....	E-2	Munson et al. (1966)
Brass	annealed	3-2	30-80 mm+	E-7	Novikov et al. (1966)
Brass	.....	~8	6 mmø	E-5	Benedick (1965)
Beryllium, crystal	c-axis	40	*	G-6	Taylor (1968)
Beryllium, crystal	a-axis	4	*	G-6	Taylor (1968)
Beryllium, sintered	.....	~2 (ramp)	ø	G-6	Taylor (1968)
Tantalum	annealed	.....	.....	G-6	Taylor (1968)
Niobium	annealed	.....	.....	G-6	Taylor (1968)
Thorium	.....	.....	.....	G-6	McQueen (1964)
Uranium	.....	.....	ø	G-6	Taylor (1968)
Bismuth, crystal	.....	3	1-3 mm	E, G-5	Larson (1967)
Bismuth, polycrystal	cast	~2 (ramp)	2-13 mmø	E, G-5	Larson (1967)
Bismuth, polycrystal	cast	~4 (ramp)	2 mmø	G-5	Present work
Tungsten	annealed	38	10 mm	G-5	Rohde (1968b)
Antimony	cast	17-2	5-49 mm+	E-1	Warnes (1967)
BRITTLE SINGLE CRYSTALS					
Quartz (SiO_2)	*x*-cut	94-48	5-25 mm+*	E-9	Wackerle (1962)
Quartz (SiO_2)	*x*-cut	66-55	6 mm*	E-11	Fowles (1967)
Quartz (SiO_2)	*y*-cut	110-82	10 mm*	E-9	Wackerle (1962)
Quartz (SiO_2)	*y*-cut	86-65	3-6 mm*	E-11	Fowles (1967)
Quartz (SiO_2)	*z*-cut	145-120	10 mm*	E-9	Wackerle (1962)

8. Appendix—Table A. Summary of Hugoniot Elastic Limit Measurements—Continued

Material	Condition [a]	σ_{HEL}, kbar [b]	Remarks [c]	Technique [d]	Reference
Quartz (SiO_2)	*z*-cut	148–100	3–6 mm*	E–11	Fowles (1967)
Quartz (SiO_2)	*z*-cut	145–60	.....	E–12	Peyre et al. (1965)
Quartz (SiO_2)	fused	98 (ramp)	10–13 mm ø	E–9	Wackerle (1962)
Sapphire (Al_2O_3)	60° cut	120–170	10–13 mm	E–9	Brooks et al. (1966)
Sapphire (Al_2O_3)	*z-cut*	120–200	10–13 mm	E–9	Brooks et al. (1966)
Sapphire (Al_2O_3)	*x*-cut	135–180	10–13 mm	E–9	Brooks et al. (1966)
Germanium	[111]	44	8 mm	G–?	Graham et al. (1966)
Germanium	[111]	41–35	6–12 mm*	E–12	McQueen (1964)
Germanium	[100]	53–46	6–12 mm*	E–12	McQueen (1964)
Germanium	[100]	45	7 mm*	E–5	Kennedy (1968)
Germanium	[100]	47	6 mm*	G–8	Graham (1967b)
Germanium	[114]	.....	6–12 mm*	E–12	McQueen (1964)
Silicon	crystal	free surface velocities 50% higher than Ge values.		E–12	McQueen (1964)
Cadmium sulfide (CdS)	*c*-axis	> 32	(*)	E–5	Kennedy et al. (1966)
Cadmium sulfide (CdS)	*a*-axis	> 28	(*)	E–5	Kennedy et al. (1966)
Indium antimonide (InSb)	[100]	> 20	.....	E–5	Kennedy et al. (1965)
Indium antimonide (InSb)	[111]	> 17	.....	E–5	Kennedy et al. (1965)
Indium antimonide (InSb)	[110]	> 20	.....	E–5	Kennedy et al. (1965)
Titania (TiO_2)	[100]	70	6 mm	E–13	Linde et al. (1968)
Titania (TiO_2)	[001]	100	6 mm	E–13	Linde et al. (1968)
Sodium Chloride (NaCl)	[100]	~ 0.3	5–14 mm*	E–5	Benedick (1968)
POLYCRYSTALLINE CERAMICS					
Lucalox (Al_2O_3, $\rho_0 = 3.98$)	.....	99–123	3–13 mm	E–11	Ahrens et al. (1968)
Alumina (Al_2O_3, $\rho_0 = 3.92$)	.....	140	.....	E–11	Gust et al. (1968)
Alumina (Al_2O_3, $\rho_0 = 3.81$)	.....	67–100	6 mm	E–11	Ahrens et al. (1968)
Alumina (Al_2O_3, $\rho_0 = 3.76$)	.....	58–72	13 mmø	G–5, 9	Present work
Alumina (Al_2O_3, $\rho_0 = 3.72$)	.....	8.0	.....	E–11	Gust et al. (1968)
Magnesium Oxide (MgO, $\rho_0 = 3.58$)	.....	89–35	4–10 mm	E–11	Ahrens (1966)
Boron Carbide (B_4C, $\rho_0 = 2.50$)	.....	150	.....	E–11	Gust et al. (1968)
Barium titanate ($BaTiO_3$)	.....	25	13 mm	E–9	Reynolds et al. (1962)
Barium titanate ($BaTiO_3$)	.....	~ 30	3–13 mm+	E–10	Doran (1968)
Lead zirconate titanate (PZT 95/5)	.....	~ 40	4–13 mm+	E–10, 11	Doran (1968)
Lead zirconate titanate (PZT 52/48)	.....	19	13 mm	E–9	Reynolds et al. (1962)
Manganese-zinc ferrite	.....	23	14 mmø	E–5	Present work
Yttrium iron garnet ($\rho_0 = 5.07$)	.....	> 60	8 mm	G–5	Present work
Polycrystal quartz rocks	.....	47–130	3–13 mm+	E–11	Ahrens et al (1966)
Titania (TiO_2, $\rho_0 = 4.24$)	.....	75	6 mm	E–13	Linde et al. (1968)

[a] AR denotes as-received.

[b] When a range of sample thicknesses is given and + is noted in remarks, the larger HEL value corresponds to the smaller sample thickness, and vice-versa.

[c] Numbers refer to sample thickness. Symbols: + sample thickness effect observed; * stress relaxation observed; ø poorly defined elastic wavefront.

[d] Letters denote method of loading: E explosive loading, and G gun impact. Numbers denote measurement techniques:

1. Pins, Minshall (1955).
2. Slanted resistance wire, Barker et al. (1964a).
3. Interferometer, Barker et al. (1965).
4. Velocity interferometer, Barker (1967).
5. Quartz gauge, Graham et al. (1965).
6. Capacitor, Rice (1961).
7. Capacitor, Ivanov et al. (1963).
8. Solid dielectric capacitor, Graham et al. (1967).
9. Optical knife-edge, Davis et al. (1961).
10. Optical lever-oblique shock, Fowle (1961).
11. Inclined mirror, Doran (1963).
12. Optical lever, McQueen (1964).
13. Manganin wire, Keough et al. (1964).
14. Capacitor, Hughes et al. (1961).

References Cited in Table A

Ahrens, T. J., J. Appl. Phys. **37**, 2532 (1966).
Ahrens, T. J., Gust, W. H., and Royce, E. B., accepted for publication, J. Appl. Phys. (1968).
Ahrens, T. J., and Duvall, G. E., J. Geophys. Research **71**, 4349 (1966).
Bancroft, D., Peterson, E. L., and Minshall, S., J. Appl. Phys. **27**, 291 (1956).
Barker, L. M., and Hollenbach, R. E., Rev. Sci. Instr. **35**, 742 (1964a).
Barker, L. M., Lundergan, C. D., and Herrmann, W., J. Appl. Phys. **35**, 1203 (1964b).
Barker, L. M., and Hollenbach, R. E., Rev. Sci. Instr. **36**, 1617 (1965).
Barker, L. M., Butcher, B. M., and Karnes, C. H., J. Appl. Phys. **37**, 1989 (1966).
Barker, L. M., Proc. IUTAM Colloq. on the Behavior of Dense Media under High Dynamic Pressures, Paris, France, Sept. 11–15, 1967.
Benedick, W. B., Rev. Sci. Instr. **36**, 1309 (1965).
Benedick, W. B., private communication (1968).
Butcher, B. M., and Canon, J. R., AIAA Journal **2**, 2174 (1964).
Butcher, B. M., and Karnes, C. H., J. Appl. Phys. **37**, 402 (1966).
Butcher, B. M., and Munson, D. E., in Dislocation Dynamics, ed. A. R. Rosenfield, G. T. Hahn, A. L. Bement, Jr., and R. I. Jaffee (McGraw-Hill, New York, 1968a).
Butcher, B. M., private communication (1968b).
Brooks, W. P., and Graham, R. A., Bull. Am. Phys. Soc. **II 11**, 414 (1966).
Champion, A. R., private communication (1968).
Costello, E. L., in Proc. Conf. on The Properties of Materials at High Rates of Strain, The Institution of Mechanical Engineers, London, 1957.
Curran, D. R., J. Appl. Phys. **32**, 1811 (1961).
Davis, W. C., and Craig, B. G., Rev. Sci. Instr. **32**, 579 (1961).
Doran, D. G., in High Pressure Measurement, ed. A. A. Giardini and E. C. Lloyd (Butterworth, London, 1963).
Doran, D. G., J. Appl. Phys. **39**, 40 (1968).
Fowles, G. R., J. Appl. Phys. **32**, 1475 (1961).
Fowles, R., J. Geophys. Research **72**, 5729 (1967).
Graham, R. A., Neilson, F. W., and Benedick, W. B., J. Appl. Phys. **36**, 1775 (1965).
Graham, R. A., Jones, O. E., and Holland, J. R., Phys. Chem. Solids **27**, 1519 (1966).
Graham, R. A., Anderson, D. H., and Holland, J. R., J. Appl. Phys. **38**, 223 (1967a).
Graham, R. A., and Ingram, G. E., Proc. IUTAM Colloq. on the Behavior of Dense Media under High Dynamic Pressures, Paris, France, Sept. 11–15, 1967b.
Gust, W. H., and Royce, E. B., Bull. Am. Phys. Soc. **II 13**, 901 (1968).
Halpin, W. J., Jones, O. E., and Graham, R. A., in Symp. Dynamic Behavior of Materials, ASTM Special Technical Publication No. 336, American Society for Testing and Materials, Philadelphia, 1963.
Holland, J. R., Acta Metallurgica **15**, 691 (1967).
Ivanov, A. G., Novikov, S. A., and Sinitsyn, V. A., Soviet Physics, Solid State **5**, 196 (1963).
Jones, O. E., Neilson, F. W., and Benedick, W. B., J. Appl. Phys. **33**, 3224 (1962).
Jones, O. E., and Holland, J. R., J. Appl. Phys. **35**, 1771 (1964).
Jones, O. E., and Holland, J. R., Acta Metallurgica **16**, 1037 (1968).
Karnes, C. H., in Proc. Symp. on the Mechanical Behavior of Materials under Dynamic Loads, San Antonio, Texas, 1967.
Kennedy, J. D., and Benedick, W. B., Bull. Am. Phys. Soc. **II 10**, 1112 (1965).
Kennedy, J. D., and Benedick, W. B., J. Phys. Chem. Solids **27**, 125 (1966).
Kennedy, J. D., private communication (1968).
Keough, D. D., Williams, R. F., and Bernstein, D., Am. Soc. Mech. Engrs., Paper 64–WA/PT–5 (1964).
Larson, D. B., J. Appl. Phys. **38**, 1541 (1967).
Linde, R. K., and DeCarli, P. S., private communication (1968).
Loree, T. R., Fowler, C. M., Zukas, E. G., and Minshall, F. S., J. Appl. Phys. **37**, 1918 (1966).
Lundergan, C. D., and Herrmann, W., J. Appl. Phys. **34**, 2046 (1963).
McQueen, R. G., in Metallurgy at High Pressures and High Temperatures, ed. K. A. Gschneidner, Jr., M. T. Hepworth, and N. A. D. Parlee (Gordon and Breach, New York, 1964).
Minshall, S., J. Appl. Phys. **26**, 463 (1955).
Minshall, F. S., in Response of Metals to High Velocity Deformation, ed. P. G. Shewmon and V. F. Zackay (Interscience Publishers, New York, 1961.
Mote, J. D., private communication (1968).
Munson, D. E., and Barker, L. M., J. Appl. Phys. **37**, 1652 (1966).
Novikov, S. A., Sinitsyn, V. A., Ivanov, A. G., and Vasilyev, L. V., The Physics of Metals and Metallurgy **21**, 135 (1966).
Peyre, C., Pujol, J., and Thouvenin, J., in Proc. Fourth Symp. on Detonation, U.S. Naval Ordnance Laboratory, White Oak, Maryland, Office of Naval Research, ACR–126 (U.S. Government Printing Office, 1965).
Reynolds, C. E., and Seay, G. E., J. Appl. Phys. **33**, 2234 (1962).
Rice, M. H., Rev. Sci. Instr. **32**, 449 (1961).
Rohde, R. W., accepted for publication, Acta Metallurgica (1968a)
Rohde, R. W., private communication (1968b).
Taylor, J. W., and Rice, M. H., J. Appl. Phys. **34**, 364 (1963).
Taylor, J. W., in Dislocation Dynamics, ed. A. R. Rosenfield, G. T. Hahn, A. L. Bement, Jr., and R. I., Jaffee (McGraw-Hill, New York, 1968).
Wackerle, J., J. Appl. Phys. **33**, 922 (1962).
Warnes, R. H., J. Appl. Phys. **38**, 4629 (1967).

DISCUSSION

M. Contre (*Commissariat a l'Energie Atomique, Paris, France*): For the static transition pressure in iron you have given Drickamer's value of 133 kbar when, in fact, this value derives from Bancroft's shock measurements. In this regard, I have recently obtained a value, in a belt-type apparatus, of 150 kbar or more. The transition occurred slowly—in four or five hours.

G. E. Duvall (*Washington State University, Pullman, Washington*): You have made a point of comparing the strains that were obtained. It does appear to me that there may be one circumstance in which the measured strain is not representative of the curve in transition: If an elastic precursor takes the material to some Hugoniot elastic limit, and before the arrival of the transition shock a relaxation occurs, the state into which the transition shock advances is not necessarily the state that existed immediately behind the elastic precursor. The results you give for cadmium sulfide and indium antimonide are particularly interesting in this regard.

D. I. Decker (*Brigham Young University, Provo, Utah*): You say you saw no shear effects on the iron transition, but even for the materials with lower Hugoniot elastic limits the amount of shear might still be considerable compared to that observed in hydrostatic-type systems. For instance, you may

always have had a large amount of shear compared to what Contre had.

F. R. Boyd, Jr. (*Geophysical Laboratory, Carnegie Institution of Washington, Washington, D.C.*): With regard to the results that you have quoted on the cadmium sulfide and the indium antimonide, isn't this the first time that an equilibrium boundary has been shown to be displaced by shearing stress? There has been an argument about this in geological circles for 50 years. In general the minerals which used to be thought of as "stress minerals," geologically, have turned out simply to be high-pressure phases.

I would be interested in knowing in what kind of high-pressure apparatus the static results on those phases were obtained. It would be very interesting to look at results obtained in two types of high-pressure apparatus in which there are wide differences in the degree of shear that is present.

G. A. Samara (*Sandia Laboratories, Albuquerque, New Mexico*): The static measurements referred to on cadmium sulfide and indium antimonide were obtained in the cubic apparatus at Fort Monmouth three or four years ago. At Sandia one of our staff members has been studying the transition of cadmium sulfide under hydrostatic conditions. I believe his results show a transition at 23 ± 0.1 kbar for samples which have initial resistivities over a range of seven or eight decades. A range of values up to about 30 kbar has been given in the literature, and so I think this value is one of the lower ones obtained.

C. W. Beckett (*National Bureau of Standards, Washington, D.C.*): You mentioned a transition in antimony at around 90 kbar. Is that transition well-behaved?

AUTHORS' CLOSURE

With regard to Dr. Contre's comments, it is likely that Drickamer's value was strongly influenced by the early shock measurements. However as noted in the paper our current estimate of the shock transition pressure for iron is 125 kbar. I'm unable to critically assess the significance of the 150 kbar value observed by Contre. If the implication is that previous quasi-hydrostatic values have been low because of shear effects nucleating the transition at lower pressures, then I am surprised that the shock transition value for iron is unaffected by shear changes (different Hugoniot elastic limits).

I agree with Dr. Duvall's point. In the paper we have discussed how such complications resulting from time-dependent phenomena can be identified. Our point is that a material exhibiting such effects would be a poor candidate for a pressure calibration standard. With regard to cadmium sulfide and indium antimonide, our characterization of these materials is incomplete at present; however, their behavior does appear to be complex.

Dr. Decker's point may well be true that shock experiments may always involve much more shear than exists in quasi-hydrostatic experiments. However, my impression is that it is difficult to assess the shear stresses existing in many quasi-hydrostatic experiments. In the case of shock compression, shear stresses can be accurately evaluated.

In reply to Dr. Boyd, I don't know whether this is the first report of shear stress displacement of an equilibrium phase boundary. My guess is that it isn't because transformations that are martensitic in nature might be expected to show such effects. For example, Dr. J. Corll of Sandia Laboratories has suggested from ultrasonic pressure measurements that the cadmium sulfide transition is of a martensite-type. I believe Dr. Samara can better answer the apparatus question than I.

The transition in antimony, asked about by Dr. Beckett, shows a range of transition pressures of about 25 kbar out of 100 kbar depending upon the propagation distance and the driving stress. It is one in which the kinetics are definitely important, and so would appear to be a poor choice as a reference transition.

Study of Phase Transitions in Insulators by the Dielectric Constant Technique*

G. A. Samara and W. L. Chrisman

Sandia Laboratories, Albuquerque, New Mexico 87115

This paper proposes the measurement of the dielectric constant and dielectric loss as a probe for detecting and studying the properties of pressure-induced phase transformations in insulators. The measurement is very sensitive, relatively simple, and can be adapted for use in many types of high pressure apparatus. To illustrate the general usefulness of the technique, results on a variety of substances (solids and liquids) obtained from measurements in three different pressure apparatus will be presented and discussed. The substances investigated include a number of alkali and thallous halides, strontium titanate, and water.

1. Introduction

The study of pressure-induced phase transitions is of interest from the standpoint of lattice stability and kinetics of phase transformations as well as for determining the influence of crystal structure on physical properties. In addition, the transition pressures in many substances have been used, or are potentially useful, as "fixed points" for pressure calibration purposes.

The detection and study of pressure-induced phase transitions in insulators have been limited to techniques—usually the direct measurement of volume change—which are not well suited for many of the high pressure apparatus now in use. In this paper we suggest the measurement of the dielectric constant as a probe for studying such transitions. The measurement is very sensitive and relatively simple. Results on a variety of substances (solids and liquids) obtained from measurements in both hydrostatic and quasi-hydrostatic (cubic multianvil and Bridgman anvil) pressure apparatus will be presented and discussed. Whalley and coworkers [1][1] have been using the same technique for studying the pressure-temperature phase diagram of ice and have also suggested its use for the study of other phase transitions.

Aside from the above considerations, the study of the pressure (volume) dependence of the dielectric constant and dielectric loss is of interest because these quantities enter into the theoretical treatment of various physical properties, e.g., the theories of electron-phonon interactions and infrared dispersion and dielectric relaxation. Combined with temperature measurements, the pressure results make it possible to separate the temperature dependence of the dielectric constant into its volume-dependent and volume-independent contributions. The latter contributions are determined entirely by anharmonic lattice effects [2].

[1] Figures in brackets indicate the literature references at the end of this paper.

*This work was supported by the U.S. Atomic Energy Commission.

Paper presented at the Symposium on Accurate Characterization of the High-Pressure Environment, held at the National Bureau of Standards, Gaithersburg, Md., October 14–18, 1968.

2. Theoretical Considerations

The purpose of this section is to give a brief discussion of dielectric properties. This should serve to define the quantities and relationships to be used later.

When a dielectric (insulator) slab is placed in a static applied electric field, it acquires a surface charge. The polarization so induced arises from the displacement of positive and negative charges in the dielectric. For an isotropic, linear dielectric, the polarization $\mathbf{P}$ is proportional and parallel to the applied field $\mathbf{E}$. The electric flux density or electric displacement $\mathbf{D}$ is defined by (cgs units)

$$\mathbf{D}=\mathbf{E}+4\pi\mathbf{P}=\epsilon\mathbf{E} \tag{1}$$

where ϵ is the static dielectric constant. The dielectric susceptibility χ is defined by $\mathbf{P}=\chi\mathbf{E}$, and from eq (1) it is seen that

$$\epsilon=1+4\pi\chi. \tag{2}$$

For isotropic dielectrics ϵ and χ are scalar quantities. They are dependent on the molecular properties of the dielectric and, at low fields (i.e., in the linear range), are independent of the magnitude of the macroscopic field $\mathbf{E}$.

The polarizability α of an atom (or molecule) is defined by

$$\mu=\alpha\mathbf{F} \tag{3}$$

where μ is the electric dipole moment, and $\mathbf{F}$ is the local, or effective, field seen by the atom. The polarization $\mathbf{P}$ is defined as the net dipole moment per unit volume and is given by

$$\mathbf{P}=\sum_i N_i\mu_i=\sum_i N_i\alpha_i\mathbf{F}_i, \tag{4}$$

where N_i is the number of dipoles per unit volume.

The local field $\mathbf{F}$ at a given lattice site i is generally written as

$$\mathbf{F}_i = \mathbf{E} + \mathbf{E}_{\text{int.}}$$
$$= \mathbf{E} + 4\pi \sum_j \phi_{ij} \mathbf{P}_j, \tag{5}$$

where $\mathbf{E}$ is the applied field, and $\mathbf{E}_{\text{int.}}$ is the internal field acting on the ion i due to the other ions j and is expressed in terms of the polarization. ϕ_{ij} is the internal field coefficient, which is a dimensionless quantity that depends on the arrangement of the ions in the lattice. For diagonal cubic crystals, i.e., crystals in which all ions have cubic environments, the Lorentz internal field is applicable and $\phi_{ij} = 1/3$. In this case the above eqs yield

$$\mathbf{P} = \frac{\sum N_i \alpha_i}{1 - \frac{4\pi}{3} \sum N_i \alpha_i} \mathbf{E} = \frac{\epsilon - 1}{4\pi} \mathbf{E}. \tag{6}$$

From eq (6) it is easily shown that

$$\frac{\epsilon - 1}{\epsilon + 2} = \frac{4\pi}{3} \sum N_i \alpha_i, \tag{7}$$

which is the familiar Clausius-Mossotti equation.

The individual ionic polarizabilities are difficult to determine, and it has become customary to use eq (7) in its macroscopic form which can be written as

$$\frac{\epsilon - 1}{\epsilon + 2} = \frac{4\pi}{3} \left(\frac{\alpha}{V} \right). \tag{8}$$

Here α is the total polarizability of a macroscopic element of the material of volume V. Equation (8) is applicable for cubic or isotropic substances [3].

For anisotropic, linear dielectrics, ϵ, χ, and α are tensors and eq (1) must be written as

$$\mathbf{D} = \epsilon \cdot \mathbf{E}, \tag{9}$$

with components

$$D_k = \sum_{l=1}^{3} \epsilon_{kl} E_l \cdot (k = 1, 2, 3). \tag{10}$$

Other quantities follow similarly.

Up to now we have considered only the static case. When a dielectric is subjected to an alternating field, both $\mathbf{D}$ and $\mathbf{P}$ will vary periodically with time. In general, however, $\mathbf{D}$ and $\mathbf{P}$ cannot follow the electric field instantaneously. There will always be relaxation effects and losses in the dielectric, and these cause a lag in phase between $\mathbf{E}$ and the response of the material. Thus for example if

$$\mathbf{E} = \mathbf{E}_0 \cos \omega t, \tag{11}$$

we have

$$\mathbf{D} = \mathbf{D}_0 \cos (\omega t - \delta), \tag{12}$$

where δ is the loss angle which is independent of $\mathbf{E}_0$, but generally depends on frequency [4]. Under these conditions the dielectric function is written as a complex quantity

$$\epsilon^* = \epsilon' - i\epsilon''. \tag{13}$$

The loss angle is defined by

$$\tan \delta = \epsilon''/\epsilon'. \tag{14}$$

$\tan \delta$ is simply related to the quality or Q factor of the dielectric by $Q = 1/\tan \delta$. It is obtained rather directly from experiment.

3. Measurement Technique

A real dielectric can be represented by an ideal capacitance (loss-free) plus a parallel resistance which expresses the sum total of all the dissipative processes occurring in the dielectric when subjected to an applied field. The static dielectric constant ϵ is usually determined from capacitance measurements at audio frequencies, which also yield values of the dielectric loss in terms of $\tan \delta$, Q, or the parallel resistance R, depending on the method of measurement. The dielectric constant of the sample is measured relative to that of free space. For a parallel-plane capacitor of large area to thickness ratio (i.e., negligible fringe field), ϵ is related to the measured capacitance C by

$$\epsilon = Cd/\epsilon_0 A. \tag{15}$$

Here d is the separation between planes, A is the area of the capacitor and $\epsilon_0 = 8.85 \times 10^{12}$ farads/meter is the dielectric constant (permittivity) of free space. For capacitors of small area to thickness ratio, corrections for fringe fields can be made, or a guard-ring arrangement requiring three-terminal measurements can be employed. However, when the primary interest in the measurement is the detection of a phase transformation, then the absolute accuracy is not important, and two-terminal measurements without regard to fringe field effects are adequate. At frequencies up to several hundred kHz the measurements can be made using a variety of commercially available capacitance and impedance bridges.

Electrode attachment to the surfaces of solid samples is very important since even small air gaps can introduce serious errors. Vapor coated metal electrodes are best, but carefully prepared conducting paint brushed or sprayed-on, or fired-on silver electrodes are often satisfactory. For measurements in certain apparatus such as Bridgman anvils, the faces of the anvils themselves can serve as electrodes.

In the present study a transformer ratio-arm type capacitance bridge (General Radio Type 1615–A) with three-terminal connections was used.

The use of shielded electrical leads and sample holders eliminated ground capacitance effects.

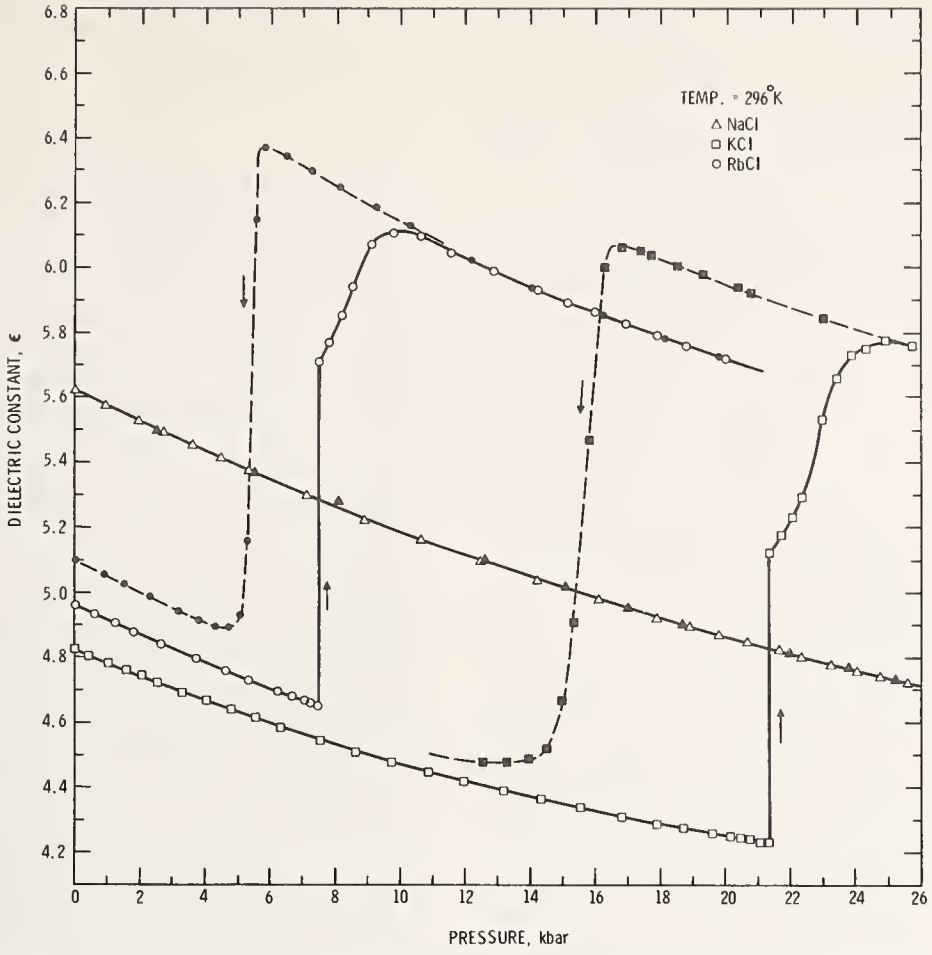

FIGURE 1. *The dielectric constants of single crystal samples of* NaCl, KCl, *and* RbCl *as functions of hydrostatic pressure.*
KCl and RbCl transform from the NaCl-type structure to the CsCl-type structure in the pressure range covered.

Sample capacitance and dielectric loss tan δ were measured at frequencies between 1 and 100 kHz. Measurements were made as functions of pressure and/or temperature in three different pressure apparatus: a hydrostatic piston-cylinder using a 50–50 mixture of *n*-pentane and *iso*-pentane as pressure fiuid, a cubic multianvil, and a Bridgman anvil apparatus. The anvils were shielded from each other to eliminate stray capacitances.

4. Results and Discussion

In the following we present and discuss results on a variety of substances to illustrate the usefulness of the technique. It is readily seen from eqs (8) and (15) that a discontinuity in ϵ, and hence the measured sample capacitance, can be expected at a first-order phase transition.

4.1. Alkali Halides

The alkali halides, with the exception of cesium chloride, bromide, and iodide which crystallize in the **CsCl**-type structure, crystallize in the **NaCl**-type structure at standard conditions. However, it is well known [5] that several of them, particularly the chlorides, bromides, and iodides of potassium and rubidium, undergo transitions from the **NaCl** to the **CsCl** structure at high pressure. We have studied the pressure dependence of the dielectric properties of many of these compounds to 25 kbar with emphasis on the behavior near phase transitions. The measurements were made in the hydrostatic apparatus.

Figure 1 shows the effect of pressure on the dielectric constant of single crystal samples of NaCl, KCl and RbCl. The latter two crystals undergo the **NaCl**→**CsCl** transition in the pressure range covered. For all three crystals the dielectric constant ϵ in the **NaCl** phase decreases monotonically with increasing pressure. For RbCl and KCl a sudden discontinuous increase in ϵ is observed at the start of the transition. The onset of the transition is also accompanied by a loud burst-like sound. It is quite remarkable that the sound of the transformation in the relatively small crystals used (about 1 cm^2 $\times$0.07cm thick) could be heard outside the massive steel apparatus. On further increasing the pressure, ϵ rises at a rate which increases with increasing pressure and finally goes through a maximum which corresponds to the end of the transition. In the **CsCl** phase ϵ again decreases monotonically with increasing pressure. The reverse transformation exhibits a large hysteresis, and the calculated value

of ϵ at 1 bar often does not return to its exact original value, probably because of small changes in sample geometry caused by the transition.

Our measurements on RbBr, RbI, KBr, and KI show features very similar to those for RbCl and KCl shown in figure 1.

The macroscopic Clausius-Mossotti relationship, eq (8), is applicable for the alkali halides in both the **NaCl** and **CsCl** phases. Its application at the transition shows that, although ϵ for each of the above K and Rb salts increases by 35 to 40 percent at the **NaCl** → **CsCl** transition, the total polarizability per molecule is not strongly dependent on crystal structure. Thus, for example, the data on RbCl and KCl in figure 1 combined with volume changes of 13.7 and 11.4 percent at their respective transitions, [5] yield for the ratio $(\alpha_{NaCl}/\alpha_{CsCl})$ values of 1.00 for RbCl and 0.96 for KCl. Comparable values are obtained for the bromides and iodides. These results indicate that changes in ϵ at these transitions are mostly due to changes in volume.

The question of whether or not NaCl undergoes a pressure-induced transition around 20 kbar has received considerable attention in the recent literature [6]. The results in figure 1 along with elastic constant measurements [6] show no evidence of a transition under hydrostatic conditions up to 26 kbar at 23 °C. Recent measurements using a diamond anvil x-ray cell [7] indicate that the NaCl → CsCl transition in NaCl does not occur until ≃ 300 kbar at room temperature.

We have also investigated KCl in a 1.25cm (flat) Bridgman anvil apparatus. The samples were ≃ (0.020–0.040) cm thick × 0.64 cm diam., fused powder discs enclosed in a pyrophyllite ring. Typical results, reported as capacitance versus hydraulic ram pressure, are shown in figure 2. The onset of the transformation is fairly well defined, but the transition is spread over a wide range. This difficulty arises, of course, because of the large pressure gradients across the flats of the anvils.

4.2. Thallous Halides

We have studied the pressure and temperature dependence of the dielectric properties of TlCl, TlBr, and TlI in some detail [2]. TlCl and TlBr have the **CsCl** structure and do not exhibit any transformations. TlI, on the other hand, crystallizes under normal conditions in a double-layered orthorhombic structure ($D_{2h}^{17}-C_{mcm}$) with four molecules per unit cell. It transforms to the cubic **CsCl** structure on increasing temperature (170 °C at 1 bar) and/or pressure (4.7 kbar at 25 °C) [8].

The dielectric constant of TlI increases by 35 percent at the transition, [2] and this is reflected by a large discontinuous increase in the measured capacitance of the sample. Figure 3 shows typical results. The two isotherms are for two differcent samples, and the differences in the values of the capacitance are due to differences in sample geometries. The transformation is characterized by a large hysteresis which decreases with increasing temperature. The transition temperature decreases very rapidly with pressure with an initial slope $dT_0/dp = -53 \pm 3$ °C/kbar [8].

In a number of isothermal pressure experiments we followed the progress of the TlI transformation as a function of time at constant pressure (the pressure being that at which the first indication of the start of the transformation was noted) by monitoring the change in sample capacitance. Figure 4 shows the results of one such experiment. The

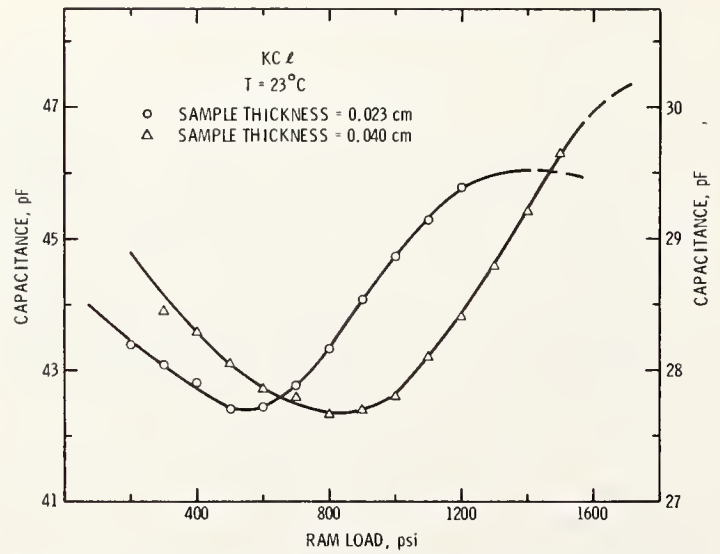

FIGURE 2. *Capacitance versus applied load for* KCl *samples run in a Bridgman anvil apparatus.*

The transformation is spread over a wide pressure range due to pressure gradients across the anvil faces.

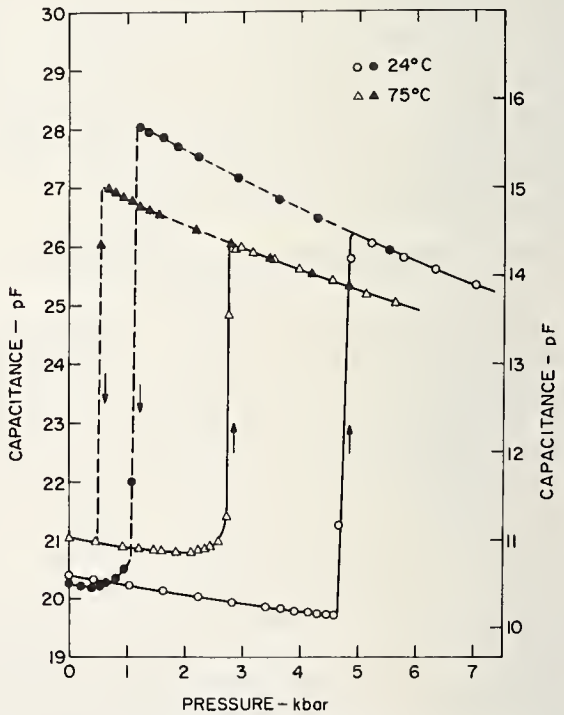

FIGURE 3. *Capacitance versus hydrostatic pressure isotherms for two different* TlI *samples.*

The 24 °C isotherm data are read against the left ordinate, and the 75 °C isotherm data are read against the right ordinate.

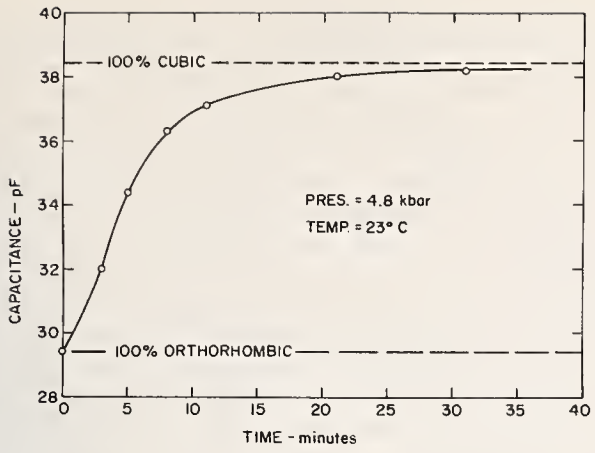

FIGURE 4. *Progress of the orthorhombic → cubic transformation in* TlI *as a function of time at constant pressure and temperature.*

transformation proceeds as a reaction rate process approaching completion asymptotically. The percent completion can be taken as the fractional change in capacitance between the limiting values of the two phases. Thus it is seen that the technique can be used for studying the kinetics of phase transitions.

At high temperatures, the dielectric constant and the dielectric loss, tan δ, of the thallous halides as well as those of many other ionic crystals, [9] increase exponentially with increasing temperature and decrease with increasing frequency. In this temperature region polarization effects associated with dipoles produced by impurities and lattice defects predominate, and the dielectric loss is dominated by the conductivity of the sample [2]. The relationship is

$$\tan \delta = \epsilon''/\epsilon' = 4\pi\sigma/\epsilon'\omega, \qquad (16)$$

where

$$\sigma = \sigma_0 \exp\ (-\mathscr{E}/kT). \qquad (17)$$

Here ω is the angular frequency, σ is the d-c conductivity, σ_0 is a constant, and $\mathscr{E}$ is the activation

TABLE 1. *Values of the activation energy (for the formation and motion of defects) of the thallous halides at 1 bar obtained from dielectric loss, tan δ, measurements at high temperatures*

Present results are compared with literature values obtained from ionic-conductivity measurements.

	TlCl	$\mathscr{E}$(eV) TlBr	TlI (ortho.)	TlI (cubic)
Samara [a]	0.84 ± 0.05	0.85 ± 0.04	0.62 ± 0.04	[b] ≈ 0.50
Lehfeldt [c]	.79 ± 0.03	.80 ± 0.05		
Others [d]	.75 to 0.87	.75 to 0.84		

[a] Ref. [2].
[b] Evaluated at 3 kbar.
[c] W. Lehfeldt, Z. Physik **85**, 717 (1933).
[d] Values quoted by Lehfeldt.

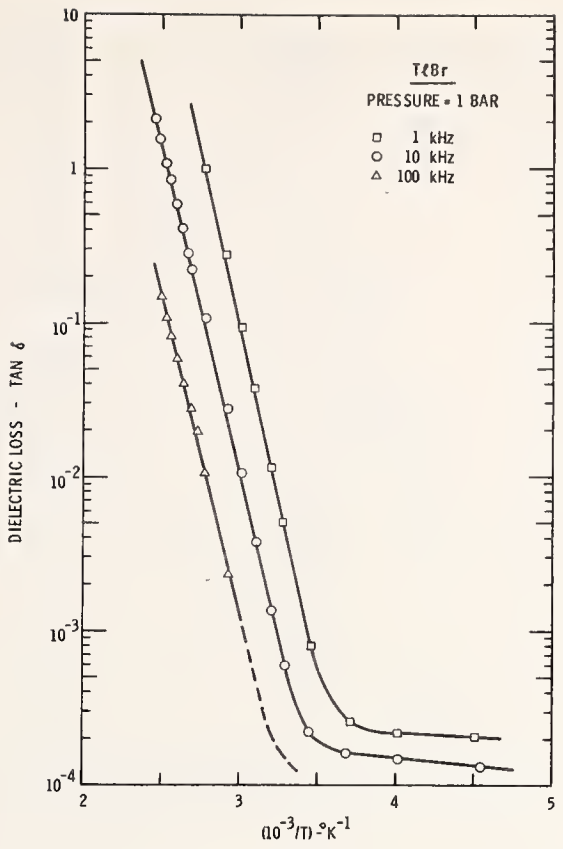

FIGURE 5. *The temperature dependence of the dielectric loss of* TlBr.

In the high-temperature region tan δ is proportional to the conductivity.

energy for the formation and motion of defects. It is seen from eqs (16) and (17) that activation energy can be determined from tan δ versus temperature measurements at constant frequency.

Figure 5 shows log tan δ versus $1/T$ plots for TlBr at three frequencies. At high temperatures the results exhibit the expected linear dependence with the slopes very nearly independent of ω. Similar results were obtained for TlCl and TlI. Table 1 summarizes for the three compounds the activation energies calculated from the slopes of the linear portions of the curves at high temperature. For comparison we also list in table 1 values of $\mathscr{E}$ for TlCl and TlBr obtained from ionic conductivity measurements. It is seen that the agreement is quite good.

We did not extend the high temperature measurements of tan δ to high pressures, but it is a simple matter to do so, and thus study the effect of pressure on the activation energy.

4.3. Strontium Titanate

At standard conditions, $SrTiO_3$ crystallizes in the ideal cubic perovskite structure and exhibits normal dielectric behavior (i.e., it is not ferroelectric or antiferroelectric). Although it does not exhibit any phase transitions in the pressure and temperature ranges of the present measurements, the data on it extended to 50 kbar [10] and serve to illustrate the

385-762 O - 71 - 17

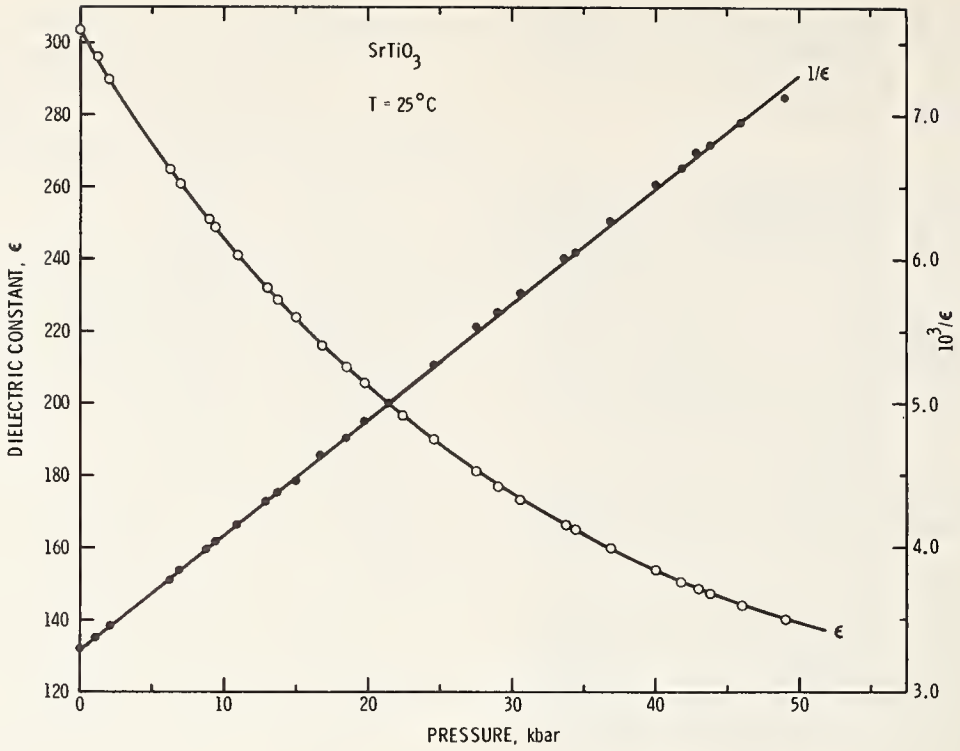

FIGURE 6. *The pressure dependence of the dielectric constant* ϵ *and* $1/\epsilon$ *for single crystal* $SrTiO_3$.

general usefulness of the dielectric constant technique. In addition, the results have interesting implications for pressure calibration purposes.

The measurements were made on single crystals and were performed in a cubic multianvil pressure apparatus [11]. The samples were suspended in a nylon-teflon container filled with a low viscosity silicone pressure fluid—a technique similar to that described by Jayaraman [12]. The fluid undoubtedly solidifies at the high pressure end, but this had no apparent influence on the results. The pressure dependence of ϵ is shown in figure 6. A reversible monotonic decrease of ϵ with increasing pressure is observed over the whole range.

It is known [13] that the temperature dependence of ϵ of $SrTiO_3$ at constant pressure obeys a Curie-Weiss law, $\epsilon = C/(T-T_0)$. The results in figure 6 show that the pressure dependence of ϵ at constant temperature obeys a similar relationship expressed in terms of pressure, i.e.,

$$\epsilon = C^*/(P-P_0). \qquad (18)$$

At 25 °C, $C^* = 12{,}600$ kbar and $P_0 = -40$ kbar.

The linear dependence of $1/\epsilon$ on pressure over a wide pressure range suggests that $SrTiO_3$ can be used as an accurate pressure gauge. In fact, this feature of the results was used in determining the pressure calibration in the range 0 to 15 kbar in the present experiment. It is recalled here that the usual calibration curves (i.e., sample pressure versus load curves based on "fixed" pressure points) for multianvil, belt, and similar apparatus exhibit anomalous behavior in this low pressure range. For example, such curves do not extrapolate to zero pressure for zero applied load [11]. In the present experiment, the $1/\epsilon$ versus pressure data above 15 kbar fell on a straight line which extrapolated back to the zero pressure $1/\epsilon$ value. Pressures in the 0 to 15 kbar range were then determined from the linear $1/\epsilon$ versus pressure response.

4.4. Water

The measurements of the dielectric constant and dielectric loss are well-suited for studying liquid-solid transformations under pressure. We have chosen water to illustrate this point. Water exhibits a truly remarkable pressure-temperature phase diagram. In addition to the liquid-ice transformation, at least eight different phases of ice have been identified [1, 14].

The present experimental setup was quite simple. An empty parallel-plate capacitor was immersed in triply distilled water contained in a glass tube open at the top. The assembly was then placed in a sample holder inside the pressure chamber of the hydrostatic pressure apparatus. A 50–50 mixture of *n*-pentane and *iso*-pentane was used as pressure fluid. Water is heavier than the pentane mixture, and the two fluids have a very low miscibility so that, for the present purposes, it was not necessary to keep them isolated from each other.

Sample capacitance and tan δ were measured at 100 kHz as functions of pressure at room temperature. The results are shown in figure 7. Although the water used was triply distilled, the dielectric loss was very high, probably due to dissolved CO_2. Both

the capacitance and tan δ increased initially with increasing pressure. The leveled-off region (especially in tan δ) between ≃ 8 and 10 kbar represents the upper limit for the sensitivity of the measuring apparatus. Large discontinuous decreases in capacitance and tan δ were observed at the water-ice VI transition. This is mostly due to the large decrease in orientational polarizability on freezing. Sharp decreases in capacitance and tan δ were also observed at the ice VI-ice VII transition. A hysteresis of ~ 0.5 kbar was observed at this transition. The hysteresis at the water-ice VI boundary was not measured because the glass tube broke on lowering the pressure at this transition. This difficulty could be avoided by using a plastic or metallic liquid container.

Whalley and co-workers [1] have been studying the water-ice phase diagram in some detail using the dielectric constant technique. Some of their measurements were made in a Bridgman anvil apparatus at pressure to over 100 kbar. The water was contained inside a thin mica ring between the anvils. In addition to the determination of phase boundaries, their results yielded information about the nature of the relaxation processes in the various phases of ice.

5. Summary

In this paper we have presented a brief account of the experimental and theoretical considerations concerning the use of measurement of the dielectric constant and dielectric loss as a probe for studying pressure- and temperature-induced phase transformations in insulators. The general usefulness of the technique was demonstrated by results obtained from measurements in three different pressure apparatus: a 30-kbar hydrostatic unit, a cubic multi-anvil, and a Bridgman anvil apparatus. Measurements on a number of alkali and thallous halides, strontium titanate and water were presented and discussed. The technique is one of the most sensitive means for studying phase transformation in insulators and can be easily applied.

6. References

[1] Whalley, E., Heath, J. B. R., and Davidson, D. W., J. Chem. Phys. **48**, 2362 (1968) and references therein.
[2] See, e.g., Samara, G. A., Phys. Rev. **165**, 959 (1968).

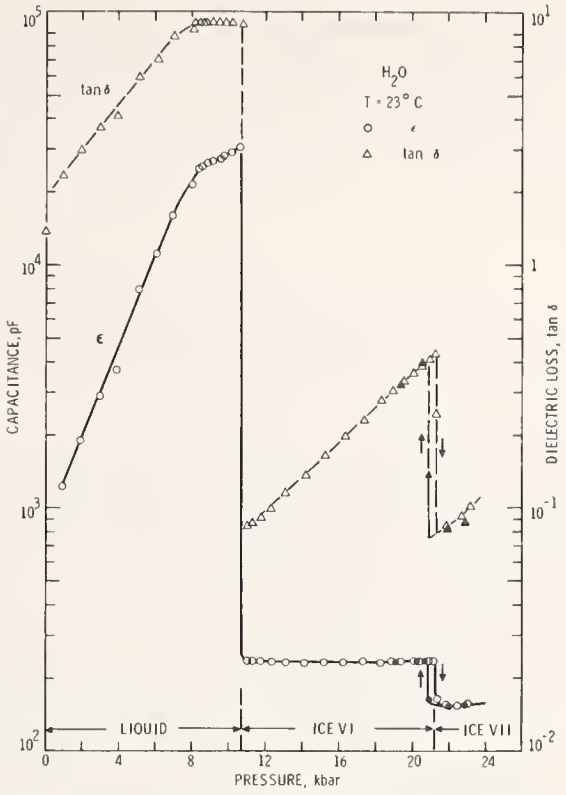

FIGURE 7. *Changes in the capacitance and dielectric loss of a triply distilled water sample as functions of hydrostatic pressure.* The liquid → ice VI and the ice VI → ice VII transitions are clearly exhibited.

[3] Fröhlich, H., Theory of Dielectrics (Clarendon Press, Oxford, England, 1949), Appendix 3, p. 169.
[4] In an ideal dielectric (loss-free) the current leads the voltage by a phase angle ϕ of exactly 90°. In a real dielectric with losses $\phi < 90°$. The loss angle δ measures the angle between the current through the dielectric and that which would flow through an ideal dielectric, i.e., $\delta + \phi = 90°$.
[5] Bridgman, P. W., Proc. Am. Acad. Arts Sci. **74**, 21 (1940).
[6] See e.g., Corll, J. A., and Samara, G. A., Solid State Comm. **4**, 283 (1966) and references therein.
[7] Bassett, W. A., Takahashi, T., Mao, H., and Weaver, J. S., J. Appl. Phys. **39**, 319 (1968).
[8] Samara, G. A., Walters, L. C., and Northrop, D. A., J. Phys. Chem. Solids **28**, 1875 (1967).
[9] Rao, K. V., and Smakula, A., J. Appl. Phys. **36**, 3953 (1965).
[10] Samara, G. A., and Giardini, A. A., Phys. Rev. **140**, A954 (1966).
[11] Samara, G. A., Henius, A., and Giardini, A. A., ASME Trans., J. Basic Engr. **86**, 729 (1964).
[12] Jayaraman, A., Proceedings of this conference.
[13] See e.g., Samara, G. A., Phys. Rev. **151**, 378 (1966) and references therein.
[14] Bridgman, P. W., J. Chem. Phys. **3**, 597 (1935).

DISCUSSION

Y. A. Atanov (*All-Union Research Institute for Physical and Radiotechnical Measurements, Moscow*): What is your estimation of the reproducibility of the pressure coefficient of the dielectric constant of $SrTiO_3$? It is my understanding that the dielectric loss of water increases very rapidly with pressure, when you raise the pressure. Could you explain the mechanism for this dielectric loss and why it increases?

G. S. Kell (*National Research Council of Canada, Ottawa, Ontario, Canada*): I would like to point out that as far as the behavior of water is concerned, the permanent dipole moment makes a major contribution.

I would also like to mention that there are at least eleven or twelve solid phases established for water. The paper by Whalley (your ref. 1) lists nine. Two of these are metastable. In addition to that there

is, I think, a phase in which the X-ray structure was determined by McFarlan some place in the region of two or three kilobars. There is cubic ice in the low-pressure region. Thus there are eleven phases which can be prepared in bulk, and in addition there is the amorphous phase which can be prepared by evaporation in small quantities.

Question from the floor: In the transformation of the alkali halides, I was interested in the noise you heard. Was this a result of the fracturing of the crystal or what? Are the crystals intact afterwards?

AUTHORS' CLOSURE

Reply to Atanov: We have not made a systematic study of the reproducibility of the pressure coefficient of the dielectric constant of $SrTiO_3$. Results from four or five independent measurements by us and others yield values of $[\partial(1/\epsilon)/\partial P]_T$ that fall in the range $7.7-8.0\times10^{-5}$/kbar. On individual samples I think the reproducibility should be better than ±1 percent. It should, of course, be remembered that ϵ is a strong function of temperature, and good temperature control is required.

The dielectric loss of the water used was quite high even though the sample was triply distilled. We did not look into the cause of this because we selected water simply to demonstrate the sensitivity of the technique. Water is a highly polar substance and dipolar relaxation effects are important. The presence of some carbon dioxide dissolved in the water may contribute to the high loss. The increase of the loss with pressure is of course associated with the increase of sample conductivity, but we do not know at present whether this increase is an intrinsic property of the sample or is due to impurities.

Reply to Kell: The total macroscopic polarizability α in eq (8) can of course be written as the sum of three contributions, i.e.,

$$\alpha=\alpha_{op}+\alpha_{ir}+\alpha_d.$$

These contributions exhibit different frequency response and can, therefore, be separated. The optical, or high-frequency contribution, α_{op}, arises from displacements of the electronic charge relative to the nucleus of each atom. The infrared contribution (often referred to as ionic contribution), α_{ir}, arises from the combined effects of the displacements of the atoms and the resulting distortion of the electronic charge. The dipolar contribution, α_d, is present in substances possessing permanent dipole moments (e.g., water), and it is operative in the dc to millimeter frequency range. Even though it is possible to effect a separation of α into the above contributions on the basis of frequency response, each contribution remains a macroscopic quantity which generally does not tell us much about the polarizabilities of the individual atoms or ions.

Reply to question from the floor: The sound one hears during the transformation of the alkali halides is characteristic of martensitic transformations and is quite familiar to people working on steels and other alloys exhibiting such diffusionless transformations. It is associated with the rapid slip that occurs during the transformation.

These transitions involve large volume changes (14% in the case of RbCl) and after a crystal has gone through the transition twice (on the up-and-down cycle), one recovers a polycrystalline mass, but the sample holds its integrity.

Experimental Determination of Curie Points of Ferromagnets up to 90 Kilobars—Possible Use For Calibration of High Pressure

J. M. Leger, C. Susse, and B. Vodar

C.N.R.S.—Laboratoire des Hautes Pressions—Bellevue, France

Second-order phase transformations which occur without volume discontinuity and theoretically without any hysteresis are suggested as secondary pressure gauges and for interpolation under high pressure in different temperature ranges. Results are presented concerning the shifts of Curie temperatures of some ferromagnets up to 90 kbar. The pressure effect is generally small but may be accurately determined.

Direct measurement of pressures above 20 kbars is only possible in devices of the piston cylinder type for which, in principle, the relation $p =$ applied force/piston area, applies. However even in these devices, when a solid pressure transmitting medium surrounds the sample, the measure of the pressure is made inaccurate because it is impossible to determine the influence of the frictional forces by increasing and decreasing pressure experiments. This arises from the fact that the friction which comes from the transmitting medium is unsymmetrical [1].[1] It is then necessary, in these devices as in apparatuses of the compressible gasket type, to make a pressure calibration. This is usually achieved either in a continuous manner in situ by measuring the crystalline parameter of a standard by x-ray diffraction, or more simply and more frequently by monitoring some polymorphic 1st order transitions such as those occuring in bismuth, thallium, cesium, barium, iron, tin, lead . . .. These transitions are generally observed at room temperature by the resistance discontinuity method, which is the easiest to handle. The direct measurements of the pressure transitions of these elements are made by volumetric measurements in a piston cylinder device without any pressure transmitting medium. This has only been made for the first four elements mentioned above.

The use of first-order transitions as fixed points, however, offers the following inconveniencies:

(a) The sudden contraction of volume of the standard at the instant of the transition cannot be compensated for instantaneously by flow of the surrounding material since it has a non zero resistance to shear; this "cavitation" effect, well known to the users, results in a spread of the transitions and makes their location, imprecise. This effect can lead to an apparent shift of the transitions when the standard cell contains several standards or when a standard suffers successive transitions (bismuth, barium).

(b) There is another major disadvantage in using first order transformations; these transitions always exhibit some hysteresis range related to the nucleation processes of the different phases, the amplitude of which depends on various parameters (shape, purity of the sample . . .). This hysteresis is not negligible as is clearly shown by the following values [2], in kbars, obtained at room temperature by x-ray diffraction using an internal standard.

Bi I—II	2.8 to 5.3	Ba I—II	2.6
Tl II—III	1.6	Bi III—V	3.8

This hysteresis must necessarily be taken into account in calibrations made at increasing pressure (belts . . .) making use of data obtained by a mean process in reversible working devices (piston-cylinder).

1. Second-Order Transformations in Solids as a Means of Characterizing the High Pressure Environment

The inconveniences quoted above of using first order transformations are eliminated if instead, second order ones are employed as fixed points for calibration. By definition the latter proceed without any volume discontinuity, and theoretically without hysteresis.

Little work at high pressures has been done so far on these transformations, probably because the two most popular methods, the volume and the electrical resistivity discontinuity methods are not well suited for their observation. However exploration of their respective capabilities as secondary pressure gauges would be most valuable. At first sight these capabilities are quite different according to the considered type of transformation:

—order-disorder transformations in binary alloys (a typical example is $AuCu_3$) offer the disadvantage of being very slow.

—transitions to a superconducting state, without magnetic field applied, which occur at very low temperatures would be of limited use.

—Curie points of ferromagnets or some ferroelectrics,

[1] Figures in brackets indicate the literature references at the end of this paper.

Paper presented at the Symposium on Accurate Characterization of the High-Pressure Environment, held at the National Bureau of Standards, Gaithersburg, Md., October 14–18, 1968.

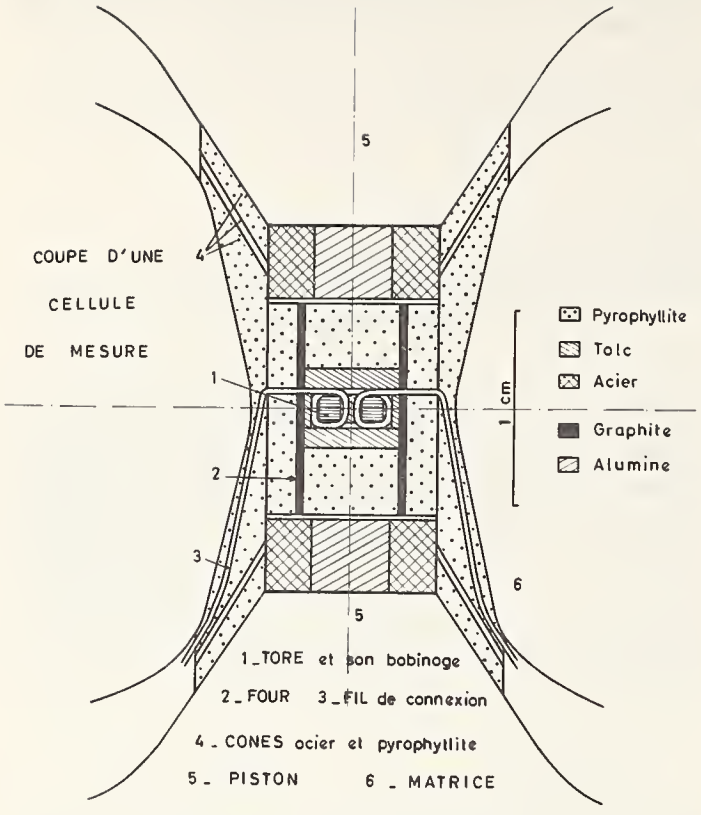

FIGURE 1. *Measurement cell.*

Neel points of antiferromagnets appear to be the most promising.

In the next section, we present our first results concerning the effect of pressure on Curie temperatures of several ferromagnets. Their possible use as pressure gauges is discussed below.

2. Curie Points of Some Ferromagnets as a Function of Pressure

2.1. Present Theoretical State

For every second-order phase change, the behaviour of the transition temperature as a function of pressure can be described by the general relations established by Ehrenferst and which correspond to the Clapeyron equation for first order transformations:

$$\frac{dT}{dp}=\frac{\chi_2-\chi_1}{\alpha'_2-\alpha'_1}=TV\frac{\alpha'_2-\alpha'_1}{C_{p2}-C_{p1}}$$

- index 1 old phase
- index 2 new phase
- α^1 isobaric thermal expansion coefficient
- χ isothermal compressibility
- C_p isobaric specific heat

These relations do not allow calculation of the pressure effect, because the necessary data (C_p, α'. . .) have not been determined under pressure. It is also impossible to compute this effect from the Landau's theory in which the thermodynamic potential is expanded in powers of an order parameter, because this expansion involves coefficients only known at ordinary pressure (magnetostriction constant . . .). On the other hand, work based on microscopic models is very scarce. The Heisenberg model does not allow understanding of the pressure effect in detail for the transition metals of the first period. A model with itinerant electrons has been proposed in the case of nickel [4], but the result, though giving the right sign for the variations, is still approximative.

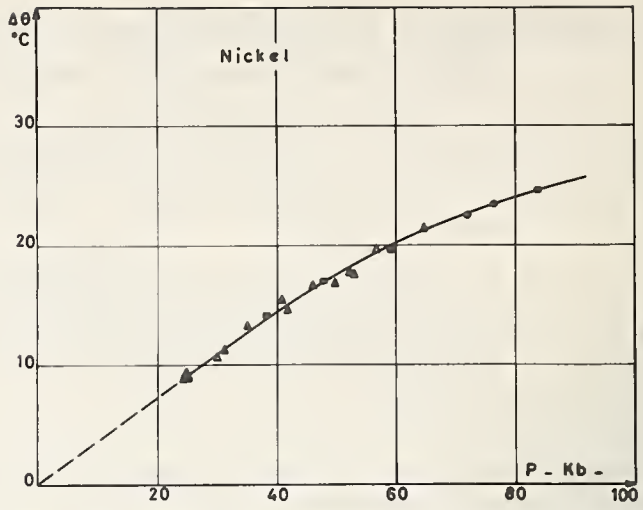

FIGURE 2. *Shift of the Curie temperature of nickel under pressure.*

Thus so far it has been impossible to predict the pressure effect on Curie temperatures from a theoretical point of view, so that they cannot be used as primary pressure gauges. However for the reasons mentioned earlier they are well suited to be employed as secondary standards.

2.2. Experimental Method

To determine the shifts of the Curie temperatures under the effect of pressure we have employed the transformer method, formerly used by several authors [5, 6, 7]: without magnetic field applied, one notes the variations of the permeability μ of the sample as a function of temperature; in our experiments this sample has the shape of a torroid on which the primary and secondary windings are made from a coaxial cable. The primary is supplied with an ac current of constant intensity; the secondary voltage and the temperature are fed onto an XY recorder and we directly obtain the $\mu=f(T)$ curves at different constant pressures. The inflexion points of these curves determine the Curie points.

This transformer method is easy to handle under pressure and allows us the determination of small shifts of Curie points, even at rather high temperatures; it must be noticed that it does not always give the exact value of the Curie temperature; generally we get a value a little too low, because the method using a low magnetic field is not very conventional.

We performed all our experiments in profiled piston devices [8] of the belt type, calibrated at

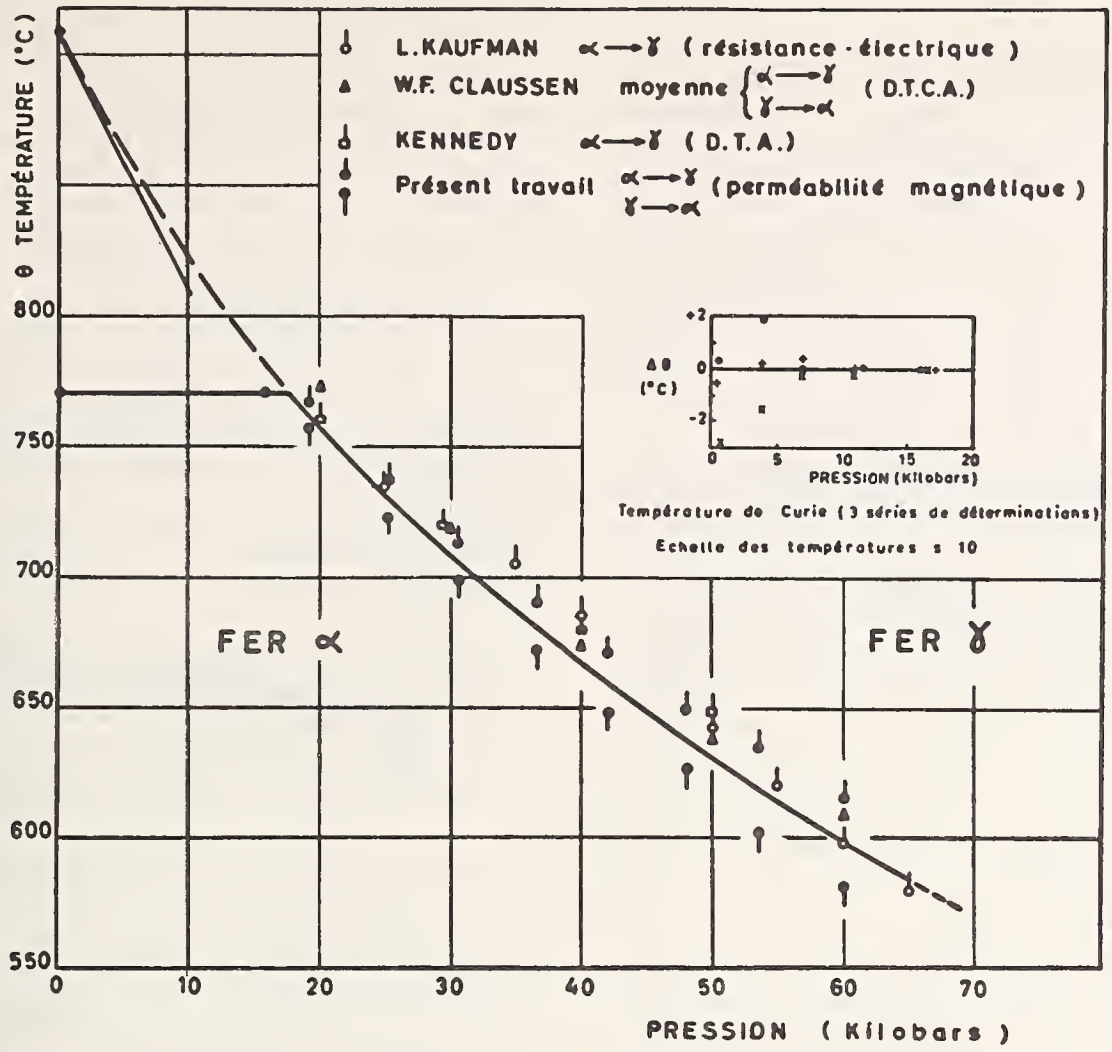

FIGURE 3. *Curie point and α-γ transformation of iron under pressure.*

room temperature according to the usual technique by monitoring the variations of the electrical resistivity of bismuth and barium. The corresponding transition pressures have been chosen equal to 25.4 kbar for Bi I–II, 58.6 kbar for Ba I–II, 82 kbar for Bi III–V.

The design of the measurement cell is shown in figure 1; the sample is completely surrounded by talc for moderate temperatures or boron nitride for high temperatures. The temperature is measured with a chromel-alumel thermocouple made of a "thermocoax" cable. The use of such couples seems to be desirable in high pressure experiments because the outer jacket, made of stainless steel, protects the wires and prevents ruptures. In no case was a correction made to take account of the pressure effect on the emf of thermocouples. The pressure and temperature ranges so covered are 15 to 90 kbar and 200 to 1,500 K.

2.3. Experimental Results

Most of the results we obtained [9, 10, 11] concerning the shifts of Curie points as a function of pressure are shown in figures 2 to 9. The corresponding Curie temperatures measured at atmospheric pressure are given in table 1.

TABLE 1. *Curie temperatures measured at ordinary pressure (in K) by the transformer method*

Fe 1044	30Ni–70Fe	334	30Ni–70Co	1209
	36Ni–64Fe	486	45Ni–55Co	1132
	53Ni–47Fe	788	60Ni–40Co	1022
Ni 627	64Ni–36Fe	863	75Ni–25Co	900
Co 1388	75Ni–25Fe	852	93Ni– 7Co	726
	93Ni– 7Fe	708		

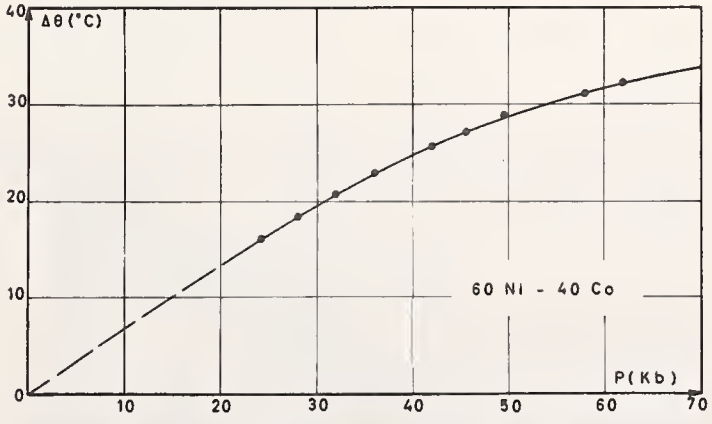

FIGURE 4. *Shift of the Curie temperature of an alloy 60* Ni–40 Co *under pressure.*

The experimental method and the features of the transformations themselves allow accurate determination of the transitions for the following reasons:

(1) It is possible to heat or cool the high pressure cell at any given speed; particularly one can proceed very slowly so that the phenomena associated with the kinetics of the transformations are eliminated. In our case, as Curie points correspond to rapid transitions, a low rate of heating simply permits a better measurement of the temperature of the sample. Therefore the situation is more favorable than when differential thermal analysis is used in a high pressure apparatus where thermal losses are large and so require high rates of heating.

(2) The shape of the sample is such that the temperature gradient present is negligible; no evidence of it was found at 1400 K during the study of cobalt.

(3) The geometry of the sample is also such that its internal pressure gradient is very small; further, since it has been shown [12] that an uniaxial stress has the same effect on Curie points as an isotropic stress of the same intensity, divided by three, the error introduced due to pressure gradient is very small. The pressure gradient shows its effect on the $\mu = f(T)$ curves by the appearance of a "tail"—for instance, in the case of nickel, the transition width is about 1.5 °C at $p = 0$ and about 3 °C above $p = 25$ kbar. It is possible to take account of this phenomenon to define the Curie point. (fig. 10).

(4) The Curie temperature is not very sensitive to nonmagnetic impurities, in contrast to the magnetic permeability or electrical resistivity.

(5) The results for iron, nickel, and cobalt confirm the absence of hysteresis effect at all pressures as predicted by Landau's theory. This is displayed in the curves (fig. 10) obtained on cooling and heating.

(6) In all cases the results were found to be perfectly reproducible.

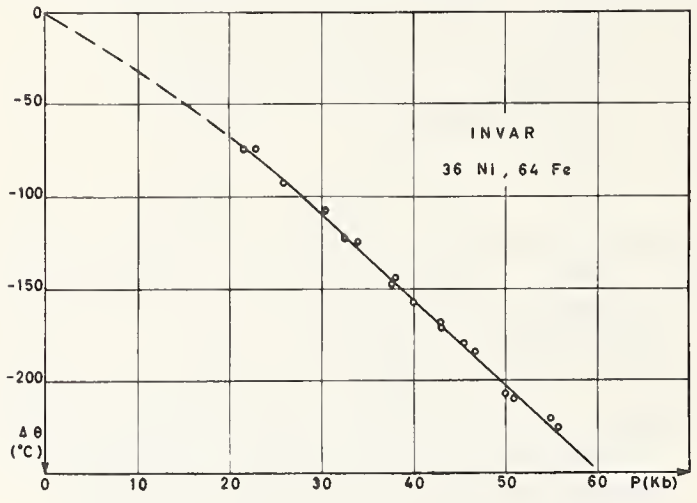

FIGURE 5. *Shift of the Curie temperature of invar under pressure.*

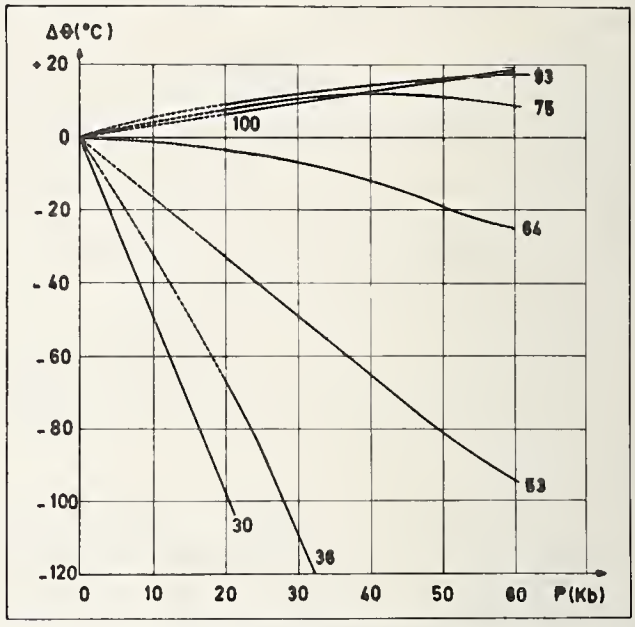

FIGURE 6. *Shifts of the Curie temperature of iron nickel alloys under pressure (the weight composition in nickel is indicated near each curve).*

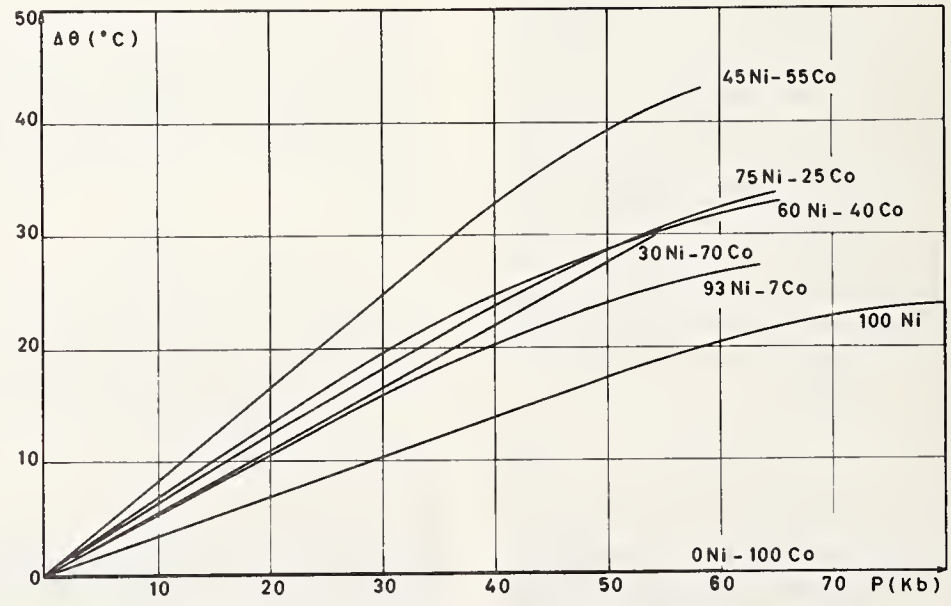

FIGURE 7. *Shifts of the Curie temperatures of nickel-cobalt alloys under pressure.*

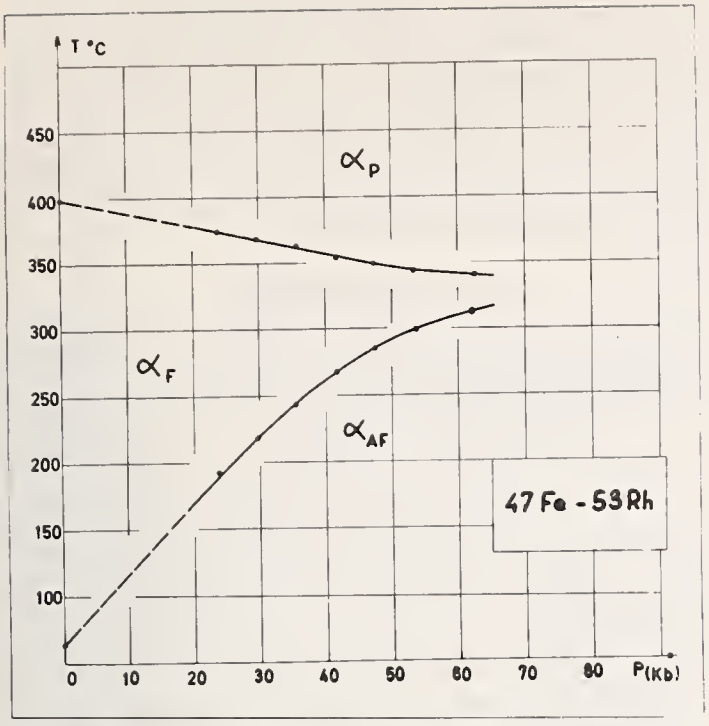

FIGURE 8. *Phase transformations under pressure for an iron rhodium alloy.*

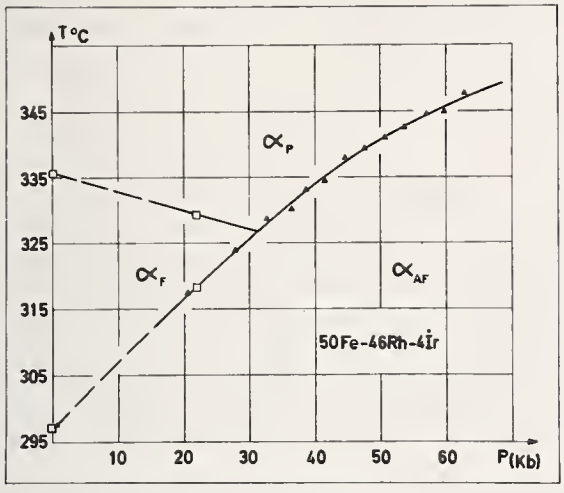

FIGURE 9. *Phase transformations under pressure for a ternary alloy* 50 Fe – 46 Rh – 4 Ir.
(▲ D.T.A.; □ permeability method).

The following remarks regarding the results ought to be mentioned:

– In most cases the shifts of the Curie temperature are small. Their use as pressure gauges would therefore require a very careful control of the temperature. Per contra by a suitable choice of the metal or alloy (table 1), it should be possible to pressure calibrate a device at any given quasi-constant temperature; this would be an advantage in certain cases.

– The sharpest transitions are observed for pure metals. Unfortunately for iron and cobalt the shifts of the Curie points are practically zero. In any case the $\alpha - \gamma$ transition in iron would preclude its use above 15 kbar. On the other hand, nickel would be useable. For this metal dT_c/dp is constant up to 60 kbar and equal to +0,35°/kbar.

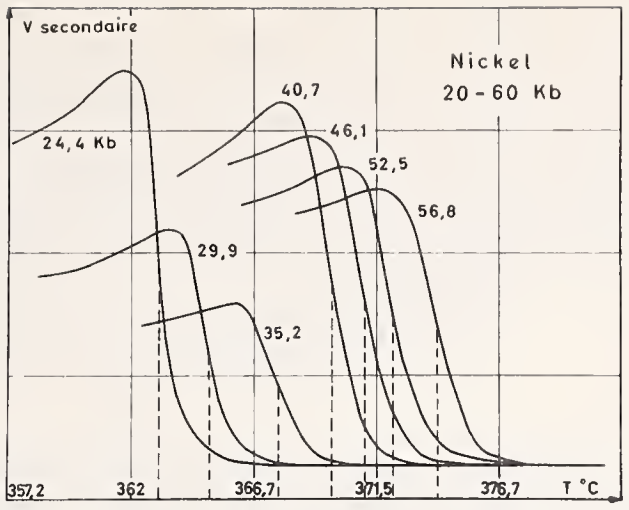

FIGURE 10. *Changes in permeability for nickel under various pressures in the vicinity of Curie point.*

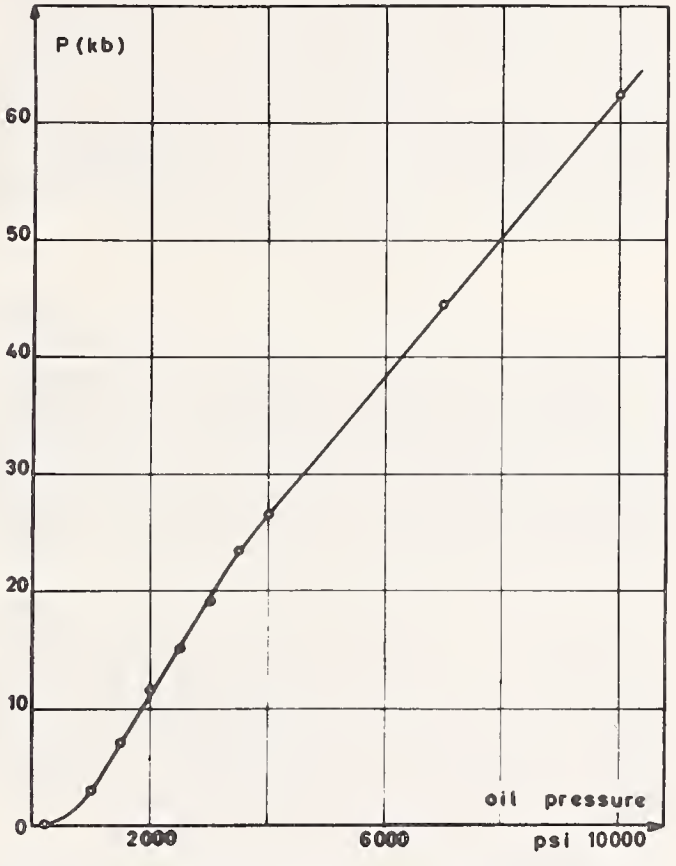

FIGURE 11. *Calibration curve of a belt type apparatus determined from shifts of Curie temperatures.*

– Alloys seem to be less favourable because they generally present a small range of hysteresis; this is particularly noticeable for Ni-Fe alloys and precludes their use. Co-Ni alloys offer greater capabilities, the hysteresis being smaller and the shifts of the Curie points larger.

– The preceding results can be related to those of McWhan [6] on rare earths metals and alloys. The order points behaviour of these materials under pressure is rather complex due to the presence of first-order transitions and sometimes of metastable states. Therefore one cannot think of using them as

pressure gauges no more than the iron-rhodium based alloys we studied and which equally show a first-order transition. (fig. 8–9).

In the course of our work we had the opportunity of using the Curie point of nickel as a pressure gauge to determine the calibration curve of one of our apparatuses in the range 0–25 kbar where there is no convenient standard. The obtained curve (fig. 11) effectively shows a shape characteristic of devices with compressible gaskets.

3. Conclusion

Compared to first order phase transformations the second order ones exhibit two major advantages as possible pressure gauges: they occur without any volume discontinuity and theoretically without hysteresis.

In the particular case of Curie points of ferromagnets the shifts so far measured under pressure are unfortunately small. However it is possible to determine them accurately because they are generally rapid and reproducible. Moreover it is possible, in principle, to fix the Curie temperature of the standard at a given value by proper choice of the alloy composition, which allows calibration in the neighbourhood of a given temperature.

It would be necessary to follow up this research on other ferromagnets for which pressure would possibly bring larger changes in the Curie points. More generally the study of other types of second order transformations, particularly in certain ferroelectrics and antiferromagnets, should be developed under very high pressure and would perhaps lead to the discovery of new pressure gauges.

4. References

[1] Pistorius, C. W. F. T., Rapoport, E., Clark, J. B., Rev. Sci. Inst. **38**, 12, 1741 (1967).
[2] Jeffery, R. N., Barnett, J. D., Vanfleet, H. B., Hall, H. T., J. Appl. Phys. **37**, 8, 3172 (1966).
[3] Belov, K. P., in Magnetic Transitions, Consultants Bureau N.Y. (1961).
[4] Lang, N. D., Ehrenreich, H., J. Appl. Phys. **38**, 1316 (1967).
[5] Patrick, L., Phys. Rev. **93**, 3, 384 (1954).
[6] McWhan, D. B., Stevens, A. L., Phys. Rev. **139**, 3A, A682 (1965).
[7] Samara, G. A., Giardini, A. A., Rev. Sci. Instr. **36**, 1, 108 (1965).
[8] Susse, C., Epain, R., Vodar, B., C.R. Acad. Sci. Paris **258**, 4513 (1964).
[9] Leger, J. M., Susse, C., Vodar, B., Solid State Com. **4**, 503 (1966).
[10] Leger, J. M., Susse, C., Vodar, B., Solid State Com. **5**, 755 (1967).
[11] Leger, J. M., Susse, C., Vodar, B., C.R. Acad. Sci. Paris **265**, C, 17, 892 (1967).
[12] Belov, K. P., Kadomtseva, A. M., Vecm. Mock. Ynib. **2**, 133 (1958).

DISCUSSION

G. A. Samara *(Sandia Laboratory, Albuquerque, New Mexico):* In figure 10, I believe that the "tailing" off of the curves at temperatures above the Curie point is most likely due to the fact that although the long-range order is lost there are still short-range order effects. We have found this "tailing" effect even under hydrostatic pressure.

O. E. Jones *(Sandia Laboratory, Albuquerque, New Mexico):* We have made some shock compression studies on a ferromagnetic 70% iron-30% nickel alloy. The shift of Curie temperature was comparable to that obtained in hydrostatic experiments, showing that here the effect of shear is not particularly important.

D. B. McWhan *(Bell Telephone Laboratories, Murray Hill, New Jersey):* On a curve of initial susceptibility versus temperature, the Curie point is sometimes taken as the inflection point, and sometimes as the intercept of the extrapolation to the background susceptibility. Defined either way, it is not clear that your values of the pressure dependence are free of an uncertainty due to possible changes in the shape of the curves with pressure.

I would also like to note that if the Curie temperature shift is plotted as a function of volume, much of the curvature in the curves for nickel would be eliminated.

AUTHORS' CLOSURE

On the results of our work on nickel, at the beginning we felt that the curves for the shift of the Curie temperature would be found to be linear; but this was not so at the highest pressure range, whatever may be the pressure scale and even if this shift is plotted as a function of the volume. We think that a maximum most probably occurs at a higher pressure; this could be deduced from the curves obtained for alloys, particularly iron-nickel ones where we did observe that maximum for one of the alloys we studied. More work on this matter is needed. Although comparison with data obtained by shock techniques are useful, the experiments should preferably be performed in conditions of pressure not too far from hydrostatic ones.

Fixed Points on the High-Pressure Scale Identified by Phase Transitions in Ammonium Fluoride

R. Kaneda, S. Yamamoto, and K. Nishibata

National Research Laboratory of Metrology, Japan

The I-II and II-III transitions in NH_4F, as fixed points on the high-pressure scale, have been investigated under purely hydrostatic conditions at the temperatures of 0, 25 and 50 °C. By means of manganin resistance gages, the transition pressures at 25 °C have been determined to be 3605 ±10 bar for the I-II and 11531 ±23 bar for the II-III. Their respective dependences on temperature are +2.5 bar/°C and +20.7 bar/°C. The realization of both transition points is easy at and above room temperature, but at low temperatures the II-III transition is very sluggish.

1. Introduction

In almost all high-pressure works, usually manganin resistance and other secondary gages are used for measuring fluid pressures, and for gage-calibrations up to 20 kbar, fixed points identified by liquid-solid phase transitions in Hg and H_2O have commonly been used. However, the accurate realization of these fixed points would not be easy, because the pressures depend strongly on temperature. The realization of triple points in H_2O is also complex and much use of them may be doubtful. This requires a new fixed point.

In view of insensitivity to temperature and easiness in detection of transitions, it may be argued that solid-solid phase transitions in NH_4F, which occur twice at pertinent pressure intervals with associated large volume changes, offer convenient fixed points.

Of the phase transitions in NH_4F, the first study was done by Stevenson [1][1] who discovered a high-pressure modification NH_4F II at about 3.8 kbar. Later, Swenson and Tedeschi [2] reported the second high-pressure phase NH_4F III formed at 11.5 kbar at room temperature. Recently, Kuriakose and Whalley [3] investigated the phase diagram to 340 °C and 20 kbar, and found a new phase NH_4F IV at temperatures over 160 °C. All these investigations were made with simple piston-cylinder equipments, in which NH_4F samples were assumed to act as pressure-transmitting media and subjected to stress fields with non-hydrostatic components. Only one previous work carried out under purely hydrostatic conditions was of Morosin and Schirber [4]. Except some suggestion on the crystal structure, their x-ray investigation of NH_4F II gave no information on behavior of the transition.

The purpose of our study is to evaluate the feasibility of the NH_4F I-II and II-III transitions for the fixed points, as well as to give more light upon their behaviors in purely hydrostatic conditions.

[1] Figures in brackets indicate the literature references at the end of this paper.

Paper presented at the Symposium on Accurate Characterization of the High-Pressure Environment, held at the National Bureau of Standards, Gaithersburg, Md., October 14–18, 1968.

2. Experimental Method

The experiments are based on the volume change method, which is the usual method to locate polymorphic transitions under pressure. Briefly, the experiment consists in pressurizing an NH_4F sample hydrostatically to observe the phase transition, as detected by the discontinuity in pressure corresponding to the change in volume of the sample, and in measuring the equilibrium pressure by means of a manganin resistance gage calibrated against a free-piston gage.

2.1. Apparatus

The arrangement of the apparatus excluding its auxilliary parts is shown in figure 1. The pressure-transmitting fluid used was pure white gasoline. The pressure in the system is generated by two intensifiers; one is the priming for compressing gasoline to about 3 kbar, and the other for producing steady pressures up to 20 kbar. For monitoring the

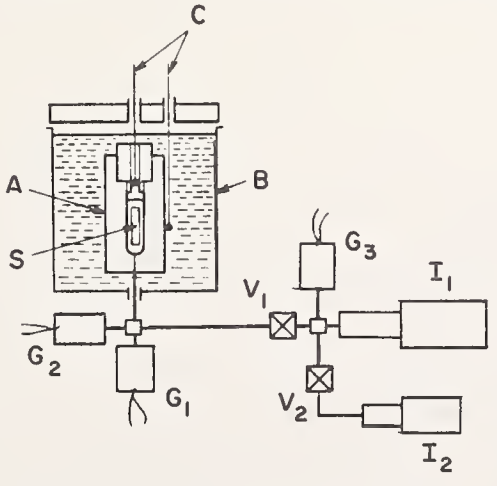

FIGURE 1. *Arrangement of apparatus.*

A: Pressure vessel
B: Bath
C: Thermocouple
I_1: 20kb Intensifier
I_2: 5kb Intensifier
G_1, G_2, G_3: Manganin resistance gages
S: Sample
V_1, V_2: Valves

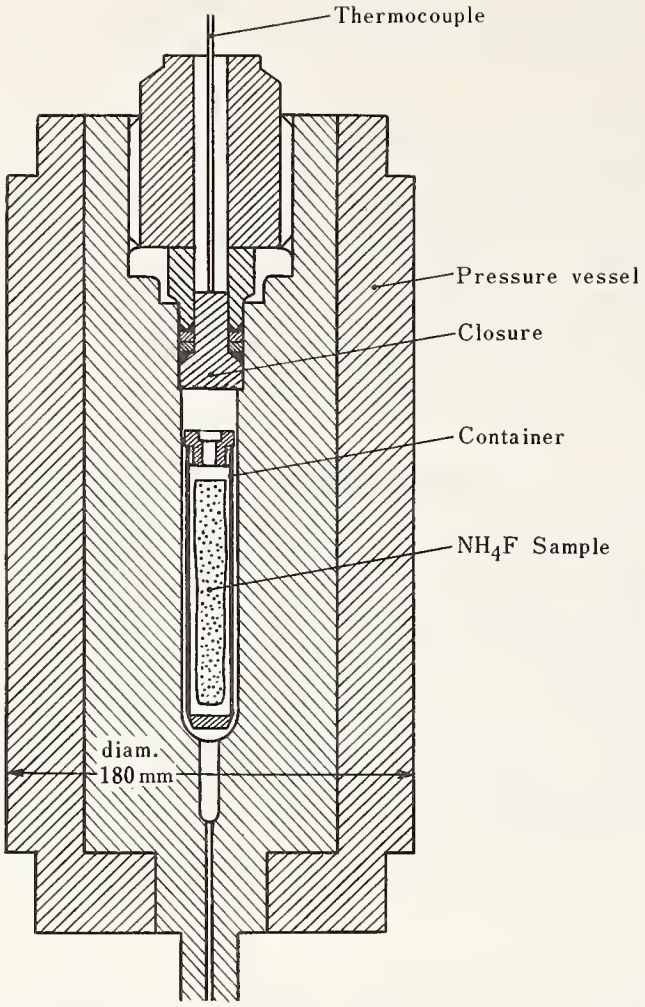

FIGURE 2. *Details of pressure vessel.*

advance of the piston, the 20 kbar intensifier is provided with an electrical displacement transducer connected to a multi-pen recorder. As the lengths of connection lines composed by tubings of 2 mm i.d. are reduced to a minimum, no time effect in pressure transmission is present.

As shown in figure 2, the pressure vessel having a cavity 15 mm diam by 140 mm long is of 18 percent Ni maraging steel, with a pressure port at the lower end, and the upper end a mashroom-type closure, The NH_4F sample of about 5 g was hermetically enclosed, together with white gasoline of nearly a half amount of the sample, in a pliant bag made of a polyethylene sheet of 0.05 mm thick. Care was taken to flush out all air bubbles. The sample was then set in a thin-walled stainless-steel container, which was in turn placed in the pressure vessel. The container, with a threaded cap holed so as to provide free access of the fluid, acts as a sample holder preventing loss of the NH_4F in the event of breakage of the bag. In the experimental runs, the bag was sometimes broken; nevertheless it kept the sample free from the constraints exerted by the walls of the container. Thus, such arrangement as above secured the sample all right, being subjected to purely hydrostatic pressures.

The pressure vessel containing the sample was thermostatically regulated by immersing it completely in a PID-controlled liquid (methyl-alcohol) bath. The bath, having a capacity of 128 liters, provided with heaters, refrigerators, and a motor-driven stirrer, is able to keep the temperature of the pressure vessel constant to ± 0.01 °C at any desired temperature in the range from -30 to 60 °C. Two copper-constantan thermocouples calibrated against a standard platinum resistance thermometer were used; one was for monitoring the bath temperature, and the other for measuring the temperature of the sample. The latter thermocouple was inserted in the pressure vessel so as to attach to the upper side of the mashroom-type closure about 100 mm from the sample. From the subsidiary experiments carried out at atmospheric pressure, the relation between the temperature of the sample and that of the upper side of the closure was obtained. By applying this relation to the actual runs, the temperatures of the sample were determined within the accuracy of ± 0.05 °C.

All significant pressure measurements were made with the manganin resistance gages calibrated against the Laboratory's standard 15 kbar free-piston gage. The apparatus is provided with three manganin resistance gages as shown in figure 1, two of which are connected to the pressure vessel for measuring the pressure on the NH_4F sample at any time, and the remaining one, acting as a reference standard, connected to the high-pressure side of the intensifier.

The gage G_1, for monitoring the pressure, was connected to the preceding recorder, with which the transition was located. For more precise determinations, the gages G_2 and G_3 were used and connected to a Leeds and Northrup G-3 Mueller bridge. There might be undesirable temperature effects in the gage G_2, as it was situated close to the bath. On the other hand, the gage G_3 was, some 2 m apart from the bath, always kept at room temperature, at which all gage-calibrations were carried out, but it could not be used directly for the purpose of determinations, since the complete equilibrium state in the NH_4F was attained with a valve V_1 closed. Therefore, during the experimental run, occasional intercomparisons of these two gages were made, and the equilibrium pressure was determined by the gage G_2. Before every experimental run, the gage G_3, as the reference standard, was usually calibrated with the free-piston gage.

Several manganin coils for the present work were prepared and examined. However, in some coils, the pressure-resistance relationship was not so consistent as had been expected. The inconsistency of p-r relationship was almost entirely due to the lack of reproducibility of resistance in the lower pressure range up to about 3 kbar. In the higher pressure range, the fractional resistance change with the pressure variation was sufficiently consistent. With a few exceptions the reproducibility or uncertainty

of the manganin resistance gages, which scarcely depended on pressure, was found to be ±4 bar.

The free-piston gage is of the controlled-clearance type and has the estimated accuracy of ±0.05 percent of the pressure to be measured. The total errors in the pressure measurements near 4 kbar and 12 kbar may therefore be assumed to be ± 6 bar and ± 10 bar, respectively.

2.2. Observational Procedure

Prior to a final experimental run, with building up pressure, the NH_4F sample was exposed to a few runs through the I-II and II-III transitions. Through these subsidiary runs, the sample resulted in a fine grain size and subsequent transformations became more smooth.

Firstly, the bath was set up at a constant temperature, and the pressure in the system was raised to the extent a little lower than needed to initiate a transition. With keeping this state for awhile (until temperature disturbances due to the compression heat disappeared), the gage G_2 was checked by comparing it with the reference standard G_3. Then the pressure was increased step by step until the transition began as indicated by the drop in pressure due to the loss in volume of the NH_4F; and with the valve V_1 closed, the pressure vessel was isolated from the rest of the system. The sample in the pressure vessel was thus allowed to reach automatically the exact equilibrium state and the equilibrium pressure was determined by the gage G_2. After that, the valve was opened and the pressure, if necessary, was increased further in order to make all amount of the NH_4F transform completely, and the intercomparison of G_2 and G_3 was made again.

The pressure was now decreased for observing the reverse transition. With releasing pressure below the equilibrium pressure and the valve closed, the system was allowed to make its pressure rise automatically to the equilibrium line from below, and the equilibrium pressure reestablished was determined.

In an experimental run, repeated observations of both the I-II and II-III equilibrium pressures attained in this way were usually made several times. For the purpose of locating the I-II and II-III transitions, pressure steps about 100 bar and 200 bar, respectively, were adopted. The magnitudes of these steps were, of course, much smaller as compared with those of the "carry back" pressure ranges of the transitions, which depended on total volume changes of the sample, compressibility of the fluid, etc. The respective "carry back" pressure ranges were roughly 800 bar and 600 bar.

2.3. Sample

The sample used was the special-grade-reagent NH_4F supplied from Wako Pure Chemical Industries, Ltd., Tokyo. To the sample, no special refining treatment was made.

3. Experimental Results

The experiments were performed at 0, 25 and 50 °C. Further, a few experiments were attempted at −25 °C and the I-II transition was surely observed at about 3.47 kbar, but the II-III transition could not be detected in spite of raising pressure on the sample up to 14 kbar.

The experimental data are summarized in table 1, which shows the equilibrium pressures attained from both lower and higher directions. The equilibrium pressure is taken as that pressure at which the rate of change in pressure is reduced to less than 0.1 bar/min. For each experimental run, the pressure value is the mean of 3 to 5 observations, except the II-III at 0 °C, and the dispersion of the observations is represented by the maximum deviation from the mean. The temperature value is the mean of all readings during the run. The dispersion of these readings, not shown in table 1, did not exceed ±0.02 °C.

TABLE 1. *Experimental results*

Run No.	Temp. (°C)	Equilibrium pressure (bar)			
		I → II	II → I	II → III	III → II
1	−0.05	3541 ± 1	3537 ± 1	.....	.....
2	0.03	3540 ± 1	3538 ± 1	11382	10596 ± 112
3	−0.01	3536 ± 1	3535 ± 1	11173 ± 75	10756
4	25.11	3607 ± 1	3603 ± 1	11540	11526
5	25.10	3607 ± 1	3605 ± 1	11540 ± 2	11528 ± 3
6	25.00	3604 ± 1	3602 ± 1	11533 ± 3	11525 ± 2
7	50.25	3662 ± 1	3661 ± 1	12014 ± 2	12007 ± 3
8	49.92	3668 ± 1	3666 ± 1	12015 ± 2	12011 ± 3

In the experimental run, the dispersion of observed values for the I-II did not exceed ±1 bar, and that for the II-III, except at 0 °C, was in the limits of ±3 bar. There was no recognizable dependence of the equilibrium pressure on the fraction of the NH_4F sample transformed. However, a slight difference in the pressure value was present between the different runs. The magnitude of the difference, i.e., several bars, corresponded nearly to the uncertainty of the manganin resistance gages. Therefore, it might be supposed that the difference was mainly due to the characteristics of the gages and not due to the nature of the transition. The reproducibility of the I-II transition on all occasions and that of the II-III at room temperature or higher were fairly good. On the other hand, the II-III transition at 0 °C was so sluggish that only one or two observations were made in the run. The dispersion and the difference in the pressure value amounted to 112 bar and 284 bar, respectively. This proved the whimsical character of the II-III transition at low temperatures.

TABLE 2. *Equilibrium and transition pressures*

Temp. (°C)	Equilibrium pressure (bar)		Transition pressure (bar)
	I → II	II → I	I-II
0	3539 ± 9	3537 ± 9	3538 ± 10
25	3606 ± 9	3604 ± 8	3605 ± 10
50	3665 ± 11	3663 ± 9	3664 ± 12
	II → III	III → II	II-III
0	11278 ± 190	10676 ± 203	10977 ± 504
25	11536 ± 17	11525 ± 17	11531 ± 23
50	12013 ± 16	12008 ± 19	12011 ± 22

From the data shown in table 1, the optimum transition pressures at just 0, 25 and 50 °C were deduced. The results are given in table 2. The transition pressure is the mean of the equilibrium pressures. The uncertainty of the transition pressure is evaluated by adding a half width of the "region of indifference" to the maximum limit of estimated uncertainty of the equilibrium pressure. The values of 3605 ± 10 bar and 11531 ± 23 bar are ascribed to the NH_4F I-II and II-III transition pressures at 25 °C, respectively. The widths of the region of indifference or the hystereses of the transitions at 25 °C are the order of 0.1 percent of the respective transition pressures, while the II-III transition at 0 °C has the region as great as some 600 bar, or about 5.5 percent. It is recognized that the region of indifference becomes narrower at higher temperature.

The dependence of transition pressure on temperature, dp/dT, calculated from table 2 is shown in table 3. The dp/dT at 25 °C or the average values of dp/dT in the range from 0 to 50 °C are +2.5 bar/°C for the I-II and +20.7 bar/°C for the II-III. Table 3 shows that both the dependences become smaller at higher temperature.

The other characteristics of the transitions observed are as follows.

At room temperature or higher, both the I-II and II-III transitions run rapidly. Particularly, the transition velocity of the I-II was much greater than had been anticipated; that is, once the transition was initiated, the volume change followed so rapidly the advance of the piston of the intensifier that the gage G_1 connected to the recorder did not show any change in pressure. At the low temperature (0 °C), the II-III transition was intolerably sluggish. Table 4 lists the observed equilibrium times which depend on not only temperature but also the direction of the transition.

Figure 3 presents the typical transition curves obtained from an experimental run at 25 °C. As these unsymmetrical "pressure-time" curves indicate, there is considerable difference in behavior between the directions of the transition. As to the I-II transition, the I → II reaction was inferior to the reverse II → I in such characteristics as the velocity of reaction, the width of the super (sub)-pressing region or the overshoot pressure range, and perhaps the reproducibility of the equilibrium pressure. Oppositely, in the II-III transition, the II → III reaction was far superior to the reverse III → II in such characteristics as mentioned above. The approximate magnitudes of the overshoot pressure ranges at 25 °C were 100 bar for the I → II, 50 bar for the II → I, 200 bar for the II → III and 350 bar for the III → II, respectively.

TABLE 3. *Dependences of transition pressures on temperature*

Temp. range (°C)	dp/dT (bar/°C)	
	I-II	II-III
0–25	+2.7	+22.2
25–50	+2.4	+19.2
Average	+2.5	+20.7

TABLE 4. *Equilibrium times*

Temp. (°C)	Equilibrium time (min)			
	I → II	II → I	II → III	III → II
0	25	15	60 ~	200 ~
25	15	10	25	90
50	10	5	15	50

TABLE 5. *Volume and entropy changes at transitions*

Transition	$\Delta V/V_0$ (%)	ΔS(cal $K^{-1} \cdot mol^{-1}$)
I-II	−24.0	−0.53
II-III	−9.5	−1.78

Although the present work was not designed for precise determinations of volume changes ΔV, the total piston displacements observed on the recorder allowed rough determinations of ΔV at the transitions. The results are shown in table 5. In conjunction with dp/dT, ΔV allow to calculate entropy changes $\Delta S (= \Delta V \cdot dp/dT)$, which are also shown in table 5. The initial volume of the NH_4F sample was measured by a Beckman air comparison pycnometer.

4. Discussion and Conclusions

The determinations of the transition pressures of NH_4F have been carried out under purely hydrostatic conditions, and the values of 3605 ± 10 bar for the I-II and 11531 ± 23 bar for the II-III have been obtained at 25 °C. Our values are not incon-

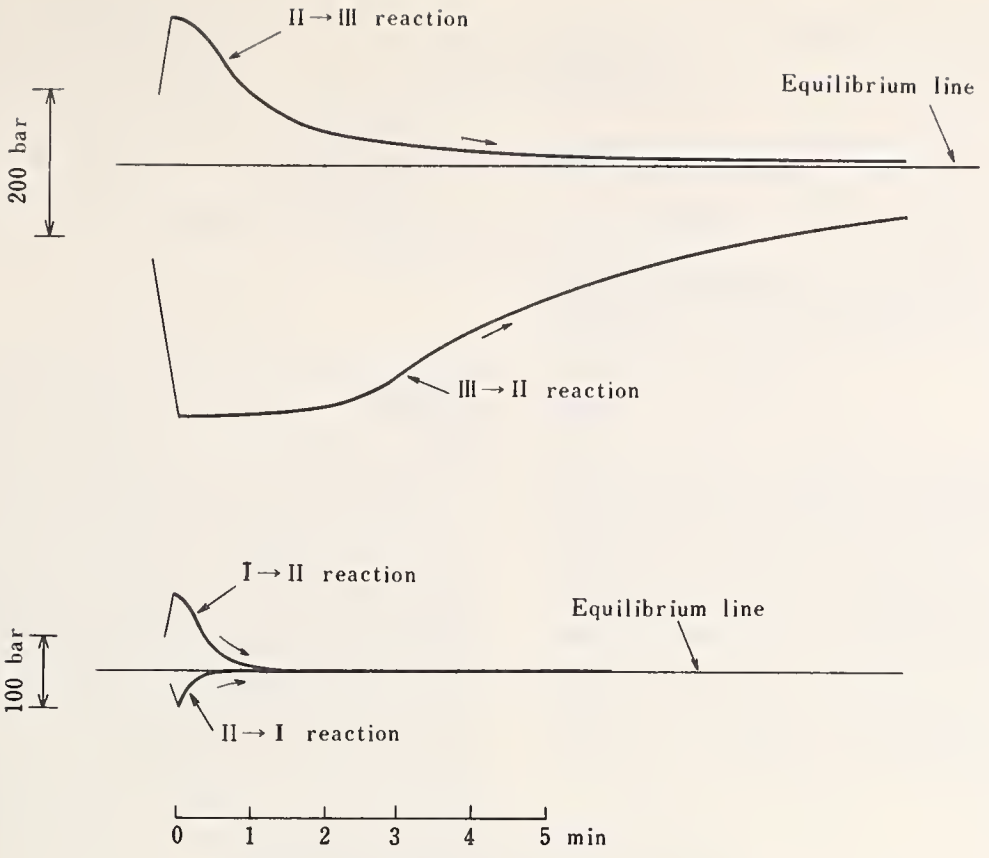

FIGURE 3. *Pressure-time curves at transitions.*

sistent with previous workers', though seldom agreeing in detail. For the I-II transition, Stevenson's value is 3.8 ± 0.3 kbar and that of Swenson and Tedeschi is 3.8 ± 0.2 kbar, both at room temperature. Kuriakose and Whalley have reported the value of 3648 bar at 22.5 °C. Their value, extrapolated to 25 °C, is 3653 bar. Morosin and Schirber's value of 3.63 ± 0.02 kbar, which was obtained at 23 ± 1 °C under purely hydrostatic conditions, is fairly close to our value. For the II-III transition, the value at 21.5 °C is 11.61 ± 0.09 kbar according to Kuriakose and Whalley. Their value, extrapolated to 25 °C, is 11.67 ± 0.09 kbar. Swenson and Tedeschi's value of 11.5 kbar at room temperature is almost identical to our value, though the uncertainty involved in their value is unknown.

The other data for the transitions, i.e., dp/dT, ΔV and ΔS, given in this paper are fairly close to those of Kuriakose and Whalley [3], except the sign of $d/dT(dp/dT)$. The sign of $d/dT(dp/dT)$ for the II-III transition is positive according to them, while that of ours is negative. This conflict may be caused by the great uncertainty involved in our value of the II-III transition pressure at 0 °C.

A principal virtue of the present experiments lies in observing the true behaviors of the NH_4F transitions, which was secured by the satisfactory arrangement of the sample having been subjected to purely hydrostatic pressure, complete freedom from pressure leak and precise monitoring of pressure and temperature. Through the experiments, it has been confirmed that both the I-II and II-III transitions have the following characteristic natures which mostly satisfy the necessary conditions for the fixed points.

(a) The transition pressures have fairly good reproducibilities, i.e., about ± 0.1 percent, and the widths of the region of indifference are narrow, i.e., about 0.1 percent of the respective transition pressures.

(b) The dependences of the transition pressures on temperature are very small, i.e., the respective dp/dT are the orders of 1/80 and 1/10 of that of the freezing point of Hg.

(c) The transitions run rapidly. The approximate equilibrium times are 10 min and 30 min, respectively.

(d) The transitions are easily detected by the volume change method. The relative ΔV are roughly 24 percent and 9.5 percent, respectively.

However, the II-III transition is very sluggish and whimsical at low temperatures, so that the transition points should be realized at and above room temperature. To improve the accuracy of realization of the transition points, it is desirable to select the direction of transitions; the II → I and II → III reactions are more satisfactory.

Thus, it may be concluded that the solid-solid phase transitions in NH_4F offer most convenient fixed points. Moreover, they may be conductive to realize an idea for a "self-calibrated" pressure gage or a working device accompanied with fixed points.

As additional remarks, it was recognized that the lack of reproducibility of manganin resistance

gages, which put some restrictions on the accuracy of the present work, was mainly due to insufficient consistency of pressure-resistance relationship in the low pressure range. This means that the manganin resistance gage, even if it is used only in the higher pressure region, should be checked once with a fixed point in the lower pressure region like the NH_4F I-II transition point.

It is expected that further determinations by the direct use of the free-piston gage will be carried out.

5. References

[1] Stevenson, R., J. Chem. Phys. **34**, 346 (1961).
[2] Swenson, C. A., and Tedeschi, J. R., J. Chem. Phys. **40**, 1141 (1964).
[3] Kuriakose, A. K., and Whalley, E., J. Chem. Phys. **48**, 2025 (1968).
[4] Morosin, B., and Schirber, J. E., J. Chem. Phys. **42**, 1389 (1965).

DISCUSSION

F. R. Boyd, Jr. (*Geophysical Laboratory, Carnegie Institution of Washington, Washington, D.C.*): I am impressed by the large volume changes of these two transitions, the total change in going from phase I to phase III being something like 35 percent. I know of no other substance that shows that high a change. It might be a useful substance in the supporting stage of a two-stage device, in which alkali halides have frequently been used to give a big volume change in order to get a long stroke.

D. B. McWhan (*Bell Telephone Laboratories, Murray Hill, New Jersey*): I think that Pauling showed some time ago that ammonium fluoride can form a solid solution with ice. It is one of few such materials, and for this reason there could be a problem due to the water content.

AUTHORS' CLOSURE

The authors quite agree with Dr. Boyd's point of view, but as yet they have made no attempt at using ammonium fluoride as a supporting material for a two-stage device.

In reply to Dr. McWhan's comments, there is probably some difference in water content among samples, as this substance is extremely hygroscopic. The authors wish to point out that subsequent to the presentation of the paper, additional experiments were carried out for a different sample of ammonium fluoride (1st-grade-reagent from Kanto Chemical Co., Inc.) which had been stored without a dessicator for a few years. Of this sample, the transition pressures obtained at 25 °C were 3606 bar and 11533 bar for the I-II and II-III, respectively. These values compare with those of the sample given in the paper and the close agreement might be an indication that the water does not greatly affect the transition pressures. However, further work under more examined conditions would be necessary in order to solve the problem due to the water content.

A Review of Resistance-Jump Phase Changes Useful for High-Pressure Calibration

F. P. Bundy

General Electric Research and Development Center
Schenectady, New York 12301

1. Introduction

Because of the limited strength of the best construction materials, apparatus capable of developing more than about 30 or 40 kbar has to be more complicated than a simple piston sliding into a simple cylinder. The necessary gasketing and side-support arrangements always absorb a sizable fraction of the force applied to the pistonlike part, or parts, of an ultra-high-pressure apparatus, making it impossible to determine exactly how much of the applied force is directed against the material enclosed in the high-pressure chamber. Thus a direct force/area determination of the pressure in the chamber is not available. In such apparatus it is much more convenient to establish the chamber pressure in respect to the applied force by inserting in the material enclosed in the chamber small wires or ribbons of substances which have, at known pressures, abrupt phase changes manifested by electrical resistance jumps. By observing three or four such resistance-jump phenomena spread over the force range of the apparatus, the chamber pressure can be calibrated. It is therefore important to have available a number of substances which exhibit such sharp and reversible phase changes at reasonable intervals up the pressure scale. It is also very desirable that the true absolute value of the pressures of these transitions be known in order that the experimental data can be used for absolute thermodynamic calculations, and so that workers using this type of calibration in different laboratories in the world can meaningfully compare their results.

The purpose of this article is to list the most commonly used calibrating materials and to summarize the pertinent information about them. A discussion will be given of the absolute accuracy to which the various transition pressures are known, and the precautions that must be used in applying this method of pressure calibration to different kinds of cell geometries in various apparatuses.

2. Phase Transformations Useful for Calibration

Some of the phase transformations which have been used most widely are listed in table 1. In the table, $\Delta R/R_1$ is the ratio of the change of the resistance to the resistance at the low pressure.

Paper presented at the Symposium on Accurate Characterization of the High-Pressure Environment, held at the National Bureau of Standards, Gaithersburg, Md., October 14–18, 1968.

The room-temperature resistance behavior versus pressure of most of these substances is shown graphically in figure 1. Of all the transitions, the Bi ones are probably the most sharp and reversible. The Bi (I-II) transition is remarkably large and abrupt. Of the group, the (α, ϵ) transitions in Fe and the Fe-Co alloys are probably the most sluggish. In apparatuses which are capable of only barely reaching the Fe transition pressure, the transition is difficult to observe.

The transitions in the Fe-Co alloys were first observed as volume discontinuities in shock com-

TABLE 1. (refs. 16, 1, 20)

Substance	Transition	Pressure	$\Delta R/R_1$
		kbar	
Bi	"low" (I-II)	25.4	−0.8
Tl	(II-III)	37	−0.3
Cs	(II-III-IV)	42	Sharp cusp formed by rapid increase followed by abrupt drop
Ba	"low" (I-II)	58	+0.2
Bi	"high" (III-V)	83	−0.5
Sn	(I-II)	100	+0.05
Fe	($\alpha-\epsilon$)	130	+1.0
Ba	"high" (II-Liq?)	~ 140	+0.3
Pb	(I-II)	~ 160	+0.15
Rb	(II-Liq?)	~ 190	+1.5
Fe15Co	($\alpha-\epsilon$)	~ 240	>+0.1
Fe20Co	($\alpha-\epsilon$)	~ 290	>+0.1

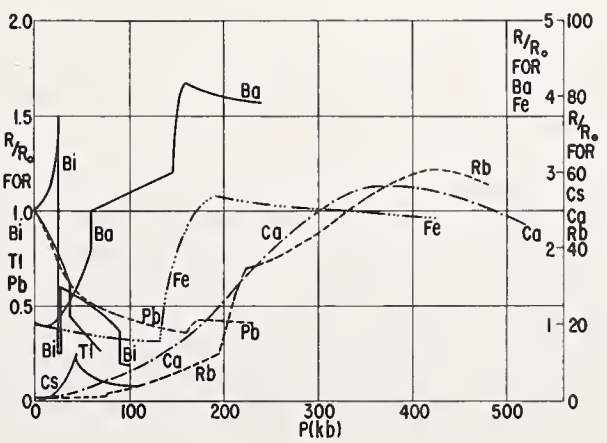

FIGURE 1. R/R₀ *versus* P, *at 25 °C, for a number of calibrating substances.*

385-762 O - 71 - 18

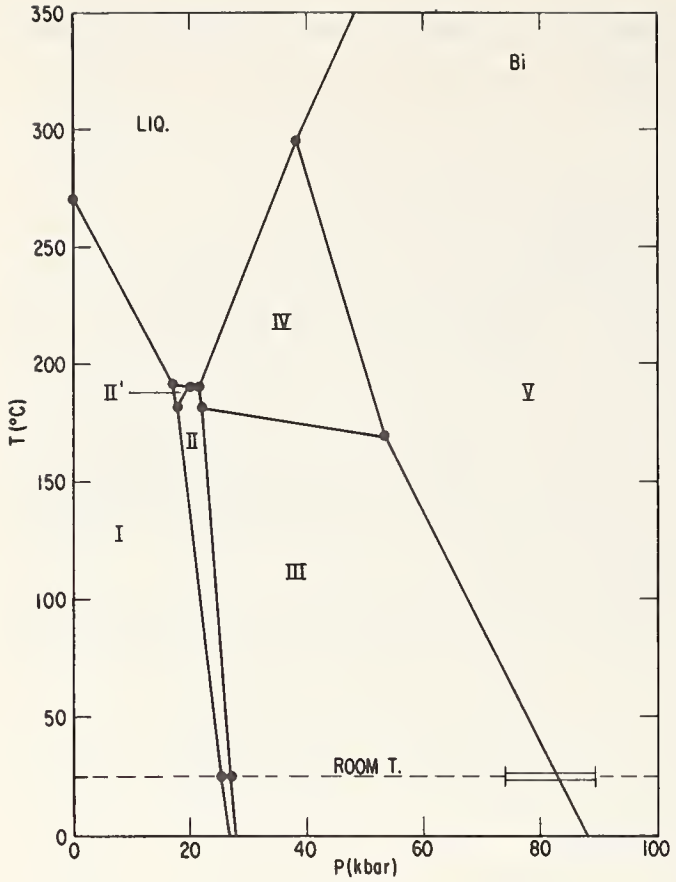

FIGURE 2. P,T *phase diagram for* Bi.

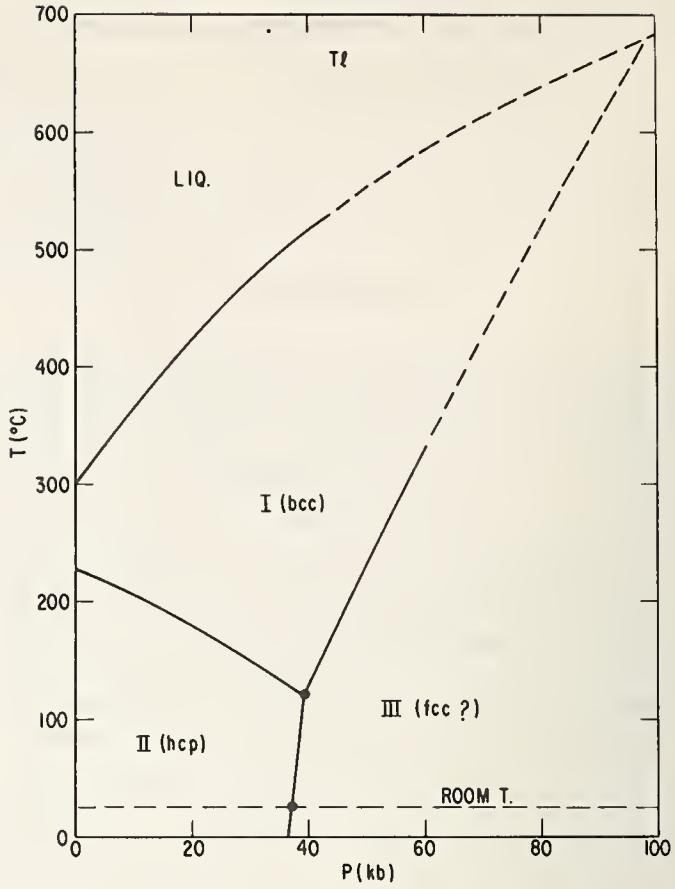

FIGURE 3. P,T *phase diagram for* Tl.

pression experiments by Loree et al. [42].[1] They appeared to be the (α-ϵ) transition, as in pure Fe, and the pressure of transition increased smoothly upward as the Co content of the alloys increased. Bundy [20] then tested the behavior of these alloys in static pressure apparatus to determine whether the transitions were accompanied by changes in resistance. Resistance jumps were found, as in Fe, at pressures which also increased smoothly with Co content. In the tests pure Fe showed the usual ΔR transition, starting at 130 kbar. However, with the alloys, the pressures at which the ΔR transitions occurred increased with the Co content much more rapidly than for the ΔV transitions as reported in the shock-compression tests. For example, at 20 percent Co content the ΔV shock-pressure transition was reported at 185 kbar, while in the ΔR tests in the static pressure apparatus the transition came at 290 kbar. It is improbable that the ΔV and ΔR events are different. It is also improbable that a shock-pressure-induced transition would initiate at a lower pressure than under static pressure conditions. This discrepancy could be examined effectively by x-ray diffraction experiments similar to those of Mao et al. [43].

The pressures at which some of the listed transitions occur are quite temperature-dependent. For this reason it seems appropriate in this article to present what is known about the P,T phase diagrams of these substances.

[1] Figures in brackets indicate the literature references at the end of this paper.

The P,T phase diagram of Bi is presented in figure 2. The data used in constructing this diagram were collected and evaluated from references [12, 14, 25, 26, 28, 33, 40, 44, 48, 50]. The points of greatest interest for calibration work are the I-II, II-III, and III-V transitions at 25 °C, room temperature. It is important to note that the pressures of all these transitions decrease as the temperature increases. The III-V transition is especially sensitive, −0.2 kbar/°C. Furthermore, although this is a sharp, reversible transition, there is still lack of agreement on its pressure among those who have tried to establish its absolute value by using approximations to free-piston gages [48], or by monitoring its electrical resistance simultaneously with x-ray diffraction of surrounding well-behaved crystalline materials, like NaCl [33]. The observed "absolute" values range from 89 kbar down to 74 kbar; 82–83 kbar is a good probable value to use until more definitive absolute pressure methods become available.

The P,T phase diagram for Tl, taken primarily from [32], is shown in figure 3. The II-III transition, which is manifested by a sharp drop in resistance, is seen to be relatively insensitive to pressure. The triple point for I-II-III occurs at the relatively low temperature of 120 °C. In the triple-point region, phase II has the highest resistivity and phase III the lowest.

Cesium has a very interesting P,T phase diagram, as shown in figure 4 [27, 32(a), 37, 49]. According to [37], the melting point of Cs I reaches a maximum

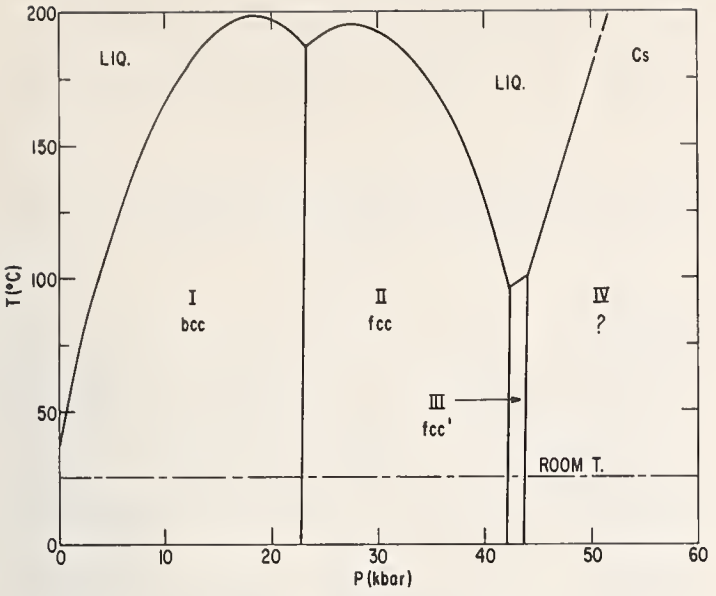

FIGURE 4. P,T *phase diagram for* Cs.

of 199 °C at 18 kbar, then decreases to 187 °C at the triple point with Cs II at 23.5 kbar. Again the melting point of the Cs II increases with pressure to a maximum at about 27 kbar, 195 °C, then decreases to another triple point at 42.5 kbar, 98 °C. As reported first by Hall et al. [27], and later by Jayaraman et al. [32(a)], a third phase exists over a pressure band only about 0.5 to 1.0 kbar wide. At pressures above this a fourth, solid phase becomes the stable one. The melting temperature of this fourth phase increases with pressure in the more normal way. Phase I is known to be bcc, while phases II and III are fcc [27]. The crystal structure of phase IV has not been established yet from the complicated x-ray diffraction pattern. In [27] it is shown that at the 42.2 kbar, 25 °C transition the resistance versus pressure curve is more than a cusp (as it is shown in fig. 1, herein). Instead, at 42.2 kbar the resistance jumps up to a relatively high level, remains constant until 42.7 kbar is reached, whereupon it drops abruptly and then continues to decrease with pressure while in the fourth phase. In an ordinary pressure apparatus, with only moderate pressure resolution, this double phase transition is usually blurred into a single resistance cusp centered at about 42.5 kbar. The data given in [32(a)] indicate that the pressures of the II-III-IV transition complex are nearly independent of the temperature, as is also the case for the I-II transition.

A P,T phase diagram for Ba is given in figure 5, based on data from references [1, 12, 23(a), 50, 30 and 47]. Ba I exhibits the unusual phenomenon of having a maximum in its melting line (at about 15 kbar, 770 °C) [30]. The two room-temperature transitions at about 58 and 140 kbar are quite well known. On the basis of the R versus P behavior of Ba at low temperatures and very high pressures, Stager and Drickamer [47] suggested that the 140 kbar transition is a melting phenomenon. Later, on the basis of x-ray diffraction, Drickamer [23(a)]

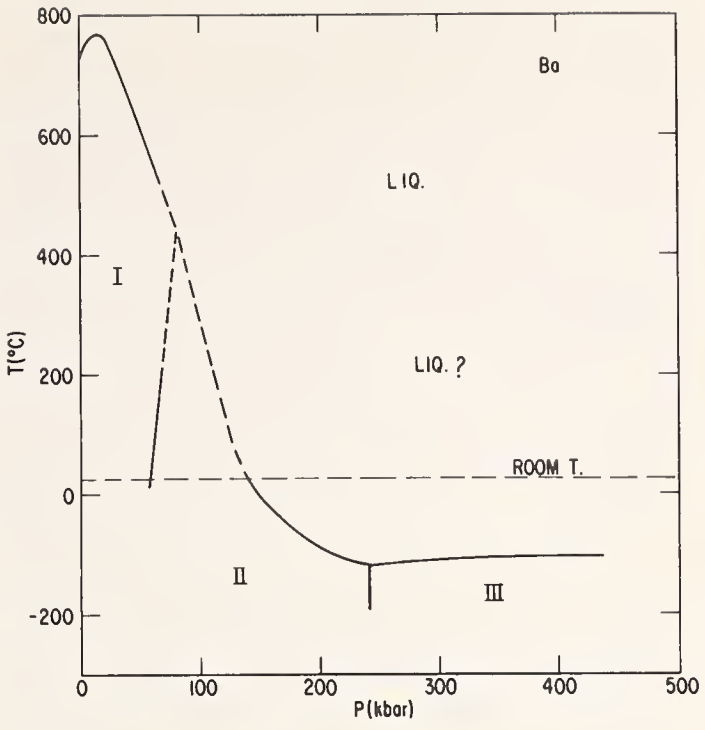

FIGURE 5. P,T *phase diagram for* Ba.

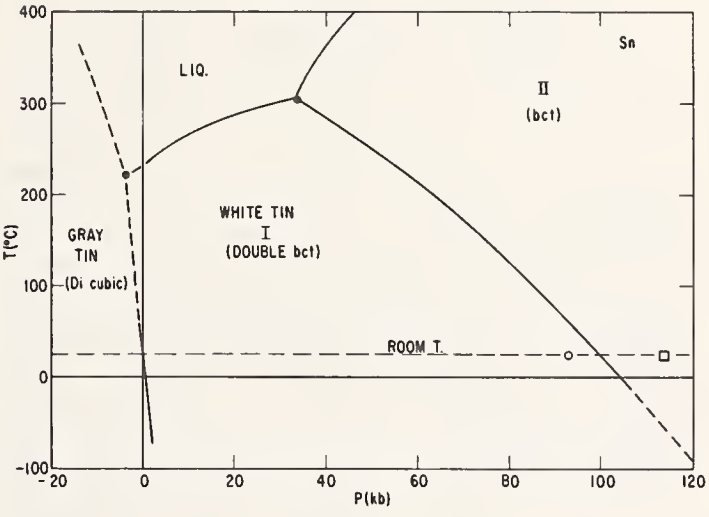

FIGURE 6. P,T *phase diagram for* Sn.

reported that the high-pressure phase at room temperature is definitely crystalline, probably fcc, so it certainly cannot be liquid. There is a real opportunity here to explore experimentally the P,T diagram above 80 kbar at temperatures well above room value.

The true pressure values for the commonly used Ba (I-II) transition range from 53 kbar ([33], based upon Decker's equation of state for NaCl), to 58.5 kbar ([50], free-piston gage). The true value of the "high" Ba transition at around 140 kbar is still not firmly established. In Drickamer-type apparatus, or high compression belt apparatus, it is definitely higher than the Fe (α-ϵ) transition, and distinctly lower than the Pb transition at about 160 kbar.

The P,T diagram for Sn is relatively simple, (fig. 6). The pressure values shown for the (I-II) transition at 25 °C range from about 114 kbar [46],

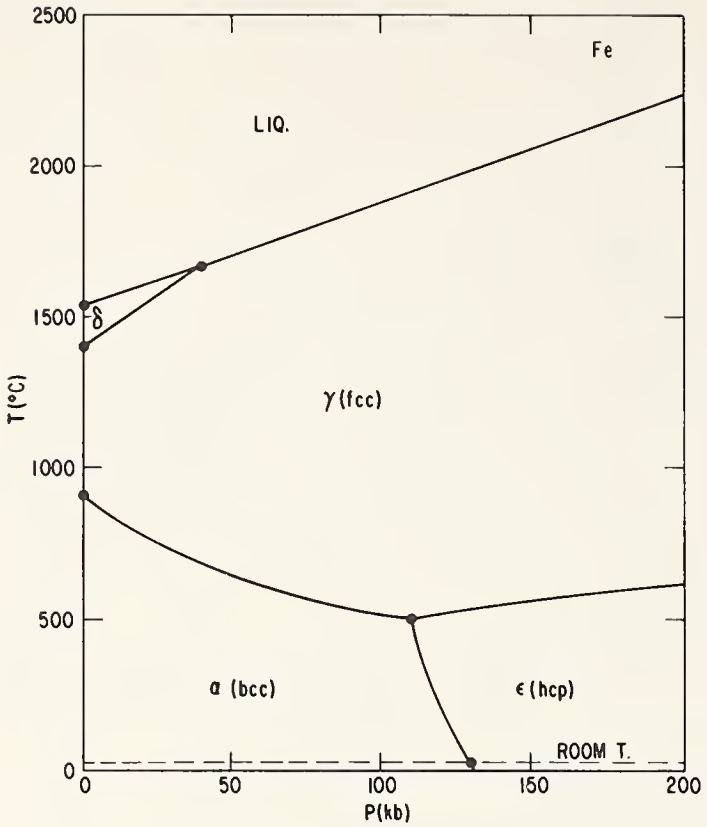

FIGURE 7. P,T *phase diagram for* Fe.

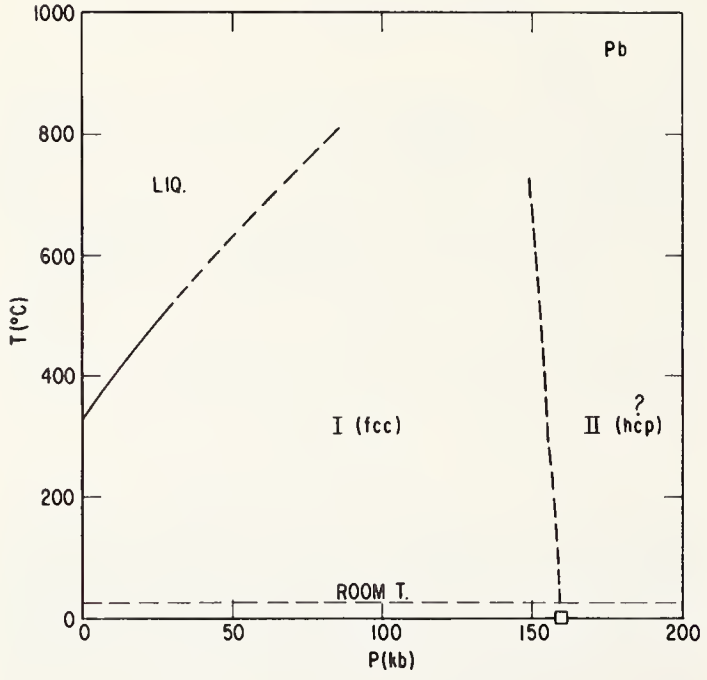

FIGURE 8. P,T *phase diagram for* Pb.

to about 92 kbar ([4], referred to Decker's equation of state for NaCl). A good probable value is about 100 kbar, in order to be in fair agreement with Bi 83 and Fe 130. At low (and negative) pressure and low temperature is the region of stability of "gray tin," which has diamond cubic structure. The transition from "white" to "gray" tin occurs only at quite low temperatures and is quite sluggish.

Data on the *P,T* phase diagram for Fe (fig. 7) have been obtained by a number of workers. Refer-

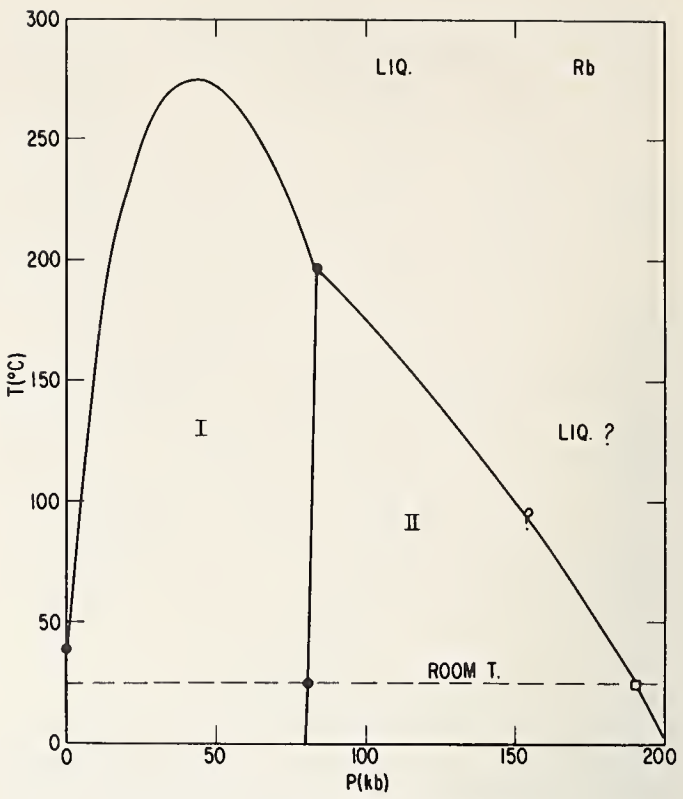

FIGURE 9. P,T *phase diagram for* Rb.

ences [2, 21, 34, 38, 35, 19, 43] cover the reports which relate most directly to this diagram. At room temperature there is only the α to ϵ transition, which is accompanied by doubling of the resistance. Increase in temperature decreases the pressure at which this transition runs. The α, ϵ, γ triple point has been established with fair accuracy at 110 kbar, 500 °C [34, 38, 35, 19]. The α, γ transition involves about a 30 percent increase of resistance as well as a marked change in thermoelectric power. H. M. Strong has used this α, γ transition to calibrate cells for pressure in the 50 kbar range at temperatures around 600 °C by monitoring the Fe/Pt thermocouple emf against that of Pt/PtRh. This type of pressure calibration at higher temperatures will be discussed by Strong in another paper in this Symposium.

The phase diagram for Pb is quite simple as far as it is known (fig. 8). The melting temperature has been explored to at least 30 kbars. Over this range the melting temperature rises smoothly about 200 °C. At room temperature there is a sharp transition at about 160 kbar [1], which gives a sharp rise of over 15 percent in resistance. While it has not been proved by direct x-ray diffraction, it is highly probable that the high-pressure phase of Pb is hcp [41]. The boundary line between the fcc and hcp phases would be expected to have a large dT/dP slope [41] and consequently the pressure of this calibration transition is probably not very temperature-sensitive.

Rubidium has a *P,T* phase diagram (fig. 9) that is somewhat similar to those of Cs and Ba in that it has a maximum in the melting point and the possibility of a number of phases at very high pressures,

room temperature. The 80 and 190 kbar transitions at 25 °C are well-established phenomena [15, 1], although the true values of the pressures may be subject to revision, as is the case for the "high" Bi and "high" Ba transitions.

3. Determination of Absolute Pressures of the Transitions

In 1942 [9], and later in 1948 [11], Bridgman reported his measurements on the volume compressibilities of a large number of substances in a two-stage piston-and-cylinder apparatus, up to pressures approaching 100 kbar. The apparatus was made and used in such a manner that its action approximated that of a free piston gage. During his investigations he discovered a number of volume discontinuities which corresponded to abrupt phase changes in the test materials. The ones which relate to the subject of the present paper were Bi at 24.9 kbar, Tl at 39 kbar, Cs at 44 kbar, Ba at 59 kbar, and Bi at 89 kbar. In 1952 [12] Bridgman reported on the resistance behavior of a large number of materials, as measured in an opposed anvil apparatus, which has an internal pressure distribution which is far from that of a perfect free-piston gage. According to his estimates of the pressures in this apparatus, there was a large abrupt resistance drop in Bi at 24.9 kbar (the same pressure at which the volume discontinuity occurred), but for Tl the resistance discontinuity came at an estimated 44 kbar, Cs at 54 kbar, and Ba at 74 kbar. Bridgman had expected any resistance discontinuities to coincide with volume discontinuities in a given material, but in the cases of Tl, Cs, and Ba he concluded that the differences in "observed" pressures of the ΔV and ΔR events were too great to allow them to be the same event. At the time, however, he knew that the pressures in his piston-and-cylinder apparatus were known to much greater absolute accuracy than in the opposed anvil apparatus. Later, Boyd and England [6], Kennedy and LaMori [36], Hall et al. [27], and others demonstrated that Bridgman's pressure estimates in the opposed anvil apparatus, above about 25 kbar, were progressively too high, and that the ΔV and ΔR events in Tl, Cs, and Ba do indeed occur at the same pressures and are the same physical events. The question now has become one of establishing the actual absolute pressures of the transitions, and of determining the effects of such disturbing factors as local pressure gradients in the specimen and the surrounding solid material, the over-pressures or under-pressures required to start the transformations in the forward and backward directions, and pressure gradients generated by local heating within cells.

There have been a number of significant efforts in this direction. Vereshchagin et al. [50] devised a rotatable free-piston arrangement in the center of a larger piston of a multipiston apparatus. This apparatus was reported to work as a free-piston up to pressures approaching 100 kbar but no details of the techniques were given. With this method they established the following absolute pressures of transition at 25 °C: Bi(I–II), 25.4 kbar; Bi(II–III) 26.9 kbar; Tl(II–III), 36.9 kbar; Ba(I–II), 58.5 kbar; and Bi(III–V), 89.3 kbar. Quite recently Haygarth, Getting, and Kennedy [26], using an improved piston-and-cylinder apparatus, have done extensive measurements on the Ba(I–II) transformation. They have found the value 55.0 ± 0.5 kbar at 22 °C, and a transition pressure coefficient of 0.015 kbar/°C near room temperature. Samples from three different sources, all of purity better than 99.5 percent, gave essentially the same results.

Another approach taken by Decker [23], and developed by Jeffrey et al. [33], has been to work out a semi-empirical theoretical equation of state for the simple, well-behaved, ionic material NaCl, and through this relate pressure and temperature to lattice parameter. Then in a pressure apparatus capable of providing simultaneous x-ray diffraction patterns of the resistance specimen and the adjacent NaCl, determine the pressure at which the transition of the resistance specimen goes. Using an x-ray tetrahedral apparatus Jeffery et al. [33] investigated the Bi, Tl, and Ba transitions. They found some hysteresis between loading and unloading which depended upon the specimen material and its geometrical shape. Relative to the "NaCl pressure scale" of Decker they found Bi(I–II) at 24.8 ± 0.8, Bi(II–III) at 28.0 ± 0.8, Tl(II–III) at 34.6 ± 2.1, Ba(I–II) at 53.3 ± 1.2, and Bi(III–V) at 73.8 ± 1.3 kbar. The Decker equation of state for NaCl agrees closely with the compressibility of NaCl at room temperature as found by Bridgman [7, 10] to 100 kbar. However, Bridgman's measurements of the compressibility of Ba [9], made in the same apparatus under essentially the same conditions as NaCl, yielded the transition pressure at 59 kbar. Thus the 1966 results of Jeffery et al. show either that there was a discrepancy between Bridgman's values for NaCl versus Ba, or that there are some very localized pressure differences in the specimen region of the x-ray-resistance cell. The fact remains that among all the most sophisticated methods of establishing absolute pressures of the transitions the scatter of values obtained is about 5 percent at 50 kbar and around 10 percent at 100 kbar. As pointed out in 1967 by Bassett et al. [5], when the most recent value of the initial compressibility of NaCl (by Slagle and McKinstry [45] is inserted in Decker's equation it yields slightly higher pressure; not enough, however, to match the free-piston values of Vereshchagin et al. or of Haygarth et al. Figure 10 is a P,T phase diagram of NaCl based upon the most recent data.

At pressures higher than those that are attainable by any kind of free-piston apparatus, absolute pressure calibration becomes dependent upon compari-

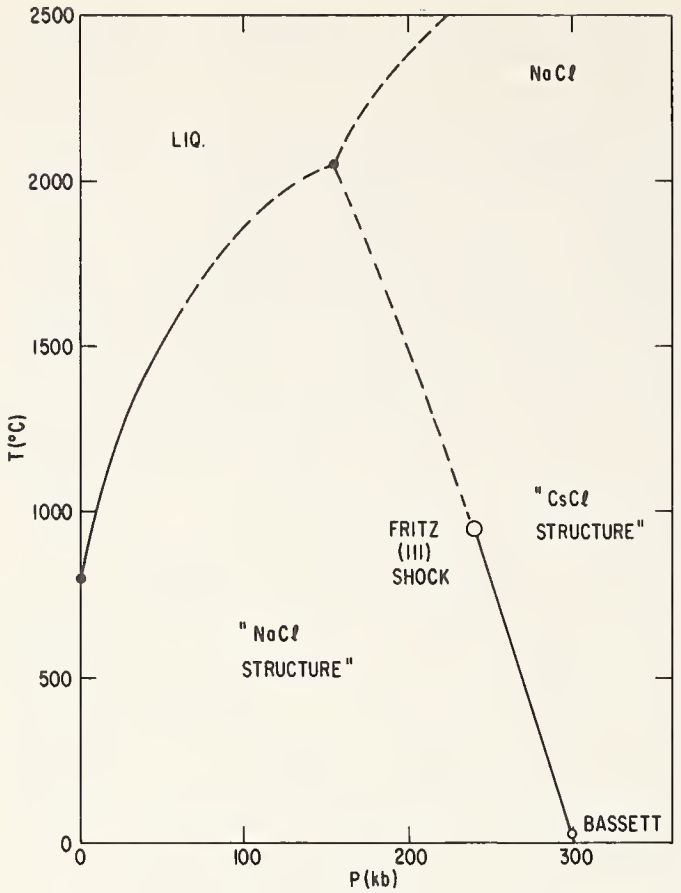

FIGURE 10. P,T *phase diagram for* NaCl.

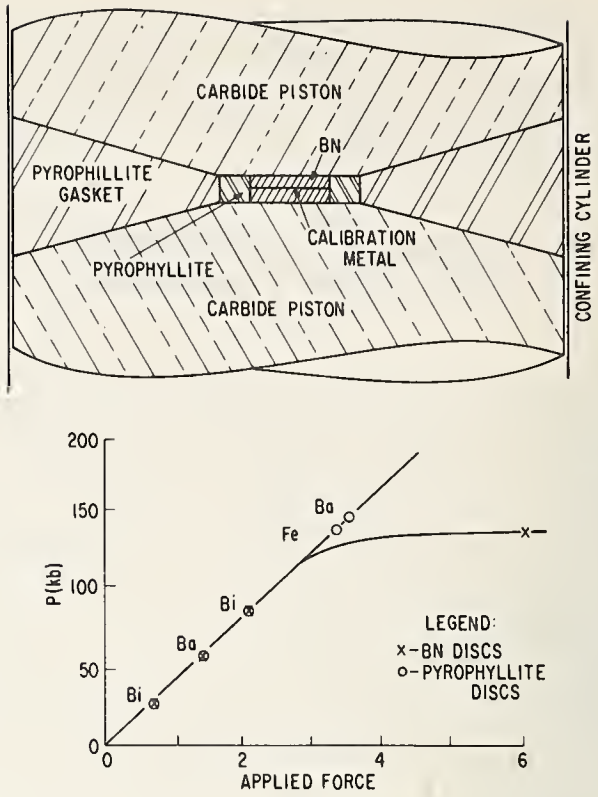

FIGURE 11. *Cell pressure anomally in Drickamer apparatus due to phase collapse of* BN *disks.*

son with shock compression data. In shock compression the shock wave velocity and the particle velocity are measured. By application of conservation of momentum and of mass through the shock front, one calculates the pressure and density attained. One also can calculate to some degree of accuracy the temperature reached during the abiabatic compression of the material. From these P, V, T conditions one can correct back to the P, V values for room temperature. The lattice spacings obtained from x-ray diffraction patterns of specimens observed under pressure in a static apparatus can then be compared to the shock-compression data to calibrate the pressure. There are varied opinions about the accuracy attainable in each step of this measurement sequence. The situation is complicated even more in those compressions in which a phase change occurs, because of the complexity of the wave velocities and additional temperature rise due to volume collapse.

4. Some Causes of Discrepancies and Anomalies

After one has had a number of years of experience with ultra-high-pressure equipment of different types, he becomes aware of various kinds of discrepancies and anomalies that can occur in pressure calibration. It may be helpful to discuss a few examples.

If the cell which goes into the high-pressure vessel incorporates a material which may undergo a volume-reducing phase change, the cell-pressure versus applied-force curve for the apparatus may take disappointing turns toward cell-pressures less than anticipated. A good example of this, in the author's experience, was with a Drickamer-type apparatus which had the usual pyrophyllite flared gasket, but which contained BN disks in the center of the cell. The BN was being used for its refractory characteristics (see fig. 11a). When the BN disks were used, the cell-pressure calibration showed a linear pressure increase with applied force up through the high Bi transition; but the (α-ϵ) Fe transition could be initiated only by loading the apparatus to near its breaking point (see fig. 11b). By contrast, when pyrophyllite disks were used, the Fe transition occurred at a loading corresponding to a linear cell-pressure increase with applied force. With pyrophyllite disks the high Ba and the Pb transitions came "on schedule" on the same straight line, while with BN disks these transitions could not be produced at all. It was found that this anomalous behavior was caused by the transformation, at room temperature, of the graphitic type BN to the much more dense wurtzite and zincblende forms [17].

A similar effect is obtained in a high-compression belt apparatus, or a Drickamer-type apparatus, when thin, hard, steel shims are used on the piston faces to increase the compression ratio of the sample zone relative to the gasket zone. In this case, the rate of rise of cell pressure with applied force decreases in the 130 kbar region as the steel in the shims transforms to the ϵ phase.

Frequently, high-pressure cells incorporate materials which are refractory and chemically inert in order to satisfactorily contain specimens under high-temperature conditions. Materials like MgO, Al_2O_3, ThO_2, etc., are frequently used. These materials also have very high compressional strength and may shield the contained specimen from the pressure generated in the more plastic parts of the surrounding cell. In such cases resistance-jump transitions may be long and drawn out with respect to the applied force, indicating large and variable pressure gradients. Later, when the core of a cell of this type is heated relative to the refractory walls, the local pressure in the specimen may rise higher than that ambient in the outer parts of the cell. In such cells a pressure calibration carried out at room temperature should not be assumed to apply to the hot-core operating condition. In a paper which comes later in this Symposium, H. M. Strong will discuss the use of Fe for determining some of the higher P,T points, utilizing the α, γ and α, ϵ transitions at higher temperatures.

At our laboratory we also have found the melting point of Ge to be useful in establishing pressure rises produced by heating the core of a cell at constant applied force to the apparatus [18]. Melting of diamond-cubic Ge causes an abrupt large drop in its resistance. Because the liquid phase is more dense than the solid, the melting point decreases with pressure. The dT/dP slope of the melting line can be calculated with considerable accuracy by inserting in the Clausius-Clapeyron relationship, $dT/dP = \Delta V/\Delta S$, the experimental values of ΔV and ΔS [29]. Assuming this calculated melting line for Ge (which cross-compares quite well with measurements made utilizing the calculated $\alpha - \gamma$ transition in Fe), P,T points in a given apparatus can be established by observing the melting of Ge in the cell and apparatus of interest. The pressure rise with temperature varies considerably with the geometry and materials of the pressure cell, and hence no general formula for the magnitude of the effect can be given a priori. In the author's work with a "high-compression belt" apparatus it was found that the pressure rise caused by heating the specimen at the core of the cell was roughly proportional to the product of the initial (cold) pressure and the temperature rise. For example, a ΔT of 500 °C from an initial pressure of 100 kbar would cause a ΔP of about 16 kbar.

The question of the initiation and the reversibility of phase transformations has been raised by many workers in the field of high pressure, and experimentally studied by some. It is important in the pressure calibration problem because overpressures or under-pressures required to start forward or reverse phase transitions add to the overall "hysteresis" effect. It is well recognized that in most pressure apparatuses there is considerable frictional and mechanical hysteresis inherent in the moving parts of the mechanical system. Also, the fact that most of the resistance-jump calibration situations consist of a solid sensor surrounded by solid cell materials of finite shear and compressional strength, means that pressure shielding of the sensor material is always a factor. Experimentally, it is very difficult to separate these factors of apparatus hysteresis, pressure gradient in the cell material surrounding the sensor, and inherent phase-change hysteresis. In his detailed study of the Bi (I-II) transition as a primary pressure calibration point, and manganin as a secondary gage, Bridgman [8] found that the "band of indifference" of the Bi (I-II-I) transition as determined in a fluid environment, monitored with a manganin gage, was about 0.06 to 0.10 kbar at 30 °C. In Bridgman's measurements, both phases were present simultaneously, so this is essentially a measurement of pressure-shielding effect (or shear strength) within the Bi specimen itself. In 1964, Davidson and Lee [22] reported results on Bi tested in a fluid environment monitored with a manganin pressure gage in which they observed the hysteresis of the Bi (I-II) transformation from completely one phase to completely the other, thus involving the nucleation of the new phase. They found hysteresis of 0.55 to 0.90 kbar. Once started, the transition proceeded isobarically to completion. In this case the observed hysteresis must be the overpressure required for nucleation of the new phase. Jeffery et al. [33], in connection with their x-ray diffraction experiments of Bi specimens in NaCl enclosures, discuss this nucleation hysteresis phenomenon quite fully, as well as the effect of pressure gradients in the material surrounding the transition specimen. The hysteresis found by Jeffery et al. in their observations of the Bi (I-II) transition ranged from 2.8 to 5.3 kbar, depending upon the geometry of the Bi-NaCl arrangement. The excess hysteresis, over that found by Davidson and Lee, is probably a result of the pressure gradients in the NaCl environment. This illustrates the effect of the geometry and kind of material which surrounds the specimen of interest.

5. References

[1] Balchan, A. S., and Drickamer, H. G., Rev. Sci. Instr. **32**, 308 (1961).
[2] Bancroft, D., Peterson, E. L., and Minshall, S., J. Appl. Phys. **27**, 557 (1956).
[3] Barnett, J. D., Benion, R. B., and Hall, H. T., Science **141**, 1041 (1963).
[4] Barnett, J. D., Bean, V. E., and Hall, H. T., J. Appl Phys. **37**, 875 (1966).
[5] Bassett, W. A., Takahashi, T., Mao, H.-K., and Weaver, J. S., J. Appl. Phys. **39**, 319 (1967).
[6] Boyd, F. R., and England, J. L., J. Geophys. Res. **65**, 741 (1960).
[7] Bridgman, P. W., Proc. Am. Acad. Arts Sci. **74**, 21 (1940).
[8] Bridgman, P. W., Proc. Am. Acad. Arts Sci. **74**, 1 (1940).
[9] Bridgman, P. W., Proc. Am. Acad. Arts Sci. **74**, 425 (1942).
[10] Bridgman, P. W., Proc. Am. Acad. Arts Sci. **76**, 1 (1945).
[11] Bridgman, P. W., Proc. Am. Acad. Arts Sci. **76**, 55 (1948).
[12] Bridgman, P. W., Proc. Am. Acad. Arts Sci. **81**, 165 (1952).
[13] Bridgman, P. W., Proc. Am. Acad. Arts Sci. **84**, 63 (1955).

[14] Bundy, F. P., Phys. Rev. **110**, 314 (1958).
[15] Bundy, F. P., Phys. Rev. **115**, 274 (1959).
[16] Bundy, F. P., Trans. ASME, J. Engg. Indus. **83**, 207 (1961).
[17] Bundy, F. P., and Wentorf, R. H., Jr., J. Chem. Phys. **38**, 1144 (1963).
[18] Bundy, F. P., J. Chem. Phys. **41**, 3809 (1964).
[19] Bundy, F. P., J. Appl. Phys. **36**, 616 (1965).
[20] Bundy, F. P., J. Appl. Phys. **38**, 2446 (1967).
[21] Claussen, W. L., Rev. Sci. Instr. **31**, 878 (1960).
[22] Davidson, T. E., and Lee, A. P., Trans. Met Soc. AIME **230**, 1035 (1964).
[23] Decker, D. L., J. Appl. Phys. **36**, 157 (1965); ibid. **37**, 5012 (1966).
[23(a)] Drickamer, H. G., Solid State Phys. **17**, 103 (1965).
[24] Dudley, J. D., and Hall, H. T., Phys. Rev. **118**, 1211 (1960).
[25] Giardini, A. A., and Samara, G. A., ASME 1964 Symposium on High Pressure Technology, ed. E. C. Lloyd and A. A. Giardini (June 1965).
[26] Haygarth, J. C., Getting, I. C., and Kennedy, G. C., J. Appl. Phys. **38**, 4557 (1967).
[27] Hall, H. T., Merrill, L., and Barnett, J. D., Science **146**, 1297 (1964).
[28] Heydemann, P. L. M., J. Appl. Phys. **38**, 2640 (1967).
[29] Horn, F. H., and Hall, R. N., Gen. Elec. Res. Lab., private communication, 1964; also Bradshaw, S. E., Wembley Laboratories, Wembley, Middlesex, England, private communication, 1964.
[30] Jayaraman, A., Klement, W., Jr., and Kennedy, G. C., Phys. Rev. Letters **10**, 387 (1963).
[31] Jayaraman, A., Klement, W., Jr., and Kennedy, G. C., Phys. Rev. **130**, 540 (1963).
[32] Jayaraman, A., Klement, W., Jr., Newton, R. C., and Kennedy, G. C., J. Phys. Chem. Solids **24**, 7 (1963).
[32(a)] Jayaraman, A., Newton, R. C., and McDonough, J. M., Phys. Rev. **159**, 527 (1967).
[33] Jeffery, R. N., Barnett, J. D., Vanfleet, H. B., and Hall, H. T., J. Appl. Phys. **37**, 3172 (1966).
[34] Johnson, P. C., Stein, B. A., and Davis, R. S., J. Appl. Phys. **33**, 557 (1962).
[35] Kaufman L., Clougherty, E. V., and Weiss, R. J., Acta Met. **11**, 323 (1963).
[36] Kennedy G. C., and LaMori, P. N., Progress in Very High Pressure Research, ed. F. P. Bundy, W. R. Hibbard, Jr., and H. M. Strong (John Wiley & Sons, New York, 1961), p. 304.
[37] Kennedy, G. C., Jayaraman, A., and Newton, R. C., Phys. Rev. **126**, 1363 (1962).
[38] Kennedy, G. C., and Newton, R. C., Solids Under Pressure (McGraw-Hill Book Co. Inc., New York, 1962).
[39] Kennedy, G. C., and Newton, R. C., Solids Under Pressure, (McGraw-Hill Book Co. Inc., New York, 1963) Chapt. 7, p. 172.
[40] Klement, W., Jr., Jayaraman, A., and Kennedy, G. C., Phys. Rev. **131**, 632 (1963).
[41] Klement, W., Jr., J. Chem. Phys. **38**, 298 (1963).
[42] Loree, T. R., Fowler, C. M., Zukas, E. G., and Minshall, F. S., J. Appl. Phys. **37**, 1918 (1966).
[43] Mao, H. K., Bassett, W. A., and Takahashi, T., J. Appl. Phys. **38**, 272 (1967).
[44] Phillips, D., and Jura, G., Trans. Met. Soc. AIME **239**, 120 (1967).
[45] Slagle, O. D., and McKinstry, H. A., J. Appl. Phys. **38**, 437 (1967).
[46] Stager, R. A., Balchan, A. S., and Drickamer, H. G., J. Chem. Phys. **37**, 1154 (1962).
[47] Stager, R. A., and Drickamer, H. G., Phys. Rev. **131**, 2524 (1963).
[48] Stark, W., and Jura, G., ASME 1964 Symposium on High Pressure Technology, ed. E. C. Lloyd and A. A. Giardini (June 1965).
[49] Stishov, S. M., and Makarenko, I. N., J. Theor. Exper. Phys. **54**, 708 (1968).
[50] Vereshchagin, L. F., Zubova, E. V., Buimova, I. P., and Burdina, K. P., Sov. Phys.-Dokl. **11**, 585 (1967).

DISCUSSION

C. Susse (*Laboratoire des Hautes Pressions, Centre National de la Recherche Scientifique, Bellevue, France*): I think we have a partial answer to the problem of the melting curve for barium at 144 kbar. Recent work performed by differential thermal analysis seems to show that the melting curve doesn't go down regularly with pressure. After the first known maximum at about 15 kbar, there is a triple point Ba I – Ba II – liquid at 500 °C – 67 kbar followed by a maximum at 525 °C – 75 kbar and by a cusp at 380 °C – 85 kbar, which is most probably related to a phase transition in the solid. Above this pressure the MP increases with pressure at least up to 95 kbar.* We intend to do some additional work in this area.

G. A. Samara (*Sandia Laboratory, Albuquerque, New Mexico*): Although there seem to be some problems in the use of the lead transition, I think it is one of the sharpest and most reproducible transitions above 100 kbar, and I would urge that lead not yet be given up as a possible reference material.

*Bastide, J. P., Susse, C., Epain, R., C. R. Acad. Sci. Paris **267**, 857 (1968).

A. Taylor (*Westinghouse Research Laboratories, Pittsburgh, Pennsylvania*): Do you find any appreciable difference in the transformation pressure of zone-refined iron as against iron of thermocouple purity?

D. Decker (*Brigham Young University, Provo, Utah*): We have made one measurement only on the iron triple point, which appears to be considerably lower than 110 kbar.

It appears that an extrapolation of the data that Madame Susse gave earlier on barium would show a transition well below 110 kbar, perhaps at 80 kbar, around 550 °C.

J. Haygarth (*Institute of Geophysics and Planetary Physics, University of California, Los Angeles*): I would like to comment on the phase diagram of barium below 100 kbar. Our findings differ somewhat from the results given earlier by Madame Susse.

We have been fairly careful to obtain barium of very low hydrogen content. It is apparent that it is rather difficult to get the hydrogen out. We

had two samples, one which contained one atomic percent hydrogen, and the other which contained four percent hydrogen. On the one containing four percent hydrogen, we obtained a second maximum in the melting curve around 47 or 48 kbar. When we ran the experiment with the sample which originally contained one percent hydrogen, we did not find this maximum.

Now there is a question about the purity of the sample which initially contained one percent hydrogen because, unfortunately, the capsule in which it had been stored was found to have become open to the air, so the hydrogen content was in question. But from this work I think that it is important to make sure that the barium, especially for melting point purposes, is very pure.

I would also like to state that the slope of the barium melting curve after the second maximum seemed to be the same as the slope just before it, agreeing with the diagram Dr. Bundy showed.

AUTHOR'S CLOSURE

Replying to Samara: I have always found the lead transition to be sharp and clean when there is good electrical contact with the sample.

Replying to Dr. Taylor: We haven't made a systematic investigation of it, but we can say that we have had to use the purest iron we could make ourselves, usually "carbonyl iron" that has been remelted in vacuum. This proves to be superior to thermocouple grade iron.

Chairman: R. Roy
The Pennsylvania State University
University Park, Pennsylvania

The Coesite–Stishovite Transition*

Syun-iti Akimoto and Yasuhiko Syono

Institute for Solid State Physics
University of Tokyo, Roppongi, Tokyo, Japan

The coesite-stishovite transition curve has been determined over the temperature range 550 to 1,200 °C in the pressure range 82.0 to 98.0 kbar by means of a tetrahedral-anvil type of high-pressure apparatus. Amorphous anhydrous silica, α-quartz, coesite, and stishovite were used as starting materials. The transition curve was fitted by the linear equation P(kbar) = 69 + 0.024 T(°C) using pressure scale proposed by Jeffery et al. This determination was found to be in a reasonable agreement with the previous data, if the common pressure scale is used. Experimental information for the coesite-stishovite transition was also compared with the stability relation derived from enthalpies and entropies of coesite and shishovite. It was suggested that the pressure scale proposed by Jeffery et al. was underestimated considerably around 100 kbar.

1. Introduction

The rutile-type polymorph of SiO_2 now known as stishovite was first synthesized by Stishov and Popova [1961][1] at high pressures in excess of 100 kbar. Since stishovite is accepted to be a probable major constituent of the earth's lower mantle, there has been much interest in determining the properties and stability of stishovite. Wentorf [1962], Sclar et al. [1962], Ringwood and Seabrook [1962], Bendelyany and Verestshagin [1964] and Minomura et al. [1964] have described the synthesis of stishovite using different types of high-pressure apparatus, but they provide no detailed data on its stability range. The first attempt to determine the coesite-stishovite transition curve was made by Stishov [1963]. He derived the standard entropy of stishovite from the linear relationship between entropy and density empirically found in the rutile-type oxides, and calculated the transition curve passing through the equilibrium point 130 ± 5 kbar, 1600 °C ± 100 °C experimentally determined. Further data on the direct experimental determination of the transition curve in the temperature range 410 to 830 °C were provided by Ostrovsky [1965, 1967]. Ryabinin [1964] also reported a stability diagram of SiO_2 including the coesite-stishovite transition curve, which differs markedly from the estimation by Stishov and Ostrovsky. It is one purpose of the present work to extend the determination of the coesite-stishovite curve to the wider range of temperatures and to provide an improved estimate of its position and slope, using several kinds of starting materials including coesite and stishovite.

Another aim of the present work is to examine the possibility that the coesite-stishovite transition could be used as a pressure calibration point at high temperatures. Most calibrations of high-pressure apparatus utilizing solid pressure-media are carried out on the basis of the phase transitions in Bi, Tl, Ba, Sn, etc., which are known rather precisely at room temperature. This method is not satisfactory for high-temperature work on account of the change in the shear strength of the pressure media with temperature. Boyd et al. [1967] recommended the quartz-coesite transition as a promising calibration point in the pressure range 30 to 40 kbar at high temperatures. Recent development of the capabilities of the high-pressure apparatus requires a higher calibration point at high temperatures. The present information on the coesite-stishovite transition might contribute to pressure calibration around 100 kbar at high temperatures.

Very recently, thermodynamic properties of coesite and stishovite were reported by Holm et al. [1967]. Experimental information for the coesite-stishovite transformation obtained in this work will be compared with the stability relation derived thermodynamically from their data. Some contributions to the establishment of an accurate pressure scale may also be expected through such a comparison.

2. Experimental Procedure

All the high-pressure and high-temperature experiments were made using the tetrahedral-anvil type of high-pressure apparatus described previously

*Reprinted by permission from J. Geophys. Research 74, No. 6 (March 15, 1969).

[1] Figures in brackets indicate the literature references at the end of this paper.

Paper presented at the Symposium on Accurate Characterization of the High-Pressure Environment, held at the National Bureau of Standards, Gaithersburg, Md., October 14–18, 1968.

[Akimoto et al., 1965]. Two different sizes of cemented tungsten carbide anvils containing 5 percent of cobalt were used. For most runs from 83 to 96 kbar the 9-mm-edge anvils were used with a 15-mm-edge tetrahedron of pyrophyllite sample container. A combination of 7-mm-edge anvils and a 13-mm-edge pyrophyllite tetrahedron was also adopted for several auxiliary runs. The pyrophyllite tetrahedron which served as the pressure-media was fired at 700 °C for 30 min before use, and its surface was painted with thick suspension of αFe_2O_3 in ethanol to enhance the surface friction. Pressure values in the tetrahedral press were calibrated at room temperature by measuring sharp resistance change in the flat strip samples of Bi, Ba, and Sn on the pressure-increase cycle. The values of transition pressure, 26 kbar for Bi I-II, 55 kbar for Ba I-II, 76 kbar for Bi III-V, and 92 kbar for Sn I-II were adopted as fixed calibration points following the proposal of Jeffery et al. [1960]. The transition pressure was confirmed to be reproducible within an accuracy of ±3 percent.

A graphite tubing, 4.0 mm long, 2.5 mm in outside diameter, and 1.7 mm in inside diameter, was used for heating the samples in the runs with the 15-mm-edge pyrophyllite tetrahedron. Smaller tubing, 3.0 mm long, 2.2 mm in outside diameter, and 1.4 mm in inside diameter, was used for the runs with the 13-mm-edge tetrahedron. The tubular graphite furnace so prepared was placed diagonally with the axis of the cylinder between opposite edges of the tetrahedron. SiO_2 powder samples were embedded in the center of the graphite furnace. A pair of boron nitride disks was placed on both ends of the sample to reduce the uncertainties resulting from the temperature gradient within the furnace.

Temperatures were measured with Pt/Pt−13%Rh thermocouple, 0.2 mm in diameter, without any correction for the effect of pressure on the emf of the thermocouple. The hot junction was placed in the center of the samples. Thermocouple leads were brought out to the faces of the pair of anvils not used for the graphite furnace contacts. The run temperatures were corrected for the increase of surface temperature of the tungsten carbide anvils.

Determination of the coesite-stishovite transition curve was made by the usual quenching method. Pressure was applied to the sample first, then the temperature was brought to the desired value and held for the desired interval of time. Then the sample was quenched isobarically by turning off the heating power. After quenching, only the central part of the samples, less than 1 mm thick, adjacent to the head of thermocouple, was used for the phase-equilibrium experiments. Identification of phases present was made chiefly by the x-ray diffraction method. In order to establish the transition curve accurately and to examine the reversibility of the reactions, runs with different kinds of starting materials were practised. Amorphous anhydrous silica, α-quartz, coesite, and stishovite were used as the starting materials. Mineralizers, such as H_2O, were not used in the present work.

3. Results

Results of experimental runs on which the location of the transition curve is based are given in table 1 and figure 1. The percentages of the phases present in the run products, shown in the last column of table 1, are roughly estimated from the peak intensity ratio of the x-ray diffraction chart. When α-quartz was used as the starting material, phases other than coesite and stishovite were not observed in the run products at temperatures above 800 °C. However, metastable α-quartz was observed in addition to coesite and stishovite in the run product at 88.5 kbar and at 650 °C. Maximum conversion to stishovite in the present pressure-temperature-time condition was about 80 percent. On the other hand, when amorphous anhydrous silica was used as the starting material, complete conversion to stishovite or coesite was achieved even at temperatures as low as 550 °C. Synthesis of stishovite was also confirmed in the run in which the starting material was coesite. Successful reverse reactions from stishovite to coesite were demonstrated at two different temperatures, and using single-phase stishovite obtained in the present work

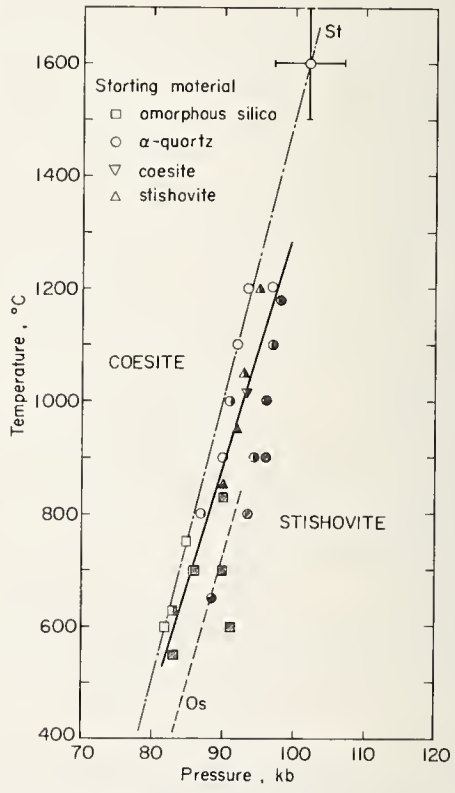

FIGURE 1. *Pressure-temperature stability fields for the coesite-stishovite equilibrium.*

The dashed line designated by O_s represents the transition curve determined by Ostrovsky [1965, 1967]. The chain line designated by St represents the transition curve estimated by Stishov [1963].

TABLE 1. *Results of runs on the coesite-stishovite transition*

Run No.	Temperature	Pressure [a]	Time	Phases present
	Starting Material, Amorphous Anhydrous Silica			
	°C	*kbar*	*min*	
S29	550± 5 [b]	83.0	100	Stishovite
S25	600±10	82.0	65	Coesite
S22	600± 5	91.0	60	Stishovite
S31	630± 5	83.0	40	70% Coesite+30% Stishovite
S27	700± 5	86.0	60	95% Stishovite+5% Coesite
S26	700± 5	90.0	60	Stishovite
S28	750± 5	85.0	45	Coesite
S30	830± 5	90.0	20	Stishovite
	Starting Material, α-Quartz			
S1	650±10	88.5	60	50% α-Quartz+30% Coesite +20% Stishovite
S12	800± 5	87.0	60	95% Coesite+5% Stishovite
S4	800± 5	93.5	60	70% Stishovite+30% Coesite
S6	900± 5	90.0	45	90% Coesite+10% Stishovite
S14	900±10	94.5	45	60% Stishovite+40% Coesite
S11	900± 5	96.0	45	80% Stishovite+20% Coesite
S13	1,000± 5	91.0	30	90% Coesite+10% Stishovite
S2	1,000±10	96.0	30	70% Stishovite+30% Coesite
S10	1,100±5	92.0	30	Coesite
S8	1,100±10	97.0	32	60% Stishovite+40% Coesite
S35	1,180±20	98.0	15	80% Stishovite+20% Coesite
S5	1,200±10	93.5	20	Coesite
S7	1,200±10	97.0	20	Coesite
	Starting Material, Coesite			
S23	1,015±10	93.5	60	60% Stishovite+40% Coesite
	Starting Material, Stishovite			
S20	850± 5	90.0	70	Stishovite
S21	950± 5	92.0	60	Stishovite
S18	1,050±10	93.0	40	50% Coesite+50% Stishovite
S24	1,200±10	95.0	30	60% Coesite+40% Stishovite

[a] Precision of pressure control is ±0.5 kbar.

[b] Precision of temperature control.

as the starting material. Summarizing all the experimental data, the boundary curve for coesite-stishovite transition was fitted by the linear relation $P(\text{kbar}) = 69 + 0.024\ T(°\text{C})$.

The unit cell dimensions of the stishovite obtained at 97.0 kbar and at 1100 °C (S8 run in table 1) were determined to be $a = 4.178 \pm 0.001$ *A* and $c = 2.665 \pm 0.001$ *A*. This determination is in quite a good agreement with those values, $a = 4.1790 \pm 0.0004$ *A*, and $c = 2.6649 \pm 0.0004$ *A*, published by other investigators [Stishov and Popova, 1961; Chao et al., 1962].

4. Discussion

In figure 1 the transition curve obtained in this work is compared with those reported by Stishov [1963] and Ostrovsky [1965]. Since pressure values used by these investigators are based on Bridgman's "volume-scale," in which Bi III-V transition was fixed as 89 kbar, their curves in figure 1 are represented after some corrections to the pressure scale by Jeffery et al. [1966] were made. The transition curve determined in this work is found to be located between Stishov's and Ostrovsky's curve and to have the slope dP/dT which is nearly consistent with Ostrovsky's determination but is slightly larger than Stishov's calculation.

Taking the accuracy of the pressure measurement (±3~5 kbar) in these investigations into consideration, we cannot find any significant difference between the curves determined with different types of high-pressure apparatus, i.e., opposed anvil type and multiple anvil type, if the common pressure scale is used. The slope of the coesite-stishovite transition curve established in this work, about 40~50°/kbar, indicates that the transition is very sensitive to pressure. Any minor errors in temperature measurement will have a small effect on the results. These situations suggest that the coesite-stishovite transition is usable as a pressure-calibration point at high temperatures. Since the pressure value in this work was calibrated at room temperature by the conventional resistance method, absolute value of pressure used at high temperatures remains still uncertain. In case of the quartz-coesite transition, the transition curve determined by Takahashi [1963] by means of the tetrahedral press with the pressure calibration method similar to this work was found to accord well with the value of transition determined carefully by Boyd et al. [1967] with the piston-cylinder type apparatus. Accordingly, if the uncertainty of ±3 kbar was taken for granted, the coesite-stishovite transition curve determined in this work using the tetrahedral press may serve as a pressure-calibration point at high temperatures.

When information is available on the thermodynamic properties of coesite and stishovite, we can estimate quite independently the pressure-temperature stability fields for the coesite-stishovite equilibrium by means of thermodynamical methods developed by Ahrens and Syono [1967]. Very recently, direct determination of the thermodynamic functions of coesite and stishovite over a wide range of temperature was reported by Holm et al. [1967]. Enthalpy changes of transformation at 298 K of quartz to coesite and to stishovite are determined to be 1.21 kcal/mole and 11.79 kcal/mole, respec-

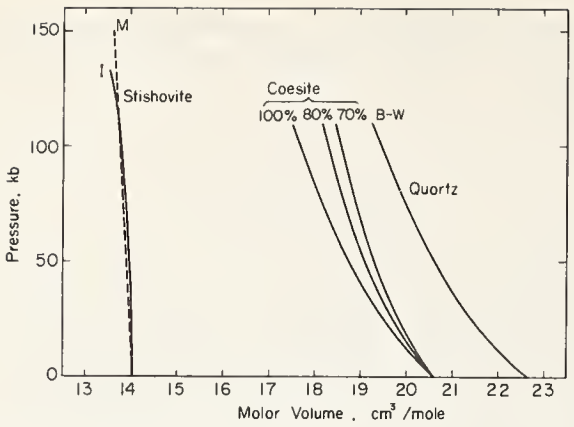

FIGURE 2. *Pressure-volume curves for quartz, coesite, and stishovite used in free energy calculation.*

Ouartz: B–W, after linear compression data by Bridgman [1949] and shock-wave compression data by Wackerle [1962].
Coesite: Numerals attached to the curves means that the compressibility of coesite was assumed to be 100 percent, 80 percent, 70 percent of that of quartz.
Stishovite: I, after Ida et al. [1967]; M, after the estimation by McQueen et al. [1963] using shock wave compression data of SiO_2 at higher pressures than 150 kbar by Wackerle [1962].

tively. Entropy changes at 298 K are also determined to be -0.23 and -3.24 cal/mole K for the transformations of quartz to coesite and to stishovite.

The increase of free energy ΔG^0_{298} at zero pressure and 298 K of a transformation is generally given by

$$\Delta G^0_{298} = \Delta H^0_{298} - 298\Delta S^0_{298} \qquad (1)$$

where ΔH^0_{298} and ΔS^0_{298} are the change in enthalpy and entropy of the transformation at zero pressure and 298 K. The equilibrium pressure P between low-pressure and high-pressure polymorph of a material is determined at 298 K by putting free energy change ΔG^P_{298} given by the following equation zero

$$\Delta G^P_{298} = \int_0^P \Delta V dp + \Delta G^0_{298} \qquad (2)$$

where ΔV is the volume change associated with the transformation. Combining (1) and (2) we can obtain

$$-\int_0^P \Delta V dp = \Delta H^0_{298} - 298\Delta S^0_{298}. \qquad (3)$$

On the basis of the thermodynamic data just mentioned, the values of right-hand side of eq (3) are now known for the transformations from coesite to stishovite as 11.48 kcal/mole. In order to obtain the equilibrium pressure at 298 K, the value of the left-hand side of eq (3) was numerically integrated. In this calculation we adopted the shock wave compression data of quartz by Wackerle [1962], which was smoothly connected with the static compressibility data by Bridgman [1949]. Recent linear compression data of α-quartz reported by McWhan [1967] are in a reasonable agreement with the present compression curve, at least for low-pressure region. The pressure-volume relation for stishovite

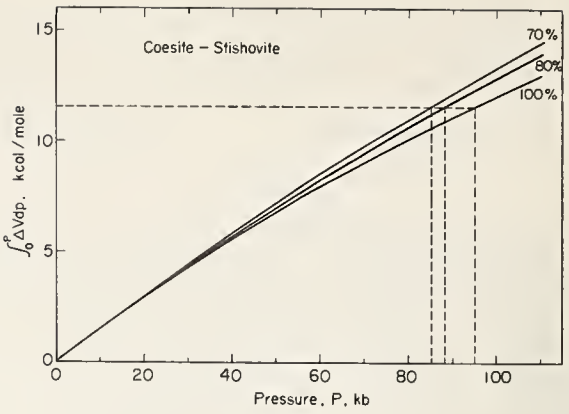

FIGURE 3. *The values of* $-\int_0^P \Delta Vdp$ *versus pressure for the coesite-stishovite transition.*

determined by Ida et al. [1967] by means of high-pressure x-ray analysis based on the compression data of NaCl [Perez-Albuerne and Drickamer, 1965] was also used. Since no compressibility data for coesite are available, we estimated the bulk modulus of coesite to be 70 percent of that of quartz, based on the logarithmic linear relationship between bulk modulus and volume per ion pair reported by Anderson and Nafe [1965]. We also tentatively calculated for comparison the compression curves of coesite, assuming the compressibility of coesite to be 80 percent and 100 percent of that of quartz. In figure 2, volume versus pressure data of three SiO_2 polymorphs used for the free-energy calculation were graphically shown.[2]

In figure 3 the values of $-\int_0^P \Delta Vdp$ for transformation of coesite to stishovite were plotted versus pressure. The equilibrium pressures between coesite and stishovite are 85, 88, 95 kbar, corresponding to the assumption of 70 percent, 80 percent, 100 percent compressibility of quartz as that of coesite. Since errors in the enthalpy measurements are reported as 0.15 and 0.3 kcal/mole for the quartz-coesite and quartz-stishovite transformation, the uncertainties of the calculated equilibrium pressure between coesite and stishovite were estimated to be ± 4 kbar.

The calculated equilibrium pressure at 298 K between coesite and stishovite, 85 ± 4 kbar (assumption of 70 percent), is remarkably higher than the experimentally determined value of 70 kbar based on the NaCl pressure scale by Jeffery et al. [1966]. The value is almost comparable to the equilibrium pressure at 298 K around 82 kbar obtained by adopting Bridgman's volume-scale for the pressure values of the present phase equilibrium experiments, but is considerably smaller than the predicted value, 97.5 kbar, by Stishov [1963].

[2] Similar calculations were carried out by Holm et al. [1967], in which the compressibility of coesite was assumed to be 80 percent of that of quartz. Furthermore, the pressure-volume relation of quartz given by them shows quite a large offset at higher pressures than 90 kbar from Wackerle's compression data. For these reasons we have done more detailed calculation.

On the other hand, the value of dP/dT can be calculated by means of Clausius-Clapeyron equation $dP/dT = \Delta S/\Delta V$, and is estimated to be 0.019 kbar/K at 298 K using the observed entropy change by Holm et al. [1967]. The slope determined experimentally at higher temperatures is 0.024 kbar/K on the basis of the pressure scale by Jeffery et al. [1966], and 0.036 kbar/K on the basis of Bridgman's volume-scale. When the effects of pressure and temperature on the slope are ignored, the former value is almost comparable to that of the calculated one, but the latter is too much higher than the calculated one.

Although there exist some ambiguities on the pressure-volume data of coesite and on temperature measurement at high pressures, it may be safely concluded from the above results that the pressure scale proposed by Jeffery et al. [1966] is too low, while Bridgman's volume-scale is too high to give consistent explanation on the stability field of coesite-stishovite equilibrium derived from thermodynamic data. In the present argument the effect of the correction for the thermocouple emf at high pressures on the phase boundary curve was completely ignored. Since the correction has generally been accepted to be positive, the value of dP/dT will be decreased, while the equilibrium pressure at 298 K will be increased after these corrections are made. Such procedure will reduce the inconsistency between independent conclusions which were derived from comparing two thermodynamic properties, enthalpy and entropy change during phase transformation, with the experimentally determined equilibrium pressure and value of dP/dT, respectively.

5. References

Ahrens, T. J., and Syono, Y., Calculated mineral reactions in the earth's mantle, J. Geophys. Res. **72,** 4181–4188 (1967).

Akimoto, S., Fujisawa, H., and Katsura, T., The olivine-spinel transition in Fe_2SiO_4 and Ni_2SiO_4, J. Geophys. Res. **70,** 1969–1977 (1965).

Anderson, O. L., and Nafe, J. E., The bulk modulus–volume relationship for oxide compounds and related geophysical problems, J. Geophys. Res. **70,** 3951–3963 (1965).

Bendelyany, N., and Verestshagin, L., The synthesis of dense modifications of silica at presence of water under pressure 150×10^3 kg/cm², Dokl. Akad. Sci. USSR **158,** No. 4, 819 (1964) (In Russian). Soviet Physics Doklady **9,** No. 10, 870–871 (1965) (English transl.).

Boyd, F. R., Bell, P. M., England, J. L., and Gilbert, M. C., Pressure measurement in single-stage apparatus, Carnegie Inst. Wash. Year Book **65,** 410–414 (1967).

Bridgman, P. W., Linear compression to 30,000 kg/cm², including relatively incompressible substances, Proc. Am. Acad. Arts Sci. **77,** 187–234 (1949).

Chao, E. C. T., Fahey, J. J., and Littler, J., Stishovite, SiO_2, a very high pressure new mineral from meteor crater, Arizona, J. Geophys. Res. **67,** 419–421 (1962).

Holm, J. L., Kleppa, O. J., and Westrum, E. F., Jr., Thermodynamic properties of polymorphic transformations in silica. Thermal properties from 5 to 1070 K and pressure-temperature stability fields for coesite and stishovite, Geochim. Cosmochim. Acta **31,** 2289–2307 (1967).

Ida, Y., Syono, Y., and Akimoto, S., Effect of pressure on the lattice parameters of stishovite, Earth Planet. Sci. Letters **3,** 216–218 (1967).

Jeffery, R. N., Barnett, J. D., Vanfleet, H. B., and Hall, H. T., Pressure calibration to 100 kbar based on the compression of NaCl J. Appl. Phys. **37,** 3172–3180 (1966).

McQueen, R. G., Fritz, J. N., and Marsh, S. P., On the equation of state of stishovite, J. Geophys. Res. **68,** 2319–2322 (1963).

McWhan, D. B., Linear compression of α-quartz to 150 kbar J. Appl. Phys. **38,** 347–352 (1967).

Minomura, S., Ito, K., and Okai, B., Pressure and temperature measurements in Drickamer's resistance cell up to 161 kbar and 4000 °C, ASME Publication 64–WA/PT–6 (1964).

Ostrovsky, I. A., Experimental fixation of the position coesite-stishovite equilibrium curve, Izv. Akad. Sci. USSR (ser. geol.) No. 10, 132–135 (1965) (In Russian).

Ostrovsky, I. A., On some sources of errors in phase-equilibria investigations at ultra-high pressure: Phase diagram of silica, Geol. J. **5,** Pt. 2, 321–328 (1967).

Perez-Albuerne, E. A., and Drickamer, H. G., Effect of pressures on the compressibilities of seven crystals having the NaCl or CsCl structures, J. Chem. Phys. **43,** 1381–1387 (1965).

Ringwood, A. E., and Seabrook, M., Some high-pressure transformations in pyroxenes, Nature **196,** 883–884 (1962).

Ryabinin, Y. N., The influence of pressure on some properties of the substance, Tectonophys. **1,** 227–232 (1964).

Sclar, C. B., Young, A. P., Carrison, L. C., and Schwartz, C. M., Synthesis and optical crystallography of stishovite, a very high pressure polymorph of SiO_2, J. Geophys. Res. **67,** 4049–4054 (1962).

Stishov, S. M., On the equilibrium line between coesite and rutile like modification of silica, Dokl. Akad. Sci. USSR **148,** No. 5, 1186–1188 (1963) (In Russian).

Stishov, S. M., and Popova, S. V., A new modification of silica, Geokhimiya, No. 10, 837–839 (1961) (In Russian); Geochemistry, No. 10, 923–926 (1961) (English transl.).

Takahashi, T., Discussion in High Pressure Measurement, edited by A. A. Giardini and E. C. Lloyd, pp. 240–244, Butterworths, Washington (1963).

Wackerle, J., Shock-wave compression of quartz, J. Appl. Phys. **33,** 922–937 (1962).

Wentorf, R. H., Stishovite synthesis, J. Geophys. Res. **67,** 3648 (1962).

DISCUSSION

W. A. Bassett (*University of Rochester, Rochester, New York*): I have made some measurements on the compression, both of coesite and stishovite on the tetrahedral x-ray press at Brigham Young University, and my coesite data when plotted on the diagram (fig. 2) would be roughly 60 percent of that shown for quartz. This would tend to bring the phase transition pressure even lower, and closer to Dr. Akimoto's experimental pressure.

I also measured stishovite and found it to be somewhat more compressible than indicated by the curve of figure 2. The value that I got for the bulk modulus would be approximately three megabars. In this work, I did not see the peculiar expansion along the *C*-axis which Dr. Akimoto reported in an earlier paper. The *C*-axis seems to contract very slightly up to a hundred kilobars, but along a straight line.

F. R. Boyd, Jr. (*Geophysical Laboratory, Carnegie Institution of Washington, Washington, D.C.*): Can you tell us how fast the reaction goes, that is, how long it will run?

J. D. Barnett (*Brigham Young University, Provo, Utah*): I understand that you determined pressures from a room-temperature calibration, with no correction made due to increased temperature in the cell.

I suggest that at a cell temperature of 500 °C to 600 °C the pressure will increase at least five or six kilobars, perhaps even 10 kilobars at the higher pressures. This has been our experience in x-ray studies.

As a second point, the value you used for the tin transition as reported in our paper by Jeffery et al. was not intended as a transition calibration point at all. There is strong indication that this is somewhere around 100 kbar rather than 92 kbar.

Thirdly, you used calibration points based on Decker's NaCl theory before a recent correction of the initial compressibility of NaCl in the theory. This will increase the pressure by approximately 2 percent.

I think when you take these three things into consideration the agreement with other measurements is really not bad at all.

AUTHORS' CLOSURE

In reply to Dr. Bassett: I don't know why there is some discrepancy in the compression curves of stishovite determined by Drickamer-type high pressure x-ray apparatus and tetrahedral-anvil type high-pressure apparatus. But if we use the revised data by Dr. Bassett for stishovite and coesite, the discrepancy between the experimentally determined transition curve of coesite-stishovite and the thermodynamically determined curve will be reduced.

The reaction time is about 20 to 30 minutes at high temperatures above 1000 °C.

The Use of Solid-Solid Transitions at High Temperatures for High-Pressure Calibration

Phillip N. La Mori

Battelle Memorial Institute, Columbus Laboratories, 505 King Avenue, Columbus, Ohio 43201

Transition pressures have been determined for bismuth $1 \rightarrow 2$ and bismuth $2 \rightarrow 3$ to the melting point (183 °C). The transitions parameters of thallium $2 \rightarrow 1$, $1 \rightarrow 3$ and $2 \rightarrow 3$ have been measured to 40 kbar and 220 °C. The thallium $1 \rightarrow 2 \rightarrow 3$ triple point has been determined as 114 ± 1 °C and 37.4 ± 0.4 kbar. The use of the determined transition parameters as high-pressure, high-temperature fixed points is discussed.

1. Introduction

The purpose of this paper is to make some initial attempts to provide pressure calibration points above room temperature. This higher temperature calibration is of extreme interest because most high-pressure experiments also are made with concomitant high temperature. At the present time (almost) all high-pressure calibrations in solid media devices are made at room temperature. Possible changes in the pressure calibration with temperature are generally ignored. In the few cases where it has been considered, the conclusions have not been testable against experimental data.

The status of high-pressure calibrations has been dealt with extensively in another paper, Decker et al. [1],[1] and will not be reviewed here. Additionally, the reader should remember that the comments in this paper are directed toward solid media devices, even though they are not necessarily restricted to them.

Fixed points for pressure calibration are accurate enough below 40 kbar to allow accurate determination of thermodynamic quantities. The calibration in the 40 to 60 kbar range is less certain but probably accurate enough, when combined with the lower pressure points, to again provide reasonable determination of thermodynamic quantities. However, a critical assumption in using these pressure calibrations is that they remain constant at higher temperatures, i.e., the temperature-pressure regime of interest in most experiments.

Decker's [1] review paper on high-pressure calibration discusses in detail criteria for selection of materials for and methods of measurement of fixed pressure points. It is assumed that the reader is familiar with Decker's review, and only a few additional comments will be necessary in this paper. After applying all of Decker's "criteria," in order for a fixed point to be of value, it must be measurable in the many different apparatus and experimental setups that are in use. Solid (because solids are easier to handle than liquids) transitions which can be measured by volume, resistance, and DTA techniques appear to be most easily adaptable to apparatus and experimental conditions. Thus, metals which exhibit solid transitions appear to be the most useful materials for study.

Thallium and bismuth were chosen for this initial study of high-pressure fixed points at high temperature. Both materials are used for fixed points at room temperature, and the solid transitions in these materials have been studied by volume, resistance, and DTA techniques. La Mori [2] has shown that the volume and resistance transitions do, in fact, occur at the same pressure.

2. Experimental

In order to attempt the measurements outlined above, it is necessary to have an apparatus capable of accurate pressure measurement at higher temperatures. Until recently, such an apparatus has not been available. The development of the externally heated piston-cylinder apparatus, La Mori [3], has permitted the determination of pressure to an accuracy of about one part per 1000 to 400 °C and pressures of 30 kbar.

The technique used to measure the transition pressure is the same as described by Kennedy and La Mori [4]. The piston is inserted into the cylinder and rotated by means of a lever arm attached to the tool stack. This has the effect of relieving friction somewhat in the manner of a free piston gage. Pressure is calculated by force/area of the main hydraulic ram relative to that of the area of the high-pressure piston. Appropriate corrections are made for the weight of the ram and tool stack, and dilation of the pressure vessel with pressure.

Figure 1 is a schematic of the X–Y plot of an actual experiment. The sample is first cycled completely through the transition. On the second upstroke, the cycle is stopped just after the transition is entered (point 1). The piston is rotated until the pressure drops to a constant value (point 2). Pressure is increased and then released (point 3). The piston

[1] Figures in brackets indicate the literature references at the end of this paper.

Paper presented at the Symposium on Accurate Characterization of the High-Pressure Environment, held at the National Bureau of Standards, Gaithersburg, Md., October 14–18, 1968.

385-762 O - 71 - 19

TABLE 1. *Data for bismuth transitions*

Temperature, °C	Pressure, kbar		Temperature, °C	Pressure, kbar	
	Compression	Release		Compression	Release
Bismuth I → Bismuth II			Bismuth II → Bismuth III		
23.3	25.39		22.9	27.02	
23.3		25.25	22.6		26.74
24.2	25.48		24.8	27.04	
24.7		25.28	24.7		26.68
35.2	24.9		33.5	26.78	
34.7		24.72	32.2		26.46
35.7		24.70	48.0	26.46	
47.7	24.2		48.0		26.14
47.8		24.14	73.2	25.76	
48.0	24.28		73.0		25.58
48.2		24.16	98.8	24.97	
73.1	23.13		98.8		24.85
73.0		23.05	127.5	24.08	
110.6	21.45		127.2		24.00
110.7		21.35	151.5	23.32	
127.0	20.61		151.3		23.21
127.5	20.57		163.9	22.95	
127.2		20.51	163.9		22.91
151.5	19.45		172.2	22.5	
151.6		19.35			
163.5	18.84				
163.7		18.78			
173.0	18.21				
173.0		18.15			

is rotated until the pressure rises to a constant value (point 4). The actual pressure of the transition must lie somewhere between points 2 and 4. These are the points that are reported in the Results section. For purposes of drawing a phase diagram, the transition line is drawn through the mean of compression and release values.

The high temperature is obtained by placing an external heater around the outside of the 11-in. diameter by 2-in.-thick pressure plate. The 6-in.-thick heater also heats 2-in.-thick aluminum plates on both sides of the pressure plate. These aluminum heat sinks are efficient enough so that there is no measurable temperature gradient over the sample at 500 °C. Heating of the pressure plate assembly causes the binding rings to expand away from the carbide pressure vessel. This and the decreased strength of the carbide at higher temperatures reduce the operating pressures of the device from 40 kbar at room temperature to 28 kbar at 500 °C. Additionally, corrections for the increase in diameter of the pressure vessel due to temperature and expansion of the binding rings, as well as the decrease in elastic constants, must be included in the determination of the diameter of the pressure vessel. This is discussed by La Mori [3].

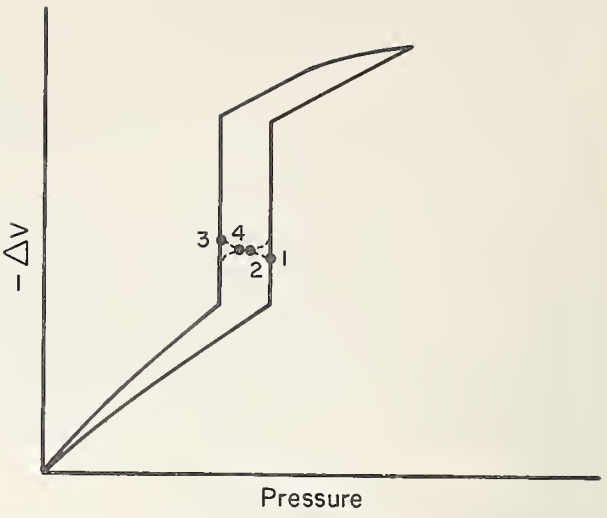

FIGURE 1. *Schematic of piston rotation experiment.*

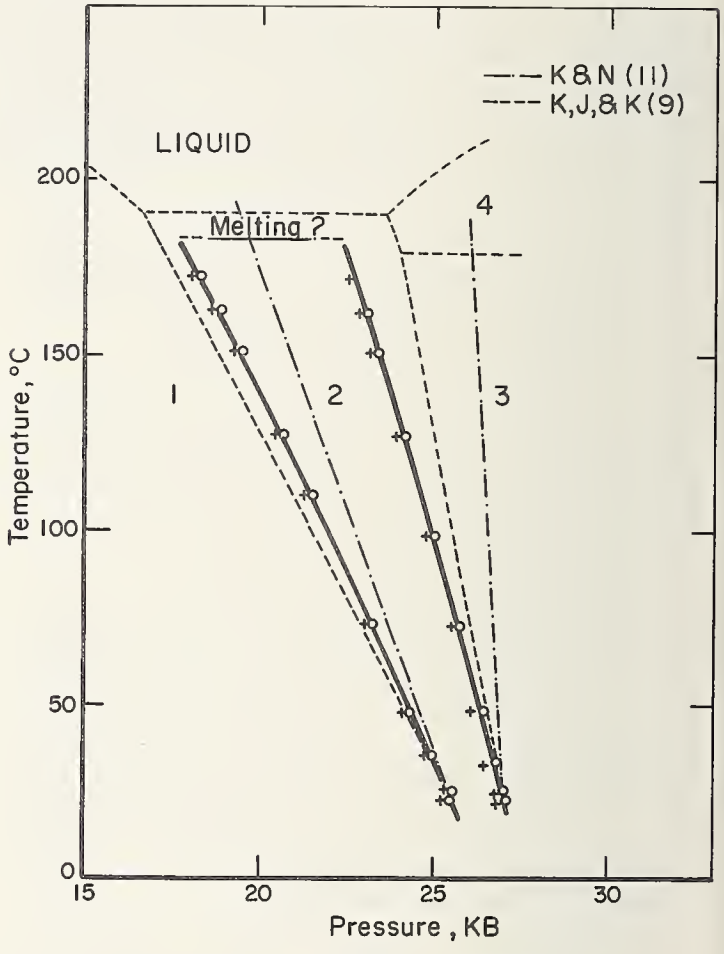

FIGURE 2. *Phase diagram of bismuth.*

3. Results

The results of this investigation on bismuth and thallium are given in tables 1 and 2, and figures 2 and 3. Corrections have been applied to the raw

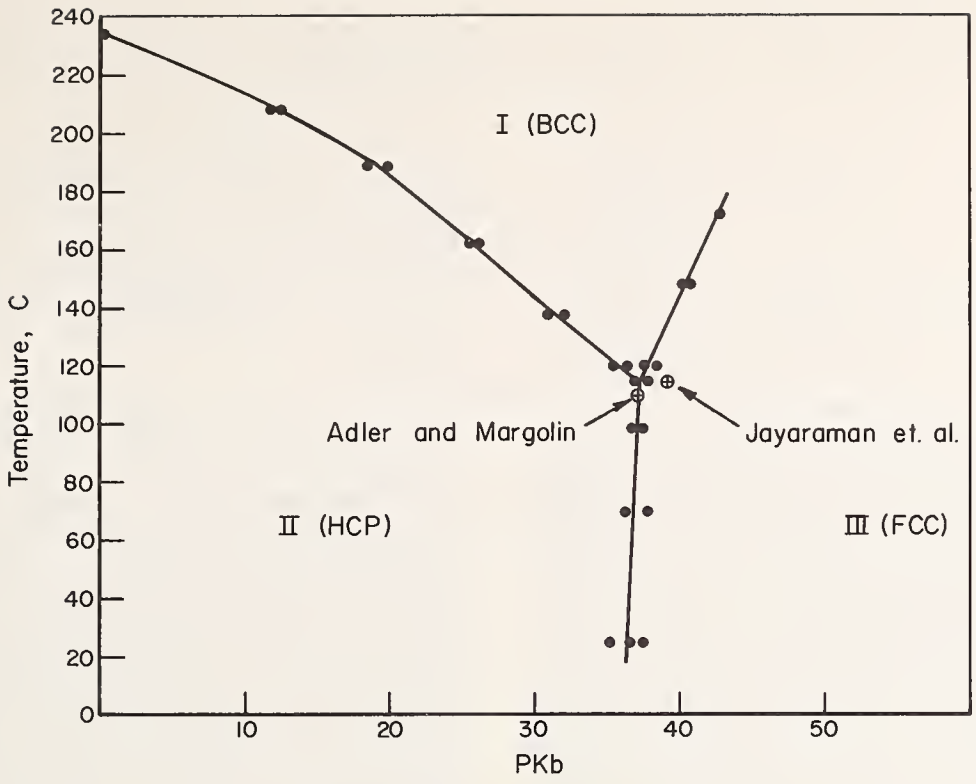

FIGURE 3. *Thallium phase diagram.*

TABLE 2. *Data for thallium transitions*

Temperature, °C	Pressure, kbar	
	Compression	Release
Thallium II → Thallium III		
25.5	37.54	35.37
70.0	37.74	36.25
98.5	37.36	36.74
114.5	37.70	36.98
Thallium II → Thallium I		
137.8	32.05	30.89
161.0	26.14	25.74
184.2	19.80	19.37
208.0	12.36	11.67
120.0	36.40	35.51
Thallium I → Thallium III		
120.0	38.63	37.90
148.5	40.49	40.25
172.0	42.61	

data as described previously. These pressure corrections amount to about 400 bars at 40 kbar. The accuracy of the pressure measurements is about 1 part in 100, while the precision is about 100 bars. The latter arises from uncertainty in the measured quantities; the former from uncertainties in the pressure measurements of the hydraulic ram. Temperature measurements are accurate to 0.1 °C (see ref. [3]).

3.1. Bismuth

The bismuth 1→bismuth 2 transition has been used as a high-pressure standard since Bridgman [5] first accurately measured it. He reported a value of 25.155 kbar at 25 °C; examination of his data shows an uncertainty of about 5 percent. Later Kennedy and La Mori [4] reported a value of 25.410 kbar ± 95 bars and using the same data they reported a "best value" of 25.380 kbar ± 20 bars. This best value was computed from the lowest pressure found on the series of compression values and the highest pressure found on the series of release values. The value of 25.41 ± .10 kbar is considered by the authors to be most representative of their work. Heydemann [6] reported a value of 25.499 kbar ± 60 bars (corrected from 25.306 kbar, Heydemann [7]).

The present work finds a value of 25.37 ± 0.2 kbar with an uncertainty large enough to agree with the previous determinations. The reason for the larger uncertainty reported here than that found by Kennedy and La Mori is that the pressure gage was not calibrated as accurately in the present experiments. Because of the presumed greater accuracy of the true free piston gage, the data on figure 1 are forced through Heydemann's value of 25.50 kbar at 25 °C.

The bismuth 2→bismuth 3 transition was previously determined by Kennedy and La Mori [4]

TABLE 3. *Triple points in bismuth*

Reference	[11]	[9]	This work
Bismuth 1-2-Liquid	19.4 kbar 184 °C	16.7 kbar 191 °C	17.6 kbar 183 °C
Bismuth 2-4-Liquid	27.5 kbar 175 °C	23.6 kbar 191 °C	21.9 kbar* 183 °C

*This does not take into account the bismuth 2-4 phase boundary, which will decrease the transition pressure slightly.

at 25 °C as 26.96 ± 0.20 kbar. This value is thought to be better than Bridgman's [5] value of 26.54 kbar which has 5 percent uncertainty. The value found here is 26.82 ± 0.20 kbar.

The bismuth experiments always ended in catastrophic failure of the pressure vessel at 183 °C. Since the bismuth filled the entire bore of the pressure vessel, this phenomenon is what one would expect on melting. If one accepts this inference as evidence for melting, then the 183 °C is in good agreement with Ponyatovskii [8] and not in agreement with Klement, Jayaraman, and Kennedy's [9] value of 191 °C.

Bridgman [10] and Ponyatovskii [8] have previously examined the bismuth 1–2 and 2–3 transitions. They are in close agreement. Our data for bismuth $1 \rightarrow 2$ are at a slightly higher pressure than the others and in close agreement for bismuth $2 \rightarrow 3$. Kennedy and Newton [11] and Klement, Jayaraman, and Kennedy [9] have inferred the transition boundaries by drawing straight lines between inflections in their melting curve determinations (DTA) and the values of Kennedy and La Mori [4]. The differences between these data, as well as their differences with the present data, are believed to be caused by the unfavorable pressure determination that is probable in their experiment, as compared to the present method. See figure 2.

These experimental differences result in significant differences in the triple point determination. The triple points inferred from this work are compared with other values in table 3. Even if our determination of the melting temperature of bismuth 2 is low, significant pressure differences will exist in the triple point determinations.

3.2. Thallium

Of the four previously reported studies of the solid transitions in thallium, the work of Jayaraman et al. [12] and Adler and Margolin [13] is considered to be valid. The data of Bridgman [10] and Ponyatovskii [14] have several errors. The data are shown on figure 3. Thallium $2 \rightarrow 3$ transforms very slowly at 25 °C. The data at 25 °C were not taken over as long a time as that of Kennedy and La Mori [4]. This caused a wider region of uncertainty. The thallium phase diagram therefore uses the previous value of 36.69 ± 0.10 kbar at 25 °C as the best value.

The 1–2–3 triple point as determined by the present experiments is 114 ± 1 °C and 37.4 ± 0.4 kbar. This is in agreement with Adler and Margolin; the value found by Jayaraman (115 °C, 39.5 kbar) is outside our experimental error. The major difference in our data and Alder and Margolin is in the 1–2 and 1–3 transitions at pressures near the triple point. These differences are outside our limit of error.

4. Discussion

Solid transition pressures and temperatures have been accurately determined for bismuth and thallium. These solid transitions should provide fixed points for high-pressure experiments at pressures up to 50 kbar and temperatures approaching 250 °C. A gap exists in the calibration at about 10 kbar. This is in the range attainable by hydrostatic methods where pressure measurement is easy and can be done with great accuracy. Therefore, use of the hydrostatic apparatus should be encouraged for accurate data in this pressure range.

Further work of this type can be done to 500 °C and 30 kbar. This is the present limit on externally heated piston-type apparatus. Specially designed cells with AgCl or other salt pressure media and internally heated systems may permit determination of less accurate pressure points to 1000 °C.

5. References

[1] Decker, D. L., Bassett, W. A., Merrill, L., Hall, H. T., and Barnett, J. D., High pressure calibration: A critical review, NBS National Standard Reference Data System Publication, in press.

[2] La Mori, Phillip N., Calibration experiments in a piston-cylinder apparatus, in *High Pressure Measurement*, ed. Giardini and Lloyd (Butterworths, Washington, 1963).

[3] La Mori, Phillip N., Compressibility of Rocks and Minerals to 450 °C and 36 kb and Their Application to the Upper Mantel, Ph. D. Thesis, Northwestern University (1967), 205 pp.

[4] Kennedy, George C., and La Mori, Phillip N., J. Geop. Res. **67,** 851 (1962).

[5] Bridgman, P. W., Proc. Am. Acad. **74,** 1 (1940).

[6] Heydemann, Peter L. M., J. Appl. Phys. **38,** 3424 (1967).

[7] Heydemann, Peter L. M., J. Appl. Phys. **38,** 2640 (1967).

[8] Ponyatovskii, E. G., Soviet Physics Crystallography (translation) **5,** 147 (1960).

[9] Klement, W., Jr., Jayaraman, A., and Kennedy, G. C., Phys. Rev. **131,** No. 2, 632 (1963).

[10] Bridgman, P. W., Phys. Rev. **48,** 893 (1935).

[11] Kennedy, George C., and Newton, Robert C., Phase Transition in Some Pure Metals in *Solids Under Pressure*, ed. Paul and Warsehauer (McGraw-Hill, New York, 1963).

[12] Jayaraman, A., Klement, W., Jr., Newton, R. C., and Kennedy, G. C., J. Phys. Chem. Solids **24,** 7 (1963).

[13] Adler, Philip N., and Margolin, Harold, Trans. Met. Soc. AIME **230,** 1048 (1964).

[14] Ponyatovskii, E. G., Soviet Physics Crystallography (translation) **4,** 237 (1959).

The Use of Iron and Gold for Calibration of Higher Pressure and Temperature Points

H. M. Strong and F. P. Bundy

General Electric Research and Development Center
Schenectady, New York 12301

1. Introduction

The calibration of pressure cells at room temperature by reference to the phase transitions in Bi, Tl, and Ba is now a fairly settled procedure. But temperature excursions away from room temperature, especially to high temperatures, quickly obscure the familiar landmarks and both pressure and temperature become uncertain. Because there are no sure reference points established in this region, navigation on the P–T plane is something like groping in a fog. High temperature affects the pressure in a number of ways: (1) it tends to increase the pressure due to restraint of thermal expansion of the heated parts of the cell by the surrounding cooler parts of the cell and pressure vessel; (2) it tends to decrease pressure when it causes phase transformations to more dense structures to occur in the sample holder or its contents; (3) it may decrease pressure by accelerating gasket leakage; and (4) it may decrease pressure by accelerating the relaxation of tension in the high-pressure chamber. It is usually impossible to estimate the net effect of these pressure-modifying factors, nor is there a simple direct monitoring method for the pressure. Temperature can be monitored by a thermocouple, but unfortunately, high pressure changes the calibration of thermocouples in an incompletely known manner. It is the purpose of this paper to describe a few techniques for improving the accuracy of pressure and temperature estimates in a static high-pressure cell.

One of the methods for obtaining more useful high-pressure, high-temperature data is to associate the high-pressure phenomenon under study with some other familiar and easily observable phenomenon, recording both simultaneously. In this way the experimenter can standardize his own experiments, and he can offer data which make it easier for another experimenter to duplicate or compare results of similar type. The reference phenomenon is likely to be one for which there is a good deal of accurate data which help very much in more closely describing the pressure and temperature conditions used in his own experiments. In this paper, the use of iron, gold, and germanium as a pressure and temperature reference material is described.

Paper presented at the Symposium on Accurate Characterization of the High-Pressure Environment, held at the National Bureau of Standards, Gaithersburg, Md., October 14–18, 1968.

2. Iron as a Pressure-Sensing Element

Iron is a rather remarkable element for measurements of high pressure because it has several features which vary with pressure in a known manner in different regions of the P–T plane. Also, it is easy for the experimenter to use iron in high-pressure cells. Some of its most useful features are shown in the Fe phase diagram for the region below 910 °C in figure 1. When any one of the solid-solid phase boundaries shown in figure 1 is crossed, the Fe responds by conveniently changing its resistance sharply, its thermoelectric properties, or its heat content, anyone of which is rather easily detected. Because the slopes (dT/dP) of the three phase lines are quite different, not all of these boundary lines are equally useful for pressure measurement. The ϵ, γ transformation above 110 kbar, 500 °C has such a small slope [1] (+1.8°/kbar) that it is not a particularly sensitive pressure probe for that region. Because its temperature of transformation is nearly the same for a wide range of pressures above 110 kbar, it might better be used as a temperature reference point for approximately relating temperature in the cell to power input. The α, ϵ transformation boundary is so steep (~25°/kbar) that it is primarily sensitive to pressure in the narrow range between about 130 and 110 kbar. The α, ϵ transformation is in fact one of the most valuable pressure reference points now known for the higher pressure region in static apparatuses. Certain alloys of Fe with Co or with V have α, ϵ type transitions at pressures in the range 160 to 300 kbar. Details about these higher transitions are given by Bundy [1] [2] and by Loree et al. [2].

The α, γ transformation is in a more popular region of the high-pressure spectrum. It has a satisfactory pressure sensitivity of about −4°/kbar in the pressure range 20 to 60 kbar. Furthermore it is quite versatile in signaling the occurrence of the transformation by electrical resistance change ($\Delta R/R_\alpha \approx 0.5$), latent heat ($\Delta H = 217$ cal/mol) or thermoelectric change (an easily identified sharp maximum in emf output of an Fe/Pt10Rh junction versus temperature). In addition, Fe has one other feature not shown in figure 1. It has a relatively large thermoelectric pressure error effect which is

[1] This value is less than the +2.8°/kbar given in ref. [4]. This new lower value is based on the latest, most accurate, values of the ΔV's published by Mao, Bassett, and Takahashi, J. Appl. Phys. **38**, 272 (1967), and the experimental slope of −2.3°/kbar for the γ, α line near the triple point.

[2] Figures in brackets indicate the literature references at the end of this paper.

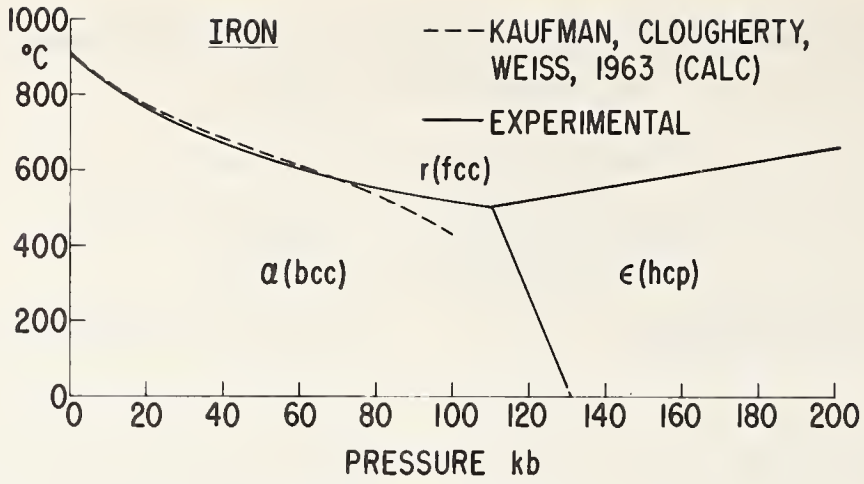

FIGURE 1. Fe *phase diagram.*

Solid lines: experimental data; broken line: calculated α, γ boundary, Kaufman et al.

useful for pressure probing in a limited range of temperature from about 1000 to about 1500 °C in the pressure region from 0 to at least 60 kbar, possibly much higher. (The authors have explored the effect in the region 30 to 60 kbar). This latter effect will be described in more detail in a later section.

The establishment of the Fe phase diagram illustrated in figure 1 is the result of the efforts of many people over a period of about 10 years. It involved a variety of experimental techniques including high-pressure x-ray probing, metallography, dynamic shock techniques, and theoretical approaches. It is not useful to describe details of all this work here but the reader can find summaries and detailed references to former work in articles by Kaufman et al. [3] and Bundy [4]. The α, γ transition, being in a more accessible pressure region, has received the most attention with established techniques and is the most accurately known boundary. In figure 1, the solid line was determined by experiment using a chromel-alumel thermocouple for temperature measurement. This thermocouple is known to have quite a small pressure calibration error. The dashed line is the calculated curve of Kaufman et al. The difference between the two curves over the span 20 to 60 kbar is probably due to thermocouple pressure effect. The portion in the upper pressure region (>80 kbar) is in a far more difficult region experimentally and naturally is less accurately known than the region below about 80 kbar.

The high-temperature phase boundaries of Fe, (γ, δ), (δ, liquid) and (γ, liquid) will not be covered in this article because they are in an experimentally difficult region and lack reliable techniques for accurate observations.

For pressure (or temperature) measurement in the regions defined by the Fe diagram shown in figure 1, it is a simple matter to install a small piece of iron in the pressure cell adjacent to the sample under investigation. A wire, disk, or thermoelectric junction may be used, depending on the mode of detection to be applied. The electrical resistance changes associated with the three phase boundaries

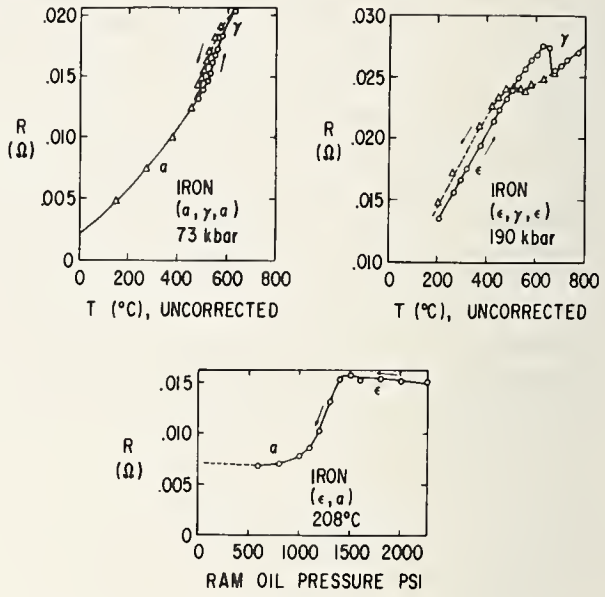

FIGURE 2. *Resistance changes at* Fe(α, γ), (α, ϵ), (ϵ, γ) *boundaries.*

are illustrated in figure 2. (The Fe probe should have a very small volume relative to the cell so that its transformation with $-\Delta V$ will not change the cell pressure significantly.) For experiments conducted under conditions very close to a phase boundary line, for example, close to the α, γ transformation, the probe will give absolute pressure readings. If the temperature of the experiment is considerably different from the phase line, especially the α, γ boundary, then absolute pressure readings cannot be obtained because temperature has a significant effect on cell pressure due to thermal expansion and other effects mentioned previously. Even under this circumstance, the iron probe is useful for establishing relative pressures between experiments.

In this laboratory, the Fe α, γ transition at ~ 650 °C was used extensively for pressure calibration and cross-comparison of experiments on diamond growth at ~ 1400 °C. The iron reading was taken during the preheats for the diamond growth runs to measure the pressure differences at the ~ 650 °C stage of different experiment runs. The

iron probe (thermocouple-grade Fe wire) was in the form of a thermoelectric junction with Pt and Pt10Rh. The three wires were connected at a common point, forming a "thermotriplet," and the millivolt output of Fe/Pt10Rh was plotted against the output of the Pt/Pt10Rh junction on an $X-Y$ recorder. The α, γ transition, which occurred at temperatures between 670 and 630 °C for these experiments, was marked by a rather sharp maximum in the output of the Fe/Pt10Rh couple. (See figure 3. In practice, the α, γ transition is displayed on a larger scale for better resolution.) The temperature at the center of this maximum was obtained from the Pt/Pt10Rh junction. To correlate this temperature with the α, γ solid curve of figure 1, it was necessary to add a relative correction, ΔT(C/A-Pt/Pt10Rh) of 18 to 20 deg to allow for the relative pressure error between Pt/Pt10Rh and chromel-alumel (C/A) under these conditions [5, 6]. The temperature so obtained was referred to the α, γ transition solid curve of figure 1 for a pressure reading. This pressure corresponded to the cell pressure at approximately 650 °C (40 to 50 kbar) and was invariably several kilobars below the pressures needed for diamond growth, which were (50 to 60 kbar), at the temperatures required, 1300 to 1500 °C. Nevertheless, the iron probe measurement was very useful for detecting the inevitable pressure variations between experiments, which were not due to varying the applied load, but which were caused by differences in gasket behavior, cell packing, relative humidity, etc.

While using this thermotriplet junction as an Fe α, γ pressure probe, it was discovered that it had the properties needed to measure relative pressures at ~1000 to 1500 °C by the thermocouple pressure error method. This two-thermocouple pressure-probe method is described in detail in the next section. It is also described in an article of this same Symposium by Hanneman et al.

In the work described here, the Fe probe was always used for pressure calibration when the transitions were running in the forward direction $\alpha \rightarrow \gamma$, $\alpha \rightarrow \epsilon$, and $\epsilon \rightarrow \gamma$. There was hysteresis in recycling the transitions. Part of this hysteresis was due to pressure-press load behavior, part to reaction kinetics in the Fe. On the second pass in the forward direction, the transitions sometimes occurred at slightly lower press load. This difference can be caused by an effect called "pressure ratcheting"—a pressure increase obtained by cycling the cell temperature up and down. The difference could also be caused by reaction kinetic differences in the Fe probe. On the second cycle, some seeds of the high-pressure modification may be on hand, for example. These are inherent weaknesses in the method. Nevertheless, using the probes in the forward transformations, quite consistent pressure measuring results were obtained. For more detailed discussions of hysteresis effects see Bundy [4].

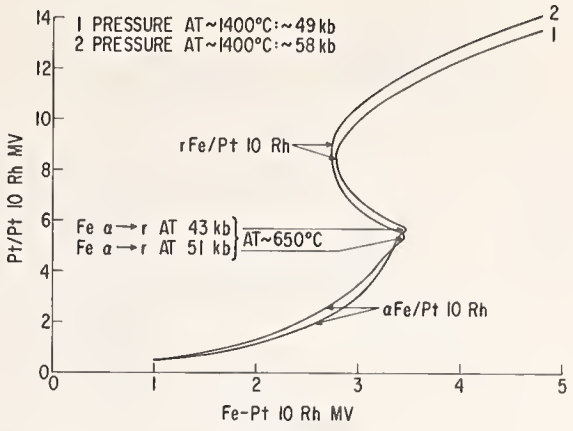

FIGURE 3. *Plot of* Fe/Pt10Rh *versus* Pt/Pt10Rh *millivolts at two pressures.*

Fe is in bcc cubic form below about 650 °C, in fcc cubic form above 650 °C.

3. The Two-Thermocouple Method for Pressure Measurement

It is well known that thermocouples change calibration under pressure, but that no two thermocouples change calibration in the same way [5, 6, 7, 8]. It is possible therefore to use the difference in temperature readings between two thermocouples under pressure as a measure of pressure. For reliability of measurements and convenience, it is desirable to have the differences in thermocouple readings to be as large as possible. But the requirement of having thermoelectric materials which are chemically stable under high temperature in a high-pressure environment limits the choice of materials that can be used. For example, chromel-alumel junctions were found to be unreliable above about 800 °C. The higher the temperature, the faster was its decay from normal calibration. Pt and Pt10%Rh alloy has been found satisfactorily stable up to about 1700 °C or more for brief periods and stable at 1400 °C for hours. Pt-Pt10Rh is satisfactory for one of a pair of the junctions for pressure measurement. Other metals found to be stable enough for use at 1000 °C to at least 1300 °C were Au, Ir, and Fe. Various combinations of Pt, Pt10Rh, Pt40Rh, Au, Ir, did show calibration differences due to pressure, but the differences were too small to be of practical use. The combination Fe/Pt10Rh with Pt/Pt10Rh proved to be stable for short periods up to about 1400 °C and for quite long periods at 1200 to 1300 °C. (The cleaner and drier the environment of the thermocouples, the longer they were stable.) Also, the pressure effect was large enough to be useful. A large number of pressure observations have been made using the thermotriplet Pt-Pt10Rh-Fe in diamond growth experiments.

In using this triplet combination, an X-Y recorder was connected to Fe/Pt10Rh and to Pt/Pt10Rh terminals. The millivolt output of the one junction plotted in terms of the millivolt output of the other junction produced a family of curves in which each curve was characteristic of the pressure. In a high-

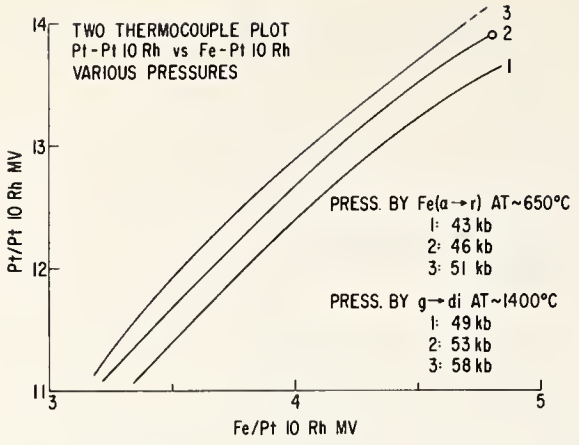

FIGURE 4. γFe/Pt10Rh *versus* Pt/Pt10Rh *millivolts at 11 to 14 mv* Pt/Pt10Rh *for three pressures.*

The cell pressure near the α, γ transition (~ 650 °C) is lower than at ~ 1400 °C by about 6 to 7 kbar.

pressure experiment, it was then possible to read from the *X-Y* plot both the relative pressure and the temperature from this three-wire junction. The types of *X-Y* plots obtained are illustrated in figure 3. The upper portions of the curves represent the thermoelectric behaviors of γFe/Pt10Rh; the lower portions show the characteristics of αFe/Pt10Rh.

From these plots it will be seen that this thermojunction has a limited range for pressure measurement which lies between ~1000 and 1500 °C at ~40 to 60 kbar. Below ~1000 °C the curves were complicated by the peculiar thermoelectric behavior associated with the α, γ transition. At this transition, the Fe/Pt10Rh passes through a peak output. The position of this peak is also a measure of pressure because as described above, the α, γ transition shifts to lower temperatures with increase in pressure.

While it is clear from figure 3 that the α, γ transition is related to the path of the curve above 1000 °C, it does not follow that they both indicate the same pressure. The additional heating beyond the α, γ transition causes cell expansion and possibly increase of pressure unless the compression pistons are pushed out correspondingly. Since the piston or anvil friction is usually very high, the piston motion, if any, does not normally fully compensate for expansion. On the other hand there may be phase transitions to denser forms within the cell which cause loss of internal pressure also not compensated by piston motion. The curves in figure 3 were made under circumstances in which there was a simple pressure increase due to restrained expansion. Curves showing a sharp shift to the right due to sudden pressure loss in a phase transformation have been observed. For these reasons the α, γ transition does not furnish an absolute calibration for the curves above 1000 °C.

The curves in figures 3 and 4 were assigned approximate pressures by comparison with the diamond-graphite equilibrium (di/g) and by other studies, to be described below, on the effects of heating on cell pressures. Figures 3 and 4 have tables which show the characteristic pressures for each curve, the pressures obtained by the α, γ transitions for the low-temperature portions of the curves shown only in figure 3, and the pressures for the high-temperature portions after allowing for cell expansion. The circled point on curve (2), figure 4, marks an experimental point lying on the di/g equilibrium. In finding the pressure corresponding to this point it was necessary to apply a thermocouple pressure correction, and the one used was obtained from those published by Hanneman and Strong [5, 6].

Ideally, the curves of figure 4 could be assigned absolute pressures so that they could be universally applicable. Unfortunately different apparatuses can have different pressure and temperature gradients along the thermocouple wires as they leave the pressure cell. This affects the apparent temperature error so that the curves of figures 3 and 4 will be more or less characteristic of a particular apparatus. But the phenomenon illustrated here is very useful for the experimenter to compare pressures at high temperature in a series of individual experiments. The method also has a distinct advantage in that it provides a means by which pressure changes can be followed in a continuous manner at high temperature.

4. The Effect of Heating on Cell Pressure

The effect of heating and thermal expansion on the pressure in a rigidly confined material can be quite remarkable. A simple example is that of sodium chloride, sometimes used as a pressure medium [5, 6, 9, 10]. Referring to the work of Decker [11] on the equation of state of sodium chloride, its cubical expansion coefficient at 50 kbar is about 105×10^{-6}. Raising its temperature by 1000° will therefore result in a volume expansion, $+\Delta V/V_0$, of 0.105 at constant pressure. The compressibility at 1000 °C and 50 kbar is about 3.5×10^{-3} kb^{-1}. Therefore to confine the sodium chloride rigidly while heating at 1000 °C would require a pressure increase of about 30 kbar.

In a practical pressure cell, confinement is not strictly rigid because gaskets do leak, pistons move some, and the pressure chamber does yield some. Furthermore, there may be internal phase changes in the sample or sample holder material to more dense forms. All of these effects influence the pressure in a direction opposite to that of thermal expansion. It is therefore necessary to measure directly the effects of heating on cell pressure in particular situations.

In this work, several methods were used for observing the influence of cell temperature and internal phase transformations on cell pressures. One of the most effective of these was to observe the variation of the melting point of a tiny, independently heated germanium element while the internal

cell temperature was varied. The schematic experimental arrangement is illustrated in figure 5 along with the Ge fusion curve [12]. The portion of the fusion curve used in this work was that part between about 30 and 60 kbar. The Ge element was heated independently by a tiny strip of carbon in contact with the Ge bar (dimensions: 1×1×5 mm). When melting occurred, the resistance of the heating element decreased sharply and the thermocouple recorded a latent heat arrest. (Liquid Ge is a metallic conductor; solid cubic Ge is semiconducting.) When the cell pressure increased, the Ge melting point decreased.

A test on cell pressure variation with heating was started with no heat applied to the central carbon tube heater and the first observation on the melting point of the Ge bar was made. Then with heat increased in the core of the cell, frequent Ge melting-point checks were made. After maximum temperature was reached, the variation of the melting temperature with time was observed. In this way a number of observations were made on both sodium chloride and pyrophyllite sample holders and in the presence of internal phase changes. Also, in a few experiments a second Ge element was placed inside the carbon tube furnace. In other experiments, Bi or Tl elements were located diametrically opposite the Ge element for observing the 25 and 37 kbar transitions in these elements. By these techniques, it was possible to gain an impression about the effects of heating on cell pressure and about internal pressure gradients.

The results obtained in this study are not applicable to all apparatuses and experimental arrangements, but they do represent the kinds of things that can happen in particular circumstances. The results did reveal sharp internal pressure gradients within the cell at relatively low temperatures. As the cell temperature increased so did the internal pressure until the core temperature reached about 1,000 to 1200 °C. This behavior was observed in both pyrophyllite and sodium chloride pressure media. At still higher core temperatures, the Ge melting point started to increase, indicating that the cell pressure was decreasing, possibly due to internal relaxations, gasket leakage, or phase transformations. For pyrophyllite the decrease in pressure with time was quite rapid and large, falling eventually below the calibrated pressure in the room-temperature cell. For sodium chloride cells the pressure always remained well above the room-temperature calibrated value and quickly reached an equilibrium value, except when the cell contained a sample which changed phase to a more dense form. In the latter case the pressure decreased until the transformation was ended. The difference in behavior of sodium chloride and pyrophyllite pressure media at high temperature is due to the fact that salt has a stable lattice while pyrophyllite does not. Pyrophyllite transforms to coesite, kyannite, and other denser structures.

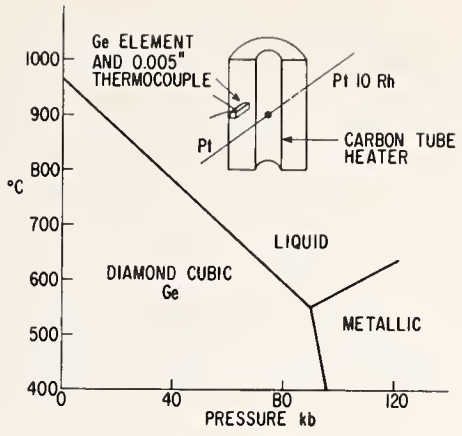

FIGURE 5. *High-pressure cell for "belt" apparatus and germanium phase diagram.*

Pressure cell contains an element for internal pressure measurement by variation of Ge melting point.

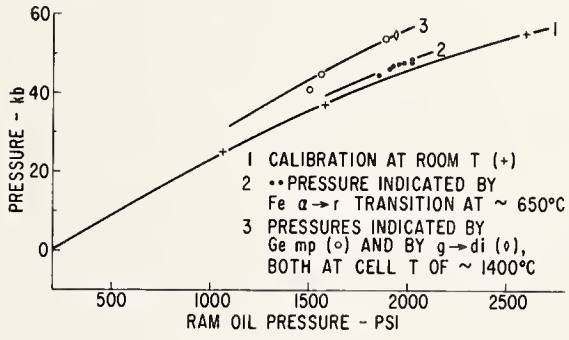

FIGURE 6. *Pressure calibration at different temperatures for a Hall belt-type apparatus.*

An illustration of the effect of temperature on internal cell pressure is shown in figure 6. The curves show cell pressure in terms of the applied load. In this case the pressure medium was largely sodium chloride. The room-temperature pressure calibration corresponds to the bottom curve in the figure. Pressures found from the α, γ transition at approximately 650 °C are shown by the middle curve. On the other hand, the internal pressure at temperatures near 1400 °C were substantially higher. The actual pressures existing were determined by the melting temperature of Ge and by the di/g equilibrium.

These results serve to emphasize the very great difficulty in knowing at all times and at all temperatures what the internal cell pressure and temperature really are. Not only do the pressure and temperature influence the normal calibrations for each other, but cell characteristics also influence the apparent values as compared to the true absolute values. If a fixed pressure-temperature reference point could be found that is located well into the region where both P and T are large, this reference point would help very much to check both pressure and temperature calibrations of various sorts of P and T probes. In the next section an attempt to locate a possible reference point using the intersection of the di/g equilibrium with the Au fusion curve is described.

5. A Possible High-Pressure High-Temperature Reference Point

Simultaneous, accurate, absolute measurement of high pressure and high temperature is not presently possible and no reliable fixed points at these conditions have been established which could be used as standard references. An approach to the problem of finding a convenient reference has recently been made, using the intersection of two phase-boundary lines which have radically different slopes. The phase lines chosen for this experiment were the melting line of gold and the diamond-graphite equilibrium line. These were chosen because they intersect at a point where both gold melting and diamond growth could be observed simultaneously. The gold fusion curve has already been experimentally observed [13, 14, 15] and some thermodynamic data were available [16, 17, 18] for approximately correcting the experimental data to the "true" curve. The di-g equilibrium has been thoroughly explored [19, 20, 21] and its location in the P-T plane is well established. The experiment consisted in finding the apparent P and T where the two curves crossed and then comparing this P and T with the "true" calculated P and T for the intersection of the two phase boundaries. The differences ΔP and ΔT between the observed and calculated intersections were then taken to be the errors in experimental calibration of pressure and temperature. Thus it was possible to compare the assumptions made about corrections of thermocouple error and pressure measurement error with another reference point determined by quite independent data and assumptions.

An experimental arrangement for melting gold and observing the di-g equilibrium is illustrated in figure 7. Experiments were run at several pressures and temperatures near 53 kbar, 1,400 °C (corrected values) so that the di-g equilibrium point could be established in relation to the gold fusion curve. The thermocouple used was Pt/Pt10Rh and melting was observed by latent heat arrests.

The fusion curve of Au was observed by three experimenters using Pt/Pt10Rh thermocouples [13, 15] and chromel-alumel thermocouples [14]. Each experimenter had a different apparatus and method of pressure determination, taking into account thermal expansion effects. It is remarkable how well the three sets of data agree when uncorrected melting temperatures were plotted in terms of corrected pressures, figure 8.

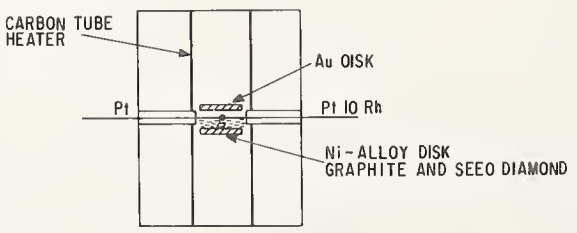

FIGURE 7. *Arrangement for simultaneously observing melting point of gold and diamond-graphite equilibrium.*

The "true" calculated melting curves in figure 8 were plotted in two ways to give upper and lower bounds to the possible location of the correct curve. The upper curve was a linear extrapolation of the initial slope obtained from Clapeyron's equation. The $\Delta S^{\alpha \rightarrow L}$ for gold at melting according to data given by Hultgren et al. [16] is 2.21 cal/deg g-atom. The $\Delta V^{\alpha \rightarrow L}$ is 0.60 cm³/g-atom [17, 18]. The slope was calculated from this data to be 6.5 deg/kbar, and extrapolated to 55 kbar, the melting point was 1,420 °C.

The lower calculated curve was plotted with the help of the Kraut and Kennedy melting law [22]:

$$T_m = T_{m_0}\left(1 + C\frac{\Delta V}{V_0}\right)$$

where T_{m_0} is the melting point at 0 kbar (1336 K) and T_m is the melting point at pressure P. $\Delta V/V_0$ is the room-temperature isothermal compression, and C is a constant to be determined from melting data at relatively low pressure, in this case 10 kbar. At 10 kbar there is very little pressure or temperature calibration error so that the experimental and calculated melting temperatures (using Clapeyron equation) agree very closely at 1,401 K. The value of C obtained from the 10 kbar melting data and Bridgman's compression data [23] was 8.94. The extrapolation of the fusion curve beyond 10 kbar then depended on the Bridgman isothermal compression data which were taken only as far as 30 kbar. There was very little curvature in the compression data and for purposes of obtaining the melting line to 55 kbar, the compression data were extrapolated to this pressure. The melting point at 55 kbar was thus found to be 1673 K.

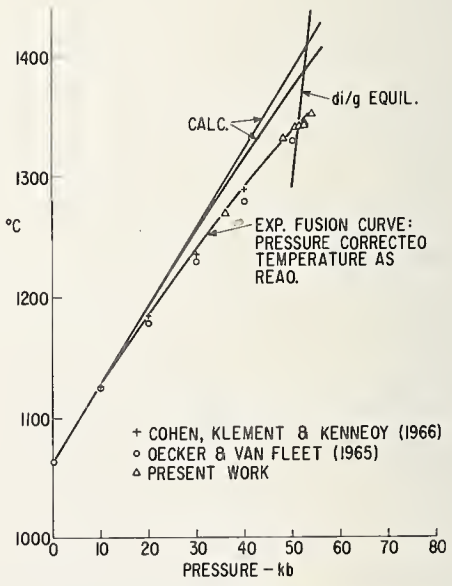

FIGURE 8. *Diamond-graphite equilibrium line and gold fusion curve.*

Upper curve: extrapolation of initial slope of gold fusion curve, 6.5°/kbar. Lower calculated curve: from Kraut and Kennedy fusion curve formula. Bottom curve: experimental data, Pt/Pt10Rh thermocouple temperatures not corrected for pressure error; cell pressure was corrected for pressure increase by internal thermal expansion.

The true di-g equilibrium and Au fusion curves thus appear to intersect at 52.5 to 53 kbar at 1388 to 1410 °C (figs. 8 and 9).

The experimental intersection of the two curves appears to occur at 42.5 to 43 kbar at 1344 to 1352 °C (fig. 9). In the experimental determination, no allowance was made for pressure error in the Pt/Pt10Rh thermocouple. Also, the pressures used for the data points were those obtained from room temperature pressure calibration by Bi, Tl, Ba-transition points.

The experimental temperature and pressure for the intersection of the two boundary lines lie below their anticipated values. The pressure requires a correction of $\sim+10$ kbar. The temperature readings were 36 to 66 degrees too low. The pressure error was consistent with the studies on effects of thermal expansion described above and the temperature error was consistent with the earlier work of Bundy, Hanneman and Strong and the recent work of Wentorf [24] on thermocouple pressure error. A more accurate fix on the intersection point could be obtained if the reliability of the Au fusion curve were to be improved.

6. Summary

Simultaneous accurate measurement of both high pressure and high temperature is not presently possible. However, a useful experimental procedure is to use one type of phase change as a reference against which other phase relations may be studied. Iron was particularly useful for this purpose because it exhibits several easily observed pressure-sensitive solid-solid type phase transformations. It also displays a large thermoelectric pressure-error behavior, which when used with Pt and Pt10Rh thermoelectric materials, provides both pressure and temperature references.

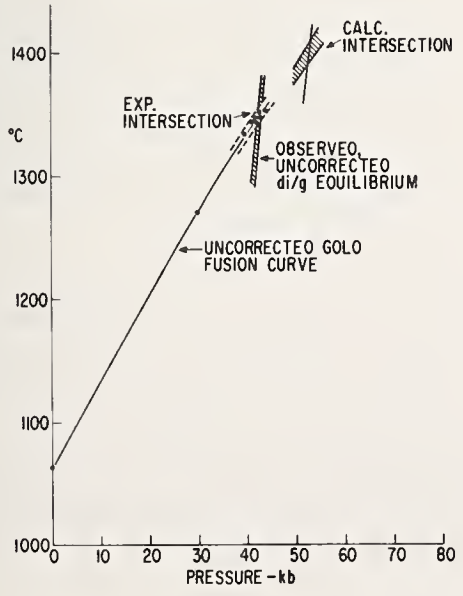

FIGURE 9. *Apparent gold fusion curve and di/g equilibrium in relation to theoretical gold fusion curve and di/g equilibrium.*
No corrections for pressure or temperature errors applied to experimental data.

It was shown that cell heating can substantially change the internal pressure in a high-pressure sample and that pressure at high temperature can decay with time at a rate dependent on cell materials used. The internal cell pressure changes were detected by changes in melting point of a tiny Ge element.

A high-pressure, high-temperature fixed reference point could be the intersection of two well-established phase boundary lines. The effectiveness of this approach to the problem of high-pressure, high-temperature measurement was illustrated using the diamond-graphite equilibrium and the gold fusion curve.

7. References

[1] Bundy, F. P., Fe-Co and Fe-V Alloys for pressure calibration in the 130 to 300 kbar region, J. Appl. Phys. **38,** 2446–2449 (1967).
[2] Loree, T. R., Fowler, C. M., Zukas, E. G., and Minshall, F. S., Dynamic polymorphism of some binary iron alloys, J. Appl. Phys. **37,** 1918–1927 (1966).
[3] Kaufman, L., Clougherty, E. V., and Weiss, R. J., The lattice stability of metals—III. Iron, Acta Met. **11,** 323–335 (1963).
[4] Bundy, F. P., Pressure-temperature phase diagram of iron to 200 kbar, 900 °C, J. Appl. Phys. **36,** 616–620 (1965).
[5] Hanneman, R. E., and Strong, H. M., Pressure dependence of the emf of thermocouples to 1300 °C and 50 kb, J. Appl. Phys. **36,** 523–528 (1965).
[6] Hanneman, R. E., and Strong, H. M., Pressure dependence of the emf of thermocouples, J. Appl. Phys. **37,** 612–614 (1966).
[7] Bridgman, P. W., Effect of pressure on thermoelectric properties, Chap. X, p. 295, in The Physics of High Pressure (G. Bell and Sons, Ltd., London, 1952). Also Proc. Am. Acad. Arts Sci. **53,** 269 (1918).
[8] Bundy, F. P., Effect of pressure on emf of thermocouples, J. App. Phys. **32,** 483–488 (1961).
[9] Strong, H. M., Pressure distribution in reaction vessels (sodium chloride sample holder), U.S. Patent 3,030,662 (1962).
[10] Jeffery, R. N., Barnett, J. D., Vanfleet, H. B., and Hall, H. T., Pressure calibration to 100 kb based on compression of NaCl (cell contained a sodium chloride insert), J. Appl. Phys. **37,** 3172–3180 (1966).
[11] Decker, D. L., Equation of state of NaCl and its use as a pressure gauge in high-pressure research, J. Appl. Phys. **36,** 157–161 (1964).
[12] Bundy, F. P., Phase diagrams of silicon and germanium to 200 kbar, 1,000 °C, J. Chem. Phys. **41,** 3809–3814 (1964).
[13] Cohen, L. H., Klement, W., Jr., and Kennedy, G. C., Melting of copper, silver and gold at high pressures, Phys. Rev. **145,** 519–25 (1966).
[14] Decker, D. L., and Vanfleet, H. B., Melting and high temperature electrical resistance of gold under pressure, Phys. Rev. **138,** A129–133 (1965).
[15] Strong, H. M., and Hanneman, R. E., unpublished work on fusion curve of gold.
[16] Hultgren, R., Orr, R. L., Anderson, P. D., and Kelley, K. K., Selected Values of Thermodynamic Properties of Metals and Alloys, John Wiley & Sons, Inc., New York, N.Y. (1963).
[17] Esser, H., Eilender, W., and Bungardt, K., Arch. Eisenhuttenwesen **12,** 157 (1938).
[18] Krause, W., and Sauerwald, F., Z. Anorg. Allg. Chem. **181,** 347 (1929).
[19] Berman, R., and Simon, Sir Francis, On the graphite-diamond equilibrium, Z. Elektrochem. **59,** 333–338 (1955).

[20] Berman, R., Thermal properties of diamond, Chapt. 14, Page 371, Physical Properties of Diamond, Ed. R. Berman (Clarendon Press, Oxford, 1965).
[21] Bundy, F. P., Bovenkerk, H. P., Strong, H. M., and Wentorf, R. H., Jr., Diamond-graphite equilibrium line from growth and graphitization of diamond, J. Chem. Phys. **35**, 383–391 (1961).
[22] Kraut, E. A., and Kennedy, G. C., New melting law at high pressures, Phys. Rev. Letters **16**, 608 (1966).
[23] Bridgman, P. W., Linear compressions to 30,000 kg/cm² including relatively incompressible substances, Proc. Am. Acad. Arts Sci. **77**, 189–234 (1949).
[24] Wentorf, R. H., Jr., Temperature measurement by thermal noise at high pressures, paper presented at this meeting.

DISCUSSION

P. M. Bell (*Geophysical Laboratory, Carnegie Institution of Washington, Washington, D.C.*): In the test cell, does iron diffuse into the platinum-platinum 10 rhodium thermocouple and affect the temperature measurement?

In determining the diamond-graphite curve, is there catalyst present and, if so, does it affect the equilibrium point?

C. W. Beckett (*National Bureau of Standards, Washington, D.C.*): I was very much interested in your remarks about gold. As you know, the gold point is one of the fixed points on the international temperature scale and at one atmosphere is reproducible to about a hundredth of a degree. One approach to this problem of thermodynamic temperatures, pressures, and so forth, would be to have a comprehensive program on the phase diagram, so to speak, which would include not only the measurements such as those you have mentioned but also measurements of the heat of fusion and the volume change at high pressures. This is much easier said than done, of course.

Before undertaking this, one has to have a carefully selected group of substances. The advantage of gold in this case is that it does not react with the carbon significantly, at least at one atmosphere, because for many years the gold-point temperature has been reproduced in graphite containers.

Another metal which behaves fairly well in these cells is copper. Now, of course, the melting point of copper is only about 20 degrees above the gold melting point at one atmosphere, but the slope of the curve with pressure is different.

Have you considered using the same technique with other metals such as copper? Platinum in graphite would not be suitable because platinum does react to graphite. However, the platinum secondary temperature point is measured in thorium dioxide containers, and it is reproducible to better than a degree at one atmosphere. Thorium is hard to use in a pressure vessel, but one could use other oxides. Beryllium might be better.

AUTHORS' CLOSURE

Response to Dr. Bell: Our platinum 10 rhodium thermocouples did not show any tendency to change calibration with time due to their being in contact with an iron wire. The temperature-heating power relations were stable for long periods. At the end of a test, the freezing and melting temperature arrests at the metal-carbon eutectic furnished a fixed check point. We did not observe an apparent shift in this check point as a result of the platinum-platinum rhodium couple sharing a contact with iron, even after several hours. The junctions were in a nearly isothermal region, so that a considerable amount of diffusion would have to occur before the effect could be felt.

On the matter of the catalyst, we have published data (H. M. Strong and R. E. Hanneman, J. Chem. Phys. **46**, 3668 (1967)) showing the displacement of the diamond graphite equilibrium due to the presence of the catalyst. The catalyst must be present in order for the reaction to run freely in either direction. The displacement of the diamond graphite equilibrium is quite small; it amounts to about 12°, which is equivalent to about one third kilobar. Allowance was made for this displacement.

Response to Dr. Beckett: Other metals have been considered for use in locating phase boundary intersections. Copper would be suitable to use for finding an intersection between its fusion curve and the diamond-graphite equilibrium. This intersection should occur about 70° below the intersection for gold. If both intersections were located, there would be three quantities to check for consistency: the two intersections and the slope of the diamond-graphite equilibrium between the intersection points. This slope should agree with the calculated slope of R. Berman and Sir Francis Simon (Z. Elektrochem. **59**, 333 (1955)).

Another possibility is to find the intersections of the well-known iron $\alpha \rightarrow \gamma$ equilibrium with the fusion curves of Al and Pb. These intersection points should occur at temperatures between 600 and 800 °C, pressures between 20 and 50 kbar, where thermocouple calibrations have smaller pressure errors. Finding these points would provide fairly accurate check points from which to reach further into the high pressure and temperature region.

Transition Pressures of Bi 3-5, Sn, and Fe

M. Contré

Commissariat à l'Energie Atomique, Centre d'Etudes de Bruyères-le-Châtel, Groupe Hautes Pressions, 29–33, Rue de la Fédération – Paris

Making use of "X type anvil," the change in resistance of two reference metals in each run was simultaneously recorded in order to compare their transition pressures. A linear extrapolation through the well-known points below 60 kbar showed inconsistencies in the most commonly used high pressure scales. The recording of the pistons displacements lead to an exponential extrapolation which gave transition pressures of 78±2 kbar for Bi 3–5, of 102±4 kbar for Sn and of 140±15 kbar for Fe.

1. Introduction

The exact measurement, or even the simple evaluation, of the pressure which is built up inside a high-pressure solid-medium apparatus has from the beginning always been a problem. It was only in piston-cylinder apparatus that a direct measurement of the pressure was possible. Thus it became feasible, making use of the phase transitions of a number of metals, to evaluate the pressure which was built up in more intricate apparatus like "belt" below 60 kbar.

Above 60 kbar there is much confusion taking into account the various data that have been published to date (table 1). Lately, during the same year 1966, two teams, one from U.S.A. working with Professor Hall [11],[1] the other from Soviet Union working with Professor Vereschagin [13] published in earnest that the high Bismuth transition occurred at 76.5 ± 2 kbar for the first one, at 89.3 kbar ± 1 percent for the second one.

Research workers in the high-pressure field cannot remain unconcerned by that state of the art, if they wish to make more precise measurements.

The present work is an attempt to show the inconsistencies of the main pressure scales in the particular case of an apparatus called "X-type anvil", and to suggest possible values for the transition pressures of bismuth 3–5, of tin and iron. The four most widely used pressure scales, called *A*, *B*, *C*, *D* (table 2), have been chosen so as to be compared. Making the assumption that the transition pressures below 60 kbar are accurate, a linear extrapolation reveals a few inconsistencies. From the piston displacement recording, an analytical expression of the calibration curve is then derived. It is thus possible to evaluate the higher transition pressures.

2. Experimental Procedure

The apparatus called "X-type anvil" has already been described [31, 32, 35] and first presented at the Eindhoven meeting of the European High Pressure Research Group (1966). It consists of a die and of pistons with a special shape as shown on figure 1. It allows higher pressures to build without damage, inside a volume which is identical to that of a "belt." The cell body is made of pyrophyllite and the gaskets are of a mixed type, that is to say they consist of a pyrophyllite ring and of a Teflon ring (fig. 1).

The experiments have been carried out by recording simultaneously the resistance of two reference metal samples at room temperature. This procedure eliminates the lack of reproducibility of the calibration curve. The specimens were located side by side, at 1 mm from each other, inside a Teflon cylinder ($\phi = 4$ mm, $h = 3$ mm) which was in the center of the cell (fig. 2). The metal samples were wires 0.5 mm in diameter and 4 mm long. The electrical connections were established between the pistons and the chamber. The chemical analysis of the samples is given in table 3.

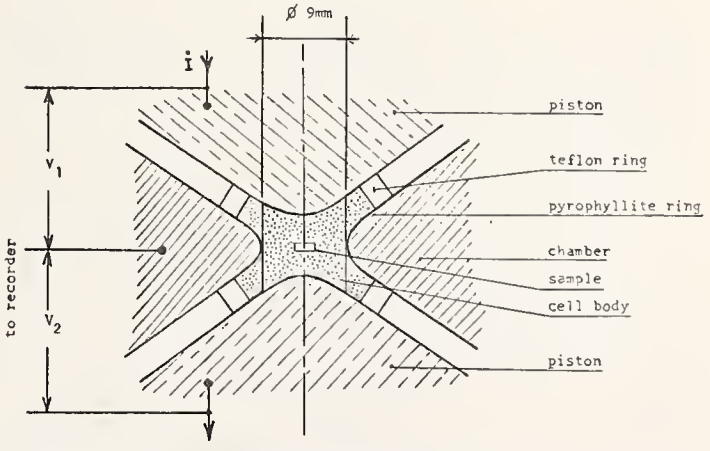

FIGURE 1. *Cross section of the cell inside the X-type anvil.*

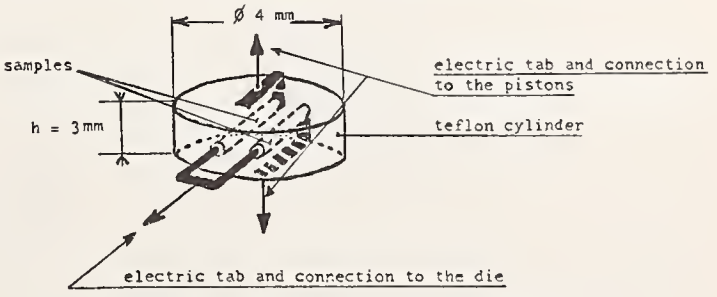

FIGURE 2. *Samples assembling, schematic.*

[1] Figures in brackets indicate the literature references at the end of this paper.

Paper presented at the Symposium on Accurate Characterization of the High-Pressure Environment, held at the National Bureau of Standards, Gaithersburg, Md., October 14–18, 1968.

TABLE 1. *Pressure transition data*

Apparatus	Year	Authors	Ref.	Pressure Transition in Kilobars								
				Bi I-II	Bi II-III	Tl II-III	Ba II-III	Yb	Bi III-V	Sn I-II	Fe $\alpha-\epsilon$	Ba
Piston-cylinder	1941 1942	Bridgman—in volume change (vol)	1	25		39.2/ 40	58.8/ 60	—	88.2/ 90	—	—	—
Bridgman's anvil	1952	Bridgman—by resistance (res)	2	25.65	27.08	45	78.4/ 80	58.8		no data below 100 kbar		
Shock	1956	Bancroft et al. (res)	5								131	
Belt	1958	Bundy (res)	17	25.65	27.08	45	78.4/ 80	58.8	122.5	114	—	—
Shock	1960	Boy and England (res)	14	25.2		37.1						
Drickamer's anvil	1961	Balchan and Drickamer (res)	4	—	—	—	59 ±1	—	90 ±2	—	133 ±1.5%	144
Piston-cylinder	1962	Kennedy-La Mori (vol)	3	25.38 ±0.02	26.96 ±0.18	36.7 ±0.1	59.6 ±1	—	—	—	—	—
Drickamer's anvil	1962	Balchan and Drickamer (res)	9							113/ 115		
Piston-cyclinder	1963	Klement-Jayaraman-Kennedy	10						~ 78			
Tetrahedral press	1963	Hall and Merrill (res)	18					39.5				
Bridgman's anvil	1964	Stark and Jura	6						81 ±4	99 ±4	118±6	
Bridgman's anvil	1964	Stromberg et al	24							107		
Piston-cylinder	1965	Roux	21	25.5 ±0.15	27.6 ±0.15	36.8 ±0.6						
Tetrahedral press	1965	Jeffery (vol) (res)	8	↑ 25.0 ↓ ±0.5	↑ 28.0 ↓ ±0.6	↑ 35.6 ±1.3	↑ 54.5 ±1.5	↑ 38.1 ±1.3	↑ 76.5 ±2	↑ 92 ±3.5	—	
Cubic press	1965	Giardina and Samara (ind. vol)	19						81–82			
Tetrahedral press	1966	Jeffery (res) Barnett —sheet Van Fleet —wire Hall	11	↑ 26.2 ±0.8 ↑ 26.5 ±1.3	↑ 29.1 ±0.8 29.7 ±1.4	35.4 ±2.1	↑ 54.6 ±0.9	↑ 38.2 ±1.5	↑ 75.7 ±1.3	↑ 92 ±3		
Piston gage	1966	Vereshchagin, Zubova, et al.	13	25.4 1%	26.9 1%	36.9 1%	58.5 1%		89.3 1%			
Dead-weight piston gage	1967	Heydemann (vol)	20	25.48 25.50	±0.06	according to grain size and purity						
Piston-cylinder	1967	Kennedy et al.	29				55.0 ±0.5					

TABLE 2. *Pressure scales*

Ref.	Year	Authors	Pressure Transition in Kilobars						
			Bi I-II	Bi II-III	Tl II-III	Ba II-III	Bi VI-VIII	Sn 1–2	Fe
A	1962	Bridgman Kennedy-La-Mori Balchan-Drickamer	25.4 ±0.1	26.8 ±0.1	36.7 ±0.1	58.5 ±0.6	89 ±1	113/ 115	133
B	1965 1966	Stark Jura—Stromberg	25.4 ±0.1	26.8 ±0.1	36.7 ±0.1	59 ±1	81 ±4	107 ±4	133
C	1965	Jeffrey Barnett Hall	25.0		35.6	54.5	76.5	92	
D	1967	Vereshchagin & al	25.4 ±1 %		36.9 ±1 %	58.5 ±1 %	89.3 ±1 %		

TABLE 3. *Chemical analysis of the samples*

Samples	Bi	Tl	Ba	Sn	Fe
Purity / Total Impurities	98.5%	99.99%	99.2%	99.9%	99.8%
	ppm	*ppm*	*ppm*	*ppm*	*ppm*
Li			< 10		
Na			100	< 10	< 25
Mg	10–50	< 10	400	25	< 50
Al	< 50	< 10	300	< 50	< 25
Si	Traces	< 50	80	200	80
K			< 10	< 10	< 10
Ca	< 100		0.1%	< 50	< 50
Ti	< 100		< 100		
Cr	< 50				< 50
Mn	< 25		250		230
Fe	< 50	< 10	< 50	< 50	
Co					< 10
Ni	< 100		< 100		350
Cu		< 10	< 50	< 50	
Zn			< 200		< 100
As					Traces
Sr			0.5%		
Zr					Traces
Mo	< 250			< 250	800
Ag	< 10				< 10
Cd		< 10			
Sn	1,000–2,000		< 50		< 50
Pb	1–1.5%	< 10	< 50		< 50
C					450 ± 50

At the same time that the resistance changes were recorded, the displacements of the pistons toward each other were measured, making use of four dial gages located at 90° angle around the high-pressure apparatus (fig. 3). All the measurements have been carried out during the first increase in pressure run and the loads have been measured with a strain-gage dynamometer.

3. Experimental Results

Fifty runs have been carried out under those conditions, among which the Fe transition was obtained 3 times, the Sn transition 10 times, and the Bi 3–5 transition 20 times. A typical resistance recording is shown on figure 4. The displacement of the pistons, as measured during each run, has the shape which is shown on figure 5. The lower part corresponds to the extrusion of the gaskets without much increase in the pressure, whereas the upper part corresponds to the real compression of the cell. Calibration curves, based on the B scale (table 2), are shown on figure 6 for two different die diameters. It is to be noted that the lower part is approximately a straight line which goes through the origin of coordinates.

From those experimental results, two types of extrapolations have been made to get the transition pressures of Bi 3–5, Sn, and Fe.

The first one is a simple linear extrapolation. The second one makes use of an analytical function. The piston displacement recordings give a clue as to the

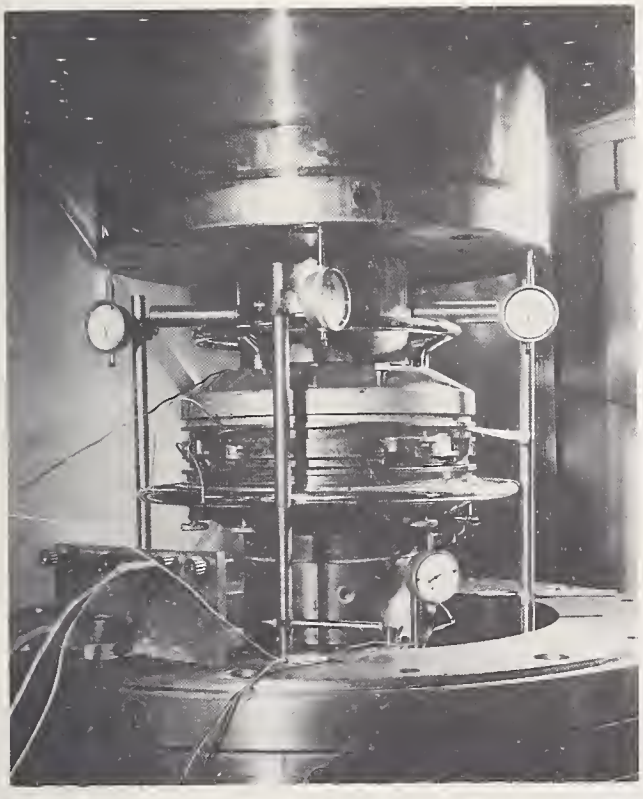

FIGURE 3. *Photograph of the "X-type anvil" showing the four dial gages used to record the piston displacements.*

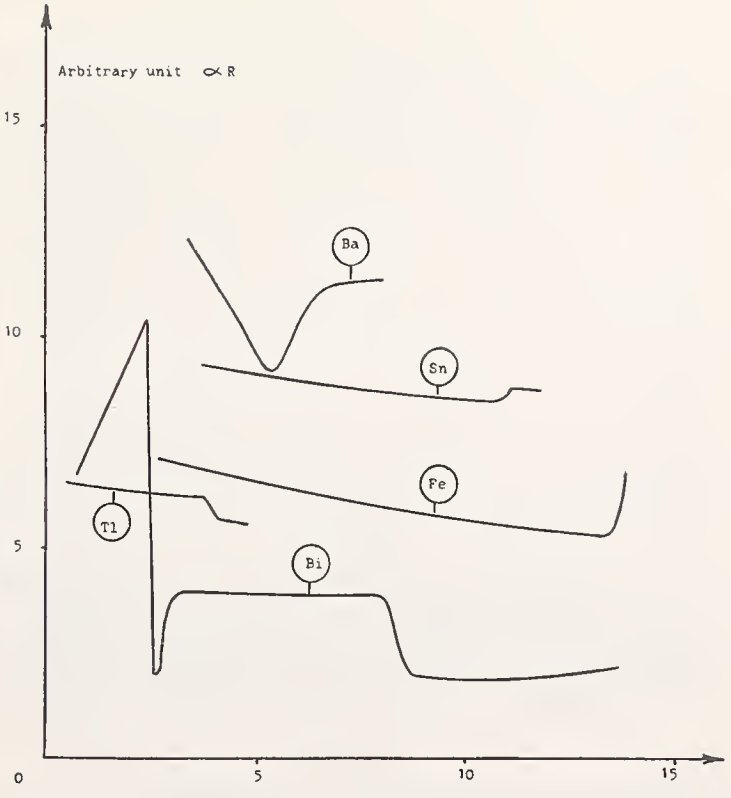

FIGURE 4. *Typical behavior of the resistance of the metals used to calibrate the pressure generated inside the cell.*

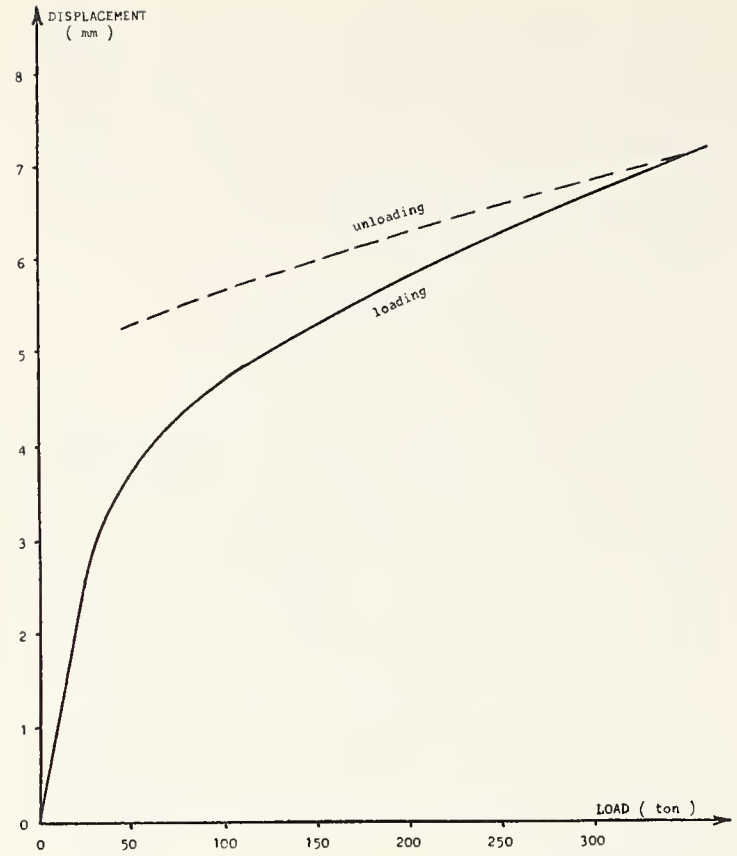

FIGURE 5. *Piston displacement curve.*

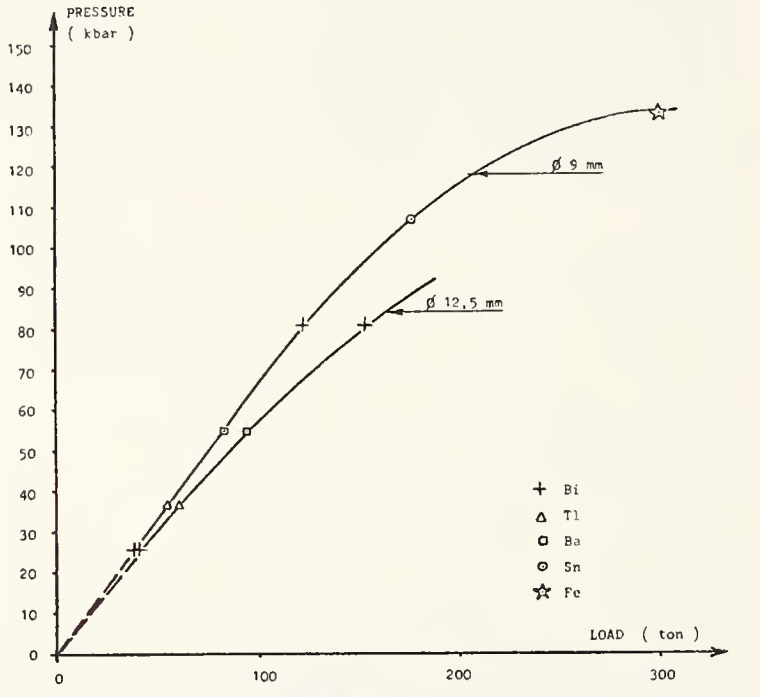

FIGURE 6. *Pressure calibration curves for two different die diameters.*

kind of function which is to be chosen. When plotted on a semilogarithmic scale those recordings are quite linear in their upper portion (fig. 7). With a slope k thus the piston displacement ϵ can be expressed as:

$$\epsilon = \epsilon_0 e^{-F/k}$$

where ϵ_0 is a constant and F is the load.

When this exponential stage is reached, the extrusion is considered as achieved and the assumption is made that the change in volume of the cell is proportional to the piston displacement. On the other hand, the pressures which are generated inside the cell are related to the overall compressibility of its components through a law, which can be shown empirically to be close to an exponential with a good approximation within the range of experimentation [28]. From these considerations an expression of the calibration curve follows:

$$P = -A \log (B + \exp -F/k).$$

A, B, and C are constants which can be evaluated knowing accurately at least three experimental values. They will be chosen among the best known transition points (Bi 1–2, Tl, Ba). It is obvious that when the load F is increased indefinitely the pressure P must go to a limiting value, which is the case with the above expression provided that B is positive. It also gives curves whose concavity is toward increasing load as expected.

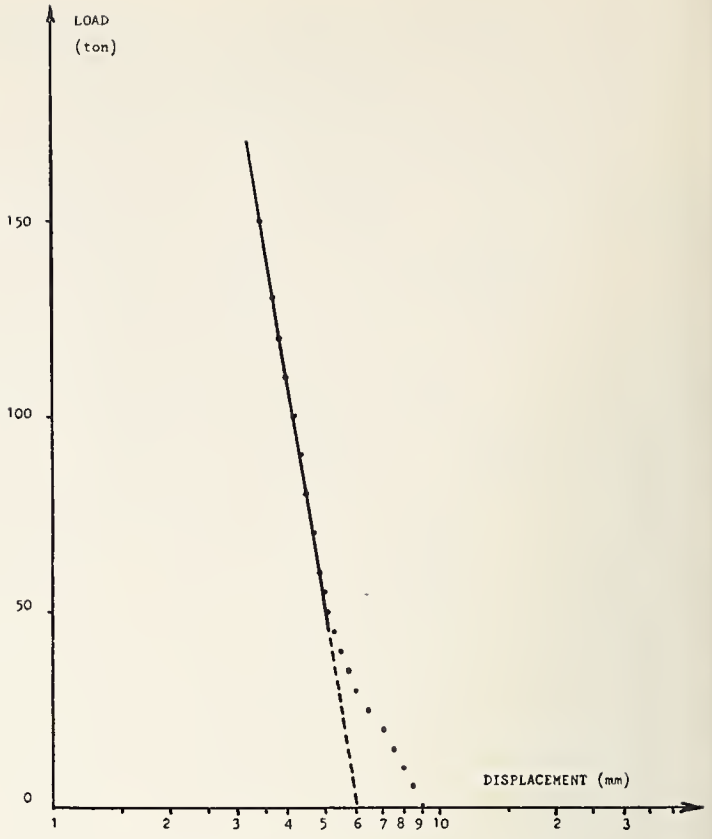

FIGURE 7. *Piston displacement curve.*

4. Discussion

4.1. Linear Extrapolation

As the true calibration curve must go to an asymptotic value when F goes to infinity, the linear extrapolation gives excess pressures. The lowest among those are gathered in table 4 together with the corresponding values of the four chosen scales A, B, C, and D.

TABLE 4. *Linear Extrapolation (pressures in kbar)*

Scales		*A*	*B*	*C*	*D*	Alined values
Bi 3→5	Nominal values	89	81	76.5	89.3	≤ 78 ± 2
	Extrapolated values	77.7	77.7	75.3	78	
Sn 1→2	Nominal values	115	107	92	(115)	≤ 104 ± 5
	Extrapolated values	118	108	118	118	
Fe α→ε	Nominal values	133	133	118	(133)	≤ 170 ± 17
	Extrapolated values	182	170	144	182	

The following remarks can be made:

(a) For the Bi 3–5 transition all these excess values are below the corresponding values of the scales. It is a striking case of inconsistency, at least for the scales *A*, *B*, and *D*. This results from the fact that the calibration curve of the present apparatus is nearly linear up to about 100 kbar.

The scale *C* is the more coherent.

(b) For the Sn transition the linear extrapolation does not reveal any inconsistency even if this extrapolation uses the scale value of the pressure transition of Bi 3–5.

(c) For the Fe transition the linear extrapolation gives a result which is very far off, even if the scale value of the pressure transition of Sn is used.

If a linear extrapolation is made through all the range the pressure transitions are found to be 78 ± 2 kbar for Bi 3–5, 104 ± 5 kbar for Sn, and 170 ± 17 kbar for Fe, which is certainly very far for the true value.

4.2. Exponential Extrapolation

The exponential extrapolation hopefully should give a better estimate of the transition pressures. Table 5 gives the calculated values.

The accuracy given next to each value takes into account the uncertainty of the pressure transition of Bi 1–2 (25.4 ± 0.1 kbar) of Tl 2–3 (36.7 ± 0.1 kbar) and of Ba using the latest value given by Kennedy [29] (55 ± 0.5 kbar), which fit better than others.

For the present apparatus, it turns out that by using the following transition pressures the calibration curve is nearly linear.

TABLE 5. *Exponential extrapolation (pressures in kbar)*

Scales		A–D	B	C
Sn	Nominal values	115	107	92
1→2	Extrapolated values	110	101.8	97.7
Fe	Nominal values	133	133	118
α→ε	Extrapolated values	–	150	106

Bi 1–2	Tl	Ba	Bi 3–5	Sn
25.4 ±0.1	36.7 ±0.1	55 ±0.5	78 ±2	102 ±4

The case of Fe is a little different because the nucleation of the transition seems to depend greatly upon the pressure gradients inside the cell, as shown by several people [26]. The present apparatus gives stresses which are of a less uniaxial character as a Drickamer or a Bridgman anvil, which might explain the high value found: 140 ± 15 kbar.[2] It thus appears that Fe does not constitute a good reference metal.

In order to fill up the gap in the high-pressure scale, it would be desirable to find another reference element such as germanium [30, 34].

5. Conclusions

With a "*X*-type anvil", inconsistencies in the high-pressure scales which are currently used have been revealed. A new pressure scale which fits better this apparatus has been established, which would locate the transition pressures of Bi 3 −5 at 78 ± 2 kbar and of Sn at 102 ± 4 kbar, and of Fe at 140 ± 15 kbar. However, many authors have discussed the influence of the apparatus shape, of sample shape (wire or ribbon), of the pressure-transmitting medium, of the pressure gradients on the nucleation of the allotropic transformations under high pressure. Thus the above conclusions may be valid only for the apparatus which was used. Rather than calibrating it would be better to evaluate the pressure at all times by the continuous change in the property of a material such as the lattice parameter with x-ray diffraction. Provided the equation of state of the material is theoretically known, an apparatus such as a hexahedral press built in our laboratory [31] should bring in the future interesting results.

[2] Recent experiments performed on iron and barium samples lying side by side in the high-pressure cell cast no doubt on the fact that the high barium transition definitely occurs at a much lower load than the iron transition, in our apparatus.

385-762 O - 71 - 20

6. References

[1] Bridgman, P. W., Proc. Am. Acad. Arts Sci. **74,** 425 (1942); Phys. Rev. **60,** 351 (1941).
[2] Bridgman, P. W., Proc. Am. Acad. Arts Sci. **81,** 165–251 (1952).
[3] Kennedy, G. C., and La Mori, P. N., J. Geophys. Res. **67,** 851 (1962).
[4] Balchan, A. S., and Drickamer, H. G., Rev. Sci. Instr. **32,** 308 (1961).
[5] Bancroft, D., Peterson, E. L., and Minshall, S., J. Appl. Phys. **27,** 291 (1956).
[6] Stark, W., and Jura, G., A.S.M.E. paper 64WA/PT–28 (presented at Winter Meeting, Nov./Dec. 1964).
[7] Bean, V. E., Master's Thesis, B.Y.U. (1964).
[8] Jeffery, R. N., Master's Thesis, B.Y.U. (1965).
[9] Stager, R. A., Balchan, A. S., and Drickamer, H. G., J. Chem. Phys. **37,** 1154 (1962).
[10] Klement, W., Jayaraman, A., and Kennedy, G. C., Phys. Rev. **131,** 632 (1963).
[11] Jeffery, R. N., Barnett, J. D., Vanfleet, H. B., and Hall, H. T., J. Appl. Phys. **37,** No. 8, 3172–3180 (1966).
[12] Lacam, A., Institut français des combustibles et de l'énergie.
[13] Vereshchagin, L. E., Zubova, E. V., Bujmova, I. P., and Burdina, Dokl. Akad. Nauk SSSR 169–174 (1966).
[14] Boy, F. R., and England, J. L., J. Geophys. Res. **65,** 741–748 (1960).
[15] Dieter, G. E., A.S.M. 279–340 (1960).
[16] Adler, P., and Margolin, H., Calibration experiments with a tetrahedral-type pressure apparatus, A.S.M.E. paper 62–WA–314 (1963).
[17] Bundy, F. P., Phys. Rev. **110,** 314 (1958); and from Modern Very High Pressure Techniques, ed.–R. H. Wentorf (1962).
[18] Hall, H. T., and Merrill, L., Inorg. Chem. **2,** 618 (1963).
[19] Giardini, A. A., and Samara, G. A., J. Phys. Chem. Solids **26,** 1523 (1965).
[20] Heydemann, P. L. M., J. Appl. Phys. **38,** No. 6, 2640–2644 (1967); Erratum, J. Appl. Phys. **38,** No. 8, 3424 (1967).
[21] Roux, C., Appareil pour hautes pressions à chambre cylindriqué, Private communication–C.E.A. (1965).
[22] Johnson, D. P., and Heydemann, P. L., Rev. Sci. Instr. **38,** No. 8, 1294–1300 (1967).
[23] Decker, D. L., J. Appl. Phys. **36,** No. 1 (1965).
[24] Stromberg, H. D., and Stephens, D. R., A.S.M.E. paper 64–WA/PT–13 (1964).
[25] Young, A. P., Robbins, P. B., and Schwartz, C. M., A.S.M.E. paper 62–WA–257 (Oct. 1963).
[26] Giardini, A. A., and Lloyd, E. C., High Pressure Measurement, Butterworths Press (1963).
[27] Bradley, R. S., High Pressure Physics and Chemistry, Acad. Press, London (1963).
[28] Contré, M., Compressibilité isotherme des milieux solides isotropes, Private communication (1963).
[29] Haygarth, J. C., Getting, I. C., and Kennedy, G. C., J. Appl. Phys. **38,** No. 12, 4557–4564 (1967).
[30] Evdokimova, V. V., Sov. Phys. USPEKHI **9,** No. 1, 54–72 (1966).
[31] Contré, M., French Patent, Dispositif pour engendrer de tres hautes pressions au sein d'un solide, Commissariat à l'Energie Atomique, France No. 1, 457, 690, 23/9/65–26/9/66.
[32] Contré, M., Enclume annulaire X, Private communication, C.E.A. (1967).
[33] Drickamer, H. G., and Minomura, S., J. Phys. Chem. Solids **23,** 451 (1962).
[34] Contre, M., French Patent, Appareil pour engendrer de très hautes pressions statiques au sein d'un solide hexaédrique, Commissariat à l'Energie Atomique, France No. 1, 395, 599, 6/12/63–8/3/65; U.S.A. No. 3, 261, 057.
[35] Contré, M., Enclume annulaire type MCX, Private communication, C.E.A. (1965).
[36] Schaufelberger, M., Diffractométrie de rayons X sous très hautes pressions, Private communication, C.E.A. (14/12/67).
[37] Schaufelberger, M., Compressibilité de l'hydrure de lithium, Private communication, C.E.A.

DISCUSSION

F. Bundy *(General Electric Research and Development Center, Schenectady, New York)*: I would like to respond to Dr. Contre's suggestion for using germanium as a calibration material near 120 kbar. Germanium does undergo a drop in resistance of 10^6 to 10^7, but my experience with it has been that the resistance change extends over an appreciable pressure range. For example, it may start falling at 110 kbar or even 105, and continue on up to a nominal 120 or 125 kbar. Thus, in my experience, it's too fuzzy for use as a calibration point. I have run germanium in the high-compression belt and in the Drickamer-type apparatus, and in both cases obtained a six orders of magnitude drop in resistance, but the change is spread out too much for a calibration point, in my opinion. Silicon is worse yet. Iron, apparently, is not much better.

I believe that you used the x-type anvil for the barium transition. I would like to ask how that result came out. I am interested because I have found the high barium transition to be a very sharp and satisfactory calibration point. The ones you showed looked quite sharp, and perhaps would fall on the curve quite well.

R. Roy *(Pennsylvania State University, University Park, Pennsylvania)*: May I recommend strongly against the use of the germanium transition. We have shown (Bates, Dachille, and Roy, Science **147,** 860 (1965) that Ge-I goes at stable equilibrium to Ge-III at less that 15 kbar at room temperature. Hence Ge-I is highly metastable in the 100 kbar regime, when it goes to Ge-II. While the transition may appear to be sharp, different samples will likely show different transition pressures in a manner similar to CdS which undergoes an analogous metastable transition. (Miller, Dachille, and Roy, J. Appl. Phys. **37,** 4913 (1966).

On Application of Mercury Melting Curve for Accurate High-Pressure Measurements

V. S. Bogdanov, Yu. L. Levin, S. S. Sekoyan, and Yu. I. Shmin

All-Union Research Institute for Physical and Radiotechnical Measurements, Moscow Region, Mendeleevo, U.S.S.R.

The successful solution of the problem of high-pressure measurement up to several hundreds of kilobars is based on the further extension of the range and the improvement of accuracy of hydrostatic pressure measurements. The maximum hydrostatic pressure achieved at present is limited to 50 kbar, while the maximum pressures that can be reliably measured by means of free piston gages do not exceed 25 kbars.

The long-term experience of VNIIFTRI in the research of the melting process under pressure shows that the above-mentioned problem can now be solved most successfully on the basis of the mercury melting curve equation as it was suggested by Zhokhovsky as far back as 1957 [1].[1] One of the merits of this method lies in the fact that under certain conditions the process of mercury melting is an equilibrium one, and can be reproduced to a high degree of accuracy. Besides the relation between pressure and temperature (measured quantity) may be represented by the universal Simon interpolation equation [2]

$$p = a\left[\left(\frac{T}{T_0}\right)^c - 1\right] \qquad (1)$$

where a and c are empirical constants and T_0 the temperature of the triple point. This equation was derived and studied in a number of investigations [3–7].

Some substances such as Rb, Cs, KNO_3, and KNO_2 however have a maximum in the melting curve and the Simon equation fits experimental data on these substances only up to pressures about 0.5 Λ (where Λ is pressure of the maximum). Therefore, the Simon equation with parameters chosen to fit experimental data in limited pressure range cannot be extrapolated to any high-pressure value.

For the development of the precision method for measuring high hydrostatic pressures up to 50 kbar based on the mercury melting curve (MMC), it is necessary to solve the following two problems:

1. The proper choice of the reliable equation for the MMC in the pressure range where free piston gages may be used.

2. Substantiation of extrapolation of chosen equation to higher pressures.

To solve both problems one needs more detailed information on the melting under pressure, and in particular the data on the volume change along the melting curve. The investigation of the volume change during melting permits one to prove experimentally the equilibrium character and reproducibility of the melting process under pressure, and reveal possible peculiarities on the melting curve.

1. The MMC Equation

The apparatus, procedure, and results of the first experiments on establishing the MMC equation are described in [8]. The experiments were carried out up to 10 kbar, pressure being measured by means of manganin gage calibrated against a free piston gage.

The later and more accurate experiments were performed on the apparatus described in [9]. In this case the measurement of P-T data was carried out together with the measurements of the volume change, the pressure up to 15 kbar being measured by a free piston gage. In addition there were used several piston-cylinder systems with different clearance developed in VNIIFTRI and Mendeleyev Metrology Institute (VNIIM). All experiments were carried out in accordance with the results of the studies of free piston deformation errors [10].

All results are divided into five sets which characteristics are given in table 1.

The analysis of the measurement errors was made by the method suggested by Dr. Dolinsky (VNIIM) and the results obtained for 281 points were processed by a computer. As a result the parameters of the Simon equation were obtained:

$$P = 39016\left[\left(\frac{T}{234.29}\right)^{1.1772} - 1\right]. \qquad (2)$$

Standard deviations of a and c are

$$\sigma\ (a) = 20\ (\mathrm{kg/cm^2}),\ \sigma(c) = 5 \cdot 10^{-4}.$$

The dispersion analysis makes it possible to estimate the validity of the relation chosen for its extrapolation to higher pressures. Table 2 summarizes standard deviations of pressure measurements $\sigma(p)$, calculated from possible errors of temperature measurements δT in different temperature intervals.

[1] Figures in brackets indicate the literature references at the end of this paper.

Paper presented at the Symposium on Accurate Characterization of the High-Pressure Environment, held at the National Bureau of Standards, Gaithersburg, Md., October 14–18, 1968.

TABLE 1

Set	Year	Pressure range	Relative error of pressure measurements	Temperature measurement error	Number of measurements	Pressure-measuring instrument
		kbar	*percent*	°C		
1	1963	0.7–15	0.35	±0.25 in the range (−35–0°C) ±0.1 in the range (0–35°C)	44	Manganin gage calibrated against free piston gage.
2	1964	0.7–15	0.1 in the range 0.7–8kbar 0.2 in the range 8–15 *k*bar	the same	116	VNIIFTRI free piston gage with re-entrant cylinder average clearance $h=6.6$
3	1965	2–15	.....do.....	±0.05	37	The same, with $h=6.3$ and $h=9.6$
4	1966	1.5–15	.....do.....	±0.05	34	The same, with $h=6.6$ and $h=11.4$
5	1967	7–15	.....do.....	0.01 in the range 0–20°C 0.05 in the range 20–30°C	50	VNIIM free piston gage with conventional cylinder.

TABLE 2

T, °C	−13.56	11.29	36.80	59.94	83.76	107.31	130.64	153.70
δT °C	±0.05	±0.05	±0.05	±0.05	±0.05	±0.1	±0.75	±1.0
P, kbar	5	10	15	20	25	30	35	40
$\sigma(p)$, bar	7	11	16	22	27	34	97	130
$\sigma(p)$, percent	0.15	0.11	0.11	0.11	0.11	0.11	0.28	0.33

$\sigma(p)$ does not change appreciably up to 40 kbar. At 40 kbar, $\sigma(p)$ is equal to 0.33 percent providing that temperature 154 °C is measured with an accuracy ±1 °C. (In practice this error can be reduced to ±0.2 °C by allowing for pressure dependence of the thermocouple e.m.f.)

It should be noted that in parallel with the determination of the melting P-T data, precision measurements of the freezing pressure of mercury at 0 °C were carried out, temperature measurement errors being about 0.002 °C. The results of the measurement sets were found to be as follows:

1965 — 7719 kg/cm²,

1966 — 7721 kg/cm²,

1967 — 7725 kg/cm²

(eq (2) gives 7725.2 kg/cm²).

The discrepancy in mercury point values turned out to be unexpectedly large, and apparently cannot be explained by the experimental errors. The cause of this discrepancy is not yet established and the experiments will be repeated soon with the best possible accuracy and utmost care.

If similar measurements were also carried out in other national laboratories, the comparison of data would provide the most reliable value of this very useful reference point. On the other hand, the results of such measurements may be considered as a mutual comparison of the national pressure scales at this point that in itself is of great importance.

2. Studies of Extrapolation of Eq (2) to 40 kbar

The estimation of accuracy and reliability of the extrapolated P-T equation can be made by comparison of the data obtained from measurement of physical phenomena of different nature. The following phenomena were chosen: the pressure dependence of electric resistance of pure metals and alloys and pressure dependence of the NaCl lattice parameter.

The validity of the equation can be also estimated from theoretical considerations of this equation and results of measurements of the volume change ΔV along the melting curve.

2.1. The Volume Change Along the MMC

The analysis of P-T melting data for substances having a maximum (T_{max}) in the melting curve shows that parameters of the Simon equation selected at the low-pressure section of the curve fit the experimental data up to $p(T_{max})/2=\Lambda/2$. Thus, if it is proved that the maximum in the MMC lies far beyond 40 kbar this will be the confirmation of correctness of extrapolation, providing no triple points exist all over pressure range.

It follows from the Clapeyron-Clausius equation

$$Tdp/dT=\lambda/\Delta V \tag{3}$$

that the maximum in the melting curve $T=f(p)$ may exist only when the volume change ΔV becomes zero (if latent heat of melting $\lambda \neq 0$).

According to Bridgman [11] the pressure dependence of ΔV of mercury is convex to the pressure axis but all other 29 substances exhibit concavity to the pressure axis. Since the solution of the problem of extrapolation requires the knowledge of exact behaviour $\Delta V=f(p)$ and $\Delta V=f_1(T)$, the measurements of ΔV were repeated. These measurements were carried out on the same apparatus that was used in studies of P-T melting parameters. For this purpose the apparatus was equipped with the special gadget. Its full description and the measurement procedure to obtain p-ΔV-T data are given in [12].

P-ΔV-T data were also obtained for benzene, nitrobenzene, and cesium up to 17 kbar [12–14]. The experiments indicated that melting of benzene, nitrobenzene, and partly cesium takes place within small finite pressure range ($T=$ const.). This range increases with pressure. In case of mercury melting process takes place at a strictly constant pressure over the entire range studied.

At the same time the experiments indicated that the volume change ΔV of mercury may vary considerably (up to 30 percent) for the same p and T values. The investigations established the direct relationship between the conditions of freezing and ΔV values [13]. Obviously this factor may account for the anomaly in the mercury ΔV dependence which was observed by Bridgman [11].

It was shown that the mercury volume change ΔV behaves in the manner similar to all other substances investigated. The pressure and temperature dependence of ΔV can be accurately represented by the empiric equations

$$\Delta V=0.01028-7.354\times 10^{-4}\ln\ (37.667+p) \tag{4}$$

and

$$\Delta V=0.0253-7.54\times 10^{-4}\ln\ (T/234.3). \tag{5}$$

From eq (4) it follows that the volume change becomes zero at about 1,000 kbar. We believe this can be regarded as a confirmation of the fact that extrapolation of eq (2) to 40 kbar is justifiable.

Eq (3) may be used for the estimation of accuracy of extrapolation. From P-ΔV-T measurements it is possible to assume that providing there are no triple points on the fusion curve, the function $\lambda/\Delta V=f(p)$ together with its first and second derivatives is a smooth continuous function of pressure, and at the maximum point ($p=\Lambda$) the following conditions are realized:

$$\Delta V(\Lambda)=0, \tag{6}$$

$$\left.\frac{\partial \Delta V}{\partial p}\right|_{p=\Lambda} \neq 0,$$

$$\lambda(\Lambda)\neq 0.$$

This means the function $\lambda/\Delta V=f(p)$ has a pole of the first order at the point Λ. So, keeping the general nature of eq (3), it can be written as

$$T\frac{dp}{dT}=\frac{\Lambda^n}{\Lambda^n-P^n}\cdot[\alpha+\beta P+\gamma(P)P^2]^* \tag{7}$$

where n, α, and β are integer parameters and $\gamma(p)$ an unknown function having no peculiarities. To estimate the accuracy of the extrapolation of the Simon equation for mercury it is sufficient to approximate $\gamma(p)$ to a constant ($\gamma(p)=\gamma_0$). Eq. (7) then takes the form

$$T\frac{dp}{dT}=\frac{\Lambda^n}{\Lambda^n-P^n}(\alpha+\beta P+\gamma_0 P^2). \tag{8}$$

The approximating capabilities of eq (8) were studied for cesium in the range from 1 kbar to $p=\Lambda$ [14, 15]. Deviations from the experimental data did not exceed 1 percent. Therefore, we can consider γ_0 to be a good approximation of the $\gamma(p)$ function for the whole pressure range studied with an accuracy not more than 1 percent. The γ_0 for mercury is found from experimental P-T data up to 15 kbar. Since Λ is estimated to be about 1,000 kbar, it is possible to eliminate from eq (8) the parameters relating to the maximum pressure without introduction of any essential errors.

Applying the obtained equation to experimental data up to 15 kbar, we find

$$\gamma_0=-3.6\times 10^{-7}\ \text{cm}^2/\text{kg}. \tag{9}$$

Using the well-known theorem of differential estimates [16] we can evaluate the deviation of the Simon equation from the exact melting curve up to 40 kbar. The calculations give

$$(\Delta p/p)\cong 1\ \text{percent}. \tag{10}$$

2.2. Electric Resistance of Metals and Alloys

The simple empirical way to confirm the correctness of extrapolation is provided by comparison of the MMC equation with the readings of some resistance gages which characteristics were carefully studied for many years [20–22], and one gold resistance gage.

The equipment, procedure and measurement results at 25 kbar are described in [17]. The comparison between the MMC equation and the readings of five resistance gages were carried out in 60 points evenly spaced in the range from 7 to 25 kbar. In most cases the results agree within ± 0.35 percent.

*The solution of eq (7) at $\gamma(P)=0$ and $P<<\Lambda$ is the Simon equation.

Similar experiments were performed with a gold resistance gage up to 40 kbar [19]. The pressure dependence of gold resistance was expressed by a semi-empiric equation taken from [23]. The parameters of the equation were determined from the results of calibration against a free piston gage. The comparison of the readings was performed at 6 points. The divergence of the data did not exceed 0.5 percent.

2.3. Equation of State for NaCl.

The MMC equation (2) was also compared with experimental data based on the equation of state for NaCl [24]. There were no attempts to intercompare directly these methods. The indirect comparison of the equation of state for NaCl with the MMC equation can be carried out by using experimental data up to 70 kbar obtained by Klement [25].

Klement's data were obtained at the quasihydrostatic apparatus that was apparently calibrated using the phase transition points in Tl II-III (~37 kbar) and Ba I-II (~60 kbar) that were taken from [26].

Jeffery and others [24] investigated the same phase transitions by the X-ray technique on the basis of the Decker's theoretical equation of state for NaCl. They reported the values 34.6 kbar and 53.3 kbar. The comparison of extrapolated MMC equation (2) with the data obtained by Klement [25] shows the same discrepancies as those between the pressure values of phase transitions determined by the two methods mentioned above. This fact may serve as an argument in favor of the MMC extrapolation equation (2). At the same time such large discrepancies cannot be ignored, so the careful analysis of the methods used for pressure determination is needed.

In our opinion the experimental error of the X-ray diffraction technique cannot be the reason for such large discrepancies. Since the pressure measurement errors in instruments of the piston-cylinder type are difficult to analyse, we tried to evaluate the merits of the equation suggested by Decker [27].

The Decker theoretical equation of state is the only microscopic equation intended for use in high-pressure measurements. To evaluate this equation we suggest another equation of state for NaCl based on the same assumptions as those of Decker but differing from the latter in the following principal features:

(1) It does not take into account Van-der-Valls interactions for they play a secondary role in comparison with both Coulomb interactions of spherically symmetric rigid ions and non-Coulomb interactions of the nearest neighbours in the lattice and can be compensated by a variation of the non-Coulomb interaction parameters [27]. Following Ghate [28] the potential energy of N elementary cells of crystal is presented in the form

$$\Phi = N\left[-\frac{Aq_{\text{eff}}^2}{2} + 6b\left(e^{-\frac{r}{\rho}} + 2e^{-\frac{\sqrt{2}\cdot r}{\rho}}\right)\right] \qquad (11)$$

where A is Madelung constant, $q_{\text{eff}} = q \cdot \epsilon$, effective ion charge, q-electron charge, r-distance between the nearest neighbours, ϵ, b, ρ unknown parameters of the theory.

(2) The parameters ϵ, b, and ρ and parameter λ which takes into account the pressure dependence of the Gruneisen constant γ[27] are determined from the latest experimental data on the effect of hydrostatic pressure on the isothermal modulus of bulk compressibility B_T. Such a choice of parameters, that is, the choice in terms of elastic and not thermal characteristics of the crystal, is more reasonable than that used in [27], since ion crystal models on which both equations of state are based, have limited possibilities to be used for discription of all thermal and mechanical properties of the crystal. Here we determined parameters of the theory from the equation of state (at $p_0 = 1$ bar, $T_0 = 298$ °K, $r_0 = 2.8205 \times 10^{-8}$ cm [27]) and conditions of coincidence of the calculated values.

$$B_{T_0} = \left\{-V\left(\frac{\partial p}{\partial V}\right)_T\right\}_{T_0, r_0}, \left(\frac{\partial B_T}{\partial p}\right)_{T_0}, \left(\frac{\partial B_T}{\partial T}\right)_{p_0}$$

with the corresponding experimental values. The equation so obtained has less unknown theory parameters and secondary interactions not covered by the present analysis, are effectively accounted for by a comparatively small number of theory parameters.

For determination of ϵ, b, ρ, and λ we selected the following initial values:

$$\left(\frac{\partial B_S}{\partial p}\right)_{T_0} = 5.38 \text{ and } B_{T_0} = 2.523 \times 10^{11} \text{ dyne/cm}^2, \qquad [28]$$

(here B_s is adiabatic modulus of bulk compressibility), which are most reliable as judged from the latest literature references.

The values $(\partial B_T/\partial p)_{T_0} = 5.46$ and $B_{T_0} = 2.396 \times 10^{11}$ dyne/cm^2 we used in the calculations were derived from [28] using the data from [29]. The value $(\partial B_T/\partial T)_{p_0} = -0.159 \times 10^9$ dyne/cm^2 was also taken from [29]. The values of the Debye temperature and γ_0 are the same as in [27].

By solving the system of four equations with four unknown quantities (ϵ, b, ρ, λ) the following parameter values were obtained: $\epsilon = 1.00288$, $b = 2.53982 \times 10^{-9}$ ergs, $\rho = 0.301719$ Å, $\lambda = 6.25$.

According to the data obtained $q_{eff} = \epsilon\, q$ is very close to q, as it is usually assumed for the crystals of NaCl type.

The value of the parameter λ differs greatly from the Decker value $\lambda = 2.55$, but is in good agreement

with $\lambda=6$ derived from the experimental data given in [30].

The coefficient of thermal expansion α calculated from the Gruneisen equation [31] was found to be 11.73×10^{-5} deg^{-1} that is close to the experimental value 12.09×10^{-5} deg^{-1} [29].

The agreement of the calculated values of elastic constants of the second and third order with experimental data carried out in [33–35] was also satisfactory. All this testifies to the applicability of our model to the description of the elastic properties of NaCl.

The equation of state obtained for NaCl was compared with the Decker equation up to 150 kbar. The comparison showed that the data practically coincide up to 60 kbar. At 150 kbar the divergence of data is about 5 percent. The pressures of the phase transitions in Tl II-III and Ba I-II calculated on the basis of our equation have coincided with those determined from the Decker equation. Hence, the pressure values of the phase transitions Tl II-III and Ba I-II obtained experimentally by Jeffery and others [24] seem to be more reasonable.

If appropriate corrections are introduced into the Klement's data on the MMC, the agreement of his corrected data will coincide within experimental errors with those calculated from eq (2). Such an agreement is an additional confirmation to the correctness of extrapolated eq (2) even over 40 kbar.

As to the theoretical analysis of the equation of state for NaCl it shows that X-ray diffraction may find wide usage in high-pressure measurements.

3. Conclusions

1. On the basis of the experimental data up to 15 kbar the MMC eq (2) is obtained. This equation is recommended for pressure measurement in the range from 7 to 40 kbar.

2. The errors of extrapolated eq (2) are estimated not to exceed 1 percent up to 40 kbar.

4. References

[1] Zhokhovsky, M. K., Izmeritel'naya Tekhnika (Measuring Technique), No. 2, 1 (1957).
[2] Simon, S. E., Glatzel, G., Z. für Anorg. Allgem. Chemie **178**, 309 (1929).
[3] Domb, C., Phil. Mag. **42**, 1316 (1951).
[4] de Boer, J., Proc. Roy. Soc. **A215**, 4 (1954).
[5] Gilvarry, J. J., Phys. Rev. **102**, 308 (1956).
[6] Babb, S. E., J. Chem. Phys. **38**, 2743 (1963).
[7] Babb, S. E., Rev. Mod. Phys. **35**, 400 (1963).
[8] Zhokhovsky, M. K., Izmeritel'naya Tekhnika No. 5 (1955).
[9] Bogdanov, V. S., Izmeritel'naya Tekhnika, No. 8 (1967).
[10] Bakhvalova, V. V., Proc. Inst. of Comm. on Stds. **104**, No. 164, 21 (1969).
[11] Bridgeman, P. W., Proc. Am. Acad. **47**, 347 (1912).
[12] Zhokhovsky, M. K., and Bogdanov, V. S., J. Phys. Chem. (USSR), **39**, 2520 (1965).
[13] Bogdanov, V. S., ibid. **40**, 2779 (1966).
[14] Bogdanov, V. S., JETR Letters **3**, 44 (1966).
[15] Kennedy, G. C., Jayaraman, A., and Newton, R. C., Phys. Rev. **126**, 1363 (1962).
[16] Kamke, E., Handbook of differential equations (Moscow, 1961).
[17] Zhokhovsky, M. K., and Razumikhin, V. N., Izmeritel'naya Tekhnika, No. 4, 43 (1957).
[18] Zhokhovsky, M. K., et al., Izmeritel'naya Tekhnika, No. 11, 26 (1959).
[19] Bogdanov, V. S., and Miroshnikov, A. P., Proc. of the Institutes of the Committee on Standards, **104 (164)** (1968).
[20] Burova, L. L., and Zolotykh, E. V., ibid. **46 (106)**, 62–67 (1960).
[21] Alexeyev, K. A., and Burova, L. L., ibid. **75 (135)**, 1 (1969).
[22] Burova, L. L., ibid. **104 (164)** (1968).
[23] Decker, D. L., and Vanfleet, H. B., Phys. Rev. **138**, 129 (1965).
[24] Jeffery, R. N., Barnett, J. D., Vanfleet, H. B., and Hall, H. T., J. Appl. Phys. **37**, 3172 (1965).
[25] Klement, W., Jayaraman, A., and Kennedy, G. C., Phys. Rev., **131**, 1 (1963).
[26] Kennedy, G. C., and LaMori, P. N., in Physics at High Pressure, Solid State Physics, Vol. **11** (New York and London, 1960).
[27] Decker, D. L., J. Appl. Phys. **36**, 157 (1965).
[28] Ghate, P. B., Phys. Rev. **139**, No. 5A, A1666 (1965).
[29] Powell, B. E., and Skovo, M. J., J. Appl. Phys. **38**, No. 1, 404 (1967).
[30] Bartels, R. A., and Shule, D. E., J. Phys. Chem. Solids **26**, 537 (1965).
[31] Born, M., and Kun, H., Dynamical Theory of Crystal Lattices (Clarendon Press, Oxford, 1954).
[32] Yates, B., and Panter, C. H., Proc. Phys. Soc. **80**, 373 (1962).
[33] Chang, Z.-P., Phys. Rev. **140**, No. 5A, A1788 (1965).
[34] Swartz, K. D., J. Acoust. Soc. Am. **41**, No. 4, Part 2, 1083 (1967).
[35] Gluyas, M., Brit. J. Appl. Phys. **18**, 913 (1967).

DISCUSSION

J. L. Cross (*National Bureau of Standards, Washington, D.C.*): It is necessary, of course, to wait a sufficient time to dissipate the latent heat. In the actual initiating of the freezing you usually have to take the pressure above the freezing point to get a seed crystal started. But once the seed crystal is started and the system allowed to come to equilibrium, the reproducibility is excellent. In the free, long duration runs that I made using two different methods for observing the existence of two phases, there was a spread of two-thirds of a bar. And for a period of 21 hours on one run where the two phases were maintained in equilibrium, the total variation in observed pressure at zero degrees, was about three-tenths of a bar.

P. N. LaMori (*Battelle Memorial Institute, Columbus, Ohio*): I would like to comment on the value of 60 kbars for the barium I-II transition, that you quote from the paper by Kennedy and myself (ref. 26). The barium point data was included in the paper as a value that we reached on one experiment just on entering the high pressure region. There was no

real attempt to determine that 60 kbars was the maximum value. All the other values in the experiment were determined both on the compression and the release strokes. So I think that you should not make a comparison between this value and results of experiments by Klement (ref. 25).

AUTHORS' CLOSURE

In agreement with comments by Mr. Cross we want to say that in our experiments the equilibrium pressure was reproducible within 0.5 bar. Obviously this variation is mainly due to the variations of temperature and manganin gage readings. In our opinion this high degree of reproducibility may be effectively utilized in the establishment of the high pressure scale. Such scale based on mercury melting curve would make all the measurements throughout the high pressure laboratories comparable, consistent and uniform.

In reply to Dr. LaMori, in the paper by Klement and co-workers [25] there is no direct indication on the actual values of fixed points used in calibrations of their apparatus. From the references given in their paper however one can suggest that Ba I-II point was taken equal to ~ 60 kbars. That is why we referred to the paper [26].

High-Pressure Scale as Determined by X-ray Diffraction Techniques up to Approximately 100 kbar

H. Tracy Hall

Brigham Young University
Provo, Utah 84601

1. Post-Bridgman Pressure-Scale Muddle

I suppose as much blame can be placed on me as on anyone for the pressure-scale muddle of the emerging post-Bridgman era. No doubt the first Ba transition observed outside of Bridgman's laboratory was observed in February of 1954 in my Belt apparatus [1].[1] Due to secrecy, these results could not be published until six years later. Meanwhile, I had managed to circumvent the Belt secrecy by the invention of the Tetrahedral Press [2]. The published calibration for this apparatus (anvil load versus pressure) used fixed points of 25, 44, 54, and 79 kbars (Bridgman's resistance points) for Bi, Tl, Cs, and Ba transitions. (NOTE: Previous work expressed in kg/cm^2 and atmospheres has been converted to kilobars in this paper). This precedent was followed by others until Prof. George C. Kennedy, at the June 1960 International High Pressure Conference held at Bolton Landing, Lake George, New York, conveyed the unsettling news that Bridgman's "resistance fixed points" were too high and should be lowered to Bridgman's "corresponding volume fixed points."

Kennedy's insight ran ahead of the experimental evidence. In hindsight one might possibly say Bridgman recognized that certain of his resistance points corresponded to lower volume points. However, a study of the crucial paper "The Resistance of 72 Elements, Alloys and Compounds to 100,000 kg/cm^2" [3] will impress the reader that Bridgman was certain that the pressures given for his electrical resistance transitions were correct.

2. Identity of Resistance and Volume Transitions Established

In view of the Nobel Laureate's 50 years of accomplishment in the field, it would have been imprudent to challenge Bridgman's results without some definitive experiments. A definitive experiment would be one in which the volume transition and the electrical resistance transition were simultaneously observed in the same sample specimen. The shapes of the resistance curves in the regions of the fixed points (for example in Tl, Cs, Ba, etc.) are very characteristic and if these were found to occur simultaneously with the volume transition, a one-to-one correspondence between the transitions, i.e., an identity, would be established.

The first one-to-one correspondence to be established at pressures beyond 30 kbar was in the instance of Ba. This work took place in the Brigham Young University high-pressure laboratory at Provo. A tetrahedral x-ray diffraction press was employed for this purpose [4]. With this equipment, the electrical resistance of Ba foil was monitored (at room temperature) simultaneously with the monitoring of its Debye-Scherrer diffraction pattern as pressure was slowly increased [4, 5]. As this was done, the characteristic electrical resistance pattern described by Bridgman [6] with an abrupt increase in electrical resistance at 70 kbar (Bridgman's resistance value) was found.

A new x-ray diffraction pattern appeared simultaneously with the crossing of this resistance discontinuity. Compressions determined 3 kbar above and 10 kbar below the discontinuity by x-ray diffraction were each only 4 percent higher than those determined from Bridgman's data [7]. (Bridgman determined his volume transition to occur at 59 kbar). The x-ray determined change in compression at the transition was the same as found by Bridgman. In addition, the overall Ba compressibility curve determined by x-ray matched a corresponding curve plotted from Bridgman's compression data quite well if a value of 59 kbar were selected for the Ba transition pressure. This furnished compelling evidence that the 79 kbar resistance and 59 kbar volume transitions were one and the same and that the correct transition pressure was about 59 kbar.

In addition to establishing the identity of the resistance and volume transitions, the x-ray work indicated the 59 kbar transition to be from the normal body-centered cubic symmetry to a hexagonal close packed symmetry with cell parameters of $a = 3.90$ Å, $c = 6.15$ Å, and $c/a = 1.58$ at about 3 kbar above the transition pressure.

Even though the above research constituted the first experimental evidence that the electrical resistance transition pressures should be lowered, most high-pressure researchers had already assumed the identity of Bridgman's 44. 54, and 79 kbar resistance transitions with his 40, 44, and 59 kbar volume transitions in Tl, Cs, and Ba respec-

[1] Figures in brackets indicate the literature references at the end of this paper.

Paper presented at the Symposium on Accurate Characterization of the High-Pressure Environment, held at the National Bureau of Standards, Gaithersburg, Md., October 14–18, 1968.

tively. Also, they assumed the volume transitions to give the approximately correct pressure values. This decision may have been influenced by P. W. Bridgman himself. It has been reported that at a Gordon Conference on High Pressure held shortly after the Bolton Landing Conference, Bridgman indicated that the pressures of discontinuities in the resistance as given in his 1952 paper were not suitable to use as fixed reference points for pressure calibration. There are no written reports of Gordon Conference proceedings and I did not attend that particular conference; consequently my information on this point is only hearsay.

Irregardless, subsequent high-pressure x-ray diffraction work has established resistance-volume change correspondences for transitions in Tl, Cs, Yb, Bi, and other metals that have been used as pressure fixed points. In all instances it has been necessary to decrease the transition pressure of Bridgman's electrical resistance transitions.

3. Establishment of Continuous Pressure Scale by X-ray

After the one-to-one correspondence between the resistance and volume transitions had been established, one could focus attention on the problem of obtaining better values for the fixed points. Of particular interest, in this connection, are the Bi III-V and Ba I-II transitions which Bridgman had established (by volume change) to occur at 88 and 59 kbar respectively.

It would be very useful to have some type of pressure calibrant that would give continuous readings. Fixed points might then be compared to this. Such a calibrant might be based on the atomic separation of the atoms of a simple substance, said separation being determined by x-ray diffraction techniques. A simple substance for which the compression can be predicted with some degree of certainty is NaCl. Jeffery, Barnett, Vanfleet, and Hall—using the previously mentioned tetrahedral x-ray diffraction press and an equation of state developed by D. L. Decker—used this approach [8]. In this work, Bi or Ba metal was imbedded in polycrystalline NaCl and the transitions were detected by the electrical resistance change of the metal while the lattice parameter of the adjacent NaCl was simultaneously measured by x-ray diffraction. The Ba I-II and Bi III-V transformations at room temperature were assigned values of 53.3 ± 1.2 kbar and 73.8 ± 1.3 kbar, respectively, corresponding to NaCl linear compression values of

$$\Delta a/a = 0.0510 \quad \text{and} \quad 0.0637.$$

These values were 9.4 and 16.2 percent smaller than Bridgman's volume values and were, at first, treated with reserve and skepticism. However, recent personal communications from other laboratories give similar values. They are listed below together with the B.Y.U. values. All x-ray values have been corrected to Decker's improved equation of state of NaCl [9].

*Laboratory**	*Method Used*	*Ba I-II, kbar*	*Bi III-V, kbar*
B. Y. U.	X-ray tet. press	54.4 ± 1.2	75.6 ± 1.3
Naval Res. Lab.[a]	X-ray tet. press		75.0
Westinghouse[b]	X-ray tet. press		
Nagoya U.[c]	"Bridgman Anvils"		76 ± 4
U.C.L.A.[d]	Piston-cylinder, vol.	55.0 ± 0.5	77.5 ± 1.0
Signal Corps, Ft. Monmouth[e]	Manganin gage	56.3	

The B.Y.U., Naval Res. Lab., Westinghouse, and Nagoya U. values all depend on Decker's equation of state for NaCl. At this juncture, the agreement among the above parties has been narrowed to about ± 3 percent. There is a Russian determination of the Ba and Bi transition in a free piston gage, for which no experimental details are supplied, of 58.5 and 89.3 kbar ± 1 percent [10]. This appears to be the only holdout for Bridgman's resistance values at the present time.

The work of Kennedy and his colleagues at U.C.L.A. and of Zeto and colleagues at Fort Monmouth is commendable in that they are using non-x-ray approaches to pressure-scale problems. Full confidence in a pressure scale will only be achieved when data from several different approaches are in agreement. Kennedy is attempting to push the pressure limit of piston-cylinder apparatus toward 100 kbar and measure volume changes, by piston displacement. Vanfleet and Zeto are utilizing a manganin wire gage immersed in a true liquid within a large pyrophyllite cubic pressure cell. The manganin gage is accurately calibrated to the Hg and Bi I-II transitions, fit by a quadratic equation, and extrapolated to higher pressures.

4. Improved X-ray Diffraction Presses

The tetrahedral x-ray diffraction press in use at B.Y.U. was designed years ago. Several improvements that could be made, particularly if the objective is to establish a pressure scale. Incidentally, duplicates of the B.Y.U. press are installed at Commissariat a l'Energie Atomique, Paris, and also at the Iron and Steel Institute of Tohoku University, Sendai, Japan. The design of these presses was completed before the invention of "anvil guide" [11]. Correct anvil position and sample location with respect to the x-ray beam are, therefore, more difficult to achieve than in presses equipped with anvil guide.

I have designed a tetrahedral press with anvil guide for use with x-ray diffraction. Two devices

*Courtesy of (a) Perry Ahlers, (b) A. Taylor, (c) H. Mii, (d) G. C. Kennedy, (e) H. Vanfleet.

of this design have been built by McCartney Manufacturing. One is located at the Westinghouse Monroeville, Pennsylvania, Laboratory; the other at the U.S. Bureau of Mines Laboratory, Albany, Oregon.

Years of experience at B.Y.U. with tetrahedral and cubic presses show that tetrahedral presses can achieve the highest pressures with the least anvil breakage. Pressures of 120 kbar on Decker's volume scale have been obtained with ¼ in (6.3 mm) on edge triangular-faced tetrahedral anvils.

Because of its higher pressure capabilities, I would choose the tetrahedral press over the cubic press in any new design for x-ray diffraction work. A new design for pressure-scale work should be built with increased ruggedness and with the highest possible precision. The stretching of the tie-bar frame under load introduces correction factors in former tetrahedral x-ray presses because the x-ray tube, goniometer track, etc., are attached to different parts of the frame. This could be eliminated in new presses based on the "ram-in-tie-bar" type equipped with the "sure-guide" mechanism [12]. In such a press, all the x-ray equipment could be mechanically connected to the "sure-guide" frame, which remains in fixed position with respect to the exact center of the press under any load. Such a press, specifically designed with pressure scale research in mind, could be built for about $50,000 (exclusive of x-ray diffraction equipment).

5. Improvement of Solid Pressure Media

In addition to excellent prospects for the improvement of high-pressure diffraction apparatus to provide more precise and accurate measurements relating to the pressure scale, there are good prospects for improving solid pressure-transmitting media. It is known that the media surrounding a wire of a fixed-point calibrant (such as Bi) influences the pressure required for onset and completion of a transition and also influences the hysteresis connected with the reverse transition. For example, Davidson and Lee [13], using a liquid media, have measured a hysteresis of from 0.55 to 0.90 kbar for the Bi I-II transition. On the other hand, Jeffery, Barnett, Hall, and Vanfleet [8] measure an average hysteresis of 5.3 kbar for a cylindrical 0.010-in-diam wire and of 2.8 kbar for a 0.002-in-thick flat strip surrounded by NaCl. Keep in mind that the pressures in the latter work were determined from atomic spacings in the NaCl *immediately adjacent* to the Bi wire or strip. Various explanations have been offered as to why transition sluggishness and hysteresis are always greater in solid media. Regardless of the explanations, the large hysteresis is undersirable. Ideally, both the NaCl and the Bi wire should be immersed in a true hydrostatic fluid in the x-ray work. For the most part, this is impractical. However, it should be possible to obtain a closer experimental approximation to the ideal situation than that of a Bi wire embedded in polycrystalline NaCl. For example, NaCl powder could be mixed with an excess of powdered material which possessed a lower coefficient of shear friction than NaCl. This mixture could then serve as the matrix for embedding the Bi or other wire. The material admixed with the NaCl must, of course, be sufficiently transparent to x-rays and meet other requirements pertinent to the experiment at hand. At 25 kbar, our shear friction measurements with rotating Bridgman anvils show NaCl powder to have a friction coefficient of 0.12. Boron nitride powder and graphite powder have coefficients of 0.07 and 0.04 respectively. Mica sheet has a coefficient of 0.07. In powdered form, mica would have an even smaller coefficient. The coefficient for powdered polyethylene is not known but should be lower than that for NaCl. The friction coefficient for NH_4F has not been measured but extrusion experiments at high pressure indicate it to be very low. If a search were conducted, no doubt a great many materials would be found with shear friction coefficients well below that of NaCl.

While solid pressure-transmitting substances offer many practical advantages in all types of high-pressure experiments, there still seems to be some unknown if not mysterious factors connected with their use. Additional research in this area is certainly needed.

6. References

[1] Hall, H. T., Rev. Sci. Instr. **31**, 125–131 (1960).
[2] Hall, H. T., Ibid. **29**, 267–275 (1958).
[3] Bridgman, P. W., Proc. Am. Acad. Arts Sci. **81**, 167–251 (1952).
[4] Barnett, J. D., and Hall, H. T., Rev. Sci. Instr. **35**, 175–182 (1964).
[5] Barnett, J. D., Bennion, Roy B., and Hall, H. T., Science **141**, 534–535 (1963).
[6] Ref. [3], pp. 198 and 199.
[7] Bridgman, P. W., Phys. Rev. **60**, 351–354 (1941).
[8] Jeffery, R. N., Barnett, J. D., Vanfleet, H. B., and Hall, H. T., J. Appl. Phys. **37**, 3172–3180 (1966).
[9] Decker, D. L., Brigham Young University, Unpublished (1968).
[10] Vereshchagin, L. F., Zuhova, E. V., Buimova, I. P., and Burdena, K. P., Dokl. Akad. Nauk SSSR **169**, 74 (1966).
[11] Hall, H. T., Rev. Sci. Instr. **33**, 1278–1280 (1962).
[12] Hall, H. T., Rev. Phys. Chem. Japan **37**, 63–71 (1967).
[13] Davidson, T. E., and Lee, A. P., Trans. Met. Soc. AIME **230**, 1035 (1964).

DISCUSSION

A. Taylor (*Westinghouse Research Laboratories., Pittsburgh, Pennsylvania*): I would like to describe some of our experience with the tetrahedral press referred to by Dr. Hall.

The stretch in the press frame under load does not concern us, nor does the fact that the assembly is "sloppy" at the joints, because a little initial pressure will take the "slop" out of the system, and the stretch can be accommodated by moving the x-ray tube up and getting a stronger beam.

The most serious difficulties with the apparatus are these: First, the sample moves off-center under load because of the extrusion of the tetrahedron, and that introduces errors in spacing which are far more serious than those produced by the stretching of the press. In measurements of pressure coefficients where one takes differences in lattice parameters, the error that is introduced can be very serious. Our procedure is to use a calibration material which is mixed with the sample. We take the press up to full pressure, take the x-ray diffraction pattern, and then bring the load down to a very small value—a couple of kilobars—and take another diffraction pattern. From the lattice parameter of the calibrating material—which is sodium chloride in this case—we are able to determine how much the sample has moved off center.

A second problem connected with x-ray diffraction measurements is associated with the large amount of incoherent scatter coming from the tetrahedron, apart from the sample. We use a mixture of 80 percent boron and 20 percent polystyrene. If we attempt to get a stronger diffraction pattern from the sample by making the diameter of the collimator a little larger, it is found that an increase in the background intensity occurs in relation to the line intensity, and a poorer line-to-background ratio is obtained. It is thus necessary to make the diameter of the collimator system quite small. We find that a diameter of about 8 or 9 thousandths of an inch is about right. But, unfortunately, when the collimator is small and the sample is very thin, there are very few crystals in the beam. Then the line profile is spotty, and it's very difficult to find the true maximum.

Until we can overcome these difficulties with the tetrahedral press, our errors in pressure in, say, the 70 to 80 kbar range might easily be plus or minus two or more kilobars.

P. N. LaMori (*Battelle Memorial Institute, Columbus, Ohio*): In your paper you have attempted to give a historical account of the "pressure scale muddle." As a participant I would like to offer a few additional comments.

You have suggested that Bridgman's results should not have been challenged without definitive experiments such as simultaneous measurement of the volume and resistance transitions. This was done as early as 1962 when I demonstrated by simultaneous volume and resistance measurements the bismuth $1 \rightarrow 2$, bismuth $2 \rightarrow 3$ and thallium $2 \rightarrow 3$ transitions. ["Calibration Experiments in a Piston-Cylinder Apparatus," *High-Pressure Measurement*, edited by A. A. Giardini and E. C. Lloyd, Butterworth's, 1963, p. 321.] In that paper the barium transition was also clearly demonstrated to be 58 ± 2 kbar by a *resistance* measurement. The additional proof that you say was necessary of Kennedy's and my earlier conclusions was thus available shortly after our original papers.

You have suggested that Kennedy's insight ran ahead of the experimental evidence. As a participant in the events leading to the discovery of the error in Bridgman resistance pressure scale, I can only say that the insight was based on solid experimental evidence. The experimental evidence consisted of accurate measurements of the bismuth, thallium and cesium transitions. It was only after all the experimental evidence was available that Professor Kennedy, myself, and Professor D. T. Griggs simultaneously and independently reached the obvious conclusion about the pressure scale. This work was presented at the Bolton Landing Conference—G. C. Kennedy and P. N. LaMori, "Some Fixed Points on the High Pressure Scale", *Progress in Very High Pressure Research*, edited by Bundy, Hibbard, and Strong, John Wiley, New York, 1960 (314 p.).

An unpublished outcome of this work shows clearly that there is a linear relationship between the differences in volume and resistance measurements above 25 kbar. This strongly suggested that the resistance measurements were incorrect. See Figure 7, P. LaMori, "The Determination of Some Solid Transition Pressures to 50,000 Bars", M. S. Thesis, U.C.L.A., 1963. However, this was known at the time of and presented at the Bolton Landing Conference (see discussion section of our paper).

Thus, the information Kennedy presented was based on (1) solid experimental evidence, and (2) a demonstrable relationship between the volume and resistance measurement.

Kennedy's insight came at a step earlier than this. This was in the conception of the piston-rotation experiment. Also important was his insistance in doing the experiment in spite of much objection from myself as well as others. The importance of this has been clearly demonstrated.

Appendix

Temperature Measurement at High Pressures

Chairman: F. P. Bundy

General Electric Research and Development Center
Schenectady, New York

P. Bell

Carnegie Institution of Washington
Washington, D.C.

P. J. Freud

Battelle Memorial Institute
Columbus, Ohio

I. Getting

University of California
Los Angeles, California

R. E. Hanneman

General Electric Research and Development Center
Schenectady, New York

G. C. Kennedy

University of California
Los Angeles, California

H. M. Strong

General Electric Research and Development Center
Schenectady, New York

R. H. Wentorf

General Electric Research and Development Center
Schenectady, New York

G. C. Kennedy: I think that there is a good deal of confusion among the audience that doesn't really exist for most experimenters in this field, in view of the apparent disagreement between the GE measurements and Getting's measurements.

Now most of the measurements are relative measurements. Relative measurements in question include measurements of the difference between an alumel-chromel couple and a platinum-platinum/rhodium couple. That experiment has been done three times, by LaMori's group, by us, and by the General Electric Research Laboratory, and all three results agree. Now, GE also has estimated the absolute effect, but because our absolute effect for platinum is positive and for alumel-chromel is negative the net absolute effect is the difference, and our absolute effect is thus half the size estimated by GE. But the three sets of measurements are all in agreement involving both the difference between two thermocouples and measurements on a single wire. So actually I think the situation is really very much under control. The only measurements which disagree are the noise experiments. So I think that, compared to other problems in high pressure, this effect of pressure on temperature measurement is in very good shape.

R. E. Hanneman: The disagreement is not quite as bad as a factor of two, up to 30 kbar and 1,000 °C. George Kennedy indicated earlier that he had little faith in use of phase transformation boundaries as

a basis for indicating temperature corrections. I think part of the problem is this question of what the pressure really is at high temperature. Another difficulty may lie in the point that we have not used simply the Clausius Clapeyron equation, but have integrated the heat capacity as a function of temperature. This does not give, of course, a linear curve, but we have tried to bring this into the calibration.

Although at GE we may have been lucky and chosen the "right" six or eight systems, we have never had the system give results in the wrong direction. There's been scatter of the order of 30 percent in experiments by using different pairs of the different kinds of materials.

I. Getting: I think that even if we can come to some agreement as to what the hydrostatic effect on calibration of thermocouples may be, this may not be the major problem facing temperature measurement in high-pressure apparatus in general. For roughly the first year that I worked on this problem, I was not able even to see the pressure effect. Chemical effects, particularly in chromel-alumel above 600 or 700 °C, were much larger. When I did the Bridgman experiment with a silver chloride pressure medium, and heated to only 400 °C at 1 kbar nominal pressure, the voltages I observed for the chromel lead itself were greater than any I have ever seen from the pressure effect. So chemical effects can be very severe.

As an example, take two identical thermocouples and don't weld the junctions together, but just put them side by side at the end of a 1/8-in- or 1/6-in-diam ceramic tubing, and put them in the location where you would normally put a thermocouple in any solid pressure medium, high-temperature, high-pressure apparatus.

Apply heat and look at the difference in the indicated temperatures. Sometimes, due to effects I don't know how to explain, we have gotten an honest 1 percent difference. That's 10 degrees at a thousand. After one has solved these problems and can get two identical thermocouples to read together, try two different composition ones, and you will find another order of magnitude difference. When these effects are all resolved, you are ready to talk about whether you are experiencing a pressure effect or not.

I think that if we are realistic about temperature corrections in the region of a thousand degrees and tens of kilobars, we will not make statements like "temperatures were measured to plus or minus five degrees." And at 1,500 degrees the situation is much worse.

P. Bell: The problem that I would like to draw attention to is the matter of contamination. While comparisons against chromel-alumel are worthwhile, I think certainly in our apparatus and in Professor Kennedy's there is boron nitride, and there is carbon. Chromel-alumel behaves very badly in a reducing atmosphere. Professor Birch mentioned this in his papers—and this is the reason why he never used it again.

R. E. Hanneman: I think that this is an appropriate place to bring up the fact that we need to search for thermocouple materials which are indeed more stable, and we might start off with this new material, platinel. We have done some work with some gold-like thermocouples, and these are not bad under some conditions. So I think that instead of driving so hard for the absolute corrections, perhaps we should spend some of our time and effort making relative measurements and looking for materials that are good and stable.

Now, one other question that was inferred today is the matter of pressure variations that occur as the temperature is changed. If you go up and down in temperature you get these hysteresis effects which Bob Wentorf very clearly showed. And these things are all so large that they are a serious pitfall for a newcomer in the field.

I. Getting: I think the point about stress distributions on the wire being unknown is important. After three years of experimentation, I claim only to have some idea of the effective pressure on the wires to within three kbar—that's 30 percent at 10 kbar.

As a further problem, in alumina ceramic tubing in a standard piston-cylinder apparatus the effective stress on the wires is so uncertain that I will no longer say that the results give the corrections for thermocouples.

I think we really would like a thermocouple, of course, which is chemically stable and which has a small pressure coefficient. But if you look at the data from Bridgman single-wire experiments to try to find a pair of materials which have the same emf's, the corrections would be zero. As it turns out, if you made a thermocouple out of platinum and alumel you would have virtually no pressure dependence; but this would be to little avail since the performance would then be dominated by the chemical susceptibility of alumel and the mechanical weakness of platinum.

R. H. Wentorf: We have been talking a lot about thermocouples, but I'd like to point out that there is another good way to measure temperature, and that's optically. If a person could get some well-defined phase transformations which aren't too sensitive to pressure, but run at a pretty high temperature where they do emit, then one could do two-color pyrometry on these samples and get, pretty well, the absolute temperature. These materials could then be run in a different configuration with thermocouples next to them without windows, and in that way one could get another grip on the problem of thermocouple calibration and the general temperature problem.

G. C. Kennedy: On the problem of chemical stability, there is a way of stabilizing the thermocouple

that works remarkably well. Platinum-rhodium at 1,500 °C in a proper environment doesn't drift. This proper environment, we have found, is in molten glass.

As an example, if an iron wire and a thermocouple beside it are placed in an ordinary environment, in a matter of 3 or 4 minutes the thermocouple will drift so fast that it may be useless. In the presence of iron or graphite at 1,500 °C it drifts so fast that it really becomes useless.

If you surround the couple by molten Pyrex or any molten high-silica glass, then it can sit for hours at 1,500 °C and it will not drift. The evidence that it does not drift is that one can repeatedly measure the same value for the melting point of iron. The pressure of molten glass seems to inhibit any migration of metallic substances to the platinum-rhodium and also inhibits any migration of carbon to platinum-rhodium.

H. M. Strong: I'll make just two short comments. Following what George Kennedy has just said, we have also found that platinum and platinum-10 percent rhodium in an environment of pure boron nitride, or in clean dry salt, is also quite stable for several hours at around 1,400 °C as indicated by the fact that for the same power input one continues to get the same reading. Also the thermocouple output at melting points of those materials remains the same.

I might amplify what Rod Hanneman said on pressure variation. We have tried to measure the pressure variation in cells as you change the temperature, using a tiny germanium element off to one side, heated independently—and with a carbon tube in the cell center to heat the cell proper. With this arrangement you can observe changes in pressure by observing changes in melting point of the germanium. The pressure may not be known absolutely, but the pressure change can be seen. By this method we have observed in pyrophyllite quite distinct changes of pressure upwards with heating amounting, at a 50-kbar level, to 10 to 20 kbars. But after a while the pyrophyllite tends to transform to a denser phase, and then the pressure will drop, sometimes quite far below the original pressure of 50 kbar. Sodium chloride environments are quite a bit more stable, but there is a distinct increase in pressure with temperature.

F. P. Bundy: A comment along this line that I would like to make on Freud's work, and also Getting's, is that in their exploration of the pressure distribution in their cell, along the temperature gradient, measurements were made at room temperature using bismuth in most cases. I would suspect from what I know of Strong's measurements under these same conditions that during the heat-up of the cell one would find that at the high temperatures the pressure goes higher than was indicated on the graphs.

P. J. Freud: The way we did the experiment was to heat up at a low loading and then increase the load.

I. Getting: One can chase this effective pressure problem, without results. I tried to do it by following piston displacement during cycling of piston load at various pressures, and got a hysteresis loop for something possibly corresponding to the average pressure in the cell as determined by the piston displacement. One can then, in temperature cycles, relieve the load on the piston as the temperature increases to try to correspond to that narrowing frictional hysteresis loop, and so on and on. I think the saving grace here is that even if you don't know the stresses in the wires to better than three kilobars it doesn't matter to more than a degree or so in the correction.

D. Decker (*Brigham Young University, Provo, Utah*): There is also another possible way of looking at temperature effects—by doing a Mossbauer experiment and looking at the Doppler shift. This effect should be independent of pressure. And since the isomer shift itself is a very slow-varying function of pressure, it gives you an estimate of the temperature. We have tried this at 80 kbar and up to 400 °C. However, we only used chromel-alumel thermocouples and found no effect. That is, measurements on thermocouples directly and by the isomer shift essentially agree.

385-762 O - 71 - 21

Fixed Points Near Room Temperature

Participants

H. Tracy Hall, *Chairman*

L. Abbot
P. B. Alers
Y. A. Atanov
J. D. Barnett
F. Bundy
R. Cavailhe
T. Clark
M. Contre
J. Cross
J. Haygarth
J. Houck
A. Jayaraman
D. P. Johnson
R. Kaneda
N. Kawai
G. S. Kell
A. Lacam
G. J. Scott
C. E. Weir
M. S. Werkema
R. J. Zeto

In our committee discussion of fixed points, we realized that several factors were of concern: Are these points equilibrium points thermodynamically? We realized that kinetics often enters into the establishment of these points. We also recognized that the apparatus plays a part in deciding where an individual person may find a fixed point in relation to his press loading or other factors.

We decided that the equilibrium value was the important value, and that we should select the fixed point data that were closest to equilibrium. Then it would be up to the individual user to worry about kinetics and apparatus factors in his own situation.

In this connection, we advise that all high-pressure workers describe their apparatus adequately. It is necessary to know what kind of device is used, and its important dimensions. If it's a piston-cylinder apparatus, the diameter of the piston and the length of the sample should be given. Materials in the cell, such as pyrophyllite, boron nitride, or silver chloride should be specified and their dimensions given. Give sufficiently detailed information so that an estimate of the pressures can be made at a later date when fixed point values become more accurate.

We decided that there were several ranges into which the pressure scale could be advantageously divided. The first range is called the Free Piston Gage Range. It was the consensus of the group that the free piston gage could be used up to pressures of about 30 kbar. The first two fixed points that we discussed—the mercury freezing pressure at 0 °C and the bismuth I-II transition—lie in the Free Piston Gage Range. There may be other points that should be included.

Our assignment was concerned with pressures at room temperature. We decided that this meant 25 degrees Centigrade, and we have shown in the accompanying list of "Pressure Fixed Points" our judgment of the best values of the pressure, in kilobars, of the fixed points at 25 degrees Centigrade.

Some measurements have been made above room temperature, and we wish to include the mercury point over a range of temperatures as a fixed point, rather than just giving it as one point. It recommended that such reference pressures be based on the Simon equation, adjusted to agree with the value 7.569 kbar at 0 °C as follows:

$$P = 38227 \left[\left(\frac{T}{234.29} \right)^{1.1772} - 1 \right]$$

where T is the temperature in K on the International Practical Temperature Scale (1948), and P is the pressure in bars.

In the case of the bismuth I-II transition, it was the consensus of the group that Heydemann's value determined at the Bureau of Standards is the best value at this time and should be 25.50 ± 0.06 kbar at 25 degrees Centigrade.

We called the next range, beginning at 30 kbar, the Upper Force-Over-Area Range, with a present upward limit of about 80 kbar. In the present state-of-the-art this limit probably cannot be exceeded in apparatus such as piston-cylinder equipment. In this range, we have selected the thallium II-III transition to have a value of 36.7 ± 0.3 kbar.

The value chosen for caesium (Cs II-III $= 42.5 \pm 1$ kbar) was the result of careful consideration. We determined who had performed experiments where the system was in a truly liquid environment, and gave considerable weight to that. We considered experiments that did not have a liquid environment but in which an attempt was made to approach a free piston condition. Here, one may have had silver chloride for the environment. We included x-ray diffraction data. We weighed these, one against the other, and came up with a good consensus as to the best value. We then tried to put some kind of an estimate on the plus or minus value. The caesium II-III value appears to be known only on an upstroke, so there could be a

question as to whether or not the caesium values are equilibrium values.

The barium I-II transition was placed at 55 ± 2 kbar, and bismuth III-V at 77 ± 3 kbar, at which point we reached the limit of our upper force-over-area range.

Then we moved into a more difficult range—the 100 Kilobar Range—in which tin, iron, barium, and lead were considered. We understand that there are no shock data on the transitions in tin, barium, and lead.

There are problems, apparently, in trying to run these transitions by shock techniques. The shock data that have been obtained pertain only to iron, and according to at least one member of our panel, the iron transition is very poorly behaved. It was the consensus of the group that iron probably ought to be left out of the system, although there were a few who objected. Iron seems to be somewhat irregular in behavior, and there is an uncertainty as to the correct transition value.

It is the consensus of this group that the tin, barium, and lead points are on much less firm ground than the points in the Force-Over-Area Range, which in turn are on less firm ground than the points of the Free Piston Gage Range. We feel that pressure is probably established up to the neighborhood of 80 kbar within plus or minus 3 kbar. In the 100 Kbar Range and above there is a great deal of uncertainty. How much is difficult to estimate. Points in this range have been chosen from older work of Drickamer's and probably should be revised downward on account of the downward revision in the barium point, and the iron point.‡

PRESSURE FIXED POINTS

Free piston gage range	Hg		7569 ± 2 bars at 0 °C
	Bi	I-II	25.50 ± 0.06 kbar at 25 °C
Upper F/A range	Tl	II-III	36.7 ± 0.3 kbar
	Cs	II-III	42.5 ± 1 (up only)
	Cs	III-IV	43.0 ± 1 (up only)
	Ba	I-II	55 ± 2
	Bi	III-V	77 ± 3
100-kbar range	Sn	I-II	100 ± 6
	Ba		140 (up only)
	Pb		110 to 160 (up only)

H. T. Hall

‡*Added in proof by the Editor:* In the following table are Drickamer's revised values based upon a later publication (Rev. Sci. Instr., Notes Section, Vol. **41**, No. 11, 1970):

Approximate Location of Transitions, kilobars

	Old	*New*
Bi	88	73–75
Sn	113–115	92–96
Fe	133	110–113
Ba	144	118–122
Eu	150–160	122–130
Pb	160	128–132
Rb	190	142–153
Cs*(max)	170–180	133–142
Ca*(max)	350–375	235–255
Rb*(max)	420–435	290–320
CdS*(max)	460	330–340
ZnS*(max)	550	410–420

*Maximum in resistance-pressure curve.

Equation-of-State Standards

Participants

O. L. Anderson, *Chairman*

J. Jamieson
George E. Duvall
D. John Pastine
G. R. Barsch
W. A. Bassett
D. L. Decker
D. McWhan
W. J. Carter
C. Beckett
R. H. Wentorf, Jr.
K. Vedam
M. van Thiel
R. Grover
Max Swerdlow
J. S. Weaver
L. Thomsen
S. E. Babb, Jr.
E. M. Compy
P. J. Freud
P. L. M. Heydemann
M. Klein
D. H. K. Mao

The appointed committee included J. Jamieson, George E. Duvall, D. John Pastine, G. R. Barsch, W. A. Bassett, D. L. Decker, D. McWhan, W. J. Carter, C. Beckett, and O. L. Anderson. The chairman made all persons attending into a committee of the whole.

The panel reached a consensus on the topics to be discussed. They were: definition of equation of state; basis for selecting a standard reference material; the reference materials themselves; properties an ideal standard should have; the theoretical problems facing the equation of state of the standard materials; special new experiments desired on standard materials.

I. Equation of state defined. The consensus was that general definitions should be avoided, and that the focus be made on the P,V,T relationship of the standard material. In particular, generalized stress and strain relationships seemed only remotely possible. However, it was recommended that a feasibility study be made on the prospect of determining shear constants as a function of pressure.

II. Basis of selecting standard materials. The primary consideration is that the material be usable as a standard in experiments. The secondary consideration is that the material be amenable to theoretical analysis. The experimental fields concerned are: (1) x-rays under pressure; (2) shock waves; (3) pressure vessels closed to x-rays. Experiments specifically not considered in the selection of the materials were low-temperature (liquid helium) high-pressure experiments, and acoustics under pressure. It was recommended that a feasibility be made for a material whose equation of state is useful for low-temperature experiments.

III. The materials selected. It was the consensus that a material must suit various kinds of experimenters. It was recognized that no one material would satisfy all experimentalists, but, on the other hand, that selecting many materials is equivalent to selecting none. The recommended materials were, in order of preference:

1. NaCl
2. Cu
3. Al

It was agreed that sodium was a material to be considered in the future. A minority viewpoint held that something should be done to choose a particular liquid as a calibrant.

These three materials were selected as the ones which were the best compromise to the ideal one which would have the following properties (in order of importance): a useful value of bulk modulus, chemical inertness, isotropic structure, the absence of phase changes, low values of atomic number, low yield points, and optical transparency.

IV. Theoretical problems to solve on recommended materials. Not necessarily in order of priority, they were: (1) Fermi-Dirac approximations; (2) quantum mechanical approaches, especially calculations in deformed lattices; (3) noncentral forces in lattice dynamic theories; (4) sixth-order anharmonic approximations in lattice dynamic theories; (5) non-equilibrium thermodynamics, especially on lattice models; (6) behavior of the Grüneisen parameter with volume; (7) uniqueness problems in the strain definition of finite strain theories.

It was further recommended that the Rochester group, the BYU group, and the Los Alamos group compromise their differences in their individual published tables of equations of state of NaCl, and together issue a common table.

It was further recommended that the equations of state of the three standard materials be cross correlated with each other, and with the recommended fixed pressure points.

V. Some special experimental problems (not presently well attended) which should be pursued. The panel urged that experiments be pursued showing the shift of vibrational frequency with volume at all frequency ranges. These include the pressure dependence of Brillouin scattering, neutron scattering, and Raman scattering. New experiments involving secondary standards were encouraged. These were: pressure shifts arising from NMR, the Mossbauer effect, and various electronic transitions.

The panel further recommended that, since all experimental values on these three materials would be of use to theoreticians working out equations of state, whenever possible experiments on these materials be performed. Of special import are those experiments that are boundary conditions of phenomological equations of state.

O. L. ANDERSON

Measurements of Pressure and Temperature in High-Pressure Apparatus

Participants

F. R. Boyd, Jr., *Chairman*

S. Akimoto
N. Asami
P. Bell
H. Bovenkerk
I. C. Getting
M. C. Gilbert
D. Hamilton
G. S. James
R. S. Kirk
I. D. MacGregor
H. O. A. Meyer
R. Roy
P. St. Pierre
F. Seifert
H. M. Strong
C. Susse
A. Taylor
H. S. Young

The measurement of pressure at high temperature includes all of the difficulties of measuring pressure at 25 degrees with a few more thrown in. Probably the biggest additional difficulty arises from the fact that at high temperatures it is difficult to get a truly hydrostatic condition. Most of the high-temperature cells that are used in high-pressure apparatus are composed of materials like lavastone, talc, and graphite, and these do not permit a very close approximation to a hydrostatic condition. There is also the problem that arises because most of the effects that one would like to study are temperature-sensitive as well as pressure-sensitive. At high temperatures, particularly above a thousand degrees centigrade, making a good pressure measurement involves the difficulty of making a good temperature measurement as well.

Now, in the last ten years or so there has been accumulated quite a large body of data on melting curves and solid-solid transitions, some of which have been most imaginatively and carefully determined. Various other effects have also been measured as a function of pressure and temperature. Nevertheless we decided at the outset of our session that we would not dignify any of these data by characterizing them as calibration curves or fixed points or anything of that sort. Thus having "disposed" of the main problem, we gave our attention to the question of which future work we or others should undertake to provide better measurements and calibrations at high temperatures.

We divided the problem into two parts: the use of phase transitions as possible calibration points; and "other effects".

We considered the "other effects" first and the discussion of these is summarized as follows: One possible calibration scheme uses thermocouples including, in particular, the iron platinum-10-rhodium couple that Dr. Strong has described. There are problems with this device in that it's hard to get a really big effect that's very sensitive to pressure.

We talked about *in situ* lattice parameter measurements, for example by x-raying a substance at both high temperature and high pressure. This is a good method, but it requires very specialized equipment, and the average high-pressure worker would not be able to readily make such a measurement in order to calibrate his device.

We talked about the effect of pressure on the index of glass. This is rather an interesting phenomenon in that many glasses, when placed under high pressure, have rather large increases in their index of refraction. With certain glasses, particularly SiO_2 glasses, this effect is large enough so that it quite possibly would provide a useful means of pressure calibration. Use of glass is also attractive in that one could run a small piece of glass with an unknown, and by measuring the index after the experiment, determine the pressure of the experiment. There are difficulties. It is a relatively low-temperature phenomenon, and there also appears to be a problem sometimes of reaching an equilibrium state in the index of the glass.

We talked also about vacancies in TiO as a function of pressure, and this can be established by a lattice parameter measurement after the event. In other words, after exposure to high pressure one can, through measurement of the lattice parameter, get an estimate of the pressure.

We discussed magnetic effects, and the largest of these Curie-point changes at present seems to be the effect of pressure on the Curie point of nickel, which Dr. Susse estimated to be about 0.35 °C per kilobar. This is thus not quite as sensitive as we would like to have.

We talked about solution phenomena which are really phase transformations of a specialized kind. There are transition loops and solvus curves which are extremely sensitive to pressure. In some cases it is possible to measure the composition of, say, phase A in equilibrium with phase B with an accuracy which would be equivalent to a change in pressure of the order of a kilobar, so that there

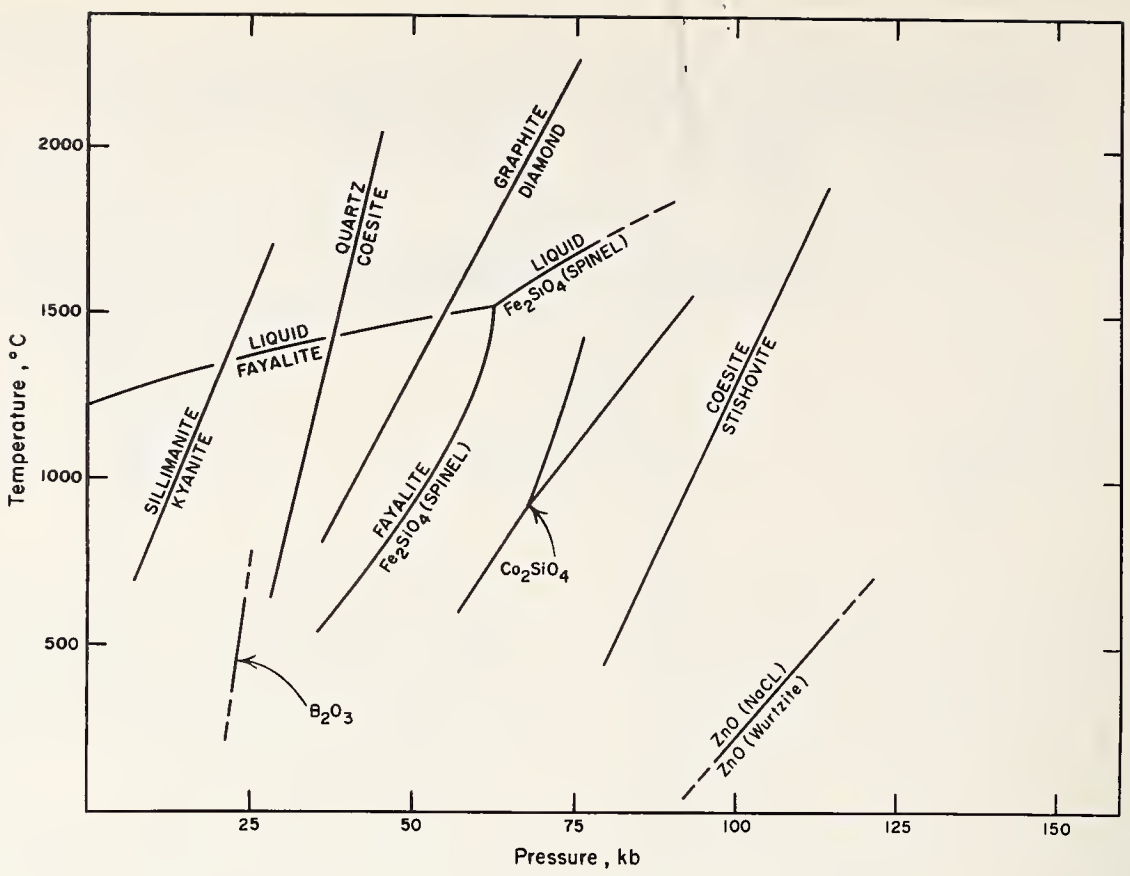

FIGURE 1. *Phase transitions which can be studied by the quenching method and which are potentially useful for calibration at high temperatures and pressures.*

Sillimanite-Kyanite: Richardson, Bell, and Gilbert (1968); Quartz-Coesite: Boyd, et al. (1966); Graphite-Diamond: Berman and Simon (1955); Fayalite-Spinel-Liquid: Akimoto, Komada, and Kushiro (1967); B_2O_3: Dachille and Roy (1959); Coesite-Stishovite: Akimoto and Syono (1960); ZnO: Bates, White, and Roy (1962); Co_2SiO_4: Akimoto and Sato (1968).

are possibilities here. And it was suggested that for very high-temperature situations one might look at solvii in oxide systems; at more moderate temperatures, silicate systems; and at low temperatures there are salt systems that could conceivably be used.

We then discussed univariant phase equilibria. We gave attention to those which, through the group's experience, were well-behaved. We felt that if we could establish some of these in a sufficiently absolute way they would make useful calibration points or curves. We divided the phase transitions into two groups according to reaction rate. There are those which require run times of the order of ten minutes to ten hours to some days in order to achieve equilibrium, and which can be studied by the quenching method; i.e. bring the material up to pressure and temperature, hold it, quench it, and then examine the results by optical, x-ray or electron probe methods. Some of these, for example quartz-coesite, can be done with high precision. We made a *P-T* diagram of phase transitions that would fall in this category.

We did the same thing for a group of phase transitions which are essentially displacive transformations, very fast ones, in which one can detect the transition either through a latent heat effect or, let's say, by a change in electrical resistance.

The accompanying diagrams illustrate the pressure and temperature ranges in which some of these transitions, both slow and fast, could be useful.

At the highest pressures there is a quenchable transition in zinc oxide (fig. 1) which goes to an NaCl structure, and there are data now on this in the range above 100 kbar and up to about 500 degrees. At a little lower pressure there is the coesite-stishovite reaction. Then further down there are three forms of Co_2SiO_4 with a triple point at 930 °C and 68 kbar.

Still further down there's a transition in Fe_2SiO_4 which goes from an olivine to a spinel form. This transition intersects the melting curve at 1520 °C and 62 kbar.

At lower pressures is the quartz-coesite transition for which we probably have better agreement and more determinations than for any other. I would say that at a temperature, for example, of 1,400 degrees the three most recent determinations of the quartz-coesite transition are within two kilobars of each other at approximately 40 kbar.

In a lower temperature range there is a transition in B_2O_3 and at pressures below quartz-coesite there is the kyanite-sillimanite transition.

These are all fairly well-behaved transitions, and it is possible to bracket many of them very closely. If we could solve some of the measurement difficulties I think almost any of these would provide useful calibration points or calibration curves.

Now, the more rapid transformations which can be observed through DTA or an electrical resistance change fall in two groups (fig. 2). Of course, all of the fixed points that we've been working with at room temperature can be extended to a greater or

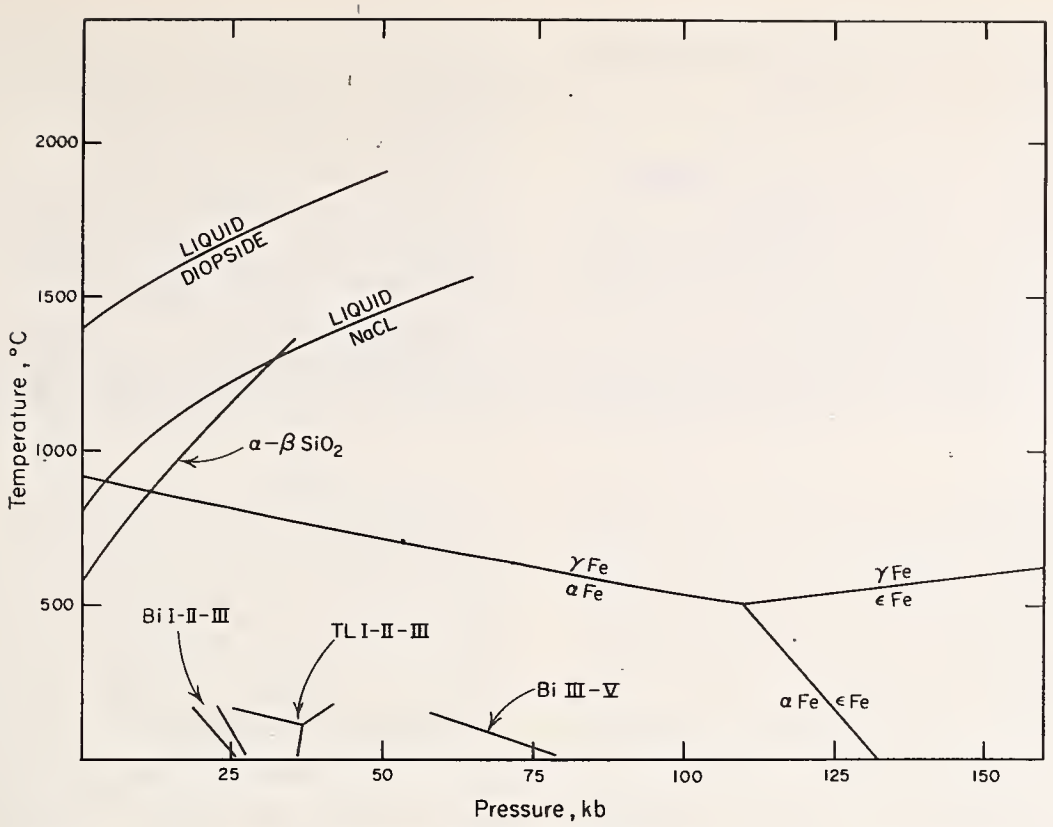

FIGURE 2. *Rapid phase transitions which can be determined by DTA, resistance-jump, etc., and which are potentially useful for calibration.*

Diopside: Williams and Kennedy (1969); NaCl: Akella, Vaidya, and Kennedy (1969); α-β Quartz: Cohen and Klement (1967); Iron: Bundy (1965); Bismuth I-II-III and Thallium I-II-III: LaMori (1970); Bismuth III-V: Haygarth, Ludemann, and Getting (1969).

lesser extent up the temperature scale. For example, Dr. LaMori earlier showed us his results up to several hundred degrees on the bismuth I-II and bismuth II-III transitions, and on the thallium transitions. Also, we have high-temperature data on the bismuth III-V transition, discussed earlier in this meeting. A second group in a higher temperature range includes the alpha-gamma iron transition which has been determined up to quite high pressures. There is also the alpha-beta quartz transition at lower pressures.

Quite a lot of work has been done on melting curves. For the most part, the melting curves of metals have slopes that are less than five degree per kilobar. Thus they are not as sensitive as would be desirable for pressure calibration at high temperature. Salts, however, exhibit much steeper melting curves. Initial slopes on the order of 20 degrees per kilobar are quite common in salts, and there would be a number of these that could be considered. One that is of current interest is sodium chloride, which also is in a reasonably manageable temperature range (fig. 2).

At higher temperatures there are silicate melting curves, which have initial slopes on the order of ten degrees per kilobar. A number of these curves have been determined and for the most part they lie in the range of 1,500 to 2,200 degrees Centigrade. Among substances of this type for which melting curves have been determined are diopside, albite, and fayalite.

There are basically three ways to improve measurements on these various equilibria to the point where one could really have confidence in them as calibration points. One is by thermochemical calculation, another by the shock wave approach, and a third I think by use of the piston-cylinder apparatus.

Much data has now been obtained with the piston-cylinder apparatus, particularly since the UCLA group found it possible to extend simple piston-cylinder measurements out to 80 kbar. But there still are problems in relating the load pressure to the actual pressure in a piston-cylinder device. Even when one can quite accurately determine the amount of the friction, there is still the possibility that in a high-temperature cell, composed of concentric layers of such materials as talc, boron nitride, and graphite, the actual load is borne disproportionately by these shells, with resulting uncertainties in the pressure on the sample.

For this reason, even though the precision of some of the measurements in this high-temperature, high-pressure, field is now very high, we are uncertain as to the absolute accuracy.

F. R. BOYD, JR.

References

Akella, J., S. N. Vaidya, and G. C. Kennedy, Melting of sodium chloride at pressures to 65 kbar, Phys. Rev. **185**, No. 3, 1135–1140, (1969).

Akimoto, S., E. Komada, and I. Kushiro, Effect of pressure on the melting of olivine and spinel polymorph of Fe_2SiO_4, J. Geophys. Research **72**, 679–686 (1967).

Akimoto, S., and Y. Sato, High pressure transformation in Co_2SiO_4 olivine and some geophysical implications, Phys. Earth and Planet Interiors **1**, 498–504 (1968).

Akimoto, S., and Y. Syono, The coesite-stishovite transition, this volume, p. 273.

Bates, C. H., W. B. White, and R. Roy, New high pressure polymorph of zinc oxide, Science, No. 3334, p. 993 (1962).

Berman, R., and F. Simon, On the graphite-diamond equilibrium, Z. Elektrochem. **59**, 333–338 (1955).

Boyd, F. R., P. M. Bell, J. L. England, and M. C. Gilbert, Pressure measurement in single-stage apparatus, Carnegie Institution of Washington Year Book 65, 410–414 (1966).

Bundy, F. P., Pressure-temperature phase diagram of iron to 200 kbar, 900 °C, J. Appl. Physics **36**, No. 2, 616–620 (1965).

Cohen, L. H., and W. Klement, Jr., High-low quartz inversion: Determination to 35 kilobars, J. Geophys. Res. **72**, 4245–4251 (1967).

Dachille, F., and R. Roy, A new high pressure form of B_2O_3 and inferences on cation coordination from infrared spectroscopy, J. Am. Ceram. Soc. **42**, 78–80 (1959).

Haygarth, J. C., H. D. Ludemann, I. C. Getting, and G. C. Kennedy, Determination of portions of the bismuth III-V and IV-V equilibrium boundaries in single-stage piston-cylinder apparatus, J. Phys. Chem. of Solids **30**, 1417–1424 (1969).

LaMori, P. N., The use of solid-solid transitions at high temperatures for high-pressure calibration, this volume, p. 279.

Richardson, S. W., P. M. Bell, and M. C. Gilbert, Kyanite-sillimanite equilibrium between 700° and 1500 °C, Am. J. Sci. **266**, 513–541 (1968).

Williams, D. W., and G. C. Kennedy, Melting curve of diopside to 50 kilobars, J. Geophys. Res. **74**, 4359–4366 (1969).

Pressure Inhomogeneity: A Possible Source of Error in Using Internal Standards for Pressure Gages*

John C. Jamieson and Bart Olinger

Department of the Geophysical Sciences
University of Chicago, Chicago, Illinois 60637

Studies have been made on two intimate mechanical mixtures of NaCl and Nb having different composition at high "pressures" using x-ray diffraction. A plot of V_p/V_o for Nb versus V_p/V_o for NaCl showed a different curve for each of the two mixtures. Our analysis and the consequences of this apparent violation of the criteria for an internal pressure gage are discussed.

It has been pointed out several times in the past that the stress configuration in compressed solids is much more complicated than the homogeneous hydrostatic case. In particular, stress differences in materials due to encapsulation have been treated by Bobrowsky [1][1] and Corll and Warren [2], while pressure differences developed by flow and geometry have been described by Jamieson and Lawson [3], Lippincott and Duecker [4], and Jamieson [5]. The encapsulation enhancement has been experimentally verified by Corll [6]. The use of an internal standard to measure pressure in high-pressure experiments implies immediately that the system under study will consist of two or more phases chemically and mechanically different in their properties. One is the material where properties are to be studied as a function of pressure; the other serves as an internal pressure gage. In the case of the present experiments the "gage" gives an x-ray diffraction pattern from which its density at any pressure may be directly calculated, in principle. Then a comparison made with data obtained by other means on the "gage's" compression gives the pressure. While this application seems straightforward, we felt that it was not at all obvious that in a system of stressed solids, stress would be sufficiently homogeneous for such a gage reading to be representative of the pressure in the second phase. This was previously stated quite clearly by Bobrowsky [1].[2] The following experiments were performed to investigate this possibility.

Two mechanical mixtures of dried NaCl and Nb were weighed and then agitated in a "Wig-L-Bug." Each was uniform to the eye under the microscope. One consisted of 89 percent NaCl by volume, the other 81 percent. These were formed into pellets and studied by *in situ* high pressure x-ray diffraction as described elsewhere [3, 7]. We chose NaCl since it is frequently used as an internal standard in such experiments. The other material chosen was Nb because of its small compressibility relative to NaCl, its simple bcc x-ray pattern, and its position next to Mo on the Periodic Table. This latter property guaranteed comparatively low absorption and high scattering power in the Mo radiation, which was used in this experiment. Absorption coefficients for the two mixtures studied were 45 cm^{-1} for the 19 percent mixture and 34 cm^{-1} for the 11 percent. For our sample diameter of 0.35 mm no serious absorption effects were to be expected using the empirical $2/\mu$ rule [7] for optimum sample size. Another reason for the choice of Nb was the fact that its Poisson's ratio of 0.35 differed grossly from the (average) one for NaCl of 0.21 as determined from handbook values.

TABLE 1. *Sample indexed pattern*

d_{obs}	*N(Nb)	d_{calc}(Nb)	*N(NaCl)	d_{calc}(NaCl)
Å		Å		Å
2.558			4	2.576
2.292	2	2.293		
1.824			8	1.822
1.618	4	1.622		
1.491			12	1.487
1.325	6	1.324		
1.283			16	1.288
1.146	8	1.147	20	1.152
1.059			24	1.057
1.023	10	1.026		
0.9950			27	0.9915
.9374	12	0.9363		
.8692	14	.8669		
.8104	16	.8109	40	.8146
.7647	18	.7645		
.7251	20	.7253		
.6916	22	.6915		
.6613	24	.6621		
.6358	26	.6361		
.5923	30	.5922		
.5578	34	.5563		

*$N = h^2 + k^2 + l^2$

*[EDITOR'S NOTE: This paper is an expanded version of the discussion presented by Professor Jamieson as part of the discussion of the paper "Calculation of the P-V Relation for Sodium Chloride up to 300 Kilobars at 25 °C," by Weaver, Takahashi, and Bassett.]

[1] Figures in brackets indicate the literature references at the end of this paper.

[2] We wish to acknowledge receipt of a letter from G. C. Kennedy, shortly after starting the experimental portion of this research, in which independently the same point was emphasized.

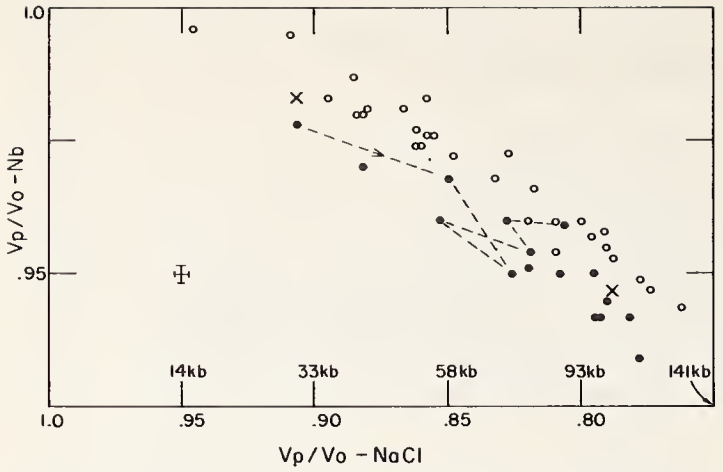

FIGURE 1. *Relative compression of mechanical mixtures of 11 percent* NB-*89 percent* NaCl (*dark circles*) *and 19 percent* NB-*81 percent* NaCl (*light circles*).

Pressures quoted are for V_p/V_0 of NaCl from reference [10]. Cross is error derived from pattern given in table 1.

In order to illustrate the pattern quality obtained, we display in table 1, an indexed pattern. From this pattern we obtain $\alpha = 3.2435 \pm 0.0016$ Å for Nb and $\alpha = 5.1520 \pm 0.0048$ Å for the NaCl unit cell edge. The error figures quoted are standard deviations for this one pattern. All in all, two runs consisting of 16 diffraction patterns at different elevated pressures were taken of the 11 percent Nb mixture. In one run, tapered face pistons were used [7]; in the other, flat face pistons. Six different runs were made of the 19 percent Nb mixture. Piston geometries were tapered face and flat-face as well as one run in which a precompressed and glued boron annulus was used with one flat piston bearing on one tapered. A total of 29 exposures were made of this composition. During each run up to its termination by sample extrusion or piston collapse pressures were increased or decreased at will. For each diffraction pattern the unit cell edges for the co-existing NaCl and Nb were calculated and the ratios V_p/V_0 calculated in which V_0 is the unit cell volume at zero pressure. All high-pressure films had been calibrated from 1-bar photographs using 1-bar values of the respective cell edges. Under these circumstances one would expect that a plot of V_p/V_0 for Nb versus V_p/V_0 for NaCl would be a smooth curve except for experimental scatter if the two co-existing phases were truly at equal pressures. We have found this not to be true on two counts. The first (and less well substantiated) is illustrated in figure 1, a composite plot of all runs. The lines connecting the points of one 11 percent run indicate successive load changes; a movement to the right is increased load, to the left is decreased. It seems apparent that there is no unique curve along which the relative compressions lie. The number of points in this run is too small to make firm statements but there does seem to be a trend that repeated cycling leads to lower V_p/V_0 for NaCl at a constant V_p/V_0 for Nb. Similiar effects can be seen in the other runs which are not individually shown to avoid confusion. The second example of aberrant behavior is also illustrated in figure 1 where it can be seen immediately that the points fall almost uniquely into two groups. The dark 11 percent Nb form a distinct set from the open circle 19 percent Nb. This is a strong violation of an imperative criteria of an internal standard, namely that the presence of the standard or its amount should not influence the behavior of the material whose state it measures. For this work we wish to present the data in figure 1 as empirical facts to illustrate phenomena which need to be taken into account in high-pressure research. For the nonce, we offer only a few qualitative comments on the possible underlying physical explanations.

As we mentioned earlier, "pressure intensification" has been predicted both theoretically and experimentally. The "Brobrowsky-Corll-Warren effect" uses as a model a sphere of one material embedded in one or more shells of a different material. In the one-shell model, pressure varies as $c + d/r^3$ in the shell. We now consider our mixture as a dissemination of Nb spheres of radius a in a matrix of NaCl and draw spherical surfaces of radius b around each, such that these spherical surfaces about each grain are in contact. We assume a uniform pressure p_e in the interstitial regions. Then [1, 2]

$$p_c/p_e = \frac{1+K}{K(1-B_1/B_0)(a/b)^3 + 1 + KB_1/B_0} \qquad (1)$$

in which p_c is the pressure at the core's exterior, B_0 its bulk modulus. B_1 is the bulk modulus of the jacket (NaCl) and K a function of its Poisson's ratio given by

$$K = \frac{2(1-2\nu)}{1+\nu} \qquad (2)$$

Using the values given in Clark [8] for the elastic constants of a quasiisotropic aggregate of NaCl averaged by the Voigt method, $\nu = 0.24$ and $K = 0.83$ at 1 bar. From Bridgman's [8] value for the compression of Nb at 30 kbar, X in figure 1, we estimate B_1/B_0 as 0.18. Numerically eq (1) becomes

$$p_c/p_c = \frac{2.69}{(a/b)^3 + 1.69}$$

and for widely spread spheres of Nb in NaCl a pressure intensification of 1.6 is predicted. If we assume the particles of Nb are uniformly separated in space, then their distances apart may be calculated to be 3.37 a and 2.81 a for the 11 percent mix and 19 percent mix, respectively. Since b as defined previously is one-half this distance, we obtain

$$p_c/p_e = 1.42 \quad \text{and} \quad 1.31$$

from substitution in eq (3). This is qualitatively in agreement with figure 1 where it is seen that a constant NaCl "pressure", i.e., $V_p/V_0 = \text{constant}$, the compression of Nb is indeed less for the 19 percent mix than the 11 percent. The coefficients in eq (3) are known only at 1 bar. In addition, flow may occur (this may explain the cycling effect shown in figure one) and alter the conditions of its derivation. Hence, no further application of the Brobrowsky theory will be made at this time.

There are further difficulties with the use of any internal standard in which x-ray diffraction is used to determine lattice spacings in a stressed polycrystalline aggregate. In order to obtain a given diffraction peak, sufficient matter must be present with its atoms arranged in a sufficiently regular fashion to give coherent radiation in a given direction. In solid pressure systems we may expect great variations in such coherency where small regions may be sufficiently coherent to diffract and transition regions with a gradually varying interplanar spacing may not. Such an effect is well known among metallurgical studies of stresses "frozen in" metals (Barrett [9]). By intuition one would expect the least stressed regions to be most coherent; hence, any lattice spacing determined by x-ray diffraction is apt to be a maximum value corresponding to lower pressure regions.

It is necessary to mention still another possible explanation for the apparently different behavior of the 11 percent and 19 percent Nb mixes as shown in figure 1 and that is the possibility of random error affecting the calibration of each individual run. Figure 1 is a composite of two 11 percent and five 19 percent runs. In each run a 1-bar diffraction pattern has been used to calibrate the camera for absorption, film shrinkage, and sample position [7]. It might be argued that sheerly by chance all measuring errors accumulated so that both 11 percent runs gave systematically low values for Nb compression while all five 19 percent gave systematically high ones. While we cannot rigorously rule out this possibility, if it did occur then many more data points and separate loadings must be made in any compressibility study than had been thought reasonable before. The points in any one run are all calibrated from the same 1-bar pattern and thus are independent of this possible random error. Yet in figure 1 we find variations within one run (and others not illustrated) ascribed to cycling and sample reworking which are well beyond any measuring error and are comparable to the 11 percent to 19 percent difference.

In conclusion, we point to the second X at 100 kbar in figure 1 which corresponds to the Los Alamos shock compression data for Nb from reference [8]. This is a Hugoniot point rather than on the isotherm, but for Nb these are almost identical. The NaCl pressure values in the graph are taken from Fritz et al. [10]. This point lies intermediate between the 11 percent and 19 percent Nb compression in this pressure region. It is obvious that much work remains to explain the rather complicated phenomena which are probably occurring not only in the mechanical mixtures studied here, but also in the two-phase system generated when a substance undergoes a polymorphic transition in a high stress environment.

Acknowledgments

This research has been supported by NSF Grant NSF GA 1270 and ARPA grant SD–89–Research and by the Petroleum Research Fund of the American Chemical Society. Grateful acknowledgment is made to the donors of that fund.

References

[1] Bobrowsky, A., in High-Pressure Measurement, ed. A. A. Giardini and E. C. Lloyd, Butterworth, Washington D.C. (1963).
[2] Corll, J. A., and Warren, W. E., J. Appl. Phys. **36**, 3655 (1965).
[3] Jamieson, J. C., and Lawson, A. W., J. Appl. Phys. **33**, 776 (1962).
[4] Lippincott, E. R., and Duecker, H. C., Science **144**, 1119 (1964).
[5] Jamieson, J. C., Bull. Geol. Soc. Am. **74**, 1067 (1963).
[6] Corll, J. A., J. Appl. Phys. **38**, 2708 (1967).
[7] Jamieson, J. C., in Metallurgy at High Pressures and High Temperatures, ed. M. T. Hepworth, N. A. D. Parlee, and K. Gschneidner, Gordon and Breach, New York (1963).
[8] Clark, S. P., ed., Handbook of Physical Constants, Geol. Soc. Am. Memoirs **97** (1966).
[9] Barrett, C. S., Structure of Metals, 2d ed., McGraw-Hill, New York (1952).
[10] Fritz, J. N., Marsh, S. P., Carter, W. J., and McQueen, R. G., The Hugoniot equation of state of sodium chloride in the sodium chloride structure, presented at this meeting.

Comparison of Four Proposed *P-V* Relations for NaCl*

J. Scott Weaver

Department of Geological Sciences and Space Science Center, The University of Rochester, Rochester, New York 14627

Some comparisons among four *P-V* relations for the B1 phase of NaCl discussed at this symposium are presented. The two scales (Models III and V) proposed by Weaver et al. (this volume) and a 1968 revision of Decker's *P-V* relation (D_{68}) are shown to agree closely. The three models yield zero-pressure thermal expansion curves in reasonable agreement with experiment, but give values for B'_{to} smaller than the measured value. This appears to be due, in part, to the form used for the lattice energy. The three models yield pressures about 2.5 percent smaller than those calculated from the pressure scale (F_{68}) based on Hugoniot data proposed by Fritz et al. (this volume). Comparison of Models III, V, and F_{68} in the $u_s - u_p$ plane suggests that part of this difference must result from either the form chosen for the lattice energy in Models III and V or from the Hugoniot data upon which F_{68} is based. Omission of part of the data used in F_{68} improves the agreement of this model with the sonic value of B'_{to} and partially removes the discrepancy between F_{68} and Models III and V. Suggestions for additional studies which may be useful in choosing a *P-V* relation for NaCl for pressure calibration purposes are presented. It is concluded that, since the differences among these scales are comparable to the experimental uncertainties involved in applying them, and since there is no compelling reason to choose one over the others, any of these scales may be used for the present.

1. Introduction

Following the discussions at this symposium, it seemed desirable to expand the treatment of the various proposed *P-V* relations for NaCl presented in Weaver et al. (this volume). In addition, the new pressure scale proposed at this symposium by Fritz et al. (this volume) differs significantly from those described in Weaver et al. In this supplementary paper, four proposed *P-V* relations for NaCl are compared in an attempt to find criteria favoring one of them, and some suggestions for additional studies bearing on the problem are made.

For convenience, the models discussed here are referred to by abbreviations: III and V refer to Models III and V presented in Weaver et al. (this volume); F_{68} refers to the 295 °K isotherm based on shock wave data reported by Fritz et al. at this symposium. The discussion here is based on the values given in tables 3 and 4 of their paper (Fritz et al., this volume). In 1968, Daniel L. Decker kindly provided a copy of computer output containing a revision of his published calculations (Decker, 1965) of the equation of state for NaCl. This revised model will be referred to as D_{68}. In general, the notations of this paper follow those in Weaver et al. (this volume). Additional notation is defined as introduced.

2. Thermal Expansion

The thermodynamic Gruneisen parameter for III, V, and D_{68} (already assumed to be a function of the volume only in both the Hildebrand and Mie-Gruneisen approximations) was assumed to be of the form: $\gamma = \gamma_0 x^A$. In III and V, the value: $A = 1.2 \pm 0.4$ was calculated from the relation: $A = 1 + (1 + \gamma\alpha T)\delta_s - B'_s + \gamma$ evaluated at $P = 0$. In D_{68}, the value: $A = 0.767$ was determined to yield the best agreement (in a least square sense) between the observed zero-pressure thermal expansion curve for NaCl and that calculated from the model. In order to compare these two different approaches to the determination of the volume dependence of the Gruneisen parameter, calculated zero-pressure thermal expansion curves for III, V, and D_{68} were compared with

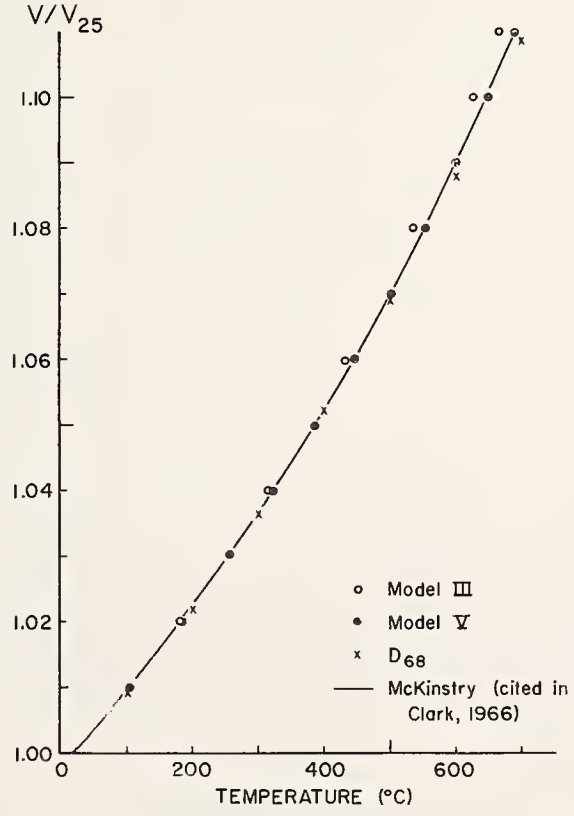

FIGURE 1. *Comparison of the zero-pressure thermal expansion for* NaCl *from models III, V, and* D_{68} *with results from experiment.*

V_{25} is the volume of NaCl at 25 °C and $P = 0$. The agreement between the calculated and measured thermal expansion curves suggests that it is not essential to use the measured thermal expansion as a boundary condition on the models (as was done for D_{68}).

*Paper and Discussion prepared subsequent to the Symposium at suggestion of Symposium organizers. Paper received in final form April 1970.

experimental results obtained by McKinstry (cited in Clark, 1966) as shown in figure 1. The points for III and V were obtained by numerically solving the P-V-T relation for V and T such that $P=0$. The points for D_{68} were calculated by three-point inverse Lagrangian interpolation in Decker's table to estimate the value of r/r_0 for which $P=0$ at various temperatures. The experimental curve was obtained by five-point Lagrangian interpolation using McKinstry's values given in Clark (1966). As can be seen in figure 1 the thermal expansion curves for V and D_{68} agree closely with the experimental results, while III yields values for the expansion about 5 percent larger at high temperatures. The general agreement among the three models suggests that the thermal expansion is insensitive to the method used to determine A, and that it is not essential that the model be forced to fit the thermal expansion curve. However, the different values of A chosen for III and V versus D_{68}, lead to different values of $(\partial P/\partial T)_V$ at high pressures. Hence, caution must be used in applying these models to pressure or temperature measurement under simultaneous conditions of high temperature and high pressure.

3. Pressure Derivatives of B_t

The values of the pressure derivatives of B_t calculated for III, V, and D_{68} may be compared with experimental values to yield a test of the models since only P and B_t are fixed by the boundary conditions at $V=V_0$, while the derivatives are then determined by the form of the model. The values for the pressure derivatives of B_t for F_{68} are largely determined by the experimental Hugoniot for NaCl and, to a lesser extent, by the procedure used to reduce the Hugoniot to an isotherm. Values for the dimensionless parameters B'_{to} and $-B_{to}B''_{to}$ for models III and V were calculated by means of seven-point finite-difference formulas to yield the results shown in table 1. Since D_{68} and F_{68} are presented in tabular form, numerical derivatives are subject to large errors due to rounding-off of the tabulated values. This difficulty may be avoided by using an approximate P-V relation such as the Murnaghan or Birch equation to convert the tabulated P-V relation to a more slowly varying function of V. For example, the parameter a obtained from the Murnaghan equation: $P=B_{to}a^{-1}(x^{-a}-1)$ is an approximately linear function of x for all of the models considered here as is shown in figure 2. A linear least squares fit to the $a-x$ relation for each model together with the relations:

$$B'_{to}=\lim_{x\to 1} a \text{ and } -B_{to}B''_{to}=\lim_{x\to 1}\frac{da}{dx}$$

(which follow easily from the Murnaghan equation) was used to compute the values shown in table 1.

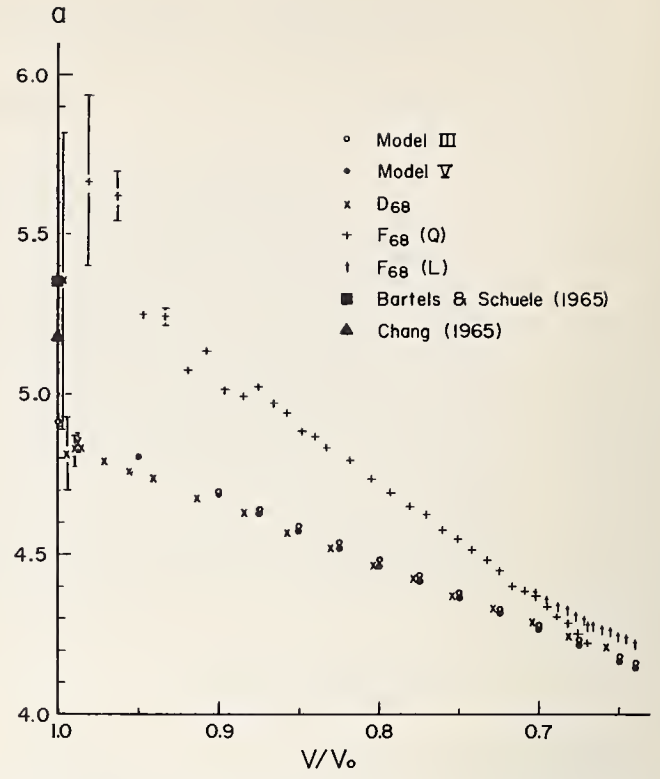

FIGURE 2. *Murnaghan equation parameter* a *versus volume for several models for* NaCl.

a was calculated from the Murnaghan equation: $P=B_{to}a^{-1}[(V/V_0)^{-a}-1]$; with $B_{to}=237.4$ kbar for III, V, and F_{68}; and $B_{to}=(0.00422)^{-1}$ kbar for D_{68}. Q and L are the quadratic and linear forms of F_{68}. The error flags show the uncertainty in a resulting from rounding off of the tabulated values of P and V for D_{68} and F_{68}. It can be shown that $a=B'_{to}$ at $V/V_0=1$. Two measured values for B'_{to} for NaCl are shown for comparison.

TABLE 1. *Values for* B'_{to} *and* $-B_{to}B''_{to}$ *calculated from models III, V,* D_{68}, *and* F_{68} *and values for* B'_{to} *determined by experiment for* NaCl.

Source	B'_{to}	$-B_{to}B''_{to}$	Method
Experiment	5.18 ± 0.09	.....	Sonic (uniaxial loading); Chang, 1965.
Experiment	5.35	.....	Sonic (hydrostatic pressure); Bartels and Schuele, 1965.
III	4.916	5.964	Numerical differentiation.
	4.902	6.217	Murnaghan equation.
V	4.894	7.169	Numerical differentiation.
	4.896	6.405	Murnaghan equation.
D_{68}	4.858	6.416	Murnaghan equation, $B_{to}=237.0$ kbar.
F_{68}	5.453	10.991	Murnaghan equation, $B_{to}=237.4$ kbar.

The values obtained for III and V using this procedure differ somewhat from those calculated by direct differentiation since the $a-x$ relation exhibits a slight curvature. The difference is probably not significant for the present purposes.

As can be seen from table 1, models III, V, and D_{68} all yield values for B'_{to} smaller than those determined experimentally. The value of the parameter $-B_{to}B''_{to}$ has not been measured for NaCl, although

the values: $-B_{so}B''_{so} \simeq 1.1B'_{so}$ found for CsCl, CsBr, and CsI (Chang and Barsch, 1967) and the value $-B_{to}B''_{to} \simeq 1.06B'_{to}$ for CsI (Barsch and Chang, this volume) suggest that the values $-B_{to}B''_{to} \simeq 1.3B'_{to}$ calculated for III, V, and D_{68} are not unreasonable. The reason for the discrepancy between the values for B'_{to} calculated from the models and that obtained from experiment is not clear. The agreement among the models shows that inclusion of the second nearest neighbor interaction does not significantly change the value calculated for B'_{to}, while the effect of the vibrational energy terms is too small to remove the discrepancy without assuming unreasonably large values for the parameter A. (For example: in model V, $B'_{to}=5.18$ would require that $A=3.42$, while $B'_{to}=5.35$ would require $A=4.85$. Either value of A is incompatible with the observed values of B'_{so} and δ_{so}.)

The value for B'_{to} calculated from F_{68} is larger than that found from experiment, and the value for $-B_{to}B''_{to} \simeq 2B'_{to}$ is larger than that expected by analogy with the cesium halides. As will be discussed in the next section, the value for B'_{to} can be brought into agreement with that measured by Bartels and Schuele (1965) if the eight lowest pressure data points are omitted from the Hugoniot determined by Fritz et al. (this volume). This procedure would also reduce the value of $-B_{to}B''_{to}$.

4. Comparison With Shock-Wave Data

In comparing F_{68} with III, V, and D_{68}, the effect of the Hugoniot to isotherm reduction used in F_{68} may be eliminated by calculating the Hugoniot corresponding to the assumptions already used in III, V, or D_{68}. For these models, the pressure, P_H, along the Hugoniot is given by:

$$P_H=\left[\frac{1}{2}\gamma(1-x)-x\right]^{-1}\left\{\frac{\gamma}{V_0}(\phi-\phi_0)+x\phi'-\frac{\gamma}{\gamma_0}\phi'_0\right\}$$

where ϕ is the lattice energy, $\phi'=d\phi/dV$, and the subscript "$_0$" refers to quantities evaluated at $V=V_0$. The corresponding shock (u_s) and particle (u_p) velocities are then determined by the Rankine-Hugoniot relations: $u_p=\rho_0^{-1/2}P_H^{1/2}(1-x)^{1/2}$; and $u_s=u_p(1-x)^{-1}$. The calculated u_s-u_p relations for III and V are compared with data from experiment in figure 3. The results for III and V are in agreement with the values obtained by Christian (1957) and by Al'tshuler et al. (1961), but lie below those found by Hauver and Melani (cited in van Thiel, 1966) and those found by Fritz et al. (this volume) which form the basis for F_{68}. (According to Fritz et al., the data from Hauver and Melani are based on the old 2024 aluminum standard, and will be brought into better agreement with the data from Fritz et al. when the new standard is used.) The difference between the

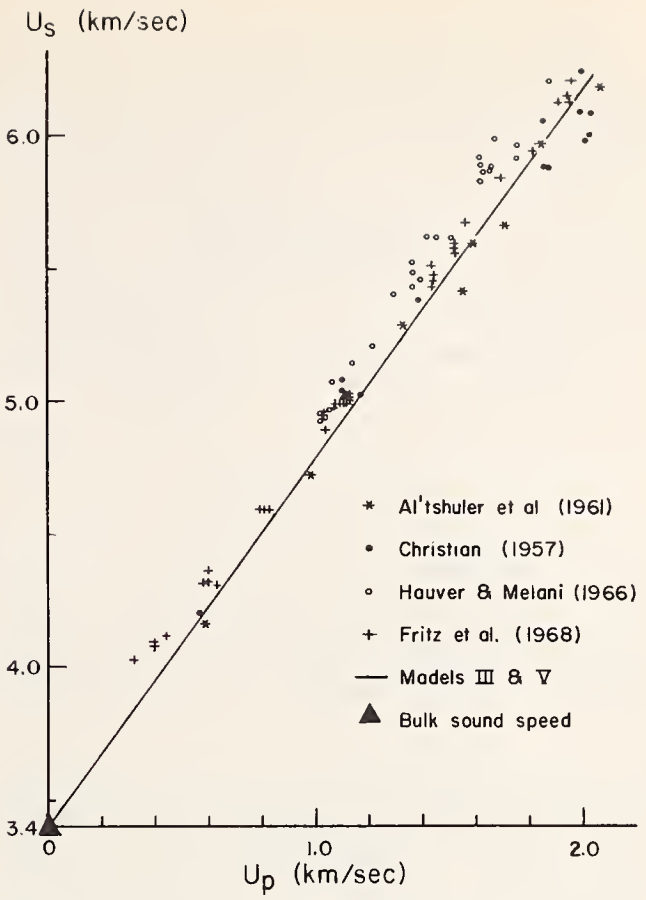

FIGURE 3. *Shock versus particle velocity for* NaCl *calculated from III and* V *compared with results from experiment.*

The calculated u_s-u_p relations for III and V are indistinguishable on the scale plotted. The bulk sound speed for NaCl measured by Slagle and McKinstry (1967) is shown by the filled triangle. The value determined by Haussuhl (1960) would be plotted within the triangle. As noted in the text, the experimental results of Hauver and Melani will be in better agreement with those found by Fritz et al. when the 2024 aluminum standard is revised.

u_s-u_p relation measured by Fritz et al. and that calculated for III and V is most pronounced for $u_p<0.7$ km/s and is somewhat reduced for larger values of u_p. Since the discrepancy between F_{68} and III or V persists when the u_s-u_p relations corresponding to these models are compared, the procedure used by Fritz et al. does not appear to be responsible for the difference.

The effect of the vibrational terms in the internal energy for III, V, and D_{68} on the Hugoniot pressure was investigated by calculating γ from the lattice energy and the observed u_s-u_p relation (Fritz et al., this volume) using the relations given above. It was found that $d\ln\gamma/d\ln V$ must have a parabolic dependence on $\ln V$ if the models and the observed u_s-u_p relation are to agree. For example, in the case of model V, the quantity $d\ln\gamma/d\ln V$ is reduced from 1.2 at $V/V_0=1.0$ to zero (or even slightly negative) at $V/V_0=0.88$ and then increases rapidly—reaching the value 3.2 at $V/V_0=0.70$. Although such behavior of γ cannot be excluded, it seems more plausible to seek to resolve the discrepancy between the calculated models and F_{68} by another means.

The data obtained by Fritz et al. are compatible with a linear u_s-u_p relation which yields a bulk sound speed about 4 percent larger than that calcu-

385-762 O - 71 - 22

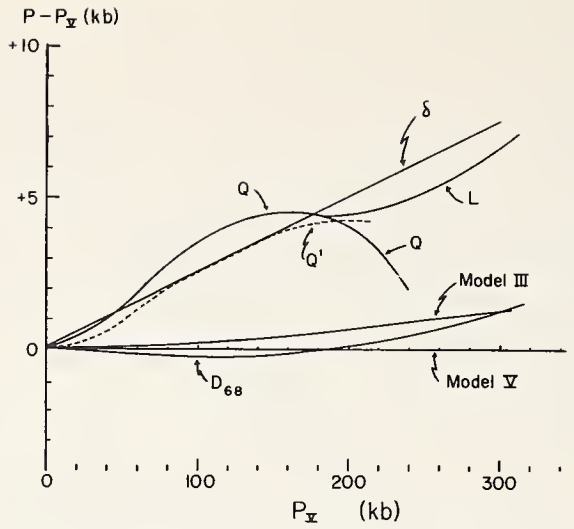

FIGURE 4. *Comparison of pressures from several models for* NaCl *with those calculated from* V.

The curve δ is an estimated upper bound on the uncertainty in the pressure calculated from V resulting from the uncertainties in the parameters used in the model. Curves Q and L are the portions of F_{68} derived from the quadratic and linear fits to the measured u_s-u_p relation for NaCl. Q' is derived from Q by omitting the 8 lowest pressure data points from the u_s-u_p relation.

lated from sonic measurements on NaCl. Hence, Fritz et al. chose to fit their data with a quadratic u_s-u_p relation constrained to pass through the measured bulk sound speed. Since the lowest pressure data points appear to deviate from the fitted u_s-u_p relation, it is interesting to examine the effect of these points on both the Hugoniot and on F_{68}. The omission of at least the four lowest data points may be justified since Fritz et al. state that these points were obtained by a different driver arrangement (using impedance mismatch to produce low shock pressures) and may have been influenced by overtaking waves. When all 43 data points listed by Fritz et al. (this volume; table 1) were fitted, the u_s-u_p relation was found to be: $u_s=3.403+1.5492u_p-0.07833u_p^2$; while, when the eight lowest pressure data points (those for which $u_p<0.70$ km/s) are omitted, the fitted relation becomes: $u_s=3.403+1.5141u_p-0.05738u_p^2$—where u_s and u_p are in km/s, and the bulk sound speed measured by Haussuhl (1960) has been used to fix the u_s-u_p relation at $u_p=0$. Most of the change results from the omission of the four lowest points, while omitting more than eight points was found to have little effect on the fitted u_s-u_p relation.

One effect of omitting the lowest points is to reduce the values for B'_{to} and $-B_{to}B''_{to}$ calculated from the u_s-u_p relation. In particular, the value of B'_{to} is reduced from 5.47 to 5.33 when the eight lowest points are excluded. The latter value is in excellent agreement with the value of 5.35 measured by Bartels and Schuele (1965) but still larger than Chang's (1965) value of 5.18. The value of $-B_{to}B''_{to}$ will also be reduced, although the lack of measured values for the second pressure and temperature derivatives of B_t for NaCl prevents calculations of the actual values. The omission of the eight lowest data points was not found to have any significant effect on the calculated temperature along the Hugoniot, so that only the change in the Hugoniot pressure need to considered in estimating the effect of these points on F_{68}. Reducing the pressure calculated from F_{68} by an amount equal to the difference in the Hugoniot pressures for the two u_s-u_p relations, yields a revised model (Q') which is compared with the others in figure 4. It can be seen that, although the discrepancy between F_{68} and III, V, and D_{68} is reduced, most of the difference remains when F_{68} is revised.

5. Conclusions

The discussions in both Weaver et al. (this volume) and the present work serve to show the close similarity among models III, V, and D_{68}. It seems that, within the quasi-harmonic formulation of the equation of state for an ionic solid, the room-temperature isotherm and the zero-pressure thermal expansion curve for NaCl are insensitive to the form chosen for the vibrational energy (Hildebrand or Mie-Gruneisen approximation), the neglect or inclusion of the repulsion between second nearest neighbors, or the exponent (A) chosen for the volume dependence of the Gruneisen parameter. However, use of these models at elevated temperatures will require that the parameter A be determined. Since A for III and V satisfies thermodynamic constraints at $P=0$, and since these models yield good approximations to the zero-pressure thermal expansion curve for NaCl, they should be useful at high temperatures.

Models III, V, and D_{68} yield pressures about 2.5 percent smaller than those calculated from F_{68} (see fig. 4). This difference cannot be attributed to the procedure used to convert the Hugoniot to an isotherm in F_{68}. Changing the form for the volume dependence of the Gruneisen parameter in III or V so as to remove the difference leads to implausible behavior of γ and its derivative with volume. Hence, either the form chosen for the lattice energy in III, V, and D_{68} or the u_s-u_p data used in F_{68} must be responsible for much of the discrepancy between these models. If the lattice energy is in error, V and F_{68} can be brought into agreement by inclusion of a term of gaussian form, suggesting that covalent bonding may be involved. However, it seems premature to include such a term without additional information.

Model F_{68} yields the value $B'_{to}=5.45$, while III, V, and D_{68} give values near 4.90. If the lowest pressure Hugoniot data (eight points) are omitted, F_{68} yields $B'_{to}=5.33$—in excellent agreement with the value measured by Bartels and Schuele (1965), but higher than that found by Chang (1965). Raising the value of B'_{to} for III, V, and D_{68} to either of the measured values probably will require modification of the form used for the lattice energy, since unreasonable

values of A are required to accomplish this with the vibrational energy terms. An additional measurement of B'_{to} for NaCl—either by sonic methods or perhaps, by means of low-pressure shock-wave techniques—would be most useful since a value near that obtained by Bartels and Schuele would tend to support F_{68}, whereas a value near Chang's would suggest that the P-V relation for NaCl lies between F_{68} and III, V, or D_{68}.

Additional determinations of the $u_s - u_p$ relation for NaCl at particle velocities less than 1.0 km/s would be useful to determine whether, as suggested here and in Fritz et al. (this volume), the low-pressure portion of F_{68} is influenced by errors in the Hugoniot data. In addition, studies on porous samples might help to determine the best choice for the parameter A. Measurement of the volume of NaCl by means of piston-cylinder techniques at pressures in the 50 to 100 kbar pressure range may be able to distinguish between F_{68} and III, V, and D_{68}.

In conclusion, I believe that it is premature to attempt to choose one of these scales over the others. Fortunately, the differences between them are, at worst, comparable to the experimental uncertainties in the application of the internal standard method of pressure determination in x-ray diffraction studies at pressures above 100 kbar. For the present, it would be desirable to report the volume for the internal standard together with the pressure based on any of these pressure scales.

6. References

Al'tshuler, L. V., Kuleshova, L. V., and Pavlovskii, M. N., The dynamic compressibility, equation of state, and electrical conductivity of sodium chloride at high pressures, Soviet Physics (JETP) **12**, 10–15 (1961).

Barsch, G. R., and Chang, Z. P., Ultrasonic and static equation of state for cesium halides, this volume.

Bartels, R. A., and Schuele, D. E., Pressure derivatives of the elastic constants of sodium chloride and potassium chloride at 295 deg. K and 195 deg. K, J. Phys. Chem. Solids **26**, 537–550 (1965).

Chang, Z. P., Third order elastic constants of sodium chloride and potassium chloride single crystals, Phys. Rev. **A140**, 1788–1799 (1965).

Chang, Z. P., and Barsch, G. R., Nonlinear pressure dependence of elastic constants and fourth-order elastic constants of cesium halides, Phys. Rev. Letters **19**, 1381–1382 (1967).

Christian, R. H., The equation of state of alkali halides at high pressure, Univ. Calif. Radiation Lab. Report 4900 (1957).

Clark, S. P., Ed., Handbook of physical constants, Geol. Soc. Am. Memoir 97, p. 80 (1966).

Decker, D. L., Equation of state of NaCl and its use as a pressure gauge in high-pressure research, J. Appl. Phys. **36**, 157–161, 1965.

Decker, D. L., personal communication (1968).

Fritz, J. N., et al., The Hugoniot equation of sodium chloride in the sodium chloride structure, this volume.

Haussuhl, S., Thermo-elastische Konstanten der Alkalihalogenide vom NaCl-Typ, Z. Phys. **159**, 223–229 (1960).

Slagle, O. D., and McKinstry, H. A., Temperature dependence of the elastic constants of the alkali halides. I. NaCl, KCl, and KBr, J. Appl. Phys. **38**, 437–446 (1967).

van Thiel, M., Compendium of Shock Wave Data, UCRL–50108 (Vol. 1) (1966).

Weaver, J. S., Takahashi, T., and Bassett, W. A., Calculation of the P-V relation for the B1 phase of NaCl up to 300 kbar at 25 °C, this volume.

DISCUSSION

D. L. Decker (*Brigham Young University, Provo, Utah*): The three equations, which are labeled III, V, and D_{68}, all assumed a volume dependence of the Gruneisen parameter to be of the form

$$\gamma = \gamma_0 (V/V_0)^A. \qquad (1)$$

Weaver compared the various choices of A and the models for these equations by comparing the volume expansion versus temperature calculated from the three equations. This is a very insensitive test for the correct value of A. A far better approach is to compare the calculated coefficient of linear thermal expansion versus temperature against the experimental results. (Enck and Dommel, 1965.) This is done in figure 1 where one observes that even at atmospheric pressure the value of A plays a definite role in thermal expansion. $A = 0.7$ gives the best fit to the experimental thermal expansion. $A = 1.4$ gives the best fit of the calculated adiabatic bulk modulus at atmospheric pressure to the measurements of Slagle and McKinstry (1967). In the modification referred to by Weaver, I used $A = 0.93$ which gives a reasonable fit to these two experimental results simultaneously.

The direct value of B'_{to} calculated in D_{68} is 4.92, which differs slightly from the interpolated value

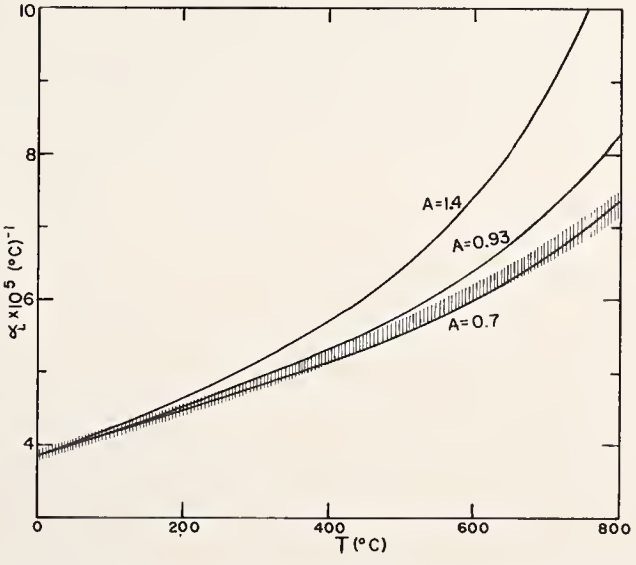

FIGURE 1. *Coefficient of linear thermal expansion versus temperature at atmospheric pressure. The solid curves are calculated using various values for the parameter A. The darkened area gives the range of the experimentally measured values.*

TABLE 1. *Comparison of calculated pressure and the pressure measured by shock techniques[a] along the Hugoniot and the 293 K isotherm.* a_0 *is the lattice parameter at 25 °C and atmospheric pressure. Pressure in kbar.*

$P(F_{68})$	Along the Hugoniot			293 K isotherm		
	a/a_0	T(K)	$P(D_{68})$	a/a_0	$P(D_{68})$	[b] $\Delta P(D_{68})$
25	0.9732	336	24.7	0.9721	24.6	±1.1%
50	0.9546	386	49.0	0.9529	48.9	±1.6%
75	0.9402	450	73.2	0.9387	73.0	±1.9%
100	0.9284	527	97.6	0.9252	97.6	±2.4%
150	0.9095	721	147.2	0.9050	146.6	±2.9%
200	0.8945	960	198.3	0.8887	197.8	±3.4%
250	0.8821	1,238	250.4	0.8746	252.2	±3.7%

[a] Fritz, J. N., S. P. Marsh, W. J. Carter, and R. G. McQueen, The Hugoniot equation of state of sodium chloride in the sodium chloride structure, this volume.

[b] The uncertainty in D_{38} due to uncertainties in the experimental parameters used in the calculation. This does not include any uncertainty due to the approximations in the theory.

given by Weaver, and is in excellent agreement with III and V. There is also another experimental measurement of B'_{to} which should be added to Weaver's table 1 and included in the discussion. This is the value 4.98 ± 0.20 measured by Drabble and Strathen (1967) which is smaller than the other measurements but agrees very well with the theoretical values in III, V, and D_{68}. There is another recent measurement yielding $B'_{to} = 3.2$ (Gluyas, 1967) but this is likely too low. The measurements of B'_{to} indicate that the theories are credible but these measurements are not precise enough to give any guidance as to how one might improve the theory.

I agree that, to within the uncertainties involved, the differences between F_{68} and III, V, or D_{68} are not related to the procedure of converting from the Hugoniot to the isotherm. This is borne out in table 1 where the calculated and measured pressures are compared along the Hugoniot as well as along the room temperature isotherm. The final column in the table gives the estimated accuracy of the calculated equation of state as limited by the uncertainties in the input parameters. These uncertainties include a variation of A ranging from 0.7 to 1.4. It is concluded that all these theoretical equations of state lie within the uncertainties given and give equally reliable approximations to the true pressure. F_{68}, however, is definitely different from D_{68} but possibly not outside the experimental error.

Bibliography

Drabble, J. R., and Strathen, R. E. B., The third-order elastic constants of potassium chloride, sodium chloride, and lithium fluoride, Proc. Phys. Soc., **92,** 1090 (1967).

Enck, F. D., and Dommel, J. G., Behavior of the thermal expansion of NaCl at elevated temperatures, J. Appl. Phys. **36,** 839 (1965).

Gluyas, M., The second- and third-order elastic constants of sodium chloride at 295 °K, Brit. J. Appl. Phys. **18,** 913 (1967).

Slagle, O. D., and McKinstry, H. A., Temperature dependence of the elastic constants of the alkali halides. I. NaCl, KCl, and KBr J. Appl. Phys. **38,** 437 (1967).

Weaver, J. S., Comparison of four proposed P–V relations for NaCl, this volume.

J. N. Fritz (*University of California, Los Alamos New Mexico*): We concur with the views and conclusions presented by Dr. Weaver. There now exists further experimental justufication for casting out the lowest pressure data points reported by us. New experiments have indicated (at least for our four lowest data points) the existence of a second compression wave in the shims that close the gap over the NaCl sample. This wave arises from the rarefaction coming back through the shim and its interaction with the NaCl. The additional particle velocity imparted to the shim results in an early gap closure and a higher apparent shock velocity in the NaCl sample. This effect becomes progressively less important at high pressures, and vanishes altogether above a certain critical pressure, and is absent for the bulk of the data we reported. The net effect of all this is well represented in Weaver's Q′ curve in his fig. 4.

Symposium Participants

L. Abbot, Harwood Engineering, Walpole, Massachusetts
P. H. Abelson, Carnegie Institution of Washington, Washington, D.C.
S. Akimoto, University of Tokyo, Tokyo, Japan
P. B. Alers, U.S. Naval Research Laboratory, Washington, D.C.
E. Ambler, National Bureau of Standards, Washington, D.C.
O. Anderson, Columbia University, Palisades, New York
N. Asami, Mitsubishi Atomic Power Ind., Inc., Saitama, Japan
Y. A. Atanov, All-Union Research Institute for Physical and Radiotechnical Measurements, Moscow
S. E. Babb, University of Oklahoma, Norman, Oklahoma
J. D. Barnett, Brigham Young University, Provo, Utah
G. R. Barsch, Pennsylvania State University, University Park, Pennsylvania
W. A. Bassett, University of Rochester, Rochester, New York
R. Bautista, Rice University, Houston, Texas
C. W. Beckett, National Bureau of Standards, Washington, D.C.
P. Bell, Carnegie Institution of Washington, Washington, D.C.
S. Block, National Bureau of Standards, Washington, D.C.
C. Bosco, U.S. Army Electronics Command, Fort Monmouth, New Jersey
H. P. Bovenkerk, General Electric Company, Detroit, Michigan
J. C. Bowen, Pressure Products Industry, Hatboro, Pennsylvania
F. R. Boyd, Jr., Carnegie Institution of Washington, Washington, D.C.
W. R. Bozman, National Bureau of Standards, Washington, D.C.
J. W. Brasch, University of Maryland, College Park, Maryland
F. Bundy, General Electric Research and Development Center, Schenectady, New York
P. D. Calvert, Massachusetts Institute of Technology, Cambridge, Massachusetts
W. J. Carter, University of California, Los Alamos, New Mexico
R. Cavailhe, Commissariat à l'Energie Atomique, Paris, France
A. Cezairliyan, National Bureau of Standards, Washington, D.C.
Z. P. Chang, Pennsylvania State University, University Park, Pennsylvania
D. H. Chung, Massachusetts Institute of Technology, Cambridge, Massachusetts
T. Clark, General Electric Company, Detroit, Michigan
N. L. Coleburn, Naval Ordnance Laboratory, White Oak, Maryland
E. M. Compy, U.S. Naval Research Laboratory, Washington, D.C.
M. Contre, Commissariat à l'Energie Atomique, Paris, France
M. Cowperthwaite, Stanford Research Institute, Menlo Park, California
J. L. Cross, National Bureau of Standards, Washington, D.C.
D. Decker, Brigham Young University, Provo, Utah
T. B. Douglas, National Bureau of Standards, Washington, D.C.
H. G. Drickamer, University of Illinois, Urbana, Illinois
G. E. Duvall, Washington State University, Pullman, Washington
D. Edwards, Naval Ordnance Laboratory, White Oak, Maryland
J. L. England, Carnegie Institution of Washington, Washington, D.C.
J. O. Erkman, Naval Ordnance Laboratory, White Oak, Maryland
J. L. Feldman, Naval Research Laboratory, Washington, D.C.
J. Forbes, Naval Ordnance Laboratory, White Oak, Maryland
P. J. Freud, Battelle Memorial Institute, Columbus, Ohio
R. C. Frisch, National Bureau of Standards, Washington, D.C.

I. Getting, University of California, Los Angeles, California
M. C. Gilbert, Virginia Polytechnic Institute, Blacksburg, Virginia
R. Grover, Lawrence Radiation Laboratory, Livermore, California
W. E. Hake, American Instrument Co., Inc., Silver Spring, Maryland
H. T. Hall, Brigham Young University, Provo, Utah
D. L. Hamilton, University of Manchester, Manchester, England
R. E. Hanneman, General Electric Research and Development Center, Schenectady, New York
J. R. Hastings, National Bureau of Standards, Washington, D.C.
G. E. Hauver, Aberdeen Proving Ground, Aberdeen, Maryland
J. Haygarth, University of California, Los Angeles, California
P. L. M. Heydemann, National Bureau of Standards, Washington, D.C.
A. Holt, Lawrence Radiation Laboratory, Livermore, California
J. Houck, National Bureau of Standards, Washington, D.C.
R. Houidobre, Air Force Office of Scientific Research, Arlington, Virginia
E. Hryckowian, U.S. Army Electronics Command, Fort Monmouth, New Jersey
R.P. Hudson, National Bureau of Standards, Washington, D.C.
U. O. Hutton, Brinklow, Maryland
J. Jackson, University of Maryland, College Park, Maryland
G. S. James, Adamant Research Laboratory, Johannesburg, South Africa
J. C. Jamieson, University of Chicago, Chicago, Illinois
A. Jayaraman, Bell Telephone Laboratories, Murray Hill, New Jersey
D. P. Johnson, National Bureau of Standards, Washington, D.C.
O. E. Jones, Sandia Laboratory, Albuquerque, New Mexico
G. Jura, University of California, Berkeley, California
R. Kaneda, National Research Laboratory of Metrology, Tokyo, Japan
N. Kawai, Osaka University, Toyonaka, Osaka, Japan
G. S. Kell, National Research Council of Canada, Ottawa, Canada
G. C. Kennedy, University of California, Los Angeles, California
R. S. Kirk, General Electric Research and Development Center, Schenectady, New York
M. C. Krupka, University of California, Los Alamos, New Mexico
I. Kushiro, Carnegie Institution of Washington, Washington, D.C.
A. S. Kusubov, Lawrence Radiation Laboratory, Livermore, California
A. Lacam, Laboratoire de Bellevue, Bellevue, Seine et Oise, France
P. N. LaMori, Battelle Memorial Institute, Columbus, Ohio
Le Neindre, Laboratoire de Bellevue, Bellevue, Seine et Oise, France
D. H. Lindsley, Carnegie Institution of Washington, Washington, D.C.
E. C. Lloyd, National Bureau of Standards, Washington, D.C.
E. Lundblad, Scandiament AB, Robertfors, Sweden
I. MacGregor, S. W. Center for Advanced Studies, Dallas, Texas
D. H. K. Mao, Carnegie Institution of Washington, Washington, D.C.
D. B. McWhan, Bell Telephone Laboratories, Murray Hill, New Jersey
R. Meister, U.S. Geological Survey, Washington, D.C.
L. Merrill, Brigham Young University, Provo, Utah
H. O. A. Meyer, Carnegie Institution of Washington, Washington, D.C.
S. Minomura, University of Tokyo, Tokyo, Japan
W. Mock, Jr., U.S. Naval Weapons Laboratory, Dahlgren, Virginia
R. L. Nuttall, National Bureau of Standards, Washington, D.C.
J. Paauwe, Naval Ordnance Laboratory, White Oak, Maryland
D. L. Pastine, Naval Ordnance Laboratory, White Oak, Maryland
L. Peselnick, U.S. Geological Survey, Washington, D.C.
E. J. Prosen, National Bureau of Standards, Washington, D.C.
S. V. Radcliffe, Case Western Reserve University, Cleveland, Ohio

C. R. Robbins, National Bureau of Standards, Washington, D.C.
E. C. Robertson, U.S. Geological Survey, Washington, D.C.
M. F. Rose, Naval Weapons Laboratory, Dahlgren, Virginia
R. Roy, Pennsylvania State University, University Park, Pennsylvania
P. St. Pierre, General Electric Company, Detroit, Michigan
G. A. Samara, Sandia Laboratory, Albuquerque, New Mexico
K. H. Schumaker, Air Force Office of Scientific Research, Arlington, Virginia
C. B. Sclar, Lehigh University, Bethlehem, Pennsylvania
G. J. Scott, University of Oklahoma, Norman, Oklahoma
F. Seifert, Institut fuer Mineralogie, Kiel, West Germany
J. V. Sengers, University of Maryland, College Park, Maryland
H. R. Shaw, U.S. Geological Survey, Washington, D.C.
E. Shull, Pennsylvania State University, University Park, Pennsylvania
E. F. Skelton, U.S. Naval Research Laboratory, Washington, D.C.
V. Sokolovskiy, All-Union Research Institute for Physical and Radiotechnical Measurements, Moscow
I. L. Spain, University of Maryland, College Park, Maryland
H. D. Stromberg, Lawrence Radiation Laboratory, Livermore, California
H. M. Strong, General Electric Research and Development Center, Schenectady, New York
C. Susse, Laboratoire de Bellevue, Bellevue, Seine et Oise, France
M. Swerdlow, Air Force Office of Scientific Research, Arlington, Virginia
T. Takahashi, University of Rochester, Rochester, New York
A. Taylor, Westinghouse Research Laboratories, Pittsburgh, Pennsylvania
L. Thomsen, Columbia University, Palisades, New York
L. C. Towle, Naval Research Laboratory, Washington, D.C.
G. Uriano, National Bureau of Standards, Washington, D.C.
M. van Thiel, Lawrence Radiation Laboratory, Livermore, California
A. van Valkenburg, National Science Foundation, Washington, D.C.
H. Vanfleet, Brigham Young University, Provo, Utah
K. Vedam, Pennsylvania State University, University Park, Pennsylvania
O. B. Verbeke, University of Maryland, College Park, Maryland
B. Vodar, Laboratoire de Bellevue, Bellevue, Seine et Oise, France
M. Waxman, National Bureau of Standards, Washington, D.C.
J. S. Weaver, University of Rochester, Rochester, New York
A. Webb, Naval Research Laboratory, Washington, D.C.
C. E. Weir, National Bureau of Standards, Washington, D.C.
R. H. Wentorf, Jr., General Electric Research and Development Center, Schenectady, New York
M. S. Werkema, Dow Chemical Company, Golden, Colorado
H. Woolley, National Bureau of Standards, Washington, D.C.
H. S. Yoder, Jr., Carnegie Institution of Washington, Washington, D.C.
H. Young, E. I. duPont de Nemours and Co., Wilmington, Delaware
R. Zeto, U.S. Army Electronics Command, Fort Monmouth, New Jersey
E. V. Zolotykh, All-Union Research Institute for Physical and Radiotechnical Measurements, Moscow

U.S. GOVERNMENT PRINTING OFFICE : 1971 OL—385–762

NBS TECHNICAL PUBLICATIONS

PERIODICALS

JOURNAL OF RESEARCH reports National Bureau of Standards research and development in physics, mathematics, chemistry, and engineering. Comprehensive scientific papers give complete details of the work, including laboratory data, experimental procedures, and theoretical and mathematical analyses. Illustrated with photographs, drawings, and charts.

Published in three sections, available separately:

• Physics and Chemistry

Papers of interest primarily to scientists working in these fields. This section covers a broad range of physical and chemical research, with major emphasis on standards of physical measurement, fundamental constants, and properties of matter. Issued six times a year. Annual subscription: Domestic, $9.50; foreign, $11.75*.

• Mathematical Sciences

Studies and compilations designed mainly for the mathematician and theoretical physicist. Topics in mathematical statistics, theory of experiment design, numerical analysis, theoretical physics and chemistry, logical design and programming of computers and computer systems. Short numerical tables. Issued quarterly. Annual subscription: Domestic, $5.00; foreign, $6.25*.

• Engineering and Instrumentation

Reporting results of interest chiefly to the engineer and the applied scientist. This section includes many of the new developments in instrumentation resulting from the Bureau's work in physical measurement, data processing, and development of test methods. It will also cover some of the work in acoustics, applied mechanics, building research, and cryogenic engineering. Issued quarterly. Annual subscription: Domestic, $5.00; foreign, $6.25*.

TECHNICAL NEWS BULLETIN

The best single source of information concerning the Bureau's research, developmental, cooperative and publication activities, this monthly publication is designed for the industry-oriented individual whose daily work involves intimate contact with science and technology—*for engineers, chemists, physicists, research managers, product-development managers, and company executives.* Annual subscription: Domestic, $3.00; foreign, $4.00*.

*** Difference in price is due to extra cost of foreign mailing.**

NONPERIODICALS

Applied Mathematics Series. Mathematical tables, manuals, and studies.

Building Science Series. Research results, test methods, and performance criteria of building materials, components, systems, and structures.

Handbooks. Recommended codes of engineering and industrial practice (including safety codes) developed in cooperation with interested industries, professional organizations, and regulatory bodies.

Special Publications. Proceedings of NBS conferences, bibliographies, annual reports, wall charts, pamphlets, etc.

Monographs. Major contributions to the technical literature on various subjects related to the Bureau's scientific and technical activities.

National Standard Reference Data Series. NSRDS provides quantitative data on the physical and chemical properties of materials, compiled from the world's literature and critically evaluated.

Product Standards. Provide requirements for sizes, types, quality and methods for testing various industrial products. These standards are developed cooperatively with interested Government and industry groups and provide the basis for common understanding of product characteristics for both buyers and sellers. Their use is voluntary.

Technical Notes. This series consists of communications and reports (covering both other agency and NBS-sponsored work) of limited or transitory interest.

Federal Information Processing Standards Publications. This series is the official publication within the Federal Government for information on standards adopted and promulgated under the Public Law 89–306, and Bureau of the Budget Circular A–86 entitled, Standardization of Data Elements and Codes in Data Systems.

Order NBS publications from:

Superintendent of Documents
Government Printing Office
Washington, D.C. 20402

☆ U. S. GOVERNMENT PRINTING OFFICE : 1971 O - 385-762

Latest developments in the subject area of this publication, as well as in other areas where the National Bureau of Standards is active, are reported in the NBS Technical News Bulletin. See following page.

HOW TO KEEP ABREAST OF NBS ACTIVITIES

Your purchase of this publication indicates an interest in the research, development, technology, or service activities of the National Bureau of Standards.

The best source of current awareness in your specific area, as well as in other NBS programs of possible interest, is the TECHNICAL NEWS BULLETIN, a monthly magazine designed for engineers, chemists, physicists, research and product development managers, librarians, and company executives.

If you do not now receive the TECHNICAL NEWS BULLETIN and would like to subscribe, and/or to review some recent issues, please fill out and return the form below.

(cut here)

Mail to: Office of Technical Information and Publications
National Bureau of Standards
Washington, D. C. 20234

Name _____

Affiliation _____

Address _____

City _____ State _____ Zip _____

☐ Please send complimentary past issues of the Technical News Bulletin.

☐ Please enter my 1–yr subscription. Enclosed is my check or money order for $3.00 (additional $1.00 for foreign mailing).
Check is made payable to: SUPERINTENDENT OF DOCUMENTS.

SP 326